frontiers | Research Topics

# Inflammation in skin-related diseases

**Edited by**
Chunmeng Shi, Zhenghua Zhang and Meredith Crosby

**Published in**
Frontiers in Immunology
Frontiers in Medicine

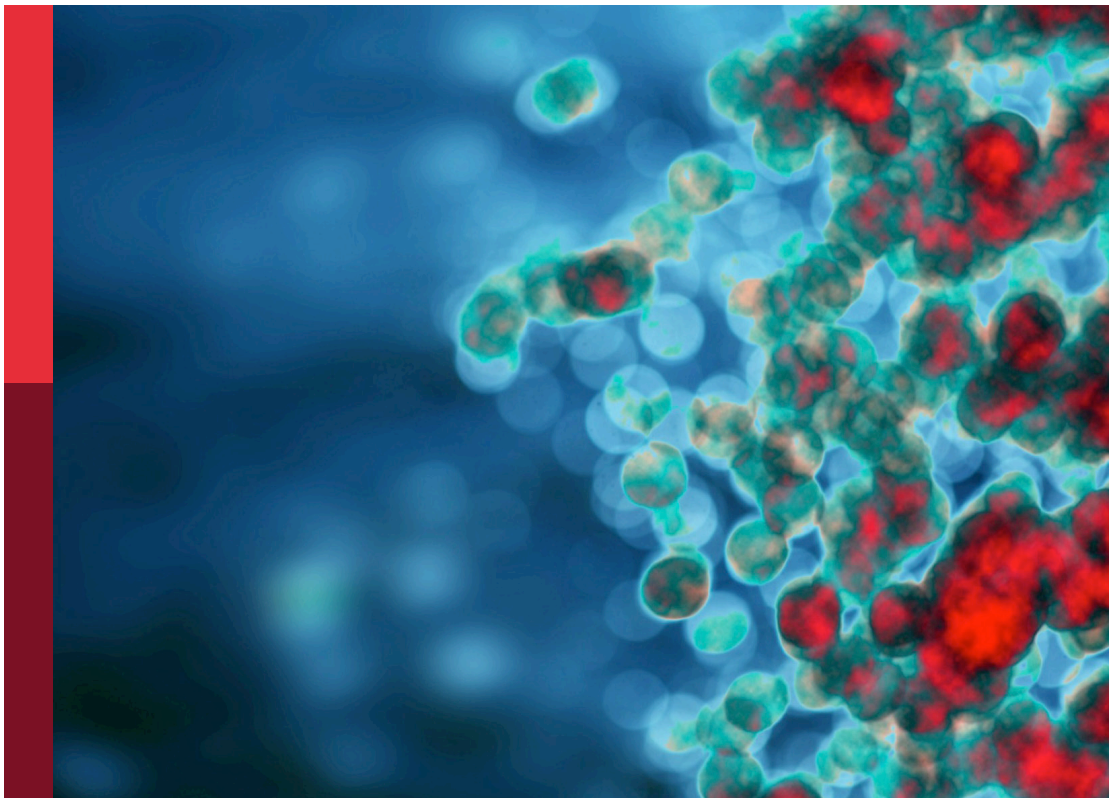

ISSN 1664-8714
ISBN 978-2-8325-5340-4
DOI 10.3389/978-2-8325-5340-4

## About Frontiers

Frontiers is more than just an open access publisher of scholarly articles: it is a pioneering approach to the world of academia, radically improving the way scholarly research is managed. The grand vision of Frontiers is a world where all people have an equal opportunity to seek, share and generate knowledge. Frontiers provides immediate and permanent online open access to all its publications, but this alone is not enough to realize our grand goals.

## Frontiers journal series

The Frontiers journal series is a multi-tier and interdisciplinary set of open-access, online journals, promising a paradigm shift from the current review, selection and dissemination processes in academic publishing. All Frontiers journals are driven by researchers for researchers; therefore, they constitute a service to the scholarly community. At the same time, the *Frontiers journal series* operates on a revolutionary invention, the tiered publishing system, initially addressing specific communities of scholars, and gradually climbing up to broader public understanding, thus serving the interests of the lay society, too.

## Dedication to quality

Each Frontiers article is a landmark of the highest quality, thanks to genuinely collaborative interactions between authors and review editors, who include some of the world's best academicians. Research must be certified by peers before entering a stream of knowledge that may eventually reach the public - and shape society; therefore, Frontiers only applies the most rigorous and unbiased reviews. Frontiers revolutionizes research publishing by freely delivering the most outstanding research, evaluated with no bias from both the academic and social point of view. By applying the most advanced information technologies, Frontiers is catapulting scholarly publishing into a new generation.

## What are Frontiers Research Topics?

Frontiers Research Topics are very popular trademarks of the *Frontiers journals series*: they are collections of at least ten articles, all centered on a particular subject. With their unique mix of varied contributions from Original Research to Review Articles, Frontiers Research Topics unify the most influential researchers, the latest key findings and historical advances in a hot research area.

Find out more on how to host your own Frontiers Research Topic or contribute to one as an author by contacting the Frontiers editorial office: frontiersin.org/about/contact

# Inflammation in skin-related diseases

**Topic editors**

Chunmeng Shi — First Affiliated Hospital of Army Medical University, China

Zhenghua Zhang — Fudan University, China

Meredith Crosby — Regeneron Pharmaceuticals, Inc., United States

**Citation**

Shi, C., Zhang, Z., Crosby, M., eds. (2024). *Inflammation in skin-related diseases*. Lausanne: Frontiers Media SA. doi: 10.3389/978-2-8325-5340-4

# Table of contents

frontiers | Frontiers in Immunology

TYPE Mini Review
PUBLISHED 11 August 2023
DOI 10.3389/fimmu.2023.1239251



OPEN ACCESS

EDITED BY
Chunmeng Shi,
First Affiliated Hospital of Army Medical University, China

REVIEWED BY
Xia Dou,
Peking University, China

*CORRESPONDENCE
Yutaka Hatano
hatano@oita-u.ac.jp

RECEIVED 13 June 2023
ACCEPTED 31 July 2023
PUBLISHED 11 August 2023

CITATION
Hatano Y and Elias PM (2023) "Outside-to-inside," "inside-to-outside," and "intrinsic" endogenous pathogenic mechanisms in atopic dermatitis: keratinocytes as the key functional cells involved in both permeability barrier dysfunction and immunological alterations.
*Front. Immunol.* 14:1239251.
doi: 10.3389/fimmu.2023.1239251



# "Outside-to-inside," "inside-to-outside," and "intrinsic" endogenous pathogenic mechanisms in atopic dermatitis: keratinocytes as the key functional cells involved in both permeability barrier dysfunction and immunological alterations

Yutaka Hatano [1]* and Peter M. Elias [2]

[1]Department of Dermatology, Faculty of Medicine, Oita University, Oita, Japan, [2]Department of Dermatology, University of California, San Francisco and Veterans Affairs Health Care System, San Francisco, CA, United States

Permeability barrier disruption has been shown to induce immunological alterations (i.e., an "outside-to-inside" pathogenic mechanism). Conversely, several inflammatory and immunological mechanisms reportedly interrupt permeability barrier homeostasis (i.e., an "inside-to-outside" pathogenic mechanism). It is now widely recognized that alterations of even a single molecule in keratinocytes can lead to not only permeability barrier dysfunction but also to immunological alterations. Such a simultaneous, bidirectional functional change by keratinocytes is herein named an "intrinsic" pathogenic mechanism. Molecules and/or pathways involved in this mechanism could be important not only as factors in disease pathogenesis but also as potential therapeutic targets for inflammatory cutaneous diseases, such as atopic dermatitis, psoriasis, and prurigo nodularis. Elevation of skin surface pH following permeability barrier abrogation comprises one of the key pathogenic phenomena of the "outside-to-inside" mechanism. Not only type 2 cytokines (e.g., IL-4, IL-13, IL-31) but also type 1 (e.g. IFN-γ), and type 3 (e.g., IL-17, IL-22) as well as several other inflammatory factors (e.g. histamine) can disrupt permeability barrier homeostasis and are all considered part of the "inside-to-outside" mechanism. Finally, examples of molecules relevant to the "intrinsic" pathogenic mechanism include keratin 1, filaggrin, and peroxisome proliferator-activated receptor-α (PPARα).

KEYWORDS

**atopic dermatitis, keratinocyte, permeability barrier dysfunction, allergic inflammation, filaggrin, keratin 1, PPAR alpha**

## Introduction

As previously described in numerous review articles, permeability barrier abrogation has been shown to induce immunological alterations (i.e., "outside-to-inside" pathogenic mechanism; Figure 1). Conversely, several inflammatory and immunological factors have been reported to disturb permeability barrier homeostasis (i.e., "inside-to-outside" pathogenic mechanism; Figure 1) (1). In this article, we will highlight additional associations between permeability barrier abrogation and inflammatory and/or immunological alterations.

Currently, multiple studies have revealed that modification in even a single molecule in keratinocytes can induce epidermal functional changes that not only disrupt permeability barrier homeostasis but also lead to immunological alterations. Here, we describe simultaneous functional changes in keratinocytes in two different directions as an "intrinsic" pathogenic mechanism (Figure 2).

## Induction of both type 2 and type 3 inflammation by the "outside-to-inside" pathogenic mechanism

Following epidermal permeability barrier abrogation, the "outside-to-inside" mechanism not only encompasses the induction and/or secretion of pro-inflammatory cytokines such as interleukin (IL)-1α, IL-1β, tumor necrosis factor (TNF)-α, and granulocyte macrophage colony-stimulating factor (GM-CSF) from epidermal keratinocytes (2), but also elevation of skin surface pH, accompanied by elevated kallikrein (KLK) activity (1), all key pathogenic phenomena for inducing inflammation, especially type 2. Initiation of production and/or secretion of so-called danger signals or alarmins, such as IL-25, IL-33, and thymic stromal lymphopoietin (TSLP), lead to immunological alterations of type 2 inflammation with or without protease-activated receptor (PAR) 2-dependent responses (3). In addition, permeability barrier abrogation reportedly induces type 2 and type 3 inflammation (e.g., IL-17 and IL-22) via activation of KLK5 and the PAR2 axis (4). In line with this theory, combined treatment with a PAR2 inhibitor and a lactobionic acid (LBA) ('super acid') exhibited therapeutic effects on hapten-induced atopic dermatitis (AD)-like dermatitis in a murine model in which elevations of epidermal TSLP paralleled development of the dermatitis (5). Application of LBA during the induction phase was also reported to prevent the initial emergence of hapten-induced AD-like dermatitis (6). Notably, both type 2 and type 3 inflammation are reported to be involved in the pathogenesis of a hapten-induced AD-like dermatitis (7), supporting the concept that a combination of permeability barrier abrogation, elevation of stratum corneum pH, and PAR2 activation could lead to the induction of type 2 and type 3 inflammation.

**Abbreviations:** IL, interleukin; TNF, tumor necrosis factor; GM-CSF, granulocyte macrophage colony-stimulating factor; KLK, kallikrein; TSLP, thymic stromal lymphopoietin; PAR, protease-activated receptor; LBA, lactobionic acid; AD, atopic dermatitis; FLG, filaggrin; LOR, loricrin; IVL, involucrin; ELOVL, elongation of very long chain fatty acids protein; CLE, cornified lipid envelope; ALOX12B, arachidonate 12-lipoxygenase, 12R type; ALOXE3, epidermis-type lipoxygenase 3; ABHD9, epoxide hydrolase 3; ZO, zonula occludens; IFN, Interferon; KRT, keratin; SC, stratum corneum; PPARs, Peroxisome proliferators-activated receptors; RANTES, Regulated upon activation, normal t cell expressed and presumably secreted cytokine; TARC, Thymus- and activation-regulated chemokine.

## Several pro-inflammatory factors are involved in the "inside to outside" pathogenic mechanism

Since we first described the "inside to outside" pathogenic mechanism (1), several inflammatory factors and pathways have been found to be involved in this mechanism.

Prototypic type 2 cytokines, IL-4 and IL-13, downregulate the expression of filaggrin (FLG), loricrin (LOR), and involucrin (IVL) (8, 9). IL-4 also reduces ceramide synthesis and compromises stratum corneum (SC) cohesion (10–12). Cutaneous permeability barrier recovery is suppressed by IL-4 (13). Recently, type 2 cytokines were reported to provoke shortening of ceramide carbon chains via down-regulation of elongase expression, such as elongation of very long chain fatty acids protein (ELOVL)3 (14). Type 2 cytokines also downregulate enzymes involved in cornified lipid envelope (CLE) formation, such as ALOX12B, ALOXE3, and ABHD9 (15). Likewise, IL-31 reportedly suppresses expression of FLG (16). Claudin-1, a tight junction-related protein, is downregulated by IL-4, IL-13, and IL-31 (17).

Considerable data demonstrating the harmful effects of a variety of inflammatory factors (besides type 2 cytokines) on the permeability barrier have been accumulated. Type 3 cytokines (e.g., IL-17 and IL-22) and histamines downregulate expression of FLG, LOR, and IVL (18, 19), R. Histamine reportedly downregulates the expression of claudin-1, claudin-4, occludin, and zonula occludens (ZO)-1 (19). Interferon (IFN)-γ, a prototypic type 1 cytokine, has been demonstrated to reduce expression of FLG, claudin-1, and ELOVL1 (20–22).

## Recognition of a newly emerging concept, an "intrinsic" pathogenic mechanism, elucidating the association between permeability barrier dysfunction and inflammatory reactions

Abundant evidence leads us to recognition of the association between permeability barrier dysfunction and inflammatory reactions. Alteration of even one molecule in epidermal keratinocytes can induce functional changes, leading to simultaneous permeability barrier dysfunction and inflammatory

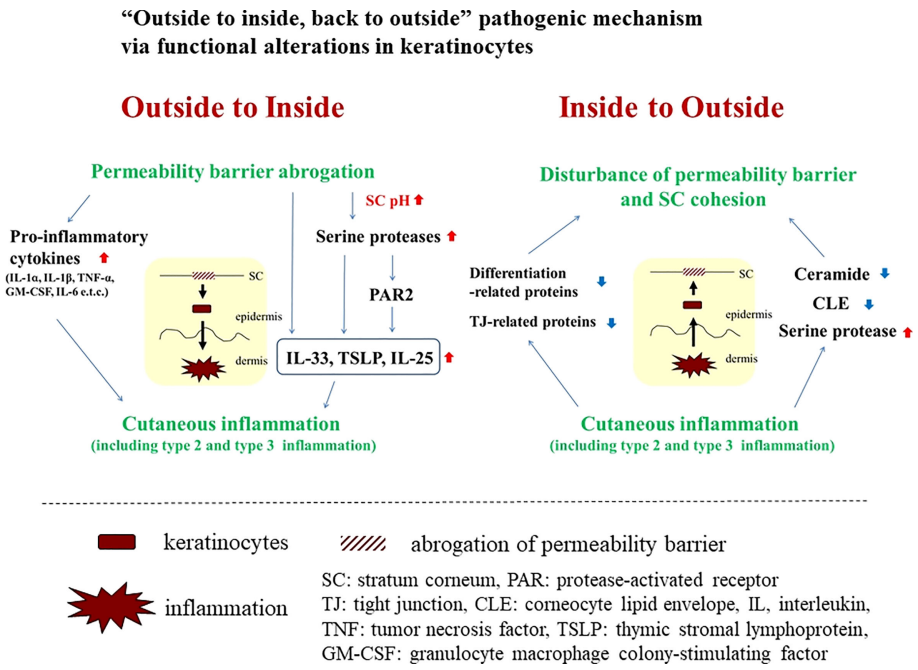


FIGURE 1
"Outside to inside, back to outside" pathogenic mechanism via functional alterations in keratinocytes.

and/or immunological dysregulation. Here, such a molecule is called an "intrinsic" participant, and the pathogenic mechanism induced by the alteration of these molecules is also called "intrinsic." Examples of "intrinsic" molecules are described below (Figure 2).

## Keratin 1

Keratins constitute the intermediate filament cytoskeleton in keratinocytes and play an important role in the mechanical integrity of corneocytes, during linkage to cornified envelopes, which is a critical process for competent permeability barrier formation (23, 24). In fact, permeability barrier abnormalities have been demonstrated in keratin (KRT)-deficient conditions (25, 26). Meanwhile, KRT1 abnormalities reportedly lead to cutaneous inflammation, accompanied by elevations of IL-18, IL-33, and TSLP (27), which are well-known danger signals in type 2 inflammation induction, a hallmark in AD pathogenesis (3, 28–30). Interestingly, IL-18 secretion is induced in *KRT1* knockout-cultured keratinocytes in a caspase-1-dependent manner,

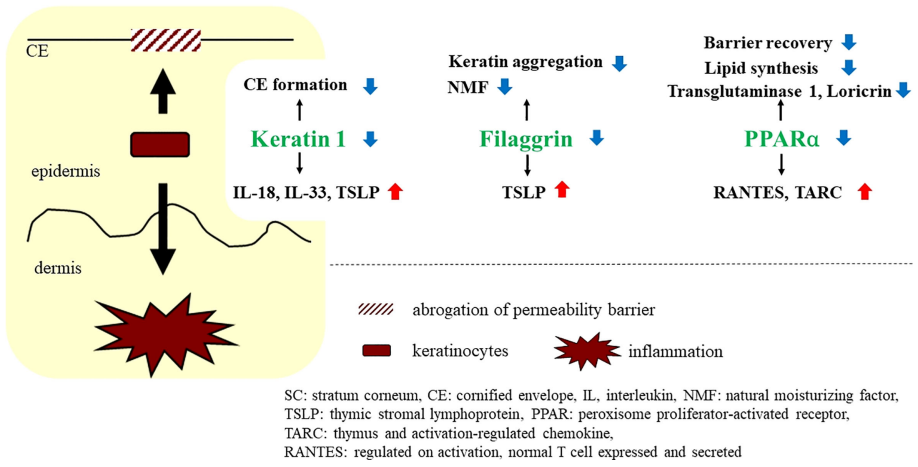


FIGURE 2
Examples of the "intrinsic" pathogenic mechanism via functional changes in keratinocytes.

suggesting that the secretion of IL-18 in *KRT1*-deficient mice could be a primary effect of *KRT1* depletion, rather than a secondary effect, following permeability barrier abrogation (27). Together, downregulation of KRT1 could cause functional, dual directional alterations in keratinocytes, leading to both permeability barrier abrogation and allergic inflammation in AD. Accordingly, expression of KRT1 reportedly is downregulated in atopic lesions due to elevated levels of inflammatory cytokines, such as IL-33, IL-4, and IL-13 (31, 32). Thus, the downregulation of KRT1 could augment not only permeability barrier abrogation but also allergic inflammation.

## Filaggrin

FLG is an epidermal differentiation-related molecule, which plays important roles in both permeability barrier homeostasis and SC hydration (33, 34). In fact, epidermis in which the filaggrin gene is knocked down exhibits substantial alterations in permeability barrier function (35). Interestingly, it has been recently shown that keratinocytes transfected with siRNA against the profilaggrin gene are able to produce greater quantities (versus control) of TSLP, which is one of the essential cytokines in the induction of type 2 immunological reactions (36). Knockdown of *FLG* reportedly increases the production of interleukin (IL)-1α, IL-8, IL-18 and GM-CSF in stratified human keratinocytes (37). It has also been reported that keratinocytes of flaky tail (versus wild-type mice), in which FLG is deficient due to a loss-of-function mutation in *profilaggrin*, produce more of the proinflammatory cytokine, IL-1β (38). In ichthyosis vulgaris, which is caused by loss of function mutations in *FLG*, expression of pro-inflammatory cytokines increases. Together, these results show that an abnormality in FLG, which has been mainly regarded as a barrier-related molecule, could simultaneously modulate processes leading to allergic inflammation in skin (39). Whether such a functional change in keratinocytes towards a proinflammatory phenotype is attributable to dysfunction of FLG in KRT aggregation remains undetermined, although in cultured epidermal keratinocytes knocked down of *FLG*, KRT1 expression was reported to be unaffected (40).

## Peroxisome proliferators-activated receptor α

Peroxisome proliferators-activated receptors (PPARs) belong to the nuclear hormone receptor class II and have three subtypes, PPARα, PPARβ/δ and PPARγ (41). They are called liposensors because their ligands are lipids or lipid derivatives. Generally, PPAR signaling has positive effects on barrier homeostasis, but it can also have anti-inflammatory effects, although there are some differences in the impact of their subtypes (41). The activation of PPARs stimulates lipid synthesis and epidermal differentiation, while also accelerating recovery after permeability barrier disruption (41). Moreover, epidermal barrier development is delayed in PPARα-deficient mice (42).

Activators of PPARα suppress both allergic and irritant cutaneous inflammation *in vivo* (43). Interestingly, it has been reported that PPARα expression in the skin is reduced in patients with AD and that PPARα-deficient mice develop more severe hapten-induced AD-like dermatitis than wild-type mice (44). RNA sequence analysis also revealed that PPARα expression is down-regulated in AD-like lesions compared with those in non-lesional flaky tail mice skin (45). In addition, PPARα expression in epidermis is reduced in similar hapten-induced murine AD models, and topical activation of PPARα exhibits a substantial therapeutic effect on murine AD, by restoring permeability barrier function and by dampening allergic inflammation (46, 47).

Awareness of physiological properties of PPARα in the skin and the association of decreased PPARα expression with AD suggests that PPARα might be one of the macromolecules that participates in "intrinsic" cross talk. In fact, reduction of PPARα expression by transfection with siRNA against *PPARα* not only up-regulates expression of the Regulated-upon-activation, normal-t cell-expressed-and-presumably-secreted cytokine (RANTES) and the Thymus- and activation-regulated chemokine (TARC) in cultured keratinocytes, but also down-regulates expression of transglutaminase 1 and LOR (48), further suggesting that PPARα modulates functions associated both with inflammation and with permeability barrier homeostasis in skin.

## Discussion

A vicious cycle involving permeability barrier dysfunction and allergic inflammation is one of the basic mechanisms leading to the pathogenesis of AD. In this article, in addition to discussing the concept of the so-called "outside-to-inside, and back-to-outside" paradigm, we offer an idea that links permeability dysfunction and allergic inflammation in the pathogenesis of AD. In the "outside-to-inside and back-to-outside" model, keratinocyte functions are modified secondarily by external stimuli, such as SC pH, or certain inflammatory factors. On the other hand, in our "intrinsic" model, primary functional changes relevant to both permeability barrier and inflammation can occur in keratinocytes by alteration of even a single molecule. Secondary alteration of such a molecule may also contribute to augment the vicious cycle between permeability barrier dysfunction and allergic inflammation. This concept demonstrates the importance of keratinocytes as a key player in the pathogenesis of AD, although it is unclear whether this concept applies equally to extrinsic and intrinsic AD.

Keratinocytes are well known to have functions related to both permeability barrier dysfunction and inflammation, meaning that keratinocytes likely are involved in both of these processes in the pathogenesis of AD. The concept "intrinsic" highlights molecules in keratinocytes which are simultaneously involved in both permeability barrier function and inflammation, and such molecules could be candidates as therapeutic targets in AD, as in the case of PPARα activators in the murine AD model. Interestingly, the Janus kinase inhibitor, JTE-052, now the main ingredient in an ointment called Delgocitinib, was originally reported to induce filaggrin expression, and this ointment has been deployed as topical therapy for AD (49, 50), suggesting that targeting keratinocyte functions is one potential strategy for treating AD.

Knowledge that changes in one molecule in keratinocytes can lead to both permeability barrier abrogation and inflammation has been already reported, as in the case of KRT1 mutations (27). Moreover, Akiyama et al. have described an autoinflammatory keratinization disease paradigm (51–53), and this disease concept seems almost identical to inflammatory aspects in our "intrinsic" mechanism described here. Therefore, seeking the pathomechanisms of autoinflammatory keratinization diseases could help to clarify the mechanism underlining our "intrinsic" paradigm, and AD might be recognized as an autoinflammatory keratinization disease in the future.

## Author contributions

YH wrote the first draft of the manuscript. PE revised the manuscript. All authors contributed to manuscript revision, read, and approved the submitted version.

## Funding

Grant-in-Aid for Scientific Research (C).

## Acknowledgments

We sincerely appreciate Ms. Joan S. Wakefield's (San Francisco Veterans Affairs Health Care System) excellent editing.

## Conflict of interest

The authors declare that the research was conducted in the absence of any commercial or financial relationships that could be construed as a potential conflict of interest.

## Publisher's note



## References

1. Elias PM, Hatano Y, Williams ML. Basis for the barrier abnorMality in atopic dermatitis. outside-inside-outside pathogenic mechanisms. *J Allergy Clin Immunol* (2008) 121:1337–43. doi: 10.1016/j.jaci.2008.01.022

2. Denda M, Wood LC, Emami S, Calhoun C, Brown BE, Elias PM, et al. The epidermal hyperplasia associated with repeated barrier disruption by acetone treatment or tape stripping cannot be attributed to increased water loss. *Arch Dermatol Res* (1996) 288:230–8. doi: 10.1007/BF02530090

3. Nakahara T, Kido-Nakahara M, Tsuji G, Furue M. Basics and recent advances in the pathophysiology of atopic dermatitis. *J Dermatol* (2021) 48:130–9. doi: 10.1111/1346-8138.15664

4. Kishibe M. Physiological and pathological roles of kallikrein-related peptidases in the epidermis. *J Dermatol Sci* (2019) 95:50–5. doi: 10.1016/j.jdermsci.2019.06.007

5. Sakai T, Hatano Y, Matsuda-Hirose H, Zhang W, Takahashi D, Jeong SK, et al. Combined benefits of a PAR2 inhibitor and stratum corneum acidification for murine atopic dermatitis. *J Invest Dermatol* (2016) 136:538–41. doi: 10.1016/j.jid.2015.11.011

6. Hatano Y, Man MQ, Uchida Y, Crumrine D, Scharschmidt TC, Kim EG, et al. Maintenance of an acidic stratum corneum prevents emergence of murine atopic dermatitis. *J Invest Dermatol* (2009) 129:1824–35. doi: 10.1038/jid.2008.444

7. Heo WI, Lee KE, Hong JY, Kim MN, Oh MS, Kim YS, et al. The role of interleukin-17 in mouse models of atopic dermatitis and contact dermatitis. *Clin Exp Dermatol* (2015) 40:665–71. doi: 10.1111/ced.12567

8. Howell MD, Kim BE, Gao P, Grant AV, Boguniewicz M, Debenedetto A, et al. Cytokine modulation of atopic dermatitis filaggrin skin expression. *J Allergy Clin Immunol* (2007) 120:150–5. doi: 10.1016/j.jaci.2007.04.031

9. Kim BE, Leung DY, Boguniewicz M, Howell MD. Loricrin and involucrin expression is down-regulated by Th2 cytokines through STAT-6. *Clin Immunol* (2008) 126:332–7. doi: 10.1016/j.clim.2007.11.006

10. Hatano Y, Terashi H, Arakawa S, Katagiri K. Interleukin-4 suppresses the enhancement of ceramide synthesis and cutaneous permeability barrier functions induced by tumor necrosis factor-alpha and interferon-gamma in human epidermis. *J Invest Dermatol* (2005) 124:786–92. doi: 10.1111/j.0022-202X.2005.23651.x

11. Hatano Y, Katagiri K, Arakawa S, Fujiwara S. Interleukin-4 depresses levels of transcripts for acid-sphingomyelinase and glucocerebrosidase and the amount of ceramide in acetone-wounded epidermis, as demonstrated in a living skin equivalent. *J Dermatol Sci* (2007) 47:45–7. doi: 10.1016/j.jdermsci.2007.02.010

12. Hatano Y, Adachi Y, Elias PM, Crumrine D, Sakai T, Kurahashi R, et al. The Th2 cytokine, interleukin-4, abrogates the cohesion of normal stratum corneum in mice. implications for pathogenesis of atopic dermatitis. *Exp Dermatol* (2013) 22:30–5. doi: 10.1111/exd.12047

13. Kurahashi R, Hatano Y, Katagiri K. IL-4 suppresses the recovery of cutaneous permeability barrier functions in *vivo*. *J Invest Dermatol* (2008) 128:1329–31. doi: 10.1038/sj.jid.5701138

14. Berdyshev E, Goleva E, Bronova I, Dyjack N, Rios C, Jung J, et al. Lipid abnorMalities in atopic skin are driven by type 2 cytokines. *JCI Insight* (2018) 22: e98006. doi: 10.1172/jci.insight.98006

15. Chiba T, Nakahara T, Kohda F, Ichiki T, Manabe M, Furue M. Measurement of trihydroxy-linoleic acids in stratum corneum by tape-stripping. Possible biomarker of barrier function in atopic dermatitis. *PloS One* (2019) 14:e0210013. doi: 10.1371/journal.pone.0210013

16. Cornelissen C, Marquardt Y, Czaja K, Wenzel J, Frank J, Lüscher-Firzlaff J, et al. IL-31 regulates differentiation and filaggrin expression in human organotypic skin models. *J Allergy Clin Immunol* (2012) 129:426–33. doi: 10.1016/j.jaci.2011.10.042

17. Gruber R, Börnchen C, Rose K, Daubmann A, Volksdorf T, Wladykowski E, et al. Diverse regulation of claudin-1 and claudin-4 in atopic dermatitis. *Am J Pathol* (2015) 185:2777–89. doi: 10.1016/j.ajpath.2015.06.021

18. Furue M. Regulation of filaggrin, loricrin, and involucrin by IL-4, IL-13, IL-17A, IL-22, AHR, and NRF2. Pathogenic implications in atopic dermatitis. *Int J Mol Sci* (2020) 21:5382. doi: 10.3390/ijms21155382

19. Gschwandtner M, Mildner M, Mlitz V, Gruber F, Eckhart L, Werfel T, et al. Histamine suppresses epidermal keratinocyte differentiation and impairs skin barrier function in a human skin model. *Allergy* (2013) 68:37–47. doi: 10.1111/all.12051

20. Hvid M, Johansen C, Deleuran B, Kemp K, Deleuran M, Vestergaard C. Regulation of caspase 14 expression in keratinocytes by inflammatory cytokines–a possible link between reduced skin barrier function and inflammation? *Exp Dermatol* (2011) 20:633–6. doi: 10.1111/j.1600-0625.2011.01280.x

21. Mizutani Y, Takagi N, Nagata H, Inoue S. Interferon-γ downregulates tight junction function, which is rescued by interleukin-17A. *Exp Dermatol* (2021) 30:1754–63. doi: 10.1111/exd.14425

22. Tawada C, Kanoh H, Nakamura M, Mizutani Y, Fujisawa T, Banno Y, et al. Interferon-γ decreases ceramides with long-chain fatty acids. possible involvement in atopic dermatitis and psoriasis. *J Invest Dermatol* (2014) 134:712–8. doi: 10.1038/jid.2013.364

23. Schweizer J, Bowden PE, Coulombe PA, Langbein L, Lane EB, Magin TM, et al. New consensus nomenclature for mamMalian keratins. *J Cell Biol* (2006) 174:169–74. doi: 10.1083/jcb.200603161

24. Candi E, Schmidt R, Melino G. The cornified envelope. a model of cell death in the skin. *Nat Rev Mol Cell Biol* (2005) 6:328–40. doi: 10.1038/nrm1619

25. Lane EB, McLean WH. Keratins and skin disorders. *J Pathol* (2004) 204:355–66. doi: 10.1002/path.1643

26. Schmuth M, Yosipovitch G, Williams ML, Weber F, Hintner H, Ortiz-Urda S, et al. Pathogenesis of the permeability barrier abnorMality in epidermolytic hyperkeratosis. *J Invest Dermatol* (2001) 117:837–47. doi: 10.1046/j.0022-202x.2001.01471.x

27. Roth W, Kumar V, Beer HD, Richter M, Wohlenberg C, Reuter U. Keratin 1 maintains skin integrity and participates in an inflammatory network in skin through interleukin-18. *J Cell Sci* (2012) 125:5269–79. doi: 10.1242/jcs.116574

28. Ihim SA, Abubakar SD, Zian Z, Sasaki T, Saffarioun M, Maleknia S, et al. Interleukin-18 cytokine in immunity, inflammation, and autoimmunity. Biological role in induction, regulation, and treatment. *Front Immunol* (2022) 13:919973. doi: 10.3389/fimmu.2022.919973

29. Konishi H, Tsutsui H, Murakami T, Yumikura-Futatsugi S, Yamanaka K, Tanaka M, et al. IL-18 contributes to the spontaneous development of atopic dermatitis-like inflammatory skin lesion independently of IgE/stat6 under specific pathogen-free conditions. *Proc Natl Acad Sci U S A* (2002) 99:11340–5. doi: 10.1073/pnas.152337799

30. Trzeciak M, Gleń J, Bandurski T, Sokołowska-Wojdyło M, Wilkowska A, Roszkiewicz J. Relationship between serum levels of interleukin-18, IgE and disease severity in patients with atopic dermatitis. *Clin Exp Dermatol* (2011) 36:728–32. doi: 10.1111/j.1365-2230.2011.04113.x

31. Dai X, Utsunomiya R, Shiraishi K, Mori H, Muto J, Murakami M, et al. Nuclear IL-33 plays an important role in the suppression of FLG, LOR, keratin 1, and keratin 10 by IL-4 and IL-13 in human keratinocytes. *J Invest Dermatol* (2021) 141:2646–2655.e6. doi: 10.1016/j.jid.2021.04.002

32. Totsuka A, Omori-Miyake M, Kawashima M, Yagi J, Tsunemi Y. Expression of keratin 1, keratin 10, desmoglein 1 and desmocollin 1 in the epidermis. possible downregulation by interleukin-4 and interleukin-13 in atopic dermatitis. *Eur J Dermatol* (2017) 27:247–53. doi: 10.1684/ejd.2017.2985

33. Brown SJ, McLean WH. One remarkable molecule. filaggrin. *J Invest Dermatol* (2012) 132:751–62. doi: 10.1038/jid.2011.393

34. Thyssen JP, Kezic S. Causes of epidermal filaggrin reduction and their role in the pathogenesis of atopic dermatitis. *J Allergy Clin Immunol* (2014) 134:792–9. doi: 10.1016/j.jaci.2014.06.014

35. Kawasaki H, Nagao K, Kubo A, Hata T, Shimizu A, Mizuno H, et al. Altered stratum corneum barrier and enhanced percutaneous immune responses in filaggrin-null mice. *J Allergy Clin Immunol* (2012) 129:1538–46.e6. doi: 10.1016/j.jaci.2012.01.068

36. Hönzke S, Wallmeyer L, Ostrowski A, Radbruch M, Mundhenk L, Schäfer-Korting M, et al. Influence of Th2 cytokines on the cornified envelope, tight junction proteins, and ß-defensins in filaggrin-deficient skin equivalents. *J Invest Dermatol* (2016) 136:631–9. doi: 10.1016/j.jid.2015.11.007

37. Sakai T, Hatano Y, Zhang W, Fujiwara S, Nishiyori R. Knockdown of either filaggrin or loricrin increases the productions of interleukin (IL)-1α, IL-8, IL-18 and granulocyte macrophage colony-stimulating factor in stratified human keratinocytes. *J Dermatol Sci* (2015) 80:158–60. doi: 10.1016/j.jdermsci.2015.09.002

38. Kezic S, O'Regan GM, Lutter R, Jakasa I, Koster ES, Saunders S, et al. Filaggrin loss-of-function mutations are associated with enhanced expression of IL-1 cytokines in the stratum corneum of patients with atopic dermatitis and in a murine model of filaggrin deficiency. *J Allergy Clin Immunol* (2012) 129:1031–9. doi: 10.1016/j.jaci.2011.12.989

39. Sakabe J, Kamiya K, Yamaguchi H, Ikeya S, Suzuki T, Aoshima M, et al. Proteome analysis of stratum corneum from atopic dermatitis patients by hybrid quadrupole-orbitrap mass spectrometer. *Allergy Clin Immunol* (2014) 134:957–60.e8. doi: 10.1016/j.jaci.2014.07.054

40. Mildner M, Jin J, Eckhart L, Kezic S, Gruber F, Barresi C, et al. Knockdown of filaggrin impairs diffusion barrier function and increases UV sensitivity in a human skin model. *J Invest Dermatol* (2010) 130:2286–94. doi: 10.1038/jid.2010.115

41. Schmuth M, Jiang YJ, Dubrac S, Elias PM, Feingold KR. Thematic review series. skin lipids. Peroxisome proliferator-activated receptors and liver X receptors in epidermal biology. *J Lipid Res* (2008) 9:499–509. doi: 10.1194/jlr.R800001-JLR200

42. Schmuth M, Schoonjans K, Yu QC, Fluhr JW, Crumrine D, Hachem JP, et al. Role of peroxisome proliferator-activated receptor alpha in epidermal development in *utero*. *J Invest Dermatol* (2002) 119:1298–303. doi: 10.1046/j.1523-1747.2002.19605.x

43. Sheu MY, Fowler AJ, Kao J, Schmuth M, Schoonjans K, Auwerx J, et al. Topical peroxisome proliferators-activated receptor-alpha activators reduce inflammation in irritant and allergic contact dermatitis models. *J Invest Dermatol* (2002) 118:94–101. doi: 10.1046/j.0022-202x.2001.01626.x

44. Staumont-Salle D, Abboud G, Brenuchon C, Kanda A, Roumier T, Lavogiez C, et al. Peroxisome proliferator-activated receptor alpha regulates skin inflammation and humoral response in atopic dermatitis. *J Allergy Clin Immunol* (2008) 121:962–8. doi: 10.1016/j.jaci.2007.12.1165

45. Sakai T, Aoki C, Mori Y, Yamate T, Matsuda-Hirose H, Hatano Y. Site-specific microarray evaluation of spontaneous dermatitis in flaky tail mice. *J Invest Dermatol* (2019) 139:2554–2557.e5. doi: 10.1016/j.jid.2019.04.024

46. Hatano Y, Man MQ, Uchida Y, Crumrine D, Mauro TM, Feingold KR, et al. Murine atopic dermatitis responds to peroxisome proliferator-activated receptors alpha and beta/delta (but not gamma) and liver X receptor activators. *J Allergy Clin Immunol* (2010) 125:160–9. doi: 10.1016/j.jaci.2009.06.049

47. Chiba T, Takeuchi S, Esaki H, Yamamura K, Kurihara Y, Moroi Y, et al. Topical application of PPARα (but not β/δ or γ) suppresses atopic dermatitis in NC/Nga mice. *Allergy* (2012) 67:936–42. doi: 10.1111/j.1398-9995.2012.02844.x

48. Adachi Y, Hatano Y, Sakai T, Fujiwara S. Expressions of peroxisome proliferator-activated receptors (PPARs) are directly influenced by permeability barrier abrogation and inflammatory cytokines and depressed PPARα modulates expressions of chemokines and epidermal differentiation-related molecules in keratinocytes. *Exp Dermatol* (2013) 22:606–8. doi: 10.1111/exd.12208

49. Amano W, Nakajima S, Kunugi H, Numata Y, Kitoh A, Egawa G, et al. The Janus kinase inhibitor JTE-052 improves skin barrier function through suppressing signal transducer and activator of transcription 3 signaling. *J Allergy Clin Immunol* (2015) 136:667–677.e7. doi: 10.1016/j.jaci.2015.03.051

50. Nakagawa H, Nemoto O, Igarashi A, Saeki H, Kabashima K, Oda M, et al. Delgocitinib ointment in pediatric patients with atopic dermatitis. A phase 3, randomized, double-blind, vehicle-controlled study and a subsequent open-label, long-term study. *J Am Acad Dermatol* (2021) 85:854–62. doi: 10.1016/j.jaad.2021.06.014

51. Akiyama M, Takeichi T, McGrath JA, Sugiura K. Autoinflammatory keratinization diseases. *J Allergy Clin Immunol* (2017) 140:1545–7. doi: 10.1016/j.jaci.2017.05.019

52. Akiyama M, Takeichi T, McGrath JA, Sugiura K. Autoinflammatory keratinization diseases. An emerging concept encompassing various inflammatory keratinization disorders of the skin. *J Dermatol Sci* (2018) 90:105–11. doi: 10.1016/j.jdermsci.2018.01.012

53. Akiyama M. Autoinflammatory keratinization diseases (AiKDs). Expansion of disorders to be included. *Front Immunol* (2020) 11:280. doi: 10.3389/fimmu.2020.00280

frontiers | Frontiers in Immunology

TYPE Original Research
PUBLISHED 23 August 2023
DOI 10.3389/fimmu.2023.1227024



OPEN ACCESS

EDITED BY
Claudia Farias Benjamim,
Federal University of Rio de Janeiro, Brazil

REVIEWED BY
Martin P. Alphonse,
Johns Hopkins Medicine, United States
Chen Fan,
University of Chinese Academy of Sciences, China

*CORRESPONDENCE
Xiqiao Wang
wxqiao2002@hotmail.com
Bo Yuan
hiyuanbo@163.com
Zengding Zhou
xueshengz@qq.com

†These authors have contributed equally to this work

RECEIVED 22 May 2023
ACCEPTED 01 August 2023
PUBLISHED 23 August 2023

CITATION
Yu J, Mao Z, Zhou Z, Yuan B and Wang X (2023) Microbiome dysbiosis occurred in hypertrophic scars is dominated by *S. aureus* colonization. *Front. Immunol.* 14:1227024. doi: 10.3389/fimmu.2023.1227024



# Microbiome dysbiosis occurred in hypertrophic scars is dominated by *S. aureus* colonization

Jiarong Yu[1†], Zhigang Mao[2†], Zengding Zhou[1*†], Bo Yuan[1*†] and Xiqiao Wang[1*†]

[1]The Department of Burn, Ruijin Hospital, Shanghai Jiaotong University School of Medicine, Shanghai, China, [2]The Department of Plastic Surgery, Ninth People's Hospital, Shanghai Jiaotong University School of Medicine, Shanghai, China

**Background:** The mechanisms of hypertrophic scar formation and its tissue inflammation remain unknown.

**Methods:** We collected 33 hypertrophic scar (HS) and 36 normal skin (NS) tissues, and detected the tissue inflammation and bacteria using HE staining, Gram staining, and transmission electronic microscopy (TEM), *in situ* hybridization and immunohistochemistry for MCP-1, TNF-α, IL-6 and IL-8. In addition, the samples were assayed by 16S rRNA sequencing to investigate the microbiota diversity in HS, and the correlation between the microbiota and the indices of Vancouver Scar Scale(VSS)score.

**Results:** HE staining showed that a dramatically increased number of inflammatory cells accumulated in HS compared with NS, and an enhanced number of bacteria colonies was found in HS by Gram staining, even individual bacteria could be clearly observed by TEM. *In situ* hybridization demonstrated that the bacteria and inflammation cells co-localized in the HS tissues, and immunohistochemistry indicated the expression of MCP-1, TNF-α, IL-6, and IL-8 were significantly upregulated in HS than that in NS. In addition, there was a significantly different microbiota composition between HS and NS. At the phylum level, *Firmicutes* was significantly higher in HS than NS. At the genus level, *S. aureus* was the dominant species, which was significantly higher in HS than NS, and was strongly correlated with VSS indices.

**Conclusion:** Microbiome dysbiosis, dominated by *S. aureus*, occurred in HS formation, which is correlated with chronic inflammation and scar formation, targeting the microbiome dysbiosis is perhaps a supplementary way for future scar management.

KEYWORDS

**microbiome dysbiosis, *S. aureus*, Vancouver Scar Score, hypertrophic scar, inflammation**

# Introduction

Human hypertrophic scars (HS), often occurring as a result of burns, trauma, or surgery, are a major clinical problem affecting over 80 million people worldwide each year (1). It appears at 1-2 months after wound healing, then develops hyperplasia within 6-24 months, which is accompanied by redness, elevation, itching, and pain. HS often causes severe cosmetic, functional, and even psychiatric impairment, greatly reducing the life quality (2). Many factors that contribute to hypertrophic scars have been reported, including delayed healing (3, 4), hypoxia microenvironment (5, 6), mechanical force, aberrant gene expression (7, 8), etc. Our understanding of HS is improving. However, these mechanisms cannot fully explain the definitive processes of scar hyperplasia, and the relevant therapies do not achieve a satisfactory effect on scar formation. Therefore, exploring the "culprit" of HS formation is of great importance.

Clinically, human adult HS was also regarded as a chronic inflammatory disease as persistent inflammation has been detected during HS formation (9). In contrast, there is no scar formation after wound healing in the fetus due to the lack of inflammatory responses in the fetus (10, 11). Thus, chronic inflammation is perhaps a "marker" that determines scar formation. Based on these observations, Ogawa and Akaishi hypothesized that HS and keloid are the same disorder depending on the extent of inflammation, and they classified keloid and HS as strong and moderate inflammation-induced scars, respectively (12). However, the factors that cause chronic inflammation in scar tissue have not been elucidated.

Currently, it is becoming increasingly evident that tissue inflammation is correlated with microbiome dysbiosis in many diseases (13, 14). Microbiota dysbiosis produces diverse metabolites that alter microbiome metabolism and host metabolism, affect adaptive immunity, and trigger inflammation (15, 16). Indeed, the skin microbiome is an ecosystem comprising commensal bacteria that not only reside in the skin surface (17), but also extend to subepidermal compartments including the skin dermis and adipose tissues (18). The pathogen invasion causes microbiota dysbiosis and inflammation. For example, Hidradenitis suppurativa is a chronic inflammatory skin disease of the hair follicle. A previous study revealed that *Propionibacterium* was the causing pathogen to induce microbiome dysbiosis (19). Atopic dermatitis (AD) is also a chronic inflammatory disease, and *S. aureus* is highly prevalent in AD skin (20, 21).

Therefore, in this study, we would like to know whether the microbiota dysbiosis occurred in scar tissues, and which bacteria dominated in the HS.

# Materials and methods

## Collection of HS and NS samples

The study was performed at the Burn Department, Ruijin Hospital, Shanghai Jiao Tong University School of Medicine, from February to December, 2021, and was approved by the Ethics Committee of Ruijin Hospital, Shanghai Jiao Tong University School of Medicine. All participants provided written informed consent.

Patients (2–61 years of age, male 19 and female 14) with burn-related HS, located on the limbs or trunks, which were featured by elevation, redness, and hardness, and needed scar excision and skin transplantation, were enrolled in this study. Meanwhile, 36 normal skin (NS) samples were harvested from these patients or other patients after skin transplantation, and all the donor sites were abdomen.

## Inclusion and exclusion criteria

The patients with scar duration ranging from 6 to 24 months were included, none of the participants received any antibiotics (systemic or oral therapy) within recent 3 months, and patients with keloids, scar ulcers, diabetes, or cardiovascular disease were excluded.

## Perform Vancouver Scar Scale score before surgery

Before surgery, the scars were assessed by Vancouver Scar Scale (VSS) score, and the indices of pigment, thickness, pliability, itching/pain, and vessel were assessed for each sample.

## Part 1: tissue processing for histochemistry experiment

During the surgery, the process was strictly disinfected to avoid bacterial contamination.

After surgery, the tissue was quickly put into the sterile specimen box, which had been irradiated under a UV light for 90 min, then tissue samples were further irradiated with UV light for 30 min, and subsequently washed 3 times with sterile PBS.

The samples were then fixed in 10% buffered formalin, embedded in paraffin blocks, and cut into 6-μm-thick sections. The sections were subjected to hematoxylin and eosin (H&E) staining, Gram staining, electron microscopy, *in situ* hybridization, and immunohistochemistry.

## H&E staining for inflammation cells

H&E staining was performed according to a standard protocol. Briefly, after deparaffinization and rehydration, sections were stained with hematoxylin solution for 5 min followed by 5 dips in 1% acid ethanol (1% HCl in 70% ethanol) and then rinsed in distilled water. Then the sections were stained with eosin solution for 3 min and followed by dehydration with graded alcohol and clearing in xylene. The mounted slides were then examined and photographed using an Olympus BX53 fluorescence microscope (Tokyo, Japan). The experiment was repeated three times, the

number of inflammation cells was calculated per view, and 8 samples were tested.

## Gram staining for bacteria detection

Gram staining was performed according to the protocol of the manufacturer (Beijing Solarbio Science& Technology, Beijing, China). Briefly, the heat-fixed smears on slides were flooded with 0.2% Victoria blue for 30 seconds and washed with tap water, smears were decolorized with 2% picric acid ethanol, and cells were counterstained with 0.004% fuchsin for 30 seconds and then washed with tap water. The positive staining was blue. The experiment was repeated three times, the area of gram-positive staining was calculated by Image J software, and 8 samples were tested.

## Transmission Electron microscopy for bacteria

Transmission Electron microscopy (TEM) was performed as previously described (22). First, tissue samples were fixed with 2.5% glutaraldehyde followed by 1% OsO4. Then, the samples underwent serial dehydration, soaking, embedding in epoxy resin, and sectioning into ultra-thin 60-nm sections. The sections were stained with a solution of uranyl acetate and lead citrate, and then a transmission electron microscope (HITACH 500, Hitachi, Ltd., Tokyo, Japan) was used at a voltage of 75 kV to observe the bacteria within the scar tissues. The experiment was repeated three times, the number of bacteria was calculated per view, and 5 samples were tested.

## *In situ* hybridization for tissue bacteria and inflammation cells

For fluorescence *in situ* hybridization, oligonucleotide probes (EUB338: 5′-GCTGCCTCCCGTAGGAGT-3′) conjugated with Alexa Flour 488 (Invitrogen, Carlsbad, CA, USA), targeting 16S rRNA, were used to label bacteria, and CD11b antibody conjugated with Alexa flour 594 (Invitrogen) was used to label the inflammatory cells. Briefly, sections were immediately fixed with RNase-free 4% formaldehyde and permeabilized, followed by dehydration with ethanol (50%, 75%, 100%). The sections were hybridized with EUB338 (5 ng/mL) overnight at 37°C, and the excess and non-specifically bound probe was washed with phosphate-buffered saline (PBS)×2. Then, sections were and incubated with rabbit anti-human CD11b primary antibody overnight at 4°C, washed with PBS×2, and incubated with Alexa Fluor 594-conjugated donkey anti-rabbit antibody at room temperature. Then the nuclei were stained with 4′,6-diamidino-2-phenylindole (DAPI; H-1200; Vector Laboratories, Burlingame, CA, USA). Images were captured using a con-focal laser scanning microscope (Carl Zeiss, Oberkochen, Germany). The experiment was repeated three times, the area of positive staining was calculated by Image J software, and 8 samples were tested.

## Immunohistochemistry for inflammation cytokines MCP-1, IL-6, IL-8, and TNF-α

VECTASTAIN Elite Avidin-Biotin Complex Kit (Maixin Biotech. Co, Fuzhou, China) was used for immunohistochemical staining of MCP-1, TNF-α, IL-6, and IL-8 according to the manufacturer's instruction. The primary and secondary antibodies used are listed in Table 1. Briefly, sections of the paraffin-embedded femurs were kept at 60°C for 24 h in the oven and then followed by deparaffinizing with xylene and hydrating with an ethanol gradient (100%–70%). After successively incubating with antigen retrieval solution (Shanghai Shunbai Biotechnology Company; Shanghai, China) and 3% $H_2O_2$ for 30 min, the slides were rinsed with water and incubated with the primary antibody MCP-1, IL-6, IL-8, and TNF-α overnight at 4°C(1:100 dilution; Santa Cruz Biotechnology Inc, Santa Cruz, CA). The next day, the slides were rinsed and incubated with the corresponding secondary antibody (1:100 dilution; Santa Cruz Biotechnology Inc)) for 30 min followed by 3,3′-diaminobenzidine (DAB) and hematoxylin staining, respectively. The slides were then examined and photographed using an Olympus BX53 fluorescence microscope (Tokyo, Japan). The experiment was repeated three times, the area of positive staining was calculated by Image J software, and 8 samples were tested.

## Part 2: tissue preparation for 16S-rRNA sequencing

As mentioned above, after the wash of the tissues, the epidermis of HS and NS were removed using a scalpel. Then the samples were stored at -80°C before genomic RNA extraction.

TABLE 1 Background information of participants.

| | Items | NS | HS | P value |
|---|---|---|---|---|
| **Basic information** | Age(years) | 18.61 ± 3.01 | 19.67 ± 3.40 | 0.82 |
| | Sample No. | 36 | 33 | - |
| | Male No. | 19 | 19 | 0.69 |
| | Female No. | 17 | 14 | |
| | Scar duration (months) | - | 10.82 ± 0.96 | - |
| **VSS scores** | Pigment | 0 | 2.15 ± 0.36 | <0.0001 |
| | Thickness | 0 | 2.52 ± 0.51 | |
| | Pliability | 0 | 2.82 ± 0.58 | |
| | Itching/pain | 0 | 1.03 ± 0.53 | |
| | Vessel | 0 | 1.48 ± 0.67 | |

## 16S-rRNA sequencing

Tissue genomic DNA was extracted from 0.1 g frozen skin and scar samples using MP Fast DNA SPIN Kit for Soil according to the manufacturer's protocol (23). Briefly, the DNA concentration and purification were measured, and the DNA quality was detected by electrophoresis. The 16S-rDNA gene were amplified using primers 341F: 5′-ACTCCTACGGGRSGCAGCAG-3′, and 806R: 5′-GGACTACVV GGGTATCTAATC-3′. PCR was performed. The reactions were performed on a thermocycler PCR system (GeneAmp 9700, ABI, USA). All PCR products were purified using an AxyPrep DNA Gel Extraction Kit (Axygen Biosciences, Union City, CA, USA) and quantified using QuantiFluor™-ST (Promega, USA). Purified and pooled amplicon libraries were paired-end sequenced (2×300) on the Illumina MiSeq platform (Illumina, San Diego, USA) according to the standard protocols by Majorbio Bio-Pharm Technology Co., Ltd. (Shanghai, China).

Raw sequence reads were demultiplexed, quality-filtered, merged, and clustered into OTUs with a 97% similarity cutoff using UPARSE (version 7.1, http://drive5.com/uparse/), and chimeric sequences were identified and removed using UCHIME. The taxonomy of the acquired OTUs was analyzed using the RDP Classifier Bayesian algorithm (http://rdp.cme.msu.edu/) against the SILVA database (version128) with a confidence threshold of 70%.

## Statistical analysis

Data generated from H&E staining, Gram staining, Masson staining, TEM, *in situ* hybridization, and immunohistochemistry analyzed by Image J software, and the data was expressed as mean ± SD, and two groups were red by two-tailed Student's t-test.

For the 16S sequencing data, all statistical analyses were performed using R packages (V·2·15·3) as follows.

Microbiota α-diversity, which represents microbial diversity within an individual group, was computed in QIIME through the whole tree phylogenetic diversity metric. And Shannon index was used.

Microbiota β-diversity, which indicates inter-variability of microbial diversity between groups, was examined through weighted UniFrac distances in QIIME and hierarchical clustering based on the unweighted pair group Method, and principal coordinates analysis (PCOA) was used.

To test the difference in microbiome composition between the two groups, the Kruskal-Wallis test was used, and phylum, genus, and species levels were selected for this analysis.

To evaluate the correlation between microbiota and clinical variables, the relationship was calculated through Spearman correlation.

For all statistical analyses, a 2-sided P <.05 was accepted as statistically significant.

# Results

## Patient characteristics

In our study, 33 HS (male 22, female 11) and 36 NS (male 24, female 12) were involved in this study, and average ages were 19.67 ± 3.50 (HS) and 18.61 ± 3.27 (NS) respectively, mainly located at the neck, trunk, and upper and lower extremity. There was no significant difference between the 2 groups in sex (p=0.83), age (p=0.20), and sample location (p=0.92), but the indices of VSS score were significantly higher in HS than that in NS (Figure 1A; Table 1).

## Higher inflammation and bacteria count in HS

H&E staining showed almost no inflammatory cells in the NS with loose collagen arrangement, however, in HS tissue, many clusters of inflammatory cells with dense collagen fibers were detected (Figure 1B).

According to Gram staining, few bacteria colonized in the sub-epidermis of NS tissue, instead, a large number of gram-positive bacteria colonizing in HS tissue was observed. (Figure 1C).

Using TEM, we confirmed the presence of bacteria in HS tissues, whereas almost no signs of bacteria were detected in NS dermis. The individual bacteria in HS tissues appeared round or elliptical with wave-like membranes. Interestingly, it was found that a bacterium was swallowed by an inflammatory cell (Figure 1D).

In addition, 16S-rRNA and CD11b staining were used to label the bacteria and inflammation cells respectively. According to the result, the bacteria clusters could be seen in HS with inflammatory cells distributed around, both were increased significantly in HS than that in NS (Figure 1E).

Immunohistochemistry revealed that NS tissues showed extremely low expression of MCP-1, IL-6, IL-8, and TNF-α. In contrast, their expression level was significantly higher in HS (Supplement Figure).

These results demonstrated that higher bacteria count and tissue inflammation were present in HS.

## α-diversity and β-diversity between two groups

The 16S rRNA amplicon sequencing analysis was used to sequence the microbiome in 36 NS and 33 HS samples. In total, 11,222 OTUs, 1 domain, 1 Kingdom, 56 Phyla, 134 Classes, 370 Orders, 691 Families, 1,652 Genera, and 3,417 Species were obtained from all samples.

In order to compare the microbiota richness and evenness between HS and NS, the a-diversity was calculated using the Chao, Shannon, and Simpson index, however, no significant difference was found between the two groups (Figure 2A). (Chao index p=0·103, Shannon index p=0·28, and Simpson index p=0·176, respectively)

β-diversity reflects the intra-group variability of the microbiome composition between two groups. When the indices of PCoA were used, the results showed that there was a clear separation between HS and NS (R=0·4970, *P*=0·001, Figure 2B), indicating a significantly different microbiota composition pattern between scar and NS.

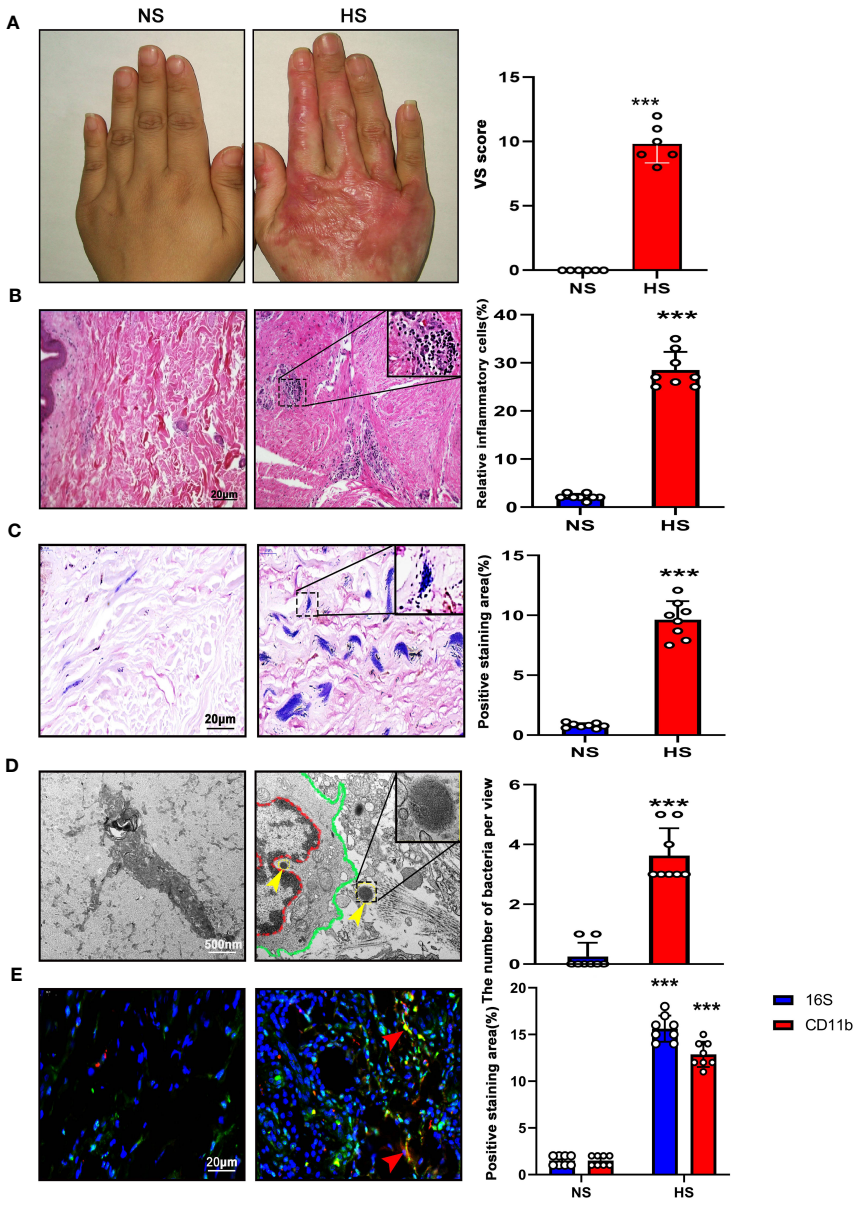


FIGURE 1
High bacterial content and inflammation in HS tissues. **(A)** Representative image of NS (left) and HS(right). HS appears red and has elevated shape compared to the NS. **(B)** H&E staining of tissue sections from NS and HS. Areas enclosed by the black box are magnified and shown in the top right corner. Scale bar: 20μm.The images are representative of three experiments with similar results. Data are shown as mean ± SD. ***P<0.001. **(C)** Gram staining of tissue sections from NS and HS. Scale bar: 20μm.The images are representative of three experiments with similar results. The area of gram positive staining was calculated by image J and shown as mean ± SD. ***P<0.001. **(D)** High-resolution transmission electron microscopy (HR-TEM) image of NS and HS tissue section. Macrophages (red line and green line) were engulfing bacteria(yellow arrow). A bacterium enclosed by the black box is magnified and shown in the top right corner. Scale bar: 500 nm. The number of bacteria was calculated by image J and shown as mean ± SD. ***P<0.001. **(E) $** Representative immunofluorent double-staining of NS and HS tissue. Staining: CD11b (green), inflammatory cell marker; 16s (red), bacteria marker; DAPI (blue). Scale bar: 20μm. The images are representative of three experiments with similar results. The area of positive staining was calculated by image J and shown as mean ± SD. ***P<0.001.

## Microbiome dysbiosis occurred in HS

The community abundance of each sample was counted at different taxonomic levels with R package, and the microbiome compositions of both groups were visualized by pie chart (Figure 2C). Then the microbiota differences between NS and HS were compared respectively at phylum, genus, and species levels.

At the phylum level, *Actinobacteria, Firmicute, Proteobacteria, and Bacteroidetes* were the major microbiota in HS and NS tissues, but the proportion varied. The *Firmicute* was significantly higher in HS than that in NS (53·2% & 5·52%, $P$=7·18×e$^{-11}$), whereas *Actinobacteria* in HS was significantly lower than NS (9·19% & 38·21%, $P$=1·735×e$^{-7}$). And the abundance of *Proteobacteria* and *Bacteroidetes* did not significantly differ between the two groups (data not shown in figure, $P$=0·065, $P$=0·59, respectively) (Figure 3A).

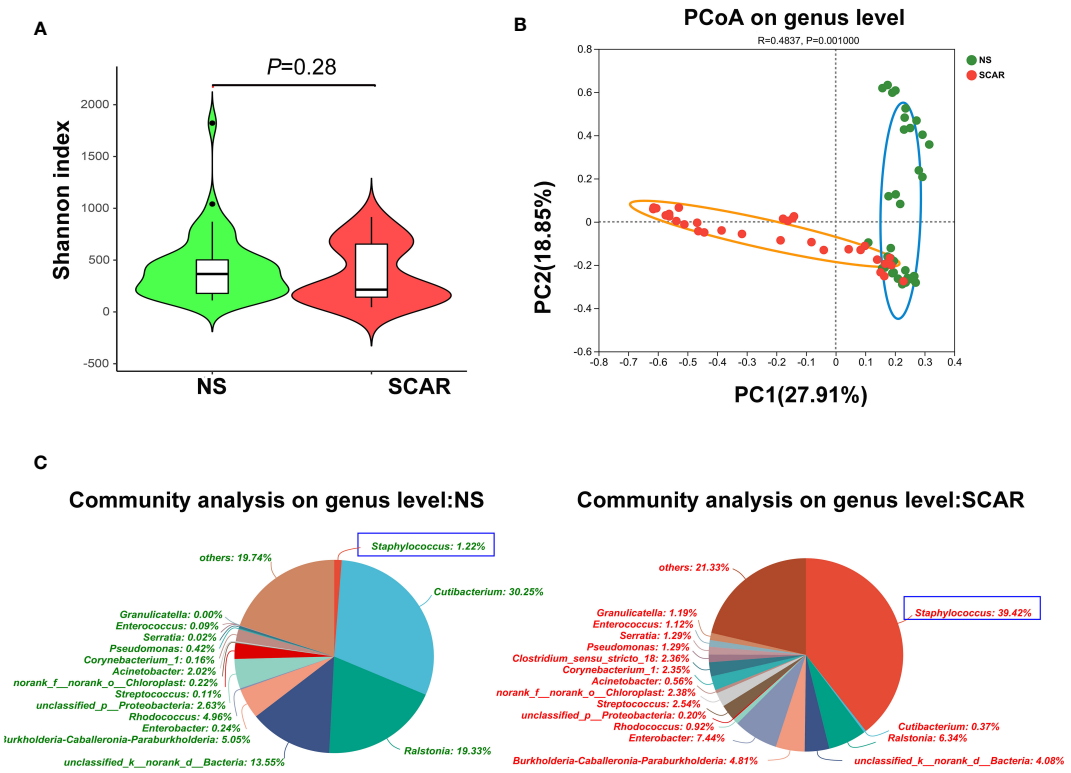


FIGURE 2
α-diversity and β-diversity of bacterial community in HS and NS. **(A)** α-diversity comparison with Shannon index showed there was no difference between HS and NS (*P*=0.210) **(B)** β-diversity comparison with PCoA showed a clear separation between HS and NS (R=0.4970, *P*=0.001). **(C)** The pie chart showed the bacteria community composition at genus level in two groups.

At the genus level, NS mainly harbored *Cutibacterium* (30·25%), *Ralstonia* (19·33%), *Rhodococcus* (4.96%), etc. Of note, HS tissues exhibited different proportions of the microbiome, named *Staphylococcus* (39·42%), *Enterobacter* (7·44%), *Ralstonia* (6·34%), *Streptococcus* (2·54%), etc. The abundances of *Staphylococcus*, *Enterobacter, and Streptococcus* in HS were significantly higher than that in the NS (39·42% & 1.22%, P=9·31×e-8; 7·44% & 0.24%, P=0·000006; 2·54% & 0.11%, P=0·0007 respectively). However, the prevalence of *Cutibacterium* and *Ralstonia* were significantly lower in HS tissues than that in NS (0.37% & 30·25%, P=1·14×e-7; 6.34% & 19·33%, P=0·0005 respectively) (Figure 3B).

At the species level, *S. aureus* had the highest prevalence in scar tissues, which was significantly greater than that in NS tissues (39·71% & 1·88%; $P$=1·13×$e^{-7}$). Secondly, unidentified *Enterobacter* and unclassified *Streptococcus* species were also significantly more prevalent in scar tissues than that in NS (7·44% & 0.22%, $P$=8·3×$e^{-5}$; 2·54% & 0.09%, $P$=3·42×$e^{-4}$, respectively), but the proportion was not high (data not shown in figure). However, *Cutibacterium acnes*, which was dominant in NS tissue, were significantly reduced in HS (28·89% & 0·33%, $P$=4·41×$e^{-8}$) (Figure 3C).

Normally, 16s sequencing could not identify species, but in our study, *S.aureus* and *Cutibacterium acnes* were identified. The above results indicate that microbiome dysbiosis occurred in HS, which was dominated by *S.aureus*.

## Genus *Staphylococcus, Enterobacter*, and *Streptococcus* are positively correlated with scar formation

In order to assess the correlation between the bacteria and the scar, the VSS indices including pigment, thickness, pliability, itching/pain, and vessel were used to evaluate HS clinical severity. For each HS patient, we calculated the Spearman correlation between the VSS scores and individual bacterial abundance, represented by a heatmap plot. Red indicates a positive correlation between bacterial content and clinical severity, and green represents a negative correlation. The results revealed that genus *Staphylococcus, Enterobacter*, and *Streptococcus* were positively correlated with clinical indices (Figure 4). However, genus *Cutibacterium, Ralstonia*, etc. were negatively correlated with scar indices. For instance, g_*Staphylococcus* had a strong correlation with chroma (r=0.6230, p<0.001), vessel (r=0.5513, p<0.001), thickness (r=0.5743, p<0.001), pliability (r=0.5965, p<0.001), itching and pain (r=0.5940, p<0.001) (Figure 4).

The spearman heatmap showed genus *Staphylococcus, Enterobacter*, and *Streptococcus* were positively correlated with these indices, and genus *Cutibacterium, Ralstonia* etc. were negatively correlated with scar indices. (**P*<0.01, ***P*<0.001, ****P*<0.0001).

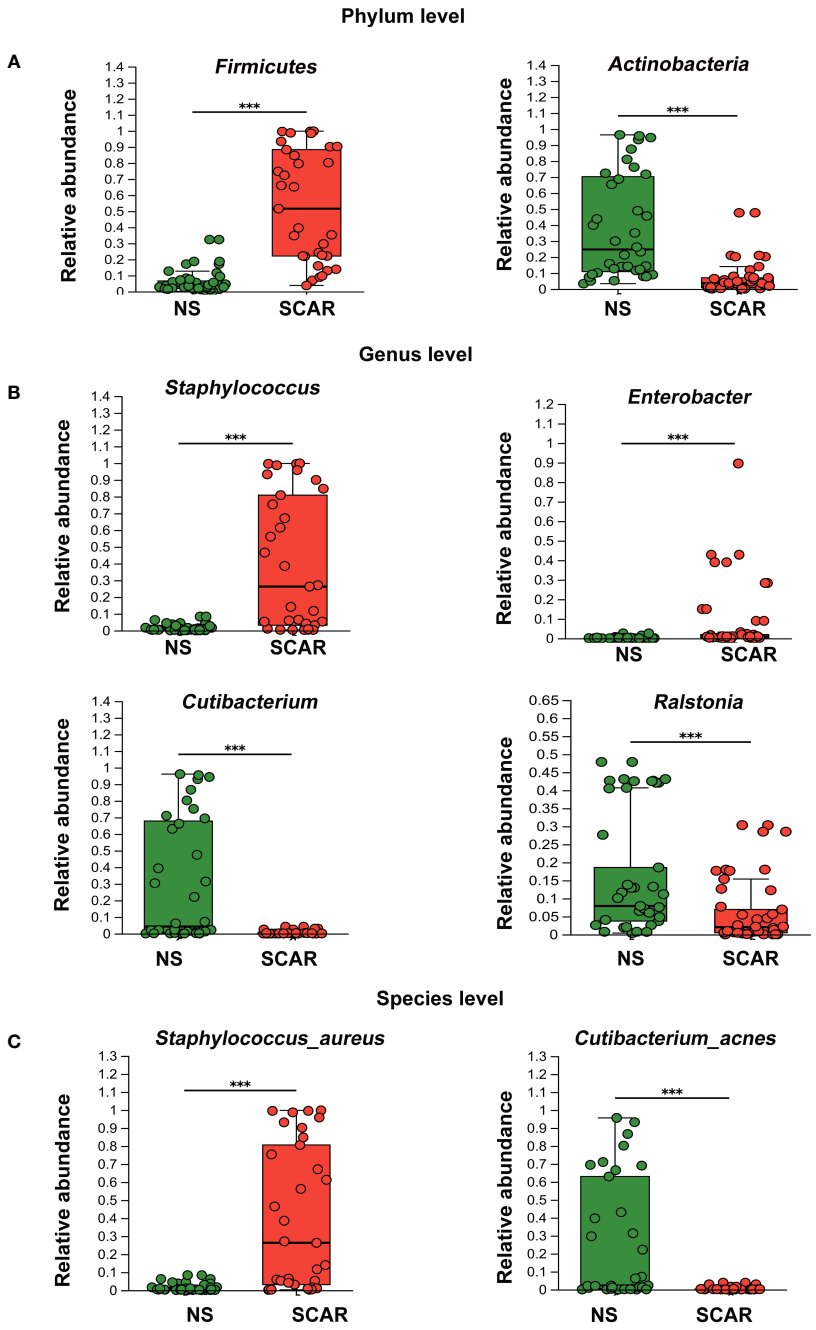


FIGURE 3
Different levels of microbiota abundance between HS and NS. **(A)** On Phylum level, the major difference of microbiota abundance between two groups. ***$P<0.001$ **(B)** On Genus level, the major difference of microbiota abundance between two groups. ***$P<0.001$ **(C)** On Species level, the major difference of microbiota abundance between two groups(the unclassified species were not listed). ***$P<0.001$.

## Discussion

Recent advances have highlighted the crucial role of microbiota in the maintenance of a healthy immune system. The pathogenic bacteria invasion or colonization will cause microbiome dysbiosis, leading to inflammation and diseases. In our study, we first observed a high count of gram-positive staining in HS, and inflammation cells co-localized with the bacteria. Meanwhile, the inflammation cytokines like MCP-1, IL-6 and IL-8, and TNF-α also increased in HS. Then using 16S sequencing, we confirmed that microbiome dysbiosis occurred in HS, which was prevalent in *S.aureus*.

Traditionally, scar tissue was regarded as a "clean site" without pathogen colonization. Where are the pathogens from? A previous study revealed that most surgical site infections arouse from the skin surface, due to the microbiome community shifting from the skin surface to the deep wound (24). A study on 312 wound swab samples from 213 patients found that the most common bacterial

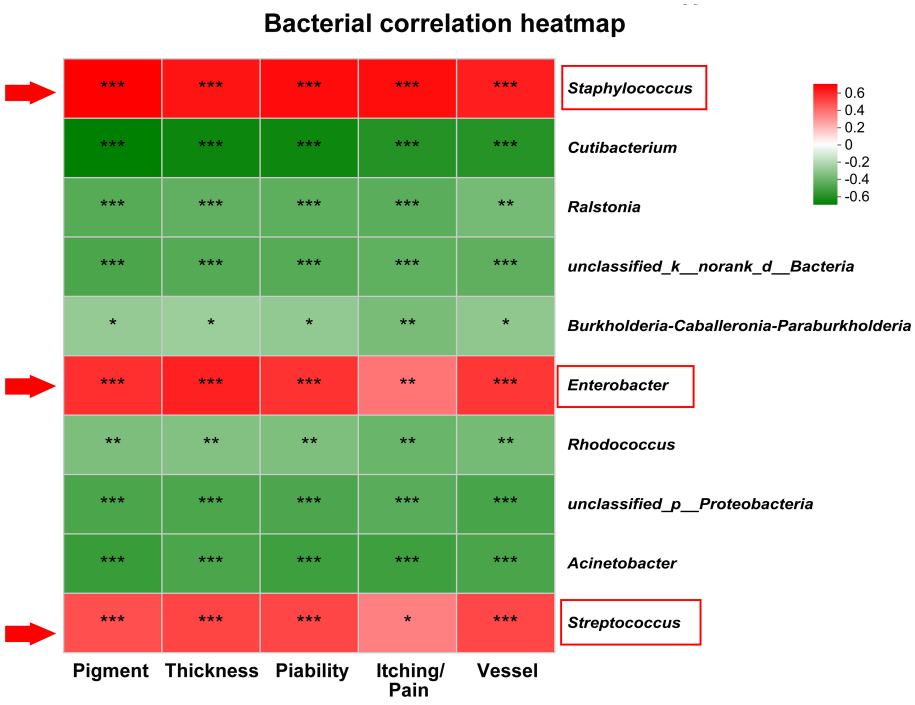


| Bacteria (Genus) | Scar index | | | | |
|---|---|---|---|---|---|
| | Pigment | Thickness | Pliability | Itching/pain | Vessel |
| g__Staphylococcus | 0.62 | 0.57 | 0.59 | 0.59 | 0.55 |
| g__Cutibacterium | -0.64 | -0.60 | -0.60 | -0.55 | -0.54 |
| g__Ralstonia | -0.42 | -0.40 | -0.40 | -0.41 | -0.34 |
| g__Enterobacter | 0.50 | 0.54 | 0.50 | 0.34 | 0.49 |
| g__Rhodococcus | -0.32 | -0.31 | -0.32 | -0.37 | -0.35 |
| g__Acinetobacter | -0.50 | -0.45 | -0.48 | -0.48 | -0.46 |
| g__Streptococcus | 0.43 | 0.45 | 0.45 | 0.31 | 0.45 |

FIGURE 4
The correlation between microbiota and scar indices. *** indicates P<0.001, ** indicates P<0.01, * indicates P<0.05.

species was *S. aureus* (37%), followed *by Pseudomonas aeruginosa* (17%), *Proteus mirabilis* (10%), *Enterobacter* spp. (6%), etc (25). Another prospective study on 1,770 wounds infection revealed that the most common causative organisms were *S. aureus* (23·7%), *Escherichia coli* (16·9%), *Staphylococcus epidermidis* (13·5%), and *Pseudomonas aeruginosa* (13·0%) (26). Similar results were reported in another study on 131 wounds, where *S. aureus*, *Pseudomonas aeruginosa*, and *Streptococci* species were the most common bacteria (27). These reports provide evidence that *S. aureus* was the major species during wound healing, which was consistent with our finding in HS. After wound healing, the tissue environment failed to remove the excess bacteria, which subsequently colonized in HS, causing microbiome dysbiosis and inducing chronic inflammation.

*S.aureus* is one of the most prevalent bacterial species causing cutaneous infections and wound inflammation (28). It is reported that *S. aureus* biofilm and toxin cause impaired granulation tissue collagen, leading to compromised wound healing (29). Moreover, previous studies have shown that *S. aureus* colonization was correlated with tissue fibrosis (30, 31). A study on bovine mammary fibrosis has found that *S. aureus* induces TLR2, TLR4, TGF-β1, and bFGF expression through AP-1 and NF-κB activation, and specific NF-κB and AP-1 inhibitors could reverse this process (32, 33). Moreover, in wound healing, *Enterobacter* could induce antibiotic resistance (34), which may be a reason for its long-term colonization and microbiota dysbiosis in scars. Furthermore, the study of intestinal fibrosis found that the inflammation caused by microbiota dysbiosis could upregulate TGFβ1, SMAD3, and α-SMA expression, and cause intestinal fibrosis (35). Thus, in our study, the higher expression of inflammation cytokines MCP-1, IL-6 and IL-8, and TNF-α may be correlated with *S. aureus* and *Enterobacter* colonization and mediate the scar formation.

It has been reported that the skin resides *Actinobacteria, Firmicutes, Proteobacteria, and Bacteroides* at the phylum level,

which are essential flora to maintain skin homeostasis (17). Our study confirmed the above findings in NS and found that in HS the abundance of the phylum *Actinobacteria* decreased significantly, indicating that the loss of *Actinobacteria* may have a close association with scar progression. Studies of *Actinobacteria* in the gut have shown its role in maintaining intestinal homeostasis by secreting beneficial metabolites (36). This suggests that *Actinobacteria* may play a protective role in scar formation, being able to maintain microbial homeostasis.

Additionally, we found that at the genus level, *Staphylococcus* and *Enterobacter* in HS were strongly correlated with VSS score indices, while *Cutibacterium* and *Ralstonia* were negatively correlated with VSS score indices. Therefore, *Cutibacterium* and *Ralstonia* may be protective communities to maintain homeostasis, while *Staphylococcus* and *Enterobacter* are pathogenic communities to promote HS formation, which may be a "biomarker" of HS to predict scar formation.

Currently, there are many modalities to treat hypertrophic scars like pressure therapy, silicon, radiotherapy, cryotherapy, laser, and so on (37–41). However, the effectiveness is not satisfied. Steroid injections show better scar inhibition due to inflammation control, however, it has a high recurrence (42), because the overload bacteria were not removed or balanced. Therefore, targeting microbiome dysbiosis perhaps is a supplementary therapy for scar treatment.

How to improve microbiota dysbiosis? Currently, there are two pathways to realize it including reducing the pathogen community and increasing the protective community. In acne research, antibiotic treatment is beneficial to improve microbiome dysbiosis and recover skin health (43). In a mouse model of *E. coli*-induced prostate fibrosis, enrofloxacin treatment completely eradicated the bacteria, resolved inflammation, and attenuated collagen content (44). Another pathway to regulate microbiome dysbiosis is the use of probiotics, which consists of beneficial organisms. Nakatusji et al. found that topical application of a protective bacteria in atopic dermatitis, the colonization of *S. aureus* decreased and improved the symptoms (45). Probiotic studies have also been shown to reduce infection and enhance wound healing in burn patients (46, 47). Therefore, more studies will be performed to test these findings in HS therapy.

In summary, our study indicates that microbiome dysbiosis occurred in HS dominated by *S. aureus* colonization, which may be the causing factor of chronic inflammation. Targeting the microbiome dysbiosis is perhaps a supplementary therapy to manage scar inflammation and its formation.

## Data availability statement

The datasets presented in this study can be found in online repositories. The names of the repository/repositories and accession number(s) can be found below: https://www.ncbi.nlm.nih.gov/bioproject/PRJNA748229.

## Ethics statement

The studies involving humans were approved by the Ethics Committee of Ruijin Hospital, Shanghai Jiao Tong University School of Medicine. The studies were conducted in accordance with the local legislation and institutional requirements. Written informed consent for participation in this study was provided by the participants' legal guardians/next of kin.

## Author contributions

XW and JY designed the research study; JY analyzed most of the data and wrote the draft of the paper; ZZ and ZM collected the hypertrophic scar and normal skin tissue from patients; JY performed most cell experiments; BY and XW revised the manuscript and contributed to the overall conclusions. All authors contributed to the article and approved the submitted version

## Funding

This work was supported by a grant from the National Natural Science Foundation of China (No. 81671914, 81170761, 81101433, 81871564, 82072173, and 81270909). And the manuscript was edited by Dr Feng Liu.

## Conflict of interest

The authors declare that the research was conducted in the absence of any commercial or financial relationships that could be construed as a potential conflict of interest.

## Publisher's note



## Supplementary material

The Supplementary Material for this article can be found online at: https://www.frontiersin.org/articles/10.3389/fimmu.2023.1227024/full#supplementary-material

# References

1. Ruppert DS, Mohammed MM, Ibrahim MM, Bachtiar EO, Erning K, Ansari K, et al. Poly(lactide-co-ϵ-caprolactone) scaffold promotes equivalent tissue integration and supports skin grafts compared to a predicate collagen scaffold. *Wound Repair Regen* (2021) 29(6):1035–50. doi: 10.1111/wrr.12951

2. Zhang T, Wang XF, Wang ZC, Lou D, Fang QQ, Hu YY, et al. Current potential therapeutic strategies targeting the TGF-β/Smad signaling pathway to attenuate keloid and hypertrophic scar formation. *BioMed Pharmacother* (2020) 129:110287. doi: 10.1016/j.biopha.2020.110287

3. Saulis AS, Mogford JH, Mustoe TA. Effect of Mederma on hypertrophic scarring in the rabbit ear model. *Plast Reconstr Surg* (2002) 110(1):177–83; discussion 184-6. doi: 10.1097/00006534-200207000-00029

4. Singer AJ, McClain SA. Persistent wound infection delays epidermal maturation and increases scarring in thermal burns. *Wound Repair Regen* (2002) 10(6):372–7. doi: 10.1046/j.1524-475X.2002.10606.x

5. Zheng J, Song F, Lu SL, Wang XQ. Dynamic hypoxia in scar tissue during human hypertrophic scar progression. *Dermatol Surg* (2014) 40(5):511–8. doi: 10.1111/dsu.12474

6. Lynam EC, Xie Y, Dawson R, Mcgovern J, Upton Z, Wang X. Severe hypoxia and malnutrition collectively contribute to scar fibroblast inhibition and cell apoptosis. *Wound Repair Regen* (2015) 23(5):664–71. doi: 10.1111/wrr.12343

7. Barnes LA, Marshall CD, Leavitt T, Hu MS, Moore AL, Gonzalez JG, et al. Mechanical forces in cutaneous wound healing: emerging therapies to minimize scar formation. *Adv Wound Care (New Rochelle)* (2018) 7(2):47–56. doi: 10.1089/wound.2016.0709

8. Hsu CK, Lin HH, Harn HI, Hughes MW, Tang MJ, Yang CC. Mechanical forces in skin disorders. *J Dermatol Sci* (2018) 90(3):232–40. doi: 10.1016/j.jdermsci.2018.03.004

9. Wang ZC, Zhao WY, Cao Y, Liu YQ, Sun Q, Shi P, et al. The roles of inflammation in keloid and hypertrophic scars. *Front Immunol* (2020) 11:603187. doi: 10.3389/fimmu.2020.603187

10. Larson BJ, Longaker MT, Lorenz HP. Scarless fetal wound healing: a basic science review. *Plast Reconstr Surg* (2010) 126(4):1172–80. doi: 10.1097/PRS.0b013e3181eae781

11. Dulay AT, Buhimschi CS, Zhao G, Oliver EA, Mbele A, Jing S, et al. Soluble TLR2 is present in human amniotic fluid and modulates the intraamniotic inflammatory response to infection. *J Immunol* (2009) 182(11):7244–53. doi: 10.4049/jimmunol.0803517

12. Ogawa R, Akaishi S. Endothelial dysfunction may play a key role in keloid and hypertrophic scar pathogenesis - Keloids and hypertrophic scars may be vascular disorders. *Med Hypotheses* (2016) 96:51–60. doi: 10.1016/j.mehy.2016.09.024

13. Gallo RL, Nakatsuji T. Microbial symbiosis with the innate immune defense system of the skin. *J Invest Dermatol* (2011) 131(10):1974–80. doi: 10.1038/jid.2011.182

14. Kong HH, Oh J, Deming C, Conlan S, Grice EA, Beatson MA, et al. Temporal shifts in the skin microbiome associated with disease flares and treatment in children with atopic dermatitis. *Genome Res* (2012) 22(5):850. doi: 10.1101/gr.131029.111

15. Minter MR, Hinterleitner R, Meisel M, Zhang C, Leone V, Zhang X, et al. Antibiotic-induced perturbations in microbial diversity during post-natal development alters amyloid pathology in an aged APPSWE/PS1ΔE9 murine model of Alzheimer's disease. *Sci Rep* (2017) 7:10411. doi: 10.1038/s41598-017-11047-w

16. Zakłos-Szyda M, Nowak A, Pietrzyk N, Podsędek A.. Viburnum opulus L. Juice phenolic compounds influence osteogenic differentiation in human osteosarcoma saos-2 cells. *Int J Mol Sci* (2020) 21(14):4909. doi: 10.3390/ijms21144909

17. Grice EA, Segre JA. The skin microbiome. *Nat Rev Microbiol* (2011) 9(4):244–53. doi: 10.1038/nrmicro2537

18. Nakatsuji T, Chiang HI, Jiang SB, Nagarajan H, Zengler K, Gallo RL. The microbiome extends to subepidermal compartments of normal skin. *Nat Commun* (2013) 4:1431. doi: 10.1038/ncomms2441

19. Ring HC, Thorsen J, Saunte DM, Lilje B, Bay L, Riis PT, et al. The follicular skin microbiome in patients with hidradenitis suppurativa and healthy controls. *JAMA Dermatol* (2017) 153(9):897–905. doi: 10.1001/jamadermatol.2017.0904

20. Biedermann T. Dissecting the role of infections in atopic dermatitis. *Acta Derm Venereol* (2006) 86(2):99–109. doi: 10.2340/00015555-0047

21. Eichenfield LF, Ellis CN, Mancini AJ, Paller AS, Simpson EL. Atopic dermatitis: epidemiology and pathogenesis update. *Semin Cutan Med Surg* (2012) 31(3 Suppl):S3–5. doi: 10.1016/j.sder.2012.07.002

22. Xi-Qiao W, Ying-Kai L, Chun Q, Shu-Liang L. Hyperactivity of fibroblasts and functional regression of endothelial cells contribute to microvessel occlusion in hypertrophic scarring. *Microvasc Res* (2009) 77(2):204–11. doi: 10.1016/j.mvr.2008.08.007

23. Guo A, Zhao Z, Zhang P, Yang Q, Li Y, Wang G. Linkage between soil nutrient and microbial characteristic in an opencast mine, China. *Sci Total Environ* (2019) 671:905–13. doi: 10.1016/j.scitotenv.2019.03.065

24. Wenzel RP. Surgical site infections and the microbiome: An updated perspective. *Infect Control Hosp Epidemiol.* (2019) 40(5):590–6. doi: 10.1017/ice.2018.363

25. Bessa LJ, Fazii P, Di Giulio M, Cellini L. Bacterial isolates from infected wounds and their antibiotic susceptibility pattern: some remarks about wound infection. *Int Wound J* (2015) 12(1):47–52. doi: 10.1111/iwj.12049

26. Twum-Danso K, Grant C, al-Suleiman SA, Abdel-Khader S, al-Awami MS, al-Breiki H, et al. Microbiology of postoperative wound infection: a prospective study of 1770 wounds. *J Hosp Infect* (1992) 21(1):29–37. doi: 10.1016/0195-6701(92)90151-B

27. Haalboom M, Blokhuis-Arkes M, Beuk RJ, Klont R, Guebitz G, Heinzle A, van der Palen J, et al. Wound swab and wound biopsy yield similar culture results. *Wound Repair Regen* (2018) 26(2):192–9. doi: 10.1111/wrr.12629

28. Huitema L, Phillips T, Alexeev V, Tomic-Canic M, Pastar I, Igoucheva O. Intracellular escape strategies of Staphylococcus aureus in persistent cutaneous infections. *Exp Dermatol* (2021) 30(10):1428–39. doi: 10.1111/exd.14235

29. Roy S, Santra S, Das A, Dixith S, Sinha M, Ghatak S, et al. Staphylococcus aureus biofilm infection compromises wound healing by causing deficiencies in granulation tissue collagen. *Ann Surg* (2020) 271(6):1174–85. doi: 10.1097/SLA.0000000000003053

30. Barbara CK. Impact of Staphylococcus aureus on the pathogenesis of chronic cystic fibrosis lung disease. *Int J Med Microbiol* (2010) 300(8):514–9. doi: 10.1016/j.ijmm.2010.08.002

31. Ahmed MI, Mukherjee S. Treatment for chronic methicillin-sensitive Staphylococcus aureus pulmonary infection in people with cystic fibrosis. *Cochrane Database Syst Rev* (2018) 2018(7):CD011581. doi: 10.1002/14651858.CD011581.pub3

32. Wu J, Ding Y, Wang J, Wang F. Staphylococcus aureus induces TGF-β1 and bFGF expression through the activation of AP-1 and NF-κB transcription factors in bovine mammary epithelial cells. *Microb Pathog* (2018) 117:276–84. doi: 10.1016/j.micpath.2018.02.024

33. Bi Y, Ding Y, Wu J, Miao Z, Wang J, Wang F. Staphylococcus aureus induces mammary gland fibrosis through activating the TLR/NF-κB and TLR/AP-1 signaling pathways in mice. *Microb Pathog* (2020) 148:104427. doi: 10.1016/j.micpath.2020.104427

34. Davin-Regli A, Lavigne JP, Pagès JM. Enterobacter spp.: update on taxonomy, clinical aspects, and emerging antimicrobial resistance. *Clin Microbiol Rev* (2019) 32(4):e00002–19. doi: 10.1128/CMR.00002-19

35. Zhao Z, Cheng W, Qu W, Shao G, Liu S., et al. Antibiotic alleviates radiation-induced intestinal injury by remodeling microbiota, reducing inflammation, and inhibiting fibrosis. *ACS Omega* (2020) 5(6):2967–77. doi: 10.1021/acsomega.9b03906

36. Binda C, Lopetuso LR, Rizzatti G, Gibiino G, Cennamo V, Gasbarrini A. Actinobacteria: A relevant minority for the maintenance of gut homeostasis. *Dig Liver Dis* (2018) 50(5):421–8. doi: 10.1016/j.dld.2018.02.012

37. So K, Umraw N, Scott J, Campbell K, Musgrave M, Cartotto R. Effects of enhanced patient education on compliance with silicone gel sheeting and burn scar outcome: a randomized prospective study. *J Burn Care Rehabil* (2003) 24(6):411–7; discussion 410. doi: 10.1097/01.BCR.0000095516.98523.04

38. O'Brien L, Pandit A. Silicon gel sheeting for preventing and treating hypertrophic and keloid scars. *Cochrane Database Syst Rev* (2006) 1):CD003826. doi: 10.1002/14651858.CD003826

39. DeBruler DM, Zbinden JC, Baumann ME, Blackstone BN, Malara MM, Bailey JK, et al. Early cessation of pressure garment therapy results in scar contraction and thickening. *PloS One* (2018) 13(6):e0197558. doi: 10.1371/journal.pone.0197558

40. Kuehlmann B, Stern-Buchbinder Z, Wan DC, Friedstat JS, Gurtner GC. Beneath the surface: A review of laser remodeling of hypertrophic scars and burns. *Adv Wound Care (New Rochelle)* (2019) 8(4):168–76. doi: 10.1089/wound.2018.0857

41. Ogawa R, Tosa M, Dohi T, Akaishi S, Kuribayashi S. Surgical excision and postoperative radiotherapy for keloids. *Scars Burn Heal* (2019) 5:2059513119891113. doi: 10.1177/2059513119891113

42. Morelli Coppola M, Salzillo R, Segreto F, Persichetti P. Triamcinolone acetonide intralesional injection for the treatment of keloid scars: patient selection and perspectives. *Clin Cosmet Investig Dermatol* (2018) 11:387–96. doi: 10.2147/CCID.S133672

43. Park SY, Kim HS, Lee SH, Kim S, et al. Characterization and analysis of the skin microbiota in acne: impact of systemic antibiotics. *J Clin Med* (2020) 9(1):168. doi: 10.3390/jcm9010168

44. Wong L, Hutson PR, Bushman W, et al. Resolution of chronic bacterial-induced prostatic inflammation reverses established fibrosis. *Prostate* (2015) 75(1):23–32. doi: 10.1002/pros.22886

45. Nakatsuji T, Chen TH, Narala S, Chun KA, Two AM, Yun T, et al. Antimicrobials from human skin commensal bacteria protect against Staphylococcus aureus and are deficient in atopic dermatitis. *Sci Transl Med* (2017) 9(378). doi: 10.1126/scitranslmed.aah4680

46. El-Ghazely MH, Mahmoud WH, Atia MA, Eldip EM. Effect of probiotic administration in the therapy of pediatric thermal burn. *Ann Burns Fire Disasters* (2016) 29:268–72.

47. Peral MC, Martinez MA, Valdez JC. Bacteriotherapy with Lactobacillus plantarum in burns. *Int Wound J* (2009) 6:73–81. doi: 10.1111/j.1742-481X.2008.00577.x

frontiers | Frontiers in Immunology

TYPE Review
PUBLISHED 29 August 2023
DOI 10.3389/fimmu.2023.1237992



OPEN ACCESS

EDITED BY
Wang Xiqiao,
Shanghai Jiao Tong University, China

REVIEWED BY
Peter S. Reinach,
Wenzhou Medical University, China
Yunsheng Chen,
Shanghai Jiao Tong University, China

*CORRESPONDENCE
Xiang He
heroxiang@hotmail.com
Qiannan Li
liqiannanyes@163.com

RECEIVED 10 June 2023
ACCEPTED 15 August 2023
PUBLISHED 29 August 2023

CITATION
Zheng Y, Huang Q, Zhang Y, Geng L, Wang W, Zhang H, He X and Li Q (2023) Multimodal roles of transient receptor potential channel activation in inducing pathological tissue scarification. *Front. Immunol.* 14:1237992. doi: 10.3389/fimmu.2023.1237992



# Multimodal roles of transient receptor potential channel activation in inducing pathological tissue scarification

Yuping Zheng, Qingrui Huang, Yanfeng Zhang, Lanxin Geng, Wuqing Wang, Huimin Zhang, Xiang He* and Qiannan Li*

Department of Dermatology, Shuguang Hospital Affiliated with Shanghai University of Traditional Chinese Medicine, Shanghai, China

Transient receptor potential (TRP) channels are a class of transmembrane proteins that can sense a variety of physical/chemical stimuli, participate in the pathological processes of various diseases and have attracted increasing attention from researchers. Recent studies have shown that some TRP channels are involved in the development of pathological scarification (PS) and directly participate in PS fibrosis and re-epithelialization or indirectly activate immune cells to release cytokines and neuropeptides, which is subdivided into immune inflammation, fibrosis, pruritus and mechanical forces increased. This review elaborates on the characteristics of TRP channels, the mechanism of PS and how TRP channels mediate the development of PS, summarizes the important role of TRP channels in the different pathogenesis of PS and proposes that therapeutic strategies targeting TRP will be important for the prevention and treatment of PS. TRP channels are expected to become new targets for PS, which will make further breakthroughs and provide potential pharmacological targets and directions for the in-depth study of PS.

KEYWORDS

**transient receptor potential channels, pathological scarification, inflammatory, fibrosis, re-epithelialization**

## 1 Introduction

Pathological scarification (PS) is a pathological result of wound healing and is caused by inflammation and trauma. Epidemiology shows that the overall prevalence of PS is 30%-90%. The incidence of hypertrophic scar (HS) in patients with full-thickness burns is as high as 80% (1). In the United States alone, the cost of treating HS is estimated to be $400 million per year (2), which brings a huge economic burden to families and society. PS is one of the important complications of tissue damage repair, including HS and keloids. It is mainly characterized by the infiltration of inflammatory cells such as macrophages, lymphocytes, mast cells and neutrophils (3). Inflammatory mediators secreted by immune cells induce fibroblasts (FBs) fibrosis and keratinocytes (KCs) re-epithelialization, resulting in excessive

deposition of a large amount of extracellular matrix (ECM) components, which is accompanied by mechanical stretching and angiogenesis and eventually develops into PS (4–6). Furthermore, recent studies have shown that oxidative stress and epigenetic regulation are involved in the occurrence of PS (7, 8). PS easily causes appearance damage and local tissue pruritus, pain, tumor-like hyperplasia or varying degrees of dysfunction, affecting the physical and mental health of patients (9). PS research has always been a challenging topic in the field of burns, plastic surgery and dermatology department (10). However, the exact pathogenesis of PS is unclear and still needs to be examined.

Recently, many studies have shown that transient receptor potential (TRP) channels are involved in many mechanisms of PS, such as participating in the development of PS fibrosis and re-epithelialization or affecting the secretion of TGF-β1 and ECM by nonimmune cells, and regulating cytokine release, cell migration and phagocytosis through immune-related mechanisms (11). Some TRP channels are involved in PS mechanical conduction, oxidative stress, epigenetics and pruritus. Therefore, the expression of TRP channels in PS deserves more attention. This review focused on specific channels in the TRP family, such as TRPV, TRPC, TRPA and TRPM, especially TRPV1-4, TRPC3, TRPC6, TRPA1 and TRPM7. These are channel proteins that play important roles in the wound healing and the development of PS.

The analysis of this information aimed to demonstrate immune inflammation and fibrosis to examine TRP channels as potential targets for inhibiting PS.

## 2 TRP channels classification and function

The TRP superfamily consists of nonselective cation channels with the ability to sense local environmental changes (12). In 1969, Cosens (13) found that light stimulation only caused a transient increase in intracellular $Ca^{2+}$ concentrations in a Drosophila mutant with light sensing defects. Subsequently, Hardie (14) found that this was due to the lack of functional copies of genes encoding ion channels and named this type of calcium-permeable cation channel the TRP channel. According to differences in amino acid sequence homology, the mammalian TRP family is divided into six groups: ankyrin (TRPA), canonical (TRPC), melastatin (TRPM), mucolipin (TRPML), polycystin (TRPP), and vanilloid (TRPV) (15).

TRP channels are abundantly expressed in various cell types (16). For example, KCs, melanocytes, FBs and a variety of immune cells express TRP channels (17). TRP channels can be activated by external stimuli or local environmental changes (including pain, pruritus, heat, warmth or cold, odor, mechanical stimulation, and osmotic pressure changes) (18). In addition, TRP channels are critical in physiological processes such as regulating skin homeostasis, melanin synthesis, wound healing, epigenetic regulation, and pathological processes such as barrier damage, vascular stress relaxation, oxidative stress, and skin cancer caused by ultraviolet irradiation (19). There is growing evidence that the TRP family plays an important role in mediating disease fibrosis (20). These results are consistent with the mechanism of PS.

The TRPV subfamily consists of six members, which can be subdivided into heat-activated TRPV (TRPV1-4) channels and $Ca^{2+}$-selective TRPV channels (TRPV5, TRPV6) (21), and these channels can be activated by different stimuli such as heat, pruritus, pain, osmotic pressure or chemical stimulation (21, 22). TRPV channels are involved in the activation and differentiation of immune cells and play an important role in activating macrophages, stimulating the type 17 immune inflammatory response and inducing neutrophil adhesion and chemotaxis (23–25). TRPV is closely related to fibrosis and is mainly involved in myofibroblasts (MFBs) differentiation and collagen deposition (26). TRPV is also an important osmotic-mechanical sensitive channel that mediates abnormal mechanical conduction into specific biochemical signals (23, 27). In addition, TRPV is related to angiogenesis (28), epigenetic regulation (29), electrolyte homeostasis (30) and the maintenance of barrier function (31).

The TRPC family can be further divided into four subgroups (TRPC1, TRPC2, TRPC4/5 and TRPC3/6/7) according to their amino acid sequence and functional homology (32). TRPC channels may mediate fibrotic diseases as mechanosensitive ion channels (33) and can sense and regulate oxidative stress responses. For example, the oxidation product OONO- upregulates the mRNA and protein expression of TRPC6 and TRPC3 in monocytes (34). In addition, TRPC channels are involved in the inflammatory response (35), mitochondrial metabolism in ageing (36), cell proliferation, wound healing (37), and angiogenesis (38). In particular, TRPC3 and TRPC6 have been shown to be crucial in the mechanical conduction of wound healing (39).

TRPA channels have been widely studied in the field of pruritus, pain and neurogenic inflammation (15). TRPA1 is the only member of the mammalian TRPA family that can be activated by cold and heat stimulation, mechanical forces, chemicals and endogenous signals associated with cell damage. TRPA1 is also an important mediator of acute and chronic itching perception. Exogenous and endogenous pruritus can produce scratching behavior by activating neuronal TRPA1 (19). In addition, TRPA1 is expressed in immune cells, KCs, melanocytes, FBs, epithelial cells and sensory neurons and plays a key role in the pathophysiology of almost all systems (40–42).

The TRPM subfamily consists of eight members (TRPM1-8), is the largest subfamily of TRP channels and has a specific structure and physical function (43). The TRPM subfamily is expressed in various organs and cells of the peripheral, central and immune systems and is vital in various biological processes, such as cold and heat stimulation, ion homeostasis, autophagy, vascular tension, epigenetics, and immune inflammation (29, 44–46). An increasing number of studies have shown that TRPM channel participates in fibrotic diseases (47, 48).

## 3 Cutaneous wound healing and the mechanism of PS

### 3.1 Physiological wound healing process

The physiological wound healing process is divided into four stages: hemostasis, inflammation, proliferation and remodeling

(49). To a certain extent, this process is mediated by growth factors and regulatory molecules (50).

① Collagen and tissue factors promote the clumping of platelet aggregation in the affected area, releasing chemotactic and growth factors and eventually forming clots (51). ② The infiltration of inflammatory cells marks the beginning of the inflammatory phase of wound healing (50). Immune cells such as neutrophils, lymphocytes, mast cells and monocytes release inflammatory mediators to defend against microorganisms and remove wound pathogens and tissue fragments (52). When proinflammatory M1 macrophages transform into anti-inflammatory M2 macrophages, the wound healing process shifts to the proliferative phase (53). The hemostasis and inflammatory phases typically take 3 days (54). ③ The proliferative phase is an important stage associated with angiogenesis, KC migration, granulation tissue formation, ECM accumulation and epithelialization (55). FBs synthesize ECM and promote the formation of granulation tissue (53). FBs activation, KCs proliferation and migration, and new epithelial differentiation jointly promote wound re-epithelialization (56). Furthermore, FBs can be activated and differentiate into MFBs, which promote matrix remodeling to promote wound healing and angiogenesis (56, 57). ④ The final step is the remodeling phase, which typically lasts for weeks or even years (58). This stage mainly involves excessive tissue degradation (59). Excessive ECM is degraded, and collagen type III (COL-3) is replaced by mature collagen type I (COL-1), eventually leading to wound healing (60), as shown in Figure 1.

TRP channels play a key role in various stages of physiological wound healing, with TRPV1-4, TRPC3, TRPC6, TRPA1, and TRPM7 being closely associated. Specifically, TRPV1, TRPV3, TRPV4, and TRPA1 are involved in the inflammatory, proliferative, and remodeling phases of physiological wound healing. For instance, TRPV1 deficiency can lead to neutrophil inflammation and NETs formation, as well as defective re-epithelialization, which can prolong wound healing (61).

TRPV3, on the other hand, can induce fibrosis through TRPV3/TSLP/Smad2/3 pathway, resulting in significantly increased expression levels of α-SMA, fibronectin, COL1A1, and TSLP (62). Additionally, the selective TRPV3 activator KS0365 has been shown to accelerate the migration of KCs and promote re-epithelialization during physiological wound healing (63). Furthermore, the presence of TRPV3 in macrophage lysosomes may play a crucial role in the inflammatory phase of PS (64).

The activation of TRPV4 has been shown to promote TGF-β1 and IL-6 induced fibrosis and inflammation (20). Conversely, the lack of TRPA1 has been found to retard macrophage infiltration, subsequent fibrotic tissue formation, and mRNA expression of α-SMA and COL-1, which may further impair fibrotic behavior in fibroblasts (65). Additionally, TRPV2, TRPC3, TRPC6, and TRPM7 have been implicated in the proliferative and remodeling phases of wound healing. Specifically, TRPV2 mediates FB differentiation and contraction by promoting TGF-β1 and α-SMA expression (66).

Inhibition of TRPC3 and TRPC6 can suppress MFBs trans-differentiation and the expression of αSMA and TGF-β1 (67, 68). Furthermore, overexpression of TRPM7 promotes fibrosis and ECM deposition in wound healing (69).

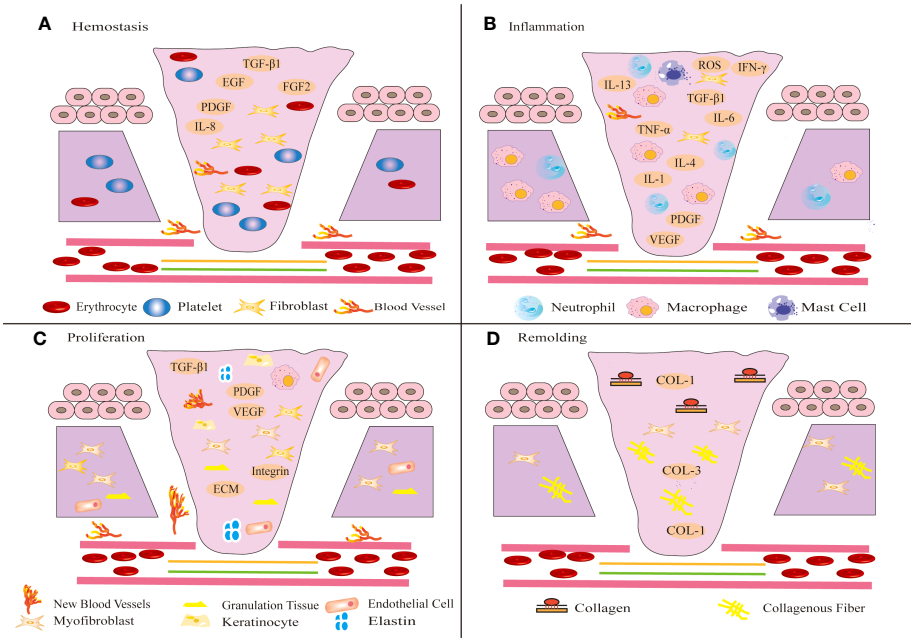


FIGURE 1
Schematic diagram of different stages of wound healing. Wound healing includes four stages: hemostasis **(A)**, inflammation **(B)**, proliferation **(C)** and remodeling **(D)**. **(A)** After injury, platelets aggregate, release chemotactic and growth factors, and eventually form clots. **(B)** Shortly thereafter, immune inflammatory cells release inflammatory mediators to resist microbial invasion and remove wound pathogens and tissue fragments. **(C)** Subsequently, FBs migrate to the wound tissue and synthesize ECM to promote the formation of granulation tissue at the wound site. The proliferation of KCs at the wound edge promotes wound re-epithelialization and migrates down to the injured dermis. **(D)** In the final remodeling stage, the tensile strength of the wound increases and the wound is completely covered by the new epidermis.

## 3.2 Mechanism of PS

PS can be induced by prolonged hemostasis and inflammatory phases, leading to an abnormal increase in activated cells and their accumulation at the injury site, abnormal proliferation of FBs and excessive collagen deposition during the proliferative phase; reduced degradation of ECM and excessive wound contraction during the remodeling phase. The mechanism of PS is complex, and current research is mainly related to immune inflammation, fibrosis, re-epithelialization, epigenetics, oxidative stress, and mechanical forces.

### 3.2.1 The mechanism by which immune cells regulate PS

Immune cells mainly prevent the invasion of pathogenic microorganisms during wound healing, and an imbalance will change the outcome of wound healing. Immune cells release cytokines or chemokines to promote fibrosis and re-epithelialization, resulting in excessive deposition of ECM and eventually leading to PS. At present, PS-related immune cells mainly include macrophages, lymphocytes, mast cells and neutrophils (Figure 2).

Macrophages are the key effector cells of innate immunity and play an important protective role in clearing pathogenic microorganisms and tissue fragments, presenting antigens, and promoting wound repair (70). Studies have shown that macrophages undergo significant phenotypic and functional changes to coordinate changes in the microenvironment at different stages of wound healing (71). In different microenvironments, macrophages can be polarized into two main phenotypes: M1 and M2. During wound healing, monocytes are polarized into the M1 phenotype by microorganisms, proinflammatory Th1 cytokines, damage-associated molecular patterns (DAMPs) and lipopolysaccharide (LPS) to initiate the inflammatory response (72, 73). Furthermore, the number of M1 macrophages begins to increase at 0-2 days after injury, peaks at 7-14 days after injury, and decreases significantly at 14-28 days after injury (72). This finding indicates that M1 cells secrete many inflammatory mediators in the early stage of normal scar formation (74, 75). During the transition from the inflammatory phase to the proliferative phase of wound healing, M1 cells are transformed into the M2 phenotype by the phagocytosis of neutrophils or the change of local wound microenvironment (76, 77). However, how M1 macrophages differentiate into M2 macrophages is not clear. The anti-inflammatory M2 phenotype is mainly involved in the proliferation and remodeling phases of wound healing. The secretion of vascular growth factors, cytokines and chemokines induces the proliferation and differentiation of FBs and MFBs, the re-epithelialization of KCs, the deposition of ECM and angiogenesis

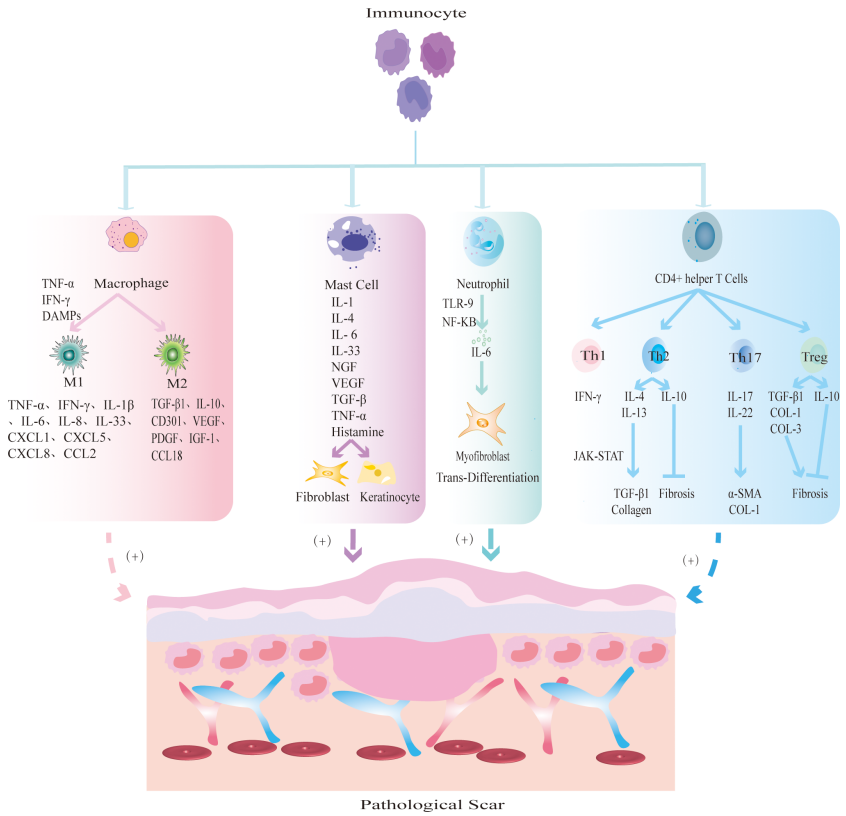


FIGURE 2
The mechanism by which different immune cells regulate PS. Macrophages are polarized into two main phenotypes: M1 and M2. M1 macrophages secrete TNF-α and IFN-γ to initiate inflammatory responses; M2 macrophages secrete TGF-β1 and IL-10 to promote tissue fibrosis. Mast cells release inflammatory mediators such as IL-1 and IL-4, and promote FBs fibrosis and KCs re-epithelialization. Neutrophils release IL-6 to induce MFBs transdifferentiation. $CD4^+$ helper T cells are further divided into Th1, Th2, Th17 and Treg subsets. Th1 releases pro-inflammatory cytokine IFN-γ; Th2 cells produce anti-inflammatory factors IL-4, IL-13 to promote fibrosis and IL-10 to inhibit fibrosis; Th17 cells secrete IL-17 and IL-22 to promote the expression of α-SMA and collagen; Treg cells secrete pro-fibrotic cytokines TGF-β1, COL-1, COL-3 and anti-fibrotic cytokine IL-10.

(71, 78–81). M2 cells are significantly increased at 28 days after injury and returned to baseline at 56 days (80). Normal wound healing is characterized by the transition from the early inflammatory stage, which is dominated by M1 macrophages, to the recovery stage, which is dominated by M2 macrophages (71). Increased secretion of inflammatory cytokines by M1 macrophages promotes the development of inflammation, or increased secretion of cytokines by M2 macrophages promotes the development of fibrosis, which leads to the formation of PS.

Most studies on lymphocytes in PS focus on T cells. Studies have shown that there may be a decrease in $CD8^+$ cytotoxic T cells in keloids, and the number and activity of FBs co-cultured with $CD8^+$ cytotoxic T cells are significantly reduced (82, 83). $CD4^+$ helper T cells can be further divided into Th1, Th2, Th17 and regulatory T (Treg) cell subsets. The dynamic balance of the proinflammatory Th1 response with the anti-inflammatory Th2 response is crucial in wound healing. Once the balance is disturbed, PS may occur. During PS, Th1 cells can produce the proinflammatory factor IFN-γ to protect against fibrosis (84, 85). Th2 cells produce IL-4 and IL-13 driven by the transcription factor GATA3, which can not only induce macrophage polarization to the M2 phenotype but also induce TGF-β1 and collagen synthesis through the JAK-STAT signaling pathway and induce pruritus (86, 87). In addition, Th2 cells can produce the anti-inflammatory mediator IL-10 to protect against fibrosis (88). Treg cells can secrete cytokines and interact with other inflammatory cells to regulate PS. The profibrotic cytokines TGF-β1, COL-3, and COL-3/COL-1, anti-fibrotic cytokine IL-10 and nuclear transcription factor Foxp3 are secreted by Treg cells, which can directly regulate PS (89). Treg cells can promote macrophage polarization to the M2 phenotype and interact with helper T cells to indirectly regulate PS (88). Th17 cells activate FBs differentiation and KCs proliferation by secreting IL-17 and IL-22 (88, 90). Overall, these studies showed that lymphocytes can induce the differentiation of FBs and KCs by releasing inflammatory mediators or participate in the development of PS by interacting with macrophages. However, there are relatively few studies, and the specific mechanism needs further study.

Mast cells are mainly involved in PS and its pruritus by releasing inflammatory mediators, promoting FBs and KCs activation and excessive collagen deposition. Mast cells release inflammatory mediators, induce degranulation, directly activate FBs fibrosis, angiogenesis and KCs re-epithelialization, recruit more immune cells to migrate to the injured site; and indirectly promote tissue repair (91, 92). Furthermore, the mast cell inhibitor DSCG can reduce the width of PS and the levels of the wound inflammatory factors IL-1α, IL-1β and CXCL1 (93). In addition, mast cells are closely related to PS pruritus. Compared with those in non-pruritus keloids, the number and degranulation of mast cells in pruritus keloids were increased (94). Therefore, number of mast cells and their storage particles are important factors affecting the PS.

Neutrophils are the first immune cells to reach the wound site and secrete various cytokines to participate in wound healing. Neutrophils kill microorganisms, remove tissue debris, and contribute to the activation of macrophages (95). However, the persistent presence of neutrophils in peripheral tissues triggers an inflammatory response. Studies have shown that neutrophil extracellular traps (NETs), which are network structures by which neutrophils kill pathogens, are highly expressed in HS and induce FBs to differentiate into MFBs through the TLR-9/NF-κB/IL-6 signaling pathway (96). It is known that the IL-6 signaling pathway is critical in the pathogenesis of PS (97, 98). At present, there is a lack of studies on the specific mechanisms by which neutrophils induce FBs differentiation and interact with other immune cells to mediate PS.

### 3.2.2 The mechanism by which nonimmune cells regulate PS

In addition to immune cells, many nonimmune cells are involved in the development of PS (Figure 3). The nonimmune cells involved in PS are mainly FBs, MFBs and KCs. During physiological wound healing, MFBs undergo apoptosis or revert to static FBs. When the mechanical environment around the wound changes or the internal environment is disordered, FBs are activated by cytokines and chemokines secreted by immune cells and differentiate into MFBs, which is accompanied by excessive secretion of ECM components which ultimately leads to PS (99). MFBs mainly mediate information exchange through autocrine and paracrine mechanisms. Autocrine signaling involves binding to its own receptor to trigger TGF-β1 and induce MFBs differentiation. When TGF-β1 is inhibited, it causes the dedifferentiation of MFBs (100). In addition, the paracrine pathway mainly recruits immune cells such as macrophages and neutrophils to achieve indirect communication and jointly promote the development of PS. KCs play an important role in the development of PS by inducing wound healing re-epithelialization and regulating FBs differentiation (101). During normal skin differentiation, KCs move from the basal layer of the epidermis. When the skin is damaged, these cells proliferate and migrate to the wound, promoting wound healing (102). In HS, the thicker the epidermis, the stronger the re-epithelialization of KCs (103). In addition, KCs upregulate the expression of profibrogenic molecules to accelerate FBs proliferation and collagen production (104). At present, the abnormal interaction between KCs and MFBs is one of the most widely recognized mechanisms in PS. In conclusion, the excessive differentiation of FBs into MFBs, which in turn promotes fibrosis and excessive re-epithelialization of KCs, leads to the occurrence of PS.

### 3.2.3 The mechanism by which other factors regulate PS

Increasing evidence shows that epigenetic modifications, represented by DNA methylation, histone modification and noncoding RNAs (ncRNAs), play a key role in the gene regulation of PS (105, 106). Many studies have focused on the expression of miRNAs in PS. The upregulation of miR-152-3p, miR-31, miR-181a, miR-21, lncRNA H19, and circRNA_0002198 (107–112) and the downregulation of miR-26a, miR-1224-5p, microRNA-152-5p, miR-29b, miR-205-5p, and circRNA_0008259 (112, 113) can promote the proliferation of FBs and the formation of collagen and ultimately induce the formation of PS (Figure 3).

There is hypoxia during PS. Compared with those in normal tissues, HIF-1α and ROS are highly expressed in PS (114, 115).

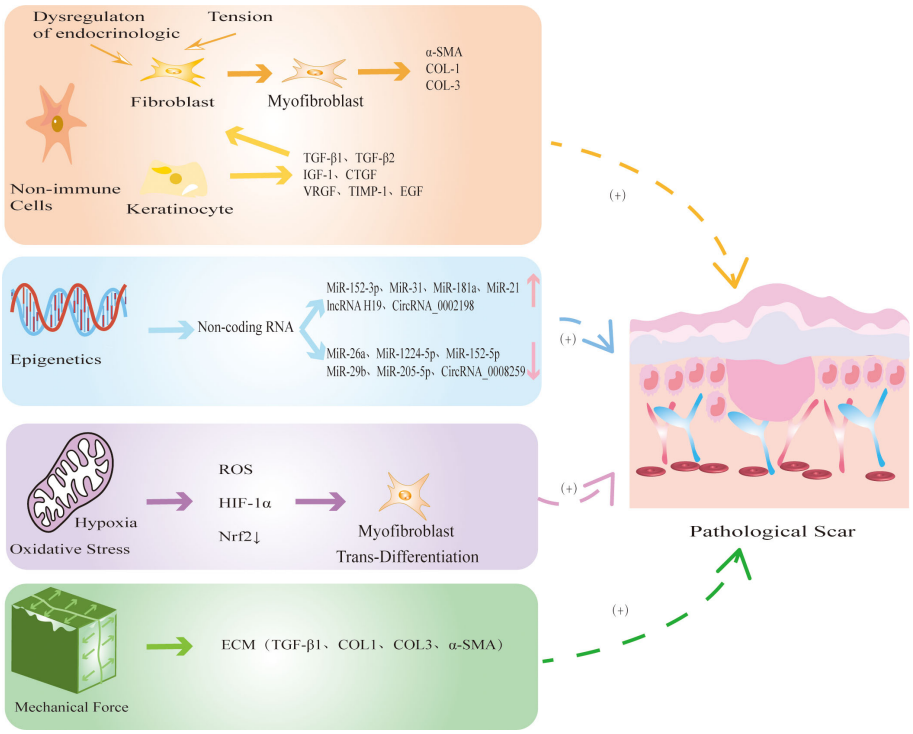


FIGURE 3
The mechanism by which non-immune cells and other factors regulate PS. Non-immune cells mainly include FBs, MFBs and KCs. When the mechanical environment around the wound changes or the internal environment is disordered, FBs differentiate into MFBs, accompanied by excessive secretion of COL-1, COL-3, α-SMA, eventually leading to PS. At the same time, KCs secretes TGF-β1 and TGF-β2 to promote re-epithelialization and FBs fibrosis. Epigenetic modification represented by noncoding RNAs is abnormally expressed in PS, which further promotes the fibrosis of FBs. Hypoxia releases ROS and HIF-1α, reduces the expression of antioxidant protein Nrf2, and induces MFBs transdifferentiation. Continuous mechanical stretching induces FBs to synthesize ECM, promotes collagen secretion and fiber synthesis.

Furthermore, hypoxia can induce the transformation of FBs to MFBs in keloids through the TGF-β1/SMAD3 pathway (114). In addition, Lee showed that antioxidant protein Nrf2 in keloids was significantly lower than that in normal skin tissue, and the protein levels of the oxidation product 2,4-dinitrophenylhydrazine were significantly higher than in normal skin (116). This finding suggests that oxidative stress is one of the mechanisms of PS (Figure 3).

Mechanical forces are important factors leading to PS (117, 118). TRP channels have been shown to play key roles in response to mechanical conduction, and TRPV2, TRPV4, TRPC3 and TRPC6 are potential mechanical force sensors involved in PS (3, 119). Studies have shown that continuous mechanical stretching can lead to the formation of PS by inducing FBs to synthesize ECM, indirectly activating the immune response to promote collagen secretion and fiber synthesis (120). In addition, local high mechanical forces are associated with abnormal skin fibrosis (1). These studies showed that mechanical forces can not only induce the release of inflammatory mediators by activating the immune response but also directly promote fibrosis in PS (Figure 3).

# 4 Modulation of TRP channels in PS

TRP channels are involved in PS (Table 1). The specific manifestations include immune inflammation, fibrosis, re-epithelialization, abnormal oxidative stress, epigenetic disorders, and excessive mechanical stretching. The factors are related to TRP channels. In addition, some TRP channels mediate PS-induced pruritus. TRP channels that are most closely related to PS are described below. Furthermore, we offer some opinions for reference in expounding the related problems.

## 4.1 TRPV1

TRPV1 is not only a heat-activated capsaicin receptor but also a multimodal receptor that is activated through multiple pathways in different microenvironments and mediates PS fibrosis, re-epithelialization and inflammatory responses, as well as being involved in PS pruritic signaling (Figure 4) (26, 148, 149).

In HS, the expression of TRPV1 is upregulated. Studies have shown that trans-epidermal water loss (TEWL) in HS is significantly higher than that in normal skin (150). This finding suggests that there is the presence of epidermal barrier dysfunction in HS, which is consistent with the clinical manifestations of skin dryness in some HS patients. Studies have shown that the barrier function of the skin is closely related to the expression of TRPV1 in KCs. Overactivation of TRPV1 delays the recovery of epidermal barrier function (151). Further studies have shown that disrupting the water barrier leads to KCs production of IL-1 and TNF-α to

10.3389/fimmu.2023.1237992

TABLE 1 The function of TRP channels in PS.

| Subfamilies | Positive biomarkers | Role of TRPs in PS | Influence mechanism | References |
|---|---|---|---|---|
| TRPV1 | IL-1 | Epidermal barrier disruption up-regulates the expression of TRPV1, promotes KCs release of IL-1, TNF-α, IL-6, IL-8 and GM-CSF to induce proliferation and re-epithelialization | Re-epithelialization | (121) |
| | TNF-α | | | |
| | IL-6 | | | |
| | IL-8 | | | |
| | GM-CSF | | | |
| | CGRP | TRPV1 activates the release of CGRP, promotes the expression of COL-1, TGF-β1 and α-SMA, upregulates the levels of macrophage-related inflammatory factors IL-1, IL-6, TNF-α and CCL2 through NF-κB and ERK signaling pathways, and promotes the release of IL-17 from type 17 inflammation | Immune inflammation, Fibrosis | (25, 122) |
| | SP | SP released by TRPV1 binds to its receptor NK1R to mediate neurogenic pruritus or activate Th2 immune cells, promoting the release of IL-4 and IL-13 to mediate pruritus | Pruritus | (87, 123–126) |
| | IL-31 | The activation of TRPV1 promotes mast cells to release IL-31 and FBs to produce Periostin to induce pruritus | | (127, 128) |
| | Periostin | | | (129–131) |
| TRPV2 | TGF-β1 | The activation of TRPV2 promotes the expression of TGF-β1 and α-SMA | Re-epithelialization | (132–134) |
| | α-SMA | | Fibrosis | |
| TRPV3 | COL-1 | The activation of TRPV3 promotes the expression of COL-1, TGF-β1, α-SMA and fibronectin in FBs through Smad2/3 signaling pathway | Fibrosis | (62) |
| | TGF-β1 | | | |
| | α-SMA | | | |
| | Fibronectin | | | |
| | NO | TRPV3 promotes the expression of COL-1 by activating iNOS to induce NO synthesis | Re-epithelialization | (135, 136) |
| | TGF-α | TRPV3 channel promotes KCs to release TGF-α, and induces KCs proliferation through TGF-α/EGFR signaling pathway | | (137) |
| | TSLP | The upregulation of TRPV3 channel increases the expression of TSLP and PAR2 to induce pruritus | Pruritus | (138–140) |
| | PAR2 | | | |
| TRPV4 | IL-6 | The activation of TRPV4 channel may promote FBs differentiation into MFBs by upregulating IL-6 | Fibrosis | (20) |
| | TSLP | TRPV4 induces KCs to release TSLP to promote pruritus | Pruritus | (141, 142) |
| | Piezo1 | TRPV4 cooperates with Piezo1 channel to promote mechanical conduction | Mechanical forces | (118, 119) |
| TRPC3 | COL-1 | Repeated mechanical stretching activates TRPC3 channel and promotes COL-1, TGF-β1, α-SMA and fibronectin through the Smad3/NF-κB signaling pathway | Mechanical forces | (33) |
| | TGF-β1 | | | |
| | α-SMA | | | |
| | Fibronectin | | | |
| | NFAT | Repeated mechanical stretching induces ET-1 in KCs to bind to EDNRB in FBs to promote the expression of TRPC3 and the profibrotic gene NFAT through Gαq-PLC-DAG signaling. | Fibrosis | (143) |
| | ROS | The activation of TRPC3 evokes ROS release to participate in FBs differentiation | Oxidative stress | (67) |
| TRPC6 | NFAT | TGF-β1 up-regulates the expression of TRPC6 to activate NFAT through p38 MAPK/SRF pathway, promotes MFBs transdifferentiation and the release of α-SMA and collagen | Fibrosis | (68, 144) |
| TRPA1 | IL-4 | IL-4 and IL-13 activate TRPA1 to mediate PS fibrosis through TGF-β/SMAD and IL-4Rα/STAT6 signaling pathways; IL-4 and IL-13 stimulate TRPA1 neuronal expression and induces pruritus | Fibrosis, Pruritus | (87) |
| | IL-13 | | | |
| | IL-17 | | | (92, 145, 146) |

*(Continued)*

TABLE 1 Continued

| Subfamilies | Positive biomarkers | Role of TRPs in PS | Influence mechanism | References |
|---|---|---|---|---|
| | IL-22 | TRPA1 activates type 17 immune cells to release IL-17, IL-22 and further recruits γδT cells to release Fgf9 | Immune inflammation | |
| | COL-1 | The activation of TRPA1 promotes COL-1 through TGF-β1 | Fibrosis | (147) |
| | TSLP | TRPA1 promotes the expression of TSLP | | (126, 147) |
| | Periostin | The activation of TRPA1 promotes FBs to produce Periostin to induce pruritus | Pruritus | (129–131) |
| TRPM7 | COL-1 | The activation of TRPM7 enhances COL-1, TGF-β1 and α-SMA through PI3K-AKT signaling pathway | Fibrosis | (145) |
| | TGF-β1 | | | |
| | α-SMA | | | |
| | HIF-1α | Hypoxia upregulates TRPM7 to activate STAT3/SMAD3/HIF-1α signaling pathway to induce fibrosis | Oxidative stress | (146) |

trigger the inflammatory response, and upregulate IL-6, IL-8, and granulocyte/macrophage colony stimulating factor (GM-CSF), promote KCs proliferation and re-epithelialization, and ultimately induce PS (121). In addition, Capsaicin induces increases in proliferation through IL-6 upregulation and TRPV1 induces the proliferation of human corneal epithelial cells through global MAPK activation (152, 153). These studies have shown that the expression of TRPV1 is related to the barrier function and inflammatory response of HS. The loss of TRPV1 inhibited inflammatory cell invasion and expression of TGF-β1 and other proinflammatory gene expression in cultured ocular fibroblasts (154). This is due to the overexpression of TRPV1 in HS which affects KCs proliferation and differentiation (20). Therefore, interfering with TRPV1 expression in KCs may become a new therapeutic strategy for PS. In addition, studies have shown that TRPV1 activation can release calcitonin gene-related peptide (CGRP) stored in vesicles from nerve endings to mediate immune inflammation and local vasodilation (155, 156). Zhou found increased CGRP levels in both human and mouse HS tissues. Furthermore, CGRP antagonists can directly reduce the expression of COL-1, TGF-β1 and α-SMA and can downregulate the levels of the macrophage-related inflammatory factors IL-1, IL-6, TNF-α and CCL2 through the NF-κB and ERK signaling pathways. Moreover, CGRP can promote PS by inducing the Th17 immune response (122). Cohen found that IL-17 expression was closely related to the Th17 immune response in light-simulated TRPV1-Ai32 mice (25). However, this process requires TRPV1 to induce CGRP release (25). The development of macrophages, the Th17 inflammatory response and fibrosis in HS induced by CGRP may be related to the release of TRPV1 from neurons. The neuroimmune mechanism by which TRPV1 regulates PS provides a new research direction. In summary, these studies have shown that TRPV1 may promote PS by directly promoting fibrosis and re-epithelialization and indirectly inducing inflammatory stimulation.

Pruritus is the most important symptom affecting the quality of life of PS patients. TRPV1 inhibitors may be one of the effective treatment strategies. The study found that the degree of scar pruritus after TRPV1 gene knockout was significantly less than that of wild type rats (152). Further studies have shown that TRPV1 can induce pruritus by promoting the expression of the pruritus mediators IL-31 and SP (127). The level of IL-31 secreted by mast cells was increased in HS compared with that in normal tissues, and the number of mast cells was also increased (128). This finding suggests that HS pruritus may be related to TRPV1-mediated promotion of mast cell degranulation and the release of inflammatory factors. In addition, the expression of SP and TRPV1 were significantly higher in HS skin than in normal skin. Furthermore, immunofluorescence analysis showed that the distribution of TRPV1 and SP was consistent (157). As a neuropeptide, SP mediates angiogenesis, macrophage polarization, mast cell degranulation, KCs proliferation and fibrosis and is an important neuromodulator of pruritus. SP can selectively bind to its specific receptor neurokinin-1 receptor (NK-1R) to mediate neurogenic pruritus (123, 125). Further studies have shown that the SP-NK1R signaling pathway promotes FBs to secrete COL-1 and is positively correlated with SP levels (157). The mechanism of skin neurogenic pruritus mediated by the TRPV1-mediated SP-NK1R signaling pathway may provide a new therapeutic target for PS pruritus conduction. Study has confirmed that hyperbaric oxygen therapy (HBOT) can alleviate the pruritus symptoms of keloid patients by reducing the expression of TRPV1 (158), but the specific mechanism is still unclear. Recently, Hashimoto found that the new pruritic Periostin was upregulated in PS (129). Periostin is produced by TGF-β1 and histamine-stimulated FBs and induces pruritus by binding to the aVb3 integrin receptor or inducing the Th2 cytokine cascade (130). However, this process requires the activation of TRPV1 and TRPA1 (130, 131). The discovery of Hashimoto provided a new direction for researching the mechanism of Periostin-mediated pruritus in PS through the activation of TRPV1 and TRPA1. Overall, these results indicate that targeting TRPV1 channels may be a prospective therapeutic strategy for PS.

## 4.2 TRPV2

TRPV2 is mainly involved in PS by promoting the release of TGF-β1 from KCs and the differentiation of FBs (Figure 4).

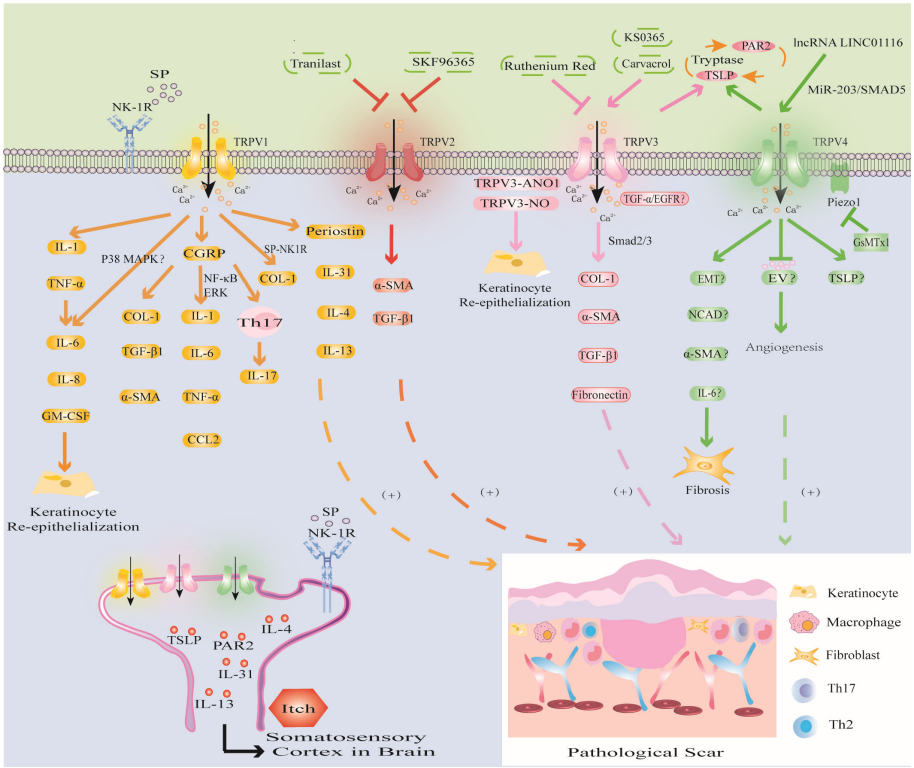


FIGURE 4
Modulation of TRPV channels in PS. TRPV1 channel activates IL-1 and TNF-α, triggers inflammatory response, promotes KCs proliferation and re-epithelialization; CGRP released by TRPV1 directly promotes PS fibrosis, and can induce PS by upregulating the levels of inflammatory factors through NF-κB and ERK signaling pathways; the SP released by TRPV1 activation mediates PS fibrosis and pruritus. The activation of TRPV1 promotes the expression of Periostin, IL-4, IL-13 and induces PS pruritus. (2) TRPV2 inhibitors SKF96365 and tranilast inhibited PS by downregulating TGF-β1 and α-SMA. (3) TRPV3 activator carvacrol promotes fibrosis through Smad2/3 pathway; activation of TRPV3 may interact with ANO1 and NO or promote PS through TGF-α/EGFR signaling pathway. PS pruritus may be related to the PAR2-TSLP positive feedback pathway mediated by TRPV3 and TRPV4 channels. (4) The activation of TRPV4 may promote the expression of EMT, NCAD, α-SMA, IL-6 to induce fibrosis, inhibit EV to inhibit abnormal angiogenesis, or release TSLP to induce PS pruritus and cooperate with Piezo1 channel to promote the formation of PS induced by mechanical stretching.

In new granulation tissue in the wound, KCs, FBs and macrophages at the edge of the wound promote wound re-epithelialization by secreting cytokines such as TGF-β1 and stimulate MFBs to produce α-SMA, eventually leading to PS (132, 133). In the cell collagen contraction model based on this theory, researchers found that the TRPV2 inhibitor SKF96365 or tranilast inhibited collagen contraction, while a TRPV2 inhibitor or TRPV2 knockdown using siRNA reduced TRPV2 agonist-induced $Ca^{2+}$ influx in FBs. It was further confirmed that the TRPV2 inhibitors SKF96365 and tranilast could induce FBs differentiation and collagen contraction by downregulating TGF-β1 and α-SMA expression (134). These studies showed that altering FBs and KCs differentiation with drugs targeting TRPV2 channels is beneficial for preventing PS and contracture.

## 4.3 TRPV3

TRPV3 plays an important role in mediating KCs re-epithelialization and FBs fibrosis and promoting ECM deposition in PS. In addition, TRPV3-mediated PS pruritus may be related to the expression of PAR2 and TSLP (Figure 4).

Studies have shown that the new TRPV3 channel activator KS0365 promotes wound healing by accelerating the re-epithelialization of KCs, while the broad-spectrum channel blocker ruthenium red and siRNA-mediated TRPV3 knockdown inhibit this process (63, 159). This finding indicates that overexpression of TRPV3 channels can promote excessive wound healing leading to the formation of PS. A clinical study showed that the TRPV3 activator carvacrol could promote the expression of COL-1, α-SMA, TGF-β1 and fibronectin in FBs through the Smad2/3 pathway, thereby promoting HS fibrosis (62). In addition, NO is an important mediator involved in biological processes such as wound healing, fibrosis, inflammation and KCs differentiation (160). Cobbold found that compared with those in normal tissues, NO levels in keloids were increased, and NO produced by nitric oxide synthase (iNOS) promoted the expression of COL-1 (135). TRPV3 induces NO synthesis by activating iNOS, thereby promoting KCs re-epithelialization and facilitating wound repair (136). This finding suggests that TRPV3-induced NO overexpression leads to PS. In addition, epidermal growth factor receptor (EGFR) can promote wound healing by promoting KCs proliferation, inflammation and angiogenesis (161). Aijima found that the phosphorylation of EGFR in the oral

epithelial cells of TRPV3-KO mice was inhibited, and TGF-α, which is a ligand of EGFR, was released from KCs through the activation of TRPV3 (137). This finding indicates that the TGF-α/EGFR signaling pathway plays a role in oral mucosal wound healing through TRPV3. Although the oral mucosa repairs faster than skin wounds and has fewer scars (137), the mechanism of oral mucosal repair suggests that the activation of TRPV3 may promote PS through the TGF-α/EGFR signaling pathway. Recent studies have shown that anoctamin1 (ANO1), a calcium-activated chloride channel, can promote the migration and proliferation of cancer cells (162). The interaction of TRPV3 with ANO1 promotes the proliferation of KCs during wound healing, while TRPV3 and ANO1 inhibitors inhibit the proliferation of KCs (162). The mechanism of the TRPV3-ANO1 interaction may provide a new target for PS.

PS pruritus may be related to the expression of PAR2 and TSLP, which is mediated by TRPV3 channels. The expression of PAR2 can be detected in burn scars with pruritus (138). Furthermore, inhibiting TRPV3 channels can reduce the expression of PAR2 and inhibit the itching of burn scars (139). In addition, compared with normal tissues, the expression of TRPV3 and TSLP in KCs in burn scars was upregulated, especially in burn scar tissues with pruritus (139). Further studies have shown that the synergistic effect of TSLP and PAR2 is particularly important in mediating pruritus signal transduction. TSLP triggers mast cell degranulation and the release of tryptase by binding to its receptor. Tryptase binds to PAR2 in KCs and activates TRPV3 channels to induce $Ca^{2+}$ influx to promote the expression of TSLP, forming a positive feedback loop. TSLP binds to its receptor and transmits to the spinal dorsal root ganglion to induce pruritus (140). Kim found that higher levels of the TRPV3 activator carvacrol were associated with higher NRS scores of the burn scar pruritus index (138). Therefore, the expression of TRPV3 in PS may be positively correlated with the degree of pruritus, and the upregulation of TRPV3 channels may be related to the increased expression of PAR2 and TSLP and the involvement of the PAR2-TSLP positive feedback pathway. The current research results provide a reference for the function of TRPV3 in PS pruritus. Further research is expected to determine whether the combination of TRPV3 with TSLP and PAR2 inhibitors can provide a feasible solution for PS pruritus.

## 4.4 TRPV4

Recent literature shows that TRPV4 may be involved in PS fibrosis, angiogenesis, pruritus, mechanical conduction and epigenetic regulation (Figure 4).

Epithelial-mesenchymal transition (EMT) plays an important role in wound healing by inducing re-epithelialization and promoting MFBs contraction and the secretion of ECM (163, 164). Sharma found that TGF-β1-induced EMT-like changes in KCs were dependent on TRPV4. Furthermore, TRPV4 promoted the expression of the mesenchymal markers N-cadherin (NCAD) and α-SMA in a bleomycin-induced mouse skin fibrosis model (165). Whether the activation of TRPV4 is involved in EMT in PS and affects the levels of NCAD and α-SMA remains to be further studied. In addition, studies have shown that IL-6 deficiency in TRPV4-deficient corneal FBs decreases MFBs differentiation, resulting in delayed corneal wound closure (20). It is well known that the IL-6 signaling pathway plays an important role in the pathogenesis of PS (97, 98). However, in the alkali burn wound healing response of TRPV4-null mice, biomarker gene expression of fibrosis, collagen1a1 and α-SMA were attenuated along with macrophage release of IL-6 whereas TGF-β release was unchanged (166). Therefore, TRPV4 channel may promote the differentiation of FBs into MFBs to mediate the development of PS, but whether the release of IL-6 promotes this process needs further study. Recent studies have shown that extracellular vesicles (EVs) are involved in skin wound healing (167). *Lactobacillus delbrueckii*-derived EVs (LDEVs) may inhibit PS fibrosis by inhibiting the expression of collagen and α-SMA (168). Furthermore, Wnt4 in mesenchymal stromal cell-derived extracellular vesicles (MSC-EVs) stimulated the proliferation and migration of FBs and KCs in a dose-dependent manner, enhanced the production of collagen and fibronectin to accelerate the process of wound healing (169, 170). In addition, studies have shown that EV induces abnormal angiogenesis by downregulating TRPV4-mediated ERK phosphorylation and activating VEGFR2 and YAP signaling (171). This finding suggests that studying the activity and participation of EVs in PS will provide new intervention targets for exploring the mechanism of TRPV4-mediated PS. In summary, these studies provide new ideas for TRPV4-induced PS fibrosis and angiogenesis, and the related mechanisms need to be further elucidated.

TRPV4 may also be involved in PS pruritus. Yang found that TRPV4 mRNA expression was significantly increased in patients with burn scar pruritus and was positively correlated with pruritus intensity compared with that in patients without scar pruritus (141). Lee found that skin dryness relied on TRPV4 channels to induce TSLP production in KCs and promote pruritus (142). This study provides a new research direction for the mechanism of TRPV4-mediated PS pruritus.

In addition, TRPV4 is related to the mechanical conduction of PS, and immune inflammatory cells and FBs fibrosis are involved. Studies have revealed the effect of TRPV4 on the reaction of implanted foreign bodies, and in the absence of TRPV4, macrophage-induced FBs differentiation into MFBs was significantly reduced (172). This finding suggests that TRPV4-mediated mechanical conduction contributes to the accumulation of MFBs. In addition, studies have shown that TRPV4 activation by some stresses (excessive mechanical, osmotic, and chemical stimulation) induces pain through ATP release in human corneal epithelial cells (173). Therefore, the interaction between mechanical conduction, immune cells and fibrosis may be related to TRPV4. In addition, a novel mechanically activated cation channel Piezo1 is overexpressed in HS, and its inhibitor GsMTx1 can protect rats from stretch-induced HS (118). Furthermore, Piezo1 interacts with TRPV4 after activation to produce a continuous $Ca^{2+}$ signal and promote mechanical conduction (119). Therefore, TRPV4 can promote PS by cooperating with the Piezo1 channel, and Piezo1 blockers may be used to treat PS. These findings provide new research targets for reducing PS mechanical contraction.

Furthermore, TRPV4 may be involved in the epigenetic regulation of PS. In liver fibrosis, TRPV4 is a direct target of miR-203 and promotes TGF-β1-induced hepatic stellate cell proliferation (174). Studies have shown that miR-203 regulates wound healing and scar formation by inhibiting Hes1 expression in epidermal stem cells (175). Furthermore, studies have shown that downregulating lncRNA LINC01116 inhibits keloid by regulating the miR-203/SMAD5 axis. Western blot analysis showed that lncRNA LINC01116 and SMAD5 were upregulated in keloids, while miR-203 expression was downregulated (176). Therefore, downregulating miR-203 expression and upregulating lncRNA LINC01116 expression may promote PS by regulating TRPV4 channel, but the specific mechanism needs further research.

## 4.5 TRPC3

TRPC3 induces mechanical stretch to promote the differentiation of FBs and KCs and regulates oxidative stress by promoting the production of ROS and $H_2O_2$ in PS (Figure 5).

Studies have shown that repeated mechanical stretching can promote the expression of TRPC3 in HS (33). TRPC3 promotes the expression of fibronectin through the Smad3/NF-κB pathway, thereby affecting FBs fibrosis in HS. In addition, TRPC3 protein and mRNA levels were positively correlated with VSS in HS patients (33). Further *in vitro* experiments showed that compared with that in Trpc3+/+ mice, the expression of TGF-β1, α-SMA, fibronectin and COL-1 in the granulation tissue of Trpc3-/- mice was significantly decreased. In addition, the TRPC3 inhibitor Pyr3 could significantly downregulate the expression of TGF-β1 (67). This finding indicates that mechanical stretching induces FBs fibrosis in PS by activating TRPC3 channels. In addition, the signal exchange between ET-1 secreted by KCs induced by mechanical stretch in PS and the ET-1 receptor EDNRB in FBs enhanced the expression of TRPC3 in FBs through Gαq-PLC-DAG signaling, promoting $Ca^{2+}$ influx and the expression of the profibrotic gene NFAT (143).

TRPC3 is involved in hypoxia-induced PS. A study showed that ROS and $H_2O_2$ was significantly enhanced and ATP was significantly reduced in HS, while the TRPC3 inhibitor Pyr3

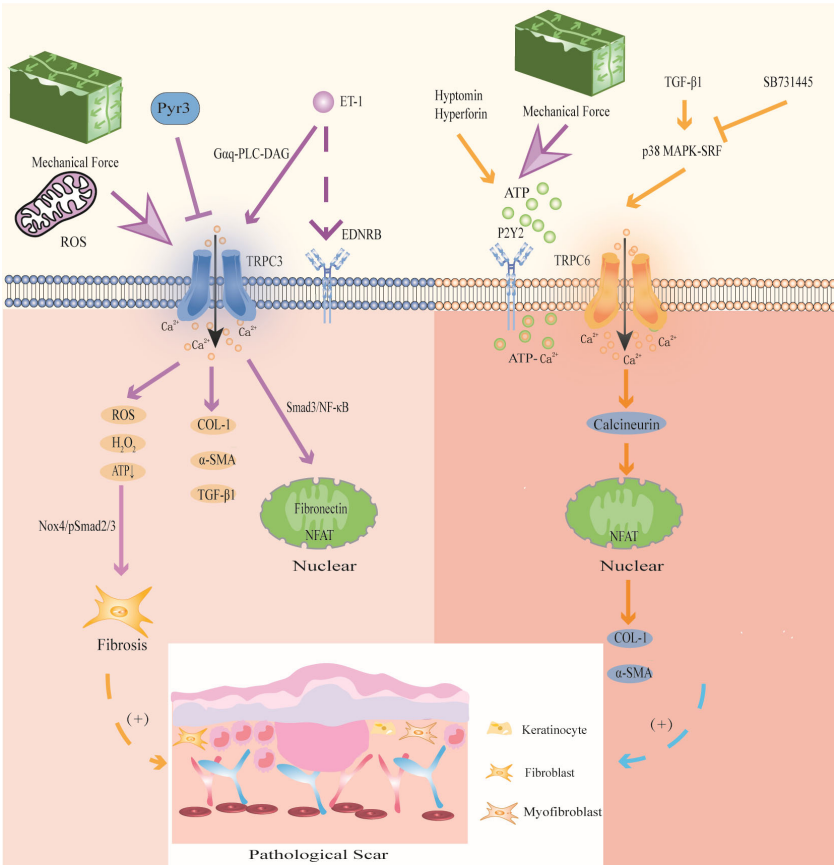


FIGURE 5
Modulation of TRPC3 and TRPC6 channels in PS. TRPC3 channel induces $Ca^{2+}$ influx accompanied by the expression of ROS, activates Nox4/pSmad2/3 pathway, and participates in FBs differentiation; activation of TRPC3 can also directly promote the expression of COL-1, α-SMA and TGF-β1;mechanical stretching and oxidative stress activate TRPC3 channels to increase $Ca^{2+}$ influx, and then activated Smad3/NF-κB migrates to the nucleus to induce fibrin expression and promote wound contraction; the signal exchange between ET-1 secreted by KCs and EDNRB activates TRPC3 channel and promotes the expression of the profibrotic gene NFAT. Mechanical stretching stimulates ATP release and activates TRPC6 channel upon binding to P2Y2 receptors, enhancing ATP- $Ca^{2+}$ influx and triggering wound healing; TGF-β1 activates TRPC6 channel through p38 MAPK-SRF signaling pathway, and promotes the expression of collagen and α-SMA through TRPC6/calcineurin/NFAT signaling pathway.

could decrease mitochondrial ROS and $H_2O_2$ and promote ATP production, thereby reducing the level of oxidative stress (67). Furthermore, the skin FBs of Trpc3-/- mice and Trpc3+/+ mice were used for detection in animal models. It was found that the levels of PDHE1α, a key subunit of the mitochondrial tricarboxylic acid cycle, and NOX4, a ROS-producing enzyme, in the skin FBs of Trpc3-/- mice, were significantly reduced compared to those of Trpc3+/+ mice (67). These results show that TGF-β1 upregulates TRPC3 expression and promotes PDHE1α phosphorylation during wound healing, resulting in increased mitochondrial ROS and $H_2O_2$ in FBs, decreased ATP production, activation of the Nox4/pSmad2/3 pathway, and thus participating in FBs differentiation in PS. We suggest that this is the mechanism by which TRPC3 promotes PS in the context of oxidative stress. Therefore, intervention with TRPC3 may be a new idea for the treatment of PS.

## 4.6 TRPC6

TRPC6 has great potential in mediating MFBs fibrosis and mechanical stretching in PS (Figure 5).

Genome-wide screening identified TRPC6 as an essential channel for MFBs transformation during wound healing and tissue remodeling, and TRPC6 overexpression activates MFBs differentiation (68). Further studies have shown that TGF-β1 induces TRPC6 expression through the p38 MAPK-serum response factor (SRF) signaling pathway to promote wound healing, and the p38 MAPK inhibitor SB731445 can completely block TRPC6 expression (68). Furthermore, TRPC6 is activated to induce $Ca^{2+}$ influx and MFBs transdifferentiation through the TRPC6/calcineurin/NFAT signaling pathway, further promoting the expression of α-SMA and collagen (68). Calcineurin inhibitors can be used to treat keloids (144). The TRPC6/calcineurin/NFAT signaling pathway, which is a key signaling pathway that mediates MFBs transdifferentiation to promote wound healing, is expected to provide new intervention targets for PS and fibrotic diseases.

In addition, TRPC6 can promote wound healing through mechanical conduction. Mechanical stimulation induces HaCaT cells to release ATP, which acts as an autocrine mediator and binds to the P2Y2 receptor, activating TRPC6 channels in HaCaT cells, promoting $Ca^{2+}$ influx, and participating in wound healing (177). Further studies have shown that the TRPC6 activators hyperforin and hypericin, which are Chinese herbal medicines that promote wound healing, can upregulate the expression of TRPC6 in HaCaT cells induced by mechanical stretching, mediate $Ca^{2+}$ influx and enhance ATP-$Ca^{2+}$ signaling to promote wound healing (177, 178). These studies suggest that mechanical stimulation enhances ATP-$Ca^{2+}$ signaling by activating TRPC6 channels, which may be a potential mechanism by which TRPC6 participates in PS.

## 4.7 TRPA1

TRPA1 mainly regulates immune inflammation and fibrosis of PS. Furthermore, this channel mediates PS pruritus (Figure 6).

Murata found that TRPA1 deficiency inhibited the infiltration of FBs, T cells and the expression of α-SMA and COL-1 during wound healing (65). TSLP, which is a Th2 cytokine, was positively correlated with TRPA1 expression (126). Studies have shown that TSLP promotes the expression of SDF-1a in FBs through the CXCR4/SDF-1 axis and promotes the synthesis of COL-1 and COL-3 through TGF-β1, thereby inducing keloids (147). In addition, TRPA1-expressing neurons stimulate dendritic cells to produce IL-23, leading to skin inflammation, which in turn activates type 17 immune cells to produce IL-17 and IL-22 to further recruit γδT cells, which release fibroblast growth factor 9 (Fgf9) to promote wound healing (92, 145, 146). Excessive upregulation of Fgf9 may lead to PS. In addition, the absence of TRPA1-induced upregulation of TGFβ1-related signaling cascades inhibits chemical injury-induced corneal wound inflammation and fibrosis in mice (20). Thus, TRPA1-mediated inflammation and fibrosis play important roles in wound healing. Targeting TRPA1 may provide a new strategy for the treatment of PS (20).

Studies have shown that the expression of TRPA1 in the scar tissue of patients with burn scar pruritus is higher than that of patients without pruritus, especially in mast cells (141). Studies have shown that IL-4 and IL-13 can upregulate the transcription of TRPV1 and TRPA1 (126). IL-4 and IL-13 can not only mediate PS fibrosis through the TGF-β/SMAD and IL-4Rα/STAT6 signaling pathways but also directly stimulate neurons through IL-4 receptors to induce PS pruritus (87). This finding suggests that IL-4 and IL-13 secreted by Th2 cells may mediate PS pruritus through TRPV1 and TRPA1 neurons. These studies provide a new direction for improving PS pruritus.

## 4.8 TRPM7

Abnormal TRPM7 expression may be involved in PS fibrosis, oxidative stress and noncoding RNA-related gene regulation (Figure 6).

Zhi found that the expression of TRPM7 was upregulated and enhanced the expression of TGF-β1, COL-1, COL-3 and α-SMA through the PI3K-AKT signaling pathway in HS (179). Furthermore, Panax Noto ginseng saponins (PNSs) can protect against HS by inhibiting TRPM7 expression, cell migration and viability, and collagen deposition by downregulating the PI3K/AKT pathway, thus inducing apoptosis and cell cycle arrest. This finding indicates that TRPM7 can promote fibrosis and collagen deposition through the PI3K/AKT signaling pathway and ultimately induce PS.

Zhang found that the overexpression of TRPM7 regulated the BAX/Bcl-2 balance and antioxidant processes through the STAT3/SMAD3/HIF-1α signaling pathway, thereby promoting FBs migration and inducing wound healing (69). This led us to hypothesize that TRPM7 may accelerate PS through the STAT3/SMAD3/HIF-1α signaling pathway.

In addition, TRPM7 may be related to the regulation of epigenetic noncoding RNA-related genes in PS. MiR-9-5p mediates endothelial cell proliferation, migration and angiogenesis by targeting TRPM7 through the PI3K/AKT/autophagy pathway (180). Studies have shown that miR-9-5p can inhibit the expression of α-SMA and COL-1 in HS by targeting PPARβ, promote the

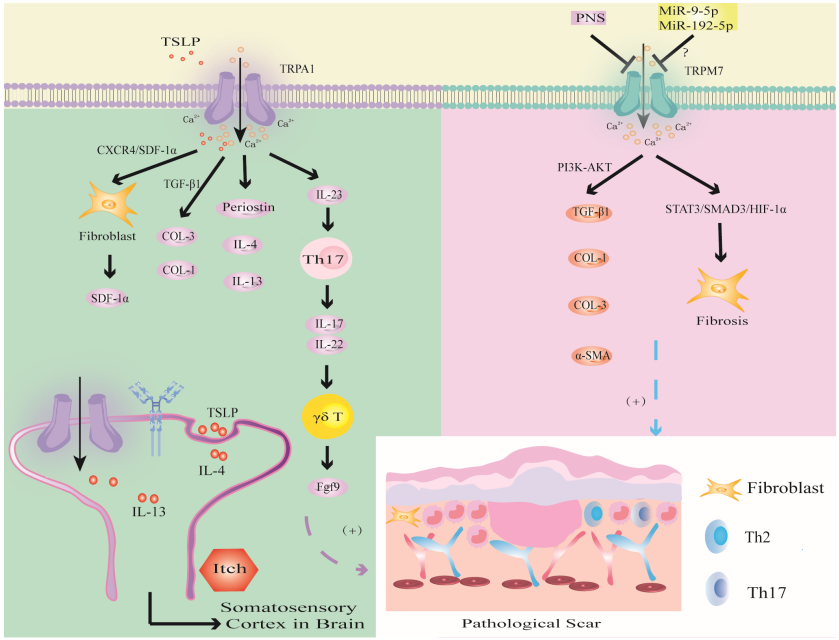


FIGURE 6
Modulation of TRPA1 and TRPM7 channels in PS. TSLP triggers TRPA1 channel to promote fibrosis through CXCR4/SDF-1 axis or promote the synthesis of COL-1 and COL-3 through TGF-β1; the activation of TRPV1 promotes the expression of Periostin, IL-4 and IL-13, which induced PS pruritus. TRPA1 activates immune cells to release inflammatory factors to promote wound healing. The activation of TRPM7 channel upregulates the expression of TGF-β1, COL-1, COL-3 and α-SMA through PI3K-AKT signaling pathway, or induces hypoxia through STAT3/SMAD3/HIF-1α signaling pathway. MiR-9-5p and miR-192-5p may inhibit PS by targeting TRPM7.

proliferation of FBs and accelerate apoptosis (181). Therefore, we hypothesize that miR-9-5p targets PPARβ to activate TRPM7 channel through the PI3K/AKT pathway, inhibit FBs fibrosis and collagen deposition, which may be an important target for PS. In addition, studies have shown that expression of the tumor suppressor miR-192-5p can be reversed by TRPM7 overexpression, thereby promoting the proliferation, migration and invasion of cervical cancer cells (182). However, miR-192-5p derived from adipose tissue-derived mesenchymal stem cell-derived exosomes (ADSC-Exos) inhibits HS by targeting IL-17 to regulate the Smad pathway (183). Therefore, inhibiting miR-9-5p to promote the expression of TRPM7 may aggravate PS fibrosis by activating the IL-17/Smad pathway. In-depth study of TRP channels may become an important research direction to determine the mechanism of PS in the context of epigenetics.

We now acknowledge that while few studies have reported on the involvement of other TRP channels in the mechanism of PS, the similarity of the structure and function of the homologous TRP channel family leads us to speculate that other TRP channels may also be related to the mechanism of PS, which needs further research and exploration in the future. In recent years, studies have found that the expression of TRPC1 is associated with renal fibrosis. CircRNA_010383 colocalized with miR-135a, and that overexpression of circRNA_010383 increased the level of TRPC1, which is a target protein of miR-135a. Additionally, the overexpression of circRNA_010383 inhibited the high glucose-induced accumulation of ECM (184). TRPC1 may have a potential relationship with the fibrosis of PS, but further research is needed to confirm this. Additionally, the study mentions that TRPM2 ablation has been found to significantly reduce renal interstitial fibrosis by decreasing TGF-β1 levels. This reduction in TGF-β1 is accompanied by a decrease in α-SMA, connective tissue growth factor (CTGF), fibronectin, and COL-1. The study also suggests that TRPM2 ablation may protect against renal fibrosis and inflammation by impeding JNK activation regulated by TGF-β1 (185). TRPM2 may be involved in inflammation and fibrosis of PS. Additionally, TRPML channels have important functional activities in immune cells such as macrophages, dendritic cells, neutrophils, NK cells, and B lymphocytes, which may provide important ideas for exploring the mechanism of TRPML in the inflammation and immunity of PS (186).In addition, TRPP1-like proteins may form mechanosensors in primary cilia. The phosphorylation of the COOH-terminus of TRPP1 may recruit TRPP2 to the cell membrane, which can promote Id2 to enter the nucleus and induce renal cell proliferation (187). The study suggests that Id2, as a key regulator of cell proliferation and differentiation, may provide a research direction for future studies on the mechanism of TRPP channel and PS.

## 5 Discussion and conclusion

In recent years, it has been found that a variety of TRP channels are involved in the development of PS, especially in immune inflammation and fibrosis, which has great research and clinical values. In this review, we introduced the specific physiological and pathological functions of TRP channels and focused on their important roles in mediating PS immune inflammation, fibrosis,

mechanical conduction, epigenetics, oxidative stress and pruritus. TRP channels promote tissue fibrosis and re-epithelialization by regulating the proliferation, migration, phagocytosis and cytokine release of immune cells or by directly activating FBs and KCs to promote the deposition of ECM and mediate the development of PS; mechanical stimulation which directly promotes fibrosis by activating TRP channels or recruiting immune cells to participate in fibrosis; noncoding RNA which regulates FBs fibrosis and collagen deposition by activating TRP channels; and the activation of TRP channels that can promote the release of oxidative stress-related factors such as ROS and H2O2, which in turn induce PS. Based on the latest reports, this review summarized the most novel concepts for the therapeutic drugs of PS from targeting TRP channels as follows: EVs are paracrine molecules that regulate cell signal transduction in the corneal scar and fibrosis, and studying how EVs participate in the development of PS through TRP channels may provide a promising treatment (167); Mechanical forces stimulate some TRP receptors on skin sensory fibers to release neuropeptides including SP and CGRP, which may provide direction for TRP-mediated PS neurogenic inflammation mechanism (122); and IL-31 mediates pruritus through TRPV1 and TRPA1 channels, indicating a new therapeutic target for the treatment of PS pruritus (127, 128). In addition, most of the current research on PS focuses on immunity. Immune signals enhance epithelial cell proliferation, differentiation and migration to accelerate skin repair (188), which suggests that targeting immune-epithelial communication to promote repair or reduce inflammation can be a new strategy for PS treatment. Therefore, studying the important role of TRP channels on account of the immune perspective may prompt novel targets for improved treatment of PS.

Although many studies have been carried out on immune inflammation in PS, the role of TRP channels in the regulation and treatment of PS is still in its infancy, mainly because it is a relatively new field involving wound healing and PS mechanisms, and many problems require further study. First, in response to different intensities of mechanical stretching, some mechanoreceptors in the TRP family promote wound healing. Excessive activated TRP in the wound site may lead to PS. Therefore, identifying the most suitable mechanical force triggering wound healing is particularly important to avoid the occurrence of PS. Second, the effects of various TRP channels on PS are different. For instance, the mechanism of TRP channels in the inflammatory, proliferative and remodeling stages of PS, TRP needs to be further explored. Finally, although several TRP agonists or antagonists have been developed for the treatment of PS, such as SKF96365 or tranilast, they have infrequently used in clinical practice due to the problems of drug permeability, side effects, and poor efficacy (189). Therefore, there is an urgent need for a comprehensive summary and in-depth evaluation of TRP channels to provide novel directions for identifying more selective and efficacious drug target to treat PS. This paper summarized the latest progress in understanding the role of TRP channels in PS, and the role of other TRP channels in PS needs to be further examined.

In the future, as the mechanisms of different TRP channels and their interactions with cytokines and growth factors become increasingly clear, TRP channels are expected to have further breakthroughs in the prevention and treatment of PS. In this article, we summarized the important roles of TRP channels in the pathogenesis of PS and proposed that drug development targeting TRP channels will be a critical topic for PS. Therefore, we hope to provide potential pharmacological targets and directions for future deeper understanding of PS and the evolution of new drugs by summarizing the mechanism of TRP channels in PS.

## Author contributions

YPZ conceived and wrote the article. QH, YFZ, and LG collected the data. WW was responsible for the idea. HZ was responsible for conceptualization and funding. XH was responsible for project administration and funding. QL were responsible for the idea, funding, and paper revision. All authors contributed to the article and approved the submitted version.

## Funding

This work was supported by grants from the National Natural Science Foundation of China (Grant Nos. 82205125), the Research on New Carrier Technology Development of Skin Barrier Repair Nursing Agent—Horizontal Project (Zhang Huimin), the Health Industry Clinical Research Special Project of Shanghai Municipal Health Commission (Grant No. 20224Y0224), Shanghai Science and Technology Commission (Grant No. 21ZR14640), Shanghai "Rising Stars of Medical Talent Youth Development Program for Youth Medical Talents-Specialist Program" (Grant No. 2022-38).

## Conflict of interest

The authors declare that the research was conducted in the absence of any commercial or financial relationships that could be construed as a potential conflict of interest.

## Publisher's note

# References


1. Finnerty CC, Jeschke MG, Branski LK, Barret JP, Dziewulski P, Herndon DN. Hypertrophic scarring: the greatest unmet challenge after burn injury. *Lancet* (2016) 388(10052):1427–36. doi: 10.1016/s0140-6736(16)31406-4

2. Aarabi S, Longaker MT, Gurtner GC. Hypertrophic scar formation following burns and trauma: new approaches to treatment. *PloS Med* (2007) 4(9):e234. doi: 10.1371/journal.pmed.0040234

3. Wang ZC, Zhao WY, Cao Y, Liu YQ, Sun Q, Shi P, et al. The roles of inflammation in keloid and hypertrophic scars. *Front Immunol* (2020) 11:603187. doi: 10.3389/fimmu.2020.603187

4. Wang X, Liang B, Li J, Pi X, Zhang P, Zhou X, et al. Identification and characterization of four immune-related signatures in keloid. *Front Immunol* (2022) 13:942446. doi: 10.3389/fimmu.2022.942446

5. Yin J, Zhang S, Yang C, Wang Y, Shi B, Zheng Q, et al. Mechanotransduction in skin wound healing and scar formation: Potential therapeutic targets for controlling hypertrophic scarring. *Front Immunol* (2022) 13:1028410. doi: 10.3389/fimmu.2022.1028410

6. Huang C, Ogawa R. The vascular involvement in soft tissue fibrosis-lessons learned from pathological scarring. *Int J Mol Sci* (2020) 21(7):2542. doi: 10.3390/ijms21072542

7. Qin H, Zhang L, Li M, Liu Y, Sun S, Nie W, et al. EGR1/NOX4 pathway regulates oxidative stress and further facilitates fibrosis progression in keloids responses to TGF-β1. *J Dermatol Sci* (2022) 108(3):138–45. doi: 10.1016/j.jdermsci.2022.12.009

8. Amjadian S, Moradi S, Mohammadi P. The emerging therapeutic targets for scar management: genetic and epigenetic landscapes. *Skin Pharmacol Physiol* (2022) 35 (5):247–65. doi: 10.1159/000524990

9. Partida-Sanchez S, BN D, Schwab A, Zierler S. Editorial: TRP channels in inflammation and immunity. *Front Immunol* (2021) 12:684172. doi: 10.3389/fimmu.2021.684172

10. Mousavizadeh SM, Torbati PM, Daryani A. The effects of kiwifruit dressing on hypertrophic scars in a rabbit ear model. *J Wound Care* (2021) 30(Sup9a):XVi–XVvii. doi: 10.12968/jowc.2021.30.Sup9a.XV

11. Khalil M, Alliger K, Weidinger C, Yerinde C, Wirtz S, Becker C, et al. Functional role of transient receptor potential channels in immune cells and epithelia. *Front Immunol* (2018) 9:174. doi: 10.3389/fimmu.2018.00174

12. Yang F, Sivils A, Cegielski V, Singh S, Chu XP. Transient receptor potential (TRP) channels in pain, neuropsychiatric disorders, and epilepsy. *Int J Mol Sci* (2023) 24(5):4714. doi: 10.3390/ijms24054714

13. Cosens DJ, Manning A. Abnormal electroretinogram from a Drosophila mutant. *Nature* (1969) 224(5216):285–7. doi: 10.1038/224285a0

14. Hardie RC, Minke B. The trp gene is essential for a light-activated Ca2+ channel in Drosophila photoreceptors. *Neuron* (1992) 8(4):643–51. doi: 10.1016/0896-6273(92)90086-s

15. Zhong T, Zhang W, Guo H, Pan X, Chen X, He Q, et al. The regulatory and modulatory roles of TRP family channels in Malignant tumors and relevant therapeutic strategies. *Acta Pharm Sin B* (2022) 12(4):1761–80. doi: 10.1016/j.apsb.2021.11.001

16. Samanta A, Hughes TET, Moiseenkova-Bell VY. Transient receptor potential (TRP) channels. *Subcell Biochem* (2018) 87:141–65. doi: 10.1007/978-981-10-7757-9_6

17. Koivisto AP, Belvisi MG, Gaudet R, Szallasi A. Advances in TRP channel drug discovery: from target validation to clinical studies. *Nat Rev Drug Discovery* (2022) 21 (1):41–59. doi: 10.1038/s41573-021-00268-4

18. Venkatachalam K, Montell C. TRP channels. *Annu Rev Biochem* (2007) 76:387–417. doi: 10.1146/annurev.biochem.75.103004.142819

19. Caterina MJ, Pang Z. TRP channels in skin biology and pathophysiology. *Pharm (Basel)* (2016) 9(4):77. doi: 10.3390/ph9040077

20. Okada Y, Sumioka T, Reinach PS, Miyajima M, Saika S. Roles of epithelial and mesenchymal TRP channels in mediating inflammatory fibrosis. *Front Immunol* (2021) 12:731674. doi: 10.3389/fimmu.2021.731674

21. Seebohm G, Schreiber JA. Beyond hot and spicy: TRPV channels and their pharmacological modulation. *Cell Physiol Biochem* (2021) 55(S3):108–30. doi: 10.33594/000000358

22. Rosenbaum T, Islas LD. Molecular physiology of TRPV channels: controversies and future challenges. *Annu Rev Physiol* (2023) 85:293–316. doi: 10.1146/annurev-physiol-030222-012349

23. Michalick L, Kuebler WM. TRPV4-A missing link between mechanosensation and immunity. *Front Immunol* (2020) 11:413. doi: 10.3389/fimmu.2020.00413

24. Lan Z, Chen L, Feng J, Xie Z, Liu Z, Wang F, et al. Mechanosensitive TRPV4 is required for crystal-induced inflammation. *Ann Rheum Dis* (2021) 80(12):1604–14. doi: 10.1136/annrheumdis-2021-220295

25. Cohen JA, Edwards TN, Liu AW, Hirai T, Jones MR, Wu J, et al. Cutaneous TRPV1(+) neurons trigger protective innate type 17 anticipatory immunity. *Cell* (2019) 178(4):919–32.e14. doi: 10.1016/j.cell.2019.06.022

26. Peng G, Tang X, Gui Y, Yang J, Ye L, Wu L, et al. Transient receptor potential vanilloid subtype 1: A potential therapeutic target for fibrotic diseases. *Front Physiol* (2022) 13:951980. doi: 10.3389/fphys.2022.951980

27. Kärki T, Tojkander S. TRPV protein family-from mechanosensing to cancer invasion. *Biomolecules* (2021) 11(7):1019. doi: 10.3390/biom11071019

28. Smani T, Gómez LJ, Regodon S, Woodard GE, Siegfried G, Khatib AM, et al. TRP channels in angiogenesis and other endothelial functions. *Front Physiol* (2018) 9:1731. doi: 10.3389/fphys.2018.01731

29. Ohya S, Kito H, Hatano N, Muraki K. Recent advances in therapeutic strategies that focus on the regulation of ion channel expression. *Pharmacol Ther* (2016) 160:11–43. doi: 10.1016/j.pharmthera.2016.02.001

30. Blanchard MG, Kellenberger S. Effect of a temperature increase in the non-noxious range on proton-evoked ASIC and TRPV1 activity. *Pflugers Arch* (2011) 461 (1):123–39. doi: 10.1007/s00424-010-0884-3

31. Szöllősi AG, Vasas N, Angyal Á, Kistamás K, Nánási PP, Mihály J, et al. Activation of TRPV3 regulates inflammatory actions of human epidermal keratinocytes. *J Invest Dermatol* (2018) 138(2):365–74. doi: 10.1016/j.jid.2017.07.852

32. Wang H, Cheng X, Tian J, Xiao Y, Tian T, Xu F, et al. TRPC channels: Structure, function, regulation and recent advances in small molecular probes. *Pharmacol Ther* (2020) 209:107497. doi: 10.1016/j.pharmthera.2020.107497

33. Ishise H, Larson B, Hirata Y, Fujiwara T, Nishimoto S, Kub T, et al. Hypertrophic scar contracture is mediated by the TRPC3 mechanical force transducer *via* NFkB activation. *Sci Rep* (2015) 5:11620. doi: 10.1038/srep11620

34. Wuensch T, Thilo F, Krueger K, Scholze A, Ristow M, Tepel M. High glucose-induced oxidative stress increases transient receptor potential channel expression in human monocytes. *Diabetes* (2010) 59(4):844–9. doi: 10.2337/db09-1100

35. Sun ZC, Ma SB, Chu WG, Jia D, Luo C. Canonical transient receptor potential (TRPC) channels in nociception and pathological pain. *Neural Plast* (2020) 2020:3764193. doi: 10.1155/2020/3764193

36. Farfariello V, Gordienko DV, Mesilmany L, Touil Y, Germain E, Fliniaux I, et al. TRPC3 shapes the ER-mitochondria Ca(2+) transfer characterizing tumour-promoting senescence. *Nat Commun* (2022) 13(1):956. doi: 10.1038/s41467-022-28597-x

37. Kim J, Moon SH, Shin YC, Jeon JH, Park KJ, Lee KP, et al. Erratum to: Intracellular spermine blocks TRPC4 channel *via* electrostatic interaction with C-terminal negative amino acids. *Pflugers Arch* (2016) 468(7):1297. doi: 10.1007/s00424-016-1824-7

38. Zhu Y, Gao M, Zhou T, Xie M, Mao A, Feng L, et al. The TRPC5 channel regulates angiogenesis and promotes recovery from ischemic injury in mice. *J Biol Chem* (2019) 294(1):28–37. doi: 10.1074/jbc.RA118.005392

39. Quick K, Zhao J, Eijkelkamp N, Linley JE, Rugiero F, Cox JJ, et al. TRPC3 and TRPC6 are essential for normal mechanotransduction in subsets of sensory neurons and cochlear hair cells. *Open Biol* (2012) 2(5):120068. doi: 10.1098/rsob.120068

40. Talavera K, Startek JB, Alvarez-Collazo J, Boonen B, Alpizar YA, Sanchez A, et al. MamMalian transient receptor potential TRPA1 channels: from structure to disease. *Physiol Rev* (2020) 100(2):725–803. doi: 10.1152/physrev.00005.2019

41. Zappia KJ, Garrison SR, Palygin O, Weyer AD, Barabas ME, Lawlor MW, et al. Mechanosensory and ATP release deficits following keratin14-cre-mediated TRPA1 deletion despite absence of TRPA1 in murine keratinocytes. *PloS One* (2016) 11(3): e0151602. doi: 10.1371/journal.pone.0151602

42. Oh MH, Oh SY, Lu J, Lou H, Myers AC, Zhu Z, et al. TRPA1-dependent pruritus in IL-13-induced chronic atopic dermatitis. *J Immunol* (2013) 191(11):5371–82. doi: 10.4049/jimmunol.1300300

43. Jimenez I, Prado Y, Marchant F, Otero C, Eltit F, Cabello-Verrugio C, et al. TRPM channels in human diseases. *Cells* (2020) 9(12):2604. doi: 10.3390/cells9122604

44. Najder K, Rugi M, Lebel M, Schröder J, Oster L, Schimmelpfennig S, et al. Role of the intracellular sodium homeostasis in chemotaxis of activated murine neutrophils. *Front Immunol* (2020) 11:2124. doi: 10.3389/fimmu.2020.02124

45. Shi R, Fu Y, Zhao D, Boczek T, Wang W, Guo F. Cell death modulation by transient receptor potential melastatin channels TRPM2 and TRPM7 and their underlying molecular mechanisms. *Biochem Pharmacol* (2021) 190:114664. doi: 10.1016/j.bcp.2021.114664

46. Wrighton KH. Epigenetics: the TRPM7 ion channel modifies histones. *Nat Rev Mol Cell Biol* (2014) 15(7):427. doi: 10.1038/nrm3824

47. Xu T, Wu BM, Yao HW, Meng XM, Huang C, Ni MM, et al. Novel insights into TRPM7 function in fibrotic diseases: a potential therapeutic target. *J Cell Physiol* (2015) 230(6):1163–9. doi: 10.1002/jcp.24801

48. Mirbod SM, Khanahmad H, Amerizadeh A, Amirpour A, Mirbod SM, Zaker E. Viewpoints on the role of transient receptor potential melastatin channels in cardiovascular system and disease: A systematic review. *Curr Probl Cardiol* (2023) 48 (2):101012. doi: 10.1016/j.cpcardiol.2021.101012

49. Orlowski P, Zmigrodzka M, Tomaszewska E, Ranoszek-Soliwoda K, Pajak B, Slonska A, et al. Polyphenol-conjugated bimetallic au@AgNPs for improved wound healing. *Int J Nanomed* (2020) 15:4969–90. doi: 10.2147/ijn.S252027

50. Kolanthai E, Fu Y, Kumar U, Babu B, Venkatesan AK, Liechty KW, et al. Nanoparticle mediated RNA delivery for wound healing. *Wiley Interdiscip Rev Nanomed Nanobiotechnol* (2022) 14(2):e1741. doi: 10.1002/wnan.1741

51. Guo S, Dipietro LA. Factors affecting wound healing. *J Dent Res* (2010) 89 (3):219–29. doi: 10.1177/0022034509359125

52. Segal AW. How neutrophils kill microbes. *Annu Rev Immunol* (2005) 23:197–223. doi: 10.1146/annurev.immunol.23.021704.115653

53. Zhang T, Wang XF, Wang ZC, Lou D, Fang QQ, Hu YY, et al. Current potential therapeutic strategies targeting the TGF-β/Smad signaling pathway to attenuate keloid and hypertrophic scar formation. *BioMed Pharmacother* (2020) 129:110287. doi: 10.1016/j.biopha.2020.110287

54. Zhang X, Shu W, Yu Q, Qu W, Wang Y, Li R. Functional biomaterials for treatment of chronic wound. *Front Bioeng Biotechnol* (2020) 8:516. doi: 10.3389/fbioe.2020.00516

55. Pignet AL, Schellnegger M, Hecker A, Kohlhauser M, Kotzbeck P, Kamolz LP. Resveratrol-induced signal transduction in wound healing. *Int J Mol Sci* (2021) 22 (23):12614. doi: 10.3390/ijms222312614

56. Qiang L, Yang S, Cui YH, He YY. Keratinocyte autophagy enables the activation of keratinocytes and fibroblastsand facilitates wound healing. *Autophagy* (2021) 17 (9):2128–43. doi: 10.1080/15548627.2020.1816342

57. Rodrigues M, Kosaric N, Bonham CA, Gurtner GC. Wound healing: A cellular perspective. *Physiol Rev* (2019) 99(1):665–706. doi: 10.1152/physrev.00067.2017

58. Wang PH, Huang BS, Horng HC, Yeh CC, Chen YJ. Wound healing. *J Chin Med Assoc* (2018) 81(2):94–101. doi: 10.1016/j.jcma.2017.11.002

59. Lee HJ, Jang YJ. Recent understandings of biology, prophylaxis and treatment strategies for hypertrophic scars and keloids. *Int J Mol Sci* (2018) 19(3):711. doi: 10.3390/ijms19030711

60. Reinke JM, Sorg H. Wound repair and regeneration. *Eur Surg Res* (2012) 49 (1):35–43. doi: 10.1159/000339613

61. Ueno K, Saika S, Okada Y, Iwanishi H, Suzuki K, Yamada G, et al. Impaired healing of cutaneous wound in a Trpv1 deficient mouse. *Exp Anim* (2023) 72(2):224–32. doi: 10.1538/expanim.22-0124

62. Um JY, Kang SY, Kim HJ, Chung BY, Park CW, Kim HO. Transient receptor potential vanilloid-3 (TRPV3) channel induces dermal fibrosis *via* the TRPV3/TSLP/Smad2/3 pathways in dermal fibroblasts. *J Dermatol Sci* (2020) 97(2):117–24. doi: 10.1016/j.jdermsci.2019.12.011

63. Maier M, Olthoff S, Hill K, Zosel C, Magauer T, Wein LA, et al. KS0365, a novel activator of the transient receptor potential vanilloid 3 (TRPV3) channel, accelerates keratinocyte migration. *Br J Pharmacol* (2022) 179(24):5290–304. doi: 10.1111/bph.15937

64. Sahu RP, Goswami C. Presence of TRPV3 in macrophage lysosomes helps in skin wound healing against bacterial infection. *Exp Dermatol* (2023) 32(1):60–74. doi: 10.1111/exd.14683

65. Murata S, Yamanaka M, Taniguchi W, Kajioka D, Suzuki K, Yamada G, et al. Lack of transient receptor potential ankyrin 1 (TRPA1) retards cutaneous wound healing in mice: A preliminary study. *Biochem Biophys Rep* (2022) 31:101322. doi: 10.1016/j.bbrep.2022.101322

66. Ishii T, Uchida K, Hata S, Hatta M, Kita T, Miyake Y, et al. TRPV2 channel inhibitors attenuate fibroblast differentiation and contraction mediated by keratinocyte-derived TGF-beta1 in an *in vitro* wound healing model of rats. *J Dermatol Sci* (2018) 90(3):332–42. doi: 10.1016/j.jdermsci.2018.03.003

67. Xia W, Wang Q, Lu Y, Hu Y, Zhang X, Zhang J, et al. Transient receptor potential channel canonical type 3 deficiency antagonizes myofibroblast transdifferentiation *in vivo*. *BioMed Res Int* (2020) 2020:1202189. doi: 10.1155/2020/1202189

68. Davis J, Burr AR, Davis GF, Birnbaumer L, Molkentin JD. A TRPC6-dependent pathway for myofibroblast transdifferentiation and wound healing *in vivo*. *Dev Cell* (2012) 23(4):705–15. doi: 10.1016/j.devcel.2012.08.017

69. Zhang H, Li H, Wang H, Lei S, Yan L. Overexpression of TRPM7 promotes the therapeutic effect of curcumin in wound healing through the STAT3/SMAD3 signaling pathway in human fibroblasts. *Burns* (2023) 49(4):889–900. doi: 10.1016/j.burns.2022.06.016

70. Moretti L, Stalfort J, Barker TH, Abebayehu D. The interplay of fibroblasts, the extracellular matrix, and inflammation in scar formation. *J Biol Chem* (2022) 298 (2):101530. doi: 10.1016/j.jbc.2021.101530

71. Hesketh M, Sahin KB, West ZE, Murray RZ. Macrophage phenotypes regulate scar formation and chronic wound healing. *Int J Mol Sci* (2017) 18(7):1545. doi: 10.3390/ijms18071545

72. Chen L, Wang J, Li S, Yu Z, Liu B, Song B, et al. The clinical dynamic changes of macrophage phenotype and function in different stages of human wound healing and hypertrophic scar formation. *Int Wound J* (2019) 16(2):360–9. doi: 10.1111/iwj.13041

73. Sim SL, Kumari S, Kaur S, Khosrotehrani K. Macrophages in skin wounds: functions and therapeutic potential. *Biomolecules* (2022) 12(11):1659. doi: 10.3390/biom12111659

74. van den Broek LJ, van der Veer WM, de Jong EH, Gibbs S, Niessen FB. Suppressed inflammatory gene expression during human hypertrophic scar compared to normotrophic scar formation. *Exp Dermatol* (2015) 24(8):623–9. doi: 10.1111/exd.12739

75. Jung BK, Roh TS, Roh H, Lee JH, Yun CO, Lee WJ. Effect of mortalin on scar formation in human dermal fibroblasts and a rat incisional scar model. *Int J Mol Sci* (2022) 23(14):7918. doi: 10.3390/ijms23147918

76. Greenlee-Wacker MC. Clearance of apoptotic neutrophils and resolution of inflammation. *Immunol Rev* (2016) 273(1):357–70. doi: 10.1111/imr.12453

77. Das A, Sinha M, Datta S, Abas M, Chaffee S, Sen CK, et al. Monocyte and macrophage plasticity in tissue repair and regeneration. *Am J Pathol* (2015) 185 (10):2596–606. doi: 10.1016/j.ajpath.2015.06.001

78. Pavlou S, Lindsay J, Ingram R, Xu H, Chen M. Sustained high glucose exposure sensitizes macrophage responses to cytokine stimuli but reduces their phagocytic activity. *BMC Immunol* (2018) 19(1):24. doi: 10.1186/s12865-018-0261-0

79. Smigiel KS, Parks WC. Macrophages, wound healing, and fibrosis: recent insights. *Curr Rheumatol Rep* (2018) 20(4):17. doi: 10.1007/s11926-018-0725-5

80. Xu X, Gu S, Huang X, Ren J, Gu Y, Wei C, et al. The role of macrophages in the formation of hypertrophic scars and keloids. *Burns Trauma* (2020) 8:tkaa006. doi: 10.1093/burnst/tkaa006

81. Feng Y, Sun ZL, Liu SY, Wu JJ, Zhao BH, Lv GZ, et al. Direct and indirect roles of macrophages in hypertrophic scar formation. *Front Physiol* (2019) 10:1101. doi: 10.3389/fphys.2019.01101

82. Xu H, Zhu Z, Hu J, Sun J, Wo Y, Wang , et al. Downregulated cytotoxic CD8(+) T-cell identifies with the NKG2A-soluble HLA-E axis as a predictive biomarker and potential therapeutic target in keloids. *Cell Mol Immunol* (2022) 19(4):527–39. doi: 10.1038/s41423-021-00834-1

83. Shan M, Liu H, Hao Y, Song K, Feng C, Wang Y. The role of CD28 and CD8(+) T cells in keloid development. *Int J Mol Sci* (2022) 23(16):8862. doi: 10.3390/ijms23168862

84. Ley K. M1 means kill; M2 means heal. *J Immunol* (2017) 199(7):2191–3. doi: 10.4049/jimmunol.1701135

85. Arenas-Ramirez N, Woytschak J, Boyman O. Interleukin-2: biology, design and application. *Trends Immunol* (2015) 36(12):763–77. doi: 10.1016/j.it.2015.10.003

86. Knipper JA, Willenborg S, Brinckmann J, Bloch W, Maaß T, Wagener R, et al. Interleukin-4 receptor α Signaling in myeloid cells controls collagen fibril assembly in skin repair. *Immunity* (2015) 43(4):803–16. doi: 10.1016/j.immuni.2015.09.005

87. Nguyen JK, Austin E, Huang A, MaMalis A, Jagdeo J. The IL-4/IL-13 axis in skin fibrosis and scarring: mechanistic concepts and therapeutic targets. *Arch Dermatol Res* (2020) 312(2):81–92. doi: 10.1007/s00403-019-01972-3

88. Short WD, Wang X, Keswani SG. The role of T lymphocytes in cutaneous scarring. *Adv Wound Care (New Rochelle)* (2022) 11(3):121–31. doi: 10.1089/wound.2021.0059

89. Chen Y, Jin Q, Fu X, Qiao J, Niu F. Connection between T regulatory cell enrichment and collagen deposition in keloid. *Exp Cell Res* (2019) 383(2):111549. doi: 10.1016/j.yexcr.2019.111549

90. Zaharie RD, Popa C, Schlanger D, Vălean D, Zaharie F. The role of IL-22 in wound healing. Potential implications in clinical practice. *Int J Mol Sci* (2022) 23 (7):3693. doi: 10.3390/ijms23073693

91. Komi DEA, Khomtchouk K, Santa Maria PL. A review of the contribution of mast cells in wound healing: involved molecular and cellular mechanisms. *Clin Rev Allergy Immunol* (2020) 58(3):298–312. doi: 10.1007/s12016-019-08729-w

92. Chesko DM, Wilgus TA. Immune cells in cutaneous wound healing: A review of functional data from animal models. *Int J Mol Sci* (2022) 23(5):2444. doi: 10.3390/ijms23052444

93. Chen L, Schrementi ME, Ranzer MJ, Wilgus TA, DiPietro LA. Blockade of mast cell activation reduces cutaneous scar formation. *PloS One* (2014) 9(1):e85226. doi: 10.1371/journal.pone.0085226

94. Lee SS, Yosipovitch G, Chan YH, Goh CL. Pruritus, pain, and small nerve fiber function in keloids: a controlled study. *J Am Acad Dermatol* (2004) 51(6):1002–6. doi: 10.1016/j.jaad.2004.07.054

95. Shih B, Garside E, McGrouther DA, Bayat A. Molecular dissection of abnormal wound healing processes resulting in keloid disease. *Wound Repair Regener* (2010) 18 (2):139–53. doi: 10.1111/j.1524-475X.2009.00553.x

96. Shao Y, Guo Z, Yang Y, Liu L, Huang J, Chen Y, et al. Neutrophil extracellular traps contribute to myofibroblast differentiation and scar hyperplasia through the Toll-like receptor 9/nuclear factor Kappa-B/interleukin-6 pathway. *Burns Trauma* (2022) 10:tkac044. doi: 10.1093/burnst/tkac044

97. Chen ZH, Yu B, Ye QF, Wang YF. [Research advances on interleukin-6 in hypertrophic scar formation]. *Zhonghua Shao Shang Za Zhi* (2022) 38(9):874–7. doi: 10.3760/cma.j.cn501120-20210331-00111

98. Kurachi I, Kurita E, Takushima A, Suga H. Human CD206+ Macrophages Show Antifibrotic Effects on Human Fibroblasts through an IL-6-Dependent Mechanism *in vitro*. *Plast Reconstr Surg* (2021) 147(2):231e–9e. doi: 10.1097/prs.0000000000007563

99. Zhou B, Tu T, Gao Z, Wu X, Wang W, Liu W. Impaired collagen fibril assembly in keloids with enhanced expression of lumican and collagen V. *Arch Biochem Biophys* (2021) 697:108676. doi: 10.1016/j.abb.2020.108676

100. Kosla J, Dvorakova M, Dvorak M, Cermak V. Effective myofibroblast dedifferentiation by concomitant inhibition of TGF-β signaling and perturbation of MAPK signaling. *Eur J Cell Biol* (2013) 92(12):363–73. doi: 10.1016/j.ejcb.2013.10.013

101. Russo B, Brembilla NC, Chizzolini C. Interplay between keratinocytes and fibroblasts: A systematic review providing a new angle for understanding skin fibrotic disorders. *Front Immunol* (2020) 11:648. doi: 10.3389/fimmu.2020.00648

102. Pastar I, Stojadinovic O, Yin NC, Ramirez H, Nusbaum AG, Sawaya A, et al. Epithelialization in wound healing: A comprehensive review. *Adv Wound Care (New Rochelle)* (2014) 3(7):445–64. doi: 10.1089/wound.2013.0473

103. Yang S, Sun Y, Geng Z, Ma K, Sun X, Fu X. AbnorMalities in the basement membrane structure promote basal keratinocytes in the epidermis of hypertrophic scars to adopt a proliferative phenotype. *Int J Mol Med* (2016) 37(5):1263–73. doi: 10.3892/ijmm.2016.2519

104. Li B, Gao C, Diao JS, Wang DL, Chu FF, Li Y, et al. Aberrant Notch signalling contributes to hypertrophic scar formation by modulating the phenotype of keratinocytes. *Exp Dermatol* (2016) 25(2):137–42. doi: 10.1111/exd.12897

105. Nyika DT, Khumalo NP, Bayat A. Genetics and epigenetics of keloids. *Adv Wound Care (New Rochelle)* (2022) 11(4):192–201. doi: 10.1089/wound.2021.0094

106. Stevenson AW, Melton PE, Moses EK, Wallace HJ, Wood FM, Rea S, et al. A methylome and transcriptome analysis of normal human scar cells reveals a role for FOXF2 in scar maintenance. *J Invest Dermatol* (2022) 142(5):1489–98.e12. doi: 10.1016/j.jid.2021.08.445

107. Wang R, Bai Z, Wen X, Du H, Zhou L, Tang Z, et al. MiR-152-3p regulates cell proliferation, invasion and extracellular matrix expression through by targeting FOXF1 in keloid fibroblasts. *Life Sci* (2019) 234:116779. doi: 10.1016/j.lfs.2019.116779

108. Zhang J, Xu D, Li N, Li Y, He Y, Hu X, et al. Downregulation of microRNA-31 inhibits proliferation and induces apoptosis by targeting HIF1AN in human keloid. *Oncotarget* (2017) 8(43):74623–34. doi: 10.18632/oncotarget.20284

109. Rang Z, Wang ZY, Pang QY, Wang YW, Yang G, Cui F. MiR-181a targets PHLPP2 to augment AKT signaling and regulate proliferation and apoptosis in human keloid fibroblasts. *Cell Physiol Biochem* (2016) 40(3-4):796–806. doi: 10.1159/000453139

110. Li Y, Zhang J, Lei Y, Lyu L, Zuo R, Chen T. MicroRNA-21 in skin fibrosis: potential for diagnosis and treatment. *Mol Diagn Ther* (2017) 21(6):633–42. doi: 10.1007/s40291-017-0294-8

111. Wang Z, Feng C, Song K, Qi Z, Huang W, Wang Y. lncRNA-H19/miR-29a axis affected the viability and apoptosis of keloid fibroblasts through acting upon COL1A1 signaling. *J Cell Biochem* (2020) 121(11):4364–76. doi: 10.1002/jcb.29649

112. Zhang Z, Yu K, Liu O, Xiong Y, Yang X, Wang S, et al. Expression profile and bioinformatics analyses of circular RNAs in keloid and normal dermal fibroblasts. *Exp Cell Res* (2020) 388(1):111799. doi: 10.1016/j.yexcr.2019.111799

113. An G, Liang S, Sheng C, Liu Y, Yao W. Upregulation of microRNA-205 suppresses vascular endothelial growth factor expression-mediated PI3K/Akt signaling transduction in human keloid fibroblasts. *Exp Biol Med (Maywood)* (2017) 242(3):275–85. doi: 10.1177/1535370216669839

114. Zhao B, Guan H, Liu JQ, Zheng Z, Zhou Q, Zhang J, et al. Hypoxia drives the transition of human dermal fibroblasts to a myofibroblast-like phenotype *via* the TGF-β1/Smad3 pathway. *Int J Mol Med* (2017) 39(1):153–9. doi: 10.3892/ijmm.2016.2816

115. De Felice B, Garbi C, Santoriello M, Santillo A, Wilson RR. Differential apoptosis markers in human keloids and hypertrophic scars fibroblasts. *Mol Cell Biochem* (2009) 327(1-2):191–201. doi: 10.1007/s11010-009-0057-x

116. Lee YJ, Kwon SB, Kim CH, Cho HD, Nam HS, Lee SH, et al. Oxidative damage and nuclear factor erythroid 2-related factor 2 protein expression in normal skin and keloid tissue. *Ann Dermatol* (2015) 27(5):507–16. doi: 10.5021/ad.2015.27.5.507

117. Harn HI, Ogawa R, Hsu CK, Hughes MW, Tang MJ, Chuong CM. The tension biology of wound healing. *Exp Dermatol* (2019) 28(4):464–71. doi: 10.1111/exd.13460

118. He J, Fang B, Shan S, Xie Y, Wang C, Zhang Y, et al. Mechanical stretch promotes hypertrophic scar formation through mechanically activated cation channel Piezo1. *Cell Death Dis* (2021) 12(3):226. doi: 10.1038/s41419-021-03481-6

119. Peng S, Poole DP, Veldhuis NA. Mini-review: Dissecting receptor-mediated stimulation of TRPV4 in nociceptive and inflammatory pathways. *Neurosci Lett* (2022) 770:136377. doi: 10.1016/j.neulet.2021.136377

120. Wang Z, Huang X, Zan T, Li Q, Li H. A modified scar model with controlled tension on secondary wound healing in mice. *Burns Trauma* (2020) 8:tkaa013. doi: 10.1093/burnst/tkaa013

121. Kloeters O, Schierle C, Tandara A, Mustoe TA. The use of a semiocclusive dressing reduces epidermal inflammatory cytokine expression and mitigates dermal proliferation and inflammation in a rat incisional model. *Wound Repair Regener* (2008) 16(4):568–75. doi: 10.1111/j.1524-475X.2008.00404.x

122. Zhou Y, Hua T, Weng X, Ma D, Li X. Calcitonin gene-related peptide alleviates hypertrophic scar formation by inhibiting the inflammation. *Arch Dermatol Res* (2022) 314(1):53–60. doi: 10.1007/s00403-020-02179-7

123. Chiang RS, Borovikova AA, King K, Banyard DA, Lalezari S, Toranto JD, et al. Current concepts related to hypertrophic scarring in burn injuries. *Wound Repair Regener* (2016) 24(3):466–77. doi: 10.1111/wrr.12432

124. Dong J, Feng F, Xu G, Zhang H, Hong L, Yang J. Elevated SP/NK-1R in esophageal carcinoma promotes esophageal carcinoma cell proliferation and migration. *Gene* (2015) 560(2):205–10. doi: 10.1016/j.gene.2015.02.002

125. Leal EC, Carvalho E, Tellechea A, Kafanas A, Tecilazich F, Kearney C, et al. Substance P promotes wound healing in diabetes by modulating inflammation and macrophage phenotype. *Am J Pathol* (2015) 185(6):1638–48. doi: 10.1016/j.ajpath.2015.02.011

126. Meng J, Li Y, Fischer MJM, Steinhoff M, Chen W, Wang J. Th2 modulation of transient receptor potential channels: an unmet therapeutic intervention for atopic dermatitis. *Front Immunol* (2021) 12:696784. doi: 10.3389/fimmu.2021.696784

127. Tang L, Gao J, Cao X, Chen L, Wang H, Ding H. TRPV1 mediates itch-associated scratching and skin barrier dysfunction in DNFB-induced atopic dermatitis mice. *Exp Dermatol* (2022) 31(3):398–405. doi: 10.1111/exd.14464

128. Lee MY, Shin E, Kim H, Kwak IS, Choi Y. Interleukin-31, interleukin-31RA, and OSMR expression levels in post-burn hypertrophic scars. *J Pathol Transl Med* (2018) 52(5):307–13. doi: 10.4132/jptm.2018.08.03

129. Yin SL, Qin ZL, Yang X. Role of periostin in skin wound healing and pathologic scar formation. *Chin Med J (Engl)* (2020) 133(18):2236–8. doi: 10.1097/cm9.0000000000000949

130. Hashimoto T, Mishra SK, Olivry T, Yosipovitch G. Periostin, an emerging player in itch sensation. *J Invest Dermatol* (2021) 141(10):2338–43. doi: 10.1016/j.jid.2021.03.009

131. Hashimoto T, Nattkemper LA, Kim HS, Kursewicz CD, Fowler E, Shah SM, et al. Dermal periostin: A new player in itch of prurigo nodularis. *Acta Derm Venereol* (2021) 101(1):adv00375. doi: 10.2340/00015555-3702

132. Tomasek JJ, Gabbiani G, Hinz B, Chaponnier C, Brown RA. Myofibroblasts and mechano-regulation of connective tissue remodelling. *Nat Rev Mol Cell Biol* (2002) 3(5):349–63. doi: 10.1038/nrm809

133. Yang L, Chan T, Demare J, Iwashina T, Ghahary A, Scott PG, et al. Healing of burn wounds in transgenic mice overexpressing transforming growth factor-beta 1 in the epidermis. *Am J Pathol* (2001) 159(6):2147–57. doi: 10.1016/s0002-9440(10)63066-0

134. Ishii T, Uchida K, Hata S, Hatta M, Kita T, Miyake Y, et al. TRPV2 channel inhibitors attenuate fibroblast differentiation and contraction mediated by keratinocyte-derived TGF-β1 in an *in vitro* wound healing model of rats. *J Dermatol Sci* (2018) 90(3):332–42. doi: 10.1016/j.jdermsci.2018.03.003

135. Cobbold CA. The role of nitric oxide in the formation of keloid and hypertrophic lesions. *Med Hypotheses* (2001) 57(4):497–502. doi: 10.1054/mehy.2001.1373

136. Miyamoto T, Petrus MJ, Dubin AE, Patapoutian A. TRPV3 regulates nitric oxide synthase-independent nitric oxide synthesis in the skin. *Nat Commun* (2011) 2:369. doi: 10.1038/ncomms1371

137. Aijima R, Wang B, Takao T, Mihara H, Kashio M, Ohsaki Y, et al. The thermosensitive TRPV3 channel contributes to rapid wound healing in oral epithelia. *FASEB J* (2015) 29(1):182–92. doi: 10.1096/fj.14-251314

138. Kim HO, Jin Cheol K, Yu Gyeong K, In Suk K. Itching caused by TRPV3 (Transient receptor potential vanilloid-3) activator application to skin of burn patients. *Medicina (Kaunas)* (2020) 56(11):560. doi: 10.3390/medicina56110560

139. Park CW, Kim HJ, Choi YW, Chung BY, Woo SY, Song DK, et al. TRPV3 channel in keratinocytes in scars with post-burn pruritus. *Int J Mol Sci* (2017) 18(11):2425. doi: 10.3390/ijms18112425

140. Ikoma A, Steinhoff M, Ständer S, Yosipovitch G, Schmelz M. The neurobiology of itch. *Nat Rev Neurosci* (2006) 7(7):535–47. doi: 10.1038/nrn1950

141. Yang YS, Cho SI, Choi MG, Choi YH, Kwak IS, Park CW, et al. Increased expression of three types of transient receptor potential channels (TRPA1, TRPV4 and TRPV3) in burn scars with post-burn pruritus. *Acta Derm Venereol* (2015) 95(1):20–4. doi: 10.2340/00015555-1858

142. Lee WJ, Shim WS. Cutaneous neuroimmune interactions of TSLP and TRPV4 play pivotal roles in dry skin-induced pruritus. *Front Immunol* (2021) 12:772941. doi: 10.3389/fimmu.2021.772941

143. Kawai K, Ishise H, Kubo T, Larson B, Fujiwara T, Nishimoto S, et al. Stretching promotes wound contraction through enhanced expression of endothelin receptor B and TRPC3 in fibroblasts. *Plast Reconstr Surg Glob Open* (2023) 11(4):e4954. doi: 10.1097/gox.0000000000004954

144. Memariani H, Memariani M, Moravvej H, Shahidi-Dadras M. Emerging and Novel Therapies for Keloids: A compendious review. *Sultan Qaboos Univ Med J* (2021) 21(1):e22–33. doi: 10.18295/squmj.2021.21.01.004

145. Wei JJ, Kim HS, Spencer CA, Brennan-Crispi D, Zheng Y, Johnson NM, et al. Activation of TRPA1 nociceptor promotes systemic adult mamMalian skin regeneration. *Sci Immunol* (2020) 5(50):eaba5683. doi: 10.1126/sciimmunol.aba5683

146. Li S, Hu M, Lorenz HP. Treatment of full-thickness skin wounds with blood-derived CD34(+) precursor cells enhances healing with hair follicle regeneration. *Adv Wound Care (New Rochelle)* (2020) 9(5):264–76. doi: 10.1089/wound.2019.0974

147. Shin JU, Kim SH, Kim HNoh JY, Jin S, Park CO, et al. TSLP is a potential initiator of collagen synthesis and an activator of CXCR4/SDF-1 axis in keloid pathogenesis. *J Invest Dermatol* (2016) 136(2):507–15. doi: 10.1016/j.jid.2015.11.008

148. Nilius B, Voets T. TRP channels: a TR(I)P through a world of multifunctional cation channels. *Pflugers Arch* (2005) 451(1):1–10. doi: 10.1007/s00424-005-1462-y

149. Li F, Wang F. TRPV1 in pain and itch. *Adv Exp Med Biol* (2021) 1349:249–73. doi: 10.1007/978-981-16-4254-8_12

150. Dolivo D, Rodrigues A, Sun L, Hou C, Li Y, Chung E, et al. Simvastatin cream alleviates dermal fibrosis in a rabbit ear hypertrophic scar model. *J Cosmet Dermatol* (2023) 22(2):534–41. doi: 10.1111/jocd.15142

151. Denda M, Sokabe T, Fukumi-Tominaga T, Tominaga M. Effects of skin surface temperature on epidermal permeability barrier homeostasis. *J Invest Dermatol* (2007) 127(3):654–9. doi: 10.1038/sj.jid.5700590

152. Sumioka T, Okada Y, Reinach PS, Shirai K, Miyajima M, Yamanaka O, et al. Impairment of corneal epithelial wound healing in a TRPV1-deficient mouse. *Invest Ophthalmol Vis Sci* (2014) 55(5):3295–302. doi: 10.1167/iovs.13-13077

153. Yang H, Wang Z, Capo-Aponte JE, Zhang F, Pan Z, Reinach PS. Epidermal growth factor receptor transactivation by the cannabinoid receptor (CB1) and transient receptor potential vanilloid 1 (TRPV1) induces differential responses in corneal epithelial cells. *Exp Eye Res* (2010) 91(3):462–71. doi: 10.1016/j.exer.2010.06.022

154. Okada Y, Reinach PS, Shirai K, Kitano A, Kao WW, Flanders KC, et al. TRPV1 involvement in inflammatory tissue fibrosis in mice. *Am J Pathol* (2011) 178(6):2654–64. doi: 10.1016/j.ajpath.2011.02.043

155. Pinho-Ribeiro FA, Baddal B, Haarsma R, O'Seaghdha M, Yang NJ, Blake KJ, et al. Blocking neuronal signaling to immune cells treats streptococcal invasive infection. *Cell* (2018) 173(5):1083–97.e22. doi: 10.1016/j.cell.2018.04.006

156. Spekker E, Körtési T, Vécsei L. TRP channels: recent development in translational research and potential therapeutic targets in migraine. *Int J Mol Sci* (2022) 24(1):700. doi: 10.3390/ijms24010700

157. Zhang S, Li K, Yu Z, Chai J, Zhang Z, Zhang Y, et al. Dramatic effect of botulinum toxin type A on hypertrophic scar: A promising therapeutic drug and its mechanism through the SP-NK1R pathway in cutaneous neurogenic inflammation. *Front Med (Lausanne)* (2022) 9:820817. doi: 10.3389/fmed.2022.820817

158. Li WB, Liu S, Zhang MZ, Liu H, Dong XH, Hao Y, et al. Hyperbaric oxygen therapy relieved pruritus and pain of keloid patients. *Am J Transl Res* (2020) 12(2):574–82.

159. Moore CL. Specific inhibition of mitochondrial Ca++ transport by ruthenium red. *Biochem Biophys Res Commun* (1971) 42(2):298–305. doi: 10.1016/0006-291x(71)90102-1

160. Cals-Grierson MM, Ormerod AD. Nitric oxide function in the skin. *Nitric Oxide* (2004) 10(4):179–93. doi: 10.1016/j.niox.2004.04.005

161. Repertinger SK, Campagnaro E, Fuhrman J, El-Abaseri T, Yuspa SH, Hansen LA. EGFR enhances early healing after cutaneous incisional wounding. *J Invest Dermatol* (2004) 123(5):982–9. doi: 10.1111/j.0022-202X.2004.23478.x

162. Yamanoi Y, Lei J, Takayama Y, Hosogi S, Marunaka Y, Tominaga M. TRPV3-ANO1 interaction positively regulates wound healing in keratinocytes. *Commun Biol* (2023) 6(1):88. doi: 10.1038/s42003-023-04482-1

163. Shu DY, Lovicu FJ. Myofibroblast transdifferentiation: The dark force in ocular wound healing and fibrosis. *Prog Retin Eye Res* (2017) 60:44–65. doi: 10.1016/j.preteyeres.2017.08.001

164. El Ayadi A, Jay JW, Prasai A. Current approaches targeting the wound healing phases to attenuate fibrosis and scarring. *Int J Mol Sci* (2020) 21(3):1105. doi: 10.3390/ijms21031105

165. Sharma S, Goswami R, Zhang DX, Rahaman SO. TRPV4 regulates matrix stiffness and TGFβ1-induced epithelial-mesenchymal transition. *J Cell Mol Med* (2019) 23(2):761–74. doi: 10.1111/jcmm.13972

166. Okada Y, Shirai K, Miyajima M, Reinach PS, Yamanaka O, Sumioka T, et al. Loss of TRPV4 function suppresses inflammatory fibrosis induced by alkali-burning mouse corneas. *PloS One* (2016) 11(12):e0167200. doi: 10.1371/journal.pone.0167200

167. Yeung V, Boychev N, Farhat W, Ntentakis DP, Hutcheon AEK, Ross AE, et al. Extracellular vesicles in corneal fibrosis/scarring. *Int J Mol Sci* (2022) 23(11):5921. doi: 10.3390/ijms23115921

168. Han F, Wang K, Shen K, Wang J, Han S, Hu D, et al. Extracellular vesicles from Lactobacillus druckerii inhibit hypertrophic scar fibrosis. *J Nanobiotechnol* (2023) 21(1):113. doi: 10.1186/s12951-023-01861-y

169. An Y, Lin S, Tan X, Zhu S, Nie F, Zhen Y, et al. Exosomes from adipose-derived stem cells and application to skin wound healing. *Cell Prolif* (2021) 54(3):e12993. doi: 10.1111/cpr.12993

170. Hade MD, Suire CN, Mossell J, Suo Z. Extracellular vesicles: Emerging frontiers in wound healing. *Med Res Rev* (2022) 42(6):2102–25. doi: 10.1002/med.21918

171. Guarino B, Katari V, Adapala R, Bhavnani N, Dougherty J, Khan M, et al. Tumor-derived extracellular vesicles induce abnormal angiogenesis *via* TRPV4 downregulation and subsequent activation of YAP and VEGFR2. *Front Bioeng Biotechnol* (2021) 9:790489. doi: 10.3389/fbioe.2021.790489

172. Goswami R, Arya RK, Sharma S, Dutta B, Stamov DR, Zhu X, et al. Mechanosensing by TRPV4 mediates stiffness-induced foreign body response and giant cell formation. *Sci Signal* (2021) 14(707):eabd4077. doi: 10.1126/scisignal.abd4077

173. Lapajne L, Lakk M, Yarishkin O, Gubeljak L, Hawlina M, Krizaj D. Polymodal sensory transduction in mouse corneal epithelial cells. *Invest Ophthalmol Vis Sci* (2020) 61(4):2. doi: 10.1167/iovs.61.4.2

174. Zhan L, Yang Y, Ma TT, Huang C, Meng XM, Zhang L, et al. Transient receptor potential vanilloid 4 inhibits rat HSC-T6 apoptosis through induction of autophagy. *Mol Cell Biochem* (2015) 402(1-2):9–22. doi: 10.1007/s11010-014-2298-6

175. Zhou Z, Shu B, Xu Y, Liu J, Wang P, Chen L, et al. microRNA-203 modulates wound healing and scar formation *via* suppressing hes1 expression in epidermal stem cells. *Cell Physiol Biochem* (2018) 49(6):2333–47. doi: 10.1159/000493834

176. Yuan W, Sun H, Yu L. Long non-coding RNA LINC01116 accelerates the progression of keloid formation by regulating miR-203/SMAD5 axis. *Burns* (2021) 47(3):665–75. doi: 10.1016/j.burns.2020.07.027

177. Takada H, Furuya K, Sokabe M. Mechanosensitive ATP release from hemichannels and $Ca^{2+}$ influx through TRPC6 accelerate wound closure in keratinocytes. *J Cell Sci* (2014) 127(Pt 19):4159–71. doi: 10.1242/jcs.147314

178. Takada H, Yonekawa J, Matsumoto M, Furuya K, Sokabe M. Hyperforin/HP-β-cyclodextrin enhances mechanosensitive ca(2+) signaling in haCaT keratinocytes and in atopic skin ex vivo which accelerates wound healing. *BioMed Res Int* (2017) 2017:8701801. doi: 10.1155/2017/8701801

179. Zhi Y, Wang H, Huang B, Yan G, Yan LZ, Zhang W, et al. Panax Notoginseng Saponins suppresses TRPM7 *via* the PI3K/AKT pathway to inhibit hypertrophic scar formation *in vitro*. *Burns* (2021) 47(4):894–905. doi: 10.1016/j.burns.2020.10.003

180. Zhou DM, Sun LL, Zhu J, Chen B, Li XQ, Li WD. MiR-9 promotes angiogenesis of endothelial progenitor cell to facilitate thrombi recanalization *via* targeting TRPM7 through PI3K/Akt/autophagy pathway. *J Cell Mol Med* (2020) 24(8):4624–32. doi: 10.1111/jcmm.15124

181. Chai CY, Tai IC, Zhou R, Song J, Zhang C, Sun S. MicroRNA-9-5p inhibits proliferation and induces apoptosis of human hypertrophic scar fibroblasts through targeting peroxisome proliferator-activated receptor β. *Biol Open* (2020) 9(12):bio051904. doi: 10.1242/bio.051904

182. Dong RF, Zhuang YJ, Wang Y, Zhang ZY, Xu XZ, Mao YR, et al. Tumor suppressor miR-192-5p targets TRPM7 and inhibits proliferation and invasion in cervical cancer. *Kaohsiung J Med Sci* (2021) 37(8):699–708. doi: 10.1002/kjm2.12398

183. Li Y, Zhang J, Shi J, Liu K, Wang X, Jia Y, et al. Exosomes derived from human adipose mesenchymal stem cells attenuate hypertrophic scar fibrosis by miR-192-5p/IL-17RA/Smad axis. *Stem Cell Res Ther* (2021) 12(1):221. doi: 10.1186/s13287-021-02290-0

184. Peng F, Gong W, Li S, Yin B, Zhao C, Liu W, et al. circRNA_010383 acts as a sponge for miR-135a, and its downregulated expression contributes to renal fibrosis in diabetic nephropathy. *Diabetes* (2021) 70(2):603–15. doi: 10.2337/db20-0203

185. Wang Y, Chen L, Wang K, Da Y, Zhou M, Yan H, et al. Suppression of TRPM2 reduces renal fibrosis and inflammation through blocking TGF-beta1-regulated JNK activation. *BioMed Pharmacother* (2019) 120:109556. doi: 10.1016/j.biopha.2019.109556

186. Spix B, Chao YK, Abrahamian C, Chen CC, Grimm C. TRPML cation channels in inflammation and immunity. *Front Immunol* (2020) 11:225. doi: 10.3389/fimmu.2020.00225

187. Li X, Luo Y, Starremans PG, McNamara CA, Pei Y, Zhou J. Polycystin-1 and polycystin-2 regulate the cell cycle through the helix-loop-helix inhibitor Id2. *Nat Cell Biol* (2005) 7(12):1202–12. doi: 10.1038/ncb1326

188. Guenin-Mace L, Konieczny P, Naik S. Immune-epithelial cross talk in regeneration and repair. *Annu Rev Immunol* (2023) 41:207–28. doi: 10.1146/annurev-immunol-101721-062818

189. Chien PN, Jeong JH, Nam SY, Lim SY, Long NV, Zhang XR, et al. Nanomicelle-generating microneedles loaded with tranilast for treatment of hypertrophic scars in a rabbit model. *In Vivo* (2022) 36(4):1734–44. doi: 10.21873/invivo.12886

frontiers | Frontiers in Immunology

TYPE Original Research
PUBLISHED 26 October 2023
DOI 10.3389/fimmu.2023.1240714



OPEN ACCESS

EDITED BY
Wang Xiqiao,
Shanghai Jiao Tong University, China

REVIEWED BY
Kazufumi Kunimura,
Kyushu University, Japan
Zhang Yong,
Shanghai Jiao Tong University, China

*CORRESPONDENCE
Yunxiang Wu
Wyx841106@163.com

RECEIVED 15 June 2023
ACCEPTED 12 October 2023
PUBLISHED 26 October 2023

CITATION
Luo Q, Cao Q, Guo J, Chang S and Wu Y (2023) Genetically predicted levels of circulating cytokines and the risk of six immune skin diseases: a two-sample Mendelian randomization study. *Front. Immunol.* 14:1240714. doi: 10.3389/fimmu.2023.1240714



# Genetically predicted levels of circulating cytokines and the risk of six immune skin diseases: a two-sample Mendelian randomization study

Qinghua Luo[1], Qiurui Cao[1], Jinyan Guo[1], Shuangqing Chang[1] and Yunxiang Wu[2]*

[1]Department of Anorectal Surgery, Jiangmen Wuyi Hospital of Traditional Chinese Medicine, Jiangmen, China, [2]Department of Anorectal Surgery, Affiliated Hospital of Jiangxi University of Chinese Medicine, Nanchang, China

**Background:** Circulating cytokines play a crucial role in the onset and progression of immune skin diseases. However, the causal relationships and the direction of causal effects require further investigation.

**Methods:** Two-sample Mendelian randomization (MR) analyses were conducted to assess the causal relationships between 41 circulating cytokines and six immune skin diseases including alopecia areata, chloasma, hidradenitis suppurativa (HS), lichen planus (LP), seborrheic dermatitis, and urticaria, using summary statistics from genome-wide association studies. Reverse MR analyses was performed to test for the reverse causation. Pleiotropy and heterogeneity tests were conducted to assess the robustness of the findings.

**Results:** Twelve unique cytokines showed a suggestive causal relationship with the risk of six immune skin diseases. Among them, the causal effects between 9 unique cytokines and immune skin diseases have strong statistical power. Additionally, the concentrations of six cytokines might be influenced by LP and urticaria. After Bonferroni correction, the following associations remained significant: the causal effect of beta-nerve growth factor on HS (odds ratio [OR] = 1.634, 95% confidence interval [CI] = 1.226-2.177, p = 7.97e-04), interleukin (IL)-6 on LP (OR = 0.615, 95% CI = 0.481-0.786, p = 1.04e-04), IL-4 on LP (OR = 1.099. 95% CI = 1.020-1.184, p = 1.26e-02), and IL-2 on urticaria (OR = 0.712, 95% CI = 0.531-0.955, p = 2.33e-02).

**Conclusion:** This study provides novel perspectives on the relationship between circulating cytokines and immune skin diseases, potentially providing valuable insights into their etiology, diagnostic approaches, and treatment.

KEYWORDS

**Mendelian randomization, circulating cytokines, immune skin diseases, genome-wide association studies, causal relationship**

# 1 Introduction

The skin, being the body's largest immune organ, serves as a protective barrier against external threats. Numerous skin diseases are associated with the overall homeostasis of the body, including inflammatory response, immune status, metabolic level, and gut flora homeostasis (1, 2). Immune skin diseases, such as alopecia areata (AA), chloasma, hidradenitis suppurativa (HS), lichen planus (LP), seborrheic dermatitis (SD), and urticaria, are highly prevalent and contribute significantly to the global health burden. However, due to their complex and diverse pathogenesis, effective treatments for these conditions are limited (3–8). Genetic research, particularly through genome-wide association studies (GWAS), has identified several single-nucleotide polymorphisms (SNPs) associated with skin diseases (9). However, translating these findings into clinically relevant therapeutic targets and treatments still requires substantial efforts.

Skin diseases often exhibit systemic inflammatory changes (10, 11). Circulating cytokine levels, as crucial inflammatory regulators, exert a significant influence on immune and inflammatory responses *in vivo* (12). Over 300 cytokines have been identified, primarily including chemokines, interleukins (ILs), interferons (IFNs), and growth factors. These small soluble molecules, secreted by cells, play roles in differentiation, proliferation, and apoptosis promotion (13). Disturbances in cytokine expression are a prominent feature during skin disease episodes (14). During exacerbations, patients with AA show increased levels of serum pro-inflammatory factors such as IFN-γ, IL-2, IL-7, and IL-15 (15). Furthermore, there have been reports on the association between chloasma, HS, LP, SD, and urticaria and cytokines (16–20). However, the existing evidence linking cytokines to these immune skin diseases stems from cross-sectional studies, which are susceptible to confounding factors, such as environment, age, dietary preferences, and lifestyles. Therefore, the causal association between cytokines and these immune skin diseases, as well as the direction of the causal effect remain unknown.

Mendelian randomization (MR) is currently a popular means for exploring causal relationships between exposures and outcomes of interest (21). It leverages the fundamental principles of Mendel's law, which entail the "random assignment of parental alleles to offspring", resembling the random assignment of participants in a randomized controlled trial. Thus, MR has emerged as a valuable tool for exploring causal relationships between complex traits, diseases, and phenotypes (22).

In the present study, genetic variants associated with 41 circulating cytokines were obtained from a large GWAS (23). Furthermore, a bidirectional two-sample MR analysis was conducted to investigate the relationship between cytokines and six immune skin diseases. Our findings might help elucidate the association between systemic inflammation and these immune skin diseases, offering new diagnostic biomarkers and revealing new targets for drug therapy.

# 2 Materials and methods

## 2.1 Study design

In the MR analysis, SNPs were treated as valid instrumental variables (IVs). These IVs had to fulfil three key assumptions, as shown in Figure 1: (1) a strong correlation between SNPs and exposure; (2) absence of association between SNPs and confounding factors that might influence the association between exposure and outcome; (3) exposure being the only pathway through which SNPs exert an effect on the outcome (24).

## 2.2 Data sources

The GWAS conducted by Ahola-Olli et al. provided the genome-wide association summary statistics for 41 systemic inflammatory regulators (23). The study population comprised 8,293 individuals from three different Finnish cohorts, namely the FINRISK1997, FINRISK2002, and the Young Finns Cardiovascular Risk Study (YFS) (Supplementary Table S1). Cytokines and growth factors in plasma were measured for participants in the FINRISK1997 cohort, while heparin plasma and serum cytokine measurements were performed for individuals in the FINRISK2002 and YFS cohorts. The circulating cytokine levels were expressed as standard deviations. Genetic associations were adjusted for the first ten genetic principal components, age, sex, and body mass index. Complete GWAS summary statistics were obtained from https://www.ebi.ac.uk/gwas/downloads/summary-statistics.

The summary statistics for the six immune skin diseases were obtained from FinnGen GWAS available at https://r8.finngen.fi/ (25). The numbers of cases and controls for each phenotype was as follows: 682 patients with AA and 361,140 controls, 95 patients with chloasma and 329,443 controls, 931 patients with HS and 361,140 controls, 3,597 patients with LP and 364,071 controls, 2,688 patients with SD and 336,589 controls, and 3,495 patients with urticaria and 364,583 controls.(More details as) These skin diseases were defined based on the International Classification of Diseases, 10$^{th}$ revision.

## 2.3 Selection of IVs

A genome-wide statistical significance threshold of $<5.0 \times 10^{-8}$ was established to extract the SNPs robustly associated with the studied exposures. Additionally, the $r^2$ threshold of 0.001 and a clump window size of 10,000 kb were set to eliminate linkage disequilibrium (26). As a result, 27 cytokines were retained based on these criteria. In a secondary analysis, the genome-wide significance threshold was relaxed to $5.0 \times 10^{-6}$ to allow for the inclusion of all 41 cytokines.

For the reverse direction, the significance threshold employed was $p < 5 \times 10^{-8}$, with consistent clumping parameter with the forward-direction analysis. However, due to the lack of sufficient SNPs, four diseases, namely AA, chloasma, HS, and SD, were not subjected to the reverse MR analysis. Consequently, the revere MR analyses were only conducted for LP and urticaria.

## 2.4 Statistical analysis

The Wald ratio test was used to estimate the association between identified IVs and skin diseases for cases containing only one SNP (27).

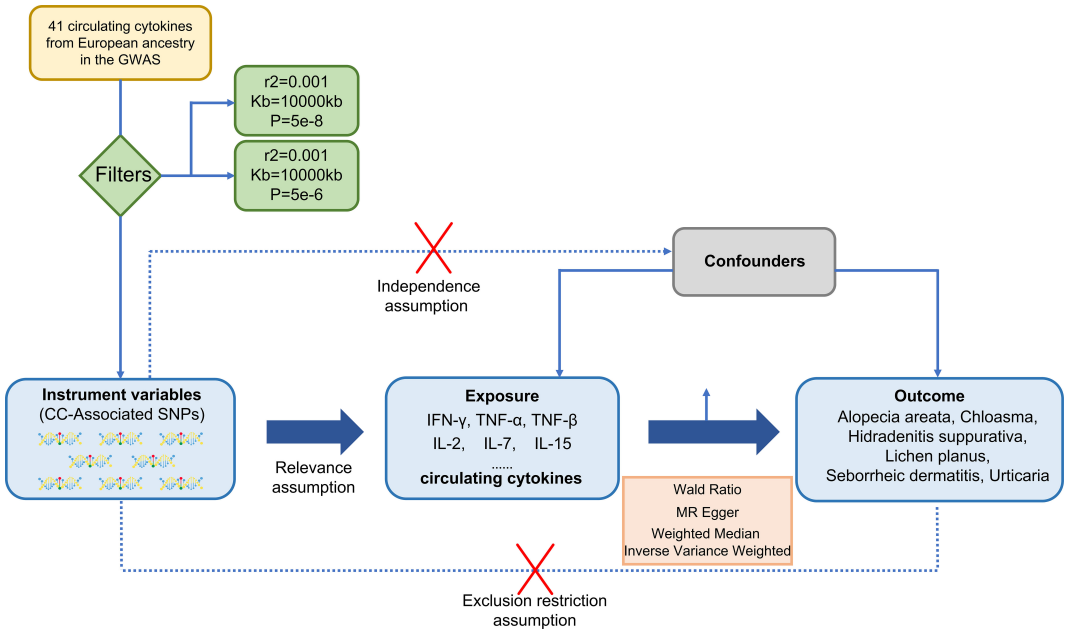


FIGURE 1
A design of three basic assumptions of Mendelian-randomization analysis: (1) a strong correlation between SNPs and exposure; (2) absence of association between SNPs and confounding factors that might influence the association between exposure and outcome; (3) exposure being the only pathway through which SNPs exert an effect on the outcome. CC, circulating cytokines; IFN-γ, Interferon-gamma; TNF-α, Tumor necrosis factor-alpha; TNFβ, Tumor necrosis factor-beta; IL-2, Interleukin-2; IL-7, Interleukin-7; IL-15, Interleukin-15.

For multiple SNPs, three MR analysis methods were used, including inverse variance weighted (IVW), MR-Egger and weighted median (WM), with the IVW method being the predominant method. The IVW method, which is the classical approach for MR analysis, incorporates inverse variances of each IV as weights to calculate a weighted average while ensuring the validity of all IVs (28). MR-Egger, on the other hand, employs a form of weighted linear regression analysis. Estimates derived from this method are robust and independent of IV validity, although they might have lower statistical precision and are susceptible to outlying genetic variations (29). The WM method addresses the issue of a large variation in estimation precision. Similar to the IVW method, this approach assigns inverse weights based on the variance of each genetic variant, and it demonstrates reliability even in the presence of violated causal effects (30). When significant causal correlations are evaluated using the IVW method, the MR egger and WM methods serve as supplementary methods and directional validation.

MR-Egger regression was used to assess pleiotropy. Moreover, the presence of pleiotropy and identification of outlying SNPs could be determined through the MR-Pleiotropy RESidual Sum and Outlier (PRESSO) test (31). The Cochran's Q was used to assess heterogeneity. A p-value of <0.05 indicates the presence of heterogeneity.

The strength of IVs can be evaluated using the F- statistic, which is calculated as follows: $F = \beta^2/SE^2$, where β is the effect size of the allele and SE is the standard error (32). An F statistic greater than 10 suggests the absence of weak IV bias (33). When analyzing multiple outcomes, significance thresholds are adjusted using the Bonferroni method. A p value smaller than the Bonferroni-corrected threshold indicates statistical significance. Additionally, correlations not exceeding the Bonferroni-corrected significance level but <0.05 were considered suggestively significant. All analyses were performed using R version 4.2.2, with the software packages "TwoSampleMR" (34) and "MRPRESSO" (28).

Due to the limited variability of phenotypic characteristics and the small proportion of patients in the outcome trait GWAS data, statistical ability is crucial. In order to calculate the statistical power, an online tool called mRnd (35) was used. In the case of a Type I error of 5%, we determined the expected OR threshold for each circulating cytokine and immune skin disease, which should meet a minimum power requirement of>80%.

# 3 Results

## 3.1 Causal effects of circulating cytokines on six immune skin diseases

Figure 2 illustrates the results, with 14 sets of suggestively significant associations (p <0.05) identified at a significance threshold of $<5.0 \times 10^{-8}$. Based on the significant correlation between circulating cytokines and immune skin diseases assessed by Mendelian randomization, further statistical efficacy analysis examined the threshold range of OR that needs to be reached when meeting sufficient statistical efficacy. It is worth noting that six cytokines meet the OR threshold for statistical efficacy analysis (IL-18, IL-17, IL-16, IL2α, TNFβ, Eotaxin). The details of statistic power analyses are presented in Supplementary Table 6. The above results do not meet the threshold range corrected by Bonferroni

10.3389/fimmu.2023.1240714

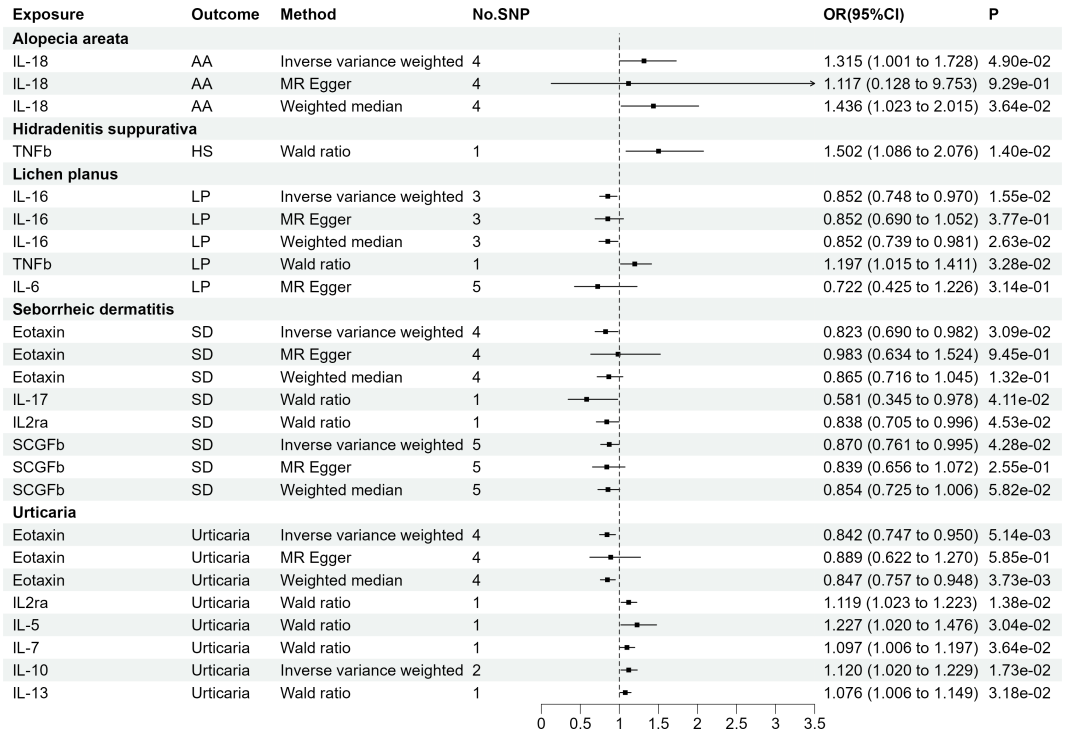


FIGURE 2
The 14 causal relationships (SNPs reaching $P<5\times10^{-8}$). AA, Alopecia areata; HS, Hidradenitis suppurativa; LP, Lichen planus; SD, Seborrheic dermatitis; IL-18, Interleukin-18; TNFβ, Tumor necrosis factor-beta; IL-16, Interleukin-16; IL-17, Interleukin-17; IL2rα, Interleukin-2 receptor, alpha subunit; SCGFβ, Stem cell growth factor beta.

(p = 0.05/27 = 1.85e-03). The specific SNP profiles, as well as the pleiotropy and heterogeneity results of these 14 groups, are presented in Supplementary Tables S3, 4. No evidence was observed in terms of heterogeneity and pleiotropy (p >0.05). The F-statistics for all groups were >10, indicating the absence of weak IV bias. Supplementary Table S5 presents the MR analyses involving 27 cytokines and six immune skin diseases.

As presented in Figure 3, employing a significance threshold of $<5.0 \times 10^{-6}$, 14 sets of suggestively significant correlations (p <0.05) were obtained. Based on the significant correlation between circulating cytokines and immune skin diseases assessed by Mendelian randomization, further statistical power analysis examined the threshold range of OR that needs to be reached when meeting sufficient statistical efficacy. Among the 14 pairs of suggestive significantly correlated traits, 4 pairs of suggestive significantly correlated traits that meet sufficient statistical efficacy were obtained through screening. The details of statistic power analyses are presented in Supplementary Table 10. Following Bonferroni correction (p = 0.05/41 = 1.22e-03), bNGF remained statistically significant in HS (OR = 1.634, 95% CI = 1.226-2.177, p = 7.97e-04) and IL6 remained statistically significant in LP (OR = 0.615, 95% CI = 0.481-0.786, p = 1.04e-04). Supplementary Tables S7, 8 provide detailed information on the SNP profiles, as well as the details of pleiotropy and heterogeneity. No heterogeneity or pleiotropy was observed, and there was no evidence of weak IV bias. The details of MR analyses involving 41 cytokines and six immune skin diseases are presented in Supplementary Table S9.

## 3.2 Causal effects of six immune skin diseases on circulating cytokines

As AA, chloasma, HS, and SD did not have genome-wide significant SNPs, our assessment was limited to LP and urticaria. Finally, seven sets of suggestively significant correlations (p <0.05) involving six cytokines (eotaxin, IL-12p70, IL-2, IL-4, IL-16, and MCP-1) were obtained. The association of LP with IL-4 (OR = 1.099, 95% CI = 1.020-1.184, p = 1.26e-02) and urticaria with IL-2 (OR = 0.712, 95% CI = 0.531-0.955, p = 2.33e-02) remained significant at the Bonferroni-corrected significance threshold (p = 0.05/2 = 0.025). Figure 4 shows the Mendelian randomization randomized forest map results of circulating cytokines and immune skin diseases with statistically significant (P<0.05) IVW method using multiple methods. Supplementary Tables S9, 10 provide information on SNPs, heterogeneity, and pleiotropy for these groups. Moreover, the F-statistics indicate the absence of weak IV bias. Detailed results of the specific reverse MR analyses involving LP and urticaria are presented in Supplementary Table S11.

10.3389/fimmu.2023.1240714

| Exposure | Outcome | Method | No.SNP | OR(95%CI) | P |
|---|---|---|---|---|---|
| **Alopecia areata** | | | | | |
| bNGF | AA | Inverse variance weighted | 7 | 1.623 (1.160 to 2.271) | 4.70e-03 |
| bNGF | AA | Weighted median | 7 | 1.594 (1.016 to 2.501) | 4.26e-02 |
| bNGF | AA | MR Egger | 7 | 1.252 (0.241 to 6.504) | 8.00e-01 |
| IL-9 | AA | Inverse variance weighted | 6 | 0.669 (0.456 to 0.981) | 3.96e-02 |
| IL-9 | AA | MR Egger | 6 | 0.430 (0.176 to 1.049) | 1.37e-01 |
| IL-9 | AA | Weighted median | 6 | 0.785 (0.472 to 1.305) | 3.51e-01 |
| IL2ra | AA | Inverse variance weighted | 6 | 0.737 (0.571 to 0.952) | 1.96e-02 |
| IL2ra | AA | MR Egger | 6 | 0.852 (0.573 to 1.267) | 4.73e-01 |
| IL2ra | AA | Weighted median | 6 | 0.756 (0.562 to 1.018) | 6.57e-02 |
| **Chloasma** | | | | | |
| RANTES | Chloasma | Inverse variance weighted | 9 | 2.308 (1.041 to 5.118) | 3.96e-02 |
| RANTES | Chloasma | MR Egger | 9 | 3.149 (0.395 to 25.129) | 3.15e-01 |
| RANTES | Chloasma | Weighted median | 9 | 2.108 (0.828 to 5.368) | 1.18e-01 |
| PDGFbb | Chloasma | Inverse variance weighted | 13 | 0.479 (0.239 to 0.958) | 3.74e-02 |
| PDGFbb | Chloasma | MR Egger | 13 | 0.531 (0.138 to 2.046) | 3.77e-01 |
| PDGFbb | Chloasma | Weighted median | 13 | 0.433 (0.174 to 1.077) | 7.18e-02 |
| MIF | Chloasma | Inverse variance weighted | 6 | 0.380 (0.151 to 0.957) | 4.00e-02 |
| MIF | Chloasma | MR Egger | 6 | 0.554 (0.110 to 2.797) | 5.14e-01 |
| MIF | Chloasma | Weighted median | 6 | 0.282 (0.090 to 0.884) | 2.99e-02 |
| **Hidradenitis suppurativa** | | | | | |
| bNGF | HS | Inverse variance weighted | 7 | 1.634 (1.226 to 2.177) | 7.97e-04 |
| bNGF | HS | MR Egger | 7 | 1.443 (0.353 to 5.896) | 6.31e-01 |
| bNGF | HS | Weighted median | 7 | 1.728 (1.180 to 2.530) | 4.97e-03 |
| **Lichen planus** | | | | | |
| IL2ra | LP | Inverse variance weighted | 6 | 0.872 (0.778 to 0.976) | 1.73e-02 |
| IL2ra | LP | MR Egger | 6 | 0.891 (0.747 to 1.062) | 2.66e-01 |
| IL2ra | LP | Weighted median | 6 | 0.860 (0.752 to 0.984) | 2.80e-02 |
| IL-6 | LP | Inverse variance weighted | 5 | 0.615 (0.481 to 0.786) | 1.04e-04 |
| IL-6 | LP | MR Egger | 5 | 0.722 (0.425 to 1.226) | 3.14e-01 |
| IL-6 | LP | Weighted median | 5 | 0.603 (0.440 to 0.827) | 1.70e-03 |
| MCP1 | LP | Inverse variance weighted | 14 | 1.151 (1.018 to 1.301) | 2.44e-02 |
| MCP1 | LP | MR Egger | 14 | 1.248 (0.935 to 1.665) | 1.58e-01 |
| MCP1 | LP | Weighted median | 14 | 1.129 (0.953 to 1.337) | 1.60e-01 |
| **Seborrheic dermatitis** | | | | | |
| SCGFb | SD | Inverse variance weighted | 14 | 0.894 (0.808 to 0.988) | 2.78e-02 |
| SCGFb | SD | MR Egger | 14 | 0.790 (0.659 to 0.948) | 2.61e-02 |
| SCGFb | SD | Weighted median | 14 | 0.860 (0.748 to 0.989) | 3.38e-02 |
| **Urticaria** | | | | | |
| Eotaxin | urticaria | Inverse variance weighted | 15 | 0.888 (0.826 to 0.955) | 1.41e-03 |
| Eotaxin | urticaria | MR Egger | 15 | 0.788 (0.670 to 0.926) | 1.26e-02 |
| Eotaxin | urticaria | Weighted median | 15 | 0.873 (0.786 to 0.970) | 1.18e-02 |
| GROa | urticaria | Inverse variance weighted | 9 | 0.947 (0.897 to 0.999) | 4.57e-02 |
| GROa | urticaria | MR Egger | 9 | 0.887 (0.787 to 0.999) | 8.94e-02 |
| GROa | urticaria | Weighted median | 9 | 0.970 (0.903 to 1.042) | 4.09e-01 |
| IL-10 | urticaria | Inverse variance weighted | 10 | 1.101 (1.009 to 1.201) | 3.13e-02 |
| IL-10 | urticaria | MR Egger | 10 | 1.138 (0.940 to 1.378) | 2.21e-01 |
| IL-10 | urticaria | Weighted median | 10 | 1.114 (1.019 to 1.218) | 1.80e-02 |

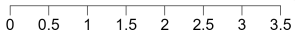


FIGURE 3
The 14 causal relationships (SNPs reaching $P<5\times10^{-6}$). AA: Alopecia areata, HS, Hidradenitis suppurativa; LP, Lichen planus; SD, Seborrheic dermatitis; βNGF, Beta nerve growth factor; IL-9, Interleukin-9; IL2rα, Interleukin-2 receptor; MIF, Macrophage migration inhibitory factor; PDGFbb, Platelet derived growth factor BB; RANTES, Regulated on Activation, Normal T Cell Expressed and Secreted; IL-6, Interleukin-6; MCP1, Monocyte chemotactic protein-1; SCGFβ, Stem cell growth factor beta; GROα, Growth regulated oncogene-α; IL-10, Interleukin-10.

The four groups that remained statistically significant after Bonferroni correction in this bidirectional MR analysis were selected for scatter plotting, as presented in Figure 5.

## 4 Discussion

This is the first study performing a bidirectional MR analysis to explore the relationship between 41 circulating cytokines and six immune skin diseases (AA, chloasma, HS, LP, SD, and urticaria). When cytokines were considered the exposure variable ($p < 5.0 \times 10^{-6}$), potential associations were observed between 3 cytokines and the risk of immune skin diseases. Specifically, bNGF was associated with AA and HS, and RANTES was associated with chloasma, IL-6 was associated with LP. On the other hand, when immune skin diseases served as the exposure variable, LP affected eotaxin, IL-12p70, IL-4, IL-16, and MCP-1 and urticaria affected IL-2 and MCP-1. Due to the limited number of cases available in the FinnGen database for the remaining four skin diseases, the genetic variation was insufficient for effective exploration. Therefore, a reanalysis should be performed in the future when an adequate number of patients become available. Although there are some circulating cytokines that have causal associations with immune skin diseases that have not been analyzed through statistical efficacy, some of these cytokines may have predictive value for disease risk and diagnostic purposes. Considering the complexity and complexity of the cytokine network in the body, it is necessary to conduct further clinical and basic experiments to verify these hypotheses.

Healthy skin comprises three layers, namely the epidermis, dermis, and subcutaneous fat. These layers harbor resident cell

10.3389/fimmu.2023.1240714

| Exposure | Outcome | Method | No.SNP | OR(95%CI) | P |
|---|---|---|---|---|---|
| **Lichen planus** | | | | | |
| LP | Eotaxin | Inverse variance weighted | 7 | 1.082 (1.005 to 1.165) | 3.73e-02 |
| LP | Eotaxin | MR Egger | 7 | 0.955 (0.680 to 1.340) | 8.00e-01 |
| LP | Eotaxin | Weighted median | 7 | 1.069 (0.977 to 1.171) | 1.47e-01 |
| LP | IL-12p70 | Inverse variance weighted | 7 | 1.078 (1.002 to 1.161) | 4.50e-02 |
| LP | IL-12p70 | MR Egger | 7 | 0.848 (0.605 to 1.187) | 3.80e-01 |
| LP | IL-12p70 | Weighted median | 7 | 1.051 (0.953 to 1.160) | 3.15e-01 |
| LP | IL-4 | Inverse variance weighted | 7 | 1.099 (1.020 to 1.184) | 1.26e-02 |
| LP | IL-4 | MR Egger | 7 | 0.896 (0.638 to 1.259) | 5.55e-01 |
| LP | IL-4 | Weighted median | 7 | 1.112 (1.010 to 1.224) | 3.11e-02 |
| LP | IL-16 | Inverse variance weighted | 7 | 1.182 (1.021 to 1.368) | 2.54e-02 |
| LP | IL-16 | MR Egger | 7 | 0.820 (0.425 to 1.580) | 5.79e-01 |
| LP | IL-16 | Weighted median | 7 | 1.091 (0.930 to 1.280) | 2.83e-01 |
| LP | MCP1 | Inverse variance weighted | 7 | 1.092 (1.002 to 1.189) | 4.46e-02 |
| LP | MCP1 | MR Egger | 7 | 0.983 (0.646 to 1.494) | 9.38e-01 |
| LP | MCP1 | Weighted median | 7 | 1.038 (0.935 to 1.151) | 4.87e-01 |
| **Urticaria** | | | | | |
| urticaria | IL-2 | Inverse variance weighted | 3 | 0.712 (0.531 to 0.955) | 2.33e-02 |
| urticaria | IL-2 | MR Egger | 3 | 0.633 (0.222 to 1.807) | 5.50e-01 |
| urticaria | IL-2 | Weighted median | 3 | 0.729 (0.518 to 1.026) | 7.03e-02 |
| urticaria | MCP1 | Inverse variance weighted | 3 | 1.303 (1.014 to 1.675) | 3.85e-02 |
| urticaria | MCP1 | MR Egger | 3 | 1.126 (0.399 to 3.177) | 8.60e-01 |
| urticaria | MCP1 | Weighted median | 3 | 1.323 (1.018 to 1.719) | 3.62e-02 |

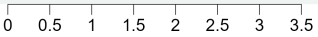


FIGURE 4
The 7 causal relationships (SNPs reaching $P<5\times10^{-8}$). LP, Lichen planus; IL-12p70, Interleukin-12p70; IL4, Interleukin-4; IL16, Interleukin-16; MCP1, Monocyte chemotactic protein-1; IL2, Interleukin-2.

populations, both immune and non-immune cells, which play crucial roles in maintaining a strong barrier against foreign substances. Moreover, these cells are involved in various inflammatory processes, contributing to an immune response against infections, autoimmunity, tumor immunity, and allergies (10). It can be stated that the pathogenesis of skin diseases is, to a certain extent, linked to inflammatory responses.

AA, a prevalent autoimmune disease, is characterized by non-scarring alopecia. The pathological process of AA involves a shift in the hair follicle microenvironment from a state of immune homeostasis to an active inflammatory state (15). Several GWASs have identified IL2ra as a cytokine gene associated with AA (36–38). IL2ra functions through regulatory T cells, playing a crucial role in maintaining immune homeostasis and suppressing autoantigen-mediated immune responses (39, 40). Notably, the *in vivo* IL-9 levels are significantly decreased in patients who exhibit effective responses to tetraphenyl cyclopentadienone treatment (41). These findings align with the results obtained in the current study. At present, no research has revealed the biological association and mechanism between bNGF and AA. Our study suggests for the first time that bNGF may have the potential to become an early screening biomarker for AA in the future and provide assistance in exploring the biological mechanisms and therapeutic targets of AA.

Chloasma, a prevalent light-induced pigmentation disorder, results in skin inflammation and the release of melanogenic cytokines and growth factors in response to ultraviolet (UV) radiation. These factors play a crucial role in the hyperpigmentation and reactivation of chloasma lesions (42). MIF is considered a key player in skin biology and wound healing and is negatively correlated with cellular and tissue ageing (43). MIF might serve as a key mediator in photoaging. *In vivo* and *in vitro* studies have shown that UVB radiation (UVB) induces the expression of MIF messenger ribonucleic acid in the skin and keratinocyte MIF production *in vivo* and *in vitro* (44). Moreover, UVB has been found to inhibit skin inflammation by inhibiting the production of RANTES in epidermal keratinocytes. This provides a new direction for the treatment of skin inflammation (45). PDGFbb production is reduced in terms of quantity and activity by UVB radiation (46). In addition, it promotes wound healing (47). Furthermore, UV irradiation induces RANTES overgrowth, resulting in inflammation (45).

HS, a chronic and inflammatory skin disease, imposes a significant burden on individuals and predominantly affects the axillae, groin, buttocks, and perianal areas. It is characterized by abnormal activation of the innate immune system (48, 49). While specific studies exploring the association between HS and bNGF are currently lacking, the observed relationship between the two cytokines remains significant even after correction. Moreover, a recent study on the relationship between bNGF and chloasma reported higher bNGF levels in affected areas compared with the normal sites (50). Therefore, the relationship between HS and bNGF warrants further investigation.

LP is a T cell-mediated autoimmune disease, specifically $CD8^+$ T cells, which are recruited into the skin and contribute to interface dermatitis (51). Impairment of IL2ra function in patients with oral LP (OLP) results in an increased inflammatory response (52). MCP-1, a chemokine present in LP lesions, plays a crucial role in aggregating monocytes to the skin interface and inducing toxic effects (53). LP and MCP-1 exhibit a bidirectional causal association that warrants further investigation. Reverse MR studies have demonstrated elevated cytokine IL-4 levels in the blood and saliva of patients with OLP (54). The relationship between LP and eotaxin, IL-12p70, and IL163 is novel and requires further investigation.

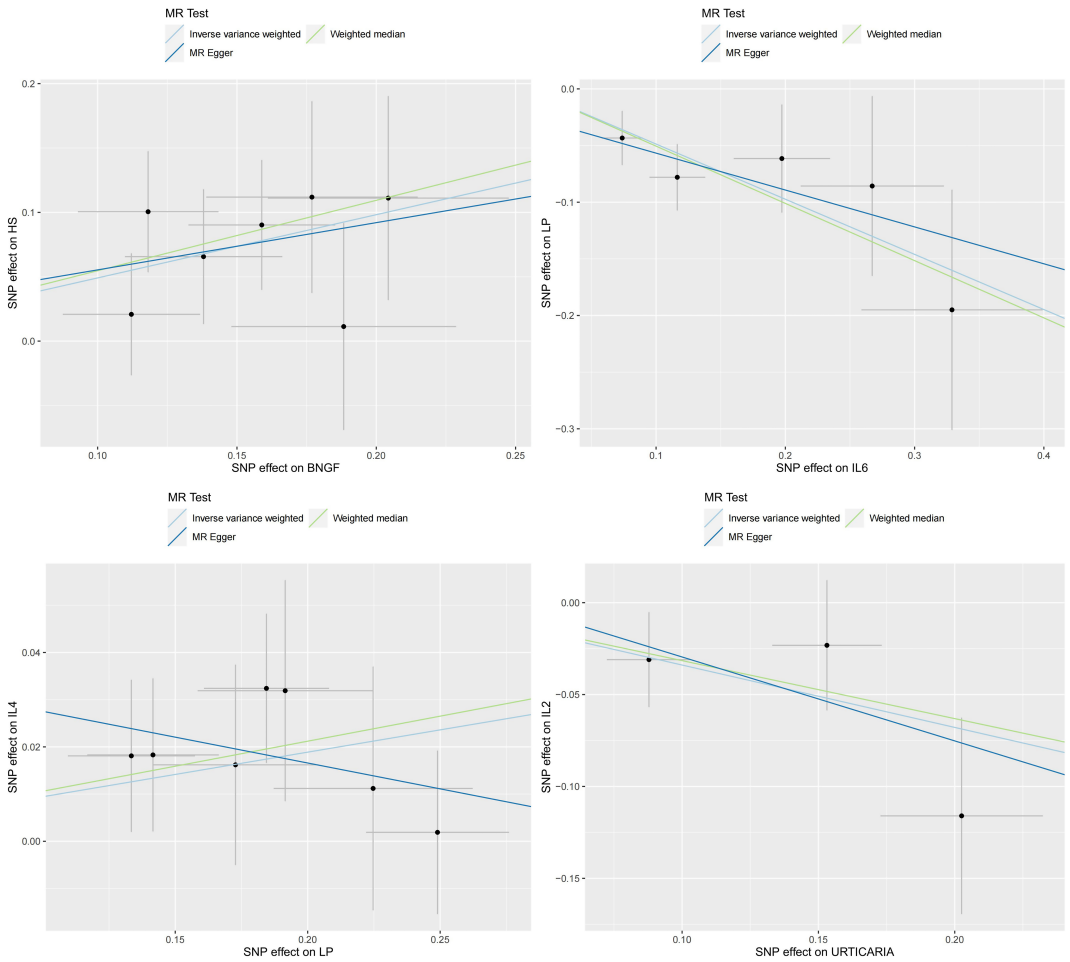


FIGURE 5
Scatter plots for the 4 significant associations at the Bonferroni corrected significance threshold. β NGF: Beta nerve growth factor, HS, Hidradenitis suppurativa; IL2, Interleukin-2; IL4, Interleukin-4; IL6, Interleukin-6; LP, Lichen planus; SD, Seborrheic dermatitis.

SD is a chronic, recurrent inflammatory skin disease. SCGFb is a newly discovered protein-secreting sulphated glycoprotein that serves as a growth factor in early hematopoiesis (55). Study have shown that SCGFb may be able to inhibit the pathogenesis of proliferative diabetic retinopathy(PDR) (55). However, the underlying mechanism remains to be elucidated.

Urticaria is a skin disease characterized by clinical symptoms such as wheal and angioedema. The pathogenesis of urticaria involves the activation of mast cells, which in turn release multiple cytokines, leading to sensory nerve activation, vasodilation, and plasma extravasation (56). Chronic urticaria is characterized by increased eotaxin and MCP-1, which are indicative of an inflammatory response (57, 58). Urticaria is mediated by mixed T helper (Th) 1/Th2-reactive lymphocytes, with Th1 cells primarily secreting IL-2 and Th2 cells secreting IL-10. In patients with urticaria, there is an observed increase in IL-10 production and a decrease in IL-2 levels, consistent with the findings of the present study (59).

The present study has certain limitations. Our study elucidates the intricate relationship between circulating cytokines and the risk of six immune skin diseases. However, it's imperative to recognize its limitations, which warrant attention in subsequent research. Despite our meticulous selection of instrumental variables (IVs) and the deployment of statistical tests, such as MR-PRESSO and MR-Egger intercept, to address potential pleiotropy and confounding, these concerns are not entirely eliminable. Future endeavors should place greater emphasis on understanding and rectifying these challenges, bolstering the validity of conclusions drawn from such data. Moreover, the representativeness of our results is constrained by the limited sample sizes for specific diseases and inflammatory markers. Although F-statistics indicate the potential insignificance of weak IVs, the precision of our inferences, particularly for these diseases and markers, remains ambiguous.

The primary scope of our findings pertains to European populations, given the Finnish origin of our dataset. The mosaic of genetic variations across ethnicities and geographies underscores the need for more comprehensive studies. Genetic disparities have profound implications in clinical scenarios, necessitating the analysis of more heterogeneous GWAS data in the future. Of the 41 cytokines we scrutinized, a mere six demonstrated a pronounced association with skin immune diseases. This underscores their specialized role in disease pathogenesis. However, the magnitude

of these associations can be contingent upon factors like sample size, genetic heterogeneity, and disease-specific nuances. The cellular dynamics within skin immune diseases demand further exploration. Deciphering the interactions between various skin cell populations and their associated cytokines will enrich our understanding of disease etiology. Cutting-edge techniques, such as single-cell RNA sequencing and spatial transcriptomics, promise to be revelatory in this domain.

While our Mendelian stochastic approach was instrumental in inferring causality, clinical implications necessitate a more direct approach. This entails measuring cytokine levels in both the affected and healthy populace, juxtaposing them with observed gene polymorphisms. Longitudinal assessments, which monitor the influence of these polymorphisms on cytokine levels across diverse conditions, are paramount.

In conclusion, our study provides a preliminary framework on the cytokine dynamics in immune skin diseases. To fully harness its translational potential, it's pivotal to address the aforementioned limitations, broaden the scope of datasets, and employ sophisticated methodologies. The potential biomarkers identified warrant rigorous validation in expansive, diverse cohorts and systematic clinical evaluations before they can be integrated into clinical practice guidelines.

## 5 Conclusion

In summary, this bidirectional MR analysis indicates potential causal associations between specific circulating cytokines and the six immune skin diseases. These findings coffer insights into potential targets and novel biomarkers for their diagnosis and treatment of immune skin diseases in clinical settings.

## Data availability statement

Publicly available datasets were analyzed in this study. This data can be found here: Data for 41 circulating cytokines are available at https://www.ebi.ac.uk/gwas/downloads/summary-statistics. Data for the six immune skin diseases can be downloaded from https://r8.finngen.fi.

## Ethics statement

Ethical review and approval were not required for the study on human participants in accordance with the local legislation and institutional requirements. Written informed consent from the participants' legal guardian/next of kin was not required to participate in this study in accordance with the national legislation and the institutional requirements.

## Author contributions

QL: Conceptualization, methodology, formal analysis, data curation, writing-original draft preparation; QC: Data curation, writing-original draft preparation, visualization; JG: Writing-original draft preparation, visualization; SC: Data curation, visualization; YW: Supervision, writing-review and editing. All authors contributed to the article and approved the submitted version.

## Acknowledgments

The authors thank the studies or consortiums referenced and included in the present analysis for providing public datasets. The authors thank Bullet Edits Limited for the linguistic editing and proofreading of the manuscript.

## Conflict of interest

The authors declare that the research was conducted in the absence of any commercial or financial relationships that could be construed as a potential conflict of interest.

## Publisher's note



## Supplementary material

The Supplementary Material for this article can be found online at: https://www.frontiersin.org/articles/10.3389/fimmu.2023.1240714/full#supplementary-material

## References

1. Karimkhani C, Dellavalle RP, Coffeng LE, Flohr C, Hay RJ, Langan SM, et al. Global skin disease morbidity and mortality: an update from the global burden of disease study 2013. *JAMA Dermatol* (2017) 153:406–12. doi: 10.1001/jamadermatol.2016.5538

2. Hay RJ, Johns NE, Williams HC, Bolliger IW, Dellavalle RP, Margolis DJ, et al. The global burden of skin disease in 2010: an analysis of the prevalence and impact of skin conditions. *J Invest Dermatol* (2014) 134:1527–34. doi: 10.1038/jid.2013.446

3. Handel AC, Miot LDB, Miot HA. Melasma: a clinical and epidemiological review. *Bras Dermatol* (2014) 89:771–82. doi: 10.1590/abd1806-4841.20143063

4. Zhou C, Li X, Wang C, Zhang J. Alopecia areata: an update on etiopathogenesis, diagnosis, and management. *Clin Rev Allergy Immunol* (2021) 61:403–23. doi: 10.1007/s12016-021-08883-0

5. Saunte DML, Jemec GBE. Hidradenitis suppurativa: advances in diagnosis and treatment. *JAMA* (2017) 318:2019–32. doi: 10.1001/jama.2017.16691

6. Solimani F, Forchhammer S, Schloegl A, Ghoreschi K, Meier K. Lichen planus - a clinical guide. *J Dtsch Dermatol Ges* (2021) 19:864–82. doi: 10.1111/ddg.14565

7. Clark GW, Pope SM, Jaboori KA. Diagnosis and treatment of seborrheic dermatitis. *Am Fam Phys* (2015) 91:185–90.

8. Zuberbier T. Urticaria. *Allergy* (2003) 58:1224–34. doi: 10.1046/j.1398-9995.2003.00327.x

9. Moitinho-Silva L, Degenhardt F, Rodriguez E, Emmert H, Juzenas S, Möbus L, et al. Host genetic factors related to innate immunity, environmental sensing and cellular functions are associated with human skin microbiota. *Nat Commun* (2022) 13:6204. doi: 10.1038/s41467-022-33906-5

10. Richmond JM, Harris JE. Immunology and skin in health and disease. *Cold Spring Harb Perspect Med* (2014) 4:a015339. doi: 10.1101/cshperspect.a015339

11. Pasparakis M, Haase I, Nestle FO. Mechanisms regulating skin immunity and inflammation. *Nat Rev Immunol* (2014) 14:289–301. doi: 10.1038/nri3646

12. Becher B, Spath S, Goverman J. Cytokine networks in neuroinflammation. *Nat Rev Immunol* (2017) 17:49–59. doi: 10.1038/nri.2016.123

13. Liszewski W, Gniadecki R. The role of cytokine deficiencies and cytokine autoantibodies in clinical dermatology. *J Eur Acad Dermatol Venereol* (2016) 30:404–12. doi: 10.1111/jdv.13303

14. Whiteside TL. "Introduction to cytokines as targets for immunomodulation,". In: House RV, Descotes J, editors. *Cytokines in Human Health: Immunotoxicology, Pathology, and Therapeutic Applications Methods in Pharmacology and Toxicology*. Totowa, NJ: Humana Press (2007). p. 1–15. doi: 10.1007/978-1-59745-350-9_1

15. Lensing M, Jabbari A. An overview of JAK/STAT pathways and JAK inhibition in alopecia areata. *Front Immunol* (2022) 13:955035. doi: 10.3389/fimmu.2022.955035

16. Nassar AAE, Ibrahim A-SM, Mahmoud AA. Efficacy and safety of intralesional steroid injection in the treatment of melasma. *J Cosmet Dermatol* (2021) 20:862–7. doi: 10.1111/jocd.13628

17. Fletcher JM, Moran B, Petrasca A, Smith CM. IL-17 in inflammatory skin diseases psoriasis and hidradenitis suppurativa. *Clin Exp Immunol* (2020) 201:121–34. doi: 10.1111/cei.13449

18. Shao S, Tsoi LC, Sarkar MK, Xing X, Xue K, Uppala R, et al. IFN-γ enhances cell-mediated cytotoxicity against keratinocytes *via* JAK2/STAT1 in lichen planus. *Sci Transl Med* (2019) 11:eaav7561. doi: 10.1126/scitranslmed.aav7561

19. Molinero LL, Gruber M, Leoni J, Woscoff A, Zwirner NW. Up-regulated expression of MICA and proinflammatory cytokines in skin biopsies from patients with seborrhoeic dermatitis. *Clin Immunol* (2003) 106:50–4. doi: 10.1016/s1521-6616(03)00003-2

20. Hinden S, Klukowska-Rötzler J, Janda J, Marti EI, Gerber V, Roosje PJ. Characterization of the inflammatory infiltrate and cytokine expression in the skin of horses with recurrent urticaria. *Vet Dermatol* (2012) 23:503–e99. doi: 10.1111/j.1365-3164.2012.01117.x

21. Davey Smith G, Hemani G. Mendelian randomization: genetic anchors for causal inference in epidemiological studies. *Hum Mol Genet* (2014) 23:R89–98. doi: 10.1093/hmg/ddu328

22. Long Y, Tang L, Zhou Y, Zhao S, Zhu H. Causal relationship between gut microbiota and cancers: a two-sample Mendelian randomisation study. *BMC Med* (2023) 21:66. doi: 10.1186/s12916-023-02761-6

23. Ahola-Olli AV, Würtz P, Havulinna AS, Aalto K, Pitkänen N, Lehtimäki T, et al. Genome-wide association study identifies 27 loci influencing concentrations of circulating cytokines and growth factors. *Am J Hum Genet* (2017) 100:40–50. doi: 10.1016/j.ajhg.2016.11.007

24. Hartwig FP, Davies NM, Hemani G, Davey Smith G. Two-sample Mendelian randomization: avoiding the downsides of a powerful, widely applicable but potentially fallible technique. *Int J Epidemiol* (2016) 45:1717–26. doi: 10.1093/ije/dyx028

25. Kurki MI, Karjalainen J, Palta P, Sipilä TP, Kristiansson K, Donner K, et al. FinnGen: Unique genetic insights from combining isolated population and national health register data. *medRxiv* (2022). doi: 10.1101/2022.03.03.22271360

26. Sanna S, van Zuydam NR, Mahajan A, Kurilshikov A, Vich Vila A, Võsa U, et al. Causal relationships among the gut microbiome, short-chain fatty acids and metabolic diseases. *Nat Genet* (2019) 51:600–5. doi: 10.1038/s41588-019-0350-x

27. Burgess S, Small DS, Thompson SG. A review of instrumental variable estimators for Mendelian randomization. *Stat Methods Med Res* (2017) 26:2333–55. doi: 10.1177/0962280215597579

28. Burgess S, Butterworth A, Thompson SG. Mendelian randomization analysis with multiple genetic variants using summarized data. *Genet Epidemiol* (2013) 37:658–65. doi: 10.1002/gepi.21758

29. Bowden J, Davey Smith G, Burgess S. Mendelian randomization with invalid instruments: effect estimation and bias detection through Egger regression. *Int J Epidemiol* (2015) 44:512–25. doi: 10.1093/ije/dyv080

30. Bowden J, Davey Smith G, Haycock PC, Burgess S. Consistent estimation in mendelian randomization with some invalid instruments using a weighted median estimator. *Genet Epidemiol* (2016) 40:304–14. doi: 10.1002/gepi.21965

31. Verbanck M, Chen C-Y, Neale B, Do R. Detection of widespread horizontal pleiotropy in causal relationships inferred from Mendelian randomization between complex traits and diseases. *Nat Genet* (2018) 50:693–8. doi: 10.1038/s41588-018-0099-7

32. Bowden J, Del Greco MF, Minelli C, Davey Smith G, Sheehan NA, Thompson JR. Assessing the suitability of summary data for two-sample Mendelian randomization analyses using MR-Egger regression: the role of the I2 statistic. *Int J Epidemiol* (2016) 45:1961–74. doi: 10.1093/ije/dyw220

33. Burgess S, Thompson SGCRP CHD Genetics Collaboration. Avoiding bias from weak instruments in Mendelian randomization studies. *Int J Epidemiol* (2011) 40:755–64. doi: 10.1093/ije/dyr036

34. Hemani G, Tilling K, Davey Smith G. Orienting the causal relationship between imprecisely measured traits using GWAS summary data. *PloS Genet* (2017) 13:e1007081. doi: 10.1371/journal.pgen.1007081

35. Brion MJ, Shakhbazov K, Visscher PM. Calculating statistical power in Mendelian randomization studies. *Int J Epidemiol* (2013) 42:1497–501. doi: 10.1093/ije/dyt179

36. Moravvej H, Tabatabaei-Panah P-S, Abgoon R, Khaksar L, Sokhandan M, Tarshaei S, et al. Genetic variant association of PTPN22, CTLA4, IL2RA, as well as HLA frequencies in susceptibility to alopecia areata. *Immunol Invest* (2018) 47:666–79. doi: 10.1080/08820139.2018.1480032

37. Mosallaei M, Simonian M, Esmaeilzadeh E, Bagheri H, Miraghajani M, Salehi AR, et al. Single nucleotide polymorphism rs10889677 in miRNAs Let-7e and Let-7f binding site of IL23R gene is a strong colorectal cancer determinant: Report and meta-analysis. *Cancer Genet* (2019) 239:46–53. doi: 10.1016/j.cancergen.2019.09.003

38. Olayinka JJT, Richmond JM. Immunopathogenesis of alopecia areata. *Curr Res Immunol* (2021) 2:7–11. doi: 10.1016/j.crimmu.2021.02.001

39. Malek TR, Castro I. Interleukin-2 receptor signaling: at the interface between tolerance and immunity. *Immunity* (2010) 33:153–65. doi: 10.1016/j.immuni.2010.08.004

40. Redler S, Albert F, Brockschmidt FF, Herold C, Hanneken S, Eigelshoven S, et al. Investigation of selected cytokine genes suggests that IL2RA and the TNF/LTA locus are risk factors for severe alopecia areata. *Br J Dermatol* (2012) 167:1360–5. doi: 10.1111/bjd.12004

41. Manimaran RP, Ramassamy S, Rajappa M, Chandrashekar L. Therapeutic outcome of diphencyprone and its correlation with serum cytokine profile in alopecia areata. *J Dermatolog Treat* (2022) 33:324–8. doi: 10.1080/09546634.2020.1752887

42. Rodríguez-Arámbula A, Torres-Álvarez B, Cortés-García D, Fuentes-Ahumada C, Castanedo-Cázares JP. CD4, IL-17, and COX-2 are associated with subclinical inflammation in malar melasma. *Am J Dermatopathol* (2015) 37:761–6. doi: 10.1097/DAD.0000000000000378

43. Welford SM, Bedogni B, Gradin K, Poellinger L, Broome Powell M, Giaccia AJ. HIF1alpha delays premature senescence through the activation of MIF. *Genes Dev* (2006) 20:3366–71. doi: 10.1101/gad.1471106

44. Scordi IA, Vincek V. Timecourse study of UVB-induced cytokine induction in whole mouse skin. *Photodermatol Photoimmunol Photomed* (2000) 16:67–73. doi: 10.1034/j.1600-0781.2000.d01-6.x

45. Arakawa S, Hatano Y, Katagiri K, Terashi H, Fujiwara S. Effects of ultraviolet B irradiation on the production of regulated upon activation normal T-cell expressed and secreted protein in cultured human epidermal keratinocytes. *Arch Dermatol Res* (2006) 297:377–80. doi: 10.1007/s00403-005-0620-6

46. Evrova O, Kellenberger D, Scalera C, Calcagni M, Giovanoli P, Vogel V, et al. Impact of UV sterilization and short term storage on the in *vitro* release kinetics and bioactivity of biomolecules from electrospun scaffolds. *Sci Rep* (2019) 9:15117. doi: 10.1038/s41598-019-51513-1

47. Barrientos S, Stojadinovic O, Golinko MS, Brem H, Tomic-Canic M. Growth factors and cytokines in wound healing. *Wound Repair Regener* (2008) 16:585–601. doi: 10.1111/j.1524-475X.2008.00410.x

48. Chopra D, Arens RA, Amornpairoj W, Lowes MA, Tomic-Canic M, Strbo N, et al. Innate immunity and microbial dysbiosis in hidradenitis suppurativa - vicious cycle of chronic inflammation. *Front Immunol* (2022) 13:960488. doi: 10.3389/fimmu.2022.960488

49. Sabat R, Jemec GBE, Matusiak Ł, Kimball AB, Prens E, Wolk K. Hidradenitis suppurativa. *Nat Rev Dis Primers* (2020) 6:18. doi: 10.1038/s41572-020-0149-1

50. Byun JW, Park IS, Choi GS, Shin J. Role of fibroblast-derived factors in the pathogenesis of melasma. *Clin Exp Dermatol* (2016) 41:601–9. doi: 10.1111/ced.12874

51. Boch K, Langan EA, Kridin K, Zillikens D, Ludwig RJ, Bieber K. Lichen planus. *Front Med* (2021) 8. doi: 10.3389/fmed.2021.737813

52. Zhou L, Cao T, Wang Y, Yao H, Du G, Chen G, et al. Frequently increased but functionally impaired CD4+CD25+ Regulatory T cells in patients with oral lichen planus. *Inflammation* (2016) 39:1205–15. doi: 10.1007/s10753-016-0356-9

53. Spandau U, Toksoy A, Goebeler M, Bröcker EB, Gillitzer R. MIG is a dominant lymphocyte-attractant chemokine in lichen planus lesions. *J Invest Dermatol* (1998) 111:1003–9. doi: 10.1046/j.1523-1747.1998.00426.x

54. Mozaffari HR, Zavattaro E, Saeedi M, Lopez-Jornet P, Sadeghi M, Safaei M, et al. Serum and salivary interleukin-4 levels in patients with oral lichen planus: A systematic review and meta-analysis. *Oral Surg Oral Med Oral Pathol Oral Radiol* (2019) 128:123–31. doi: 10.1016/j.oooo.2019.04.003

55. Sukowati CHC, Patti R, Pascut D, Ladju RB, Tarchi P, Zanotta N, et al. Serum stem cell growth factor beta for the prediction of therapy response in

hepatocellular carcinoma. *BioMed Res Int* (2018) 2018:6435482. doi: 10.1155/2018/6435482

56. Church MK, Kolkhir P, Metz M, Maurer M. The role and relevance of mast cells in urticaria. *Immunol Rev* (2018) 282:232–47. doi: 10.1111/imr.12632

57. Tedeschi A, Asero R, Lorini M, Marzano AV, Cugno M. Serum eotaxin levels in patients with chronic spontaneous urticaria. *Eur Ann Allergy Clin Immunol* (2012) 44:188–92.

58. Wang J, Zhao Y, Yan X. Effects of desloratadine citrate disodium on serum immune function indices, inflammatory factors and chemokines in patients with chronic urticaria. *J Coll Phys Surg Pak* (2019) 29:214–7. doi: 10.29271/jcpsp.2019.03.214

59. Li N, Cao N, Niu Y-D, Bai X-H, Lu J, Sun Y, et al. Effects of the polysaccharide nucleic acid fraction of bacillus Calmette-Guérin on the production of interleukin-2 and interleukin-10 in the peripheral blood lymphocytes of patients with chronic idiopathic urticaria. *BioMed Rep* (2013) 1:713–8. doi: 10.3892/br.2013.130

frontiers | Frontiers in Immunology

TYPE Original Research
PUBLISHED 05 January 2024
DOI 10.3389/fimmu.2023.1285951



OPEN ACCESS

EDITED BY
Zhenghua Zhang,
Fudan University, China

REVIEWED BY
Guang Li,
University of Pittsburgh, United States
Kepeng Wang,
UCONN Health, United States

*CORRESPONDENCE
Xiaofan Chen
littlecanva@163.com
Bo Yu
yubomd@hotmail.com

RECEIVED 30 August 2023
ACCEPTED 07 December 2023
PUBLISHED 05 January 2024

CITATION
Tang S, Hu H, Li M, Zhang K, Wu Q, Liu X, Wu L, Yu B and Chen X (2024) OPN promotes pro-inflammatory cytokine expression via ERK/JNK pathway and M1 macrophage polarization in Rosacea.
*Front. Immunol.* 14:1285951.
doi: 10.3389/fimmu.2023.1285951



# OPN promotes pro-inflammatory cytokine expression via ERK/JNK pathway and M1 macrophage polarization in Rosacea

Siyi Tang[1], Hao Hu[1], Manhui Li[1], Kaoyuan Zhang[2], Qi Wu[3], Xiaojuan Liu[1], Lin Wu[2], Bo Yu[2]* and Xiaofan Chen[1]*

[1]Shenzhen Key Laboratory for Translational Medicine of Dermatology, Biomedical Research Institute, Shenzhen Peking University - The Hong Kong University of Science and Technology Medical Center, Shenzhen, Guangdong, China, [2]Department of Dermatology, Peking University Shenzhen Hospital, Shenzhen, China, [3]Greater Bay Biomedical Innocenter, Shenzhen Bay Laboratory, Shenzhen, China

Rosacea is a chronic inflammatory dermatosis that involves dysregulation of innate and adaptive immune systems. Osteopontin (OPN) is a phosphorylated glycoprotein produced by a broad range of immune cells such as macrophages, keratinocytes, and T cells. However, the role of OPN in rosacea remains to be elucidated. In this study, it was found that OPN expression was significantly upregulated in rosacea patients and LL37-induced rosacea-like skin inflammation. Transcriptome sequencing results indicated that OPN regulated pro-inflammatory cytokines and promoted macrophage polarization towards M1 phenotype in rosacea-like skin inflammation. *In vitro*, it was demonstrated that intracellular OPN (iOPN) promoted LL37-induced IL1B production through ERK1/2 and JNK pathways in keratinocytes. Moreover, secreted OPN (sOPN) played an important role in keratinocyte-macrophage crosstalk. In conclusion, sOPN and iOPN were identified as key regulators of the innate immune system and played different roles in the pathogenesis of rosacea.

KEYWORDS

**Rosacea, OPN, keratinocyte, macrophage, inflammation**

## 1 Introduction

Rosacea is a chronic inflammatory skin disorder primarily affecting the midface (1), which is characterized by recurrent flushing or persistent erythema, pustules, papules, phymatous changes, and telangiectasia (2). There are three clinical types of rosacea, including erythematotelangiectatic (ETR) type, papulopustular (PPR) type,

and phytates (PhR) type (3). Recent research into the pathogenesis of rosacea suggested that dysregulation of the immune system as well as neurovascular played a key role in the development of rosacea (1). As the "initiator" of rosacea, activated keratinocytes secreted large numbers of inflammatory factors that function as important signal transmitters between keratinocytes and other immune cells. Multiple innate immune cells including macrophages, neutrophils, and mast cells (4), were infiltrated in rosacea lesions and contributed significantly to the pathophysiology of rosacea (5, 6). Moreover, proinflammatory cytokines are also key effectors of the inflammatory response in rosacea. Cathelicidin LL37 may induce the production of characteristic cytokines and chemokines via mTORC1 signaling pathway in rosacea (7). Due to its role in inflammation and angiogenesis, IL-1β is one of the most important pro-inflammatory cytokines in the pathogenesis of rosacea (8). However, there was need to demonstrate the mechanism of elevated IL-1β in rosacea.

As part of the innate immune system, macrophages differentiated from monocytes were recruited from the blood into inflamed tissues (9, 10), which play a vital role in regulating local inflammatory response. Macrophages are capable of changing their phenotypes in response to many different stimuli, including classically activated macrophages (M1 macrophages) and alternatively activated macrophages (M2 macrophages) (11). M1 macrophages are pro-inflammatory and play a central role in host defense against infection, whereas M2 macrophages are associated with anti-inflammatory responses and tissue remodeling (11). Macrophages regulate the initiation and progression of inflammatory diseases through the transformation of different phenotypes (12). Selective depletion of M1 macrophages in transgenic mice inhibits chronic skin inflammation (13), while selective activation of M2 macrophages ultimately attenuates atopic dermatitis (14). These studies illustrate that the reduction of the M1/M2 ratio suppresses skin inflammation. Recruitment and activation of macrophages have been reported in the skin lesions of rosacea patients (5), and the polarization of macrophages towards the M1 phenotype may exacerbate rosacea inflammation (15). Crosstalk between macrophages and keratinocytes may participate in macrophage polarization in rosacea pathogenesis. However, the exact signal transmitter between them still needs to be investigated in depth.

Osteopontin (OPN) is a phosphorylated glycoprotein produced by a broad range of cells including osteoclasts (16), T cells (17), macrophages (18), and fibroblasts (19). Previous studies have revealed the roles of OPN in the process of immune response (20), tumorigenesis (21), and biomineralization (22). Many studies have shown that secreted OPN (sOPN) has a chemotactic effect on macrophages and neutrophils during acute and chronic inflammation processes (23). However, another intracellular form of OPN (iOPN) without a signal sequence has recently attracted considerable attention in immune cell signaling (23). Different forms of OPN may exist in different cells (24). Which forms of OPN exist in keratinocytes and how they regulate the inflammatory signaling pathways and macrophage polarization in rosacea remain unclear.

In the present study, we focused on the role of epidermal OPN in the pathogenesis of rosacea. Firstly, it was found that OPN was upregulated in the epidermis of rosacea patients and promoted LL37-induced skin inflammation. OPN promoted rosacea-like skin inflammation by increasing the infiltration of macrophages and angiogenesis. Furthermore, it was demonstrated that iOPN promoted pro-inflammatory cytokine IL1B expression via ERK1/2 and JNK signaling pathways in keratinocytes, while sOPN played a key role in keratinocyte-macrophage crosstalk by promoting M1 macrophage polarization. These results indicated that OPN might be a promising therapeutic target in rosacea treatment.

# 2 Materials and methods

## 2.1 Datasets

The epidermal rosacea transcriptome dataset (GSE65914) of rosacea lesions and healthy controls was downloaded from the Gene Expression Omnibus (GEO) database (https://www.ncbi.nlm.nih.gov/gds/).

## 2.2 Patient and specimen collection

All skin biopsy samples (three rosacea patients and three healthy controls) included in this study were obtained from the Department of Dermatology, Peking University Shenzhen Hospital (Shenzhen, China). In this study, all the patients were not treated with systemic treatment before skin biopsy. The control groups were obtained from biopsies of non-inflamed skin from healthy subjects. The collected samples were fixed with 4% paraformaldehyde and embedded for tissue sectioning and staining. This study was conducted in accordance with the Declaration of Helsinki and approved by the Ethics Committee of Peking University Shenzhen Hospital. Informed consent was obtained from all participants.

## 2.3 Cell culture and treatment

HaCaT and THP-1 cells were obtained from the China Center for Type Culture Collection (China). HaCaT and THP-1 cells were cultured in DMEM (Gibco, USA) and RPMI-1640 (Gibco, USA) growth medium containing 10% FBS (Gibco, USA) in a humidified atmosphere with 5% $CO_2$ at 37°C. For LL37 treatment, HaCaT cells were stimulated with LL37 (QYAOBIO, China) (80, 100μg/ml) in serum-free medium for 12 hours. For siRNA treatment, HaCaT cells at 70% confluence were transfected with small interfering RNA targeting OPN mRNA (si-OPN) or negative controls (si-NC) by Lipofectamine™ RNAiMAX Transfection Reagent (Thermo Scientific, USA) according to the manufacturer's instructions. siRNAs were bought from Ribobio (China). The siRNA sequence that targeted OPN mRNA was as follows: 5'-GAACGACTCTGA TGATGTA-3'. For inhibitor treatment, ERK1/2 inhibitor

(SCH772984) (MedChemExpress, USA) and JNK inhibitor II (Thermo Fisher Scientific, USA) were used to inhibit ERK1/2 and JNK signaling pathways in HaCaT cells. THP-1 cells were incubated with 50 ng/ml phorbol 12-myristate 13-acetate (PMA; Sigma-Aldrich, USA) for 48 hours to differentiate into macrophages (M0), and then stimulated with 1000ng/ml recombinant human OPN (rhOPN) (Sino Biological, China) for 48 hours. The endotoxin level of rhOPN is less than 1.0 EU/μg as determined by the LAL method in the manual from its manufacturer.

## 2.4 Animal experiments

OPN knockout (OPN KO) mice on C57BL/6 background were obtained from The Jackson Laboratory (USA). Female C57BL/6 wild-type (WT) mice (6-8 weeks of age) were kept under specific pathogen-free conditions at 24°C. All procedures were approved and supervised by Shenzhen Perking University - the Hong Kong University of Science and Technology Medical Center Animal Care and Use Committee. LL37 was synthesized in QYAOBIO (China). For the rosacea-like mouse model (23), the backs of the mice were shaved 24 hours before treatment, and then injected with LL37 by intradermal injection every 12 hours for 2 days to induce a rosacea-like inflammatory phenotype. Erythema on the lesions was photographed and evaluated 24 hours after the last injection.

## 2.5 RNA sequencing and analysis

RNA qualification, library preparation, sequencing, quality control, read mapping to the reference genome, and expression analysis were performed by BGI Genomics (Wuhan, China). In brief, the total RNAs from the mouse skin tissues were extracted with TRIzol reagent (Sigma-Aldrich, USA) according to the manufacturer's instructions. The RNA samples were denatured at appropriate temperature to reveal its secondary structure, and oligo (dT) magnetic beads were used to enrich the mRNA. Fragmentation reagents were added to the mRNA to fragment the mRNA. Then one-strand and two-strand cDNA were synthesized. The ends of the double-stranded cDNA were repaired. A single "A" nucleotide is added to the 3' end to connect the adapter to the cDNA, then the product is amplified. After the PCR product was denatured into a single-stranded product, a cyclization reaction system was prepared to obtain a single-stranded circular product and digest the uncirculated linear DNA molecules. Single-stranded circular DNA molecules replicated through rolling circles form DNA nanoball (DNB) containing multiple copies. DNBs were added to the mesh holes on the chip using high-density DNA nanochip technology, and sequenced through combined probe-anchored polymerization technology. To obtain clean data, the raw data were filtered with SOAPnuke. HISAT2 was used to align the clean data to the reference genome. Bowtie2 was used to align the clean data to the reference gene set. The expression levels of genes were calculated by RSEM.

Using $|\log2FC| \geq 1$, p value $< 0.05$ as the thresholds, differentially expressed genes (DEGs) were identified with the DESeq R package. Kyoto Encyclopedia of Genes and Genomes (KEGG) pathway analysis was performed by R clusterProfiler package. For immune infiltration analysis, relative levels of different immune cell types in WT mice and OPN KO mice were quantified by using the CIBERSORT algorithm (https://cibersort.stanford.edu).

## 2.6 Isolation and culture of primary mouse keratinocytes

C57BL/6 wildtype (WT) mice and OPN knockout (OPN KO) mice neonates from post-natal days 0 to 2 were sacrificed, of which limbs were removed then. After washed with 70% ethanol and PBS, the whole skins were peeled off and floated in ice-cold dispase digestion buffer overnight at 4°C. The next day, the epidermis and dermis were mechanically separated with forceps, and then CnT-Accutase-100 (CellnTec, Switzerland) was added to detach keratinocytes from the separated epidermis. The primary keratinocytes were seeded in the six-well plate with CnT-07 Epithelial Proliferation Medium (CellnTec, Switzerland) and CnT-07.S (CellnTec, Switzerland), which were cultivated at 37°C with 5% $CO_2$ for 48 hours. All animal studies were approved and supervised by Shenzhen Perking University - the Hong Kong University of Science and Technology Medical Center Animal Care and Use Committee.

## 2.7 Generation of stable cell lines expressing sOPN and iOPN

The 903 nucleotide (nt) coding sequence (CDS) of sOPN was cloned into the lentiviral vector pLVX-IRES-Hyg (Addgene, USA), which encodes a polypeptide of 300 amino acids. Similarly, the 855 nt CDS of iOPN, lacking the first 48 nt signal peptide of sOPN, was cloned into the pLVX-IRES-Hyg vector. The nucleotide and protein sequences of OPN are listed in Figure S1, and primers used for cloning are shown in Table S1. An empty vector without fragment insert was also used to produce a control lentivirus. To generate sOPN and iOPN expressing lentivirus, the lentiviral vector Lenti-iOPN (LV-iOPN), Lenti-sOPN (LV-sOPN), or LV-negative control (LV-NC) co-transfected with psPAX2 and pMD2.G plasmids (Addgene, USA) into 293T packaging cells. 12 hours after transfection, cells were supplied with fresh medium and cultured for an additional 36 hours. The lentivirus-containing supernatant was filtered and used for cell infection. Then HaCaT cells were infected by the lentivirus mentioned above. After antibiotic selection for a week, the stable HaCaT cells expressing sOPN (LV-sOPN HaCaTs), iOPN (LV-iOPN HaCaTs), and LV-NC HaCaTs as negative control were obtained.

## 2.8 Co-culture assay

Firstly, the HaCaT cells and the THP-1 cells were cultured separately. THP-1 cells cultured in RPMI 1640 growth medium

were seeded into transwell inserts (Corning, USA) with a 0.4μm pore size polycarbonate permeable membrane and differentiated with 50 ng/ml PMA for 48 hours. The LV-sOPN HaCaTs, LV-iOPN HaCaTs, and si-OPN-treated HaCaTs cultured in DMEM growth medium were seeded in 6-well plates and stimulated by LL37 (100μg/ml) for 24 hours in serum-free media. After washed with PBS, THP-1-derived macrophages were co-cultured with HaCaT cells for another 48 hours. Then macrophage mRNA was collected.

## 2.9 RNA extraction and real-time quantitative PCR

The total RNA was extracted with TRIzol reagent (Sigma-Aldrich, USA) according to the manufacturer's instructions. RNA concentration was detected using Nanodrop-2000 (Thermo Scientific, USA). Reverse transcription was carried out with the High Capacity cDNA Reverse Transcription Kit (BioRad, USA). Then mRNA expression was determined with real-time quantitative PCR (qRT-PCR). The qRT-PCR reaction mix contained 5 μl SYBR Green qPCR Master Mix, 3 μl diluted primer mix, and 2 μl diluted cDNA. Bio-Rad CFX96 real-time fast PCR system was used to perform qRT-PCR amplification. β-Actin was an internal control, and the relative expression of mRNA was calculated according to the $2^{-\triangle\triangle Ct}$ method. All the sequences of primers used for qRT-PCR in this study are listed in Table S1.

## 2.10 Western blot analysis

Briefly, cells were harvested on ice with ice-cold RIPA lysis buffer containing protease inhibitor cocktails. Proteins were separated by 10% SDS-PAGE gel and transferred into PVDF membranes for western blot assay. The membranes were blocked with 5% BSA and then incubated with appropriate primary and horseradish peroxidase (HRP)-conjugated secondary antibodies. Finally, the immunosignals were detected using the SuperSignal West Femto Chemiluminescent Substrate Kit (Thermo Scientific, USA). Antibodies from Cell Signaling Technology (USA) are as follows: β-Actin (8H10D10) Mouse mAb (#3700), p44/42 MAPK (Erk1/2) (137F5) Rabbit mAb (#4695), Phospho-p44/42 MAPK (Erk1/2) (Thr202/Tyr204) Antibody (#9101), Phospho-SAPK/JNK (Thr183/Tyr185) (98F2) Rabbit mAb (#4671), SAPK/JNK Antibody (#9252), HRP-linked Antibody (#7074).

## 2.11 Flow cytometry

The skin samples of the LL37-induced rosacea mice model were cut into small pieces and processed in digestion buffer (1 mg/ml collagenase) for 2 hours at 37°C. Cells from the skin samples were passed through 40 μm nylon mesh to obtain a single-cell suspension, then the single cells were resuspended in 30% Percoll solutions and centrifuged. Subsequently, the single-cell suspension was stained with Zombie Aqua (Biolegend, USA) for 20 minutes, blocked with Fc block for 10 minutes (anti-mouse CD16/32 mAbs; Biolegend, USA), and finally stained with the fluorochrome-conjugated antibodies for 20 minutes. Cells were then washed and measured on CytoFLEX (Beckman Coulter, USA) flow cytometer and analyzed by CytExpert (Beckman Coulter, USA) software. M1 macrophages were defined as $CD45^+CD11b^+F4/80^+CD86^+$cells. M2 macrophages were defined as $CD45^+CD11b^+F4/80^+CD206^+$ cells.

The following antibodies from BioLegend (CA, USA) were used: FITC anti-mouse/human CD11b (M1/70), APC/Cyanine7 anti-mouse CD45 (S18009F), APC anti-mouse F4/80 (BM8), PE/Cyanine7 anti-mouse CD206 (C068C2), Brilliant Violet 421 anti-mouse CD86 (GL-1).

## 2.12 Histology and immunohistochemistry

Skin tissues were fixed in 4% paraformaldehyde, embedded in paraffin, and sectioned. Sections were stained with hematoxylin and eosin (H&E). For immunohistochemistry, skin tissues were dewaxed with xylene and hydrated with ethanol, then subjected to antigen retrieval and blocked endogenous peroxidase activity with 3% hydrogen peroxide. After incubation with blocking buffer for 1 hour at room temperature, tissue sections were incubated with primary antibody and peroxidase-conjugated secondary antibody (Beyotime Biotechnology, China). The staining results were visualized using SignalStain® DAB Substrate Kit (Cell Signaling Technology Inc., USA) and finally counterstained with Mayer's hematoxylin.

The following primary antibodies were used: Anti-Osteopontin antibody (ab8448) was from Abcam (USA). F4/80 (D2S9R) Rabbit mAb, CD4 (D2E6M) Rabbit mAb, and CD31 (D8V9E) Rabbit mAb were from Cell Signaling Technology (USA).

## 2.13 Immunofluorescence analysis

For confocal studies, HaCaT cells were grown in a glass chamber and fixed with 10% buffered formalin for 30 minutes, and then incubated with blocking buffer at 4°C overnight. The next day, HaCaT cells were incubated with Anti-Osteopontin antibody (1:500, ab8448, Abcam, USA), GM130 Antibody (1:50, Santa Cruz, USA) for two hours, and incubated with appropriate fluorescence-conjugated secondary antibodies for 1 hour at room temperature. DAPI (Sangon Biotech, China) was used to manifest nuclei. Images were captured using confocal microscopy. Secondary antibodies (Thermo Fisher Scientific, USA) used in immunofluorescence were Alexa Fluor 488 donkey anti-rabbit IgG and Alexa Fluor 555 donkey anti-mouse IgG.

## 2.14 Enzyme-linked immunosorbent assay

The concentrations of OPN in the supernatant of HaCaTs were quantified using the Human Osteopontin/OPN ELISA Kit (KE00233) (Proteintech, USA) according to the protocol provided by the manufacturers.

### 2.15 Statistical analysis

Statistical analysis was performed using GraphPad Prism software (GraphPad Software, USA), and data were presented as the mean ± SEM. All experiments were repeated at least three times unless otherwise mentioned. Data were analyzed for significance using T-test, one-way ANOVA and two-way ANOVA, and the value of $P<0.05$ was considered to be statistically significant.

## 3 Results

### 3.1 OPN expression is increased in rosacea patients and LL37-induced rosacea inflammation in mice

To determine the expression pattern of OPN in rosacea, rosacea transcriptome data (GSE65914) was obtained from the GEO database. Firstly, we analyzed the mRNA expression of OPN in rosacea transcriptome data. Results showed that OPN was significantly upregulated in all three types of rosacea (Figure 1A). Meanwhile, LL37 was administrated to mice by intradermal injection to induce rosacea-like inflammation (25). Consistently, it was shown that the OPN level was significantly increased in mice injected with LL37 compared with the control group (Figure 1B). In addition, IHC results confirmed that OPN protein levels were significantly increased in skin biopsies of rosacea patients (Figure 1C) and LL37-induced rosacea-like skin inflammation (Figure 1D). Together, these results suggested that OPN has a potential role in rosacea pathogenesis.

### 3.2 OPN promotes LL-37-induced macrophage infiltration and angiogenesis in mice

To explore the role of OPN in rosacea, OPN KO mice and WT mice were used to establish LL37-induced rosacea-like skin inflammation models (Figure 2A). Rosacea-like features, including the redness area (Figure 2B) and redness score (Figure 2C), were obviously reduced in OPN KO mice. In addition, histological analysis revealed that the number of inflammatory cell infiltration in the dermis was significantly reduced in OPN KO mice (Figures 2D, E). Macrophage infiltration and Th1/Th17 polarized inflammation are considerable symbols in all rosacea subtypes, so we wondered whether OPN regulates cutaneous immune dysfunction in rosacea. As depicted in Figure 2F, an obvious accumulation of $F4/80^+$ macrophages was observed in LL37-induced rosacea-like skin inflammation, whereas much fewer macrophages were found in OPN KO mice treated with LL37 (Figure 2G). Next, we evaluated $CD4^+$ T cells in mice skin lesions to determine whether OPN participated in the adaptive immune response. An increasing number of $CD4^+$ T cells were observed in LL37-induced skin inflammation. However, there was no significant difference between the OPN KO mice and the WT mice with LL37 treatment (Figure 2H). Thus, our data above demonstrated that OPN promotes rosacea-like inflammation through increased infiltration of macrophages and angiogenesis in rosacea.

Angiogenesis and vasodilation were other distinguishing traits of rosacea (26). Therefore, the effect of OPN on angiogenesis in rosacea was assessed by CD31 immunostaining (Figure 2F). As illustrated in Figure 2I, dermal vessel density was significantly increased in the WT mice, whereas relatively reduced angiogenesis was found in the OPN KO mice. It demonstrated that OPN contributes to rosacea-like inflammation through angiogenesis in rosacea.

### 3.3 OPN promotes the progression of rosacea by regulating the expression of pro-inflammatory factors in the rosacea-like animal model

To reveal the potential mechanism that OPN promotes rosacea-like inflammation, RNA-seq was performed to identify genes regulated by OPN in rosacea-like skin inflammation. The WT-PBS group and WT-L37 group have 1580 DEGs, including 954 upregulated genes and 626 downregulated genes ($|\log2FC| \geq 1$, p value < 0.05) (Figure 3A). The OPN KO-PBS group and OPN KO-LL37 group have 1772 DEGs, including 1181 upregulated genes and 591 downregulated genes ($|\log2FC| \geq 1$, p value < 0.05) (Figure 3B). The KEGG enrichment analyses have showed the deregulated pathways including IL-17, NF-κB, and MAPK pathways (Figures 3C, D), which are known to drive skin inflammation. DEGs from WT group treated or not with LL37 were enriched in MAPK signaling pathway, while DEGs from OPN KO group were not enriched in this signaling pathway. Therefore, more concerned about MAPK signaling pathway had been paid in the following experiments.

IL1B, IL6, NLRP3, and TNFa were important characteristic factors and critical mediators in the inflammation of rosacea (8, 27, 28). Rosacea transcriptome data (GSE65914) was analyzed to further understand the relationship between the expression of OPN and pro-inflammatory factors in healthy controls and rosacea patients. All the samples were included to analyze the correlation between the level of OPN and pro-inflammatory factors. Interestingly, the rosacea patients who expressed higher OPN also expressed higher IL6, IL1B, NLRP3, and TNFa (Figure 3E), suggesting that there was a correlation between the expression of OPN and pro-inflammatory factors in rosacea. The pro-inflammatory cytokines including IL1B, NLRP3, and TNFa were also significantly upregulated in rosacea-like skin lesions of WT mice and remarkably downregulated in those of OPN KO mice (Figure 3F). Collectively, these results indicated that epidermal OPN contributes to the pathogenesis of rosacea skin disorders by regulating the expression of pro-inflammatory factors.

### 3.4 iOPN promotes the progression of rosacea by regulating IL1B expression via ERK1/2 and JNK signaling pathways in keratinocytes

Keratinocytes are the most prominent cells within the epidermis. To further understand how OPN functions in keratinocytes, a specific siRNA targeting OPN gene was

10.3389/fimmu.2023.1285951

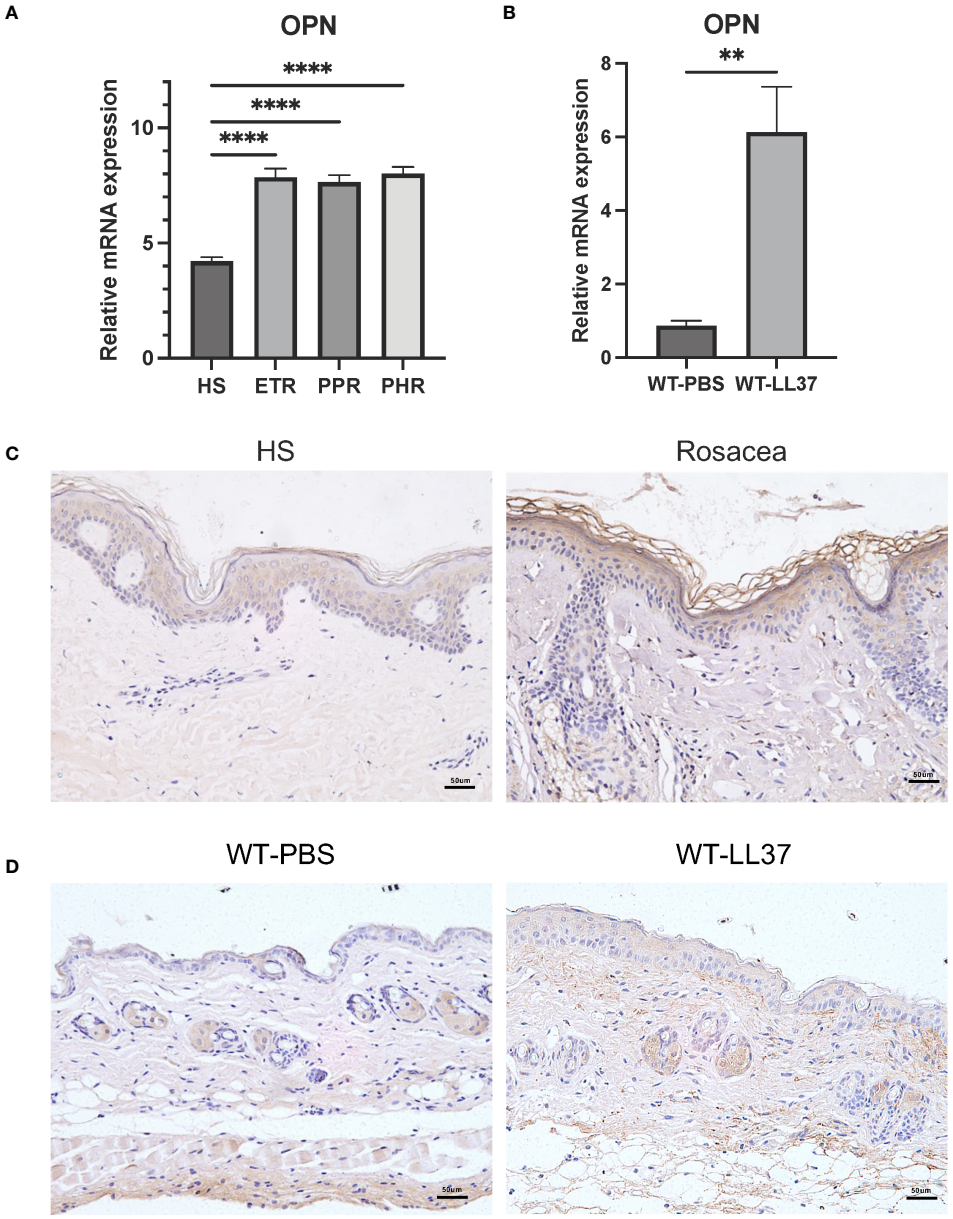


FIGURE 1
OPN expression in rosacea patients and LL37-induced rosacea-like skin inflammation. **(A)** Relative mRNA expression of OPN was from the GSE65914 dataset, which contains healthy controls (n = 20) and three clinical types of rosacea, including Erythematotelangiectatic (ETR) type (n = 14), papulopustular (PPR) type (n =12), and phytates (PHR) type (n= 12). Data represent the mean ± SEM. One-way ANOVA with Tukey's *post hoc* test was used for statistical analyses. ****p < 0.0001. **(B)** Relative mRNA expression of OPN in rosacea-like skin lesions of WT mice injected with PBS or LL37 (n = 4 for each group). Data represent the mean ± SEM. T-test was used for statistical analyses. **p < 0.01. **(C)** Representative images of immunohistochemistry of OPN on skin lesions from healthy individuals (HS) and rosacea patients. Scale bar: 50μm. **(D)** Representative images of immunohistochemistry of OPN in skin lesions of WT mice injected with PBS or LL37. Scale bar: 50μm.

transfected into keratinocytes. The knockdown efficiency of si-OPN was up to 90% in the HaCaT cells (P < 0.0001) (Figure 4A). Consistent with the result *in vivo*, OPN deletion markedly inhibited the expression of LL37-induced pro-inflammatory cytokine IL1B in both HaCaTs (Figure 4B) and primary mouse keratinocytes (Figure 4C). As shown in Figures 4D, E, LL37 treatment significantly increased the phosphorylated ERK1/2 and JNK in both HaCaTs and primary mouse keratinocytes, whereas OPN knockdown significantly decreased p-ERK/ERK and p-JNK/JNK ratios (Figures S2A, B).

To analyze the expression pattern of OPN in keratinocytes, dual immunofluorescence staining of OPN and Golgi matrix protein 130 (GM130) was performed. It was shown that HaCaT contains both secretory and intracellular forms of OPN (Figure 4F). Next, we sought to determine whether sOPN or iOPN regulates inflammatory signaling pathways. The

10.3389/fimmu.2023.1285951

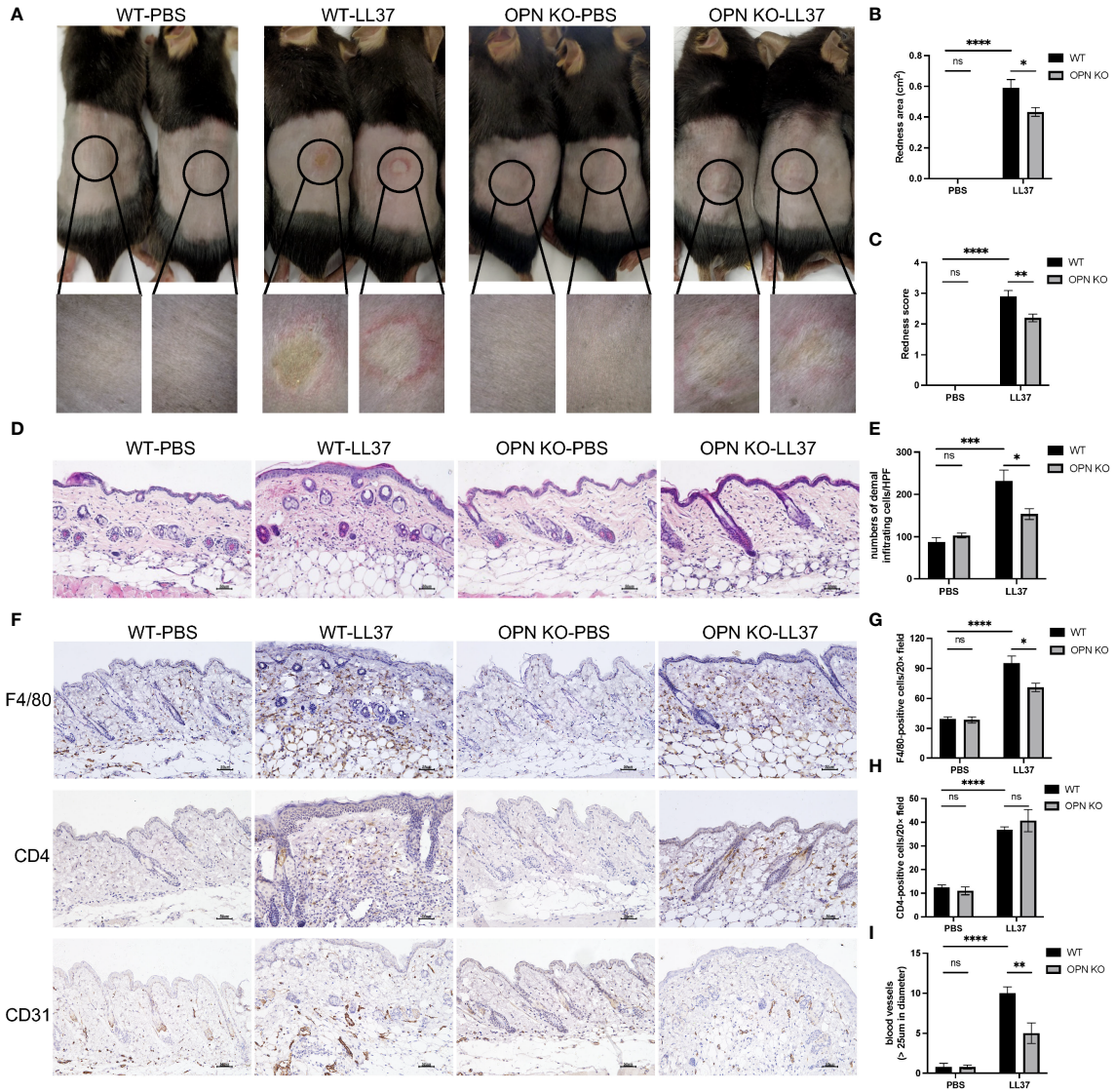


FIGURE 2
OPN knockdown attenuated rosacea-like skin redness and inflammatory cell infiltration in mice. **(A)** LL37 was injected intradermally into the dorsal skin of WT mice and OPN KO mice to induce a rosacea-like phenotype. The skin lesions were collected two days after injection with PBS or LL37. The lower panel is a magnified image of the circular area in the upper panel. The severity of the rosacea-like phenotypes was assessed according to the redness area **(B)** and redness score **(C)**. Data represent the mean ± SEM. *p < 0.05, **p < 0.01, ****p < 0.0001. Ns, no significance. **(D)** HE staining for the histological analysis of WT mice and OPN KO mice injected with PBS or LL37. Scale bar: 50mm. **(E)** The number of dermal inflammatory infiltration in each group was quantified (n = 4 for each group). Data represent the mean ± SEM. Two-way ANOVA with Tukey's *post hoc* test was used for statistical analyses. *p < 0.05, ***p < 0.001. Ns, no significance. **(F)** Representative images of immunohistochemistry of F4/80, CD4, and CD31 in WT mice and OPN KO mice injected with PBS or LL37. Scale bar: 50mm. **(G)** The infiltration of F4/80-positive cells was quantified in each group (n = 4 for each group). Data represent the mean ± SEM. Two-way ANOVA with Tukey's *post hoc* test was used for statistical analyses. *p < 0.05, ****p < 0.0001. Ns, no significance. **(H)** The infiltration of CD4-positive cells was quantified in each group (n = 4 for each group). Data represent the mean ± SEM. Two-way ANOVA with Tukey's *post hoc* test was used for statistical analyses. ****p < 0.0001. Ns, no significance. **(I)** The number of CD31-positive blood vessels (>25um in diameter) was quantified in each group (n = 4 for each group). Data represent the mean ± SEM. Two-way ANOVA with Tukey's *post hoc* test was used for statistical analyses. **p < 0.01, ****p < 0.0001. Ns, no significance.

lentivirus-mediated overexpression of sOPN and iOPN was constructed in HaCaT cells, and the expression level of OPN mRNA was detected in these infected cells (Figure 4G). The intracellular and extracellular OPN overexpression levels were detected by western blot and ELISA respectively. Results showed that the intracellular protein level was remarkably increased in LV-iOPN HaCaTs (Figure 4H), and OPN concentration in the supernatant was significantly increased in the LV-sOPN HaCaTs (Figure 4I). It was confirmed that overexpression of iOPN significantly increased the expression of pro-inflammatory IL1B

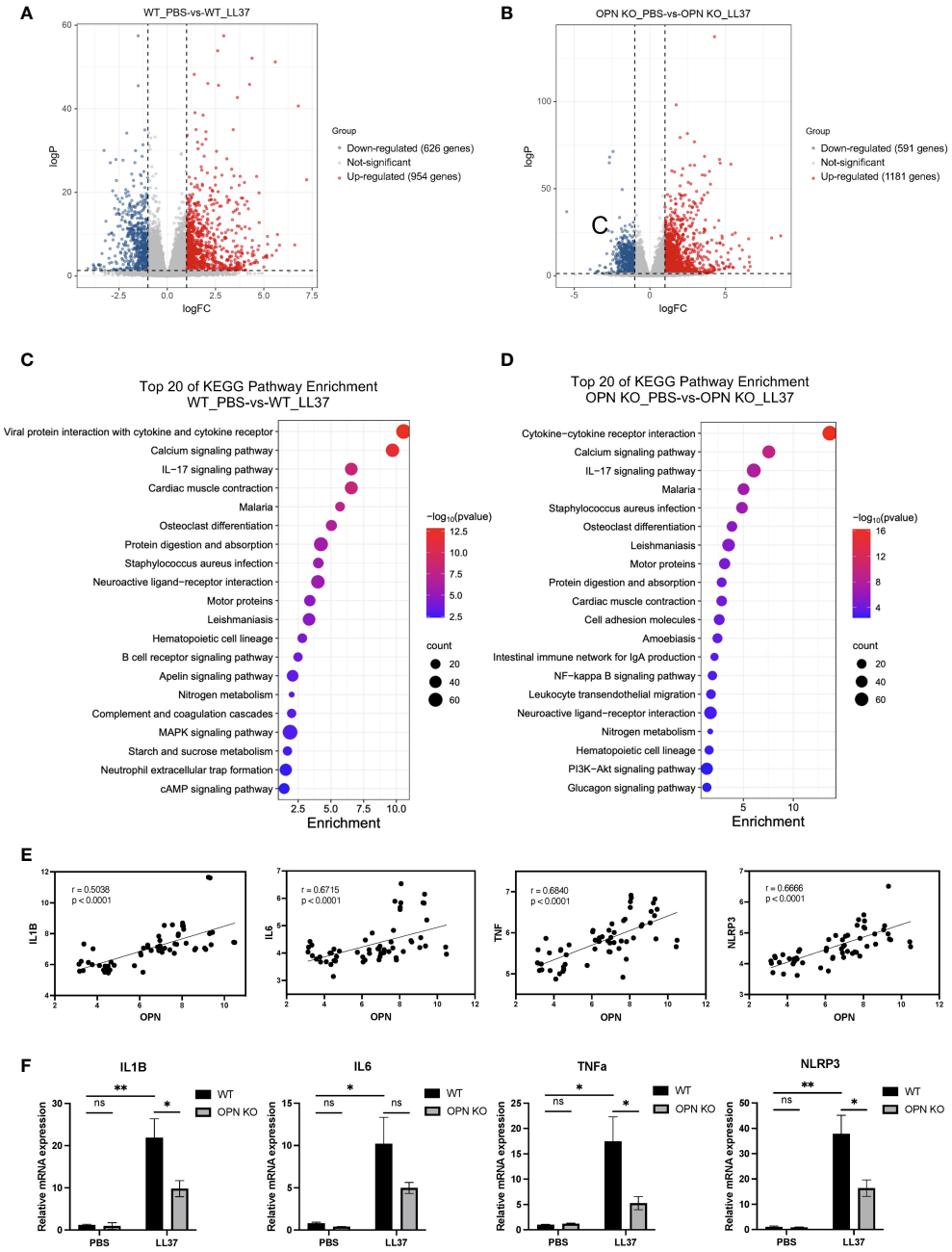


FIGURE 3
OPN promotes the expression of IL1B in the rosacea-like mice. **(A)** Volcano plots showed the differentially expressed genes between the WT_PBS and WT_LL37 groups. The red, gray, and blue dots represented up-regulated, insignificant, and down-regulated genes, respectively. **(B)** Volcano plots showed the differentially expressed genes between the OPN KO_PBS and OPN KO_LL37 groups. The red, gray, and blue dots represented up-regulated, insignificant, and down-regulated genes, respectively. **(C)** KEGG pathway analysis of DEGs between WT_PBS and WT_LL37 group for functional enrichment analysis. **(D)** KEGG pathway analysis of DEGs between OPN KO_PBS and OPN KO_LL37 groups for functional enrichment analysis. **(E)** Pearson's correlation analysis was performed to analyze the correlation between the expression level of OPN and IL1B, IL6, TNFA, NLRP3 in GSE65914 rosacea dataset, which includes all the healthy controls (n=20) and rosacea patients (n=38). **(F)** The mRNA expression levels of IL1B, IL6, TNFa, and NLRP3 in skin lesions from WT and OPN KO mice injected with LL37 or PBS (n ≥ 4 for each group). Data represent the mean ± SEM . Two-way ANOVA with Tukey's *post hoc* test was used for statistical analyses. *p < 0.05, **p < 0.01. Ns, no significance.

in HaCaT cells. Meanwhile, both the ERK1/2 inhibitor (SCH772984) and JNK inhibitor II effectively inhibited the expression of *IL1B* in LV-iOPN HaCaTs (Figure 4J).

Because LV-sOPN HaCaTs show slight expression of intracellular OPN (Figure 4H), it was not appropriate for further identification of the role of sOPN in the IL1B expression. Instead, rhOPN was added to si-OPN-treated HaCaTs, of which the intracellular OPN was almost eliminated. It was found that extracellular OPN could not increase the expression of IL1B (Figure 4K). Together, these findings demonstrated that iOPN

10.3389/fimmu.2023.1285951

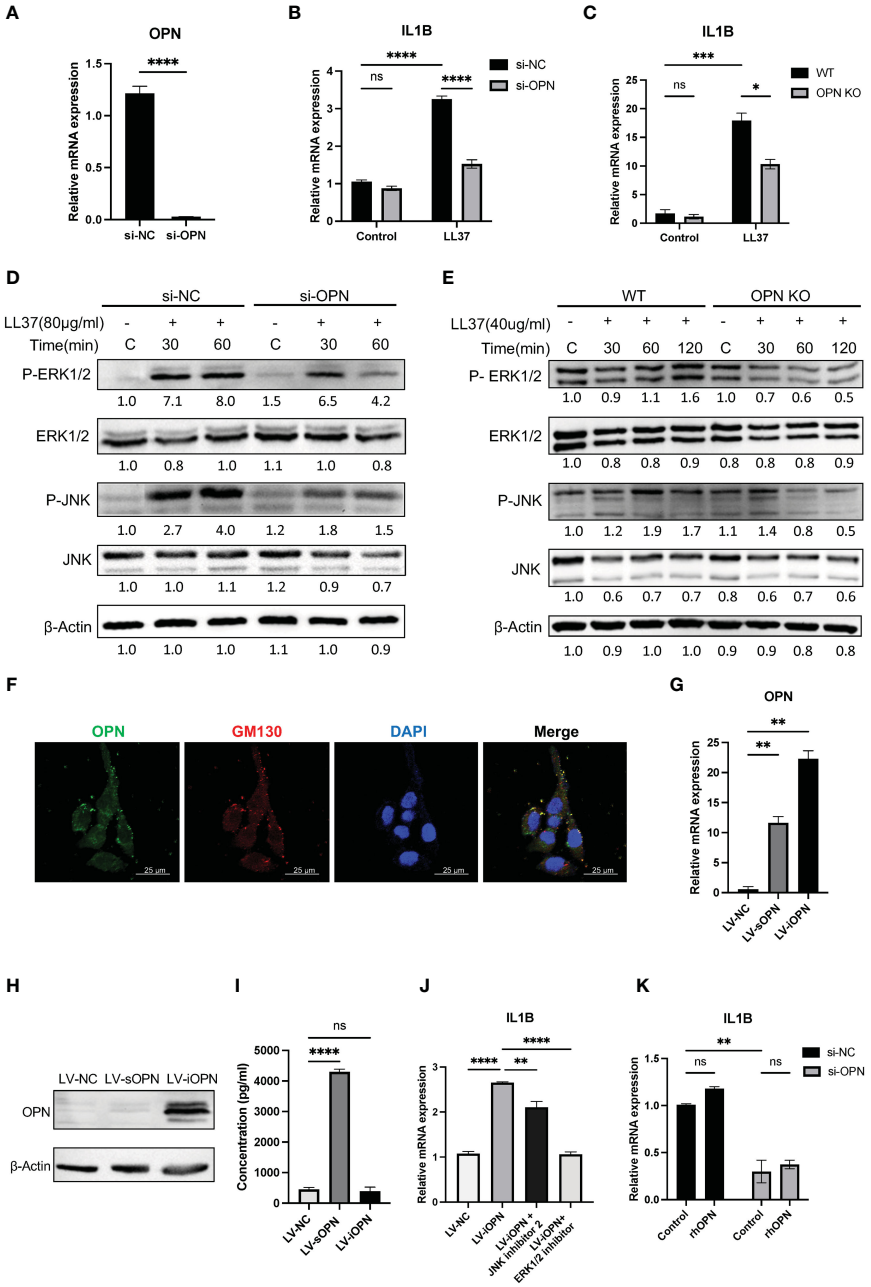


FIGURE 4
OPN knockdown downregulated the expression of IL1B via ERK1/2 and JNK pathways in keratinocytes. **(A)** The knockdown efficiency of OPN in HaCaT cells was detected by qRT-PCR. Data represent the mean ± SEM. T-test was used for statistical analyses. ****p < 0.0001. **(B)** The mRNA expression level of IL1B in LL37-induced HaCaT cells after si-OPN treatment. Data represent the mean ± SEM. Two-way ANOVA with Tukey's *post hoc* test was used for statistical analyses. ****p < 0.0001. Ns, no significance. **(C)** The mRNA expression level of IL1B in LL37-induced WT and OPN KO mice primary keratinocytes. Data represent the mean ± SEM. Two-way ANOVA with Tukey's *post hoc* test was used for statistical analyses. *p < 0.05, ***p < 0.001. Ns, no significance. **(D)** Cultured HaCaT cells treated with si-OPN were stimulated with LL37 (80ug/ml) for various time points. Total cellular proteins were extracted to determine the phosphorylated and total ERK1/2 and JNK by western blot. β-Actin was selected as an internal control. **(E)** WT and OPN KO mice primary keratinocytes were stimulated with LL37 (40 ug/ml) for various time points. Total cellular proteins were extracted to determine the phosphorylated and total ERK1/2 and JNK by western blot. β-Actin was selected as an internal control. **(F)** Co-localization of OPN and GM130 in HaCaT cells was observed by confocal microscopy. Green indicates OPN. Red indicates GM130. Blue indicates DAPI. Scale bar, 25 μm. **(G)** The overexpression efficiency of sOPN and iOPN in HaCaT cells was detected by qRT-PCR. Data represent the mean ± SEM. One-way ANOVA with Dunnett's *post hoc* test was used for statistical analyses. **p < 0.0001. **(H)** The overexpression levels of OPN in HaCaT cells were detected by Western blotting. β-Actin was selected as an internal control. **(I)** The overexpression levels of sOPN in the supernatant of HaCaT cells were detected by ELISA. Data represent the mean ± SEM. One-way ANOVA with Tukey's *post hoc* test was used for statistical analyses. ****p < 0.0001. Ns, no significance. **(J)** LV-iOPN HaCaTs were treated with ERK1/2 inhibitor (SCH772984) (200nM) and JNK inhibitor II (100nM) for 20 hours, and the mRNA expression level of IL1B was detected by qRT-PCR. Data represent the mean ± SEM. One-way ANOVA with Tukey's *post hoc* test was used for statistical analyses. **p <0.01, ****p < 0.0001. **(K)** HaCaT cells with si-OPN treatment were stimulated with rhOPN (2500ng/ml) in serum-free medium, and the mRNA expression level of IL1B was detected by qRT-PCR. Data represent the mean ± SEM. Two-way ANOVA with Tukey's *post hoc* test was used for statistical analyses. **p <0.01. Ns, no significance.

10.3389/fimmu.2023.1285951

promotes the progression of rosacea by regulating IL1B expression via ERK1/2 and JNK signaling pathways in keratinocytes.

## 3.5 OPN knockdown inhibits the polarization of M1 macrophages in rosacea lesions

The polarization of M1 macrophages promoted rosacea inflammation. M1 macrophage infiltration was significantly increased in rosacea and positively correlated with CEA and IGA scores (15, 29). Our results revealed that OPN promoted the infiltration of F4/80+ macrophages in LL37-induced rosacea-like skin inflammation. To further investigate the role of OPN in immune cell infiltration, CIBERSORT was used to assess immune cell infiltration in lesional tissues from rosacea-like mice based on our transcriptome data (Figure 5A). Compared with the WT_LL37 group, the percentage of M1 macrophage infiltration in OPN KO_LL37 group was significantly reduced (Figure 5B). Next, flow cytometry were performed to quantitatively analyze the percentage of M1 and M2 macrophages in LL37-induced rosacea-like lesions from WT and OPN KO mice, with gating strategy provided in Figure S3A. Phenotypically, M1 macrophage expressed higher levels of CD86, whereas CD206 was commonly associated with M2 macrophage (30). Flow cytometry analysis showed that compared with the PBS group, the percentage of CD86-positive M1

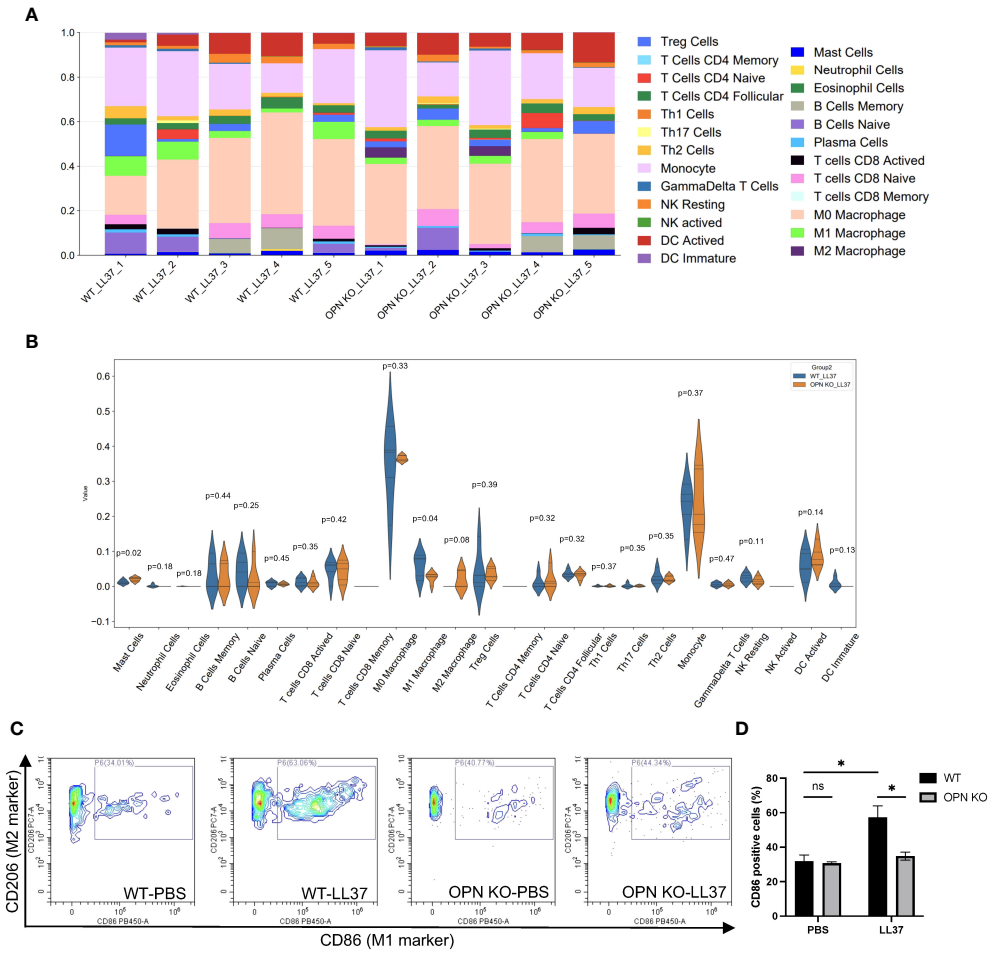


FIGURE 5
OPN knockdown inhibited M1 macrophage polarization in LL37-induced rosacea mice. **(A)** Analysis of immune cells infiltration using CIBERSORT in skin lesions from WT mice and OPN KO mice injected with LL37 (n = 5 for each group). **(B)** Statistical analysis of immune cells infiltration in WT-LL37 group (blue bar) and OPN KO-LL37 group (yellow bar) was shown in the violin plot. T-test was used for statistical analyses. **(C)** Flow cytometry was performed to quantitatively analyze the percentage of CD86-positive cells in skin lesions of the WT-PBS group (n = 3), OPN KO-PBS (n = 3), WT-LL37 group (n = 6), and OPN KO-LL37 group (n = 6). CD86 was identified as an M1 macrophage marker and CD206 was identified as an M2 macrophage marker. **(D)** CD86-positive cells in each group were quantified. Data represent the mean ± SEM. Two-way ANOVA followed by Sidak's multiple comparison test was used for statistical analyses. *p < 0.05. Ns, no significance.

macrophages increased from 32% to 57% of total macrophages in rosacea-like lesions of WT mice, whereas the percentage of the CD86+ macrophages increased from 31% to 35% in OPN KO mice (Figures 5C, D). However, there was no significant difference in the percentage of CD206-positive cells (Figures S3B, C). Together, these results indicated that OPN promotes the M1 polarization of macrophages in the rosacea-like mice model.

### 3.6 Keratinocytes-derived sOPN promotes M1 macrophage polarization

Keratinocyte-immune cell crosstalk has been considered to contribute to skin homeostasis (31). To explore whether the activated keratinocytes affect the differentiation of the macrophages in rosacea, THP-1-derived macrophages (M0) were co-cultured with LL37-induced HaCaTs for 48 hours. Co-cultured with si-OPN-treated HaCaTs significantly inhibited the mRNA expression levels of the M1 macrophage markers (Figure 6A). Since OPN deficiency eliminates both intracellular and secreted forms of OPN, the regulation role of OPN in macrophage polarization still needs to be investigated in depth. It was wondered whether the extracellular OPN affects the polarization of the macrophages. The results showed that co-cultured with LV-sOPN HaCaTs, not LV-iOPN HaCaTs, significantly increased the mRNA expression levels of the M1 macrophage markers, including IL6, CCL2, and TNFa (Figure 6B). Moreover, as extracellular OPN *in vitro*, rhOPN was added to macrophages (M0). It was found that rhOPN potentiated the expression of M1 macrophage signature genes (Figure 6C). These findings indicated that sOPN plays a vital role in keratinocyte-macrophage crosstalk. Communication between keratinocytes and immune cells may provide new insight into the pathogenesis of rosacea.

## 4 Discussion

Rosacea is a chronic inflammatory facial disease occurring worldwide. It was well recognized that dysregulation of the innate and adaptive immune response as well as neurovascular dysregulation contribute to rosacea pathophysiology significantly (32). The expression of cytokines including IL-1β, IL-6, and IL-17, was associated with PPR type (5, 8, 33). Multiple studies suggested that IL-1β may be a major driver of rosacea for its increased expression (8). In this study, OPN was an inducer for the production of pro-inflammatory cytokine IL-1β in rosacea pathogenesis. Besides, it was reported that IL-1β also interacts with pro-angiogenic factor VEGF in angiogenic responses. Overall, increased expression of IL-1β may contribute to the aggravation of rosacea inflammation and blood vessel formation.

OPN plays a vital role in increasing inflammatory cell infiltration and promoting inflammation in acute and chronic inflammatory diseases (34). Although OPN was generally classified as a pro-inflammatory cytokine, it may also had anti-inflammatory effects. OPN inhibited the expression of iNOS by promoting the degradation of Stat1 in macrophages (35, 36). Most studies regarded OPN as a secreted protein, that binds to integrins or CD44 (37) receptors and activates multiple signaling pathways, including NFκB and MAPK signaling pathways (38, 39). However, an alternative translation of different start codons from a single OPN mRNA can generate another OPN isoform called iOPN (40). These OPN isoforms may exist in different cells and mediate different biological functions. Natural killer (NK) cells expressed higher levels of iOPN, and iOPN deficiency promoted NK cell death and impaired NK cell differentiation (41). In anti-fungal responses, iOPN was involved in the TLR2 pathway and enhanced MAPK activation (42). Our study reveals that keratinocyte contains both sOPN and iOPN. Instead of sOPN, iOPN upregulates the expression of cytokine IL-1β via ERK1/2 and JNK signaling pathways in LL37-induced inflammation. iOPN plays a pro-inflammatory role and contributes to rosacea pathogenesis.

Activation and infiltration of macrophages have been reported in the skin lesions of rosacea patients (5). It was found that M1 macrophage polarization promoted rosacea inflammation (15, 29). M1 macrophage polarization in rosacea may be the result of multiple factors. Previous studies showed that GBP5 and ADAMDEC1 played a pro-inflammatory role in rosacea-like skin inflammation by regulating the M1 macrophage polarization (15, 29). However, OPN plays an increasingly important role in macrophage polarization, and whether or not OPN regulates macrophage polarization remains controversial (43). Recently, it was reported that macrophage polarity defined by CXCL9 and OPN expression, rather than traditional M1 and M2 markers, was strongly associated with tumor prognosis (44). In nonalcoholic fatty liver disease, OPN promoted macrophage M1 polarization by activation of the JAK1/STAT1/HMGB1 signaling pathway (45). Another study indicated that OPN served a protective role and downregulated M1 macrophage markers in hypertension and vascular calcification (46). In the present study, we demonstrated that OPN promoted macrophage infiltration and M1 macrophage polarization in rosacea lesions, which may be one of the important factors contributing to the exacerbation of rosacea inflammation.

Since OPN deficiency in keratinocytes eliminates both intracellular and secreted forms of OPN, the regulation role of sOPN and iOPN in macrophage polarization still needs to be investigated in depth. Previous studies have highlighted that dynamic epithelial-immune crosstalk fine-tunes epithelial homeostasis (47). In rosacea skins, infiltrated immune cells produce inflammatory mediators that lead to the activation of keratinocytes (48). The activated keratinocytes may further affect the polarization of the macrophages. In this study, the co-culture assay was performed to investigate whether sOPN or iOPN affected keratinocyte-macrophage crosstalk in rosacea inflammation. It was identified that instead of iOPN, keratinocyte-derived sOPN played a crucial role in promoting M1 macrophage polarization *in vitro*. It was shown that iOPN promoted IL1B expression in keratinocytes. IL1B was one

10.3389/fimmu.2023.1285951

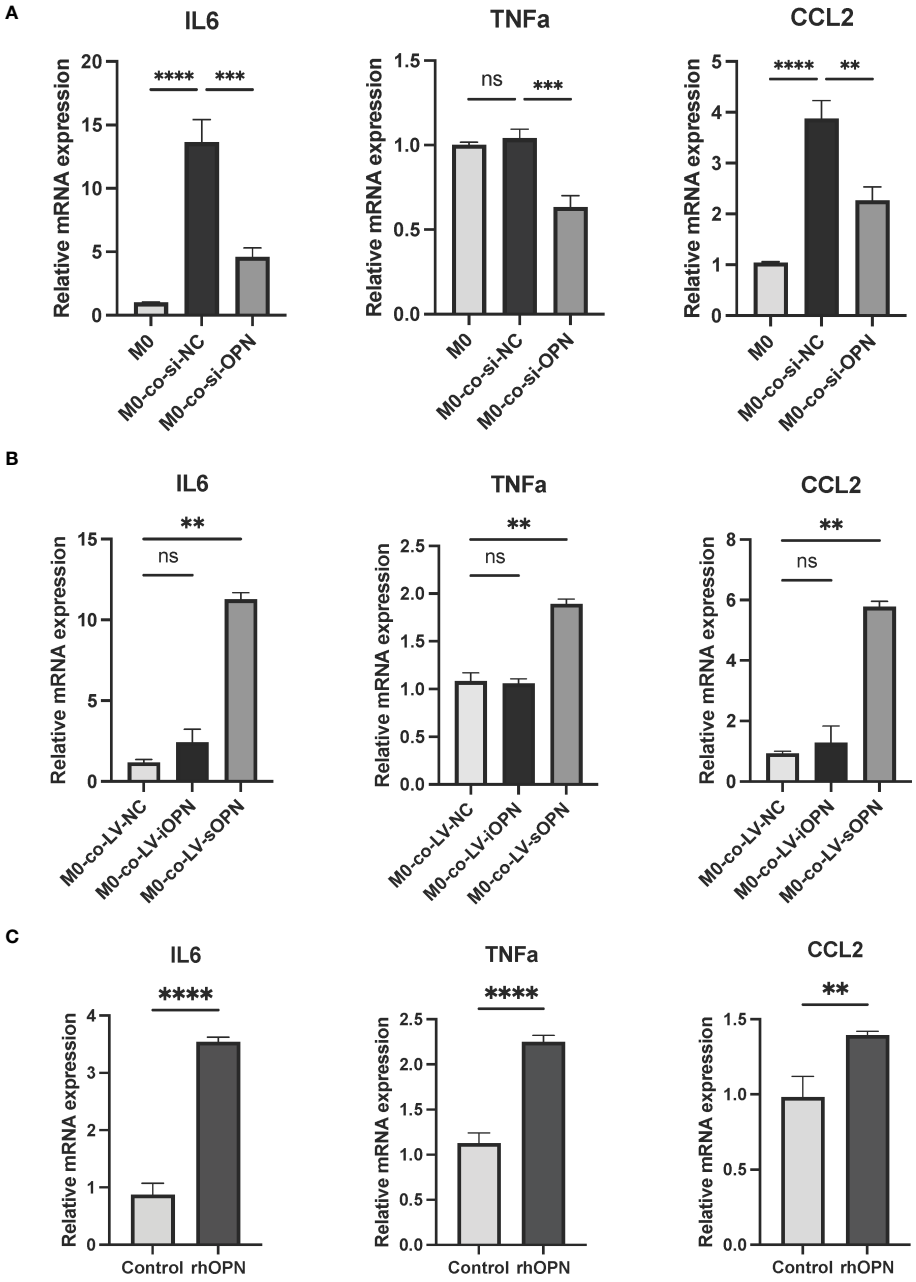


FIGURE 6
OPN secreted by LL37-induced keratinocytes promoted M1 macrophage polarization. **(A)** THP-1-derived macrophages (M0) were co-cultured with LL37-induced and si-OPN-treated HaCaTs for 48 hours, and the mRNA expression levels of IL6, TNFa, and CCL2 were determined by qRT-PCR. Data represent the mean ± SEM. One-way ANOVA with Tukey's *post hoc* test was used for statistical analyses. **p < 0.01, ***p < 0.001, ****p < 0.0001. Ns, no significance. **(B)** THP-1-derived macrophages (M0) were co-cultured with LL37-induced LV-NC HaCaTs, LV-sOPN HaCaTs, and LV-iOPN HaCaTs for 48 hours, and the mRNA expression levels of IL6, TNFa, and CCL2 were determined by qRT-PCR. Data represent the mean ± SEM. One-way ANOVA with Tukey's *post hoc* test was used for statistical analyses. **p < 0.01. Ns, no significance. **(C)** THP-1-derived macrophages(M0) were stimulated with rhOPN for 48 hours, and the mRNA expression levels of IL6, TNFa, and CCL2 were determined by qRT-PCR. Data represent the mean ± SEM. T-test was used for statistical analyses. **p < 0.01, ****p < 0.0001.

of the M1 macrophage marker. However, the role of extracellular IL1B in macrophage polarization remained unclear. RhOPN was added to si-OPN-treated HaCaTs to study the role of sOPN in keratinocytes. The results showed that sOPN could not promote IL1B expression in keratinocytes. Similarly, the level of IL1B expression was not changed in macrophages treated with rhOPN. Moreover, some inflammatory mediators regulated by iOPN may also indirectly affect macrophage polarization and need to be further clarified. Some studies have revealed IL-1, IL-10, IL-12, IL-17, and IFN-γ (37, 49), of which secretion was regulated by OPN in different cells and tissues. Disruption of the crosstalk between keratinocytes and immune cells is expected to be a promising therapeutic target for rosacea treatment. In addition, sOPN or iOPN-specific knock-in mice will be helpful to better understand the different roles of iOPN and sOPN *in vivo*.

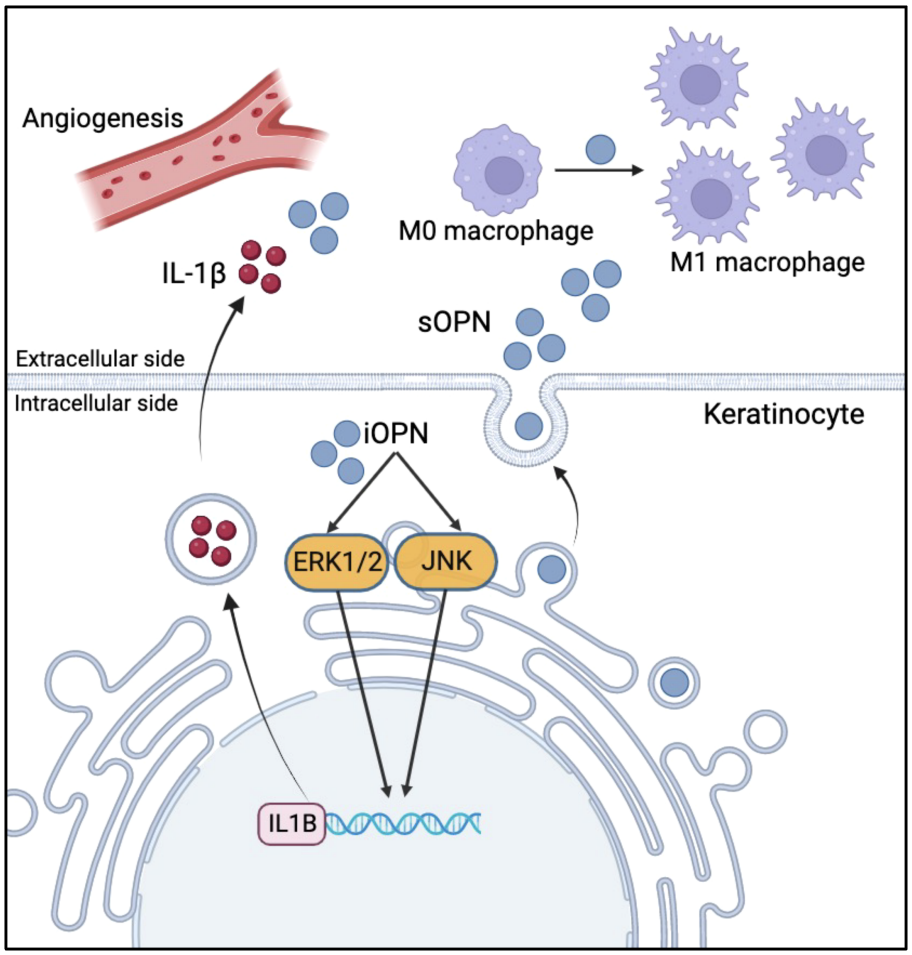


FIGURE 7
Schematic diagram of sOPN and iOPN in the pathogenesis of rosacea. sOPN and iOPN play different roles in the pathogenesis of rosacea. iOPN plays a crucial role in the upregulation of pro-inflammatory cytokine IL1B expression via ERK1/2 and JNK signaling pathways. sOPN participates in keratinocyte-macrophage crosstalk by promoting M1 macrophage polarization.

In conclusion, our study sheds light on the pivotal role of sOPN and iOPN in the pathogenesis of rosacea (Figure 7). Understanding the role of iOPN and sOPN may provide evidence for their use as biomarkers and therapeutic targets in rosacea.

## Data availability statement

The datasets of GSE65914 can be found in online repositories. Mice RNA-seq gene expression data can be found in the Supplementary Material.

## Ethics statement

The studies involving humans were approved by Medical Ethics Committee of Peking University Shenzhen Hospital. The studies were conducted in accordance with the local legislation and institutional requirements. The participants provided their written informed consent to participate in this study. The animal study was approved by Shenzhen Perking University - the Hong Kong University of Science and Technology Medical Center Animal Care and Use Committee. The study was conducted in accordance with the local legislation and institutional requirements. Written informed consent was obtained from the individual(s) for the publication of any potentially identifiable images or data included in this article.

## Author contributions

ST: Data curation, Formal analysis, Methodology, Writing – original draft. HH: Data curation, Methodology, Writing – original draft. ML: Methodology, Writing – review & editing. KZ: Data curation, Methodology, Writing – original draft. QW: Funding acquisition, Methodology, Writing – review & editing. XL: Data curation, Methodology, Writing – original draft. LW: Conceptualization, Methodology, Writing – review & editing. BY: Funding acquisition, Supervision, Writing – review & editing. XC:

Conceptualization, Funding acquisition, Methodology, Writing – review & editing.

## Funding

The author(s) declare financial support was received for the research, authorship, and/or publication of this article. This work was supported by National Natural Science Foundation of China (81874249), Guangdong Basic and Applied Basic Research Foundation (2020A1515011125), Shenzhen Bay Laboratory Open Program (SZBL2019062801001), Shenzhen Basic Research Grants (JCYJ20220530160207016) and Scientific Research Foundation of Peking University Shenzhen Hospital (KYQD2021049).

## Acknowledgments

We would like to thank the Biomedical Research Institute of Shenzhen Peking University - The Hong Kong University of Science and Technology Medical Center for providing platform support and technical assistance. We would also like to acknowledge the availability of the preprint version of this manuscript on Research Square under the DOI:10.21203/rs.3.rs-3651651/v1 (50).

## Conflict of interest

The authors declare that the research was conducted in the absence of any commercial or financial relationships that could be construed as a potential conflict of interest.

## Publisher's note



## Supplementary material

The Supplementary Material for this article can be found online at: https://www.frontiersin.org/articles/10.3389/fimmu.2023.1285951/full#supplementary-material

## References

1. van Zuuren EJ, Arents BWM, van der Linden MMD, Vermeulen S, Fedorowicz Z, Tan J. Rosacea: new concepts in classification and treatment. *Am J Clin Dermatol* (2021) 22(4):457–65. doi: 10.1007/s40257-021-00595-7

2. Oge LK, Muncie HL, Phillips-Savoy AR. Rosacea: diagnosis and treatment. *Am Fam Physician* (2015) 92(3):187–96.

3. Steinhoff M, Schauber J, Leyden JJ. New insights into rosacea pathophysiology: a review of recent findings. *J Am Acad Dermatol* (2013) 69(6 Suppl 1):S15–26. doi: 10.1016/j.jaad.2013.04.045

4. Piipponen M, Li D, Landén NX. The immune functions of keratinocytes in skin wound healing. *Int J Mol Sci* (2020) 21(22):8790. doi: 10.3390/ijms21228790

5. Buhl T, Sulk M, Nowak P, Buddenkotte J, McDonald I, Aubert J, et al. Molecular and morphological characterization of inflammatory infiltrate in rosacea reveals activation of Th1/Th17 pathways. *J Invest Dermatol* (2015) 135(9):2198–208. doi: 10.1038/jid.2015.141

6. Muto Y, Wang Z, Vanderberghe M, Two A, Gallo RL, Di Nardo A. Mast cells are key mediators of cathelicidin-initiated skin inflammation in rosacea. *J Invest Dermatol* (2014) 134(11):2728–36. doi: 10.1038/jid.2014.222

7. Deng Z, Chen M, Liu Y, Xu S, Ouyang Y, Shi W, et al. A positive feedback loop between mTORC1 and cathelicidin promotes skin inflammation in rosacea. *EMBO Mol Med* (2021) 13(5):e13560. doi: 10.15252/emmm.202013560

8. Harden JL, Shih YH, Xu J, Li R, Rajendran D, Hofland H, et al. Paired transcriptomic and proteomic analysis implicates IL-1β in the pathogenesis of papulopustular rosacea explants. *J Invest Dermatol* (2021) 141(4):800–9. doi: 10.1016/j.jid.2020.08.013

9. Coillard A, Segura E. *In vivo* differentiation of human monocytes. *Front Immunol* (2019) 10:1907. doi: 10.3389/fimmu.2019.01907

10. Watanabe S, Alexander M, Misharin AV, Budinger GRS. The role of macrophages in the resolution of inflammation. *J Clin Invest* (2019) 129(7):2619–28. doi: 10.1172/JCI124615

11. Yunna C, Mengru H, Lei W, Weidong C. Macrophage M1/M2 polarization. *Eur J Pharmacol* (2020) 877:173090. doi: 10.1016/j.ejphar.2020.173090

12. Liu YC, Zou XB, Chai YF, Yao YM. Macrophage polarization in inflammatory diseases. *Int J Biol Sci* (2014) 10(5):520–9. doi: 10.7150/ijbs.8879

13. Hristodorov D, Mladenov R, von Felbert V, Huhn M, Fischer R, Barth S, et al. Targeting CD64 mediates elimination of M1 but not M2 macrophages in *vitro* and in cutaneous inflammation in mice and patient biopsies. *MAbs* (2015) 7(5):853–62. doi: 10.1080/19420862.2015.1066950

14. Shin D, Choi W, Bae H. Bee venom phospholipase A2 alleviate house dust mite-induced atopic dermatitis-like skin lesions by the CD206 mannose receptor. *Toxins (Basel)* (2018) 10(4):146. doi: 10.3390/toxins10040146

15. Zhou L, Zhao H, Zhao H, Meng X, Zhao Z, Xie H, et al. GBP5 exacerbates rosacea-like skin inflammation by skewing macrophage polarization towards M1 phenotype through the NF-κB signalling pathway. *J Eur Acad Dermatol Venereol* (2023) 37(4):796–809. doi: 10.1111/jdv.18725

16. Si J, Wang C, Zhang D, Wang B, Zhou Y. Osteopontin in bone metabolism and bone diseases. *Med Sci Monit* (2020) 26:e919159. doi: 10.12659/MSM.919159

17. Klement JD, Paschall AV, Redd PS, Ibrahim ML, Lu C, Yang D, et al. An osteopontin/CD44 immune checkpoint controls CD8+ T cell activation and tumor immune evasion. *J Clin Invest* (2018) 128(12):5549–60. doi: 10.1172/JCI123360

18. Rittling SR. Osteopontin in macrophage function. *Expert Rev Mol Med* (2011) 13:e15. doi: 10.1017/S1462399411001839

19. Hunter C, Bond J, Kuo PC, Selim MA, Levinson H. The role of osteopontin and osteopontin aptamer (OPN-R3) in fibroblast activity. *J Surg Res* (2012) 176(1):348–58. doi: 10.1016/j.jss.2011.07.054

20. Rittling SR, Singh R. Osteopontin in immune-mediated diseases. *J Dent Res* (2015) 94(12):1638–45. doi: 10.1177/0022034515605270

21. Zhao H, Chen Q, Alam A, Cui J, Suen KC, Soo AP, et al. The role of osteopontin in the progression of solid organ tumour. *Cell Death Dis* (2018) 9(3):356. doi: 10.1038/s41419-018-0391-6

22. Singh A, Gill G, Kaur H, Amhmed M, Jakhu H. Role of osteopontin in bone remodeling and orthodontic tooth movement: a review. *Prog Orthod* (2018) 19(1):18. doi: 10.1186/s40510-018-0216-2

23. Bastos A, Gomes AVP, Silva GR, Emerenciano M, Ferreira LB, Gimba ERP. The intracellular and secreted sides of osteopontin and their putative physiopathological roles. *Int J Mol Sci* (2023) 24(3):2942. doi: 10.3390/ijms24032942

24. Jia R, Liang Y, Chen R, Liu G, Wang H, Tang M, et al. Osteopontin facilitates tumor metastasis by regulating epithelial-mesenchymal plasticity. *Cell Death Dis* (2016) 7(12):e2564. doi: 10.1038/cddis.2016.422

25. Yamasaki K, Di Nardo A, Bardan A, Murakami M, Ohtake T, Coda A, et al. Increased serine protease activity and cathelicidin promotes skin inflammation in rosacea. *Nat Med* (2007) 13(8):975–80. doi: 10.1038/nm1616

26. Lee HJ, Hong YJ, Kim M. Angiogenesis in chronic inflammatory skin disorders. *Int J Mol Sci* (2021) 22(21):12035. doi: 10.3390/ijms222112035

27. Yoon SH, Hwang I, Lee E, Cho HJ, Ryu JH, Kim TG, et al. Antimicrobial peptide LL-37 drives rosacea-like skin inflammation in an NLRP3-dependent manner. *J Invest Dermatol* (2021) 141(12):2885–94.e5. doi: 10.1016/j.jid.2021.02.745

28. Shih YH, Xu J, Kumar A, Li R, Chang ALS. Alterations of immune and keratinization gene expression in papulopustular rosacea by whole transcriptome analysis. *J Invest Dermatol* (2020) 140(5):1100–3.e4. doi: 10.1016/j.jid.2019.09.021

29. Liu T, Deng Z, Xie H, Chen M, Xu S, Peng Q, et al. ADAMDEC1 promotes skin inflammation in rosacea via modulating the polarization of M1 macrophages. *Biochem Biophys Res Commun* (2020) 521(1):64–71. doi: 10.1016/j.bbrc.2019.10.073

30. Xu HT, Lee CW, Li MY, Wang YF, Yung PS, Lee OK. The shift in macrophages polarisation after tendon injury: A systematic review. *J Orthop Translat* (2020) 21:24–34. doi: 10.1016/j.jot.2019.11.009

31. Rebholz B, Haase I, Eckelt B, Paxian S, Flaig MJ, Ghoreschi K, et al. Crosstalk between keratinocytes and adaptive immune cells in an IkappaBalpha protein-mediated inflammatory disease of the skin. *Immunity* (2007) 27(2):296–307. doi: 10.1016/j.immuni.2007.05.024

32. Woo YR, Lim JH, Cho DH, Park HJ. Rosacea: molecular mechanisms and management of a chronic cutaneous inflammatory condition. *Int J Mol Sci* (2016) 17 (9):1562. doi: 10.3390/ijms17091562

33. Dajnoki Z, Béke G, Kapitány A, Mócsai G, Gáspár K, Rühl R, et al. Sebaceous gland-rich skin is characterized by TSLP expression and distinct immune surveillance which is disturbed in rosacea. *J Invest Dermatol* (2017) 137(5):1114–25. doi: 10.1016/j.jid.2016.12.025

34. Lund SA, Giachelli CM, Scatena M. The role of osteopontin in inflammatory processes. *J Cell Commun Signal* (2009) 3(3-4):311–22. doi: 10.1007/s12079-009-0068-0

35. Rollo EE, Laskin DL, Denhardt DT. Osteopontin inhibits nitric oxide production and cytotoxicity by activated RAW264. *7 macrophages. J Leukoc Biol* (1996) 60(3):397–404. doi: 10.1002/jlb.60.3.397

36. Gao C, Guo H, Mi Z, Grusby MJ, Kuo PC. Osteopontin induces ubiquitin-dependent degradation of STAT1 in RAW264.7 murine macrophages. *J Immunol* (2007) 178(3):1870–81. doi: 10.4049/jimmunol.178.3.1870

37. Icer MA, Gezmen-Karadag M. The multiple functions and mechanisms of osteopontin. *Clin Biochem* (2018) 59:17–24. doi: 10.1016/j.clinbiochem.2018.07.003

38. Xu G, Nie H, Li N, Zheng W, Zhang D, Feng G, et al. Role of osteopontin in amplification and perpetuation of rheumatoid synovitis. *J Clin Invest* (2005) 115 (4):1060–7. doi: 10.1172/JCI200523273

39. Cui J, Wang J, Lin C, Liu J, Zuo W. Osteopontin mediates cetuximab resistance via the MAPK pathway in NSCLC cells. *Onco Targets Ther* (2019) 12:10177–85. doi: 10.2147/OTT.S228437

40. Shinohara ML, Kim HJ, Kim JH, Garcia VA, Cantor H. Alternative translation of osteopontin generates intracellular and secreted isoforms that mediate distinct biological activities in dendritic cells. *Proc Natl Acad Sci USA* (2008) 105(20):7235–9. doi: 10.1073/pnas.0802301105

41. Leavenworth JW, Verbinnen B, Wang Q, Shen E, Cantor H. Intracellular osteopontin regulates homeostasis and function of natural killer cells. *Proc Natl Acad Sci USA* (2015) 112(2):494–9. doi: 10.1073/pnas.1423011112

42. Inoue M, Moriwaki Y, Arikawa T, Chen YH, Oh YJ, Oliver T, et al. Cutting edge: critical role of intracellular osteopontin in antifungal innate immune responses. *J Immunol* (2011) 186(1):19–23. doi: 10.4049/jimmunol.1002735

43. Shirakawa K, Endo J, Kataoka M, Katsumata Y, Yoshida N, Yamamoto T, et al. IL (Interleukin)-10-STAT3-galectin-3 axis is essential for osteopontin-producing reparative macrophage polarization after myocardial infarction. *Circulation* (2018) 138(18):2021–35. doi: 10.1161/CIRCULATIONAHA.118.035047

44. Bill R, Wirapati P, Messemaker M, Roh W, Zitti B, Duval F, et al. CXCL9: SPP1 macrophage polarity identifies a network of cellular programs that control human cancers. *Science* (2023) 381(6657):515–24. doi: 10.1126/science.ade2292

45. Xu Z, Xi F, Deng X, Ni Y, Pu C, Wang D, et al. Osteopontin promotes macrophage M1 polarization by activation of the JAK1/STAT1/HMGB1 signaling pathway in nonalcoholic fatty liver disease. *J Clin Transl Hepatol* (2023) 11(2):273–83. doi: 10.14218/JCTH.2021.00474

46. Ge Q, Ruan CC, Ma Y, Tang XF, Wu QH, Wang JG, et al. Osteopontin regulates macrophage activation and osteoclast formation in hypertensive patients with vascular calcification. *Sci Rep* (2017) 7:40253. doi: 10.1038/srep40253

47. Larsen SB, Cowley CJ, Fuchs E. Epithelial cells: liaisons of immunity. *Curr Opin Immunol* (2020) 62:45–53. doi: 10.1016/j.coi.2019.11.004

48. Deng Z, Liu F, Chen M, Huang C, Xiao W, Gao S, et al. Keratinocyte-immune cell crosstalk in a STAT1-mediated pathway: novel insights into rosacea pathogenesis. *Front Immunol* (2021) 12:674871. doi: 10.3389/fimmu.2021.674871

49. Oh K, Seo MW, Kim YW, Lee DS. Osteopontin potentiates pulmonary inflammation and fibrosis by modulating IL-17/IFN-γ-secreting T-cell ratios in bleomycin-treated mice. *Immune Netw* (2015) 15(3):142–9. doi: 10.4110/in.2015.15.3.142

50. Tang S, Hu H, Zhang K, Liu X, Wu L, Yu B, et al. OPN promotes proinflammatory cytokine expression via ERK/JNK pathway and M1 macrophagepolarization in Rosacea. *Preprint host on Research Square* (2023). doi: 10.21203/rs.3.rs-3651651/v1

frontiers | Frontiers in Immunology

TYPE Correction
PUBLISHED 29 February 2024
DOI 10.3389/fimmu.2024.1382092



OPEN ACCESS

EDITED AND REVIEWED BY
Zhenghua Zhang,
Fudan University, China

*CORRESPONDENCE
Xiaofan Chen
littlecanva@163.com
Bo Yu
yubomd@hotmail.com

RECEIVED 05 February 2024
ACCEPTED 20 February 2024
PUBLISHED 29 February 2024

CITATION
Tang S, Hu H, Li M, Zhang K, Wu Q, Liu X, Wu L, Yu B and Chen X (2024) Corrigendum: OPN promotes pro-inflammatory cytokine expression via ERK/JNK pathway and M1 macrophage polarization in Rosacea. *Front. Immunol.* 15:1382092. doi: 10.3389/fimmu.2024.1382092



# Corrigendum: OPN promotes pro-inflammatory cytokine expression via ERK/JNK pathway and M1 macrophage polarization in Rosacea

Siyi Tang[1], Hao Hu[1], Manhui Li[1], Kaoyuan Zhang[2], Qi Wu[3], Xiaojuan Liu[1], Lin Wu[2], Bo Yu[2*] and Xiaofan Chen[1*]

[1]Shenzhen Key Laboratory for Translational Medicine of Dermatology, Biomedical Research Institute, Shenzhen Peking University - The Hong Kong University of Science and Technology Medical Center, Shenzhen, Guangdong, China, [2]Department of Dermatology, Peking University Shenzhen Hospital, Shenzhen, China, [3]Greater Bay Biomedical Innocenter, Shenzhen Bay Laboratory, Shenzhen, China

KEYWORDS

**Rosacea, OPN, keratinocyte, macrophage, inflammation**

A Corrigendum on

OPN promotes pro-inflammatory cytokine expression via ERK/JNK pathway and M1 macrophage polarization in Rosacea

By Tang S, Hu H, Li M, Zhang K, Wu Q, Liu X, Wu L, Yu B and Chen X (2024) *Front. Immunol.* 14:1285951. doi: 10.3389/fimmu.2023.1285951

In the published article, there was an error in Figure 2A as published. The magnified image for the WT-PBS group was misused in the OPN KO-PBS group in the lower panel of Figure 2A. The corrected Figure 2 and its caption appear below.

The authors apologize for this error and state that this does not change the scientific conclusions of the article in any way. The original article has been updated.

## Publisher's note

All claims expressed in this article are solely those of the authors and do not necessarily represent those of their affiliated organizations, or those of the publisher, the editors and the reviewers. Any product that may be evaluated in this article, or claim that may be made by its manufacturer, is not guaranteed or endorsed by the publisher.

10.3389/fimmu.2024.1382092

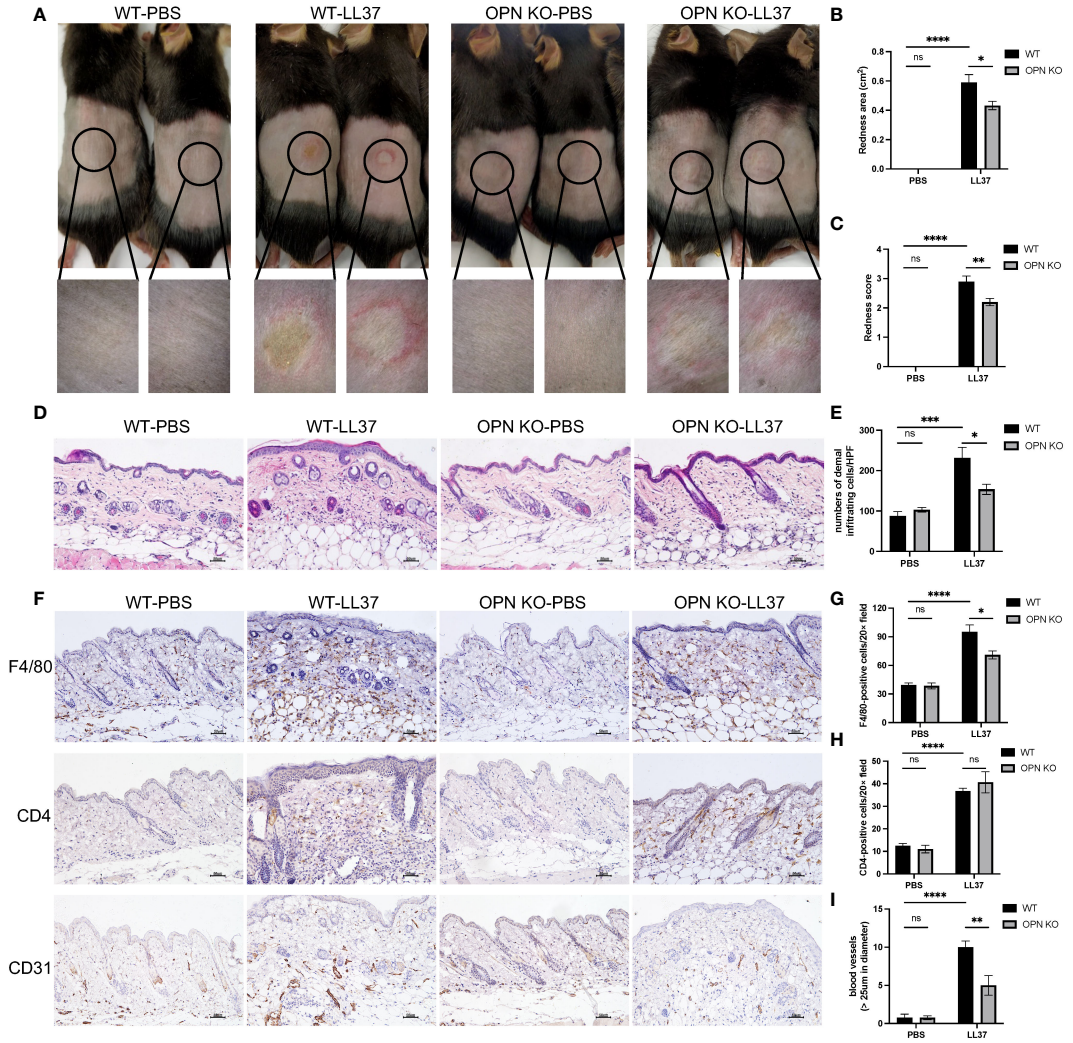


FIGURE 2
OPN knockdown attenuated rosacea-like skin redness and inflammatory cell infiltration in mice. **(A)** LL37 was injected intradermally into the dorsal skin of WT mice and OPN KO mice to induce a rosacea-like phenotype. The skin lesions were collected two days after injection with PBS or LL37. The lower panel is a magnified image of the circular area in the upper panel. The severity of the rosacea-like phenotypes was assessed according to the redness area **(B)** and redness score **(C)**. Data represent the mean ± SEM. *p < 0.05, **p < 0.01, ****p < 0.0001. Ns, no significance. **(D)** HE staining for the histological analysis of WT mice and OPN KO mice injected with PBS or LL37. Scale bar: 50μm. **(E)** The number of dermal inflammatory infiltration in each group was quantified (n = 4 for each group). Data represent the mean ± SEM. Two-way ANOVA with Tukey's *post hoc* test was used for statistical analyses. *p < 0.05, ***p < 0.001. Ns, no significance. **(F)** Representative images of immunohistochemistry of F4/80, CD4, and CD31 in WT mice and OPN KO mice injected with PBS or LL37. Scale bar: 50μm. **(G)** The infiltration of F4/80-positive cells was quantified in each group (n = 4 for each group). Data represent the mean ± SEM. Two-way ANOVA with Tukey's *post hoc* test was used for statistical analyses. *p < 0.05, ****p < 0.0001. Ns, no significance. **(H)** The infiltration of CD4-positive cells was quantified in each group (n = 4 for each group). Data represent the mean ± SEM. Two-way ANOVA with Tukey's *post hoc* test was used for statistical analyses. ****p < 0.0001. Ns, no significance. **(I)** The number of CD31-positive blood vessels (>25um in diameter) was quantified in each group (n = 4 for each group). Data represent the mean ± SEM. Two-way ANOVA with Tukey's *post hoc* test was used for statistical analyses. **p < 0.01, ****p < 0.0001. Ns, no significance.

frontiers | Frontiers in Immunology

TYPE Original Research
PUBLISHED 09 January 2024
DOI 10.3389/fimmu.2023.1263646



OPEN ACCESS

EDITED BY
Zhenghua Zhang,
Fudan University, China

REVIEWED BY
Seung-Hyo Lee,
Korea Advanced Institute of Science and Technology (KAIST), Republic of Korea
Fatemeh Navid,
National Institute of Arthritis and Musculoskeletal and Skin Diseases (NIH), United States

*CORRESPONDENCE
Tai-Gyu Kim
kimtg@catholic.ac.kr

†These authors have contributed equally to this work and share first authorship

RECEIVED 20 July 2023
ACCEPTED 18 December 2023
PUBLISHED 09 January 2024

CITATION
Kim C-H, Hong S-M, Kim S, Yu JI, Jung S-H, Bang CH, Lee JH and Kim T-G (2024) Skin repair and immunoregulatory effects of myeloid suppressor cells from human cord blood in atopic dermatitis.
*Front. Immunol.* 14:1263646.
doi: 10.3389/fimmu.2023.1263646



# Skin repair and immunoregulatory effects of myeloid suppressor cells from human cord blood in atopic dermatitis

Chang-Hyun Kim[1†], Seung-Min Hong[1†], Sueon Kim[1], Jae Ik Yu[1], Soo-Hyun Jung[1], Chul Hwan Bang[2], Ji Hyun Lee[2] and Tai-Gyu Kim[1,3*]

[1]ViMedier Platform Group, ViGenCell Inc., Seoul, Republic of Korea, [2]Department of Dermatology, Seoul St. Mary's Hospital, College of Medicine, The Catholic University of Korea, Seoul, Republic of Korea, [3]Department of Microbiology, College of Medicine, The Catholic University of Korea, Seoul, Republic of Korea

**Introduction:** Previously, we achieved large-scale expansion of bone marrow-derived suppressor cells (MDSCs) derived from cluster of differentiation (CD)34$^+$ cells cultured in human umbilical cord blood (hUCB) and demonstrated their immunomodulatory properties. In the present study, we assessed the therapeutic efficacy of hUCB-MDSCs in atopic dermatitis (AD).

**Methods:** *Dermatophagoides farinae* (Df)-induced NC/Nga mice (clinical score of 7) were treated with hUCB-MDSCs or a control drug. The mechanisms underlying the therapeutic effects of hUCB-MDSCs were evaluated.

**Results and discussion:** hUCB-MDSCs demonstrated immunosuppressive effects in both human and mouse CD4$^+$ T cells. hUCB-MDSCs significantly reduced the clinical severity scores, which were associated with histopathological changes, and reduced inflammatory cell infiltration, epidermal hyperplasia, and fibrosis. Furthermore, hUCB-MDSCs decreased the serum levels of immunoglobulin E, interleukin (IL)-4, IL-5, IL-13, IL-17, thymus- and activation-regulated chemokines, and thymic stromal lymphopoietin. Additionally, they altered the expression of the skin barrier function-related proteins filaggrin, involucrin, loricrin, cytokeratin 10, and cytokeratin 14 and suppressed the activation of Df-restimulated T-cells via cell–cell interactions. hUCB-MDSCs promoted skin recovery and maintained their therapeutic effect even after recurrence. Consequently, hUCB-MDSC administration improved Df-induced AD-like skin lesions and restored skin barrier function. Our findings support the potential of hUCB-MDSCs as a novel treatment strategy for AD.

KEYWORDS

**atopic dermatitis, inflammatory responses, myeloid-derived suppressor cells, skin repair, T-cells**

# 1 Introduction

Atopic dermatitis (AD) is characterized by complex interactions among genetic, pharmacological, environmental, and psychological factors (1, 2). Its pathogenesis involves systemic immune dysregulation, epidermal barrier dysfunction, and allergen-specific immunoglobulin E (IgE) hypersensitivity; however, the underlying mechanisms remain unclear (3, 4). T-Helper (Th)2 cell differentiation from naïve cluster of differentiation (CD)4$^+$ T cells increases interleukin (IL)-4, IL-5, and IL-13 production. Additionally, Th2 cytokines promote mast cell and eosinophil proliferation and activation, thereby increasing IgE level (5). Severe AD may lead to the excessive use of topical or systemic anti-inflammatory and immunosuppressive agents (6, 7), with long-term toxicity and short-term efficacy. Moreover, complete AD suppression is not feasible with recently developed treatments (6–8). Therefore, safer and more effective alternative therapies are needed.

Myeloid-derived suppressor cells (MDSCs) represent a heterogeneous population of hematopoietic cell precursors—macrophages, granulocytes, and dendritic cells—in various maturation states that accumulate in the bone marrow, spleen, and blood (9). MDSCs have garnered attention owing to their increased activity during cancer and inflammatory responses and involvement in tissue damage in an immunosuppressive environment. Their distinctive characteristics are heterogeneous morphology, phenotypes, and functions. Gr-1$^+$CD11b$^+$ cells in mice and lineage-human leukocyte antigen-DR isotype-low/CD11b$^+$CD33$^+$ cells in humans are MDSC markers (10). These cells induce immunomodulatory mediators such as indoleamine 2,3-deoxygenase (IDO), inducible nitric oxide synthase (iNOS), and arginase-1 (ARG1) (11, 12). MDSCs inhibit T and NK cell immune responses and promote regulatory T (Treg) cell generation (13, 14). Several receptor–ligand interactions between MDSCs and immune cells regulate immune responses (15). The immunomodulatory and anti-inflammatory properties of these cells have been demonstrated in experimental inflammatory and autoimmune disease models (16–18). Additionally, MDSCs play a role in wound healing (19–21). Among MDSC secretions, transforming growth factor-β and ARG1 contribute to wound healing by producing collagen from fibroblasts (19). Moreover, nitric oxide, generated from inducible nitric oxide synthase (iNOS), contributes to wound healing via several mechanisms (22).

We recently reported that human umbilical cord blood (hUCB)-MDSCs suppress graft-versus-host disease (GVHD) development in mice by selectively suppressing Th2- and Th17-mediated immune responses (23). However, the effects of hUCB-MDSCs and underlying mechanisms in experimental AD mouse models remain to be elucidated. Therefore, in the present study, we investigated the mechanisms underlying the skin-repair and immunomodulatory effects of hUCB-MDSC therapy in a mouse model of *Dermatophagoides farinae* (Df)-induced AD-like skin lesions.

# 2 Materials and methods

## 2.1 Culture of hUCB-MDSCs

All experimental procedures using human cord blood derivatives, including hUCB-MDSCs, were conducted following the guidelines approved by the Korea National Institute for bioethics policy (IRB no. P01-202010-31-008). hUCB-MDSCs were isolated and cultured as previously described (Figure 1A) (23, 24).

## 2.2 Animals and reagents

Five-week-old female *NC/Nga* mice (Japan SLC, Hamamatsu, Japan) were allowed to acclimatize for 1 week before the experiments. The mice were maintained under specific pathogen-free conditions in the animal care facility of the Catholic University of Korea. The Animal Care and Use Committee of the Research Institute at the Catholic University of Korea approved the experiments (IACUC no.: CUMC-2021-0114-04). Df body ointment was prepared by Biostir, Inc. (Kobe, Japan). One gram of the ointment contained 136.4 mg protein, 234 μg Df 1, and 7 μg Df 2.

## 2.3 *In vitro* T cell assay

Splenocytes from NC/Nga mice were seeded at a density of $1 \times 10^6$ cells/well into 24-well plates (Falcon, Corning, NY, USA) and stimulated with CD3/CD28 DYNABEADS (Gibco, Thermo Fisher Scientific, Waltham, MA, USA) to analyze T cell proliferation. hUCB-MDSCs were cocultured with spleen cells at ratios of 0.5:1, 0.25:1, and 0.1:1. Thereafter, cell proliferation was assessed using the Cell Trace CFSE Cell Proliferation Kit (Invitrogen, Thermo Fisher Scientific) per the manufacturer's instructions.

To analyze T-cell differentiation, purified CD4$^+$ T cells from NC/Nga mice were seeded at a density of $3.12 \times 10^5$ cells/well into 24-well plates (Falcon) and differentiated using the Th2 differentiation kit (STEMCELL Technologies, Vancouver, Canada) or Th17 differentiation kit (R&D systems, Minneapolis, MN, USA). hUCB-MDSCs were cocultured with CD4$^+$ T cells at ratios of 1:1, 0.5:1, and 0.25:1. Th2 and Th17 cell cultures were incubated for 6 and 5 days, respectively, according to the manufacturer's instructions.

## 2.4 Flow cytometry

Splenocytes or lymph node (LN) cells were harvested and stained with eFluor780-fixable viability dye (eBioscience), Pacific Blue-anti-CD3e (BioLegend, San Diego, CA, USA), PE-cyanine (Cy)7-anti-CD8 (BioLegend), and PerCP-Cy5.5-anti-CD4 (BioLegend) antibodies. After fixation and permeabilization, the cells were stained with PE-anti-IL-13, PE-anti-IL-22, allophycocyanin-anti-IL-5, PE-Cy7-anti-IL-4, Alexa Fluor 488-anti-IL-17A, and BV785-anti-IFN-γ antibodies (BioLegend). The data were analyzed using FlowJo (Tree Star, Ashland, OR, USA).

10.3389/fimmu.2023.1263646

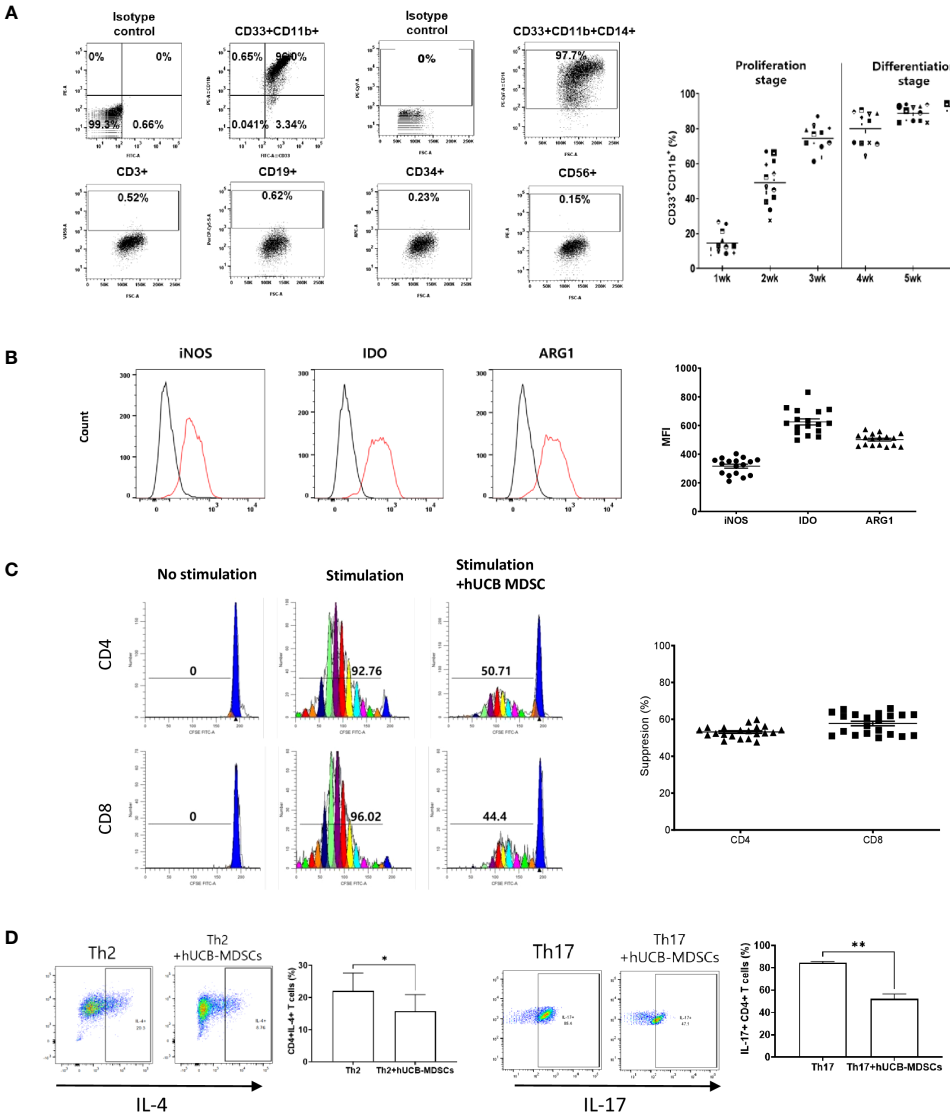


FIGURE 1
Immunobiological characterization of human umbilical cord blood (hUCB) myeloid-derived suppressor cells (MDSCs) *in vitro* using human T cells. **(A)** The proliferation- and differentiation-stage $CD33^{+}CD11b^{+}$ MDSC markers during the 6-week culture period of hUCB-MDSCs. Flow cytometric analysis of hUCB-MDSCs stained with individual MDSC-positive or -negative surface marker antibodies. ($CD33^{+}CD11b^{+} \geq 70\%$, $CD14^{+} \geq 90\%$) **(B)** The expression of immune suppressive molecules by hUCB-MDSCs was analyzed using FITC anti-inducible nitric oxide synthase (iNOS)2 antibody, PE anti-indoleamine 2,3-deoxygenase (IDO) antibody, and PerCP-Cy5.5 anti-arginase-1 (ARG1) antibody staining. Cells were analyzed using a FACS Lyric device after two washes in stain buffer and incubation on ice for 30 min. Black, isotype control antibody. Red, each specific antibody. (iNOS $\geq$ 200 MFI, IDO $\geq$ 450 MFI, ARG1 $\geq$ 400 MFI) **(C)** hUCB-MDSC-mediated immune suppression of T cells, stimulated by anti-CD3/CD28 beads for 6 days in human peripheral blood mononuclear cells (PBMCs), was tested at a PBMC–hUCB-MDSC ratio of 1:1. (Suppression $\geq$ 45%). **(D)** hUCB-MDSC-mediated immunoregulation of human $CD4^{+}$ T-cell differentiation, stimulated using Th2 or Th17 differentiation kits for 13 or 6 days in human $CD4^{+}$ T cells, was tested at a human $CD4^{+}$ T cells–hUCB-MDSC ratio of 1:1. $^{*}p < 0.05$, $^{**}p < 0.01$.

## 2.5 Induction of AD in NC/Nga mice

AD was induced using Df body ointment (25). The back hair of NC/Nga mice was shaved, and the mice were subjected to skin hair removal treatment (Niclean, Ildong, Korea). The skin barrier was disrupted by treating the shaved dorsal skin and surfaces of both ears with 4% sodium dodecyl sulfate 3 h before the application of Df body ointment (100 mg/mouse). These procedures were repeated two times a week for 4 weeks. After 14 days of the initial Df sensitization, the mice were randomly divided into six groups (n = 5 mice per group): normal (untreated), Df-alone (negative control), Df+Dexa (positive control), Df+hUCB-MDSCs ($1 \times 10^{4}$ cells per mouse), Df+hUCB-MDSCs ($1 \times 10^{5}$ cells per mouse), and Df+hUCB-MDSCs ($1 \times 10^{6}$ cells per mouse). hUCB-MDSCs were intravenously administered to these mice two times a week for 2 weeks. Dexa (2 mg/kg) in water was orally administered to these mice five doses per week for 3 weeks by gavage (oral-zoned needle). Additional information is provided in the Supplementary Materials and Methods.

## 2.6 Skin lesion scoring

Erythema/hemorrhage, scarring/dryness, edema, and excoriation/erosion were scored as 0 (none), 1 (mild), 2 (moderate), or 3 (severe) per the observed symptoms. The total skin score was defined as the sum of individual scores (26).

## 2.7 Serum IgE, cytokine, and chemokine assays

Mouse serum was collected 1 week after the final administration of hUCB-MDSCs, and total IgE concentration was measured using an enzyme-linked immunosorbent assay (ELISA) kit (Yamasa, Tokyo, Japan), per the manufacturer's instructions. IL-4, IL-5, IL-13, IL-17, TSLP, and TARC levels were measured using ELISA kits (R&D Systems).

## 2.8 Histological analyses

The dorsal skin was resected, fixed in 10% formalin solution, and embedded in paraffin. The embedded specimens were then serially sectioned (5 μm) with a microtome (HM 325; Thermo Fisher Scientific) and stained with hematoxylin–eosin to observe the histopathological features or with Masson's trichrome stain to examine the variable deposition of collagen fibers (blue) and skin fibrosis in the lesioned skin. Mast cells and eosinophils were stained with toluidine blue and Congo red, respectively. Additional information is provided in the Supplementary Materials and Methods.

## 2.9 *In vitro* Df restimulation assay

Axillary LNs from normal or Df-induced AD-NC/Nga mice were isolated, and a single-cell suspension was prepared. Cell proliferation was assessed using the Cell Trace CFSE Cell Proliferation Kit (Invitrogen), per the manufacturer's instructions. LN cells ($1 \times 10^6$ cells) were stimulated with 1 mg/mL Df in a 24-well flat-bottom microplate at 37°C for 4 days. hUCB-MDSCs ($5 \times 10^5$ cells) were co-cultured either directly on LN cells or in a Transwell of pore size 0.4 μm (Costar, Corning Inc., Corning, NY, USA). ARG1 (Nor-NOHA 0.5 mM; Selleckchem, Houston, TX, USA) or iNOS inhibitor (1400W 0.1 mM; Medchem Express, Monmouth, NJ, USA) and hUCB-MDSCs was simultaneously treated. After incubation, the cells were harvested for flow cytometry.

## 2.10 Statistical analysis

Data were analyzed for statistical significance using Prism 6.0 (GraphPad Software, San Diego, CA, USA). Unless otherwise indicated, a two-sided unpaired Student's *t*-test was used to compare two groups, and a one-way analysis of variance with a Dunnett *post-hoc* test was used for multiple group comparisons. The results are presented as mean ± standard deviation. Results with $p < 0.05$ were considered significant.

# 3 Results

## 3.1 *In vitro* immunobiological characterization of hUCB-MDSCs

hUCB-MDSCs cultured with hGM-CSF/hSCF for 6 weeks were immune-positive for CD11b, CD33, and CD14, but negative for CD3, CD19, CD34, and CD56 (Figure 1A). The levels of ARG1, IDO, and iNOS, the main factors involved in MDSC-mediated immune suppression, were increased in these cells (Figure 1B).

The carboxyfluorescein succinimidyl ester (CFSE) dilution assay confirmed that hUCB-MDSCs effectively inhibited human $CD4^+$ and $CD8^+$ T cell proliferation (Figure 1C). hUCB-MDSCs downregulated the differentiation of human $CD4^+$ T cells into Th2 and Th17 cells (Figure 1D). Furthermore, they markedly inhibited mouse $CD4^+$ and $CD8^+$ T cell proliferation stimulated with anti-CD3/CD28 beads at a 1:0.5 (mouse T-cell:hUCB-MDSC) ratio (Figure 2A). The addition of hUCB-MDSCs at ratios of 1:1 and/or 1:0.5 to Th2- and Th17-polarizing conditions significantly decreased the IL-4, IL-13, and IL-17 levels compared with those of the untreated group (Figure 2B). These results demonstrate the *in vitro* immunosuppressive properties of hUCB-MDSCs against human and mouse T cells.

## 3.2 Migration of hUCB-MDSCs to damaged skin

To investigate the distribution of hUCB-MDSCs, PKH26-labeled hUCB-MDSCs were injected into both atopic and normal control mice and subsequently identified in various organs. Notably, although hUCB-MDSCs were observed in the lungs, spleen, and LNs of both groups, infiltration of hUCB-MDSCs in skin tissue was found only in atopic dermatitis mice (Supplementary Figure S1).

## 3.3 Effects of hUCB-MDSCs on Df-induced AD-like skin lesions

The schematic diagram of the experiment is illustrated in Figure 3A. Dexamethasone (Dexa), an anti-inflammatory and immunosuppressive drug used for treating AD, served as a positive control. The symptom severity scores of the Df+hUCB-MDSC ($1 \times 10^5$ and $1 \times 10^6$ cells) and Df+Dexa groups were considerably improved compared with those of the Df-alone group (Figure 3B), whereas no difference was observed compared with those of the Df+hUCB-MDSC ($1 \times 10^4$ cells) group. When hUCB-MDSCs were injected once or twice, the effect of hUCB-MDSCs ($1 \times 10^5$ and $1 \times 10^6$ cells) was not observed (Supplementary Figure S2). Df-induced skin inflammation in mice presented as epidermal

10.3389/fimmu.2023.1263646

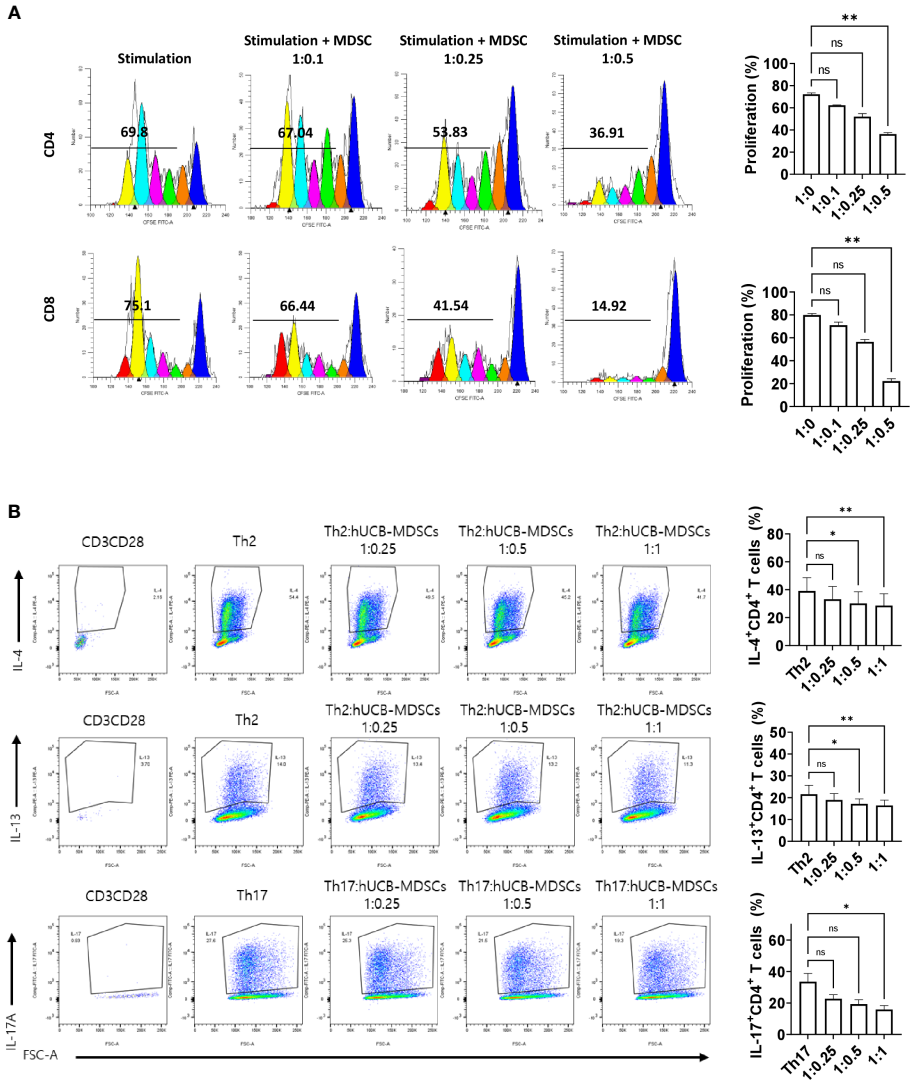


FIGURE 2
Immunoregulatory capacity of human umbilical cord blood (hUCB) myeloid-derived suppressor cells (MDSCs) to mouse T cells in *in vitro*. **(A)** hUCB-MDSC-mediated immune suppression of T cells, stimulated by anti-CD3/CD28 beads for 4 days, in normal NC/Nga mice, was tested at T-cell–hUCB-MDSC ratios of 1:0, 1:0.1, 1:0.25, and 1:0.5. **(B)** Inhibition of T-helper cell differentiation by hUCB-MDSCs. Naïve $CD4^+$ T cells isolated from NC/Nga mice were cocultured with T cell:hUCB-MDSCs (1:0, 1:0.25, 1:0.5, and 1:1 ratios) in the presence of antiCD3, antiCD28, and T cell differentiation kit reagents for 5 or 6 days. Data are presented as mean ± standard error of the mean (n = 3 or 4). *$p < 0.05$ and **$p < 0.01$; ns, not significant.

hyperplasia, hyperkeratosis, and lymphocyte infiltration into the epidermis and dermis, which are typical histopathological characteristics of human AD (2, 3). The Df+hUCB-MDSC ($1 \times 10^5$ and $1 \times 10^6$ cells) and Df+Dexa groups exhibited amelioration of histopathological characteristics (Figure 4A). Epidermal thickness considerably decreased in the Df+hUCB-MDSC and Df+Dexa groups compared with that in the Df-alone group (Figure 4A). Treatment with Df+hUCB-MDSCs ($1 \times 10^5$ and $1 \times 10^6$ cells) led to a significant decrease in the number of infiltrating mast cells compared with that in the Df+Dexa and Df-alone groups (Figure 4B). Furthermore, the extent of decrease in eosinophil counts following Df+hUCB-MDSC treatment was similar to that observed in the Df+Dexa group (Figure 4C). Remarkably, even in a Df-stimulated AD animal model under relapse conditions, hUCB-MDSCs exhibited sustained therapeutic efficacy, in contrast to Dexa which rapidly lost its effectiveness, as confirmed by clinical skin scores (Supplementary Figure S3).

## 3.4 Effects of hUCB-MDSCs on skin barrier repair and skin fibrosis

Impaired skin barrier function and skin fibrosis are important targets for AD treatment (3, 27). The proportion of dermal collagen matrix considerably increased in the Df-alone group compared with that in the normal group. However, compared with the Df-alone group, the Df+hUCB-MDSC ($1 \times 10^5$ and $1 \times 10^6$ cells) and Df+Dexa groups showed a markedly reduced proportion of dermal

10.3389/fimmu.2023.1263646

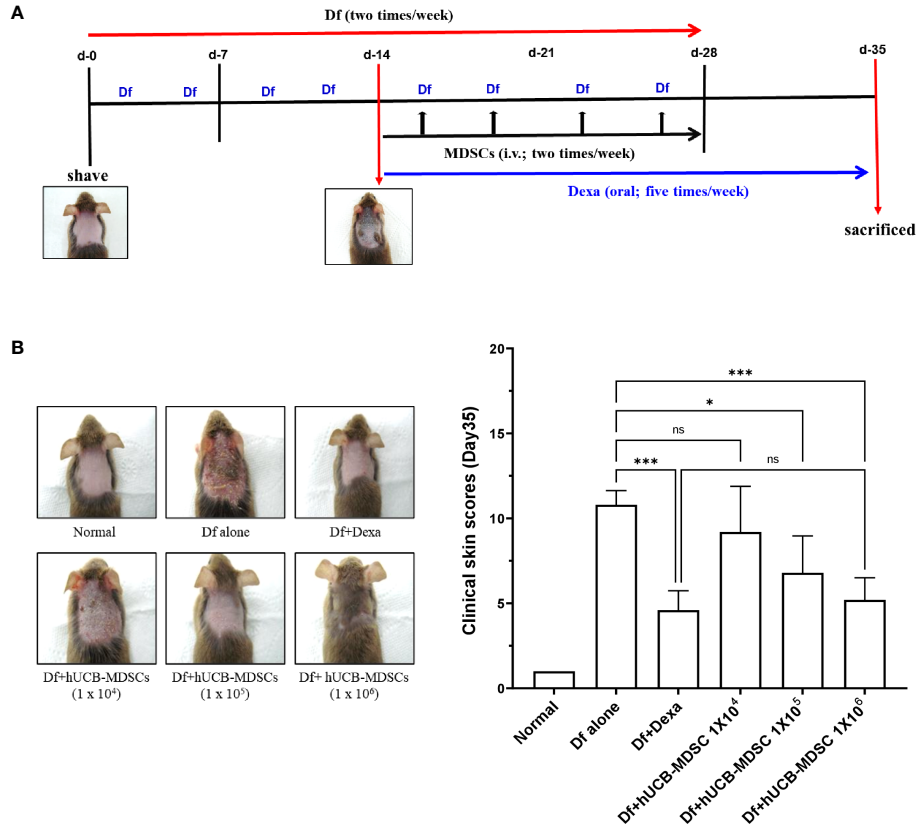


FIGURE 3
Effects of human umbilical cord blood (hUCB)-myeloid-derived suppressor cell (MDSC) therapy against *Dermatophagoides farinae* (Df)-induced atopic dermatitis skin score. **(A)** Schematic diagram of the animal experiments. After hair removal, Df body ointment (100 mg/mouse) was swabbed on the dorsal skin and surfaces of both ears twice a week for 4 weeks. Fourteen days after the first sensitization, Df-induced NC/Nga mice were either not treated (negative control; Df-alone) or treated with hUCB-MDSCs ($1 \times 10^4$, $1 \times 10^5$, or $1 \times 10^6$ cells/mouse) intravenously twice a week for 2 weeks. Dexamethasone (Dexa) (positive control; 2 mg/kg) was orally administered in five doses per week for 3 weeks. **(B)** Images of the skin of five mice (left). Clinical skin scores of mice are presented as the sum of individual scores of erythema/hemorrhage, scarring/dryness, edema, and excoriation/erosion (right). $*p < 0.05$, $***p < 0.001$; ns, not significant.

collagen matrix (Figure 5A). In both Dexa and hUCB-MDSC groups, the epidermal protein levels were higher than those in the Df-alone group (Figure 5B). Notably, the levels of epidermal proteins such as FLG, IVL, LOR, and CK10 were significantly higher in the Df+hUCB-MDSC ($1 \times 10^6$ cells) group than in the positive control group treated with Dexa (Figure 5B). Overall, hUCB-MDSCs display potential as an alternative treatment strategy to avoid the adverse effects of Dexa-associated skin atrophy.

## 3.5 Effects of hUCB-MDSCs on increased levels of IgE and inflammatory mediators

The total serum IgE level was considerably lower in the Df +hUCB-MDSC ($1 \times 10^5$ and $1 \times 10^6$ cells) and Df+Dexa groups than in the Df-alone group; however, no notable difference was observed between the Df+hUCB-MDSC ($1 \times 10^4$ cells) and Df-alone groups (Figure 6). The Th2 (IL-4, IL-5, and IL-13) and Th17 cytokine (IL-17) levels markedly decreased in the Df+hUCB-MDSC ($1 \times 10^5$ and/or $1 \times 10^6$ cells) and Df+Dexa groups compared with those in the Df-alone group. Moreover, the serum thymic stromal lymphopoietin (TSLP) and thymus- and activation-regulated chemokine (TARC) levels considerably decreased in the Df+hUCB-MDSC ($1 \times 10^5$ and/or $1 \times 10^6$ cells) and Df+Dexa groups. Conversely, there was no considerable difference between the Df+hUCB-MDSC ($1 \times 10^4$ cells) and Df-alone groups in terms of TSLP and TARC levels.

## 3.6 Effects of hUCB-MDSCs on the regulation of differentiation to CD4+ T-cell subsets

The spleen weight and size of the Df-alone group were notably higher than those of the normal control group. Compared with the Df-alone group, the Df+hUCB-MDSC ($1 \times 10^5$ and $1 \times 10^6$ cells) and Df+Dexa groups showed considerably reduced spleen weight and size (Figure 7A). Analysis of effector $CD4^+$ T cell subsets in the mouse spleen revealed that the number of IL-4-, IL-5-, IL-13-, and IL-17-producing $CD4^+$ T cells in the splenocytes of Df-induced NC/Nga mice was notably lower in the Df+hUCB-MDSC ($1 \times 10^5$ cells and/or $1 \times 10^6$ cells) group than in the Df+hUCB-MDSC ($1 \times 10^4$ cells) and Df-alone groups (Figure 7B). Additionally, IL-5

10.3389/fimmu.2023.1263646

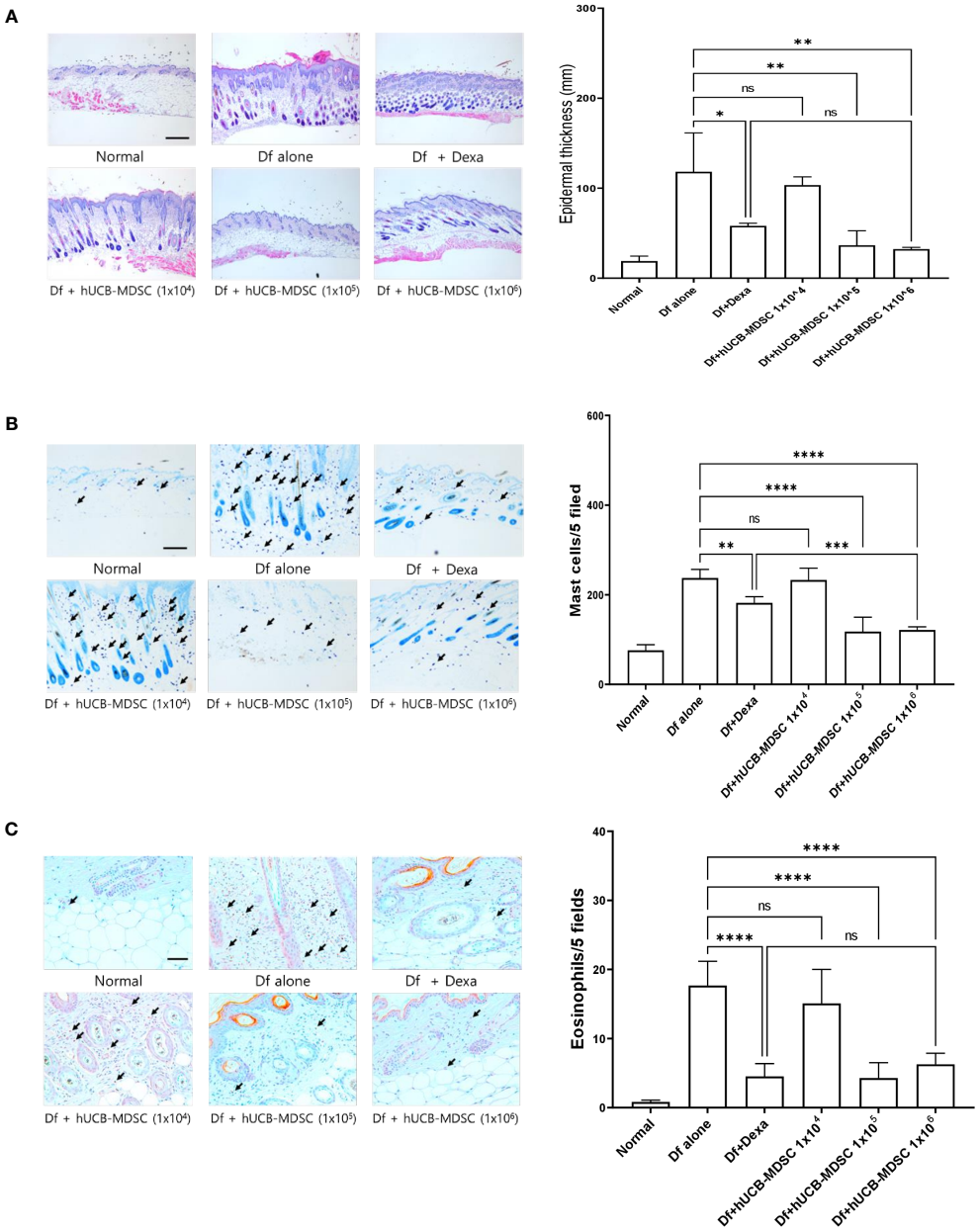


FIGURE 4
Effects of human umbilical cord blood (hUCB)-myeloid-derived suppressor cell (MDSC) therapy against *Dermatophagoides farinae* (Df)-induced atopic dermatitis-like skin lesions. **(A)** Hematoxylin- and eosin-stained sections showing epidermal thickness (hyperplasia) at five randomized sites under 100× magnification. **(B, C)** Sections were stained with toluidine blue and Congo red for visualizing mast cells and eosinophils, respectively. The cell count is expressed as the number of mast cells and eosinophils in five high-power fields (×400 for the count) for each section. Data are presented as mean ± standard error of the mean of six mice per group in a representative experiment out of two experiments. Scale bar = 400 μm **(A)**, 200 μm **(B)** and 50 μm **(C)**. *$p < 0.05$, **$p < 0.01$, ***$p < 0.001$, and ****$p < 0.0001$; ns, not significant.

production was decreased in the Df+hUCB-MDSC ($1 \times 10^4$ cells) group, whereas IFN-γ production was increased in the Df+hUCB-MDSC ($1 \times 10^5$ cells) group.

The proportion changes of effector $CD4^+$ T cell subsets caused by hUCB-MDSCs in the LNs are illustrated in Supplementary Figure S4. The number of IL-4-, IL-5-, IL-13-, and IL-17-producing $CD4^+$ T cells in the LNs of Df-induced NC/Nga mice was decreased in the Df +hUCB-MDSC ($1 \times 10^5$ cells and $1 \times 10^6$ cells) and/or Df+hUCB-MDSC ($1 \times 10^4$ cells) groups, whereas IFN-γ production was increased in the Df+hUCB-MDSC ($1 \times 10^5$ cells and $1 \times 10^6$ cells) groups.

## 3.7 Immune regulatory mechanism between hUCB-MDSCs and T cells

Restimulation of lymph node cells collected from mice with Df-induced AD increased the proliferation of $CD4^+$ and $CD8^+$ T cells, and hUCB-MDSCs downregulated the proliferation (Figure 8A). However, the Transwell assay revealed that hUCB-MDSCs no longer exhibited immunomodulatory functions in the context of blocked cell-cell interactions, suggesting that secreted immunosuppressive substances had little effect on AD mice (Figure 8A). We validated our results using

10.3389/fimmu.2023.1263646

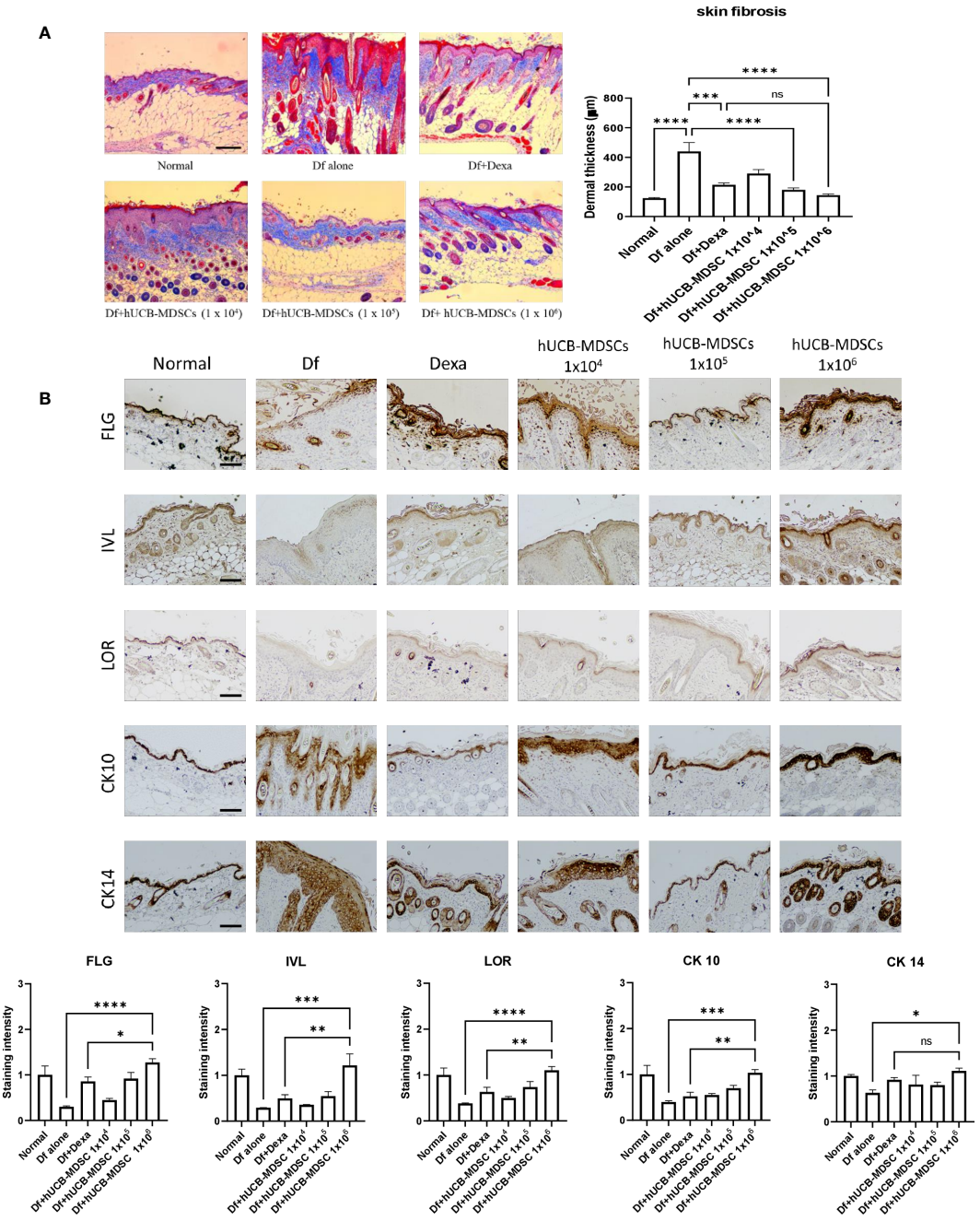


FIGURE 5
Effects of human umbilical cord blood (hUCB)-myeloid-derived suppressor cell (MDSC) therapy on skin barrier repair and skin fibrosis in *Dermatophagoides farinae* (Df)-induced atopic dermatitis-like skin lesions in NC/Nga mice. **(A)** Masson's trichrome staining (representative images) (left) and dermal thickness (right). **(B)** Immunohistochemical staining of filaggrin (FLG), involucrin (IVL), loricrin (LOR), keratin-10 (CK10), and keratin-14 (CK14) in skin equivalents from NC/Nga mice not treated (Df alone) or treated with hUCB-MDSCs ($1 \times 10^4$ cells), hUCB-MDSCs ($1 \times 10^5$ cells), hUCB-MDSCs ($1 \times 10^6$ cells), or dexamethasone (Dexa) (2 mg/kg) on day 35. Data are presented as mean ± standard error of the mean of five mice per group in a representative experiment of two experiments. Scale bar = 200 μm **(A, B)**. *$p < 0.05$, **$p < 0.01$, ***$p < 0.001$; ****$p < 0.0001$; ns, not significant.

iNOS and ARG1 inhibitors (Nor-NOHA, 1400W), which also did not affect the immunosuppressive function of hUCB-MDSCs (Figure 8A). The same results were observed in a subset of $CD4^+$ T cells (Figure 8B). These findings suggest that the suppressive function of hUCB-MDSCs in AD is primarily dependent on cell–cell interactions rather than on secreted immunosuppressive substances.

# 4 Discussion

MDSCs inhibit T-cell-mediated inflammatory responses via various mechanisms, which may alleviate the disease. However, their small population limits their clinical applications. hUCB can differentiate to immunomodulatory cells such as mesenchymal stem

10.3389/fimmu.2023.1263646

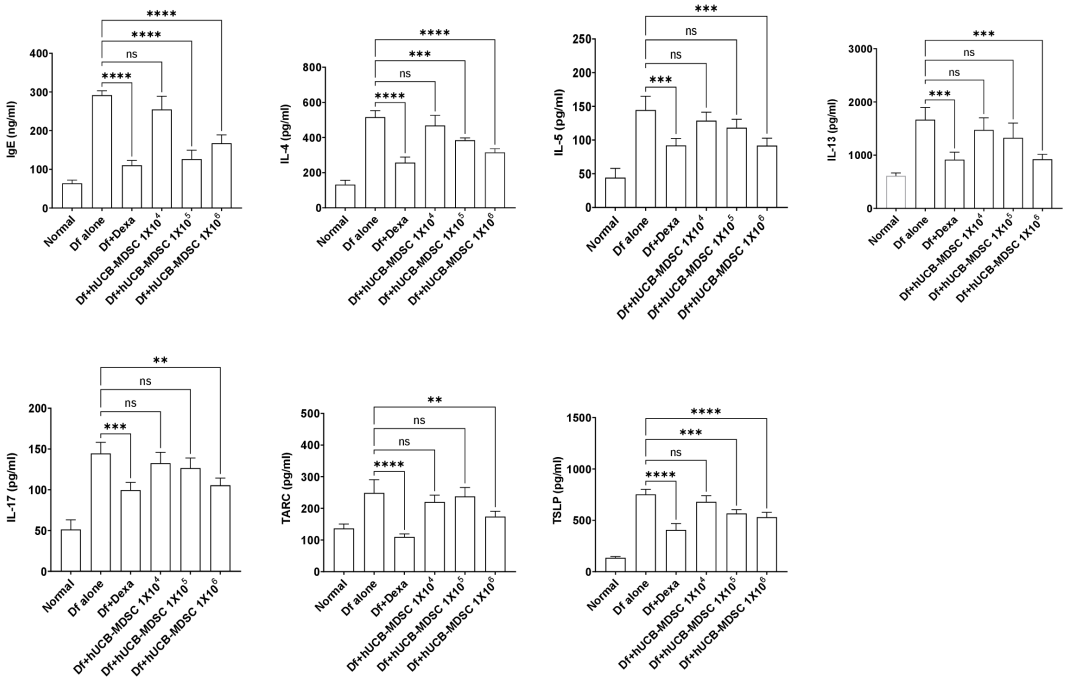


FIGURE 6
Effects of human umbilical cord blood-myeloid-derived suppressor cell therapy on the levels of IgE and inflammatory mediators in the serum of *Dermatophagoides farina* (Df)-induced NC/Nga mice. IgE, IL-4, IL-5, IL-13, IL-17, TARC, and TSLP levels were measured on day 7 after the final administration of hUCB-MDSCs. Data are presented as mean ± standard error of the mean of five mice per group in a representative experiment of two experiments. $^{**}p < 0.01$, $^{***}p < 0.001$, and $^{****}p < 0.0001$; ns, not significant.

cells (MSCs) and MDSCs (28, 29). Our MDSCs produced at a large scale from hUCB-CD34$^+$ cells suppressed the pathological features of GVHD in preclinical models by modulating T-cell-mediated immunity (23, 24).

In our mouse model, the lesioned skin exhibited erythema, scaling, thickening, and inflammatory cell infiltration into the dermis and epidermis, similar to human AD symptoms (2, 3). Inflammatory skin diseases are accompanied by epidermal hyperproliferation and inflammatory cell infiltration into the dermis and epidermis. Here, hUCB-MDSCs alleviated the overall skin lesion severity in a dose-dependent manner; however, a low dose of hUCB-MDSCs ($1 \times 10^4$ cells) was not effective. Furthermore, hUCB-MDSCs ($1 \times 10^5$ and $1 \times 10^6$ cells) reduced the epidermal thickness of skin lesions and attenuated the infiltration of inflammatory cells.

Similar to the findings of a previous study (23), viable hUCB-MDSCs administered to AD-induced mice were found in the spleen, skin, lungs, and LNs. The lungs are the most common site of invasion for intravenously injected cells, which also migrate to the spleen and lymph nodes (30–34). Therefore, hUCB-MDSCs may have infiltrated the lungs, spleens, and LNs of normal healthy mice. However, infiltration into the skin was found only in AD mice, suggesting that hUCB-MDSCs selectively infiltrated sites of inflammation (35, 36). In the future, research on chemotaxis related to these movements should be conducted.

AD is associated with skin fibrosis and barrier disruption of the stratum spinosum, stratum basale, and stratum granulosum because of epidermal protein function loss (27, 37). Skin barrier dysfunction is associated with AD-related proinflammatory mediator production in mice and patients with AD (38, 39). The levels of various AD-related proinflammatory cytokines increase in patients with AD, leading to defects in skin barrier functions by decreasing epidermal differentiation marker levels (40, 41). The skin barrier integrity of epidermal structures can be disrupted in the stratum basale and stratum spinosum of AD-lesional skin, along with decreased levels of CK10 and CK14, markers for keratinocyte differentiation (42, 43). Skin fibrosis probably results from abnormal repair in response to skin damage, which may be caused by allergic inflammatory responses (44). Skin barrier normalization is related to wound healing (45), and MDSCs are involved in wound healing. Here, hUCB-MDSCs ($1 \times 10^5$ and/or $1 \times 10^6$ cells) restored skin barrier function and improved skin fibrosis, suggesting that the anti-inflammatory effects and wound-healing capacities of hUCB-MDSC therapy are the mechanisms responsible for recovery from skin barrier impairment and dysfunction and skin fibrosis in Df-induced AD-NC/Nga mice.

The activation and overproduction of proinflammatory cytokines are observed in the serum of patients with AD, similar to that in the serum of Df-induced AD mice (46–48), and they are associated with major immunological and cellular mechanisms in AD. Consistently, we observed that the IgE and Th2- and Th17-mediated cytokine levels were increased in the serum of Df-induced NC/Nga mice; however, hUCB-MDSC administration ($1 \times 10^5$ and/or $1 \times 10^6$ cells) considerably suppressed their production. TSLP, TARC, and Th2-specific chemokines in the serum of mice and patients with AD are involved in Th2-mediated immune responses

10.3389/fimmu.2023.1263646

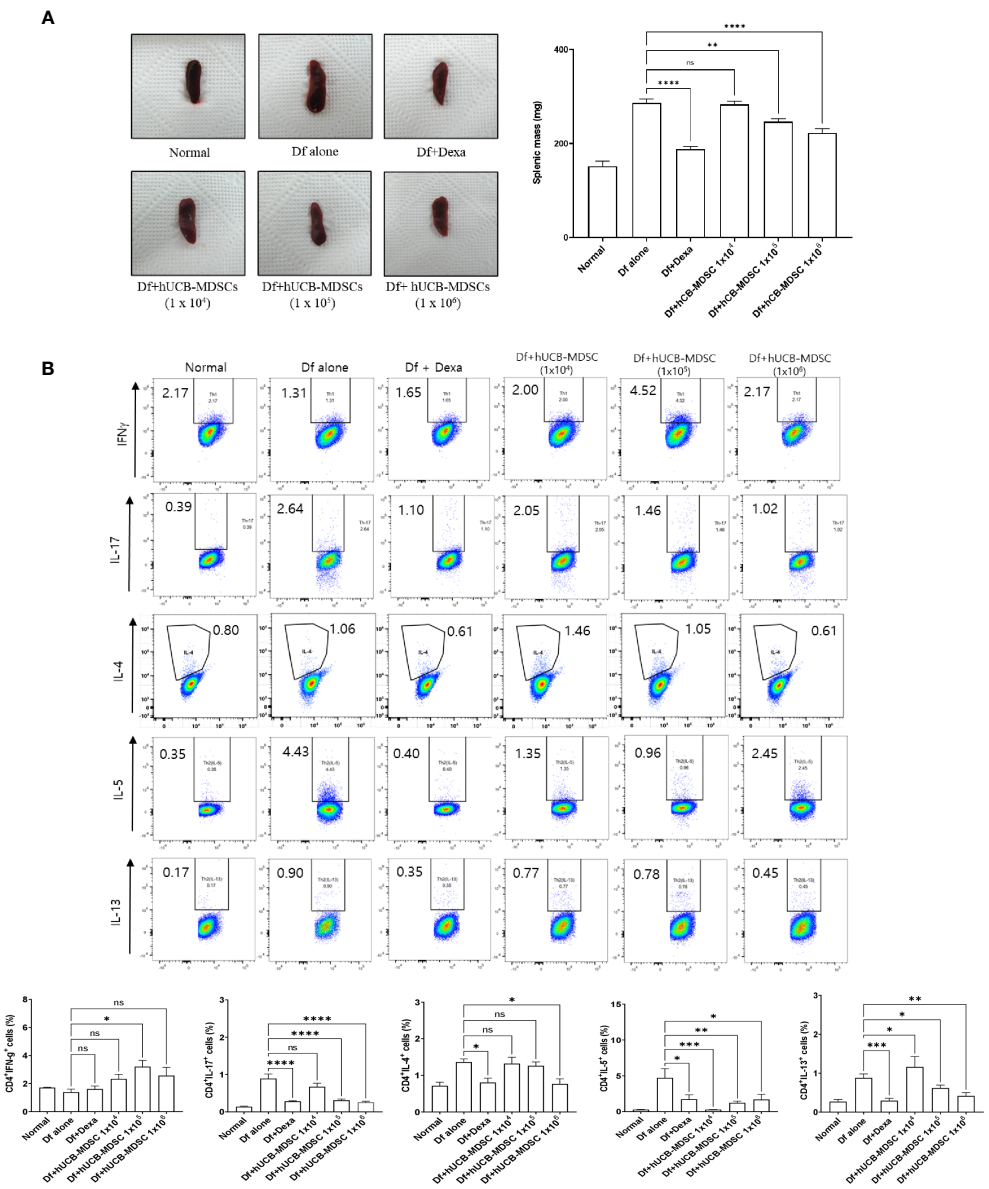


FIGURE 7
Effects of human umbilical cord blood (hUCB)-myeloid-derived suppressor cell (MDSC) therapy on the regulation of differentiation to $CD4^+$ T cell subsets. **(A)** Representative photograph of the spleen collected from untreated and treated NC/Nga mice; mice were treated with *Dermatophagoides farinae* (Df) alone, hUCB-MDSCs ($1 \times 10^4$ cells), hUCB-MDSCs ($1 \times 10^5$ cells), hUCB-MDSCs ($1 \times 10^6$ cells), or dexamethasone (Dexa) (2 mg/kg). Spleen weights of mice sacrificed on day 7 after the final administration of hUCB-MDSCs. **(B)** Flow cytometric analysis illustrating T-helper (Th)1 cells (cluster of differentiation [CD]$4^+$ interferon-$\gamma^+$), Th2 cells ($CD4^+$ interleukin [IL]-$4^+$, $CD4^+$ IL-$5^+$, and $CD4^+$ IL-$13^+$), and Th17 cells ($CD4^+$ IL-$17^+$) in the splenocytes of NC/Nga mice. The data are presented as mean ± standard error of the mean of five mice per group in a representative experiment of two experiments. *$p < 0.05$, **$p < 0.01$, ***$p < 0.001$, and ****$p < 0.0001$; ns, not significant.

while playing important roles in AD (49–51). TSLP is involved in inflammatory cell (mast cells and eosinophils) proliferation and activation and induces IgE (52). Our results showed that hUCB-MDSCs ($1 \times 10^5$ and/or $1 \times 10^6$ cells) significantly inhibited serum TSLP and TARC production. Therefore, hUCB-MDSCs can alleviate clinical symptoms and T-cell-mediated immune responses by suppressing the production of IgE, several pro-inflammatory cytokines, and chemokines involved in AD.

MDSCs regulate immune cell functions and inflammatory mediators in various autoimmune diseases. Our experiments showed that hUCB-MDSCs inhibit $CD4^+$ and $CD8^+$ T cell proliferation and Th2 and Th17 differentiation, consistent with the findings of a previous study (12). Additionally, hUCB-MDSCs attenuated Df-induced splenomegaly. These findings suggest that hUCB-MDSC therapy exerts an anti-inflammatory effect by altering the T cell proliferation rate and Th2 and Th17 cell ratio. However, the expression of IFN-γ in the spleen and LN cells was increased by hUCB-MDSCs. IFN-γ is known to exhibit therapeutic effects in AD (53, 54). Moreover, IFN-γ has the potential to enhance the immunomodulatory capabilities of MDSCs (55, 56). However, it is crucial to note that mouse-derived IFN-γ cannot bind to the human IFN-γ receptor, rendering it impossible for mouse IFN-γ to

10.3389/fimmu.2023.1263646

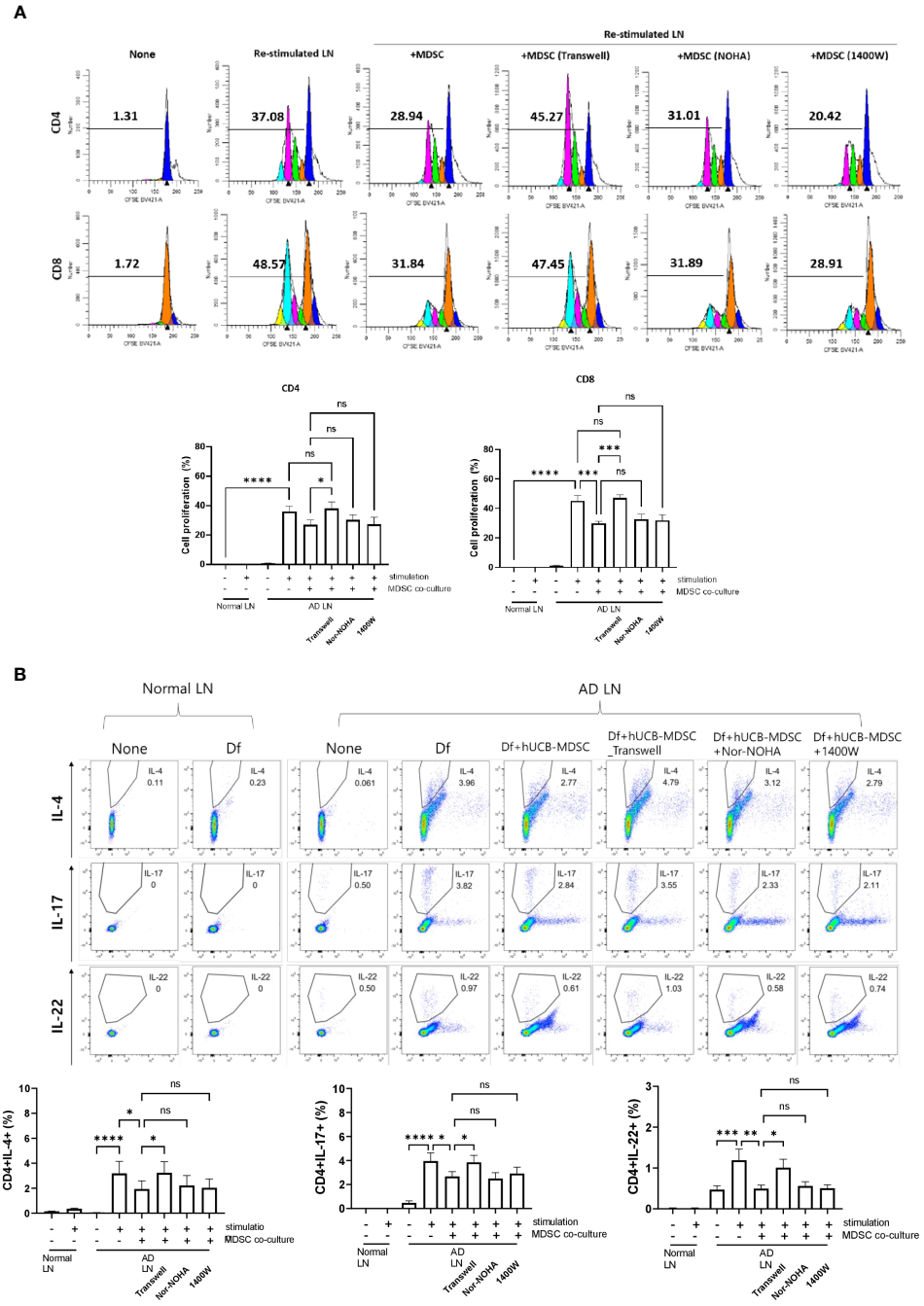


FIGURE 8
Mechanism of atopic dermatitis (AD)-associated immune cell regulation between human umbilical cord blood (hUCB)-myeloid-derived suppressor cells (MDSCs) and T cells in the AD mouse model. Lymph node (LN) cells from Nc/Nga mice were stimulated with treatments for 4 days *in vitro*. **(A)** Representative experimental data demonstrating the loss of the ability of hUCB-MDSCs to suppress T cell stimulation in the Transwell assay. The intensity of CFSE-labeled T cells was acquired using flow cytometry and further analyzed using ModFit LT 4.0 software. **(B)** Flow cytometric analysis of T-helper (Th)2 cells (cluster of differentiation [CD]4$^+$ interleukin [IL]-4$^+$), Th17 cells (CD4$^+$ IL-17$^+$), and Th22 cells (CD4$^+$ IL-22$^+$). Data are presented as mean ± standard error of the mean of three to nine mice per group. *$p < 0.05$, **$p < 0.01$, ***$p < 0.001$ and ****$p < 0.0001$; ns, not significant.

affect human MDSCs (57). Therefore, further studies are necessary to elucidate the role of IFN-γ induced by hUCB-MDSCs in AD mice.

The *in vitro* Df restimulation experiment indicated the important role of interactions between hUCB-MDSCs and immune cells, and not the secreted factors arginase-1 and iNOS, in immunomodulatory actions. Further research on these immunomodulatory mechanisms is needed.

Numerous systemic immunomodulatory agents are used to treat AD. However, the current treatments for severe AD are not always effective. Additionally, basic and preclinical studies using AD models have demonstrated the immunomodulatory and anti-

inflammatory effects of MSCs derived from hUCB, bone marrow, and adipose tissues (58). MDSCs developed here were 4–8 times smaller than MSCs, which is advantageous for dosage administration and is potentially safer than MSCs. Moreover, hUCB-MDSCs were intravenously injected, and the medium dose ($1 \times 10^5$ cells) of hUCB-MDSCs considerably reduced AD allergic progression in mice as effectively as the high dose ($1 \times 10^6$ cells). These findings suggest that MDSCs, at lower doses, can effectively treat AD.

Our study demonstrated that hUCB-MDSCs alleviated AD-like clinical symptoms by regulating interactions between several upstream and downstream immunological factors involved in progressive AD pathology. hUCB-MDSC therapy exerts immunomodulatory and anti-inflammatory effects with reduced toxicity, suppresses adverse effects, and promotes skin regeneration; therefore, it may be a novel cell therapy for AD.

## Data availability statement

The original contributions presented in the study are included in the article/Supplementary Material, further inquiries can be directed to the corresponding author.

## Ethics statement

The studies involving humans were approved by Korea National Institute for bioethics policy. The studies were conducted in accordance with the local legislation and institutional requirements. The participants provided their written informed consent to participate in this study. The animal study was approved by The Animal Care and Use Committee of the Research Institute at the Catholic University of Korea. The study was conducted in accordance with the local legislation and institutional requirements.

## Author contributions

C-HK: Conceptualization, Investigation, Writing – original draft. S-MH: Conceptualization, Investigation, Writing – original draft, Writing – review & editing. SK: Conceptualization, Writing – original draft, Writing – review & editing. JY: Investigation, Writing – original draft. S-HJ: Investigation, Writing – original draft. CB: Conceptualization, Writing – original draft. JL: Conceptualization, Writing – original draft. T-GK: Conceptualization, Project administration, Supervision, Writing – original draft, Writing – review & editing.

## Funding

The author(s) declare that no financial support was received for the research, authorship, and/or publication of this article.

## Acknowledgments

We express our gratitude to the Catholic Hematopoietic Stem Cell Bank, College of Medicine, The Catholic University of Korea.

## Conflict of interest

Authors C-HK, S-MH, SK, JY, S-HJ and T-GK were employed by the company ViGenCell Inc.

The remaining authors declare that the research was conducted in the absence of any commercial or financial relationships that could be construed as a potential conflict of interest.

## Publisher's note



## Supplementary material

The Supplementary Material for this article can be found online at: https://www.frontiersin.org/articles/10.3389/fimmu.2023.1263646/full#supplementary-material

## References

1. Sroka-Tomaszewska J, Trzeciak M. Molecular mechanisms of atopic dermatitis pathogenesis. *Int J Mol Sci* (2021) 22:4130. doi: 10.3390/ijms22084130

2. Kim J, Kim BE, Leung DYM. Pathophysiology of atopic dermatitis: Clinical implications. *Allergy Asthma Proc* (2019) 40:84–92. doi: 10.2500/aap.2019.40.4202

3. Nakajima S, Tie D, Nomura T, Kabashima K. Novel pathogenesis of atopic dermatitis from the view of cytokines in mice and humans. *Cytokine* (2021) 148:155664. doi: 10.1016/j.cyto.2021.155664

4. Patrick GJ, Archer NK, Miller LS. Which way do we go? Complex interactions in atopic dermatitis pathogenesis. *J Invest Dermatol* (2021) 141:274–84. doi: 10.1016/j.jid.2020.07.006

5. Brandt EB, Sivaprasad U. Th2 cytokines and atopic dermatitis. *J Clin Cell Immunol* (2011) 2:110. doi: 10.4172/2155-9899.1000110

6. Ratchataswan T, Banzon TM, Thyssen JP, Weidinger S, Guttman-Yassky E, Phipatanakul W. Biologics for treatment of atopic dermatitis: Current status and future prospect. *J Allergy Clin Immunol Pract* (2021) 9:1053–65. doi: 10.1016/j.jaip.2020.11.034

7. Puar N, Chovatiya R, Paller AS. New treatments in atopic dermatitis. *Ann Allergy Asthma Immunol* (2021) 126:21–31. doi: 10.1016/j.anai.2020.08.016

8. Bieber T. Atopic dermatitis: An expanding therapeutic pipeline for a complex disease. *Nat Rev Drug Discovery* (2022) 21:21–40. doi: 10.1038/s41573-021-00266-6

9. Gabrilovich DI, Ostrand-Rosenberg S, Bronte V. Coordinated regulation of myeloid cells by tumours. *Nat Rev Immunol* (2012) 12:253–68. doi: 10.1038/nri3175

10. Kong YY, Fuchsberger M, Xiang SD, Apostolopoulos V, Plebanski M. Myeloid derived suppressor cells and their role in diseases. *Curr Med Chem* (2013) 20:1437–44. doi: 10.2174/0929867311320110006

11. Gabrilovich DI, Nagaraj S. Myeloid-derived suppressor cells as regulators of the immune system. *Nat Rev Immunol* (2009) 9:162–74. doi: 10.1038/nri2506

12. Papafragkos I, Markaki E, Kalpadakis C, Verginis P. Decoding the myeloid-derived suppressor cells in lymphoid Malignancies. *J Clin Med* (2021) 10:3462. doi: 10.3390/jcm10163462

13. Tumino N, Di Pace AL, Besi F, Quatrini L, Vacca P, Moretta L. Interaction between MDSC and NK cells in solid and hematological Malignancies: Impact on HSCT. *Front Immunol* (2021) 12:638841. doi: 10.3389/fimmu.2021.638841

14. Haist M, Stege H, Grabbe S, Bros M. The functional crosstalk between myeloid-derived suppressor cells and regulatory T cells within the immunosuppressive tumor microenvironment. *Cancers (Basel)* (2021) 13:210. doi: 10.3390/cancers13020210

15. Munansangu BSM, Kenyon C, Walzl G, Loxton AG, Kotze LA, du Plessis N. Immunometabolism of myeloid-derived suppressor cells: Implications for *Mycobacterium tuberculosis* infection and insights from tumor biology. *Int J Mol Sci* (2022) 23:3512. doi: 10.3390/ijms23073512

16. Song C, Yuan Y, Wang XM, Li D, Zhang GM, Huang B, et al. Passive transfer of tumour-derived MDSCs inhibits asthma-related airway inflammation. *Scand J Immunol* (2014) 79:98–104. doi: 10.1111/sji.12140

17. Park MJ, Lee SH, Kim EK, Lee EJ, Baek JA, Park SH, et al. Interleukin-10 produced by myeloid-derived suppressor cells is critical for the induction of Tregs and attenuation of rheumatoid inflammation in mice. *Sci Rep* (2018) 8:3753. doi: 10.1038/s41598-018-21856-2

18. Kim CH, Yoo JK, Jeon SH, Lim CY, Lee JH, Koo DB, et al. Anti-psoriatic effect of myeloid-derived suppressor cells on imiquimod-induced skin inflammation in mice. *Scand J Immunol* (2019) 89:e12742. doi: 10.1111/sji.12742

19. Sanchez-Pino MD, Dean MJ, Ochoa AC. Myeloid-derived suppressor cells (MDSC): When good intentions go awry. *Cell Immunol* (2021) 362:104302. doi: 10.1016/j.cellimm.2021.104302

20. Rani M, Zhang Q, Schwacha MG. Gamma Delta T cells regulate wound myeloid cell activity after burn. *Shock* (2014) 42:133–41. doi: 10.1097/SHK.0000000000000176

21. Mahdipour E, Charnock JC, Mace KA. Hoxa3 promotes the differentiation of hematopoietic progenitor cells into proangiogenic Gr-1+CD11b+ myeloid cells. *Blood* (2011) 117:815–26. doi: 10.1182/blood-2009-12-259549

22. Man MQ, Wakefield JS, Mauro TM, Elias PM. Role of nitric oxide in regulating epidermal permeability barrier function. *Exp Dermatol* (2022) 31:290–8. doi: 10.1111/exd.14470

23. Lim JY, Ryu DB, Park MY, Lee SE, Park G, Kim TG, et al. Ex vivo generated human cord blood myeloid-derived suppressor cells attenuate murine chronic graft-versus-host diseases. *Biol Blood Marrow Transplant* (2018) 24:2381–96. doi: 10.1016/j.bbmt.2018.07.004

24. Park MY, Lim BG, Kim SY, Sohn HJ, Kim S, Kim TG. GM-CSF promotes the expansion and differentiation of cord blood myeloid-derived suppressor cells, which attenuate xenogeneic graft-vs.-host disease. *Front Immunol* (2019) 10:183. doi: 10.3389/fimmu.2019.00183

25. Kim CH, Cheong KA, Park CD, Lee AY. Therapeutic effects of combination using glucosamine plus tacrolimus (FK-506) on the development of atopic dermatitis-like skin lesions in NC/Nga mice. *Scand J Immunol* (2012) 75:471–8. doi: 10.1111/j.1365-3083.2011.02659.x

26. Suto H, Matsuda H, Mitsuishi K, Hira K, Uchida T, Unno T, et al. NC/Nga mice: A mouse model for atopic dermatitis. *Int Arch Allergy Immunol* (1999) 120 Suppl 1:70–5. doi: 10.1159/000053599

27. Bieber T, Paller AS, Kabashima K, Feely M, Rueda MJ, Ross Terres JA, et al. Atopic dermatitis: Pathomechanisms and lessons learned from novel systemic therapeutic options. *J Eur Acad Dermatol Venereol* (2022) 36:1432–49. doi: 10.1111/jdv.18225

28. Erices A, Conget P, Minguell JJ. Mesenchymal progenitor cells in human umbilical cord blood. *Br J Haematol* (2000) 109:235–42. doi: 10.1046/j.1365-2141.2000.01986.x

29. Rieber N, Gille C, Köstlin N, Schäfer I, Spring B, Ost M, et al. Neutrophilic myeloid-derived suppressor cells in cord blood modulate innate and adaptive immune responses. *Clin Exp Immunol* (2013) 174:45–52. doi: 10.1111/cei.12143

30. Kurtz A. Mesenchymal stem cell delivery routes and fate. *Int J Stem Cells* (2008) 1:1–7. doi: 10.15283/ijsc.2008.1.1.1

31. Pendharkar AV, Chua JY, Andres RH, Wang N, Gaeta X, Wang H, et al. Biodistribution of neural stem cells after intravascular therapy for hypoxic-ischemia. *Stroke* (2010) 41:2064–70. doi: 10.1161/STROKEAHA.109.575993

32. Rosado-de-Castro PH, Schmidt Fda R, Battistella V, Lopes de Souza SA, Gutfilen B, Goldenberg RC, et al. Biodistribution of bone marrow mononuclear cells after intra-arterial or intravenous transplantation in subacute stroke patients. *Regener Med* (2013) 8:145–55. doi: 10.2217/rme.13.2

33. Fabian C, Naaldijk Y, Leovsky C, Johnson AA, Rudolph L, Jaeger C, et al. Distribution pattern following systemic mesenchymal stem cell injection depends on the age of the recipient and neuronal health. *Stem Cell Res Ther* (2017) 8:85. doi: 10.1186/s13287-017-0533-2

34. Casiraghi F, Azzollini N, Cassis P, Imberti B, Morigi M, Cugini D, et al. Pretransplant infusion of mesenchymal stem cells prolongs the survival of a semiallogeneic heart transplant through the generation of regulatory T cells. *J Immunol* (2008) 181:3933–46. doi: 10.4049/jimmunol.181.6.3933

35. Cripps JG, Gorham JD. MdSc. MDSC in autoimmunity. *Int Immunopharmacol* (2011) 11:789–93. doi: 10.1016/j.intimp.2011.01.026

36. Schwacha MG, Scroggins SR, Montgomery RK, Nicholson SE, Cap AP. Burn injury is associated with an infiltration of the wound site with myeloid-derived suppressor cells. *Cell Immunol* (2019) 338:21–6. doi: 10.1016/j.cellimm.2019.03.001

37. Lefèvre-Utile A, Braun C, Haftek M, Aubin F. Five functional aspects of the epidermal barrier. *Int J Mol Sci* (2021) 22:11676. doi: 10.3390/ijms222111676

38. Aioi A, Tonogaito H, Suto H, Hamada K, Ra CR, Ogawa H, et al. Impairment of skin barrier function in NC/Nga Tnd mice as a possible model for atopic dermatitis. *Br J Dermatol* (2001) 144:12–8. doi: 10.1046/j.1365-2133.2001.03946.x

39. Kubo A, Nagao K, Amagai M. Epidermal barrier dysfunction and cutaneous sensitization in atopic diseases. *J Clin Invest* (2012) 122:440–7. doi: 10.1172/JCI57416

40. Peng W, Novak N. Pathogenesis of atopic dermatitis. *Clin Exp Allergy* (2015) 45:566–74. doi: 10.1111/cea.12495

41. Bäsler K, Bergmann S, Heisig M, Naegel A, Zorn-Kruppa M, Brandner JM. The role of tight junctions in skin barrier function and dermal absorption. *J Control Release* (2016) 242:105–18. doi: 10.1016/j.jconrel.2016.08.007

42. Totsuka A, Omori-Miyake M, Kawashima M, Yagi J, Tsunemi Y. Expression of keratin 1, keratin 10, desmoglein 1 and desmocollin 1 in the epidermis: Possible downregulation by interleukin-4 and interleukin-13 in atopic dermatitis. *Eur J Dermatol* (2017) 27:247–53. doi: 10.1684/ejd.2017.2985

43. Park G, Moon BC, Choi G, Lim HS. Cera flava alleviates atopic dermatitis by activating skin barrier function via immune regulation. *Int J Mol Sci* (2021) 22:7531. doi: 10.3390/ijms22147531

44. Meyer M, Müller AK, Yang J, Ŝulcová J, Werner S. The role of chronic inflammation in cutaneous fibrosis: Fibroblast growth factor receptor deficiency in keratinocytes as an example. *J Investig Dermatol Symp Proc* (2011) 15:48–52. doi: 10.1038/jidsymp.2011.1

45. Wikramanayake TC, Stojadinovic O, Tomic-Canic M. Epidermal differentiation in barrier maintenance and wound healing. *Adv Wound Care (New Rochelle)* (2014) 3:272–80. doi: 10.1089/wound.2013.0503

46. Grewe M, Bruijnzeel-Koomen CA, Schöpf E, Thepen T, Langeveld-Wildschut AG, Ruzicka T, et al. A role for Th1 and Th2 cells in the immunopathogenesis of atopic dermatitis. *Immunol Today* (1998) 19:359–61. doi: 10.1016/s0167-5699(98)01285-7

47. Nograles KE, Zaba LC, Shemer A, Fuentes-Duculan J, Cardinale I, Kikuchi T, et al. IL-22-producing "T22" T cells account for upregulated IL-22 in atopic dermatitis despite reduced IL-17-producing TH17 T cells. *J Allergy Clin Immunol* (2009) 123:1244–52.e2. doi: 10.1016/j.jaci.2009.03.041

48. Yamamoto M, Haruna T, Ueda C, Asano Y, Takahashi H, Iduhara M, et al. Contribution of itch-associated scratch behavior to the development of skin lesions in *Dermatophagoides farinae*-induced dermatitis model in NC/Nga mice. *Arch Dermatol Res* (2009) 301:739–46. doi: 10.1007/s00403-008-0912-8

49. Liu YJ. Thymic stromal lymphopoietin: Master switch for allergic inflammation. *J Exp Med* (2006) 203:269–73. doi: 10.1084/jem.20051745

50. Shimada Y, Takehara K, Sato S. Both Th2 and Th1 chemokines (TARC/CCL17, MDC/CCL22, and Mig/CXCL9) are elevated in sera from patients with atopic dermatitis. *J Dermatol Sci* (2004) 34:201–8. doi: 10.1016/j.jdermsci.2004.01.001

51. Kim SH, Seong GS, Choung SY. Fermented *Morinda citrifolia* (Noni) alleviates DNCB-induced atopic dermatitis in NC/Nga mice through modulating immune balance and skin barrier function. *Nutrients* (2020) 12:249. doi: 10.3390/nu12010249

52. Comeau MR, Ziegler SF. The influence of TSLP on the allergic response. *Mucosal Immunol* (2010) 3:138–47. doi: 10.1038/mi.2009.134

53. Jang IG, Yang JK, Lee HJ, Yi JY, Kim HO, Kim CW, et al. Clinical improvement and immunohistochemical findings in severe atopic dermatitis treated with interferon gamma. *J Am Acad Dermatol* (2000) 42:1033–40. doi: 10.1067/mjd.2000.104793

54. Brar K, Leung DY. Recent considerations in the use of recombinant interferon gamma for biological therapy of atopic dermatitis. *Expert Opin Biol Ther* (2016) 16:507–14. doi: 10.1517/14712598.2016.1135898

55. Mojic M, Takeda K, Hayakawa Y. The dark side of IFN-γ: Its role in promoting cancer immunoevasion. *Int J Mol Sci* (2017) 19:89. doi: 10.3390/ijms19010089

56. Yang F, Li Y, Zou W, Xu Y, Wang H, Wang W, et al. Adoptive transfer of IFN-γ-induced M-MDSCs promotes immune tolerance to allografts through iNOS pathway. *Inflammation Res* (2019) 68:545–55. doi: 10.1007/s00011-019-01237-9

57. Hess NJ, Brown ME, Capitini CM. GVHD pathogenesis, prevention and treatment: Lessons from humanized mouse transplant models. *Front Immunol* (2021) 12:723544. doi: 10.3389/fimmu.2021.723544

58. Najera J, Hao J. Recent advance in mesenchymal stem cells therapy for atopic dermatitis. *J Cell Biochem* (2023) 124:181–7. doi: 10.1002/jcb.30365

frontiers | Frontiers in Immunology

TYPE Original Research
PUBLISHED 11 January 2024
DOI 10.3389/fimmu.2023.1289788



OPEN ACCESS

EDITED BY
Zhenghua Zhang,
Fudan University, China

REVIEWED BY
Krzysztof Guzik,
Jagiellonian University, Poland
Mark Woodford,
Upstate Medical University, United States

*CORRESPONDENCE
Hakim Ben Abdallah
hba@clin.au.dk

RECEIVED 06 September 2023
ACCEPTED 11 December 2023
PUBLISHED 11 January 2024

CITATION
Ben Abdallah H, Bregnhøj A, Ghatnekar G, Iversen L and Johansen C (2024) Heat shock protein 90 inhibition attenuates inflammation in models of atopic dermatitis: a novel mechanism of action.
*Front. Immunol.* 14:1289788.
doi: 10.3389/fimmu.2023.1289788



# Heat shock protein 90 inhibition attenuates inflammation in models of atopic dermatitis: a novel mechanism of action

Hakim Ben Abdallah [1]*, Anne Bregnhøj [1], Gautam Ghatnekar [2], Lars Iversen [1] and Claus Johansen [1]

[1]Department of Dermatology and Venereology, Aarhus University Hospital, Aarhus, Denmark, [2]Regranion, Mount Pleasant, SC, United States

**Background:** Heat shock protein 90 (HSP90) is an important chaperone supporting the function of many proinflammatory client proteins. Recent studies indicate HSP90 inhibition may be a novel mechanism of action for inflammatory skin diseases; however, this has not been explored in atopic dermatitis (AD).

**Objectives:** Our study aimed to investigate HSP90 as a novel target to treat AD.

**Methods:** Experimental models of AD were used including primary human keratinocytes stimulated with cytokines (TNF/IFNγ or TNF/IL-4) and a mouse model established by MC903 applications.

**Results:** In primary human keratinocytes using RT-qPCR, the HSP90 inhibitor RGRN-305 strongly suppressed the gene expression of Th1- (*TNF*, *IL1B*, *IL6*) and Th2-associated (*CCL17*, *CCL22*, *TSLP)* cytokines and chemokines related to AD. We next demonstrated that topical and oral RGRN-305 robustly suppressed MC903-induced AD-like inflammation in mice by reducing clinical signs of dermatitis (oedema and erythema) and immune cell infiltration into the skin (T cells, neutrophils, mast cells). Interestingly, topical RGRN-305 exhibited similar or slightly inferior efficacy but less weight loss compared with topical dexamethasone. Furthermore, RNA sequencing of skin biopsies revealed that RGRN-305 attenuated MC903-induced transcriptome alterations, suppressing genes implicated in inflammation including AD-associated cytokines (*Il1b, Il4, Il6, Il13*), which was confirmed by RT-qPCR. Lastly, we discovered using Western blot that RGRN-305 disrupted JAK-STAT signaling by suppressing the activity of STAT3 and STAT6 in primary human keratinocytes, which was consistent with enrichment analyses from the mouse model.

**Conclusion:** HSP90 inhibition by RGRN-305 robustly suppressed inflammation in experimental models mimicking AD, proving that HSP90 inhibition may be a novel mechanism of action in treating AD.

KEYWORDS

Hsp90, atopic dermatitis, RGRN-305, small molecule, keratinocytes, MC903 mouse model

# Introduction

Atopic dermatitis (AD) is a common inflammatory skin disorder characterised by erythematous, scaly and itchy skin that imposes a high disease burden on patients and the healthcare system, affecting up to 20% of children and up to 5% of adults (1–3). AD is associated with atopic comorbidities (e.g., food allergy, allergic rhinitis and asthma), but other comorbidities have been reported including cardiovascular and neuropsychiatric disorders (4, 5). Although the multifactorial pathophysiology remains to be fully explored, the mechanisms underlying AD implicate a complex interaction of components involving skin barrier dysfunction, immune dysregulation, altered skin microbiome and genetic predisposition (6). Recent molecular insights into the disease mechanisms have revealed significant pathways and novel targets, enabling the vast ongoing drug development and the recent approval of therapeutics targeting IL-4, IL-13 and JAK1/2 (7). Nonetheless, some groups of patients do not achieve satisfactory long-term control or tolerate current treatments, highlighting the pressing need for novel treatments.

Heat shock protein 90 (HSP90) is a common chaperone that folds and supports the activity of client proteins including proteins involved in inflammation. Hence, HSP90 inhibition may be a wide-ranging approach targeting different inflammatory pathways, representing a novel mechanism of action for treating inflammatory skin diseases. In accordance, HSP90 inhibition demonstrated significant alleviation of skin inflammation in preclinical studies of psoriasis, irritative contact dermatitis and epidermolysis bullosa acquisita (8–11). The anti-inflammatory effects of HSP90 inhibition have also been demonstrated in several experimental models beyond dermatology including rheumatoid arthritis, systemic sclerosis, systemic lupus erythematous, encephalomyelitis and colitis (12–17). This suggests that HSP90 plays an important role in modulating inflammation. Recently, two recent proof-of-concept studies revealed that orally administered HSP90 inhibitor (RGRN-305) led to marked improvements in psoriasis (open-label study; n=13) and hidradenitis suppurativa (randomised controlled trial; n=15) (18, 19). Another recent study revealed that HSP90 serum levels were 2.79-fold increased ($P > 0.001$) in AD patients (n = 27) compared with healthy controls (n = 70) and correlated with disease severity (20). Yet, to the best of our knowledge, no studies have explored the effects of HSP90 inhibition in atopic dermatitis. Therefore, our study aimed to investigate HSP90 as a novel target for treating atopic dermatitis using experimental models.

# Materials and methods

## HSP90 inhibitor

Regranion (Mount Pleasant, SC, USA) kindly provided the HSP90 inhibitor RGRN-305 (MW = 443 g/mol), formerly named Debio 0932/CUDC-305, which inhibits HSP90α/β (IC50 ~ 0.1 μM).

## Cell culture and experiments

Primary normal human epidermal keratinocytes (NHEKs) were isolated from nine healthy donors as described previously (21). The keratinocytes were plated in 6-well plates and cultured in keratinocyte SFM (Gibco, ThermoFisher Scientific, Waltham, MA, USA) supplemented with growth factors and 5 μg/ml Gentamicin (Gibco) at 37°C in a humidified incubator containing 5% $CO_2$ until 60-70% confluency. Subsequently, the keratinocytes were starved for 24 hours in keratinocyte SFM medium without growth factors before the initiation of experiments. After 2 hours of preincubation with vehicle (0.2% ethanol diluted in water), RGRN-305 (5 μM) or dexamethasone (0.1 μM; Sigma-Aldrich, Burlington, MA, USA), the keratinocytes were stimulated with TNF (10 ng/mL; PeproTech, London, UK) in combination with IFNγ (10 ng/mL; PeproTech) or IL-4 (50 ng/mL; PeproTech) for up to 24 hours to induce an AD-like phenotype (22–24). The used concentration of RGRN-305 was based on previous concentration studies demonstrating anti-inflammatory properties and low toxicity in stimulated NHEKs (8, 10).

## Human samples

Four-millimetres punch biopsies from six AD patients were collected from lesional and non-lesional skin and stored in liquid nitrogen until RNA isolation.

## RNA isolation from NHEKs

Keratinocytes were washed with phosphate-buffered saline (PBS; Gibco) followed by RNA extraction using SV 96 Total RNA Isolation System (Promega, Madison, WI, USA) per the manufacturers' instructions. NanoDrop 2000 Spectrophotometer (ThermoFisher) was used to determine the RNA concentration and purity.

## RNA isolation from punch biopsies

Punch biopsies were stored in 750 µL RNAlater-ICE (ThermoFisher) at -80°C for 20 minutes and overnight at -20°C. Then, the biopsies were added to 175 µL SV RNA lysis buffer with β-mercaptoethanol (SV Total RNA Isolation System; Promega) followed by homogenization using TissueLyser (Qiagen, Hilden, Germany). The remaining steps including RNA purification and DNase treatment were conducted following the manufacturer's instructions.

## Reverse transcription-quantitative PCR

cDNA was generated using total RNA, TaqMan Reverse Transcription Reagents with random hexamers (ThermoFisher) and Peltier Thermal Cycler-200 (MJ Research Inc, Waltham, MA, USA) following the manufacturer's instructions. Real-time PCR was carried out with 20 ng cDNA per 20 µL reaction in StepOnePlus Real-Time PCR system (ThemoFisher) using TaqMan Universal PCR Master Mix, primers and probes (ThermoFisher) for *TNF* (Hs00174128_m1), *IL1B* (Hs01555410_m1), *IL6* (Hs00174131_m1), *TSLP* (Hs00263639_m1), *CCL17* (Hs00171074_m1), *CCL22* (Hs01574247_m1), *HSPA1A* (Hs00359163_s1), *HSPB1* (Hs00356629_g1), *Il1b* (Mm00434228_m1), *Il4* (Mm00445259_m1), *Il6* (Mm00446190_m1), *Il13* (Mm00434204_m1), *RPLP0* (Hs99999902_m1) and *Gapdh* (Mm99999915_m1). Three technical replicates for each sample underwent real-time PCR; 2 minutes at 50°C and 10 minutes at 95°C followed by 40 cycles of 15 seconds at 95°C and 1 minute at 60°C. The standard curve method with StepOne Software v2.1 and reference genes (*RPLP0* and *Gapdh)* were used to obtain normalised relative expression levels of target genes (25).

## Protein isolation from NHEKs

PBS-washed keratinocytes were added to cell lysis buffer with cOmplete Protease Inhibitor Cocktail and phenylmethylsulphonyl fluoride (Sigma-Aldrich). The lysate was centrifuged at 13,000 g for 3 minutes followed by collection of the supernatant containing the protein extract. The protein concentration was determined by Bradford Protein Assay.

## Western blot

A total of 20 µg protein extract for each sample was loaded on 10% mini-PROTEAN TGX PreCast Gel (Bio-Rad, Hercules, CA, USA) and separated by gel electrophoresis using Mini Trans-Blot Cell (Bio-Rad). The subsequent protein blotting onto nitrocellulose membranes was performed with Trans-Blot Turbo Transfer System (Bio-Rad). Membranes were incubated overnight at 4°C with the following primary antibodies from Cell Signaling Technology Danvers, MA, USA (catalog#): P-STAT1 (#9167), P-STAT3 (#9145) P-p65 (#3033), and P-STAT6 (#56554). After washing, the membranes were incubated with HRP-conjugated anti-rabbit IgG antibody (Cell Signaling Technology; catalog#7074) at room temperature for 1 hour. Protein bands were detected with an enhanced chemiluminescence (ECL) reaction using Clarity Western ECL Substrate (Bio-Rad) and digitally imaged with C-DiGit Blot Scanner (LI-COR, Lincoln, NE, USA). To normalize the protein expression to β-actin levels, the membranes were stripped and reprobed with an anti-β-actin antibody (A1978; Sigma-Aldrich), which was detected by HRP-conjugated anti-mouse IgG (p0447; Dako, Glostrup, Denmark). Relative intensities of bands were quantified by densitometric analyses using Image Studio Digits Version 3.1 (LI-COR).

## Mice

Female Balb/cAnNRj (8 weeks old) mice were purchased from Janvier Labs (Le Genest-Saint-Isle, France), and housed in animal facilities at 19-25°C with 12-hour light/dark cycles and free access to laboratory rodent diet and water. The mice had at least 1 week acclimation period before the experiments started.

## Atopic dermatitis mouse model

Mice were randomly divided to receive: vehicle and drug-vehicle (negative control); MC903 (MedChemExpress, Monmouth Junction, NJ, USA) and drug-vehicle (disease control); MC903 and topical or oral RGRN-305 (RGRN-305 treatment groups); or MC903 and topical dexamethasone (positive control; purchased from Sigma-Aldrich). Four to eight mice were allocated to each group, totalling 76 mice for all experiments.

To induce AD-like skin inflammation, 1 or 2.5 nmol of MC903 in 25 µL absolute ethanol was topically applied once daily to the ventral and dorsal surface of the right ear for six consecutive days. After MC903 challenge, the mice were treated with topical RGRN-305 (1 mg in 25 µL ethanol), oral RGRN-305 (100 mg/kg), topical dexamethasone (20 nmol in 25 µl ethanol), or drug-vehicle (topical ethanol or oral 5% kleptose [HPB, Roquette Pharma, Lestrem, France]). The topical treatments were applied 2 hours post-MC903 challenge, whereas the oral treatments were administered by oral gavage immediately post-MC903 challenge. At the end of the experiment on day 9, clinical photos of the ears were taken and the mice were euthanised by cervical dislocation. Two punch biopsies (4 mm) from the ear were collected for RNA isolation and histological assessment. Ear thickness, the primary clinical endpoint for inflammation, was measured daily with a digital caliper (Mitutoyo Corporation, Kawasaki, Japan), and body weight was measured throughout the study to monitor the

welfare of mice. During the experimental procedures, the mice were anesthetized with 2% isoflurane.

## Histology

Four-millimetres punch biopsies from the ear were fixed in 4% formaldehyde overnight at 4°C, paraffin-embedded, and serially sliced into 4 µm sections subjected to staining procedures. For haematoxylin & eosin (HE) staining, a standard protocol was followed. To detect mast cells, sections were stained with 0.1% toluidine blue solution (Sigma-Aldrich) at pH 2.3 and room temperature for 3 minutes. For immunohistochemical staining, heat-induced antigen retrieval was performed (25 minutes at 97° C) in Tris-EGTA buffer (pH 9), and stained with anti-CD4 antibody (1:1000; EPR19514, Abcam, Cambridge, UK) or anti-Ly6g antibody (1:2000; EPR22909-135, Abcam) for 1 hour at room temperature. The remaining steps for detection were performed with Ultravision Quanto Detection System (ThermoFisher) following the manufacturer's instructions. The sections were counterstained with hematoxylin.

All slides were scanned with 20× objective using the whole slide scanner NanoZoomer 2.0-HT (Hamamatsu Photonics K.K, Hamamatsu City, Japan). Quantitative image analysis was performed in QuPath 0.4.2 using the *Cell Detection* command with default settings followed by a manual review and corrections (26). The number of counted cells was normalised to the length of the section

## RNA sequencing

Paired-end RNA sequencing of total RNA was conducted by Eurofins Genomics Europe Sequencing GmbH (Konstanz, Germany) in accordance with their protocols. To prepare the RNA library, NEBNext Ultra II Directional RNA Library Prep Kit for Illumina was used with 100 ng of total RNA. The mRNA quality was assessed by Fragment Analyzer. Illumina NovaSeq 6000 platform in 2x150 Sequence mode was performed to acquire at least 20 million read pairs. Raw sequence data quality was assessed using FastQC (version 0.12.0). Read alignment to the mouse reference genome (GRCm39 primary assembly) and counting of uniquely aligned unambiguous reads were performed with the R package Subread (version 2.10.3) (27). Regularized logarithm transformation (rlog) performed with the R package DESeq2 (1.36.0) was used for library size correction and variance stabilization (28). The rlog normalized counts were used for principal component analysis (PCA) and heat map analysis (pheatmap 1.0.12). DESeq2 with independent filtering and Wald test enabled were used for the differential gene expression analyses (28). To adjust for multiple comparisons, the p-values were adjusted by setting the false discovery rate (FDR) at 0.05 with the Benjamini and Hochberg procedure. Kyoto Encyclopaedia of Genes and Genomes (KEGG) and Gene Ontology (GO) enrichment analyses were generated with DAVID and validated with ShinyGO 0.76 (29, 30).

## Statistical analysis

The statistical significance threshold was set at $P < 0.05$. Differences between treatment groups in clinical endpoints, mRNA (qPCR) and protein levels (Western blot) were analysed by unpaired t-tests for mice and paired t-tests for keratinocytes. If data were not normally distributed, Mann-Whitney and Wilcoxon signed-rank tests were performed. All statistical analyses were generated with GraphPad Prism 9.0 and R 4.2.0 software.

## Ethical statement

The experiments with NHEKs were approved by the Central Jutland Regional Committee on Health Research Ethics (M-20110027), and informed consent was obtained from the donors. Permission to obtain punch biopsies from patients with atopic dermatitis was approved by Central Jutland Regional Committee on Health Research Ethics (M-20090102).

The animal experiments were approved by The Danish Animal Experiments Inspectorate (2022-15-0201-01267) and carried out in agreement with the Danish Animal Welfare Act for the Care and Use of Animals for Scientific Purposes. The animal experiments conducted at Comparative Biosciences were approved by their institutional review board. All efforts were made to minimize the distress experienced by the laboratory animals.

# Results

## RGRN-305 robustly inhibited AD-associated cytokine expression in NHEKs

To explore the anti-inflammatory effects of HSP90 inhibition in atopic dermatitis models *in vitro*, NHEKs from healthy donors were stimulated with TNF/IFNγ or TNF/IL-4, as experimental models, to mimic an AD-related gene expression. qPCR analysis demonstrated that inflammatory cytokines (*TNF*, *IL1B*, *IL6*) and chemokines (*CCL17*, *CCL22*) were statistically significantly upregulated in these models, consistent with an observed increased expression in human AD lesional skin compared with non-lesional skin (Figure 1). Interestingly, RGRN-305 robustly inhibited the expression of these AD-associated cytokines and chemokines compared with stimulated/vehicle- and stimulated/dexamethasone-treated NHEKs. While not significantly upregulated in our models, RGRN-305 also suppressed the expression of *TSLP*, supporting a convincing anti-inflammatory effect mediated by HSP90 inhibition in keratinocytes. RGRN-305 caused low (2-5%) cytotoxicity in the stimulated primary human keratinocytes (Supplementary Figure S1).

## RGRN-305 suppresses the activity of STAT3 and STAT6 signalling pathways in NHEKs

To further elucidate the potential AD-related pathways targeted by HSP90 inhibition in keratinocytes, the phosphorylation status of

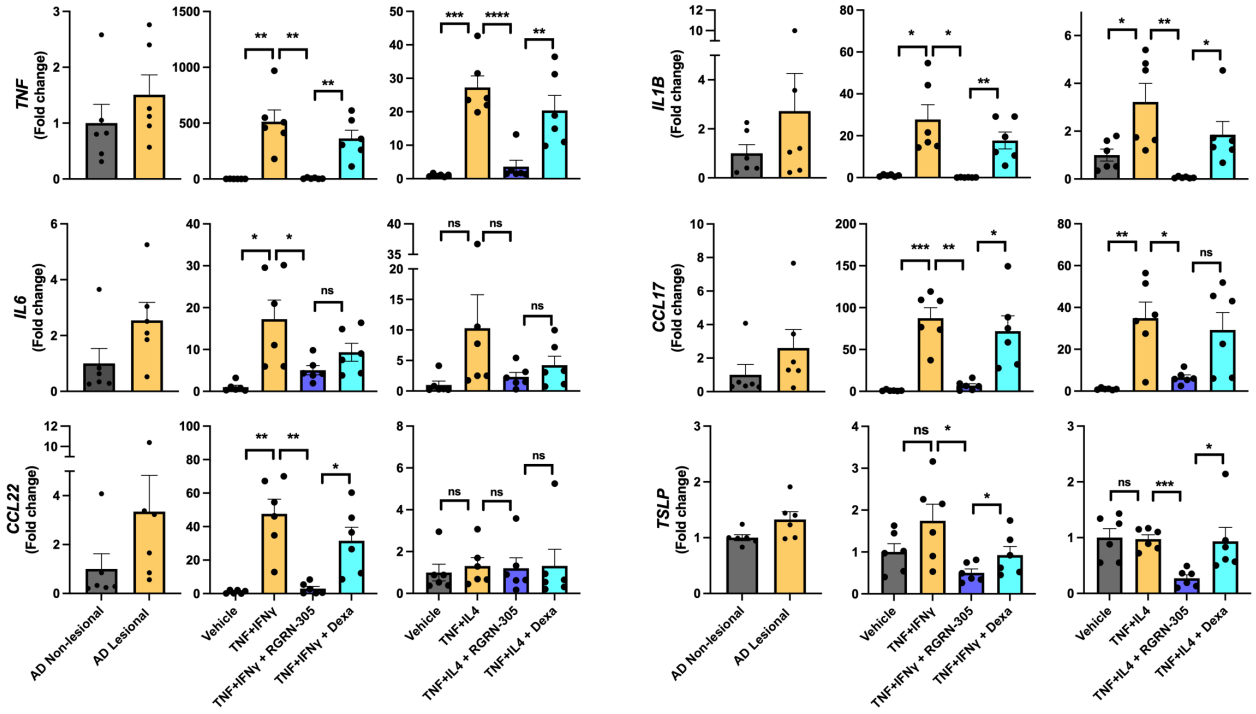


FIGURE 1
RT-qPCR analysis of AD-related gene expression in lesional/non-lesional AD skin and cytokine-stimulated primary human keratinocytes. Effects of RGRN-305 (5 μM) or dexamethasone (0.1 μM) on inflammatory gene expression in primary human keratinocytes stimulated with TNF (10 ng/ml) in combination with IFNγ (10 ng/ml) or IL-4 (100 ng/mL) for 24 hours (three independent experiments, n = 6). Data are shown as mean ± SEM. *p < 0.05, **p ≤0.01, ***p ≤0.001, ****p ≤ 0.0001. ns, not significant. AD, atopic dermatitis. Dexa, dexamethasone.

key signalling proteins, including STAT1, STAT3, STAT6 and p65 (subunit of NF-κB), was determined by Western blot (Figure 2). Importantly, RGRN-305 significantly suppressed the phosphorylation of STAT3 under TNF/IFNγ or TNF/IL-4 stimulation, and to a lesser degree STAT6 (~20% reduction) under TNF/IL-4 stimulation. However, RGRN-305 had no significant effects on the phosphorylation of STAT1 and p65.

## Topical RGRN-305 attenuates MC903-induced AD-like inflammation in mice

Next, we investigated the effects of HSP90 inhibition on AD-like skin inflammation in a mouse model for atopic dermatitis. The right ears of BALB/c mice were challenged daily with 1 nmol MC903 or vehicle for 6 days and received topical treatment with drug-vehicle (ethanol), RGRN-305 or dexamethasone throughout the experiment for 9 days. Treatment with RGRN-305 resulted in visibly reduced erythema and a highly significant reduction (55%) in ear thickness (a marker of inflammation) compared with drug-vehicle at the end of the experiment on day 9 (Figure 3A). Dexamethasone treatment was highly potent resulting in ear thickness below baseline levels and was more effective than RGRN-305. However, dexamethasone-treated mice lost significantly more weight than RGRN-305-treated mice, indicating a more favourable safety profile for RGRN-305 (Supplementary Figure S2).

Next, we repeated the experiment with 2.5 nmol (increased from 1 nmol) of MC903 challenge to observe whether RGRN-305 could suppress a stronger stimulus of inflammation (Figure 3B). Interestingly, topical RGRN-305 still significantly suppressed the MC903-induced ear thickening by 50% on day 9, which was comparable to dexamethasone treatment (P = 0.13).

## Oral RGRN-305 ameliorates MC903-induced AD-like inflammation in mice

To evaluate the feasibility of orally administered RGRN-305, mice were challenged with 2.5 nmol MC903 for six days and administered 100 mg/kg RGRN-305 by oral gavage once daily throughout the experiment. Oral RGRN-305 treatment led to visibly reduced erythema and significantly reduced ear thickening (28% reduction) compared with drug-vehicle, but RGRN-305 was less effective than dexamethasone (Figure 3C). Furthermore, an independent testing facility (Comparative Biosciences, Sunnyvale, CA, USA) demonstrated a dose-dependent improvement by oral RGRN-305 (20, 50 and 100 mg/kg) in alleviating AD-like inflammation in BALB/c mice using an alternative MC903 regimen, further supporting our findings (Supplementary Figure S3, Supplementary Appendix S1).

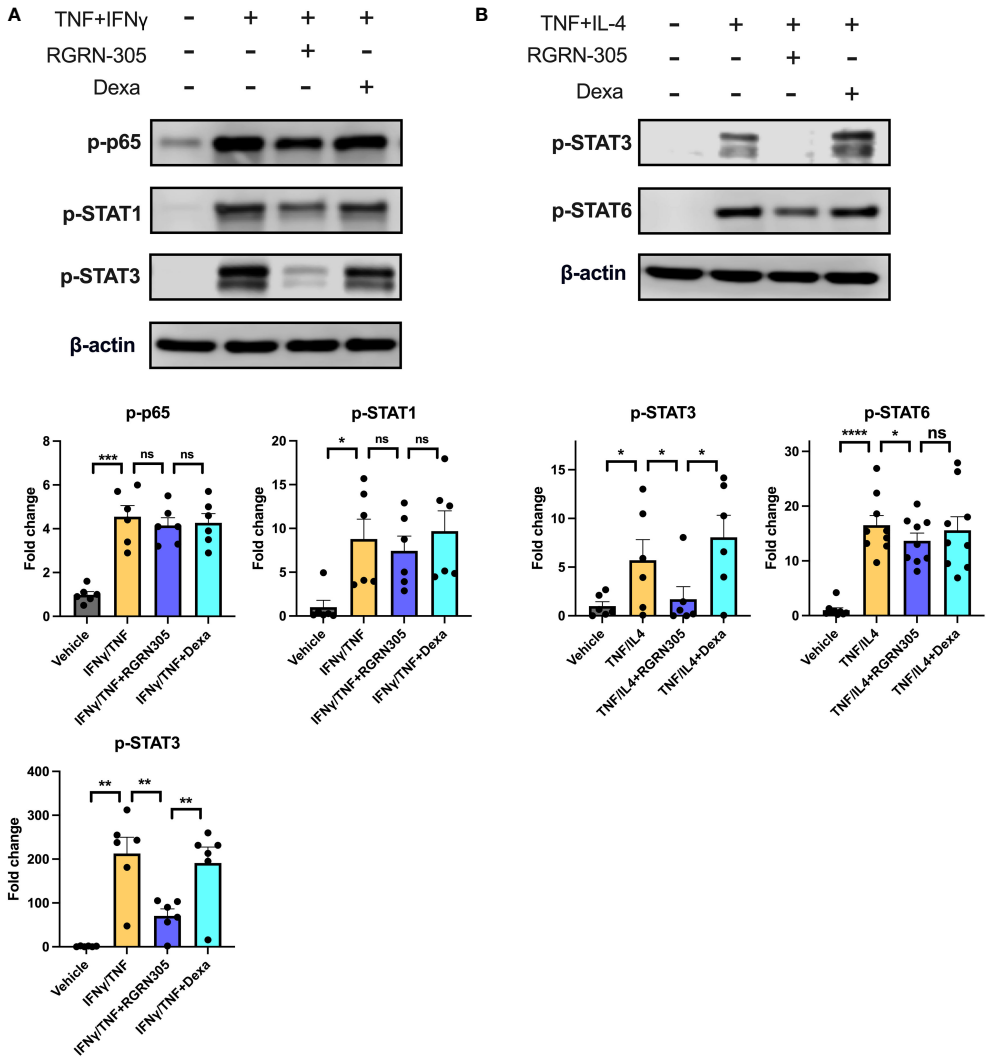


FIGURE 2
Effects of RGRN-305 (5 μM) or dexamethasone (0.1 μM) on the phosphorylation status of key signalling proteins determined by Western blot in primary human keratinocytes stimulated with TNF (10 ng/ml) in combination with **(A)** IFNγ (10 ng/ml) or **(B)** IL-4 (100 ng/mL) for 1 hour (three independent experiments, n = 6-9). Representative Western blots and densitometric results (mean ± SEM) are shown. *p < 0.05, **p ≤0.01, ***p ≤0.001, ****p ≤ 0.0001. ns, not significant. Dexa, dexamethasone.

## Topical RGRN-305 decreases MC903-induced immune cell infiltration in mice

To gain insight into the mechanisms of HSP90 inhibition, punch biopsies derived from the experiment with topical RGRN-305 and 1 nmol MC903 challenge were investigated. Histological analyses confirmed that MC903 increased the epidermal and dermal thickness, which was significantly decreased by RGRN-305 or dexamethasone (Figures 4A, B). Moreover, the total number of cells within histological sections was significantly reduced by RGRN-305 to levels broadly similar with dexamethasone (Figure 4C). In line with this, RGRN-305 significantly suppressed immune cell infiltration into the skin including mast cells, $Ly6g^+$ cells (neutrophils) and $CD4^+$ cells (T-cells; Figures 4D-G).

## Topical RGRN-305 inhibits MC903-induced transcriptome alterations and AD-associated cytokine expression in mice

To examine alterations in gene expression, RNA sequencing and qPCR analyses of ear tissue were performed and showed that topical RGRN-305-treated mice exhibited significantly reduced AD-related cytokine expression of *Il1b*, *Il4*, *Il6* and *Il13* compared with drug-vehicle-treated mice (Figure 5). Using RNA sequencing data, a principal component analysis (PCA) and a hierarchically clustered heatmap revealed that the mice clustered into their respective treatment groups (Figures 6A, B). The MC903/drug-vehicle-treated mice exhibited a distinctive expression pattern separated from the RGRN-305-treated mice,

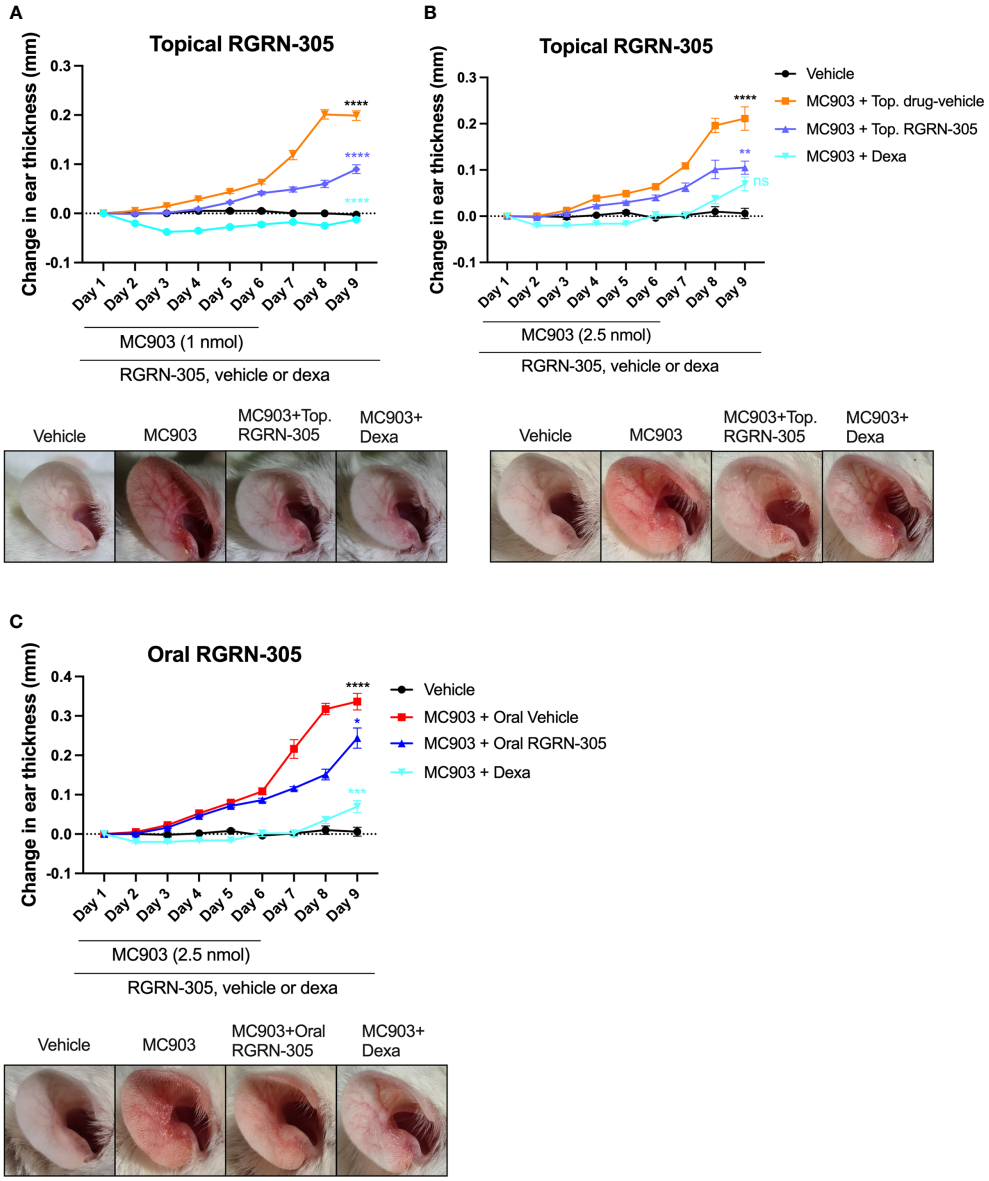


FIGURE 3
Ear thickness changes throughout the experiments and photographs on day 9 in MC903-induced atopic dermatitis mouse model. Female Balb/cAnNRj ears were challenged daily with **(A)** 1 nmol or **(B)** 2.5 nmol of MC903 for 6 days and treated once daily with topical drug-vehicle, topical dexamethasone (20 nmol) or topical RGRN-305 (1 mg). **(C)** Mice were challenged daily with 2.5 nmol for 6 days and treated once daily with oral drug-vehicle, topical dexamethasone (20 nmol) or oral RGRN-305 (100 mg/kg). Four to eight mice in each group, in total 76 mice. Two independent experiments were conducted. Data are shown as mean ± SEM. *p < 0.05, **p ≤0.01, ***p ≤0.001, ****p ≤ 0.0001. ns, not significant. Statistical significance denotes pair-wise comparison on day 9; Black, MC903+Drug-vehicle vs. Vehicle; Blue, MC903+RGRN-305 vs. MC903+Drug-vehicle; Teal, MC903+RGRN-305 vs. MC903+Dexa. Dexa, dexamethasone. Top, topical.

indicating that RGRN-305 treatment mitigates MC903-induced transcriptome alternations. In addition, volcano plots illustrate that MC903 challenge skewed the trend of differentially expressed genes (DEGs) to the right, indicating upregulation of genes (Figure 6C); whereas, RGRN-305 treatment compared with drug-vehicle, skewed the trend of DEGs to the left, indicating down-regulation of genes induced by MC903 (Figure 6D). To explore the biological functions of the DEGs, enrichment analyses were performed for down-regulated DEGs by RGRN-305 compared with drug-vehicle. The analyses revealed that the top ten significant GO biological process (BP) terms were mostly related to inflammation, revealing that RGRN-305 suppressed genes involved in inflammation (Figure 6E). Furthermore, KEGG pathway enrichment analysis showed that RGRN-305 down-regulated genes implicated in inflammatory pathways including JAK-STAT signalling (Figure 6F). Lists of all genes derived from the differential expression analyses are present in Supplementary Table S1.

10.3389/fimmu.2023.1289788

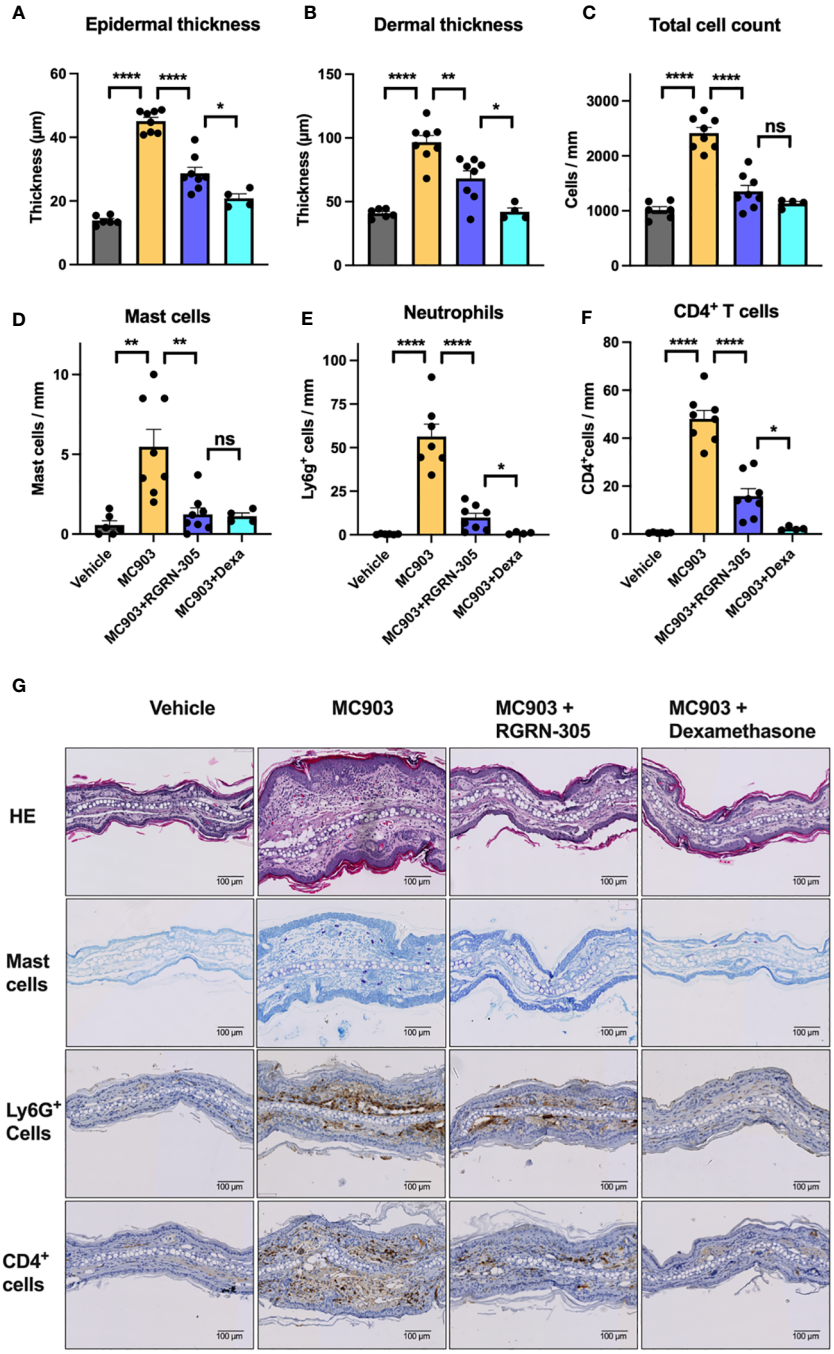


FIGURE 4
Histological analysis of ear biopsies from mice challenged daily with 1 nmol of MC903 and treated with drug-vehicle, topical RGRN-305 or topical dexamethasone. **(A)** Epidermal thickness, **(B)** dermal thickness and **(C)** total number of cells were determined from haematoxylin & eosin (HE) stained sections. **(D)** Quantification of mast cells in toluidine blue stained sections. **(E)** Quantification of Lyg6+ cells (neutrophils) and **(F)** CD4+ cells (T cells) in immunohistochemical stained sections. **(G)** Representative images of stained sections. Data are shown as mean ± SEM. *p < 0.05, **p ≤0.01, ****p ≤ 0.0001. ns, not significant. Dexa, dexamethasone.

## RGRN-305 upregulates the gene expression of *HSPA1A/Hspa1a* (HSP70)

To investigate a potential compensatory heat shock response secondary to HSP90 inhibition by RGRN-305, the gene expression of *HSPA1A* (HSP70) and *HSPB1* (HSP27) was determined by qPCR and RNA sequencing (Supplementary Figure S4). In primary human keratinocytes, RGRN-305 treatment caused a trend towards upregulation of *HSPA1A* ($P = 0.059$), whereas no change was observed for *HSPB1*. In the MC903-mouse model, RGRN-305 treatment led to a highly significant upregulation of *Hspa1a* and *Hspb1*.

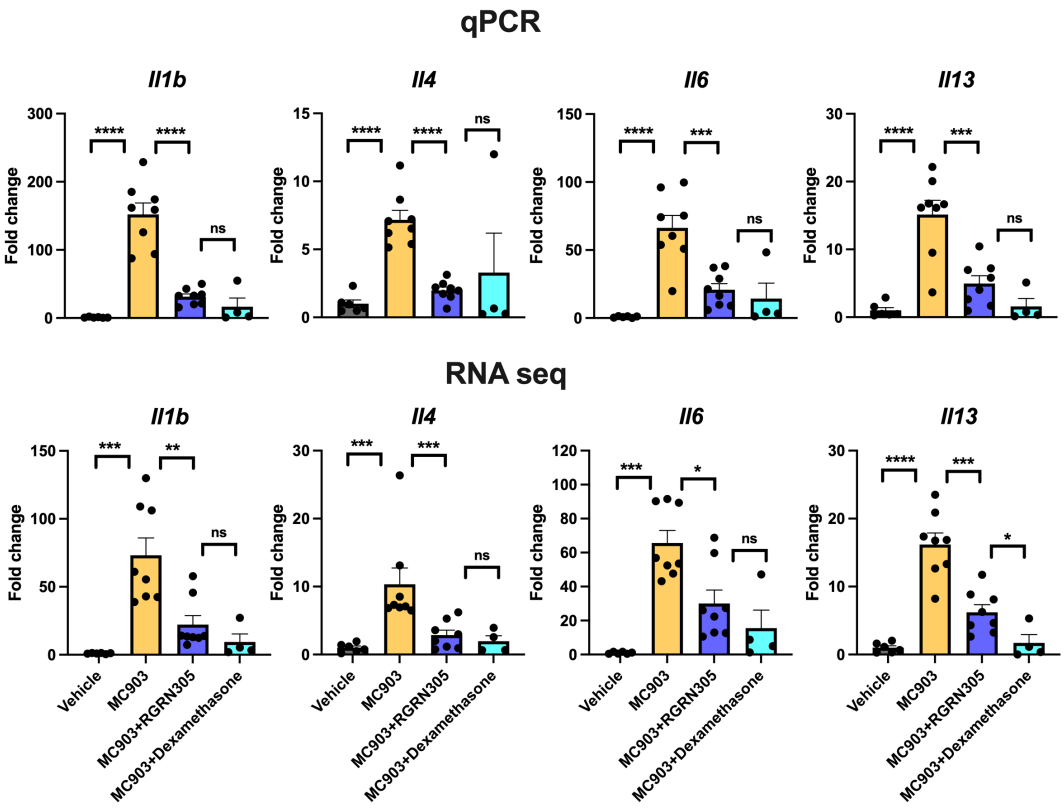


FIGURE 5
RT-qPCR (upper panels) and RNA sequencing analysis (lower panels) of AD-related cytokine gene expression in ear tissue from mice challenged daily with 1 nmol of MC903 and treated with drug-vehicle, topical RGRN-305 or topical dexamethasone. Data are shown as mean ± SEM. *p < 0.05, **p ≤0.01, ***p ≤0.001, ****p ≤ 0.0001. ns, not significant.

## Discussion

In this study, we discovered HSP90 inhibition by RGRN-305 robustly suppressed inflammation in experimental models of AD by significantly reducing clinical symptoms of dermatitis (erythema and oedema), immune cell infiltrations, expression of key cytokines (e.g., IL-4 and IL-13) and signalling pathways (STAT3 and STAT6) related to AD. Thus, our encouraging results suggest HSP90 may be considered a novel therapeutic target for AD, providing preclinical validation for further clinical investigations in patients.

While HSP90 inhibitors have been researched for oncological disorders, the therapeutic potential of HSP90 inhibitors in inflammation has been sparsely examined. To the best of our knowledge, two proof-of-concept clinical studies and a small number of preclinical studies have been conducted (18, 19, 31, 32). Our findings are in line with other preclinical studies beyond atopic dermatitis wherein HSP90 inhibition exerted anti-inflammatory effects by targeting several inflammatory cytokines (e.g. TNF, IL-1β, and IL-6) and signalling pathways (e.g. ERK1/2, p38, and JNKs) (8, 12, 14, 33).

Atopic dermatitis is routinely treated with emollients in combination with topical anti-inflammatory treatments such as corticosteroids or calcineurin inhibitors as first-line therapies, whereas systemic treatments are reserved for more severe or recalcitrant cases (34). We demonstrated that both topical and oral RGRN-305 significantly reduced AD-like skin inflammation in mice. While both routes of administration may be feasible in treating AD, topically delivered RGRN-305 may be the better option as the reduction of ear thickness was 50-54% compared with 28% for oral RGRN-305. Moreover, topical RGRN-305 demonstrated similar or slightly inferior efficacy compared with topical dexamethasone, a very potent corticosteroid (35). Yet, RGRN-305 treatment resulted in significantly less weight loss compared with dexamethasone, indicating a more favourable safety profile. In agreement, oral treatment with RGRN-305 has been well-tolerated in proof-of-concept studies with psoriasis and hidradenitis suppurative patients (18, 19). It is worth nothing that RGRN-305 has been shown to accumulate in the skin (9), thus additional time than this duration study investigated (nine days) may allow orally delivered RGRN-305 to build sufficient levels in the skin and thereby increase the efficacy. Considering that atopic dermatitis is treated frequently with topical corticosteroids, it may be relevant to consider whether treatment with RGRN-305 in combination with dexamethasone may enhance the immunosuppressive and clinical effects in AD, warranting further investigation.

In the acute phase of AD, a Th2 response is initiated and shifts towards a dominancy of Th1 response as the disease progresses into its chronic stage (36, 37). Activated keratinocytes, as key effector cells, play a crucial role in promoting immune dysregulation by secreting a variety of cytokines and chemokines (e.g. IL-1β, IL-6, CCL17, TSLP), contributing to the pathogenesis in AD (38). In primary human

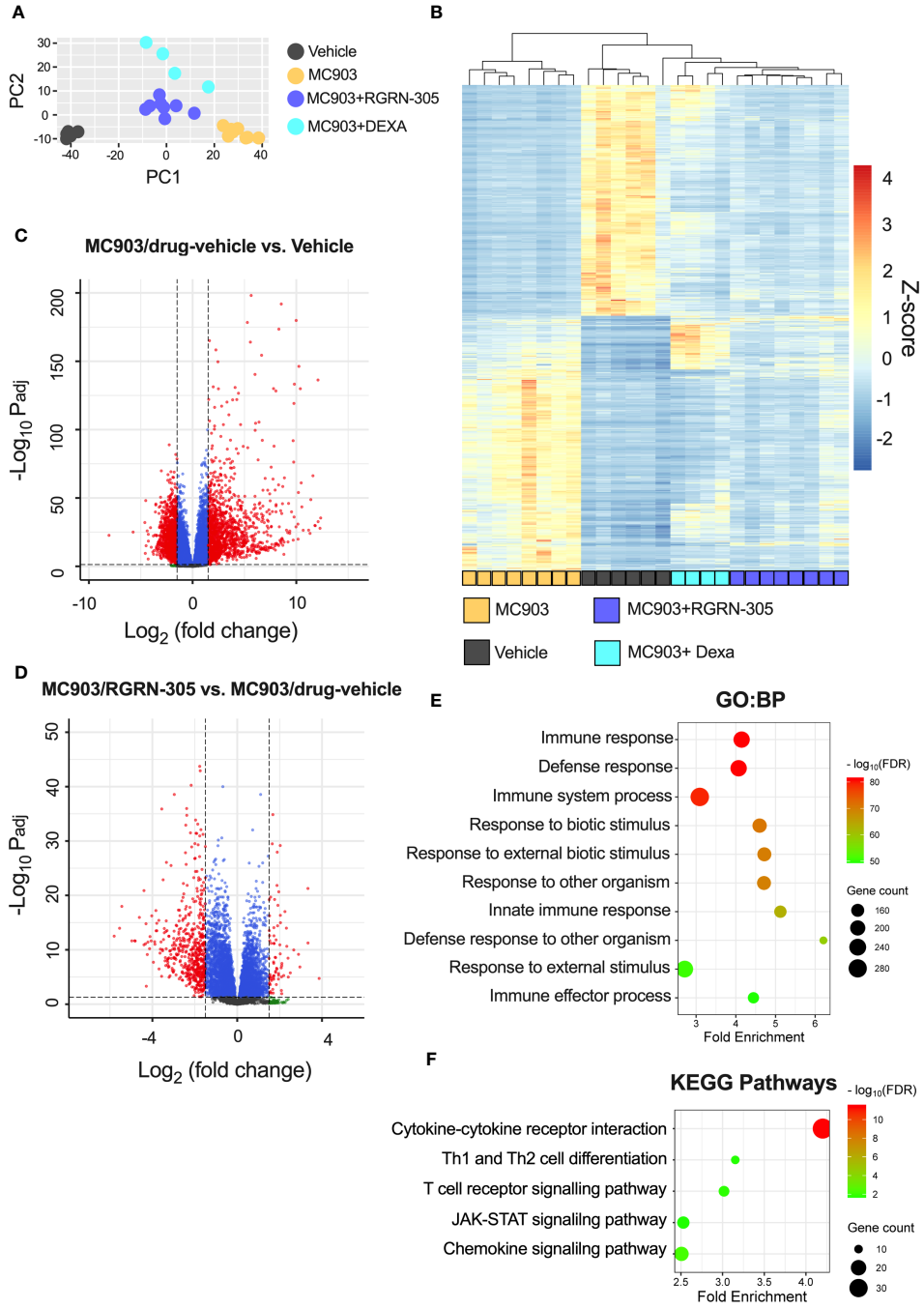


FIGURE 6
RNA sequencing analysis of ear tissue from mice challenged daily with 1 nmol of MC903 and treated with drug-vehicle, topical RGRN-305 or topical dexamethasone. **(A)** Principal component analysis (PCA) of regularized log (rlog) transformed data. **(B)** Heatmap of differentially expressed genes (DEGs; $\log_2$[foldchange] > 1.5 and FDR-adjusted p-value < 0.05) upon MC903-induced inflammation. The genes were filtered to include those with a mean of normalised counts > 25. **(C, D)** Volcano plots for two different comparisons. The dashed horizontal lines mark an FDR-adjusted p-value of 0.05, whereas the vertical lines mark a $\log_2$(fold change) of 1.5. DEGs are marked as red dots. **(E, F)** Enrichment analyses of down-regulated DEGs by RGRN-305 compared with drug-vehicle. **(E)** The top ten significant GO biological processes terms and **(F)** five relevant significantly enriched KEGG pathway terms are presented. Dexa, dexamethasone. PCA, Principal component analysis.

keratinocytes and mice, RGRN-305 treatment strongly suppressed Th1- and Th2-associated cytokines and chemokines implicated in AD (Figures 1, 5). In human keratinocytes, RGRN-305 inhibited the phosphorylation (i.e., activation) of STAT3 and, to a lesser extent, STAT6 (Figure 2); two key signalling proteins downstream of the IL-4 receptor (39). In accordance, enrichment analysis from the mouse model showed JAK-STAT signalling was highly downregulated by RGRN-305. Interestingly, another recent study (n = 7) discovered that HSP90 inhibition disrupted JAK-STAT signalling by potently decreasing JAK2 expression and the phosphorylation of STAT3 and STAT5 in patients with myeloproliferative neoplasms (40). In addition, the relation between HSP90 and activation of STAT3,

STAT5 and STAT6 have been reported in preclinical cancer studies, further supporting our findings (41–43). The recent success of therapeutics targeting JAK-STAT pathways highlights the importance of these pathways in AD, and it may be one of the mechanisms by which HSP90 inhibition ameliorates AD (44). However, considering the wide range of client proteins targeted by HSP90 inhibition, the anti-inflammatory effects are most likely attributable to other mechanisms as well.

While the pathophysiological mechanisms underlying AD are complex, it is noteworthy that inhibition of cell-surface HSP90 has been demonstrated to reduce Toll-like receptor (TLR) signalling in response to pathogen-associated molecular patterns (PAMPs) in human monocytes, suggesting that HSP90 promotes TLR signalling (45). This relationship may have implications for AD, as TLR signalling can influence various cell types with wide-ranging effects, potentially affecting vitamin D metabolism (46). Further research is warranted to investigate the significance of this potential mechanism in atopic dermatitis.

HSP90 inhibitors may trigger a heat shock response by dissociating heat shock factor 1 (HSF1) from HSP90, which may induce the expression of HSP70 and HSP27 (47, 48). RGRN-305 treatment was associated with an increased expression of *HSPA1A* (HSP70), indicating a heat shock response. However, the clinical significance of a heat shock response in inflammatory skin diseases is still not fully understood (31). HSP70 has been reported to elicit immunosuppressive effects in an animal model of atopic dermatitis, whereas HSP70 has displayed both anti- and pro-inflammatory effects in other models of inflammatory skin diseases (49–52). Further research is needed to determine the role of a heat shock response in atopic dermatitis.

Limitations of the study include the inherent nature of basic research and experimental models that may encounter challenges when translating the findings into clinical practice. Nonetheless, the accumulating evidence of HSP90 inhibition exerting broad anti-inflammatory effects together with the findings from this study increases the likelihood of clinical success in treating AD. Another limitation is that the effects of RGRN-305 in specific cell types beyond keratinocytes have not been evaluated. However, the mouse experiments capture the complex interplay and contribution of various cell types in the skin. Lastly, the permeability of mice skin varies to human skin, and therefore further studies should evaluate optimal drug formulations enhancing the permeation and efficacy of topical RGRN-305.

In conclusion, HSP90 inhibition by RGRN-305 potently suppressed inflammation using *in vitro* and *in vivo* experimental models mimicking AD, providing evidence that HSP90 inhibition may be a novel mechanism of action in treating AD.

## Data availability statement

The datasets presented in this study can be found in online repositories. The names of the repository/repositories and accession number(s) can be found below: https://www.ncbi.nlm.nih.gov/geo/query/acc.cgi?&acc=GSE246569.

## Ethics statement

The studies involving humans were approved by Central Jutland Regional Committee on Health Research Ethics (M-20110027). The studies were conducted in accordance with the local legislation and institutional requirements. The participants provided their written informed consent to participate in this study. The animal study was approved by The Danish Animal Experiments Inspectorate (2022-15-0201-01267). The study was conducted in accordance with the local legislation and institutional requirements.

## Author contributions

HB: Conceptualization, Formal analysis, Funding acquisition, Investigation, Methodology, Visualization, Writing – original draft, Writing – review & editing. AB: Methodology, Supervision, Writing – review & editing. GG: Conceptualization, Funding acquisition, Writing – review & editing. LI: Conceptualization, Funding acquisition, Methodology, Supervision, Writing – review & editing. CJ: Conceptualization, Formal analysis, Funding acquisition, Investigation, Methodology, Supervision, Writing – review & editing.

## Funding

The author(s) declare financial support was received for the research, authorship, and/or publication of this article.

## Acknowledgments

We thank Kristine Møller and Annette Blak Rasmussen for their technical assistance.

## Conflict of interest

Author LI has served as a consultant and/or paid speaker for and/or participated in clinical trials sponsored by: AbbVie, Almirall, Amgen, AstraZeneca, BMS, Boehringer Ingelheim, Celgene, Centocor, Eli Lilly, Janssen Cilag, Kyowa, Leo Pharma, MSD, Novartis, Pfizer, Regranion, Samsung, Union Therapeutics and UCB. Author LI was also employed by the company MC2 Therapeutics A/S. Author GG is the CEO of Regranion, which owns the rights to RGRN-305. Author CJ has served as a consultant and/or paid speaker for Eli Lilly, Abbvie, Leo Pharma and L'Oréal.

The remaining authors declare that the research was conducted in the absence of any commercial or financial relationships that could be construed as a potential conflict of interest.

The author(s) declare the research was financially supported by an unrestricted grant from Regranion, LLC. The funder had the following involvement in the study: interpretation of data, review of the manuscript.

## Publisher's note



## Supplementary material

The Supplementary Material for this article can be found online at: https://www.frontiersin.org/articles/10.3389/fimmu.2023.1289788/full#supplementary-material

SUPPLEMENTARY APPENDIX S1
Study report from Comparative Biosciences, Inc.

SUPPLEMENTARY FIGURE 1
Cytotoxicity of RGRN-305 in stimulated primary human keratinocytes.

SUPPLEMENTARY FIGURE 2
Relative body weights throughout the experiments.

SUPPLEMENTARY FIGURE 3
Ear thickness measures from experiments conducted at Comparative Biosciences, Inc.

SUPPLEMENTARY FIGURE 4
Gene expression of *HSPA1A/Hspa1a* and *HSPB1/Hspb1*.

SUPPLEMENTARY TABLE 1
Lists of all genes derived from the differential expression analyses.

## References

1. Langan SM, Irvine AD, Weidinger S. Atopic dermatitis. *Lancet (London England)* (2020) 396(10247):345–60. doi: 10.1016/S0140-6736(20)31286-1

2. Barbarot S, Auziere S, Gadkari A, Girolomoni G, Puig L, Simpson EL, et al. Epidemiology of atopic dermatitis in adults: Results from an international survey. *Allergy* (2018) 73(6):1284–93. doi: 10.1111/all.13401

3. Silverberg JI, Barbarot S, Gadkari A, Simpson EL, Weidinger S, Mina-Osorio P, et al. Atopic dermatitis in the pediatric population: A cross-sectional, international epidemiologic study. *Ann allergy Asthma Immunol* (2021) 126(4):417–28.e2. doi: 10.1016/j.anai.2020.12.020

4. Silverberg JI. Comorbidities and the impact of atopic dermatitis. *Ann allergy Asthma Immunol* (2019) 123(2):144–51. doi: 10.1016/j.anai.2019.04.020

5. Ben Abdallah H, Vestergaard C. Atopic dermatitis, hypertension and cardiovascular disease. *Br J Dermatol* (2022) 186(2):203–4. doi: 10.1111/bjd.20802

6. Kim J, Kim BE, Leung DYM. Pathophysiology of atopic dermatitis: Clinical implications. *Allergy Asthma Proc* (2019) 40(2):84–92. doi: 10.2500/aap.2019.40.4202

7. Bieber T. Atopic dermatitis: an expanding therapeutic pipeline for a complex disease. *Nat Rev Drug Discov* (2022) 21(1):21–40. doi: 10.1038/s41573-021-00266-6

8. Ben Abdallah H, Seeler S, Bregnhøj A, Ghatnekar G, Kristensen LS, Iversen L, et al. Heat shock protein 90 inhibitor RGRN-305 potently attenuates skin inflammation. *Front Immunol* (2023) 14:1128897. doi: 10.3389/fimmu.2023.1128897

9. Stenderup K, Rosada C, Gavillet B, Vuagniaux G, Dam TN. Debio 0932, a new oral Hsp90 inhibitor, alleviates psoriasis in a xenograft transplantation model. *Acta Derm Venereol* (2014) 94(6):672–6. doi: 10.2340/00015555-1838

10. Hansen RS, Thuesen KKH, Bregnhøj A, Moldovan LI, Kristensen LS, Grek CL, et al. The HSP90 inhibitor RGRN-305 exhibits strong immunomodulatory effects in human keratinocytes. *Exp Dermatol* (2021) 30(6):773-81. doi: 10.1111/exd.14302

11. Tukaj S, Bieber K, Kleszczyński K, Witte M, Cames R, Kalies K, et al. Topically applied Hsp90 blocker 17AAG inhibits autoantibody-mediated blister-inducing cutaneous inflammation. *J Invest Dermatol* (2017) 137(2):341–9. doi: 10.1016/j.jid.2016.08.032

12. Rice JW, Veal JM, Fadden RP, Barabasz AF, Partridge JM, Barta TE, et al. Small molecule inhibitors of Hsp90 potently affect inflammatory disease pathways and exhibit activity in models of rheumatoid arthritis. *Arthritis Rheumatism* (2008) 58 (12):3765–75. doi: 10.1002/art.24047

13. Shimp SK3rd, Chafin CB, Regna NL, Hammond SE, Read MA, Caudell DL, et al. Heat shock protein 90 inhibition by 17-DMAG lessens disease in the MRL/lpr mouse model of systemic lupus erythematosus. *Cell Mol Immunol* (2012) 9(3):255–66. doi: 10.1038/cmi.2012.5

14. Yun TJ, Harning EK, Giza K, Rabah D, Li P, Arndt JW, et al. EC144, a synthetic inhibitor of heat shock protein 90, blocks innate and adaptive immune responses in models of inflammation and autoimmunity. *J Immunol* (2011) 186(1):563–75. doi: 10.4049/jimmunol.1000222

15. Štorkánová H, Štorkánová L, Navrátilová A, Bečvář V, Hulejová H, Oreská S, et al. Inhibition of Hsp90 counteracts the established experimental dermal fibrosis induced by bleomycin. *Biomedicines* (2021) 9(6). doi: 10.3390/biomedicines9060650

16. Dello Russo C, Polak PE, Mercado PR, Spagnolo A, Sharp A, Murphy P, et al. The heat-shock protein 90 inhibitor 17-allylamino-17-demethoxygeldanamycin suppresses glial inflammatory responses and ameliorates experimental autoimmune encephalomyelitis. *J Neurochem* (2006) 99(5):1351–62. doi: 10.1111/j.1471-4159.2006.04221.x

17. Collins CB, Aherne CM, Yeckes A, Pound K, Eltzschig HK, Jedlicka P, et al. Inhibition of N-terminal ATPase on HSP90 attenuates colitis through enhanced Treg function. *Mucosal Immunol* (2013) 6(5):960–71. doi: 10.1038/mi.2012.134

18. Ben Abdallah H, Bregnhøj A, Emmanuel T, Ghatnekar G, Johansen C, Iversen L. Efficacy and Safety of the Heat Shock Protein 90 Inhibitor RGRN-305 in Hidradenitis Suppurativa: A Parallel-Design Double-Blind Trial. *JAMA Dermatol* (2023). doi: 10.1001/jamadermatol.2023.4800

19. Bregnhøj A, Thuesen KKH, Emmanuel T, Litman T, Grek Grek, Ghatnekar GS, et al. HSP90 inhibitor RGRN-305 for oral treatment of plaque-type psoriasis: efficacy, safety and biomarker results in an open-label proof-of-concept study. *Br J Dermatol* (2022) 186(5):861–74. doi: 10.1111/bjd.20880

20. Sitko K, Bednarek M, Mantej J, Trzeciak M, Tukaj S. Circulating heat shock protein 90 (Hsp90) and autoantibodies to Hsp90 are increased in patients with atopic dermatitis. *Cell Stress Chaperones* (2021) 26(6):1001–7. doi: 10.1007/s12192-021-01238-w

21. Johansen C. Generation and culturing of primary human keratinocytes from adult skin. *J Vis Exp* (2017) 130. doi: 10.3791/56863

22. Kim HJ, Baek J, Lee JR, Roh JY, Jung Y. Optimization of cytokine milieu to reproduce atopic dermatitis-related gene expression in HaCaT keratinocyte cell line. *Immune Netw* (2018) 18(2):e9. doi: 10.4110/in.2018.18.e9

23. Han J, Cai X, Qin S, Zhang Z, Wu Y, Shi Y, et al. TMEM232 promotes the inflammatory response in atopic dermatitis via NF-κB and STAT3 signaling pathways. *Br J Dermatol* (2023) 189(2):195-209. doi: 10.1093/bjd/ljad078

24. Piazza S, Martinelli G, Magnavacca A, Fumagalli M, Pozzoli C, Terno M, et al. Unveiling the ability of witch hazel (Hamamelis virginiana L.) bark extract to impair keratinocyte inflammatory cascade typical of atopic eczema. *Int J Mol Sci* (2022) 23(16). doi: 10.3390/ijms23169279

25. Biosystems A. *Applied Biosystems StepOne™ and StepOnePlus™ Real-Time PCR Systems: Applied Biosystems* (2010). Available at: https://tools.thermofisher.com/content/sfs/manuals/cms_046739.pdf.

26. Bankhead P, Loughrey MB, Fernández JA, Dombrowski Y, McArt DG, Dunne PD, et al. QuPath: Open source software for digital pathology image analysis. *Sci Rep* (2017) 7(1):16878. doi: 10.1038/s41598-017-17204-5

27. Liao Y, Smyth GK, Shi W. The R package Rsubread is easier, faster, cheaper and better for alignment and quantification of RNA sequencing reads. *Nucleic Acids Res* (2019) 47(8):e47. doi: 10.1093/nar/gkz114

28. Love MI, Huber W, Anders S. Moderated estimation of fold change and dispersion for RNA-seq data with DESeq2. *Genome Biol* (2014) 15(12):550. doi: 10.1186/s13059-014-0550-8

29. Ge SX, Jung D, Yao R. ShinyGO: a graphical gene-set enrichment tool for animals and plants. *Bioinformatics* (2020) 36(8):2628–9. doi: 10.1093/bioinformatics/btz931

30. Sherman BT, Hao M, Qiu J, Jiao X, Baseler MW, Lane HC, et al. DAVID: a web server for functional enrichment analysis and functional annotation of gene lists (2021 update). *Nucleic Acids Res* (2022) 50(W1):W216–w21. doi: 10.1093/nar/gkac194

31. Tukaj S, Sitko K. Heat shock protein 90 (Hsp90) and Hsp70 as potential therapeutic targets in autoimmune skin diseases. *Biomolecules* (2022) 12(8). doi: 10.3390/biom12081153

32. Tukaj S, Węgrzyn G. Anti-Hsp90 therapy in autoimmune and inflammatory diseases: a review of preclinical studies. *Cell Stress Chaperones* (2016) 21(2):213–8. doi: 10.1007/s12192-016-0670-z

33. Nizami S, Arunasalam K, Green J, Cook J, Lawrence CB, Zarganes-Tzitzikas T, et al. Inhibition of the NLRP3 inflammasome by HSP90 inhibitors. *Immunology* (2021) 162(1):84–91. doi: 10.1111/imm.13267

34. Flohr C. How we treat atopic dermatitis now and how that will change over the next 5 years. *Br J Dermatol* (2022) 188(6):718-25. doi: 10.1093/bjd/ljac116

35. Johnson DB, Lopez MJ, Kelley B. *Dexamethasone. StatPearls*. Treasure Island (FL: StatPearls Publishing Copyright © 2023, StatPearls Publishing LLC (2023).

36. Bieber T. Atopic dermatitis. *N Engl J Med* (2008) 358(14):1483–94. doi: 10.1056/NEJMra074081

37. Guttman-Yassky E, Krueger JG, Lebwohl MG. Systemic immune mechanisms in atopic dermatitis and psoriasis with implications for treatment. *Exp Dermatol* (2018) 27 (4):409–17. doi: 10.1111/exd.13336

38. Das P, Mounika P, Yellurkar ML, Prasanna VS, Sarkar S, Velayutham R, et al. Keratinocytes: an enigmatic factor in atopic dermatitis. *Cells* (2022) 11(10). doi: 10.3390/cells11101683

39. Dubin C, Del Duca E, Guttman-Yassky E. The IL-4, IL-13 and IL-31 pathways in atopic dermatitis. *Expert Rev Clin Immunol* (2021) 17(8):835–52. doi: 10.1080/1744666X.2021.1940962

40. Hobbs GS, Hanasoge Somasundara AV, Kleppe M, Litvin R, Arcila M, Ahn J, et al. Hsp90 inhibition disrupts JAK-STAT signaling and leads to reductions in splenomegaly in patients with myeloproliferative neoplasms. *Haematologica* (2018) 103(1):e5–9. doi: 10.3324/haematol.2017.177600

41. Schoof N, von Bonin F, Trümper L, Kube D. HSP90 is essential for Jak-STAT signaling in classical Hodgkin lymphoma cells. *Cell Commun Signal* (2009) 7:17. doi: 10.1186/1478-811X-7-17

42. Prinsloo E, Kramer AH, Edkins AL, Blatch GL. STAT3 interacts directly with Hsp90. *IUBMB Life* (2012) 64(3):266–73. doi: 10.1002/iub.607

43. Kolosenko I, Grander D, Tamm KP. IL-6 activated JAK/STAT3 pathway and sensitivity to Hsp90 inhibitors in multiple myeloma. *Curr Med Chem* (2014) 21 (26):3042–7. doi: 10.2174/0929867321666140414100831

44. Huang IH, Chung WH, Wu PC, Chen CB. JAK-STAT signaling pathway in the pathogenesis of atopic dermatitis: An updated review. *Front Immunol* (2022) 13:1068260. doi: 10.3389/fimmu.2022.1068260

45. Bzowska M, Nogieć A, Bania K, Zygmunt M, Zarębski M, Dobrucki J, et al. Involvement of cell surface 90 kDa heat shock protein (HSP90) in pattern recognition by human monocyte-derived macrophages. *J Leukoc Biol* (2017) 102(3):763–74. doi: 10.1189/jlb.2MA0117-019R

46. Tamagawa-Mineoka R. Toll-like receptors: their roles in pathomechanisms of atopic dermatitis. *Front Immunol* (2023) 14:1239244. doi: 10.3389/fimmu.2023.1239244

47. Park HK, Yoon NG, Lee JE, Hu S, Yoon S, Kim SY, et al. Unleashing the full potential of Hsp90 inhibitors as cancer therapeutics through simultaneous inactivation of Hsp90, Grp94, and TRAP1. *Exp Mol Med* (2020) 52(1):79–91. doi: 10.1038/s12276-019-0360-x

48. Yao JQ, Liu QH, Chen X, Yang Q, Xu ZY, Hu F, et al. Hsp90 inhibitor 17-allylamino-17-demethoxygeldanamycin inhibits the proliferation of ARPE-19 cells. *J BioMed Sci* (2010) 17(1):30. doi: 10.1186/1423-0127-17-30

49. Kao JK, Hsu TF, Lee MS, Su TC, Lee CH, Hsu CS, et al. Subcutaneous injection of recombinant heat shock protein 70 ameliorates atopic dermatitis skin lesions in a mouse model. *Kaohsiung J Med Sci* (2020) 36(3):186–95. doi: 10.1002/kjm2.12163

50. Seifarth FG, Lax JE, Harvey J, DiCorleto PE, Husni ME, Chandrasekharan UM, et al. Topical heat shock protein 70 prevents imiquimod-induced psoriasis-like inflammation in mice. *Cell Stress Chaperones* (2018) 23(5):1129–35. doi: 10.1007/s12192-018-0895-0

51. Raghuwanshi N, Yadav TC, Srivastava AK, Raj U, Varadwaj P, Pruthi V. Structure-based drug designing and identification of Woodfordia fruticosa inhibitors targeted against heat shock protein (HSP70-1) as suppressor for Imiquimod-induced psoriasis like skin inflammation in mice model. *Mater Sci Eng C Mater Biol Appl* (2019) 95:57–71. doi: 10.1016/j.msec.2018.10.061

52. Denman CJ, McCracken J, Hariharan V, Klarquist J, Oyarbide-Valencia K, Guevara-Patiño JA, et al. HSP70i accelerates depigmentation in a mouse model of autoimmune vitiligo. *J Invest Dermatol* (2008) 128(8):2041–8. doi: 10.1038/jid.2008.45

frontiers | Frontiers in Immunology

TYPE Opinion
PUBLISHED 19 January 2024
DOI 10.3389/fimmu.2024.1326219



OPEN ACCESS

EDITED BY
Zhenghua Zhang,
Fudan University, China

REVIEWED BY
Hayakazu Sumida,
The University of Tokyo, Japan

*CORRESPONDENCE
Teruki Dainichi
dainichi.teruki@kagawa-u.ac.jp

RECEIVED 23 October 2023
ACCEPTED 05 January 2024
PUBLISHED 19 January 2024

CITATION
Dainichi T, Matsumoto R, Sakurai K and Kabashima K (2024) Necessary and sufficient factors of keratinocytes in psoriatic dermatitis.
*Front. Immunol.* 15:1326219.
doi: 10.3389/fimmu.2024.1326219



# Necessary and sufficient factors of keratinocytes in psoriatic dermatitis

Teruki Dainichi[1,2]*, Reiko Matsumoto[2], Kenji Sakurai[2] and Kenji Kabashima[2,3]

[1]Department of Dermatology, Kagawa University Faculty of Medicine, Miki-cho, Japan, [2]Department of Dermatology, Kyoto University Graduate School of Medicine, Kyoto, Japan, [3]Agency for Science, Technology and Research (A*STAR) Skin Research Laboratories (ASRL), A*STAR, Singapore, Singapore

KEYWORDS

psoriasis, TRAF6, p38, MAPK, CXCL2, HB-EGF, keratinocyte

## Introduction

Transcriptional activation of keratinocytes plays essential roles for the specific types of immune response of the skin (1). Psoriasis is a common chronic inflammatory skin disease that develops in middle-aged individuals with genetic predisposition (2). Clinical studies have demonstrated that tumor necrosis factor (TNF), interleukin (IL)-23, and IL-17 play pivotal roles in the pathogenesis of psoriasis. In addition, genome-wide association studies (GWASs) in patients with psoriasis have demonstrated that a genetic predisposition to T helper ($T_H$) 17 responses and dysregulation of inflammatory signaling in immune and non-immune components, such as keratinocytes, contribute to the development of psoriasis. In particular, the identification of gene mutations in familial-type psoriasis suggests a unique role for keratinocyte signaling (2). However, the necessary and sufficient conditions for keratinocytes to develop psoriasis have not yet been identified.

Various animal models of psoriasis have been proposed. Among them, psoriatic dermatitis induced by daily epicutaneous application of imiquimod, a Toll-like receptor (TLR) 7/8 ligand, to mice is one of the most widely-used models. It reproduces several aspects of psoriasis including acanthosis and parakeratosis, neutrophil infiltration in the epidermis, and activation of the IL-23–IL-17 axis resulting proliferation of IL-17A-producing $CD4^+$ T cells in the lesional skin (3). In addition, we have developed a new animal model for psoriasis by daily epicutaneous application with anisomycin, a p38-MAP kinase activator (4). It also reproduces histopathological and immunological aspects of psoriasis as well as imiquimod-induced dermatitis. Transcriptome analysis of the lesional skin revealed that approximately two thirds of the genes upregulated in imiquimod-induced dermatitis were also induced in anisomycin-induced dermatitis whereas some genes, such as *Defb3*, *S100a8/a9*, and *Il19*, were dominant in the imiquimod-induced dermatitis and others including *Defb4*, *Mmp13*, and *Il24* were dominant in the anisomycin-induced dermatitis (4).

Can we predict the necessary and sufficient conditions in keratinocytes by extracting response genes that are shared between each of the necessary and sufficient conditions for psoriatic dermatitis?

## A necessary condition — the TRAF6 pathway

TNF receptor associated factor 6 (TRAF6) is an intermediate signaling molecule between various types of receptors for exogenous or endogenous mediators and activation of nuclear factor-kappa B (NF-κB) and mitogen-activated protein kinase (MAP kinase) pathways (5). We previously demonstrated that mice lacking TRAF6, specifically in keratinocytes, are resistant to psoriatic inflammation induced by imiquimod (6).

## A sufficient condition — the p38-MAP kinase pathway

Then, which of the TRAF6 pathways, NF-κB pathways or MAP kinase pathways, is essential for the development and persistence of psoriasis? Notably, epidermis-specific depletion of the canonical NF-κB pathway using *Krt14*-Cre-mediated deletion of p65 (RelA) and c-Rel in keratinocytes leads to psoriatic dermatitis after birth (7). In contrast, we have shown that daily topical treatment of mouse ear skin with anisomycin is sufficient to induce psoriatic dermatitis in an IL-17-dependent manner (4).

Therefore, TRAF6-dependent p38-MAP kinase-mediated transcriptional activation of keratinocytes is expected to generate the necessary and sufficient conditions for psoriasis.

## Necessary and sufficient factors of keratinocytes in psoriatic dermatitis

The differentially expressed genes (DEGs) shared in the two conditions — (A) psoriatic dermatitis genes *in vivo* and (B) TRAF6–p38-response genes in keratinocytes — would embody the necessary and sufficient conditions for keratinocytes in psoriatic dermatitis. Venn diagrams using microarray data deposited in the Gene Expression Omnibus (GEO) database (accession numbers: GSE 30999, GSE101077, and GSE110658) (4, 6, 8) revealed the gene sets for each group. Group (A) included fifteen genes that were shared between dermatitis induced by imiquimod (84 genes) or anisomycin (306 genes) and psoriasis (518 genes), which were four times or more higher in lesional skin than in non-lesional skin. Group (B) included nine genes that were shared between imiquimod-induced genes fully abrogated in keratinocyte-specific TRAF6-deficient mice (80 genes), anisomycin-induced genes fully abolished by treatment with the p38 inhibitor BIRB796 (282 genes), and p38-response genes two times or more higher in primary-cultured keratinocytes after treatment with anisomycin (124 genes).

Venn diagrams for groups (A) and (B) demonstrated that only two genes, *CXCL2* and *HBEGF*, were common to psoriatic dermatitis genes *in vivo* and TRAF6–p38-response genes in keratinocytes (Figure 1).

## Discussion

The condition of keratinocytes for the transcription of these two genes, *CXCL2* and *HBEGF*, in keratinocytes may contribute to the necessary and sufficient conditions for triggering inflammatory loops in the epithelial-immune microenvironment (EIME) (2) in psoriasis.

*CXCL2* encodes C-X-C motif chemokine ligand 2 (CXCL2, also known as GRO2 or MIP-2), an 8 kDa-chemokine produced by activated monocytes and neutrophils. CXCL2 is expressed at sites of inflammation and recruits inflammatory cells, such as neutrophils, via its receptor C-X-C motif chemokine receptor 2 (CXCR2). CXCL2 gene expression is NF-κB-dependent, and the enzymatic activities of both coactivator-associated arginine methyltransferase (CARM1/PRMT4) and transcriptional coactivator p300/CREB-binding protein are necessary for the NF-κB-mediated transactivation (9). p38-MAP kinase pathway is involved in the stabilization and translation of CXCL2 mRNAs (10, 11). Mechanistically, MAP kinase-activated protein kinase 2 (MK2), a downstream kinase of p38, phosphorylates heterogeneous nuclear ribonucleoprotein (hnRNP) A0, which binds to AU-rich elements (AREs) within the 3'-untranslated regions of CXCL2 mRNAs and stimulates their stabilization and translation (5, 11).

Epidermal keratinocytes produce chemoattractants, including CXCL2, and recruit neutrophils to the skin lesions of patients with psoriasis and its animal models (12). IL-17 stimulates the production of multiple chemokines, including CXCL2, in multiple cell lineages (13). In an acute trinitrobenzene sulfonic acid (TNBS)-induced colitis model, the production of CXCL2 in the colon and its severity are reduced in *Il17ra*$^{-/-}$ mice (14). Imiquimod-induced psoriatic dermatitis triggers the transcriptional expression of CXCL2 and CXCR2 in the earliest phase and is blunted by treatment with a selective CXCR2 antagonist (15). In contrast, evidence from other diseases has suggested the involvement of CXCL2 in the induction of the IL-23–IL-17 axis and the type 17 inflammatory loop. In patients with inflammatory bowel diseases, CXCR1$^{+}$ CXCR2$^{+}$ neutrophils that infiltrate the colon are the main sources of IL-23 (16). In addition, the antibody blockade of CXCR2 signaling reduces the expression levels of tissue IL-23 in the liver and intestine at the initial stage of graft-versus-host disease (GVHD) and attenuates disease severity (17). Furthermore, photodynamic therapy in BALB/c Colo26-HA tumor-bearing mice rapidly induces the accumulation of $T_H17$ cells in tumor-draining lymph nodes (TDLNs), and IL-17 promotes neutrophil migration into TDLNs across HEVs through preferential interactions between CXCR2 and CXCL2, but not CXCL1 (18). Moreover, the development of Candida-induced keratitis is blocked by anti-IL-17A or anti-IL-23p19 antibodies and is defective in nude mice. However, CXCL2 is sufficient to restore Candida keratitis in

10.3389/fimmu.2024.1326219

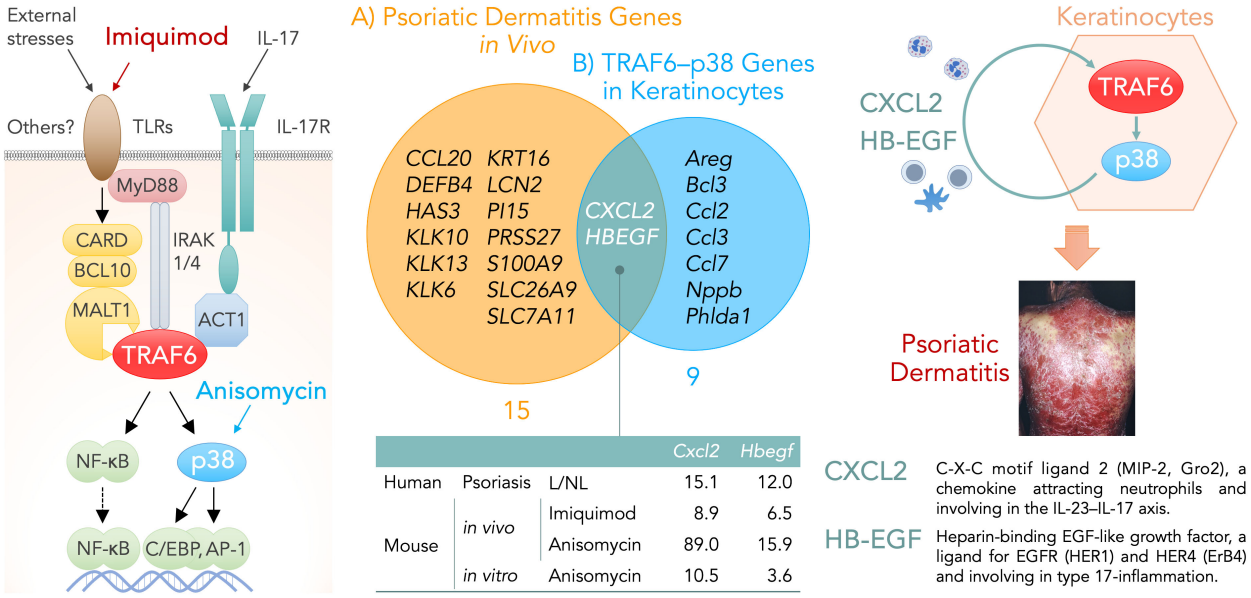


| | | | Cxcl2 | Hbegf |
|---|---|---|---|---|
| Human | Psoriasis | L/NL | 15.1 | 12.0 |
| Mouse | *in vivo* | Imiquimod | 8.9 | 6.5 |
| | | Anisomycin | 89.0 | 15.9 |
| | *in vitro* | Anisomycin | 10.5 | 3.6 |

FIGURE 1
***Left***, keratinocyte signaling pathways that are involved in the development of psoriatic dermatitis. Imiquimod binds to TLR7/8 and triggers the activation of MyD88-dependent TLR signaling pathway. External stresses promote the formation of the CARD–BCL10–MALT1 (CBM) complex and subsequent activation of the TRAF6 pathway. *CARD14* is selectively expressed in the skin and its gain-of-function mutation are found in patients with familial psoriasis although the upstream molecule of CARD14 remains unknown. Anisomycin is a p38-MAP kinase activator. ***Middle***, Venn diagrams showing genes expressed by keratinocytes under the necessary and sufficient conditions for psoriatic dermatitis: A) Psoriatic dermatitis genes *in vivo* (fifteen genes), which were shared between psoriasis and its animal models induced by imiquimod or anisomycin, were four times or more higher in lesional skin than in non-lesional skin. B) TRAF6–p38-response genes in keratinocytes (nine genes), which were shared between imiquimod-induced genes fully abrogated in keratinocyte-specific TRAF6-deficient mice, anisomycin-induced genes fully abolished by treatment with the p38 inhibitor BIRB796, and p38-response genes two times or more higher in primary-cultured keratinocytes after treatment with anisomycin. The table indicates the number of fold-increases in the gene expression levels of *Cxcl2* and *Hbegf* under each condition. ***Right***, the production of CXCL2 and HB-EGF may represent necessary and sufficient conditions for keratinocytes in the TRAF6–p38 pathway-mediated inflammatory loop of psoriatic dermatitis. ACT1, NF-κB activator 1; AP-1, activator protein 1; BCL10, B-cell lymphoma/leukemia 10; CARD, caspase recruitment domain-containing protein; C/EBP, CCAAT/enhancer binding protein; CXCL2, C-X-C motif ligand 2; HB-EGF, heparin-binding epidermal growth factor-like growth factor; HER, human epidermal growth factor receptor; IL, interleukin; IL-17R, interleukin 17 receptor; IRAK, interleukin-1 receptor-associated kinase; L, lesional skin; MALT1, mucosa associated lymphoid tissue lymphoma translocation gene 1; MAP kinase, mitogen-activated protein kinase; MyD88, myeloid differentiation primary response protein 88; NF-κB, nuclear factor kappa B; NL, nonlesional skin; TLR, Toll-like receptor; TRAF6, tumor necrosis factor receptor-associated factor 6.

nude mice (19). Therefore, it is likely that the CXCL2–IL-23–IL-17 loop in the EIME drives type 17 inflammation in patients with psoriasis.

*HBEGF* encodes a transmembrane protein called pro-heparin-binding epidermal growth factor-like growth factor (HB-EGF). The processing of pro-HB-EGF via ectodomain shedding by proteases, including a disintegrin and metalloproteinase (ADAM)17/TNF-α converting enzyme (TACE) and matrix metalloproteinases (MMPs), produces mature HB-EGF, a member of the EGF protein family (20). It is worth noting that the expression levels of several genes coding ADAMs and MMPs are significantly higher in the psoriasis lesional skin than in the nonlesional skin (8). HB-EGF is a ligand of epidermal growth factor receptor (EGFR)/human EGFR (HER)1 and HER4/ErbB4, whose activation triggers a series of signaling cascades and results in a variety of effects, including cell proliferation and migration. In contrast, a release of ATP in a challenging environment induces HB-EGF synthesis and release through the p38-MAP kinase pathway in human keratinocytes (21).

HB-EGF is involved in the development of pathological conditions associated with type 17 inflammation. $T_H17$-induced airway remodeling in a mouse asthma model leads to the epithelial overexpression of HB-EGF and is abolished by HB-EGF blockade (22). Transgenic mice that express HB-EGF throughout the intestine develop serrated polyps, in which the frequency of IL-17-producing γδ T cells is higher than in unaffected surrounding tissue or the wild-type (23).

HB-EGF is located in the basal layer of healthy and nonlesional skin, overexpressed in the suprabasal layers of uninvolved skin and marginal lesions in psoriasis, but not in the center part of psoriatic lesions (24). In human keratinocytes, HB-EGF and IL-17A synergistically induce IκBζ expression, which is essential for the induction of psoriasis signature genes *in vitro*, in a p38-MAP kinase-dependent manner (25). Notably, mice lacking HB-EGF specifically in keratinocytes show defects in wound healing (26), a process that simulates psoriatic conditions. EGFR is expressed in the basal and suprabasal layers of normal epidermis and is highly expressed throughout the epidermis in psoriatic lesions (27). Of note, there are reported cases treated for cancers with EGFR-blockade agents (cetuximab and erlotinib) resulting resolution of concomitant psoriasis (28). Expression levels of HER4 in epidermal keratinocytes are higher in the psoriasis lesional skin than those from normal skin (29). HER4 is also expressed in $CD4^+$ T cells from

patients with psoriasis, and treatment with HER4 siRNA reduced mouse IL-17A$^+$ CD4$^+$ T cells *in vitro* and imiquimod-induced dermatitis *in vivo* (30). These results suggest that HB-EGF is a critical downstream mediator of the TRAF6–p38 pathway in psoriatic dermatitis.

In conclusion, our previous findings suggest that TRAF6 in keratinocytes is a necessary factor and cutaneous activation of p38-MAP kinase is a sufficient factor for psoriatic dermatitis. Venn diagrams of their transcriptome data show that CXCL2 and HB-EGF are the only two factors produced by keratinocytes under the necessary and sufficient conditions for psoriatic dermatitis. This interpretation allows us to propose novel drug targets for psoriasis.

## Author contributions

TD: Conceptualization, Formal analysis, Supervision, Writing – original draft, Writing – review & editing. RM: Data curation, Formal analysis, Investigation, Writing – review & editing. KS: Data curation, Formal analysis, Investigation, Writing – review & editing. KK: Resources, Writing – review & editing.

## Funding

The author(s) declare that no financial support was received for the research, authorship, and/or publication of this article.

## Conflict of interest

The authors declare that the research was conducted in the absence of any commercial or financial relationships that could be construed as a potential conflict of interest.

## Publisher's note



## References

1. Dainichi T, Iwata M. Inflammatory loops in the epithelial–immune microenvironment of the skin and skin appendages in chronic inflammatory diseases. *Front Immunol* (2023) 14:1274270. doi: 10.3389/fimmu.2023.1274270

2. Dainichi T, Kitoh A, Otsuka A, Nakajima S, Nomura T, Kaplan DH, et al. The epithelial immune microenvironment (EIME) in atopic dermatitis and psoriasis. *Nat Immunol* (2018) 19(12):1286–98. doi: 10.1038/s41590-018-0256-2

3. van der Fits L, Mourits S, Voerman JS, Kant M, Boon L, Laman JD, et al. Imiquimod-induced psoriasis-like skin inflammation in mice is mediated via the IL-23/IL-17 axis. *J Immunol* (2009) 182(9):5836–45. doi: 10.4049/jimmunol.0802999

4. Sakurai K, Dainichi T, Garcet S, Tsuchiya S, Yamamoto Y, Kitoh A, et al. Cutaneous p38 mitogen-activated protein kinase activation triggers psoriatic dermatitis. *J Allergy Clin Immunol* (2019) 144(4):1036–49. doi: 10.1016/j.jaci.2019.06.019

5. Dainichi T, Matsumoto R, Mostafa A, Kabashima K. Immune control by TRAF6-mediated pathways of epithelial cells in the EIME (Epithelial immune microenvironment). *Front Immunol* (2019) 10:1107. doi: 10.3389/fimmu.2019.01107

6. Matsumoto R, Dainichi T, Tsuchiya S, Nomura T, Kitoh A, Hayden MS, et al. Epithelial TRAF6 drives IL-17-mediated psoriatic inflammation. *JCI Insight* (2018) 3 (15):e121175. doi: 10.1172/jci.insight.121175

7. Grinberg-Bleyer Y, Dainichi T, Oh H, Heise N, Klein U, Schmid RM, et al. Cutting Edge: NF-kappaB p65 and c-Rel Control Epidermal Development and Immune Homeostasis in the Skin. *J Immunol* (2015) 194(6):2472–6. doi: 10.4049/jimmunol.1402608

8. Suarez-Farinas M, Li K, Fuentes-Duculan J, Hayden K, Brodmerkel C, Krueger JG. Expanding the psoriasis disease profile: interrogation of the skin and serum of patients with moderate-to-severe psoriasis. *J Invest Dermatol* (2012) 132(11):2552–64. doi: 10.1038/jid.2012.184

9. Covic M, Hassa PO, Saccani S, Buerki C, Meier NI, Lombardi C, et al. Arginine methyltransferase CARM1 is a promoter-specific regulator of NF-kappaB-dependent gene expression. *EMBO J* (2005) 24(1):85–96. doi: 10.1038/sj.emboj.7600500

10. Xiao YQ, Someya K, Morita H, Takahashi K, Ohuchi K. Involvement of p38 MAPK and ERK/MAPK pathways in staurosporine-induced production of macrophage inflammatory protein-2 in rat peritoneal neutrophils. *Biochim Biophys Acta* (1999) 1450(2):155–63. doi: 10.1016/s0167-4889(99)00042-7

11. Rousseau S, Morrice N, Peggie M, Campbell DG, Gaestel M, Cohen P. Inhibition of SAPK2a/p38 prevents hnRNP A0 phosphorylation by MAPKAP-K2 and its interaction with cytokine mRNAs. *EMBO J* (2002) 21(23):6505–14. doi: 10.1093/emboj/cdf639

12. Furue M, Furue K, Tsuji G, Nakahara T. Interleukin-17A and keratinocytes in psoriasis. *Int J Mol Sci* (2020) 21(4):1275. doi: 10.3390/ijms21041275

13. Onishi RM, Gaffen SL. Interleukin-17 and its target genes: mechanisms of interleukin-17 function in disease. *Immunology* (2010) 129(3):311–21. doi: 10.1111/j.1365-2567.2009.03240.x

14. Zhang Z, Zheng M, Bindas J, Schwarzenberger P, Kolls JK. Critical role of IL-17 receptor signaling in acute TNBS-induced colitis. *Inflammation Bowel Dis* (2006) 12 (5):382–8. doi: 10.1097/01.MIB.0000218764.06959.91

15. Sumida H, Yanagida K, Kita Y, Abe J, Matsushima K, Nakamura M, et al. Interplay between CXCR2 and BLT1 facilitates neutrophil infiltration and resultant keratinocyte activation in a murine model of imiquimod-induced psoriasis. *J Immunol* (2014) 192(9):4361–9. doi: 10.4049/jimmunol.1302959

16. Kvedaraite E, Lourda M, Idestrom M, Chen P, Olsson-Akefeldt S, Forkel M, et al. Tissue-infiltrating neutrophils represent the main source of IL-23 in the colon of patients with IBD. *Gut* (2016) 65(10):1632–41. doi: 10.1136/gutjnl-2014-309014

17. Cho KA, Woo SY, Park YS, Park MH, Ryu KH. Macrophage inflammatory protein-2 (MIP-2)/CXCR2 blockade attenuates acute graft-versus-host disease while preserving graft-versus-leukemia activity. *Biochem Biophys Res Commun* (2012) 426 (4):558–64. doi: 10.1016/j.bbrc.2012.08.126

18. Brackett CM, Muhitch JB, Evans SS, Gollnick SO. IL-17 promotes neutrophil entry into tumor-draining lymph nodes following induction of sterile inflammation. *J Immunol* (2013) 191(8):4348–57. doi: 10.4049/jimmunol.1103621

19. Zhang H, Li H, Li Y, Zou Y, Dong X, Song W, et al. IL-17 plays a central role in initiating experimental Candida albicans infection in mouse corneas. *Eur J Immunol* (2013) 43(10):2671–82. doi: 10.1002/eji.201242891

20. Dao DT, Anez-Bustillos L, Adam RM, Puder M, Bielenberg DR. Heparin-binding epidermal growth factor-like growth factor as a critical mediator of tissue repair and regeneration. *Am J Pathol* (2018) 188(11):2446–56. doi: 10.1016/j.ajpath.2018.07.016

21. Giltaire S, Lambert S, Poumay Y. HB-EGF synthesis and release induced by cholesterol depletion of human epidermal keratinocytes is controlled by extracellular ATP and involves both p38 and ERK1/2 signaling pathways. *J Cell Physiol* (2011) 226 (6):1651–9. doi: 10.1002/jcp.22496

22. Wang Q, Li H, Yao Y, Xia D, Zhou J. The overexpression of heparin-binding epidermal growth factor is responsible for Th17-induced airway remodeling in an experimental asthma model. *J Immunol* (2010) 185(2):834–41. doi: 10.4049/jimmunol.0901490

23. Bongers G, Pacer ME, Geraldino TH, Chen L, He Z, Hashimoto D, et al. Interplay of host microbiota, genetic perturbations, and inflammation promotes local development of intestinal neoplasms in mice. *J Exp Med* (2014) 211(3):457–72. doi: 10.1084/jem.20131587

24. Zheng Y, Peng Z, Wang Y, Tan S, Xi Y, Wang G. Alteration and significance of heparin-binding epidermal-growth-factor-like growth factor in psoriatic epidermis. *Dermatology* (2003) 207(1):22–7. doi: 10.1159/000070936

25. Dai X, Murakami M, Shiraishi K, Muto J, Tohyama M, Mori H, et al. EGFR ligands synergistically increase IL-17A-induced expression of psoriasis signature genes

in human keratinocytes via IkappaBzeta and Bcl3. *Eur J Immunol* (2022) 52(6):994–1005. doi: 10.1002/eji.202149706

26. Shirakata Y, Kimura R, Nanba D, Iwamoto R, Tokumaru S, Morimoto C, et al. Heparin-binding EGF-like growth factor accelerates keratinocyte migration and skin wound healing. *J Cell Sci* (2005) 118(Pt 11):2363–70. doi: 10.1242/jcs.02346

27. Amagai M, Ozawa S, Ueda M, Nishikawa T, Abe O, Shimizu N. Distribution of EGF receptor expressing and DNA replicating epidermal cells in psoriasis vulgaris and Bowen's disease. *Br J Dermatol* (1988) 119(5):661–8. doi: 10.1111/j.1365-2133.1988.tb03480.x

28. Overbeck TR, Griesinger F. Two cases of psoriasis responding to erlotinib: time to revisiting inhibition of epidermal growth factor receptor in psoriasis therapy? *Dermatology* (2012) 225(2):179–82. doi: 10.1159/000342786

29. Huang C, Zhong W, Ren X, Huang X, Li Z, Chen C, et al. MiR-193b-3p-ERBB4 axis regulates psoriasis pathogenesis via modulating cellular proliferation and inflammatory-mediator production of keratinocytes. *Cell Death Dis* (2021) 12 (11):963. doi: 10.1038/s41419-021-04230-5

30. Tang R, Cui H, Dou R, Tao L, Tan L, Guo T, et al. ErbB4 affects Th1/Th17 cell differentiation and promotes psoriasis progression. *Cell Mol Biol (Noisy-le-grand)* (2023) 69(12):1–5. doi: 10.14715/cmb/2023.69.12.1

frontiers | Frontiers in Immunology

TYPE Original Research
PUBLISHED 13 February 2024
DOI 10.3389/fimmu.2024.1323174



OPEN ACCESS

EDITED BY
Zhenghua Zhang,
Fudan University, China

REVIEWED BY
Xiao-Yong Man,
Zhejiang University, China
Fusheng Zhou,
Anhui Medical University, China

*CORRESPONDENCE
Yuling Shi
shiyuling1973@tongji.edu.cn
Xin Wang
wx2205553@tongji.edu.cn
Qian Yu
yuervictory@163.com

†These authors have contributed equally to this work

RECEIVED 17 October 2023
ACCEPTED 30 January 2024
PUBLISHED 13 February 2024

CITATION
Ma R, Cui L, Cai J, Yang N, Wang Y, Chen Q, Chen W, Peng C, Qin H, Ding Y, Wang X, Yu Q and Shi Y (2024) Association between systemic immune inflammation index, systemic inflammation response index and adult psoriasis: evidence from NHANES. *Front. Immunol.* 15:1323174. doi: 10.3389/fimmu.2024.1323174



# Association between systemic immune inflammation index, systemic inflammation response index and adult psoriasis: evidence from NHANES

Rui Ma[1,2†], Lian Cui[1,2†], Jiangluyi Cai[1,2†], Nan Yang[1,2], Yuanyuan Wang[1,2], Qianyu Chen[1,2], Wenjuan Chen[1,2], Chen Peng[1,2], Hui Qin[1,2], Yangfeng Ding[1,2], Xin Wang[1,2*], Qian Yu[2,3*] and Yuling Shi[1,2*]

[1]Department of Dermatology, Shanghai Skin Disease Hospital, Tongji University School of Medicine, Shanghai, China, [2]Institute of Psoriasis, Tongji University School of Medicine, Shanghai, China, [3]Department of Dermatology, Shanghai Tenth People's Hospital, Tongji University School of Medicine, Shanghai, China

**Background:** The systemic immune-inflammation index (SII) and systemic inflammation response index (SIRI) are both novel biomarkers and predictors of inflammation. Psoriasis is a skin disease characterized by chronic inflammation. This study aimed to investigate the potential association between SII, SIRI, and adult psoriasis.

**Methods:** Data of adults aged 20 to 80 years from the National Health and Nutrition Examination Survey (NHANES) (2003–2006, 2009–2014) were utilized. The K-means method was used to group SII and SIRI into low, medium, and high-level clusters. Additionally, SII or SIRI levels were categorized into three groups: low ($1^{st}$-$3^{rd}$ quintiles), medium ($4^{th}$ quintile), and high ($5^{th}$ quintile). The association between SII-SIRI pattern, SII or SIRI individually, and psoriasis was assessed using multivariate logistic regression models. The results were presented as odds ratios (ORs) and confidence intervals (CIs). Restricted cubic spline (RCS) regression, subgroup, and interaction analyses were also conducted to explore the potential non-linear and independent relationships between natural log-transformed SII (lnSII) levels or SIRI levels and psoriasis, respectively.

**Results:** Of the 18208 adults included in the study, 511 (2.81%) were diagnosed with psoriasis. Compared to the low-level group of the SII-SIRI pattern, participants in the medium-level group had a significantly higher risk for psoriasis (OR = 1.40, 95% CI: 1.09, 1.81, $p$-trend = 0.0031). In the analysis of SII or SIRI individually, both SII and SIRI were found to be positively associated with the risk of psoriasis (high vs. low group OR = 1.52, 95% CI: 1.18, 1.95, $p$-trend = 0.0014; OR = 1.48, 95% CI: 1.12, 1.95, $p$-trend = 0.007, respectively). Non-linear relationships were observed between lnSII/SIRI and psoriasis (both $p$-values for overall < 0.05, $p$-values for nonlinearity < 0.05). The association between SII levels and psoriasis was stronger in females, obese individuals, people with type 2 diabetes, and those without hypercholesterolemia.

**Conclusion:** We observed positive associations between SII-SIRI pattern, SII, SIRI, and psoriasis among U.S. adults. Further well-designed studies are needed to gain a better understanding of these findings.

KEYWORDS

systemic immune-inflammation index, systemic inflammation response index, psoriasis, adults, NHANES

# Introduction

Psoriasis is a common chronic inflammatory skin disease that affects over 60 million adults and children worldwide, causing a significant burden on society (1). It is characterized by erythematous and scaly skin lesions that can appear on various parts of the body, accompanied by systemic manifestations (2). The etiology of psoriasis is not fully understood and involves complex interactions between genetic, immune, and environmental factors (3). Psoriasis is currently incurable, but the search for new factors or biomarkers to assess its risk has always attracted extensive attention and is expected to have clinical applications.

Undoubtedly, psoriasis is an inflammatory skin disease in which both systemic and local inflammatory reactions play crucial roles in its onset and progression (1). However, there is limited research available on the relationship between psoriasis and the overall chronic inflammatory status of the body. The systemic immune-inflammation index (SII) and system inflammation response index (SIRI) are integrated and innovative inflammatory biomarker have recently been proposed based on immune cell subpopulation and platelet counts (4, 5). These indices have been widely used in studies to assess the association between chronic inflammatory status and various human diseases, including cancers, metabolic disorders, and inflammatory conditions (6, 7).

The National Health and Nutrition Examination Survey (NHANES) is a comprehensive survey conducted in the United States that utilizes complex, multi-stage, and probability sampling methods to gather nutritional and health information about the population (8). Using the NHANES database, more and more factors related to human health and diseases have been discovered. For instance, recent studies have utilized the NHANES database to investigate the roles of SII and SIRI in various human diseases (9, 10).

Despite the growing body of research, the links between SII/SIRI and psoriasis remain unclear. Therefore, our study aims to explore this relationship using the NHANES database.

# Methods

## Study population

This study was conducted basing on the NHANES database (11). All NHANES protocols were approved by the NCHS Research Ethics Review Board (Protocol #98-12, Continuation of Protocol #2005-06, Continuation of Protocol #2011-17, http://www.cdc.gov/nchs/nhanes/irba98.htm), and informed consent was obtained from all participants when they were enrolled. A total of 50938 participants from five NHANES cycles (2003–2004, 2005–2006, 2009–2010, 2011–2012, and 2013–2014) were enrolled in the present study. Exclusion criteria included: 1) missing psoriasis diagnosis data, 2) age <20 years old (psoriasis data for participants <20 years of age were missing in the 2003–2004 and 2005–2006 cycles), 3) missing SII or SIRI data, and 4) missing data on other covariates. A total of 18208 participants were included for analysis (Figure 1).

## Assessment of psoriasis

Psoriasis was defined if the participants responded affirmatively to the question, "Have you ever been told by a health care provider that you had psoriasis?" or "Have you ever been told by a doctor or other health care professional that you had psoriasis (sore-eye-asis)?" (12). Participants who refused to answer or did not know were excluded (13).

## Definition of systemic immune-inflammation index and systemic inflammation response index

Peripheral blood samples of the NHANES participants were analyzed at the Mobile Examination Centers (MEC) using a Beckman Coulter HMX Hematology Analyzer. Lymphocyte, neutrophil, monocyte, and platelet counts were measured via

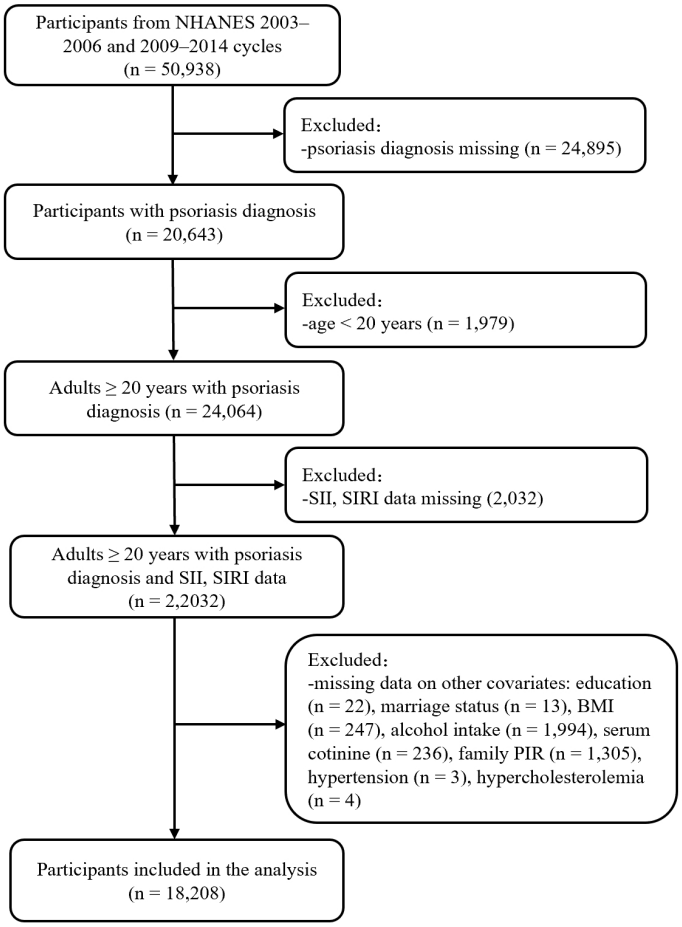


FIGURE 1
Flow chart of participant selection. BMI, body mass index; NHANES, National Health and Nutrition Examination Survey; PIR, poverty income ratio; SII, systemic immune inflammation index; SIRI, systemic inflammation response index.

complete blood count, and were presented as $\times 10^3$ cells/μL. The SII and SIRI levels were calculated using the following formulas: platelet count × neutrophil count/lymphocyte count, monocyte count × neutrophil count/lymphocyte count, respectively. These values were expressed as $\times 10^3$ cells/μL based on previous studies (4, 14, 15). SII and SIRI were considered as exposure variables in this study.

## Covariates

Based on existing literature, potential confounders that may affect psoriasis were evaluated. These variables included age (20-60, >60 years old), gender (male and female), race/ethnicity (Mexican American, other Hispanic, non-Hispanic White, non-Hispanic Black, other race/multiracial), education level (high school or lower, college or above), marital status (married/living with partner, widowed/divorced/separated, never married), family poverty income ratio (PIR), alcohol intake (mild, <1 time per week; moderate, 1-3 times per week; severe, ≥4 times per week), body mass index (BMI) (<25, 25–29.9, ≥30 kg/m$^2$), serum cotinine (ng/mL), hypertension (yes/no), type 2 diabetes (T2D) (yes/no), and hypercholesterolemia (yes/no). Hypertension was diagnosed if at least one of the following criteria were met: systolic pressure/diastolic pressure ≥140/90 mmHg, self-reported physician diagnosis of hypertension, or self-reported use of hypertension medication (16). T2D was diagnosed if at least one of the following criteria were met: glycosylated hemoglobin ≥6.5%, fasting blood glucose ≥7.0 mmol/L (126 mg/dL), self-reported physician diagnosis of diabetes, or self-reported use of insulin (16). Hypercholesterolemia was diagnosed if at least one of the following criteria were met: cholesterol ≥240 mg/dL, self-reported physician diagnosis of, or self-reported use of hypercholesterolemia medication (17).

## Statistical analysis

Results including geometric mean (GM), standard error (SE), percentiles, odds ratio (OR), and 95% confidence interval (CI), were adjusted using specific sample weights, clustering, and stratification to account for the complex survey design of NHANES and to ensure data representativeness of the noninstitutionalized U.S. population. And based on the NHANES analytic guidelines (18), the formula of calculating

sampling weight was as follows: fasting subsample 10-year MEC weight = fasting subsample 2-year MEC weight/5 (12).

Various statistical methods were employed for data analysis. GM and SEs were reported for non-normally distributed continuous variables, while categorical variables were described in terms of frequency and percentage. Baseline characteristics between different groups were compared using the Kruskal–Wallis H test and Rao-Scott chi-square test, as appropriate. In order to categorize participants into different clusters based on their SII and SIRI measurements, the SII and SIRI data were first scaled and the k-means method was then applied. The k-means algorithm is a non-model-based technique used for categorizing mixed data (11, 19). It creates clusters in such a way that the squared Euclidean distance between the row vector of any object and the centroid vector of its corresponding cluster is minimized compared to the distances to the centroids of other clusters (20). The optimal number of clusters in this study was determined using the elbow method (20), and the subgroups were reduced in dimensionality and visualized using t-Distributed Stochastic Neighbor Embedding (t-SNE). Besides, categorical analysis on SII or SIRI levels individually was also performed by categorizing participants into three groups based on the quintile of SII/SIRI levels, including low group ($1^{st}$ – $3^{rd}$ quintiles), medium group ($4^{th}$ quintile) and high group ($5^{th}$ quintile), respectively. Multivariate logistic regression models were used to calculate ORs and CIs to assess the associations between SII-SIRI pattern (by k-means algorithm)/SII/SIRI levels and psoriasis. For the right-skewed distribution of SII levels, SII levels were natural log-transformed (lnSII) when assessing the association between SII levels (continuous variable) and psoriasis risk. The crude model was adjusted for no covariates, while the fully adjusted model was adjusted for gender, age, race/ethnicity, education levels, marital status, BMI, alcohol intake, serum cotinine, family PIR, hypertension, T2D, and hypercholesterolemia. Additionally, four-knot (5th, 35th, 65th, and 95th quantiles) restricted cubic splines (RCS) were used to estimate exposure–response curves of SII/SIRI levels and psoriasis. A $p$-value <0.05 for overall and nonlinear indicated a non-linear relationship between SII/SIRI levels and psoriasis.

Finally, stratification analyses by gender (male, female), age (20–60, >60 years old), BMI (<25, 25–29.9, ≥30 kg/m$^2$), hypertension (no and yes), T2D (no and yes), and hypercholesterolemia (no and yes) were performed, as well as interaction analyses between various stratification factors and lnSII or SIRI.

All analyses were conducted using SAS 9.4 software (SAS Institute Inc., Cary, NC, USA) and R (version 4.3.1, R Development Core Team). The R package "rms" was used for RCS analysis. A two-sided $p$-value<0.05 was considered statistically significant.

# Results

## Participants characteristics

Among 18,208 adults aged 20–80 years from five NHANES cycles, 511 (2.81%) were diagnosed with psoriasis. The baseline characteristics of the study participants, both those with and without psoriasis, are shown in Table 1. In brief, there were obvious differences between participants with psoriasis and those without psoriasis, including race/ethnicity, BMI, the incidence of hypertension and hypercholesterolemia, SII levels, SIRI levels, lymphocyte and neutrophil counts.

A total of 18,208 participants were also clustered into three subgroups based on SII–SIRI pattern (by k-means algorithm, Figure 2), SII levels, and SIRI levels, respectively. As shown in Table 2, SII-SIRI pattern/SII/SIRI levels were significantly associated with gender, age, race/ethnicity, education levels, alcohol intake, marital status, serum cotinine levels, the incidence of psoriasis, hypertension, T2D and hypercholesterolemia. And the levels of SII, SIRI, lymphocyte, monocyte, neutrophil and peripheral platelet counts were significantly different among the three subgroups (Table 3). Comparing to low–level group, the high–level group had the highest levels of SII, SIRI, monocyte, neutrophil and peripheral platelet counts, and the lowest lymphocyte counts.

## Association between SII-SIRI pattern/SII/SIRI levels and the risk of psoriasis

As presented in Table 4, medium levels of SII-SIRI pattern were associated with an increased risk of psoriasis (medium vs. low, OR = 1.54, 95% CI: 1.20, 1.98, $p$-trend = 0.0002) in the crude model. The results remained robust and statistically significant (medium vs. low, OR = 1.40, 95% CI: 1.09, 1.81, $p$-trend = 0.0031) after multivariable adjustment. Compared to the low–level group of SII, multivariate-adjusted OR for participants in the high–level group tend to be higher (high vs. low, OR = 1.52, 95% CI: 1.18, 1.95, $p$-trend = 0.0014). Similar results were found for SIRI levels (high vs. low, OR = 1.48, 95% CI: 1.12, 1.95, $p$-trend = 0.007). When lnSII or SIRI levels were included as continuous variables in the multivariate logistic regression models, the positive associations still existed (OR = 1.39, 95% CI: 1.12, 1.74, $p$ = 0.0038; OR = 1.10, 95% CI: 1.02, 1.18, $p$ = 0.016, respectively).

Based on the association between the SII-SIRI pattern and psoriasis, we aimed to determine the range of SII and SIRI levels that were positively associated with an increased risk of psoriasis. As shown in Table 5, when SII levels were higher than 737.69 × $10^3$ cells/μL, and SIRI levels ranged from 1.18 to 1.65 × $10^3$ cells/μL, the risk of psoriasis increased significantly (OR = 2.17, 95% CI: 1.25, 3.79, $p$ = 0.007). No significant associations were found among other concentration ranges.

## Dose-response relationship between SII/SIRI levels and the risk of psoriasis

As shown in Figure 3, after adjusting for multiple potential confounders, the nonlinear associations between SII/SIRI levels and the risk of psoriasis were statistically significant ($p$ value for overall < 0.05 and $p$ value for nonlinear < 0.05). As SII increased from 486.75 to 1418.09 × $10^3$ cells/μL, the OR (95% CI) of psoriasis increased from 1.02 (1.01, 1.02) to 1.33 (1.00, 1.77), indicating a

10.3389/fimmu.2024.1323174

TABLE 1 Baseline characteristics of participants in the NHANES follow-up study from 2003–2006 and 2009–2014 cycles (n = 18,208).

| Characteristics | Participants | | | *p*-value |
|---|---|---|---|---|
| | Total | Without psoriasis | With psoriasis | |
| N | 18208 | 17697 | 511 | |
| Sex | | | | 0.797 |
| Male | 8909 (49.38) | 8665 (49.40) | 244 (48.81) | |
| Female | 9299 (50.62) | 9032 (50.60) | 267 (51.19) | |
| Age | | | | 0.216 |
| 20-60 | 13957 (82.53) | 13586 (82.60) | 371 (80.34) | |
| >60 | 4251 (17.47) | 4111 (17.40) | 140 (19.66) | |
| Race/ethnicity | | | | <0.0001 |
| Mexican American | 2809 (8.18) | 2767 (8.32) | 42 (3.80) | |
| Other Hispanic | 1403 (4.80) | 1364 (4.85) | 39 (3.51) | |
| Non-Hispanic White | 8546 (70.11) | 8227 (69.73) | 319 (81.92) | |
| Non-Hispanic Black | 3776 (10.59) | 3710 (10.75) | 66 (5.84) | |
| Other race/multiracial | 1674 (6.31) | 1629 (6.36) | 45 (4.94) | |
| Education level | | | | 0.093 |
| High school or lower | 8219 (37.57) | 8009 (37.71) | 210 (33.48) | |
| College or above | 9989 (62.43) | 9688 (62.29) | 301 (66.52) | |
| Alcohol intake (times/week) | | | | 0.216 |
| Mild (<1) | 12275 (62.05) | 11932 (62.12) | 343 (59.75) | |
| Moderate (1-3) | 4204 (26.25) | 4094 (26.28) | 110 (25.35) | |
| Severe (≥) | 1729 (11.70) | 1671 (11.59) | 58 (14.90) | |
| Marital status | | | | 0.565 |
| Married/living with partner | 11032 (64.49) | 10729 (31.43) | 303 (64.28) | |
| widowed/divorced/separated | 3600 (16.91) | 3474 (32.30) | 126 (18.58) | |
| Never married | 3576 (18.60) | 3494 (36.27) | 82 (17.14) | |
| BMI (kg/m2) | | | | 0.0006 |
| <25 | 5460 (31.12) | 5349 (31.43) | 111 (21.48) | |
| 25-29.9 | 5866 (32.40) | 5694 (32.30) | 172 (35.61) | |
| ≥30 | 6882 (36.48) | 6654 (36.27) | 228 (42.92) | |
| Serum cotinine (ng/mL) | 0.35 ± 0.03 | 0.36 ± 0.03 | 0.29 ± 0.06 | 0.272 |
| Family PIR | 2.42 ± 0.05 | 2.42 ± 0.04 | 2.51 ± 0.11 | 0.130 |
| Hypertension (yes) | 6824 (34.19) | 6575 (33.81) | 249 (45.88) | <0.0001 |
| T2D (yes) | 2524 (9.68) | 2270 (9.63) | 90 (11.20) | 0.289 |
| Hypercholesterolemia (yes) | 6986 (37.76) | 6734 (37.44) | 252 (47.62) | <0.0001 |
| SII ($10^3$ cells/μL) | 488.17 ± 3.70 | 486.57 ± 3.73 | 542.72 ± 14.23 | <0.0001 |
| SIRI ($10^3$ cells/μL) | 1.05 ± 0.01 | 1.05 ± 0.01 | 1.17 ± 0.04 | 0.0006 |
| Lymphocyte ($10^3$ cells/μL) | 2.01 ± 0.01 | 2.01 ± 0.01 | 1.93 ± 0.03 | 0.019 |

*(Continued)*

TABLE 1 Continued

| Characteristics | Participants | | | *p*-value |
|---|---|---|---|---|
| | Total | Without psoriasis | With psoriasis | |
| Monocyte ($10^3$ cells/μL) | 0.52 ± 0.00 | 0.52 ± 0.00 | 0.53 ± 0.01 | 0.774 |
| Neutrophil ($10^3$ cells/μL) | 4.04 ± 0.02 | 4.03 ± 0.02 | 4.25 ± 0.08 | 0.003 |
| peripheral platelet ($10^3$ cells/μL) | 242.72 ± 0.95 | 242.55 ± 0.96 | 245.73 ± 3.24 | 0.142 |

Data are expressed as geometric mean ± SE or frequency (percentage). Percentages, geometric mean, and SE were weight-adjusted using NHANES-specified sampling weights. For categorical variables, p-values were calculated using Rao-Scott chi-square test, and for continuous variables, p-values were calculated using Kruskal–Wallis H test (non-normal distribution). —, not applicable; BMI, body mass index; NHANES, National Health and Nutrition Examination Survey; PIR, poverty income ratio; Q, quantile; SE, standard error; SII, systemic immune–inflammation index; SIRI, systemic inflammation response index; T2D, type 2 diabetes.

positive association between the SII levels and psoriasis risk within this range. Similarly, a positive association existed between SIRI levels and psoriasis risk (from 1.03 (1.01, 1.04) to 1.40 (1.00, 1.96)) when SIRI ranged from 1.06 to 4.29 × $10^3$ cells/μL.

## Subgroup analysis

To further study the roles of potential confounders in the associations of SII/SIRI levels with psoriasis, we divided the participants in subgroups stratified by gender, age, BMI, hypertension, T2D, and hypercholesterolemia (Figure 4). In subgroups analysis of SII levels, a statistically significant association was only observed in females, in the 20-60 years age group, in those with a BMI ≥ 30 kg/m2, without hypertension, with T2D, or without hypercholesterolemia (all $p < 0.05$). In the subgroup analysis of SIRI levels, positive associations were found in older adults (> 60 years of age), those with T2D, or without hypercholesterolemia (all $p < 0.05$). However, we did not find any significant interactions between SII/SIRI levels and those potential confounders (all $p$ value for interaction > 0.05).

# Discussion

To our knowledge, this current cross-sectional study is the first to investigate the association between the SII-SIRI pattern, as well as SII and SIRI individually, and the risk of psoriasis in a large, nationally representative sample. The results of this study revealed that significant changes in the SII-SIRI pattern are independently associated with an increased risk of psoriasis in the NHANES population. Interestingly, the association between SII or SIRI levels and the occurrence of psoriasis exhibited a non-linear dose-response relationship. Additionally, our findings suggest that monitoring SII and SIRI levels and combining these two indexes in analysis may assist in the early identification of individuals at high risk of developing psoriasis. Furthermore,

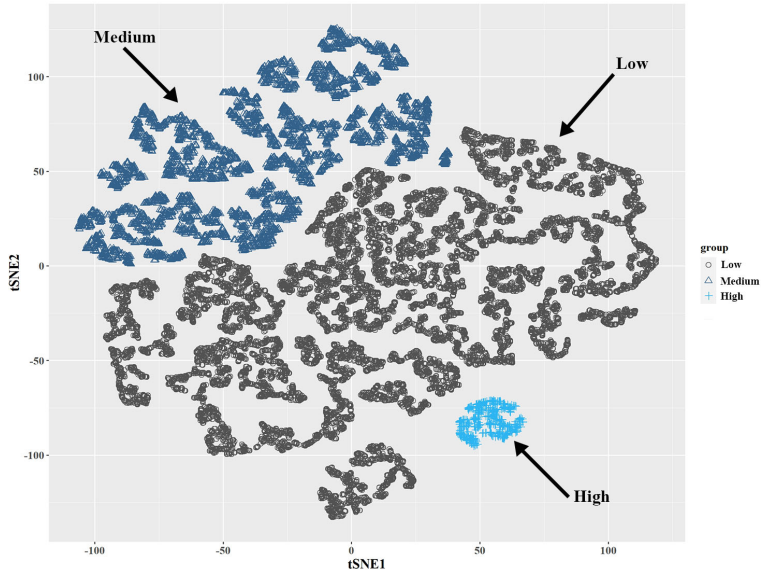


FIGURE 2
Visualization of k-means clustering using t-SNE for NHANES participants (2003-2006, 2009-2014, n = 18,208) based on SII and SIRI levels. Three sub-groups (low-, medium-, and high-level groups) were identified based on the combination of SII and SIRI levels. NHANES, National Health and Nutrition Examination Survey; SII, systemic immune–inflammation index; SIRI, systemic inflammation response index; t-SNE, t-Distributed Stochastic Neighbor Embedding.

TABLE 2 Baseline characteristics of participants based on subgroups of SII-SIRI pattern/SII/SIRI levels in the NHANES follow-up study from 2003–2006 and 2009–2014 cycles (n = 18,208).

| Characteristics | SII-SIRI pattern divided by k-means method | | | | SII levels ($10^3$ cells/μL) | | | | SIRI levels ($10^3$ cells/μL) | | | |
|---|---|---|---|---|---|---|---|---|---|---|---|---|
| | Low | Medium | High | *p*-value | Low (Q1-Q3, <549.50) | Medium (Q4, 549.50-737.69) | High (Q5, ≥737.69) | *p*-value | Low (Q1-Q3, <1.18) | Medium (Q4, 1.18-1.65) | High (Q5, ≥1.65) | *p*-value |
| N | 12606 | 5130 | 472 | | 11103 | 3492 | 3613 | | 11032 | 3458 | 3718 | |
| SII-SIRI pattern | | | | | | | | <0.0001 | | | | <0.0001 |
| Low | – | – | – | – | 10591 (95.50) | 1816 (52.78) | 199 (5.24) | | 10661 (96.47) | 1859 (53.26) | 86 (1.95) | |
| Medium | – | – | – | – | 510 (4.48) | 1673 (47.17) | 2947 (82.71) | | 371 (3.53) | 1595 (46.60) | 3164 (86.08) | |
| High | – | – | – | – | 2 (0.02) | 3 (0.06) | 467 (12.04) | | 0 (0.00) | 4 (0.14) | 468 (11.97) | |
| Sex | | | | 0.134 | | | | <0.0001 | | | | <0.0001 |
| Male | 6209 (49.42) | 2456 (48.80) | 244 (55.00) | | 5834 (52.85) | 1632 (47.49) | 1443 (40.87) | | 5137 (46.40) | 1779 (52.09) | 1993 (55.63) | |
| Female | 6397 (50.58) | 2674 (51.20) | 228 (45.00) | | 5269 (47.15) | 1860 (52.51) | 2170 (59.13) | | 5895 (53.60) | 1679 (47.91) | 1725 (44.37) | |
| Age | | | | <0.0001 | | | | 0.909 | | | | <0.0001 |
| 20-60 | 9831 (83.98) | 3805 (79.87) | 321 (72.82) | | 8451 (82.50) | 2688 (82.79) | 2818 (82.35) | | 8777 (85.23) | 2598 (81.59) | 2582 (75.38) | |
| >60 | 2775 (16.03) | 1325 (20.13) | 151 (27.18) | | 2652 (17.50) | 804 (17.21) | 795 (17.65) | | 2255 (14.77) | 860 (18.41) | 1136 (24.62) | |
| Race/ethnicity | | | | <0.0001 | | | | <0.0001 | | | | <0.0001 |
| Mexican American | 1979 (8.59) | 772 (7.39) | 58 (5.81) | | 1654 (8.22) | 568 (8.32) | 587 (7.91) | | 1711 (8.54) | 578 (8.21) | 520 (7.06) | |
| Other Hispanic | 1018 (5.12) | 358 (4.18) | 27 (3.22) | | 880 (4.93) | 276 (5.03) | 247 (4.20) | | 880 (5.11) | 2665 (4.77) | 258 (3.93) | |
| Non-Hispanic White | 5355 (67.29) | 2886 (75.95) | 305 (81.44) | | 4757 (67.59) | 1822 (73.40) | 1967 (74.40) | | 4491 (66.11) | 1838 (74.21) | 2217 (78.06) | |
| Non-Hispanic Black | 3017 (12.37) | 699 (6.68) | 60 (6.41) | | 2733 (12.72) | 545 (7.78) | 498 (7.02) | | 2825 (13.39) | 486 (6.65) | 465 (6.13) | |
| Other race/multiracial | 1237 (6.64) | 415 (5.80) | 22 (3.12) | | 1079 (6.54) | 281 (5.47) | 314 (6.46) | | 1125 (6.86) | 291 (6.16) | 258 (4.82) | |
| Education level | | | | 0.0002 | | | | 0.049 | | | | <0.0001 |
| High school or lower | 5610 (36.56) | 2370 (39.57) | 239 (42.84) | | 4972 (36.88) | 1570 (37.49) | 1677 (39.76) | | 4816 (35.87) | 1620 (38.79) | 1783 (41.48) | |
| College or above | 6996 (63.44) | 2760 (60.43) | 233 (57.16) | | 6131 (63.12) | 1992 (62.51) | 1936 (60.24) | | 6216 (64.13) | 1838 (61.21) | 1935 (58.52) | |
| Alcohol intake (times/week) | | | | 0.013 | | | | <0.0001 | | | | 0.004 |
| Mild (<1) | 8470 (61.51) | 3490 (63.31) | 315 (62.37) | | 7339 (60.15) | 2400 (64.37) | 2536 (65.44) | | 7453 (61.72) | 2322 (62.83) | 2500 (62.28) | |
| Moderate (1-3) | 2981 (27.15) | 1124 (24.33) | 99 (23.49) | | 2700 (28.11) | 763 (23.90) | 741 (23.02) | | 2610 (27.30) | 796 (25.45) | 798 (23.93) | |
| Severe (≥) | 1155 (11.34) | 516 (12.35) | 58 (14.14) | | 1064 (11.74) | 329 (11.73) | 336 (11.54) | | 969 (10.99) | 340 (11.72) | 420 (13.80) | |

*(Continued)*





10.3389/fimmu.2024.1323174

TABLE 2 Continued

| Characteristics | SII-SIRI pattern divided by k-means method | | | | SII levels ($10^3$ cells/μL) | | | | SIRI levels ($10^3$ cells/μL) | | | |
|---|---|---|---|---|---|---|---|---|---|---|---|---|
| | Low | Medium | High | *p*-value | Low (Q1-Q3, <549.50) | Medium (Q4, 549.50-737.69) | High (Q5, ≥737.69) | *p*-value | Low (Q1-Q3, <1.18) | Medium (Q4, 1.18-1.65) | High (Q5, ≥1.65) | *p*-value |
| Marital status | | | | <0.0001 | | | | <0.0001 | | | | <0.0001 |
| Married/living with partner | 7708 (65.64) | 3049 (62.12) | 275 (59.68) | | 6780 (65.74) | 2141 (64.76) | 2111 (60.45) | | 6696 (65.22) | 2134 (65.31) | 2202 (61.52) | |
| widowed/divorced/separated | 2385 (15.56) | 1102 (19.70) | 113 (22.25) | | 2119 (15.53) | 691 (17.42) | 790 (20.55) | | 2088 (15.78) | 672 (16.66) | 840 (20.54) | |
| Never married | 2513 (18.79) | 979 (18.18) | 84 (18.07) | | 2204 (18.73) | 660 (17.81) | 712 (19.00) | | 2248 (19.00) | 652 (18.04) | 676 (17.94) | |
| BMI ($kg/m^2$) | | | | <0.0001 | | | | <0.0001 | | | | <0.0001 |
| <25 | 3921 (32.51) | 1385 (27.39) | 154 (35.86) | | 3455 (32.41) | 1020 (29.78) | 985 (28.59) | | 3497 (33.37) | 946 (27.80) | 1017 (27.68) | |
| 25-29.9 | 4105 (32.91) | 1612 (31.51) | 149 (28.51) | | 3699 (33.75) | 1086 (31.86) | 1081 (28.89) | | 3542 (32.46) | 1116 (33.04) | 1208 (31.60) | |
| ≥30 | 4580 (34.58) | 2133 (41.09) | 169 (35.63) | | 3949 (33.83) | 1386 (38.36) | 1547 (42.51) | | 3993 (34.17) | 1396 (39.16) | 1493 (40.72) | |
| Serum cotinine (ng/mL) | 0.30 ± 0.02 | 0.48 ± 0.05 | 0.91 ± 0.20 | <0.0001 | 0.32 ± 0.02 | 0.36 ± 0.04 | 0.48 ± 0.05 | 0.0003 | 0.28 ± 0.02 | 0.39 ± 0.05 | 0.62 ± 0.07 | <0.0001 |
| Family PIR | 2.44 ± 0.05 | 2.39 ± 0.05 | 2.36 ± 0.11 | 0.237 | 2.44 ± 0.05 | 2.42 ± 0.05 | 2.35 ± 0.06 | 0.166 | 2.45 ± 0.04 | 2.39 ± 0.06 | 2.36 ± 0.06 | 0.134 |
| Psoriasis (yes) | 299 (2.70) | 192 (4.10) | 20 (4.11) | 0.001 | 271 (2.63) | 104 (3.57) | 136 (4.24) | 0.0007 | 255 (2.68) | 107 (3.36) | 149 (4.29) | 0.0017 |
| Hypertension (yes) | 4513 (31.64) | 2099 (39.71) | 212 (41.43) | <0.0001 | 4066 (32.45) | 1354 (35.18) | 1404 (38.41) | <0.0001 | 3831 (30.48) | 1366 (37.35) | 1627 (42.16) | <0.0001 |
| T2D (yes) | 1632 (8.55) | 811 (12.19) | 81 (12.09) | <0.0001 | 1496 (8.83) | 454 (9.34) | 574 (12.54) | <0.0001 | 1361 (7.94) | 528 (11.10) | 625 (13.47) | <0.0001 |
| Hypercholesterolemia (yes) | 4718 (36.92) | 2076 (39.80) | 192 (37.65) | 0.019 | 4217 (37.55) | 1318 (36.91) | 1451 (39.26) | 0.278 | 4043 (36.21) | 1416 (40.43) | 1527 (39.76) | 0.0001 |

Data are expressed as GM ± SE or frequency (percentage). Percentages, geometric mean, SE and cut points were weight-adjusted using NHANES-specified sampling weights. For categorical variables, p-values were calculated using Rao-Scott chi-square test, and for continuous variables, p-values were calculated using Kruskal–Wallis H test (non-normal distribution). —, not applicable; BMI, body mass index; GM, geometric mean; NHANES, National Health and Nutrition Examination Survey; PIR, poverty income ratio; Q, quantile; SE, standard error; SII, systemic immune–inflammation index; SIRI, systemic inflammation response index; T2D, type 2 diabetes.





10.3389/fimmu.2024.1323174

TABLE 3 Comparison of SII, SIRI levels and whole blood lymphocyte, monocyte, neutrophil and peripheral platelet counts of the NHANES participants (2003–2006 and 2009–2014 cycles, n = 18,208) among subgroups of SII-SIRI pattern/SII/SIRI levels ($10^3$ cells/μL).

| Characteristics | SII-SIRI pattern divided by k-means method | | | | SII levels ($10^3$ cells/μL) | | | | SIRI levels ($10^3$ cells/μL) | | | |
|---|---|---|---|---|---|---|---|---|---|---|---|---|
| | Low | Medium | High | *p*-value | Low (Q1-Q3, <549.50) | Medium (Q4, 549.50-737.69) | High (Q5, ≥737.69) | *p*-value | Low (Q1-Q3, <1.18) | Medium (Q4, 1.18-1.65) | High (Q5, ≥1.65) | *p*-value |
| N | 12606 | 5130 | 472 | | 11103 | 3492 | 3613 | | 11032 | 3458 | 3718 | |
| SII | 384.48 ± 2.23 | 784.92 ± 5.33 | 1565.58 ± 32.32 | <0.0001 | 352.91 ± 1.73 | 631.83 ± 1.21 | 997.97 ± 5.57 | <0.0001 | 384.11 ± 2.89 | 585.59 ± 5.09 | 834.97 ± 8.09 | <0.0001 |
| SIRI | 0.79 ± 0.00 | 1.81 ± 0.01 | 4.35 ± 0.06 | <0.0001 | 0.80 ± 0.01 | 1.29 ± 0.01 | 1.92 ± 0.02 | <0.0001 | 0.73 ± 0.00 | 1.38 ± 0.00 | 2.37 ± 0.02 | <0.0001 |
| Lymphocyte | 2.11 ± 0.01 | 1.83 ± 0.01 | 1.40 ± 0.03 | <0.0001 | 2.14 ± 0.01 | 1.92 ± 0.02 | 1.73 ± 0.01 | <0.0001 | 2.10 ± 0.01 | 1.99 ± 0.01 | 1.77 ± 0.01 | <0.0001 |
| Monocyte | 0.48 ± 0.00 | 0.61 ± 0.00 | 0.76 ± 0.02 | <0.0001 | 0.50 ± 0.00 | 0.53 ± 0.00 | 0.56 ± 0.01 | <0.0001 | 0.45 ± 0.00 | 0.59 ± 0.00 | 0.70 ± 0.01 | <0.0001 |
| Neutrophil | 3.47 ± 0.02 | 5.46 ± 0.03 | 8.00 ± 0.16 | <0.0001 | 3.39 ± 0.02 | 4.65 ± 0.03 | 5.92 ± 0.04 | <0.0001 | 3.37 ± 0.02 | 4.70 ± 0.03 | 5.96 ± 0.04 | <0.0001 |
| peripheral platelet | 233.56 ± 0.85 | 263.57 ± 1.52 | 273.17 ± 4.87 | <0.0001 | 222.91 ± 0.78 | 260.97 ± 1.40 | 291.40 ± 1.50 | <0.0001 | 239.21 ± 1.01 | 248.28 ± 1.67 | 247.89 ± 1.51 | <0.0001 |

Data are expressed as GM ± SE. GM and SE were weight-adjusted using NHANES-specified sampling weights. p-values were calculated using Kruskal–Wallis H test. GM, geometric mean; NHANES, National Health and Nutrition Examination Survey; SE, standard error; SII, systemic immune–inflammation index; SIRI, systemic inflammation response index.



10.3389/fimmu.2024.1323174

TABLE 4 Odds ratios (95%CI) of psoriasis and SII-SIRI pattern/SII/SIRI levels in the NHANES follow-up study from 2003–2006 and 2009–2014 cycles (n = 18,208) ($10^3$ cells/μL).

| Categories | Psoriasis incidence | | |
|---|---|---|---|
| | psoriasis/observations (n/N) | Unadjusted OR (95% CI) | Adjusted OR (95% CI) |
| **SII-SIRI pattern** | | | |
| Low | 299 (12307) | Ref. | Ref. |
| Medium | 192 (5130) | 1.54 (1.20, 1.98)*** | 1.40 (1.09, 1.81) * |
| High | 20 (472) | 1.54 (0.83, 2.88) | 1.46 (0.79, 2.70) |
| *p*-value for trend | – | 0.0002 | 0.0031 |
| **SII levels** | | | |
| Low (Q1-Q3, <549.50) | 271 (11103) | Ref. | Ref. |
| Medium (Q4, 549.50-737.69) | 104 (3492) | 1.37 (1.01, 1.86)* | 1.30 (0.96, 1.78) |
| High (Q5, ≥737.69) | 136 (3613) | 1.64 (1.27, 2.12)*** | 1.52 (1.18, 1.95)** |
| *p*-value for trend | – | 0.0002 | 0.0014 |
| Continuous (lnSII) | – | 1.51 (1.22, 1.87)*** | 1.39 (1.12, 1.74)** |
| **SIRI levels** | | | |
| Low (Q1-Q3, <1.18) | 255 (11032) | Ref. | Ref. |
| Medium (Q4, 1.18-1.65) | 107 (3458) | 1.27 (0.95, 1.68) | 1.16 (0.86, 1.55) |
| High (Q5, ≥1.65) | 149 (3718) | 1.63 (1.23, 2.15)*** | 1.48 (1.12, 1.95)** |
| *p*-value for trend | – | 0.0005 | 0.007 |
| Continuous | – | 1.14 (1.07, 1.22)*** | 1.10 (1.02, 1.18)* |

ORs were estimated using multivariate logistic regression models and were weight adjusted using NHANES-specified sampling weights. ORs were adjusted for gender, age, race/ethnicity, education levels, marital status, BMI, alcohol intake, serum cotinine, family PIR, hypertension, type 2 diabetes, and hypercholesterolemia. *p<0.05, **p<0.01, ***p<0.001. BMI, body mass index; CI, confidence interval; NHANES, National Health and Nutrition Examination Survey; OR, odds ratio; PIR, poverty income ratio; Ref, reference; SII, systemic immune–inflammation index; SIRI, systemic inflammation response index.

prioritizing the management of inflammation may be worth considering in order to mitigate the risk of psoriasis.

Psoriasis is a chronic inflammatory skin disease characterized by abnormal innate and acquired immunity (1). The presence of an abundance of neutrophils in the skin lesions of psoriasis is a typical histopathological hallmark (21), and their release of cytokines, chemokines, enzymes, and neutrophil elastase mediates chronic inflammation (22). Monocytes play a central role in innate immune system and have a significant function in orchestrating inflammation (23). Lymphocytes are key component cells for adaptive immune responses, which links the innate and adaptive responses (24). Platelets maintain homeostasis, participate in mediating acute and chronic inflammatory processes, and contribute to the creation of an inflammatory environment (25).

TABLE 5 Multivariable-adjusted OR (95% CI) of psoriasis according to subgroups of SII levels stratified by SIRI levels ($10^3$ cells/μL).

| | SII levels | | | | *p*-value for trend |
|---|---|---|---|---|---|
| | geometric mean ± SD | Low (Q1-Q3, <549.50) | Medium (Q4, 549.50-737.69) | High (Q5, ≥737.69) | |
| **SIRI levels** | | | | | |
| Low (Q1-Q3, <1.18) | 384.14 ± 2.90 | Ref. | 1.14 (0.72, 1.83) | 1.16 (0.59, 2.29) | 0.540 |
| Medium (Q4, 1.18-1.65) | 585.59 ± 5.09 | Ref. | 1.32 (0.74, 2.34) | 2.17 (1.25, 3.79)** | 0.008 |
| High (Q5, ≥1.65) | 834.97 ± 8.09 | Ref. | 1.26 (0.59, 2.67) | 1.07 (0.60, 1.92) | 0.910 |

ORs were estimated using multivariate logistic regression models and were weight adjusted using NHANES-specified sampling weights. ORs were adjusted for gender, age, race/ethnicity, education levels, marital status, BMI, alcohol intake, serum cotinine, family PIR, hypertension, type 2 diabetes, and hypercholesterolemia. **p<0.01. BMI, body mass index; CI, confidence interval; NHANES, National Health and Nutrition Examination Survey; OR, odds ratio; PIR, poverty income ratio; Ref, reference; SII, systemic immune–inflammation index; SIRI, systemic inflammation response index.

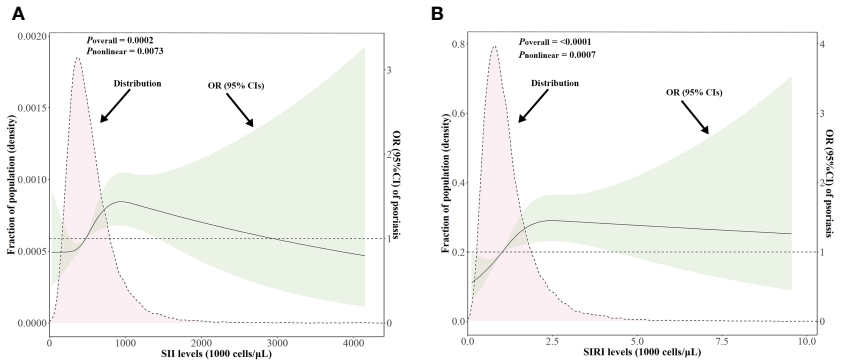


FIGURE 3
Distributions of SII and SIRI levels ($10^3$ cells/μL) and dose-response curves of SII and SIRI levels in relation to psoriasis in the NHANES follow-up study from 2003–2006 and 2009–2014 cycles (n = 18,208). Distributions of SII and SIRI levels and adjusted ORs with 95% CIs for **(A)** SII levels, **(B)** SIRI levels. ORs for SII/SIRI levels were adjusted for gender, age, race/ethnicity, education levels, marital status, BMI, alcohol intake, serum cotinine, family PIR, hypertension, type 2 diabetes, and hypercholesterolemia. BMI, body mass index; CI, confidence interval; NHANES, National Health and Nutrition Examination Survey; OR, odds ratio; PIR, poverty income ratio; SII, systemic immune–inflammation index; SIRI, systemic inflammation response index.

Previous studies have shown that changes in neutrophils, monocytes, lymphocytes, and platelet cells from peripheral blood are associated with psoriasis (26–28). SII and SIRI have been reported as promising systemic inflammatory response biomarkers in predicting stroke prognosis, colorectal cancer, gynecological and breast cancers (29–32). SII has also been found to be associated with the psoriatic comorbidities including hypertension, T2D, hyperlipidemia, nonalcoholic fatty liver disease, and psoriatic arthritis (16, 33–36). However, previous literature on the association between SII and psoriasis is limited to two small sample size cross-sectional studies that examined the predictive ability and disease severity (37, 38). Thus, we hypothesized that SII or SIRI may be associated with the occurrence of psoriasis.

In our study, we found that patients with psoriasis had significantly higher SII and SIRI levels compared to those without psoriasis. In addition to considering SII or SIRI as single exposure variables, we also conducted an unsupervised clustering model to group the SII-SIRI mixture as a pattern and studied the association between this pattern and the risk of psoriasis. We found that higher levels of SII or SIRI were associated with an increased risk of psoriasis. Besides, the medium level of the SII-SIRI pattern was positively associated with psoriasis, specifically when SII levels were higher than $737.69 \times 10^3$ cells/μL and SIRI levels ranged from 1.18 to $1.65 \times 10^3$ cells/μL. This concentration range had the highest risk of psoriasis compared to considering SII or SIRI levels individually, suggesting that the SII-SIRI pattern provides more clinical information than a single index. Interestingly, the results of the restricted cubic spline analysis demonstrated a non-linear association between SII/SIRI levels and psoriasis. It is worth noting that previous SII-related studies have reported a non-linear dose-response relationship between SII and hyperlipidemia, all-cause mortality in patients with

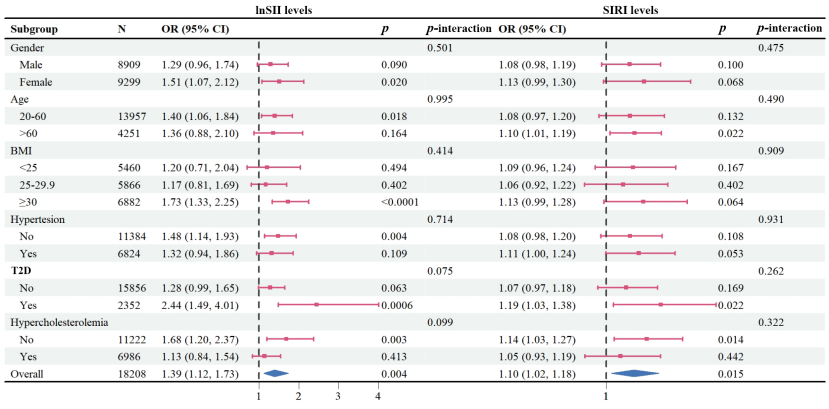


FIGURE 4
Forest plot depicting subgroup analysis of the association between lnSII/SIRI and psoriasis. The ORs were calculated using multivariate logistic regression models with adjustment for gender, age, race/ethnicity, education levels, marital status, BMI, alcohol intake, serum cotinine, family PIR, hypertension, type 2 diabetes, and hypercholesterolemia, except for the variable used for stratification. BMI, body mass index; ORs, Odds ratios; PIR, poverty income ratio; SII, systemic immune–inflammation index; SIRI, systemic inflammation response index.

nonalcoholic fatty liver disease, and a 'U-shaped' association with all-cause, cardiovascular disease, and cancer-related mortality in cardiovascular disease patients (16, 35, 39). These findings indicate that SII or SIRI levels and psoriasis occurrence is intricate and dose-dependent, which worths further studies.

In subgroup analysis, we found that the positive associations between SII and psoriasis were present in females, people aged younger than 60, obese people, and those with T2D. Similarly, positive associations were observed between SIRI and psoriasis in people aged older than 60 and those with T2D. These findings suggest that the association between SII or SIRI and psoriasis occurrence may be influenced by other confounding factors, and obesity and T2D may be risk factors for psoriasis, as previously reported by numerous studies (40–42). Similar results could be seen from the epidemiological study between SII and kidney stone (10). Further interventional/experimental research is needed to explore the potential underlying mechanisms behind these findings.

Our study has several notable advantages. Firstly, the large sample size and appropriate adjustment of covariates support the reliability and representativeness of our study. Secondly, we thoroughly assessed the individual effects of SII or SIRI on psoriasis risk, addressing previous research gaps. Furthermore, we used a SII-SIRI pattern grouping method to investigate the relationship between the SII-SIRI mixture pattern and psoriasis risk using different statistical models, obtaining relatively robust and consistent results, which increases the reliability of our study. And we found the changing threshold or ranges of SII and SIRI concentrations, which were associated with the risk of psoriasis most significantly than taking SII or SIRI into consideration individually. This finding might be hoping to support the early identification and prevention of psoriasis. Lastly, SII and SIRI were measured using common methodology, making them easily accessible and low-cost biomarkers with potential clinical utility. However, there are a few limitations worth noting. Firstly, due to the cross-sectional study design, we cannot establish a causal association between the SII-SIRI pattern/SII/SIRI and psoriasis risk. Secondly, the diagnosis of psoriasis was based on self-reported questionnaires, introducing the possibility of recall bias. Lastly, although we adjusted for a set of confounders, there may still be residual or unmeasured confounders in our findings. Therefore, it is crucial to confirm the association between the SII-SIRI pattern/SII/SIRI and psoriasis risk in future prospective studies with larger sample sizes and more comprehensive data collection.

## Conclusion

Our cross-sectional study provides evidence that SII or SIRI is positively associated with the risk of psoriasis. Additionally, we established a novel SII-SIRI pattern and observed a similar association when SII and SIRI levels fall within a specific threshold range. However, given the limitations of our study, further research with well-designed prospective designs is needed to confirm these findings.

## Data availability statement

The original contributions presented in the study are included in the article/supplementary materials, further inquiries can be directed to the corresponding author/s.

## Ethics statement

The studies involving humans were approved by Ethics Review Committee of the National Center for Health Statistics. The studies were conducted in accordance with the local legislation and institutional requirements. The participants provided their written informed consent to participate in this study.

## Author contributions

RM: Conceptualization, Formal analysis, Funding acquisition, Investigation, Methodology, Software, Writing – original draft. LC: Conceptualization, Formal analysis, Investigation, Methodology, Software, Visualization, Writing – original draft. JC: Conceptualization, Formal analysis, Investigation, Methodology, Software, Validation, Writing – original draft. NY: Data curation, Resources, Writing – original draft. YW: Data curation, Resources, Writing – original draft. QC: Data curation, Resources, Writing – original draft. WC: Data curation, Funding acquisition, Writing – original draft. CP: Data curation, Funding acquisition, Writing – original draft. HQ: Data curation, Funding acquisition, Writing – original draft. YD: Data curation, Resources, Writing – original draft. XW: Conceptualization, Funding acquisition, Investigation, Visualization, Writing – original draft. QY: Funding acquisition, Resources, Validation, Writing – review & editing. YS: Conceptualization, Formal analysis, Funding acquisition, Resources, Validation, Writing – review & editing.

## Funding

The author(s) declare financial support was received for the research, authorship, and/or publication of this article. This study was supported by funding from China Postdoctoral Science Foundation (2023M732651), National Key Research and Development Program of China (2023YFC2508106), Clinical Research Plan of SHDC (no. SHDC2020CR1014B), the National Natural Science Foundation of China (82203907, 82273510,

82103712, 82003334), the Innovation Program of Shanghai Municipal Education Commission (2019-01-07-00-07-E00046), Program of Shanghai Academic Research Leader (20XD1403300), Shanghai Pujiang Program (No. 22PJD058), Talent Plan of Shanghai Municipal Health Commission (no.2022YQ057), and Clinical Research Plan of Shanghai Municipal Health Commission (no.20214Y0337, 202340006).

## Acknowledgments

We highly appreciate NHANES for providing open-access data, and we would like to express our gratitude to Jiaxin Li from the University of Hong Kong for assisting us with data visualization.

## Conflict of interest

The authors declare that the research was conducted in the absence of any commercial or financial relationships that could be construed as a potential conflict of interest.

## Publisher's note



## References

1. Griffiths CEM, Armstrong AW, Gudjonsson JE, Barker J. Psoriasis. *Lancet* (2021) 397:1301–15. doi: 10.1016/S0140-6736(20)32549-6

2. Ghoreschi K, Balato A, Enerback C, Sabat R. Therapeutics targeting the IL-23 and IL-17 pathway in psoriasis. *Lancet* (2021) 397:754–66. doi: 10.1016/S0140-6736(21)00184-7

3. Armstrong AW, Read C. Pathophysiology, clinical presentation, and treatment of psoriasis: a review. *JAMA* (2020) 323:1945–60. doi: 10.1001/jama.2020.4006

4. Hu B, Yang XR, Xu Y, Sun YF, Sun C, Guo W, et al. Systemic immune-inflammation index predicts prognosis of patients after curative resection for hepatocellular carcinoma. *Clin Cancer Res* (2014) 20:6212–22. doi: 10.1158/1078-0432.CCR-14-0442

5. Qi Q, Zhuang L, Shen Y, Geng Y, Yu S, Chen H, et al. A novel systemic inflammation response index (SIRI) for predicting the survival of patients with pancreatic cancer after chemotherapy. *Cancer* (2016) 122:2158–67. doi: 10.1002/cncr.30057

6. Dziedzic EA, Gasior JS, Tuzimek A, Paleczny J, Junka A, Dabrowski M, et al. Investigation of the associations of novel inflammatory biomarkers-systemic inflammatory index (SII) and systemic inflammatory response index (SIRI)-with the severity of coronary artery disease and acute coronary syndrome occurrence. *Int J Mol Sci* (2022) 23:9553. doi: 10.3390/ijms23179553

7. Xia Y, Xia C, Wu L, Li Z, Li H, Zhang J. Systemic immune inflammation index (SII), system inflammation response index (SIRI) and risk of all-cause mortality and cardiovascular mortality: a 20-Year follow-up cohort study of 42,875 US adults. *J Clin Med* (2023) 12:1128. doi: 10.3390/jcm12031128

8. Akinbami LJ, Chen TC, Davy O, Ogden CL, Fink S, Clark J, et al. National health and nutrition examination survey, 2017-march 2020 prepandemic file: sample design, estimation, and analytic guidelines. *Vital Health Stat 1* (2022) 190):1–36. doi: 10.15620/cdc:115434

9. Xie R, Xiao M, Li L, Ma N, Liu M, Huang X, et al. Association between SII and hepatic steatosis and liver fibrosis: A population-based study. *Front Immunol* (2022) 13:925690. doi: 10.3389/fimmu.2022.925690

10. Di X, Liu S, Xiang L, Jin X. Association between the systemic immune-inflammation index and kidney stone: A cross-sectional study of NHANES 2007-2018. *Front Immunol* (2023) 14:1116224. doi: 10.3389/fimmu.2023.1116224

11. Wen X, Wang M, Xu X, Li T. Exposure to per- and polyfluoroalkyl substances and mortality in U.S. adults: a population-based cohort study. *Environ Health Perspect* (2022) 130:67007. doi: 10.1289/EHP10393

12. Ruan Z, Lu T, Chen Y, Yuan M, Yu H, Liu R, et al. Association between psoriasis and nonalcoholic fatty liver disease among outpatient US adults. *JAMA Dermatol* (2022) 158:745–53. doi: 10.1001/jamadermatol.2022.1609

13. Chen Y, Pan Z, Shen J, Wu Y, Fang L, Xu S, et al. Associations of exposure to blood and urinary heavy metal mixtures with psoriasis risk among U.S. adults: A cross-sectional study. *Sci Total Environ* (2023) 887:164133. doi: 10.1016/j.scitotenv.2023.164133

14. Qin Z, Li H, Wang L, Geng J, Yang Q, Su B, et al. Systemic immune-inflammation index is associated with increased urinary albumin excretion: a population-based study. *Front Immunol* (2022) 13:863640. doi: 10.3389/fimmu.2022.863640

15. Wang RH, Wen WX, Jiang ZP, Du ZP, Ma ZH, Lu AL, et al. The clinical value of neutrophil-to-lymphocyte ratio (NLR), systemic immune-inflammation index (SII), platelet-to-lymphocyte ratio (PLR) and systemic inflammation response index (SIRI) for predicting the occurrence and severity of pneumonia in patients with intracerebral hemorrhage. *Front Immunol* (2023) 14:1115031. doi: 10.3389/fimmu.2023.1115031

16. Mahemuti N, Jing X, Zhang N, Liu C, Li C, Cui Z, et al. Association between systemic immunity-inflammation index and hyperlipidemia: A population-based study from the NHANES (2015-2020). *Nutrients* (2023) 15:1177. doi: 10.3390/nu15051177

17. Qi Q, Sun K, Rong Y, Li Z, Wu Y, Zhang D, et al. Body composition of the upper limb associated with hypertension, hypercholesterolemia, and diabetes. *Front Endocrinol (Lausanne)* (2022) 13:985031. doi: 10.3389/fendo.2022.985031

18. Johnson CL, Paulose-Ram R, Ogden CL, Carroll MD, Kruszon-Moran D, Dohrmann SM, et al. National health and nutrition examination survey: analytic guidelines, 1999-2010. *Vital Health Stat 2* (2013) 161:1–24.

19. Grant RW, McCloskey J, Hatfield M, Uratsu C, Ralston JD, Bayliss E. et al: Use of latent class analysis and k-means clustering to identify complex patient profiles. *JAMA Netw Open* (2020) 3:e2029068. doi: 10.1001/jamanetworkopen.2020.29068

20. Steinley D. K-means clustering: a half-century synthesis. *Br J Math Stat Psychol* (2006) 59:1–34. doi: 10.1348/000711005X48266

21. Chiang CC, Cheng WJ, Korinek M, Lin CY, Hwang TL. Neutrophils in psoriasis. *Front Immunol* (2019) 10:2376. doi: 10.3389/fimmu.2019.02376

22. Jiang M, Fang H, Shao S, Dang E, Zhang J, Qiao P, et al. Keratinocyte exosomes activate neutrophils and enhance skin inflammation in psoriasis. *FASEB J* (2019) 33:13241–53. doi: 10.1096/fj.201900642R

23. Jakubzick CV, Randolph GJ, Henson PM. Monocyte differentiation and antigen-presenting functions. *Nat Rev Immunol* (2017) 17:349–62. doi: 10.1038/nri.2017.28

24. Gray KJ, Gibbs JE. Adaptive immunity, chronic inflammation and the clock. *Semin Immunopathol* (2022) 44:209–24. doi: 10.1007/s00281-022-00919-7

25. Koupenova M, Clancy L, Corkrey HA, Freedman JE. Circulating platelets as mediators of immunity, inflammation, and thrombosis. *Circ Res* (2018) 122:337–51. doi: 10.1161/CIRCRESAHA.117.310795

26. Herster F, Bittner Z, Codrea MC, Archer NK, Heister M, Loffler MW, et al. Platelets aggregate with neutrophils and promote skin pathology in psoriasis. *Front Immunol* (2019) 10:1867. doi: 10.3389/fimmu.2019.01867

27. Johnston A, Xing X, Wolterink L, Barnes DH, Yin Z, Reingold L, et al. IL-1 and IL-36 are dominant cytokines in generalized pustular psoriasis. *J Allergy Clin Immunol* (2017) 140:109–20. doi: 10.1016/j.jaci.2016.08.056

28. Rodriguez-Rosales YA, Langereis JD, Gorris MAJ, van den Reek J, Fasse E, Netea MG, et al. Immunomodulatory aged neutrophils are augmented in blood and skin of psoriasis patients. *J Allergy Clin Immunol* (2021) 148:1030–40. doi: 10.1016/j.jaci.2021.02.041

29. Zhang Y, Xing Z, Zhou K, Jiang S. The predictive role of systemic inflammation response index (SIRI) in the prognosis of stroke patients. *Clin Interv Aging* (2021) 16:1997–2007. doi: 10.2147/CIA.S339221

30. Lin KB, Fan FH, Cai MQ, Yu Y, Fu CL, Ding LY, et al. Systemic immune inflammation index and system inflammation response index are potential biomarkers of atrial fibrillation among the patients presenting with ischemic stroke. *Eur J Med Res* (2022) 27:106. doi: 10.1186/s40001-022-00733-9

31. Chen JH, Zhai ET, Yuan YJ, Wu KM, Xu JB, Peng JJ, et al. Systemic immune-inflammation index for predicting prognosis of colorectal cancer. *World J Gastroenterol* (2017) 23:6261–72. doi: 10.3748/wjg.v23.i34.6261

32. Ji Y, Wang H. Prognostic prediction of systemic immune-inflammation index for patients with gynecological and breast cancers: a meta-analysis. *World J Surg Oncol* (2020) 18:197. doi: 10.1186/s12957-020-01974-w

33. Xu JP, Zeng RX, Zhang YZ, Lin SS, Tan JW, Zhu HY, et al. Systemic inflammation markers and the prevalence of hypertension: A NHANES cross-sectional study. *Hypertens Res* (2023) 46:1009–19. doi: 10.1038/s41440-023-01195-0

34. Guo W, Song Y, Sun Y, Du H, Cai Y, You Q, et al. Systemic immune-inflammation index is associated with diabetic kidney disease in Type 2 diabetes mellitus patients: Evidence from NHANES 2011-2018. *Front Endocrinol (Lausanne)* (2022) 13:1071465. doi: 10.3389/fendo.2022.1071465

35. Zhao E, Cheng Y, Yu C, Li H, Fan X. The systemic immune-inflammation index was non-linear associated with all-cause mortality in individuals with nonalcoholic fatty liver disease. *Ann Med* (2023) 55:2197652. doi: 10.1080/07853890.2023.2197652

36. Kelesoglu Dincer AB, Sezer S. Systemic immune inflammation index as a reliable disease activity marker in psoriatic arthritis. *J Coll Physicians Surg Pak* (2022) 32:773–8. doi: 10.29271/jcpsp.2022.06.773

37. Dincer Rota D, Tanacan E. The utility of systemic-immune inflammation index for predicting the disease activation in patients with psoriasis. *Int J Clin Pract* (2021) 75: e14101. doi: 10.1111/ijcp.14101

38. Yorulmaz A, Hayran Y, Akpinar U, Yalcin B. Systemic immune-Inflammation index (SII) predicts increased severity in psoriasis and psoriatic arthritis. *Curr Health Sci J* (2020) 46:352–7. doi: 10.12865/CHSJ.46.04.05

39. Xiao S, Wang Z, Zuo R, Zhou Y, Yang Y, Chen T, et al. Association of systemic immune inflammation index with all-cause, cardiovascular disease, and cancer-related mortality in patients with cardiovascular disease: A cross-sectional study. *J Inflamm Res* (2023) 16:941–61. doi: 10.2147/JIR.S402227

40. Barros G, Duran P, Vera I, Bermudez V. Exploring the links between obesity and psoriasis: A comprehensive review. *Int J Mol Sci* (2022) 23:7499. doi: 10.3390/ijms23147499

41. Takeshita J, Grewal S, Langan SM, Mehta NN, Ogdie A, Van Voorhees AS, et al. Psoriasis and comorbid diseases: Epidemiology. *J Am Acad Dermatol* (2017) 76:377–90. doi: 10.1016/j.jaad.2016.07.064

42. Elmets CA, Leonardi CL, Davis DMR, Gelfand JM, Lichten J, Mehta NN, et al. Joint AAD-NPF guidelines of care for the management and treatment of psoriasis with awareness and attention to comorbidities. *J Am Acad Dermatol* (2019) 80:1073–113. doi: 10.1016/j.jaad.2018.11.058

frontiers | Frontiers in Medicine

TYPE Original Research
PUBLISHED 16 February 2024
DOI 10.3389/fmed.2024.1328765



OPEN ACCESS

EDITED BY
Andreas Recke,
University of Lübeck, Germany

REVIEWED BY
Sally Helen Ibbotson,
University of Dundee, United Kingdom
Indrashis Podder,
College of Medicine and Sagore Dutta Hospital, India

*CORRESPONDENCE
Atsushi Fukunaga
✉ atsushi.fukunaga@ompu.ac.jp

RECEIVED 31 October 2023
ACCEPTED 29 January 2024
PUBLISHED 16 February 2024

CITATION
Imamura S, Oda Y, Fukumoto T, Mizuno M, Suzuki M, Washio K, Nishigori C and Fukunaga A (2024) Solar urticaria: clinical characteristics, treatment effectiveness, long-term prognosis, and QOL status in 29 patients.
*Front. Med.* 11:1328765.
doi: 10.3389/fmed.2024.1328765



# Solar urticaria: clinical characteristics, treatment effectiveness, long-term prognosis, and QOL status in 29 patients

Shinya Imamura[1,2], Yoshiko Oda[1], Takeshi Fukumoto[1], Mayuko Mizuno[1], Mariko Suzuki[1], Ken Washio[1], Chikako Nishigori[1] and Atsushi Fukunaga[1,3]*

[1]Division of Dermatology, Department of Internal Related, Kobe University Graduate School of Medicine, Kobe, Japan, [2]Department of Dermatology, Kobe City Hospital Organization, Kobe City Medical Center West Hospital, Kobe, Japan, [3]Department of Dermatology, Osaka Medical and Pharmaceutical University, Osaka, Japan

**Introduction:** Solar urticaria (SU), a relatively rare skin inflammatory and photosensitivity disease, is often resistant to standard urticaria treatment. Quality of life (QOL) among SU patients has not been extensively explored. This study was performed to clarify the clinical features and effectiveness of therapies (e.g., hardening therapy) for SU and to determine QOL among SU patients.

**Methods:** The authors examined the characteristics, treatments, and QOL statuses of 29 Japanese SU patients using medical records and a questionnaire approach.

**Results:** Among 29 patients, H1 antihistamine therapy (H1) was effective in 22 (75.8%) patients. H2 antihistamine therapy (H2) was effective in three of seven (42.9%) patients. Ultraviolet radiation A (UVA) hardening therapy was effective in eight of nine (88.9%) patients. Visible light (VL) hardening therapy was ineffective in three of three patients. In one patient who underwent both UVA and VL hardening therapy, only UVA hardening therapy was effective. In the questionnaire, 18 patients (90%) reported some improvement compared with disease onset (four had complete remission, six had completed treatment although mild symptoms persisted, and eight were receiving treatment with moderate symptoms), whereas two patients reported exacerbation. Patients in complete remission had a mean disease duration of 4 years, whereas patients not in remission had a mean disease duration of 8.8 years. The mean Dermatology Life Quality Index (DLQI) score for the current status was 7.4. There was a correlation between DLQI and symptom/treatment status. However, neither DLQI and action spectra nor DLQI and treatments exhibited significant differences.

**Discussion:** The questionnaire revealed current QOL status and long-term prognosis in SU patients. Compared with disease onset, most patients showed improvement when assessed for this study. Both H1 and H2 should be attempted for all SU patients. UVA hardening therapy may be an option for SU patients with an action spectrum that includes UVA.

KEYWORDS

**solar urticaria, UVA, UVB, VL, MUD, IIT, rush hardening therapy, DLQI**

# Introduction

Solar urticaria (SU), a relatively rare photosensitivity disease (1), is characterized by edematous erythema and wheals on areas exposed to visible light (VL) or ultraviolet radiation (UV); it can sometimes be life-threatening (2). The exposure to UV light/VL is suspected to activate a photoantigen, possibly a chromophore-derived photoproduct, that exists in the serum of affected individuals (3). Treatments for SU are limited; they include topical sunscreen, oral H1 antihistamine therapy (H1), oral H2 antihistamine therapy (H2) (4), rush hardening therapy (hardening), immunosuppressants, and biological agents (5). However, SU is often refractory to treatment (6, 7). Hardening, a standard treatment for SU, induces tolerance by repeatedly exposing a patient to gradually increasing doses of the triggering wavelengths (8). There is some evidence that ultraviolet radiation A (UVA) hardening is effective (9–11). Several hypotheses have been proposed regarding its effectiveness, such as tolerance that arises from the depletion of mast cell mediators (12), a simple photoprotective effect from delayed tanning (13), and the binding of photoallergens to IgE-binding sites (10, 14).

Only a few studies have collected epidemiological and photobiological data for SU (15, 16). Ethnic differences in skin color affect SU incidence (17, 18), and action spectra differ among ethnicities (16, 19). However, few studies have analyzed Asian patients (16, 20, 21). Furthermore, only a few studies of SU have included prognostic data (6, 19, 21) or assessed quality of life (QOL) (22–24). Thus, the long-term prognosis of SU patients, particularly with regard to QOL, is not well known.

The first aim of this study was to clarify the clinical features and effectiveness of various therapies (e.g., hardening therapy) among Japanese SU patients. The second aim was to clarify the long-term prognosis and assess QOL using a questionnaire approach. In this study, the authors analyzed data from SU patients who visited our dermatology department over a 13-year period, and the authors evaluated the results of questionnaires regarding prognosis and QOL.

# Methods

## Patient population

Twenty-nine Japanese SU patients who visited Kobe University from April 2003 to April 2016 were analyzed in this study (Table 1). Most patients had Fitzpatrick skin color type III–IV. No patients received omalizumab or immunosuppressive drugs because omalizumab was not approved during the study period; moreover, such treatments were uncommon or not covered by public insurance in Japan. All patients in this study had been diagnosed with SU on the basis of a photo-provocation test. Data regarding background characteristics and treatment effectiveness were collected from medical records. In some cases, improvement in minimal urticarial dose (MUD) was measured; in other cases, improvement in the extent of skin lesions during daily life was determined by physician interviews. These immediate post-treatment improvement data were gathered from medical records. At a few months to a few years post-treatment, all patients were mailed a questionnaire that assessed long-term improvement. The questionnaire asked patients to review their Dermatology Life Quality Index (DLQI) score for their current status. The study protocol was approved by the Institutional Review Board of Kobe University (No. 1617).

## Photo-provocation test

Diagnoses of SU were made via photo-provocation tests that used VL, UVA, and ultraviolet radiation B (UVB) light sources. Each test used a slide projector lamp with a 250-W halogen bulb for VL (peak, 850 nm; range, 400–3,000 nm; JC24V250WS/GI; Iwasaki Electric Co. Ltd., Japan), a long-bulb fluorescent black light for UVA (peak, 350 nm; range, 310–400 nm; FL 32S; Toshiba Lighting & Technology Co., Japan), and a long-bulb fluorescent sunlamp for UVB (peak, 310 nm; range, 280–350 nm; FL 32S E-30; Toshiba Lighting & Technology Co.). The approximate flux value of narrow-band UVB (NB-UVB) was 3.9–4.5 [mW/cm$^2$], and the approximate flux value of UVA was 6.7–8.1 [mW/cm$^2$]. VL was not measured for slide projectors because appropriate measurement equipment was unavailable.

Photo-provocation tests with UVA/UVB were performed as previously described (10). Additionally, VL irradiation was administered on each patient's back at a distance of 15–30 cm for 20 min. Patients who developed a wheal after exposure were diagnosed with SU and enrolled in this study; patients who developed only erythema or itchiness were diagnosed with photosensitivity and excluded from the study. Wavelengths that caused a wheal were considered the action spectra. The MUD was defined as the lowest dose that caused obvious wheals. To detect delayed reactions in some cases, skin lesions were checked at 24 and 48 h after irradiation; if a wheal appeared within a few hours or within 1 day, the latent time result was considered positive (3). As previously reported, the presence of a latent time suggested that the patient could have an inhibition spectrum (3, 16, 25).

## Inhibition spectra

To determine the inhibition spectrum, cutoff glass filters (Toshiba Medical Supply, Japan) were used to eliminate short wavelengths. After the induction of wheals by irradiation with the action spectrum, half of the wheals were shielded (3) and the exposed wheals were irradiated with wavelengths outside of the action spectrum. Wavelengths that suppressed wheal formation were regarded as the inhibition spectrum.

## Intradermal serum injection test

To detect serum photoallergens, some patients underwent an intradermal injection test (IIT) using autologous serum that had undergone *in vitro* irradiation with their action spectra. Regarding the amount of *in vitro* irradiation, there were various details. In many cases, more than MUD was irradiated to serum *in vitro*, but up to 3.3

Abbreviations: SU, solar urticaria; UVA, ultraviolet radiation A; UVB, ultraviolet radiation B; VL, visible light; MUD, minimal urticarial dose; IIT, intradermal injection test; PUVA, psoralen-UVA; DLQI, Dermatology Life Quality Index; CR, complete remission; H1, H1 antihistamines; H2, H2 antihistamines; IQR, interquartile range.

TABLE 1 Data based on the medical record.

| No. | Sex | Age (y) | | Complications | | | IgE (IU/mL) | Phototesting | | | | | | Treatments | | |
|---|---|---|---|---|---|---|---|---|---|---|---|---|---|---|---|---|
| | | At first visit | At onset | Allergic rhinitis | Asthma | Atopic dermatitis | | Action spectrum | Inhibition spectrum | UVA MUD (J/cm2) | VL MUD min (cm) | UVB MUD (mJ/cm2) | IIT positive with irradiated serum | H1 antihistamines | H2 antihistamines | Phototherapy including hardening therapy (immediate effectiveness) |
| 1 | F | 56 | 55 | | (+) | | 223 | UVA, VL | (−) | 6 | 4 (UN) | NE | VL | Bepotastine, Cyproheptadine (partial effec.) | ND | VL (ineffec.) |
| 2 | M | 25 | 17 | | | | NE | UVA, VL | >530 nm | 8.3 | 10 (15 cm) | NE | (−) | Homochlorcyclizine (ineffec.) | ND | UVA (effec.), VL (ineffec.) |
| 3 | F | 67 | 67 | (+) | | | 28 | VL | >531 nm | NE | 20 (30 cm) | NE | VL | Olopatadine (partial effec.) | ND | VL (ineffec.) |
| 4 | M | 51 | 48 | | | | 251 | UVA, VL | (−) | 8.6 | 20 (30 cm) | NE | VL | Olopatadine (partial effec.) | ND | VL (ineffec.) |
| 5 | F | 61 | 60 | | | | 124 | UVA, UVB, VL | (−) | 10 | 0.67 (20 cm) | 169 | UVA, VL | Fexofenadine (partial effec.) | ND | UVA (effec.) |
| 6 | M | 23 | 23 | | | (+) | NE | VL | NE | NE | 40 (10 cm) | NE | NE | Loratadine (UN) | ND | ND |
| 7 | F | 21 | 21 | | (+) | | NE | UVA, VL | NE | 12 | 20 (UN) | NE | NE | Fexofenadine (ineffec.) | ND | ND |
| 8 | F | 57 | 57 | (+) | | | 322 | VL | NE | NE | 20 (15 cm) | NE | NE | Epinastine (partial effec.) | ND | ND |
| 9 | M | 28 | 23 | | | | 598 | VL | NE | NE | 30 (UN) | NE | (−) | Epinastine (partial effec.) | ND | ND |
| 10 | M | 36 | 36 | | | | NE | VL | NE | NE | 40 (UN) | NE | NE | Fexofenadine (UN) | ND | ND |
| 11 | F | 6 | 6 | | | (+) | 51 | VL | NE | NE | 35 (15 cm) | NE | NE | Epinastine (partial effec.) | Details UN (ineffec.) | ND |
| 12 | M | 56 | 56 | (+) | | | 24 | UVA, VL | Latent time | 8 | 5 (15 cm) | NE | UVA, VL | Ebastine (ineffec.) | Famotidine (ineffec.) | Oral PUVA (ineffec.) |
| 13 | F | 33 | 33 | | | | 68 | UVA, VL | >540 nm | 6 | 3 (15 cm) | NE | VL | Fexofenadine (partial effec.) | ND | UVA (effec.) |
| 14 | M | 62 | 60 | (+) | | | 274 | UVA, VL | Latent time | 0.5 | 1 (15 cm) | NE | VL | Cetirizine (partial effec.) | ND | UVA (effec.) |
| 15 | M | 17 | 17 | (+) | | | 308 | VL | 420-480 nm | NE | 10 (UN) | NE | VL | Olopatadine (partial effec.) | Lafutidine (effec.) | Natural sunbathing (effec.) |

*(Continued)*





10.3389/fmed.2024.1328765

TABLE 1 (Continued)

| No. | Sex | Age (y) | | Complications | | | IgE (IU/mL) | Phototesting | | | | | | Treatments | | |
|---|---|---|---|---|---|---|---|---|---|---|---|---|---|---|---|---|
| | | At first visit | At onset | Allergic rhinitis | Asthma | Atopic dermatitis | | Action spectrum | Inhibition spectrum | UVA MUD (J/cm2) | VL MUD min (cm) | UVB MUD (mJ/cm2) | IIT positive with irradiated serum | H1 antihistamines | H2 antihistamines | Phototherapy including hardening therapy (immediate effectiveness) |
| 16 | F | 27 | 17 | | | | NE | VL | Latent time | NE | 5 (15 cm) | NE | NE | Levocetirizine (effec.) | Lafutidine (effec.) | UVA (ineffec.) |
| 17 | M | 29 | 29 | | | | NE | VL | Latent time | NE | 6 (15 cm) | NE | NE | Ebastine (partial effec.) | Lafutidine (effec.) | ND |
| 18 | M | 38 | 35 | | | | NE | VL | Latent time | NE | 15 (15 cm) | NE | NE | Bepotastine (partial effec.) | ND | ND |
| 19 | F | 17 | 17 | (+) | | | NE | VL | NE | NE | 20 (20 cm) | NE | NE | Bepotastine (partial effec.) | ND | ND |
| 20 | M | 13 | 11 | (+) | | | 309 | VL | >450 nm | NE | 2 (15 cm) | NE | VL | Olopatadine (partial effec.) | ND | ND |
| 21 | M | 23 | 23 | (+) | | | 75 | UVA, VL | NE | 12 | 5 (30 cm) | NE | (−) | Ebastine (effec.) | Lafutidine (ineffec.) | UVA (effec.) |
| 22 | F | 19 | 17 | (+) | | (+) | 726 | UVA, VL | NE | 12 | 10 (20 cm) | NE | VL | Olopatadine (partial effec.) | ND | UVA (effec.) |
| 23 | F | 67 | 67 | | | | NE | UVA, VL | Latent time | 6 | 10 (15 cm) | NE | NE | Epinastine (partial effec.) | ND | ND |
| 24 | F | 4 | 3 | | | | 61 | VL | NE | NE | 3 (15 cm) | NE | (−) | Epinastine (effec.) | ND | ND |
| 25 | F | 51 | 51 | | (+) | | 12 | UVA, UVB, VL | NE | 0.5 | 0.083 (15 cm) | 120 | VL | Cetirizine (ineffec.) | ND | UVA (effec.) |
| 26 | F | 10 | 10 | | | | 6 | VL | NE | NE | 10 (15 cm) | NE | NE | Levocetirizine (effec.) | ND | ND |
| 27 | F | 22 | 18 | | (+) | (+) | 214 | UVA, UVB | NE | 5 | NE | 20 | NE | Fexofenadine (partial effec.) | ND | ND |
| 28 | F | 51 | 50 | | (+) | | 653 | UVA, VL | >480 nm | 2 | 7 (15 cm) | NE | VL | Fexofenadine (UN) | ND | UVA (effec.) |
| 29 | M | 49 | 46 | | | | NE | VL | (−) | NE | 5 (30 cm) | NE | VL | Levocetirizine (effec.) | Lafutidine (ineffec.) | ND |

Y, year; F, female; M, male; UVA, ultraviolet radiation A; UVB, ultraviolet radiation B; VL, visible light; MUD, minimal urticarial dose; NE, not examined; ND, not done; IIT, intradermal injection test; PUVA, psoralen-UVA; effec., effective; ineffec., ineffective.





10.3389/fmed.2024.1328765

times of MUD was irradiated *in vitro* in a case. Additionally, non-irradiated autologous serum was used as a control (26). For the IIT, 0.05 mL of serum was intradermally injected into the forearm. Natural saline was utilized as a negative control. At 15 and 30 min after injection, a wheal diameter 1.5–2.0 mm larger than the negative control was considered a positive result (27).

## Hardening therapy

The protocol for UVA hardening therapy was performed as previously described, with a maintenance dose of 10 J/cm$^2$ UVA once every 1–2 weeks (9, 10). The duration varied among patients. VL hardening therapy was conducted as follows. A slide projector was used to administer VL irradiation to 3–4 parts of the body (face, abdomen, forearms, and thighs) at a distance of 10–30 cm for 3–10 min. In each subsequent treatment, VL irradiation was administered for 1 min longer than in the previous treatment. The protocol was repeated once daily for outpatients and 2–3 times per day for inpatients. The schedule was performed every day or every second day. H1 and H2 were used alone or in combination with hardening therapy.

# Results

## Patient population

The median patient age at the first visit was 29 years (interquartile range [IQR]: 21–51 years); there were 13 men (44.8%) and 16 women (55.2%). Sixteen patients had a history of allergic disease (eight allergic rhinitis, four asthma, two atopic dermatitis, one each allergic rhinitis and atopic dermatitis, and one each asthma and atopic dermatitis). The serum total IgE level was measured in 19 patients; the median level was 213.7 IU/mL (IQR: 56.1–308.5 IU/mL). The median age at onset was 29 years (IQR: 17–51 years); it showed a bimodal distribution, with peaks at 21–25 and 51–60 years (Figure 1A). Patient characteristics are shown in Table 1.

The questionnaire response rate was 69% (20 of 29 patients) (Table 2). The median age at the time of questionnaire response was 46 years (IQR: 29–65 years). The median time from disease onset until questionnaire response was 7 years (IQR: 3.75–14 years).

## Photo-provocation test and IIT

Among the 29 patients, photo-provocation tests revealed action spectra of VL only in 15 patients (51.7%), UVA to VL in 11 patients (37.9%), UVB to VL in two patients (6.9%), and UVB to UVA in one patient (3.4%) (Figure 1B; Table 1). Because only one patient did not have an action spectrum that included VL, 28 patients (96.5%) were at least sensitive to VL.

The median MUDs were 10 min (IQR: 4.75–20) for VL, 7 J/cm$^2$ (IQR: 5–10) for UVA, and 120 mJ/cm$^2$ (IQR: 70–145) for UVB. An inhibition spectrum was confirmed in 6 of the 10 tested patients. Detailed examination of the wavelengths revealed an inhibition spectrum longer than 420 nm in all six patients. A latent time was detected in six patients. The IIT with autologous serum irradiated with their action spectrum *in vitro* was positive in 13 of 17 patients tested (76.5%): 11 patients were positive to irradiated serum with VL, and 2 patients were positive for irradiated serum with both VL and UVA.

## Treatment selection

All 29 patients underwent H1 (Table 1); 12 of these patients underwent H1 only. The dose of H1 was limited to a 2-fold increase because of insurance coverage-related restrictions in Japan. Because all patients attempted H1 only as the first step, the effectiveness of H1 only could be measured in all patients. Ten patients underwent both H1 and hardening therapy; three patients underwent both H1 and H2; and two patients underwent H1, H2, and hardening therapy. One patient underwent H1, H2, and oral psoralen-UVA (PUVA) therapy; one patient underwent H1, H2, and natural sunbathing therapy (the sunbathing protocols varied and are not described in this article).

## Treatment effectiveness

Treatment effectiveness was examined on the basis of medical records (i.e., without questionnaire responses) or via MUD measurements (Table 1). When the reviewing physician recorded improvement based on the patient's subjective symptoms or the MUD was improved after treatment, the treatment was considered effective. To eliminate subjective patient data, the authors divided patients into a "MUD-based review group" and an "Interview-based review group" (Supplementary Figures S1, S2). When treatment effectiveness was adequate and urticaria did not appear in daily life, or when urticaria was not induced during a photo-provocation test, the treatment was considered "effective." If the treatment exhibited partial effectiveness but urticaria remained present or another additional treatment was needed, or the prolonging of MUD was observed but urticaria appeared by photo-provocation test, the treatment was considered "partially effective."

The results for H1 only were as follows: five effective (17.2%), 17 partially effective (58.6%), four ineffective (13.8%), and three unknown (10.3%) (Figure 2A; Table 1). The results for H2 only were three effective (42.9%) and four ineffective (57.1%) (Figure 2B; Table 1). Hardening with UVA was effective in eight patients and ineffective in one patient (Figure 2C; Table 1). The patient with an ineffective treatment result had an unusual situation in which the action spectrum comprised VL, but UVA hardening was attempted. Hardening with VL was ineffective in three of three patients. Natural sunbathing was effective in one patient. Oral PUVA was ineffective in one patient. In one patient who underwent hardening with both UVA and VL, UVA hardening was effective, whereas VL hardening was ineffective.

## Current symptoms according to the questionnaire

Twenty of 29 patients responded to the questionnaire. Their current statuses were as follows (Table 2; Figure 3A): complete remission in four (20%), improvement with mild symptoms but not undergoing treatment in six (30%), improvement with moderate

TABLE 2 Data based on the questionnaires.

| No. | Response to questionnaire | Age (y) | | | Current status | | DLQI | |
|---|---|---|---|---|---|---|---|---|
| | | At onset | At response | At complete remission | Current improvement | Current Treatment | Current status | QOL disability |
| 1 | (+) | 55 | 69 | | Improve (mild symp.) | (−) | 2 | Mild dist. |
| 2 | (+) | 17 | 42 | | Improve (mild symp.) | (−) | 5 | Mild dist. |
| 3 | (+) | 67 | 80 | | Improve (mild symp.) | (−) | 7 | Moderate dist. |
| 4 | (+) | 48 | 63 | | Deteriorate | UN | 20 | Severe dist. |
| 5 | (+) | 60 | 77 | 71 | Complete remission | (−) | 0 | No dist. |
| 6 | NA | 23 | NA | | NA | NA | NA | NA |
| 7 | NA | 21 | NA | | NA | NA | NA | NA |
| 8 | (+) | 57 | 64 | 59 | Complete remission | (−) | 0 | No dist. |
| 9 | (+) | 23 | 37 | | Improve (moderate symp.) | Clemastine Fumarate, Fexofenadine (UAN) | 16 | Severe dist. |
| 10 | NA | 36 | NA | | NA | NA | NA | NA |
| 11 | NA | 6 | NA | | NA | NA | NA | NA |
| 12 | NA | 56 | NA | | NA | NA | NA | NA |
| 13 | (+) | 33 | 40 | 35 | Complete remission | (−) | 0 | No dist. |
| 14 | (+) | 60 | 69 | | Improve (moderate symp.) | Olopatadine | 3 | Mild dist. |
| 15 | NA | 17 | NA | | NA | NA | NA | NA |
| 16 | (+) | 17 | 31 | | Improve (moderate symp.) | Levocetirizine (UAN) | 4 | Mild dist. |
| 17 | NA | 29 | NA | | NA | NA | NA | NA |
| 18 | (+) | 35 | 43 | | Improve (mild symp.) | (−) | 3 | Mild dist. |
| 19 | (+) | 17 | 22 | | Improve (moderate symp.) | Olopatadine | 13 | Severe dist. |
| 20 | (+) | 11 | 17 | | Improve (mild symp.) | (−) | 11 | Severe dist. |
| 21 | NA | 23 | NA | | NA | NA | NA | NA |
| 22 | (+) | 17 | 21 | | Improve (mild symp.) | (−) | 10 | Moderate dist. |
| 23 | (+) | 67 | 69 | 68 | Complete remission | (−) | 0 | No dist. |
| 24 | (+) | 3 | 6 | | Improve (moderate symp.) | Epinastine | 7 | Moderate dist. |
| 25 | (+) | 51 | 53 | | Improve (moderate symp.) | Levocetirizine, Lafutidine, Montelukast, hardening | 7 | Moderate dist. |
| 26 | NA | 10 | NA | | NA | NA | NA | NA |
| 27 | (+) | 18 | 23 | | Deteriorate | Fexofenadine (UAN) | 13 | Severe dist. |
| 28 | (+) | 50 | 51 | | Improve (moderate symp.) | Fexofenadine, hardening | 17 | Severe dist. |
| 29 | (+) | 46 | 49 | | Improve (moderate symp.) | Loratadine, Lafutidine | 10 | Moderate dist. |

Y, year; DLQI, Dermatology Life Quality Index; CR, complete remission; UAN, use as needed; ND, not done; UN, unknown; NA, no answer; symp, symptom; dist., disturbance. The patients who did not answer to the questionnaires were described as gray rows. The patients' number is coincident with Table 1. The same number expresses the same patient.

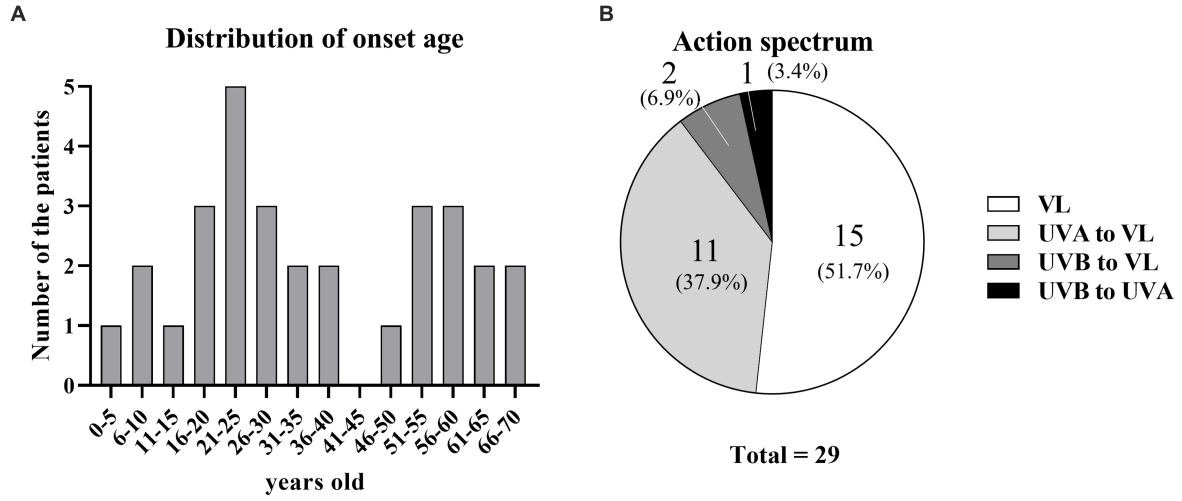


FIGURE 1
Age at onset and action spectra of SU. **(A)** Distribution of age at onset. **(B)** Percentages of action spectra.

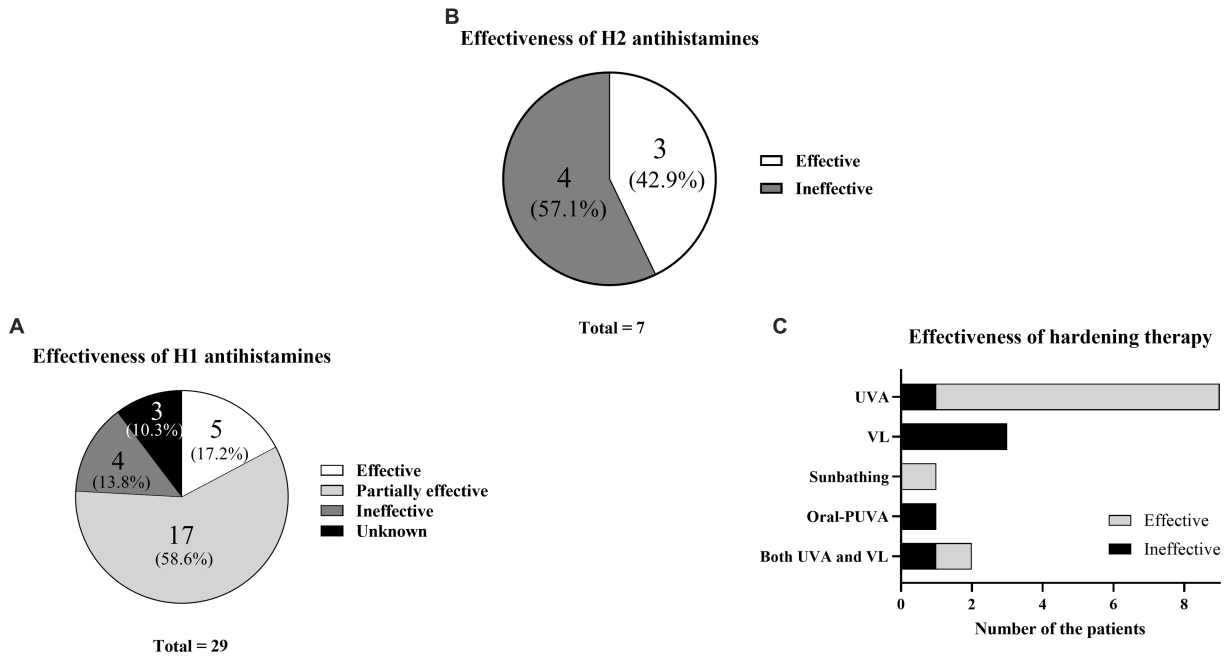


FIGURE 2
Treatment effectiveness. **(A)** Percentages of H1 antihistamine effectiveness. **(B)** Percentages of H2 antihistamine effectiveness. **(C)** Effectiveness of hardening therapy according to wavelength.

symptoms but continuing treatment in eight (40%), and deterioration in two (10%). In particular, nine patients (45%) were continuing H1, whereas two patients (10%) were continuing hardening therapy based on their current status (Table 2).

In the complete remission group, the mean disease duration from onset to complete remission was 4 years; the specific durations for each of the four patients were 1, 2, 2, and 11 years (Figure 3B; Table 2). In contrast, the mean disease durations were 11.7 years in the improvement with mild symptoms group, 6.4 years in the improvement with moderate symptoms group, and 10 years in the deterioration group (Figure 3B). The mean disease duration in the non-complete remission group (combination of mild symptoms, moderate symptoms, and deterioration groups) was 8.8 years.

## Dermatology life quality index score for current status according to the questionnaire

To analyze QOL status among SU patients, the authors collected DLQI data via questionnaire. The patients were classified into five groups depending on their DLQI scores to visualize the degree of

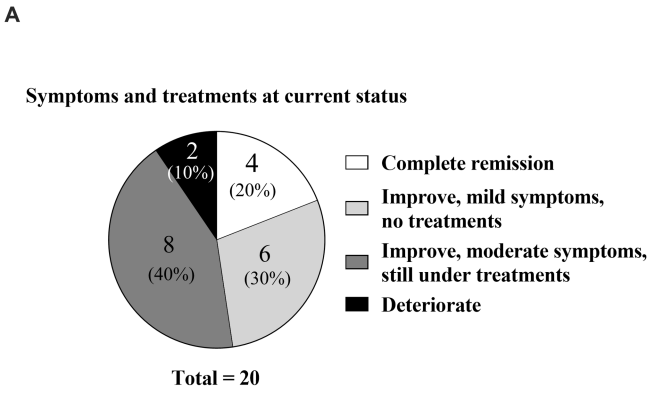


B

**Duration since disease onset until Complete remission or current status**

| Current status | Avarage duration |
|---|---|
| Complete remission | 4 years |
| Improve, mild symptoms, no treatments | 11.7 years |
| Improve, moderate symptoms, still under treatments | 6.4 years |
| Deteriorate | 10 years |

FIGURE 3
Current symptoms and time from disease onset. **(A)** Percentages of current symptoms and current treatment conditions. **(B)** Time from disease onset to complete remission or current status.

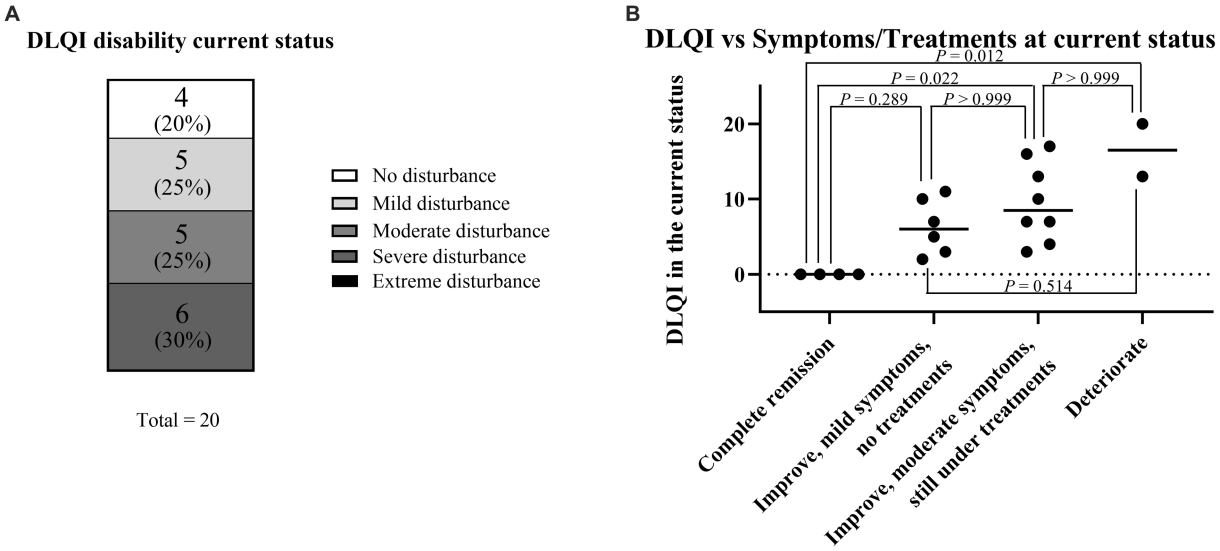


FIGURE 4
Current symptoms and comparison with DLQI score for the current status. **(A)** DLQI score for the current status. **(B)** Association between DLQI score for the current status and current symptoms/treatments. Because continuous variables showed a non-normal distribution according to the Shapiro–Wilk test and each sample was independent, statistical analyses were performed using the Kruskal–Wallis test followed by Dunn's multiple comparisons test.

QOL impairment (Figure 4A; Table 2). Briefly, DLQI scores 0–1 were classified as "no disturbance," 2–5 as "mild disturbance," 6–10 as "moderate disturbance," 11–20 as "severe disturbance," and 21–30 as "extreme disturbance" (28). Thus, four patients (20%) had "no disturbance," five patients (25%) had "mild disturbance," five patients (25%) had "moderate disturbance," six patients (30%) had "severe disturbance," and no patients had "extreme disturbance."

The association between the DLQI score for the current status and current symptoms/treatments was analyzed (Figure 4B). The median DLQI scores in each group were as follows: complete remission, 0 (IQR: 0–0); mild symptoms, 6 (IQR: 3.5–9.25); moderate symptoms, 8.5 (IQR: 6.25–13.75); and deterioration, 16.5 (IQR: 14.75–18.25). There were significant differences in DLQI score between the complete remission and moderate symptom groups ($p = 0.022$) and between the complete remission and deterioration groups ($p = 0.012$).

## Dermatology life quality index score for current status according to the action spectrum and treatments

The authors examined factors affecting the DLQI score for the current status. The action spectrum at onset did not affect the DLQI score for the current status (Figure 5A). Similarly, treatment selection (H1, UVA hardening, and/or VL hardening) did not affect the DLQI score for the current status (Figure 5B).

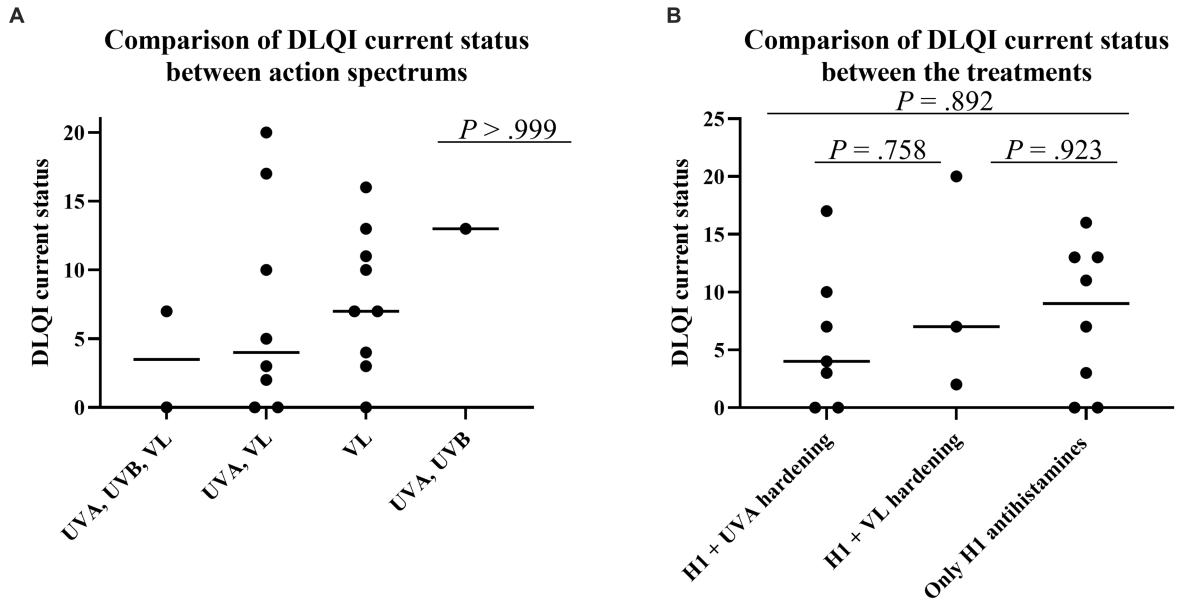


FIGURE 5
Factors affecting DLQI score for the current status. **(A)** Comparison of DLQI score for the current status according to action spectrum at onset. Because continuous variables showed a non-normal distribution according to the Shapiro–Wilk test and each sample was independent, statistical analyses were performed using the Kruskal–Wallis test followed by Dunn's multiple comparisons test. **(B)** Comparison of DLQI score for the current status according to treatment. Because continuous variables showed a non-normal distribution according to the Shapiro–Wilk test and each sample was independent, statistical analyses were performed using the Kruskal–Wallis test followed by Dunn's multiple comparisons test.

In addition to the above factors, the authors found no differences in other factors (sex, age at onset, complications, total serum IgE level, inhibition spectrum, and time from disease onset).

## Statistical analysis

As shown in Figures 4B, 5A,B, continuous variables exhibited a non-normal distribution according to the Shapiro–Wilk test and each sample was independent; thus, statistical analyses were performed using the Kruskal–Wallis test followed by Dunn's multiple comparisons test. Statistical analysis was performed with GraphPad Prism 8 software (GraphPad Software Inc., La Jolla, CA).

# Discussion

In this study, the authors used a questionnaire approach to explore long-term prognosis and QOL among SU patients. The authors examined factors affecting long-term prognosis within a few years after treatment. To our knowledge, no previous studies have compared treatment selection, immediate effectiveness based on medical records, and long-term prognosis within a few years after treatment (using a questionnaire).

Here, the authors discuss patient characteristics (Table 1). Although a previous report mentioned sex differences in SU incidence, prognostic differences were not recorded (29). In the present study, the authors analyzed sex differences; although the male-to-female ratio was 13:16, DLQI scores did not differ between men and women. Age at onset of SU was previously described as young (median ages of 32 or 35 years) (16, 29). In the present study, the median age at onset was similar but tended to be younger (29 years). Additionally, the authors found that no patient had an IgE level exceeding 1,000 IU/mL. Many patients had action spectrum to VL was also reported in another Japanese report (16). This may reflect the difference in the action spectrum between the yellow race and Caucasians.

Regarding treatment selection, H1 effectiveness has been considered insufficient compared with other treatments (6, 30, 31). However, when the authors grouped patients according to H1 effectiveness (effective/partially effective), 22 of the 29 patients (72.4%) experienced at least partial H1 effectiveness (Figure 4A). These findings suggest that H1 can be recommended as a first-line treatment. However, many patients underwent combination therapy with the addition of H1; this fact also expressed that the effectiveness of H1 was found, but it was limited and not enough (If the authors excluded the partially effective group of 55.2%, the effective group was only 17.2%) (Figure 4A).

Next, the authors analyzed treatment selection and immediate effectiveness based on medical records. Hardening therapy was selected for 17 patients. Eight of nine patients who underwent UVA hardening showed improvement, whereas three of the three patients who underwent VL hardening showed no improvement (Figure 4C). Thus, UVA hardening was considered an effective treatment in the present study. Compared with UVA hardening, very few reports have described successful VL hardening treatment outcomes (10). Nevertheless, our VL hardening protocol is experimental and requires further optimization. Thus, when an SU patient has an action spectrum that includes UVA, UVA hardening may be effective. In contrast, when the patient has an action spectrum of VL only, VL hardening is not strongly recommended; however, methods for VL hardening require further modification.

Long-term prognostic data for SU are currently limited. In the present study, when the authors combined the improvement groups (complete remission, improvement with mild symptoms, and

improvement with moderate symptoms), the authors observed that 18 (90%) of 20 patients experienced some improvement (Figure 5A). This tendency may reflect a natural recovery aspect of SU as previously mentioned (19). Notably, the complete remission group comprised only four (20%) of 20 patients, with complete remission at a mean of 4 years after disease onset (Figure 5B). This percentage was similar to the percentages in another report (12% at 5 years and 26% at 10 years after diagnosis) (19). These data imply that SU is refractory in many patients; although most patients experienced at least partial recovery, complete remission was rare and challenging to achieve. Furthermore, in terms of disease duration, complete remission occurred within a mean of 4 years after disease onset. This was a shorter duration compared with the non-complete-remission group (Figure 5B). The four patients with complete remission had the following features: female sex, various action/inhibition spectra, H1 + UVA hardening in two patients, and H1 only in two patients (Table 1).

QOL status among SU patients has rarely been evaluated using DLQI scores (32). Thus, long-term prognostic assessment and DLQI measurement are strengths of this study. The authors compared DLQI scores for the current status among patients who underwent hardening therapy; the authors found that neither action spectra nor treatment selection affected the DLQI score for the current status (Figures 2A,B). Thus, although hardening therapy showed some immediate effectiveness, such therapy did not have a long-term prognostic effect on the DLQI score for the current status.

This study had some limitations. Because SU is relatively a rare disease, only 29 patients were included. This is a limitation of the single-center design; an international multi-center study is needed to increase the number of patients. Furthermore, the DLQI score reflects subjective symptoms, rather than objective indicators. Finally, because H1 was administered to all patients, the authors could not perform comparisons with a control group of SU patients who did not undergo H1 treatment. Therefore, a larger, standardized study that prospectively collects appropriate data, including baseline information, is needed. Additionally, most judgments of treatment effectiveness were made on the basis of MUD, but a few judgments of treatment effectiveness were determined on the basis of physician-mediated patient interviews; the authors highlight the differences between these groups in Supplementary Figures S1, S2.

In conclusion, our questionnaire analysis revealed long-term prognosis and current QOL status in SU patients. Most patients showed some improvement when assessed for this study, compared with disease onset. This study confirmed the effectiveness of hardening therapy, especially UVA hardening therapy for SU patients with an action spectrum that includes UVA.

## Data availability statement

The raw data supporting the conclusions of this article will be made available by the authors, without undue reservation.

## Ethics statement

The studies involving humans were approved by the Institutional Review Board of Kobe University. The studies were conducted in accordance with the local legislation and institutional requirements. Written informed consent for participation in this study was provided by the participants' legal guardians/next of kin. Written informed consent was obtained from the individual(s) for the publication of any potentially identifiable images or data included in this article.

## Author contributions

SI: Data curation, Formal analysis, Funding acquisition, Investigation, Methodology, Project administration, Software, Visualization, Writing – original draft, Writing – review & editing. YO: Conceptualization, Data curation, Investigation, Methodology, Writing – review & editing. TF: Data curation, Methodology, Writing – review & editing. MM: Data curation, Methodology, Writing – review & editing. MS: Data curation, Methodology, Writing – review & editing. KW: Conceptualization, Data curation, Methodology, Validation, Writing – review & editing. CN: Supervision, Writing – review & editing. AF: Conceptualization, Data curation, Investigation, Methodology, Supervision, Writing – original draft, Writing – review & editing.

## Funding

The author(s) declare financial support was received for the research, authorship, and/or publication of this article. This study was supported in part by a Grant-in-Aid for Scientific Research (C) (JSPS KAKENHI Grant No. 20 K08651) to AF and a Grant-in-Aid for Early-Career Scientists (JSPS KAKENHI Grant No. 23 K15268) to SI from the Ministry of Education, Culture, Sports, Science, and Technology, Japan.

## Acknowledgments

The authors thank Edanz (https://jp.edanz.com/ac) for editing a draft of this manuscript.

## Conflict of interest

The authors declare that the research was conducted in the absence of any commercial or financial relationships that could be construed as a potential conflict of interest.

## Publisher's note



## Supplementary material

The Supplementary material for this article can be found online at: https://www.frontiersin.org/articles/10.3389/fmed.2024.1328765/full#supplementary-material

# References


1. Czarnetzki BM. The history of urticaria. *Int J Dermatol*. (1989) 28:52–7. doi: 10.1111/j.1365-4362.1989.tb01314.x

2. De Martinis M, Sirufo MM, Ginaldi L. Solar Urticaria, a disease with many dark sides: is Omalizumab the right therapeutic response? Reflections from a clinical case report. *Open Med (Wars)*. (2019) 14:403–6. doi: 10.1515/med-2019-0042

3. Fukunaga A, Horikawa T, Yamamoto A, Yamada Y, Nishigori C. The inhibition spectrum of solar urticaria suppresses the wheal-flare response following intradermal injection with photo-activated autologous serum but not with compound 48/80. *Photodermatol Photoimmunol Photomed*. (2006) 22:129–32. doi: 10.1111/j.1600-0781.2006.00213.x

4. Srinivas CR, Fergusson J, Shenoi SD, Pai S. Solar urticaria. *Indian J Dermatol Venereol Leprol*. (1995) 61:288–90.

5. Zuberbier T, Abdul Latiff AH, Abuzakouk M, Aquilina S, Asero R, Baker D, et al. The international EAACI/GA$^2$LEN/euro GuiDerm/APAAACI guideline for the definition, classification, diagnosis, and management of urticaria. *Allergy*. (2022) 77:734–66. doi: 10.1111/all.15090

6. Snast I, Lapidoth M, Uvaidov V, Enk CD, Mazor S, Hodak E, et al. Real-life experience in the treatment of solar urticaria: retrospective cohort study. *Clin Exp Dermatol*. (2019) 44:e164–70. doi: 10.1111/ced.13960

7. Grundmann SA, Ständer S, Luger TA, Beissert S. Antihistamine combination treatment for solar urticaria. *Br J Dermatol*. (2008) 158:1384–6. doi: 10.1111/j.1365-2133.2008.08543.x

8. Dawe RS, Ferguson J. Prolonged benefit following ultraviolet a phototherapy for solar urticaria. *Br J Dermatol*. (1997) 137:144–8. doi: 10.1046/j.1365-2133.1997.17861873.x

9. Beissert S, Ständer H, Schwarz T. UVA rush hardening for the treatment of solar urticaria. *J Am Acad Dermatol*. (2000) 42:1030–2. doi: 10.1067/mjd.2000.104517

10. Masuoka E, Fukunaga A, Kishigami K, Jimbo H, Nishioka M, Uchimura Y, et al. Successful and long-lasting treatment of solar urticaria with ultraviolet a rush hardening therapy. *Br J Dermatol*. (2012) 167:198–201. doi: 10.1111/j.1365-2133.2012.10944.x

11. Lyons AB, Peacock A, Zubair R, Hamzavi IH, Lim HW. Successful treatment of solar urticaria with UVA1 hardening in three patients. *Photodermatol Photoimmunol Photomed*. (2019) 35:193–5. doi: 10.1111/phpp.12447

12. Hawk JL, Eady RA, Challoner AV, Kobza-Black A, Keahey TM, Greaves MW. Elevated blood histamine levels and mast cell degranulation in solar urticaria. *Br J Clin Pharmacol*. (1980) 9:183–6. doi: 10.1111/j.1365-2125.1980.tb05831.x

13. Haylett AK, Nie Z, Brownrigg M, Taylor R, Rhodes LE. Systemic photoprotection in solar urticaria with α-melanocyte-stimulating hormone analogue [Nle 4-D-Phe7]-α-MSH. *Br J Dermatol*. (2011) 164:407–14. doi: 10.1111/j.1365-2133.2010.10104.x

14. Dawe RS. Induction of tolerance in solar urticaria by ultraviolet a 'rush hardening': is this true desensitization? *Br J Dermatol*. (2012) 167:4–5. doi: 10.1111/j.1365-2133.2012.11030.x

15. Pérez-Ferriols A, Barnadas M, Gardeazábal J, de Argila D, Carrascosa JM, Aguilera P, et al. Solar urticaria: epidemiology and clinical phenotypes in a Spanish series of 224 patients. *Actas Dermosifiliogr*. (2017) 108:132–9. doi: 10.1016/j.ad.2016.09.003

16. Uetsu N, Miyauchi-Hashimoto H, Okamoto H, Horio T. The clinical and photobiological characteristics of solar urticaria in 40 patients. *Br J Dermatol*. (2000) 142:32–8. doi: 10.1046/j.1365-2133.2000.03238.x

17. Kerr HA, Lim HW. Photodermatoses in African Americans: a retrospective analysis of 135 patients over a 7-year period. *J Am Acad Dermatol*. (2007) 57:638–43. doi: 10.1016/j.jaad.2007.05.043

18. Hamel R, Mohammad TF, Chahine A, Joselow A, Vick G, Radosta S, et al. Comparison of racial distribution of photodermatoses in USA academic dermatology clinics: a multicenter retrospective analysis of 1080 patients over a 10-year period. *Photodermatol Photoimmunol Photomed*. (2020) 36:233–40. doi: 10.1111/phpp.12543

19. Beattie PE, Dawe RS, Ibbotson SH, Ferguson J. Characteristics and prognosis of idiopathic solar Urticaria: a cohort of 87 cases. *Arch Dermatol*. (2003) 139:1149–54. doi: 10.1001/archderm.139.9.1149

20. Chong WS, Khoo SW. Solar urticaria in Singapore: an uncommon photodermatosis seen in a tertiary dermatology center over a 10-year period. *Photodermatol Photoimmunol Photomed*. (2004) 20:101–4. doi: 10.1111/j.1600-0781.2004.00083.x

21. Silpa-Archa N, Wongpraparut C, Leenutaphong V. Analysis of solar urticaria in Thai patients. *Asian Pac J Allergy Immunol*. (2016) 34:146–52. doi: 10.12932/AP0632.34.2.2016

22. Jong CT, Finlay AY, Pearse AD, Kerr AC, Ferguson J, Benton EC, et al. The quality of life of 790 patients with photodermatoses. *Br J Dermatol*. (2008) 159:192–7. doi: 10.1111/j.1365-2133.2008.08581.x

23. Rizwan M, Reddick CL, Bundy C, Unsworth R, Richards HL, Rhodes LE. Photodermatoses: environmentally induced conditions with high psychological impact. *Photochem Photobiol Sci*. (2013) 12:182–9. doi: 10.1039/c2pp25177a

24. Pherwani AV, Bansode G, Gadhia S. The impact of chronic urticaria on the quality of life in Indian patients. *Indian J Dermatol*. (2012) 57:110–3. doi: 10.4103/0019-5154.94277

25. Miyauchi H, Horio T. Detection of action, inhibition and augmentation spectra in solar urticaria. *Dermatology*. (1995) 191:286–91. doi: 10.1159/000246570

26. Oda Y, Washio K, Fukunaga A, Mizuno M, Hirai H, Imamura S, et al. Establishment of the basophil activation test to detect photoallergens in solar urticaria. *J Allergy Clin Immunol Pract*. (2020) 8:2817–2819.e1. doi: 10.1016/j.jaip.2020.04.042

27. Sabroe RA, Grattan CE, Francis DM, Barr RM, Kobza Black A, Greaves MW. The autologous serum skin test: a screening test for autoantibodies in chronic idiopathic urticaria. *Br J Dermatol*. (1999) 140:446–52. doi: 10.1046/j.1365-2133.1999.02707.x

28. Hongbo Y, Thomas CL, Harrison MA, Salek MS, Finlay AY. Translating the science of quality of life into practice: what do dermatology life quality index scores mean? *J Invest Dermatol*. (2005) 125:659–64. doi: 10.1111/j.0022-202X.2005.23621.x

29. Harris BW, Badri T, Schlessinger J. *Solar urticaria*. Treasure Island, FL: StatPearls Publishing LLC (2022).

30. Pont M, Delaporte E, Bonnevalle A, Thomas P. Solar urticaria: pre-PUVA UVA desensitization. *Ann Dermatol Venereol*. (2000) 127:296–9.

31. Bissonnette R, Buskard N, McLean DI, Lui H. Treatment of refractory solar urticaria with plasma exchange. *J Cutan Med Surg*. (1999) 3:236–8. doi: 10.1177/120347549900300503

32. Haylett AK, Koumaki D, Rhodes LE. Solar urticaria in 145 patients: assessment of action spectra and impact on quality of life in adults and children. *Photodermatol Photoimmunol Photomed*. (2018) 34:262–8. doi: 10.1111/phpp.12385

frontiers | Frontiers in Immunology

TYPE Original Research
PUBLISHED 20 February 2024
DOI 10.3389/fimmu.2024.1351513



OPEN ACCESS

EDITED BY
Wang Xiqiao,
Shanghai Jiao Tong University, China

REVIEWED BY
Masanori A. Murayama,
Kansai Medical University, Japan
Biao Cheng,
General Hospital of Southern Theater Command of PLA, China
Sha Huang,
People's Liberation Army General Hospital, China

*CORRESPONDENCE
Duyin Jiang
jdybs2@vip.163.com
Guobao Huang
huangguobao@163.com

RECEIVED 06 December 2023
ACCEPTED 30 January 2024
PUBLISHED 20 February 2024

CITATION
Wang X, Wang X, Liu Z, Liu L, Zhang J, Jiang D and Huang G (2024) Identification of inflammation-related biomarkers in keloids. *Front. Immunol.* 15:1351513. doi: 10.3389/fimmu.2024.1351513



# Identification of inflammation-related biomarkers in keloids

Xiaochuan Wang[1], Xiaoyang Wang[1], Zhenzhong Liu[1], Lei Liu[1], Jixun Zhang[1], Duyin Jiang[1]* and Guobao Huang[2]*

[1]Plastic Burn Surgery, The Second Hospital of Shandong University, Jinan, Shandong, China, [2]Burn Plastic Surgery, Central Hospital Affiliated to Shandong First Medical University, Jinan, Shandong, China

**Background:** The relationship between inflammation-related genes (IRGs) and keloid disease (KD) is currently unclear. The aim of this study was to identify a new set of inflammation-related biomarkers in KD.

**Methods:** GSE145725 and GSE7890 datasets were used in this study. A list of 3026 IRGs was obtained from the Molecular Signatures Database. Differentially expressed inflammation-related genes (DEGs) were obtained by taking the intersection of DEGs between KD and control samples and the list of IRGs. Candidate genes were selected using least absolute shrinkage and selection operator (LASSO) regression analysis. Candidate genes with consistent expression differences between KD and control in both GSE145725 and GSE7890 datasets were screened as biomarkers. An alignment diagram was constructed and validated, and in silico immune infiltration analysis and drug prediction were performed. Finally, RT-qPCR was performed on KD samples to analyze the expression of the identified biomarkers.

**Results:** A total of 889 DEGs were identified from the GSE145725 dataset, 169 of which were IRGs. Three candidate genes (*TRIM32*, *LPAR1* and *FOXF1*) were identified by the LASSO regression analysis, and expression validation analysis suggested that *FOXF1* and *LPAR1* were down-regulated in KD samples and *TRIM32* was up-regulated. All three candidate genes had consistent changes in expression in both the GSE145725 and GSE7890 datasets. An alignment diagram was constructed to predict KD. Effector memory CD4 T cells, T follicular helper cell, Myeloid derived suppressor cell, activated dendritic cell, Immature dendritic cell and Monocyte were differentially expressed between the KD and control group. Sixty-seven compounds that may act on *FOXF1*, 108 compounds that may act on *LPAR1* and 56 compounds that may act on *TRIM32* were predicted. Finally, RT-qPCR showed that the expression of *LPAR1* was significantly lower in KD samples compared to normal samples whereas *TRIM32* was significantly higher, while there was no difference in the expression of *FOXF1*.

**Conclusion:** This study provides a new perspective to study the relationship between IRGs and KD.

KEYWORDS

**inflammation-related genes, keloid disease, GEO, alignment diagram, biomarker**

# 1 Introduction

Keloid disease (KD) is a benign skin fibroplasia caused by abnormal wound healing after skin injury (1) leading to hyperplasic invasive growth, and has a high recurrence rate (2). The occurrence of KD involves trauma, chronic inflammation, and fibrosis tumor inheritance (1, 3, 4). Keloids can grow on all parts of the body (5), and are accompanied by unbearable itching and pain which seriously affects quality of life. Keloids, especially on the face, can also have a serious impact on mental health (6, 7). Although there are many studies on KD the pathogenesis is still not completely clear (8); improved understanding of the pathogenesis will likely lead to new treatments. Several studies have shown that inflammation is involved in regulating KD collagen synthesis, and the intensity of inflammation is positively correlated with the final scar size (9, 10). Therefore, study of the inflammation-related molecular pathogenesis of KD may lead to new KD prevention and treatment strategies.

It is well known that scars are the result of both inflammation and fibrosis after injury repair (1, 8, 11). In the early stage of repair, inflammatory cells play a pro-inflammatory role through cytokines. It usually enters the repair and healing stage after 72 hours and finally completes the remodeling of collagen (12). Pro-inflammatory factors such as IL-1α, IL-1β, IL-6 and TNF-α are up-regulated in KD tissue (11). It has been speculated that chronic inflammation persists in KD causing excessive deposition of extracellular matrix which is an important cause of keloid formation (13, 14). This indicates that KD is an inflammatory disease of the skin (12). In addition, Shi et al. demonstrated that IL-10 can negatively regulate collagen synthesis, thereby reducing scar formation (13, 15). Nishiguchi et al. reported that the chemokine CXCL12 can promote scar formation in mice (12, 16). A large number of studies have shown that KD is correlated with chronic inflammation (11, 12, 17). However, few studies have explored of inflammation-related genes IRGs in KD and the specific mechanism of action in KD pathogenesis. Therefore, we identified and analyzed differentially-expressed IRGs in KD in order to discover new genes that might be important in KD pathogenesis, both as biomarkers for early diagnosis and as novel drug targets.

# 2 Materials and methods

## 2.1 Data source

Two KD datasets (GSE145725 and GSE7890) were obtained from the Gene Expression Omnibus (GEO) database (https://www.ncbi.nlm.nih.gov/gds). The GSE145725 dataset contains 9 fibroblast samples from KD and 10 normal fibroblast control samples. The GSE7890 dataset contains 5 fibroblast samples from KD and 5 normal fibroblast control samples. IRGs were obtained from the Molecular Signatures Database (MSigDB, https://www.gsea-msig) by using the search term "INFLAMMATORY". A total of 57 fibrosis-related genes were shown in Supplementary Table 1.

## 2.2 Identification of inflammation-related DEGs

Differential expression analysis was performed between KD and control samples in the GSE145725 dataset using the limma R package (18) to screen differentially expressed genes (DEGs) using cutoffs of $|\log_2 FC| > 0.5$ and adj. $P < 0.05$. Gene ontology (GO) and Kyoto encyclopedia of genes and genomes (KEGG) enrichment analyses of DEGs were completed using the clusterProfiler package (19). Inflammation-related DEGs were obtained by taking the intersection of DEGs and IRGs. To explore whether interactions existed among the inflammation-related DEGs, a protein-protein interaction (PPI) network was created using STRING (https://string-db.org).

## 2.3 Acquisition of biomarkers

To obtain candidate genes, least absolute shrinkage and selection operator (LASSO) regression analysis SVM, and Boruta algorithms were performed on the inflammation-related DEGs using the glmnet (20), e1071 and Boruta packages. In addition, candidate genes were validated by checking that they were also differentially expressed in the GSE7890 dataset. Validated candidate genes were screened as biomarkers. To explore the potential mechanisms of the biomarkers, Gene Set Enrichment Analysis (GSEA) of biomarkers in GSE145725 was conducted using the h.all.v2023.1.Hs.symbols.gmt dataset in the clusterProfiler package (19). Differential analysis of fibrosis-related genes in the GSE145725 dataset and correlation analysis of differential fibrosis-related genes with biomarkers to further explore the function of biomarkers.

## 2.4 Construction and validation of alignment diagram

To predict the probability of KD from the expression of the identified biomarkers, an alignment diagram was constructed using the rms package (21) in R. In order to assess the predictive ability of the alignment diagram, a calibration curve was plotted using the calibrate function in the rms package, where the closer the slope is to 1, the more accurate the prediction. In order to evaluate the clinical effectiveness of the alignment diagram, decision curve analysis (DCA) was performed using the "rmda" package. Based on the DCA curve, the clinical impact curve (CIC) was plotted using the model to predict the risk stratification of 1000 people.

## 2.5 Immuno-infiltration analysis and drug prediction

The immune abundance of 28 immune cells in KD and control samples from GSE145725 was calculated using the ssGSEA algorithm (22) to obtain differentially expressed (DE) immune cells, and the correlation between the ssGSEA scores of DE

immune cells and biomarkers was calculated and presented using a heatmap. Compounds that may act on biomarkers were predicted using the Comparative Toxicogenomics Database (CTD) database (http://ctdbT2Dme.org/) and key gene-compound networks were constructed.

## 2.6 Protein expression analysis of biomarkers and construction of miRNA-mRNA-TFs regulatory network

The expression of the identified biomarkers was analyzed in different human skin tissues using the Bgee database (https://bgee.org/). To further explore their expression in different cell types of the skin, the Human Protein Atlas (http://www.proteinatlas.org/) was used. The miRNAs that may target the identified biomarkers were predicted using the MicroRNA Target Prediction Database (miRDB, https://mirdb.org/) and The Encyclopedia of RNA Interactomes (ENCORI, http://starbase.sysu.edu.cn/index.php), and the intersection of the predictions from the two databases was taken as the candidate miRNA. Transcription factors (TF) that regulate the expression of the identified biomarkers were predicted using the NetworkAnalyst online tool (https://www.networkanalyst.ca/ and hTFtarget database (http://bioinfo.life.hust.edu.cn). Finally, miRNA-mRNA-TF regulatory networks were constructed using Cytoscape.

## 2.7 Statistical analysis

The limma package was used to identify DEGs. Venn diagrams were constructed using the venn package. ClusterProfiler was used for enrichment analysis. STRING was used to build PPI networks. LASSO was used to screen candidate genes. ssGSEA was used to calculate the infiltration abundance of immune cells. Statistical analysis was done using R software (version 4.1.1 https://www.r-project.org/). Differences between groups were analyzed using the Wilcox test. $P < 0.05$ was considered a statistically significant difference.

## 2.8 RT-qPCR Analysis

The expression of the three biomarkers was measured using RT-qPCR. We collected KD and control samples from The Second Hospital of Shandong University department of plastic surgery with 5 samples in each group. This study was performed in line with the principles of the Declaration of Helsinki. Approval was granted by the Ethics Committee of the Second Hospital of Shandong university(Date: December 6, 2023; No: KYLL-2023LW088). Total RNA was extracted using TRIzol (Ambion, Austin USA) according to the manufacturer's instructions. The extracted RNA was reverse transcribed into cDNA using the SureScript First strand cDNA synthesis kit before RT-qPCR. RT-qPCR was performed using the 2xUniversal Blue SYBR Green qPCR Master Mix (Servicebio, Wuhan China). The *GAPDH* gene was used as a housekeeping gene and the relative expression of the biomarkers was determined using the $2^{-\Delta\Delta Ct}$ method.

# 3 Results

## 3.1 Identification of inflammation-associated DEGs in the GSE145725 dataset

A total of 889 DEGs were identified from the GSE145725 dataset, of which 433 were up-regulated in KD and 456 were down-regulated (Figures 1A, B). GO analysis revealed that DEGs were associated with skeletal system morphogenesis, regulation of animal organ morphogenesis, and cartilage development (Supplementary Figure 1A) and KEGG analysis revealed enriched in transcriptional misregulation in cancer, cGMP-PKG signaling pathway, and Wnt signaling pathway (Supplementary Figure 1B). A total of 169 inflammation-related DEGs were obtained from the overlap between the 889 DEGs and 3026 IRGs (Figure 1C). To explore whether there are any known interactions between the proteins coded for by the 169 inflammation-associated DEGs, a PPI network was created (Figure 1D) which had a confidence level of 0.4 (Confidence = 0.4) with strong interactions between A2M and SERPINF1, ABCC1 and CASP3, and ADAMTS3 and TTC12.

## 3.2 Screening and verification of biomarkers for KD

FOXF1, LPAR1, SERPINF1, TRIM32 were found as candidate genes by machine learning (SVM and Boruta) (Supplementary Figure 2A). The results of the LASSO regression analysis suggested that when $\lambda = 0.004102608$ three candidate genes (*TRIM32*, *LPAR1*, and *FOXF1*) with regression coefficients that were not penalized to 0 were obtained after tenfold cross-validation (Figure 2A). *FOXF1* and *LPAR1* were down-regulated in KD samples and *TRIM32* was up-regulated in KD samples and all three candidate genes had the same expression trends in the GSE145725 and GSE7890 datasets (Figure 2B). GSEA results showed that *FOXF1* was mainly enriched in E2f targets, G2M checkpoint, and myogenesis. *LPAR1* was mainly enriched in reactive oxygen species pathway, apoptosis, and IFN-α response. *TRIM32* was mainly enriched in IFN-α response, apoptosis, and hypoxia (Figure 2C). Correlation analysis showed that nine fibrosis-related genes were significantly different between KD and controls and showed high correlation with biomarkers (Supplementary Figure 2B).

## 3.3 Prediction of KD risk from biomarker expression

Based on the expression of the biomarkers, an alignment diagram was constructed. The score of each sample was calculated by the alignment diagram, with a higher score indicating a higher likelihood of KD (Figure 3A). The slope of the calibration curve is close to 1 and the CIC converge with the trend of the real situation suggests that the predictive efficacy of the model is excellent (Figure 3B). Expression distribution analysis of the identified biomarkers suggested that they are expressed at high levels in the skin of the abdomen (Figure 3C). In addition, *FOXF1* is expressed in endothelial cells and smooth muscle cells, *LPAR1* is expressed in endothelial cells and fibrosis, and *TRIM32* is expressed in mitotic cells (skin) (Figure 3D).

10.3389/fimmu.2024.1351513

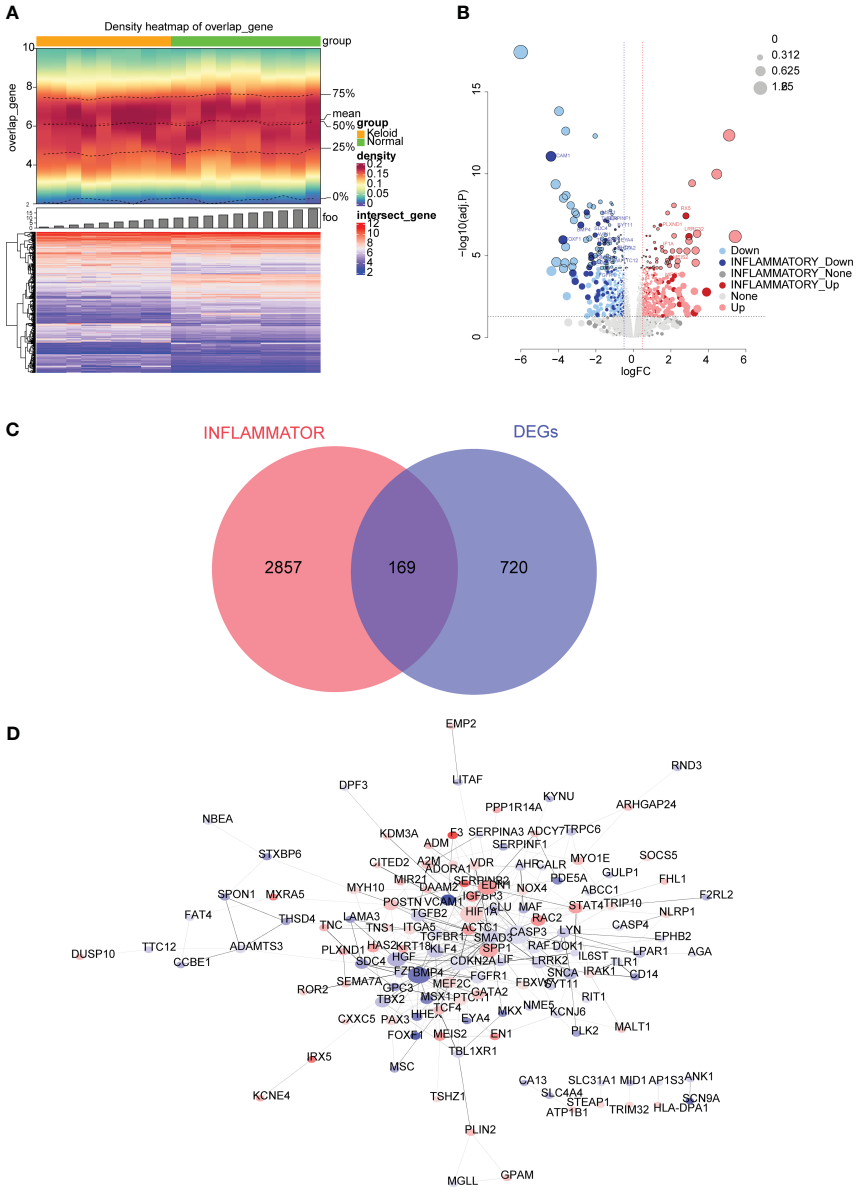


FIGURE 1
Differential expression analysis in the GSE145725 dataset. **(A)** Heatmap of differentially expressed genes (DEGs) between keloid disease (KD) and normal samples. A heat map of gene density is shown at the top, and a heat map of gene expression is shown at the bottom (red is high expression, blue is low expression). **(B)** Volcano plot of DEGs between KD and normal groups. Each dot represents a gene, the darker colored dots indicate inflammation-related genes, and the black circles indicate genes with an adjusted P value < 0.01. The names of genes associated with inflammation with very significant differences are labeled in the figure. **(C)** Venn diagram of 169 inflammation-related DEGs obtained by overlapping the DEGs and inflammation-related genes (IRGs). **(D)** Protein-protein interaction (PPI) network of 169 inflammation-associated DEGs.

## 3.4 Immune cell infiltration and its relevance with biomarkers

Six differentially abundant immune cells were identified between the KD and control group (Figure 4A). Correlation analysis between the ssGSEA scores of the differentially abundant immune cells and the biomarkers suggested that *LPAR1* was positively correlated with activated CD4 T cells, myeloid-derived suppressor cells, effector memory CD4 T cells, and type 2 T helper cells ($P < 0.01$), *TRIM32* was positively correlated with monocytes ($P < 0.01$), and *FOXF1* was positively correlated with activated CD8 T cells, and myeloid-derived suppressor cells ($P < 0.01$) (Figure 4B).

## 3.5 Prediction of potential regulatory mechanisms

A total of 32 miRNAs and 9 TFs were obtained and a miRNA-mRNA-TF regulatory network was constructed (Figure 5A; biomarkers in red, miRNAs in blue and TFs in green). *FOXF1* and *LPAR1* were regulated by E2F1 and *TRIM32* and *FOXF1* were regulated by CREB1. Sixty-seven

10.3389/fimmu.2024.1351513

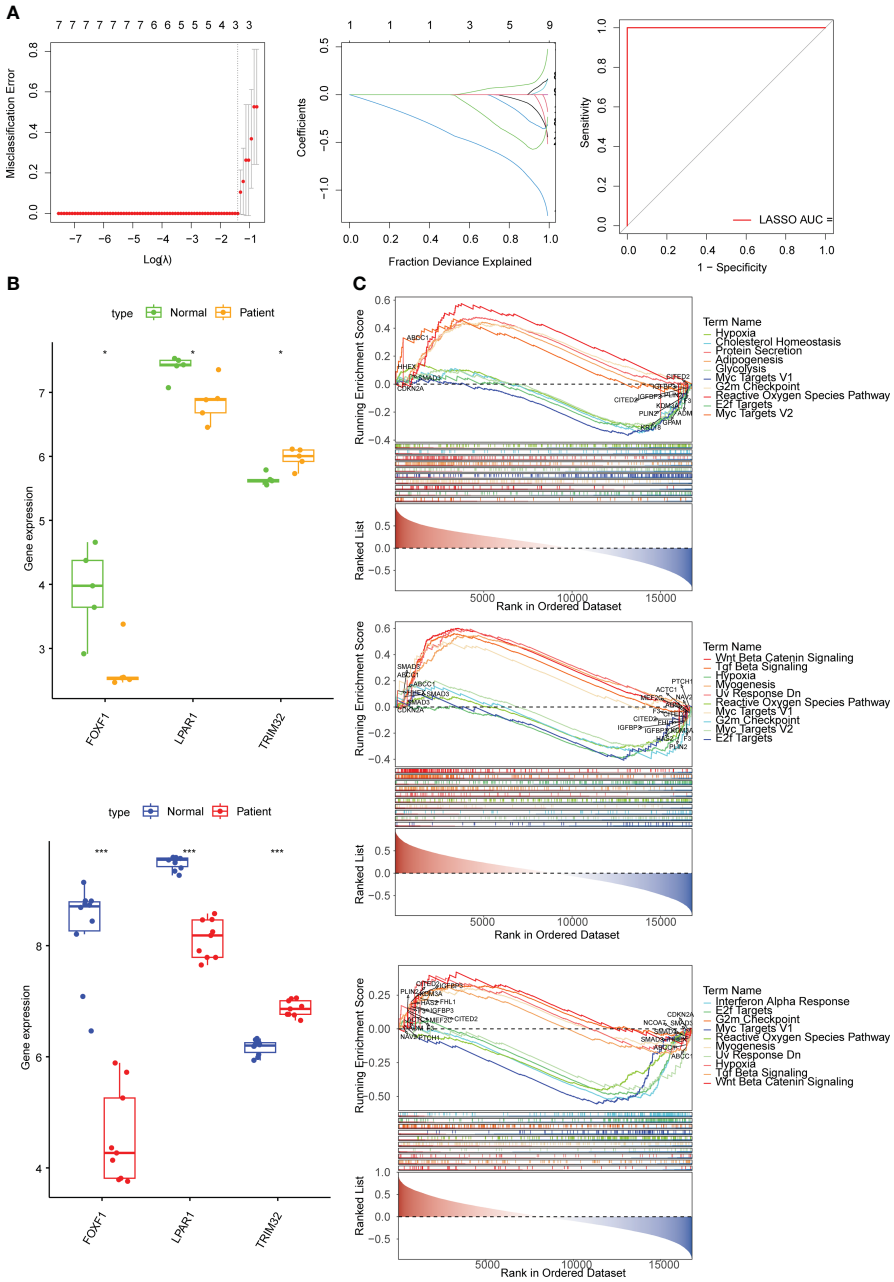


FIGURE 2
Identification of biomarkers and exploration of potential function. **(A)** Error plots for 10-fold cross-validation, plot of gene coefficients, and receiver operating characteristic (ROC) curve of the least absolute shrinkage and selection operator (LASSO) model. The different colored lines represent different genes. AUC, area under the curve. **(B)** The expression of biomarkers in the KD and normal samples in the GSE7890 and GSE145725 datasets. **(C)** The top 10 pathways significantly enriched in *FOXF1*, *LPAR1*, and *TRIM32* according to gene set enrichment analysis (GSEA) enrichment analysis. * means p<0.05, *** means p<0.001.

compounds that may act on *FOXF1*, 108 compounds that may act on *LPAR1*, and 56 compounds that may act on *TRIM32* were predicted and gene-compound action networks were constructed (Figure 5B).

## 3.6 Expression of biomarkers in clinical samples

RT-qPCR data showed that the mRNA level of *LPAR1* was significantly lower, and the mRNA level of *TRIM32* was significantly higher ($P < 0.05$) in the KD samples compared to the normal samples. There was no significant difference in the expression of *FOXF1* (Figure 6).

# 4 Discussion

KD is a benign skin tumor caused by abnormal hyperplasia of connective tissue in the skin, that occurs during prolonged abnormal wound healing. The mechanisms by which keloids form

10.3389/fimmu.2024.1351513

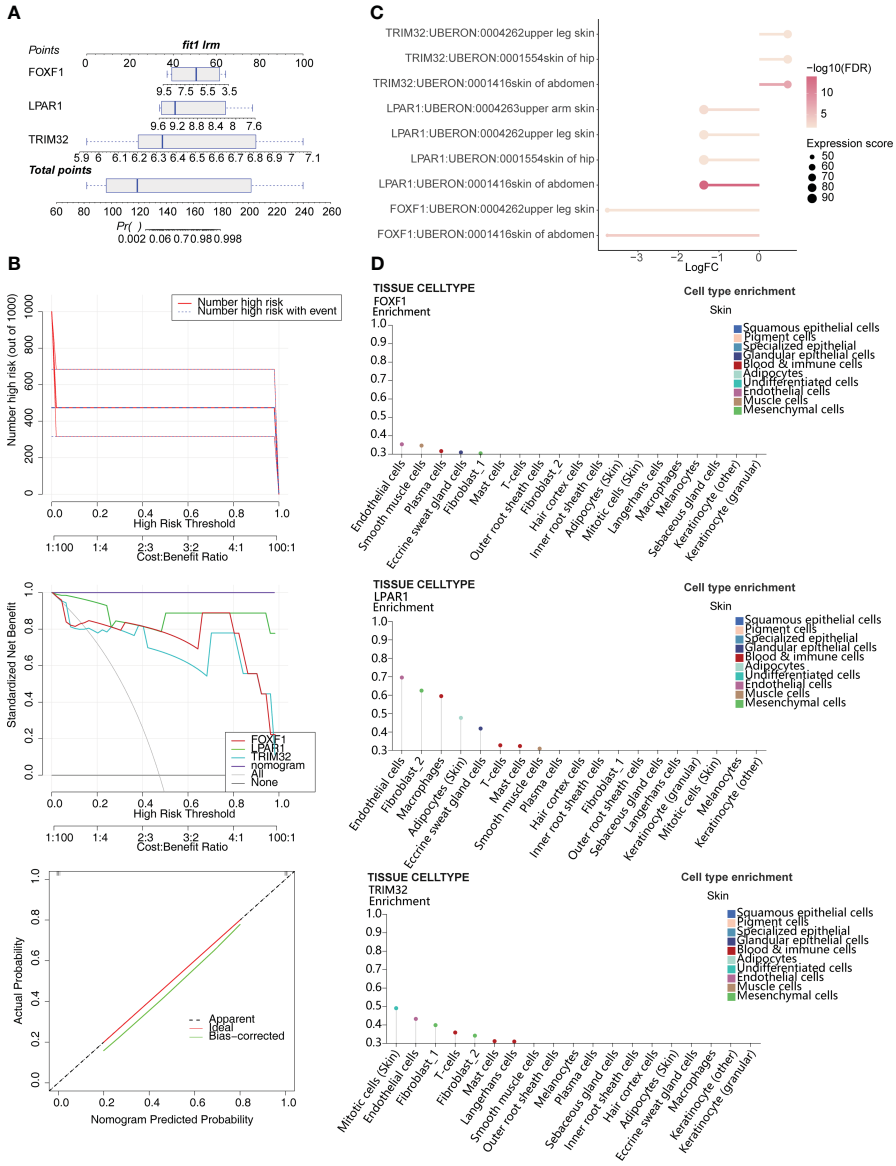


FIGURE 3
Construction of the alignment diagram to predict the risk of KD. **(A)** Alignment diagram based on expression of *FOXF1*, *LPAR1*, and *TRIM32*. **(B)** Clinical impact curve (CIC), decision curve analysis (DCA), and calibration curve of the alignment diagram. **(C)** Distribution of biomarkers in human tissues. **(D)** Expression of biomarkers in different skin cell types.

are currently unclear. Some scholars believe that the abnormal response of fibroblasts to inflammation is causes keloid formation. We propose that the inflammatory response is a significant factor in keloid pathogenesis (13–15). However, most of the current research on keloids focuses on fibroblasts and collagen with little emphasis on the importance of inflammatory genes. Therefore, finding key inflammatory genes associated with KD may help to identify new diagnostic biomarkers and drug targets.

In this study we explored the differentially expressed IRGs in two KD datasets, conducted multiple functional enrichment analyses, constructed a PPI network, and explored immune infiltration in the KD microenvironment. Finally, three keloid biomarkers were identified: *LPAR1*, *FOXF1* and *TRIM32*. In the RT-qPCR data collected from our clinical samples *LPAR1* and *TRIM32* were differentially expressed in KD samples ($P<0.05$) whereas *FOXF1* was not ($P>0.05$).

The protein encoded by *TRIM32* is a member of the tripartite motif-containing family. This protein is located in the cytoplasm and nucleus and has E3 ubiquitin ligase activity (23). TRIM32 can ubiquitinate PIAS4/PIASY and promote its degradation in UVB and TNF-α stimulated keratinocytes. In our study, the GSEA results indicated that *TRIM32* was mainly enriched in IFN-α reactions, cell apoptosis, and hypoxia. Chaudhuri et al. reported that knocking down *TRIM32* inhibited glucose-induced podocyte apoptosis, oxidative stress, and inflammatory response (24). Liu et al. reported that the gene manipulation of *Trim32* can regulate Th17 vs. Th2 immunity in response to TLR activation, suggesting that atopic dermatitis is a result of TRIM32 protein deficiency in the

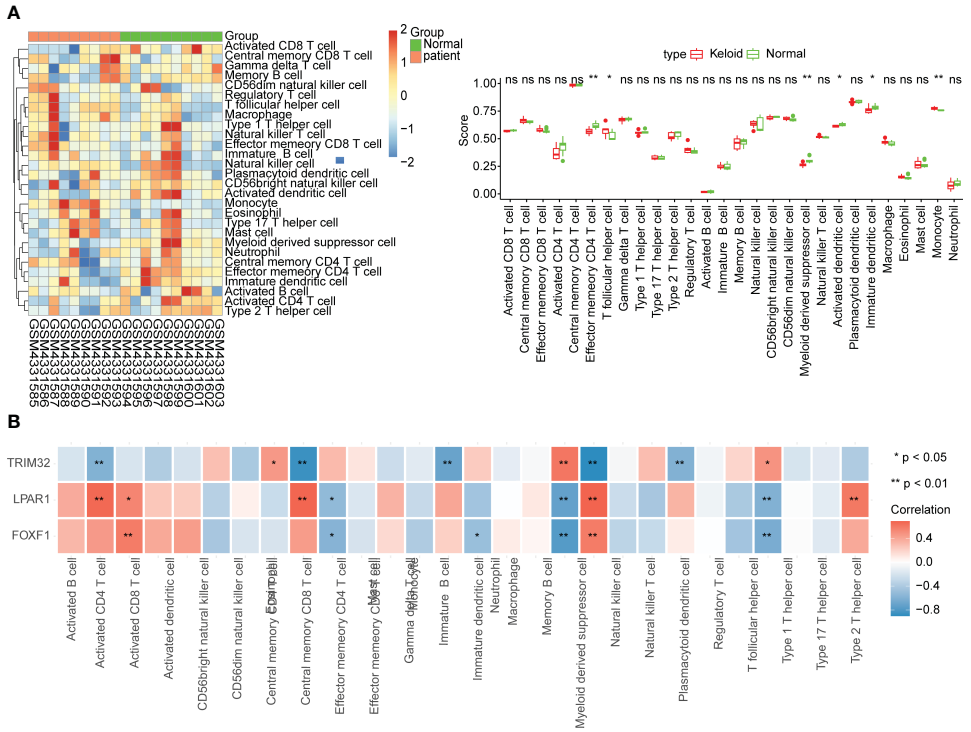


FIGURE 4
Immune infiltration analysis. **(A)** Relative abundance of immune cells and comparison between KD and normal samples. ns, not significant; *p<0.05; **p<0.01. **(B)** Correlation between biomarkers and immune cells.

skin. It was speculated that *TRIM32* plays a crucial role in inflammatory diseases and congenital immunodeficiency diseases (25). Our analysis found that *TRIM32* was upregulated in publicly available KD microarray data, and RT-qPCR from our clinical samples confirmed this ($P < 0.05$). We speculate that *TRIM32* is closely involved in the formation of keloids. Further research on the inflammatory regulation of scarring by *TRIM32* may establish *TRIM32* as a potential treatment target for keloids.

The protein encoded by *LPAR1* is an integral membrane protein in the family of lysophosphatidic acid receptors also known as EDG receptors (26, 27). LPAR1 is involved in the reorganization, migration, differentiation, and proliferation of actin cytoskeleton, as well as its response to tissue damage and infection (28–30). *LPAR1* promotes the formation of lamellar pseudopodia at the anterior edge of migrating cells by activating RAC1. This activation plays a role in chemotaxis and cell migration, which are important in injury responses (31–33). Wu et al. reported that *LPAR1* can mediate various biological functions of tumors (34) and participate in the activation, proliferation differentiation, and migration of immune cells (32). Our correlation analysis between the ssGSEA scores of the differentially abundant immune cells and biomarkers in this study showed that *LPAR1* was positively correlated with activated CD4 T cells and effector memory CD4 T cells. *LPAR1* expression was reported to be positively correlated with the expression of chemokines and chemokine receptors, suggesting that *LPAR1* may regulate immune cell migration (35). The E2F family of transcription factors regulate cell function via gene transcription. E2F was reported as a novel fibrotic gene regulating pulmonary fibrosis (36). The enrichment of single gene GSEA in this study indicated that *LPAR1* is significantly enriched in the "E2F target" pathway. *LPAR1* is most highly expressed in endothelial cells and fibroblasts in skin and soft tissues. Our analysis showed that *LPAR1* was downregulated in KD samples, and this was confirmed by our RT-qPCR data from clinical samples. We therefore speculate that *LPAR1* plays an important inflammatory and immune regulatory role in the formation of keloids.

*FOXF1* belongs to the forkhead transcription factor family and is characterized by a unique forkhead domain (37). In an immune cell analysis of infantile angiomatosis, *FOXF1* was found to be positively correlated with the degree of monocyte infiltration (38). Recent studies have shown that overexpression of *FOXF1* can inhibit the production of α-SMA, fibronectin, and type IV collagen, thereby alleviating TGF-β1-induced fibrosis (39). In addition, overexpression of *FOXF1* can promote the proliferation of BEAS-2B cells, inhibit apoptosis, and inhibit inflammation in response to TGF-β1. Fenghua et al. reported that increasing *FOXF1* expression in endothelial cells could alleviate pulmonary fibrosis (40). *FOXF1* is highly expressed in both endothelial cells and fibroblasts, suggesting that *FOXF1* is involved in chronic inflammation following tissue injury and inhibits collagen deposition and fiber proliferation in keloid formation. In this study, GSEA results showed that *FOXF1* was mainly enriched in E2f targets, G2M checkpoints and myogenesis. However, in our RT-qPCR experiment, we found no significant difference in *FOXF1* expression between KD and normal samples ($P > 0.05$). This may be due to the smaller number of samples in the verification set (5 vs. 5) compared to the microarray data (10 vs. 9).

10.3389/fimmu.2024.1351513

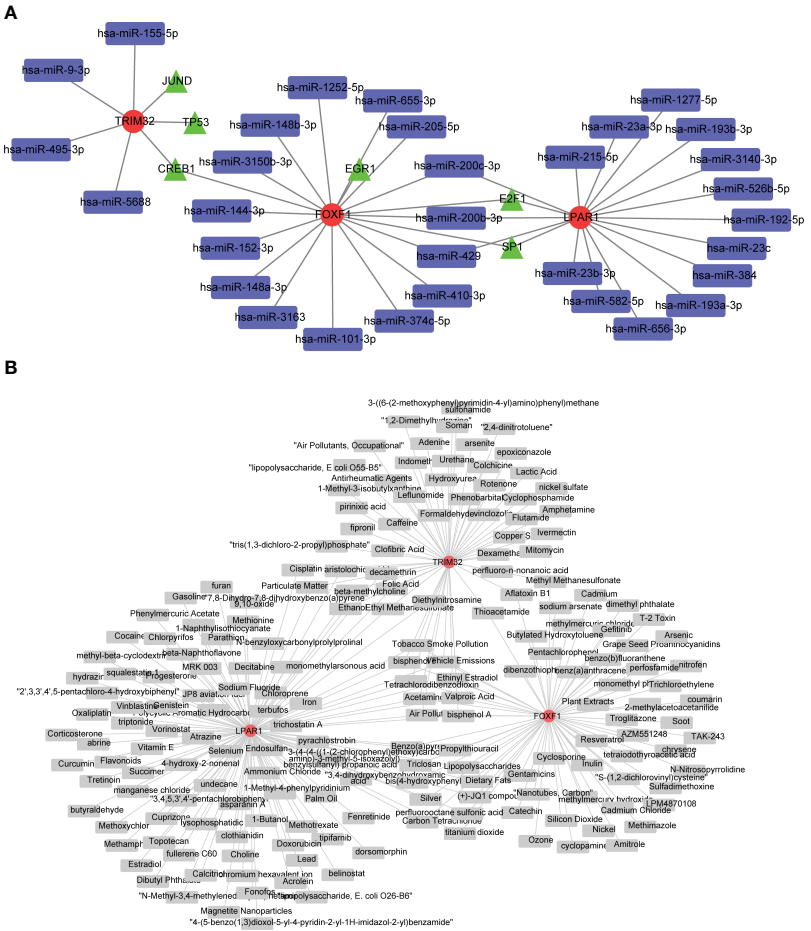


FIGURE 5
Investigation of potential regulatory mechanisms KD biomarkers, and drug predictions. **(A)** Regulatory network based on microRNAs (miRNAs), transcription factors (TFs), and biomarkers. Red circles are biomarkers, blue quadrangles are miRNAs, and green triangles are TFs. **(B)** Biomarker-drug network for KD. Red circles represent biomarkers and gray quadrangles represent drugs targeting these biomarkers.

Our clinical predictive model predicts that the risk of developing KD increases as the expression of *FOXF1* and *LPAR1* decrease and the expression of *TRIM32* increases. Previous studies on these three genes support this prediction. *FOXF1* is associated with tissue development and inhibition of *FOXF1* may cause abnormalities in the cell cycle of wound tissue leading to impaired wound healing. The inhibition of *LPAR1* leads to a decrease in chemotaxis which is crucial for the inflammatory response around the wound. Moderate migration of inflammatory cells such as macrophages, mast cells, and granulocytes helps to remove necrotic cell debris and repair fibers during wound healing. Decreased expression of *LPAR1* inhibits the formation of lamellar pseudopodia at the leading edge of migrating cells which also slows down wound healing. *TRIM32* promotes the degradation of PIAS4

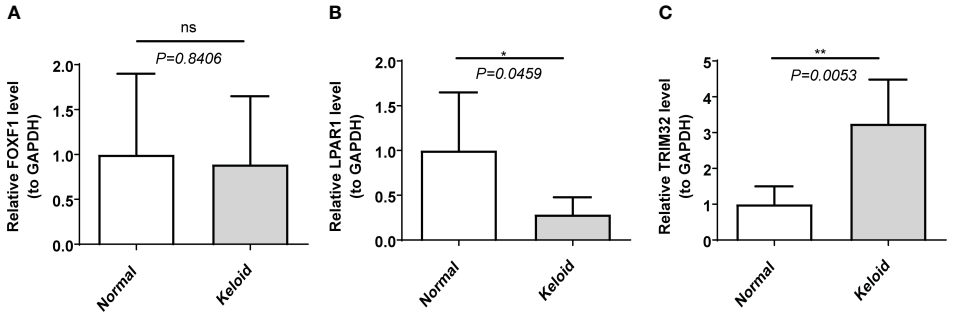


FIGURE 6
The expression of biomarkers in clinical samples by RT-qPCR. **(A)** *FOXF1*. **(B)** *LPAR1*. **(C)** *TRIM32*. ns, not significant; *p<0.05; **p<0.01.

in keratinocytes. Therefore, increased *TRIM32* expression reduces the inhibitory effect of PIAS4 on the formation of keratinocytes, resulting in a large accumulation of keratinocytes around the wound, which secrete keratin fibers that are the main components of scar tissue.

In this study, immuno-infiltration analysis showed significant differences between keloid and normal tissue in CD4+ effector T cells, myeloid-derived suppressor cells, activated dendritic cells, immature dendritic cells, follicular helper T cells, and monocytes. The levels of CD4+ effector T cells, myeloid-derived suppressor cells, activated dendritic cells, and immature dendritic cells were significantly lower in KD tissues than in control tissues while the levels of follicular helper T cells and monocytes were significantly higher. It has been confirmed that the Th2 characteristic is possessed by KD (41). Our analysis suggested that *FOXF1* and *LPAR1* were significantly negatively correlated with monocytes and follicular helper T cells, and significantly positively correlated with myeloid-derived suppressor cells, and that the levels of monocytes and follicular T helper cells at the wound were significantly increased. Henderson et al. analyzed more than 100,000 human hepatocytes and identified a subset of macrophages associated with scarring. This group of macrophages express *TRIM32* and *CD9*, are differentiated from circulating monocytes, and are known to promote fibrosis (42). Previous studies have reported that monocytes and macrophages are key components of the immune system and participate in the regulation of inflammatory immunity and tissue repair by activating T and B lymphocytes (43). Follicular helper T cells are involved in the humoral immune regulation of inflammation and play a crucial role in autoimmunity and tumor-related immunity (44). Myeloid-derived suppressor cells are a group of suppressor cells of bone marrow origin which are precursors of dendritic cells, macrophages, and granulocytes, and have the ability to significantly inhibit immune cell responses (45). Chronic inflammation and fibrosis may be caused by improper activation of the immune response mediated by macrophages, an example of which is the development of fibrosis in systemic sclerosis (46). The biomarkers we identified are related to monocytes, myeloid-derived suppressor cells, and follicular helper T cells, which may all play an important role in the formation of keloids.

In the immune infiltration analysis, we found that there were different degrees of correlation between the biomarkers and the infiltration of immune cells. In order to further explore the role of immune cells in the development of KD, we used the HPA database to explore the expression of the biomarkers in different cell types. LPAR1 was enriched in macrophages, T-cells and mast cells, TRIM32 was enriched in T cells and mast cells, while FOXF1 was not significantly expressed in any immune cells. In a mouse model of multiple sclerosis, Choi et al. found that LPAR1-3 antagonists increased cell infiltration and immune cell activation (including macrophages) (PMID:34666785). In addition, Choi et al. demonstrated that in the immune microenvironment of tumors, different LPA receptors promoted metastasis, which helped create a T cell rejection and pro-tumor microenvironment suitable for therapeutic intervention (PMID: 34788605). Wang et al. reported that in a mouse model of atopic dermatitis (AD), TRIM32 acted as a regulator of PKCζ and could control the differentiation of Th2 cells, which are very important for the pathogenesis of AD (PMID: 33096083). We believe that immune cells, in particular T cells, play an important role in the development of KD, and are expected to become a new target for KD immunotherapy. However, the molecular mechanisms involved need further investigation.

In this study the transcriptional regulatory network analysis indicated that *FOXF1* and *LPAR1* share two transcriptional regulatory factors, E2F1 and SP1. In addition, the two share three miRNAs, hsa-miR-200c-3p, hsa-miR-200b-3p, and hsa-miR-429. The downregulation of *FOXF1* and *LPAR1* in keloid patients could be caused by the inactivation of E2F1 and SP1 due to mutations or other factors, or by the effect of the three miRNAs. *TRIM32* did not share any miRNAs with the other two genes. JUND and TP53 were predicted to target *TRIM32*, which may contribute to its upregulation.

This study has several limitations. First, our analysis was based on a limited number of clinical samples from public databases, and may suffer from poor statistical power due to the small sample size. In addition, our analysis of the expression patterns of the identified biomarkers was based on public databases, and further validation is necessary, which would need to be done by collecting a larger number of clinical samples or conducting animal experiments. Given these limitations, larger datasets are needed to support further research and validation of the genes and molecular mechanisms that we identified.

In this article we analyzed IRGs in KD, leading to the identification of two new biomarkers of keloid tissue. Further studies on IRGs in KD may lead to new tools for early diagnosis as well as the identification of novel drug targets for treatment of KD.

## Data availability statement

The datasets presented in this study can be found in online repositories. The names of the repository/repositories and accession number(s) can be found in the article/Supplementary Material.

## Ethics statement

The studies involving humans were approved by Research Ethics committee of the second hospital of shandong university. The studies were conducted in accordance with the local legislation and institutional requirements. The participants provided their written informed consent to participate in this study.

## Author contributions

XCW: Data curation, Methodology, Validation, Writing – original draft, Writing – review & editing. XYW: Data curation,

Validation, Writing – review & editing. ZL: Methodology, Resources, Writing – review & editing. LL: Data curation, Resources, Writing – review & editing. JZ: Methodology, Resources, Writing – review & editing. DJ: Data curation, Writing – review & editing, Methodology. GH: Methodology, Writing – review & editing, Resources.

## Funding

The author(s) declare that no financial support was received for the research, authorship, and/or publication of this article. The study was not funded.

## Acknowledgments

Thank you. We appreciate the database mentioned in our research.

## Conflict of interest

The authors declare that the research was conducted in the absence of any commercial or financial relationships that could be construed as a potential conflict of interest.

## Publisher's note



## Supplementary material

The Supplementary Material for this article can be found online at: https://www.frontiersin.org/articles/10.3389/fimmu.2024.1351513/full#supplementary-material

## References

1. Direder M, Weiss T, Copic D, Vorstandlechner V, Laggner M, Pfisterer K, et al. Schwann cells contribute to keloid formation. *Matrix Biol* (2022) 108:55–76. doi: 10.1016/j.matbio.2022.03.001

2. Limandjaja GC, Niessen FB, Scheper RJ, Gibbs S. Hypertrophic scars and keloids: overview of the evidence and practical guide for differentiating between these abnormal scars. *Exp Dermatol* (2021) 30:146–61. doi: 10.1111/exd.14121

3. Kiprono SK, Chaula BM, Masenga JE, Muchunu JW, Mavura DR, Moehrle M. Epidemiology of keloids in normally pigmented Africans and African people with albinism: population-based cross-sectional survey. *Br J Dermatol* (2015) 173:852–4. doi: 10.1111/bjd.13826

4. Liu S, Yang H, Song J, Zhang Y, Abualhssain ATH, Yang B. Keloid: genetic susceptibility and contributions of genetics and epigenetics to its pathogenesis. *Exp Dermatol* (2022) 31:1665–75. doi: 10.1111/exd.14671

5. Knowles A, Glass DA 2nd. Keloids and hypertrophic scars. *Dermatol Clin* (2023) 41:509–17. doi: 10.1016/j.det.2023.02.010

6. Balci DD, Inandi T, Dogramaci CA, Celik E. Dlqi scores in patients with keloids and hypertrophic scars: A prospective case control study. *J Dtsch Dermatol Ges* (2009) 7:688–92. doi: 10.1111/j.1610-0387.2009.07034.x

7. Ud-Din S, Bayat A. New insights on keloids, hypertrophic scars, and striae. *Dermatol Clin* (2014) 32:193–209. doi: 10.1016/j.det.2013.11.002

8. Limandjaja GC, Niessen FB, Scheper RJ, Gibbs S. The keloid disorder: heterogeneity, histopathology, mechanisms and models. *Front Cell Dev Biol* (2020) 8:360. doi: 10.3389/fcell.2020.00360

9. Mak K, Manji A, Gallant-Behm C, Wiebe C, Hart DA, Larjava H, et al. Scarless healing of oral mucosa is characterized by faster resolution of inflammation and control of myofibroblast action compared to skin wounds in the red duroc pig model. *J Dermatol Sci* (2009) 56:168–80. doi: 10.1016/j.jdermsci.2009.09.005

10. Huang C, Akaishi S, Hyakusoku H, Ogawa R. Are keloid and hypertrophic scar different forms of the same disorder? A fibroproliferative skin disorder hypothesis based on keloid findings. *Int Wound J* (2014) 11:517–22. doi: 10.1111/j.1742-481X.2012.01118.x

11. Ogawa R. Keloid and hypertrophic scars are the result of chronic inflammation in the reticular dermis. *Int J Mol Sci* (2017) 18. doi: 10.3390/ijms18030606

12. Wang ZC, Zhao WY, Cao Y, Liu YQ, Sun Q, Shi P, et al. The roles of inflammation in keloid and hypertrophic scars. *Front Immunol* (2020) 11:603187. doi: 10.3389/fimmu.2020.603187

13. Lee SY, Lee AR, Choi JW, Lee CR, Cho KH, Lee JH, et al. Il-17 induces autophagy dysfunction to promote inflammatory cell death and fibrosis in keloid fibroblasts via the Stat3 and Hif-1α dependent signaling pathways. *Front Immunol* (2022) 13:888719. doi: 10.3389/fimmu.2022.888719

14. Hong TJ, Escribano J, Coca-Prados M. Isolation of Cdna clones encoding the 80-Kd subunit protein of the human autoantigen Ku (P70/P80) by antisera raised against ciliary processes of human eye donors. *Invest Ophthalmol Vis Sci* (1994) 35:4023–30.

15. Shi J, Wang H, Guan H, Shi S, Li Y, Wu X, et al. Il10 inhibits starvation-induced autophagy in hypertrophic scar fibroblasts via cross talk between the Il10-Il10r-Stat3 and Il10-Akt-Mtor pathways. *Cell Death Dis* (2016) 7:e2133. doi: 10.1038/cddis.2016.44

16. Nishiguchi MA, Spencer CA, Leung DH, Leung TH. Aging suppresses skin-derived circulating Sdf1 to promote full-thickness tissue regeneration. *Cell Rep* (2018) 24:3383–92.e5. doi: 10.1016/j.celrep.2018.08.054

17. Hong YK, Chang YH, Lin YC, Chen B, Guevara BEK, Hsu CK. Inflammation in wound healing and pathological scarring. *Adv Wound Care (New Rochelle)* (2023) 12:288–300. doi: 10.1089/wound.2021.0161

18. Ritchie ME, Phipson B, Wu D, Hu Y, Law CW, Shi W, et al. Limma powers differential expression analyses for Rna-sequencing and microarray studies. *Nucleic Acids Res* (2015) 43:e47. doi: 10.1093/nar/gkv007

19. Yu G, Wang LG, Han Y, He QY. Clusterprofiler: an R package for comparing biological themes among gene clusters. *Omics* (2012) 16:284–7. doi: 10.1089/omi.2011.0118

20. Li Y, Lu F, Yin Y. Applying logistic lasso regression for the diagnosis of atypical Crohn's disease. *Sci Rep* (2022) 12:11340. doi: 10.1038/s41598-022-15609-5

21. Sachs MC. Plotroc: A tool for plotting Roc curves. *J Stat Softw* (2017) 79. doi: 10.18637/jss.v079.c02

22. Chen B, Khodadoust MS, Liu CL, Newman AM, Alizadeh AA. Profiling tumor infiltrating immune cells with cibersort. *Methods Mol Biol* (2018) 1711:243–59. doi: 10.1007/978-1-4939-7493-1_12

23. Douglas B, Vesey B. Bacteroides: A cause of residual abscess? *J Pediatr Surg* (1975) 10:215–20. doi: 10.1016/0022-3468(75)90281-x

24. Chen Z, Tian L, Wang L, Ma X, Lei F, Chen X, et al. Trim32 inhibition attenuates apoptosis, oxidative stress, and inflammatory injury in podocytes induced by high glucose by modulating the Akt/Gsk-3β/Nrf2 pathway. *Inflammation* (2022) 45:992–1006. doi: 10.1007/s10753-021-01597-7

25. Liu Y, Wang Z, de la Torre R, Barling A, Tsujikawa T, Hornick N, et al. Trim32 deficiency enhances Th2 immunity and predisposes to features of atopic dermatitis. *J Invest Dermatol* (2017) 137:359–66. doi: 10.1016/j.jid.2016.09.020

26. Dharmadhikari AV, Szafranski P, Kalinichenko VV, Stankiewicz P. Genomic and epigenetic complexity of the Foxf1 locus in 16q24.1: implications for development and disease. *Curr Genomics* (2015) 16:107–16. doi: 10.2174/1389202916666150122223252

27. Katoh M, Igarashi M, Fukuda H, Nakagama H, Katoh M. Cancer genetics and genomics of human fox family genes. *Cancer Lett* (2013) 328:198–206. doi: 10.1016/j.canlet.2012.09.017

28. Plastira I, Bernhart E, Joshi L, Koyani CN, Strohmaier H, Reicher H, et al. Mapk signaling determines lysophosphatidic acid (Lpa)-induced inflammation in microglia. *J Neuroinflamm* (2020) 17:127. doi: 10.1186/s12974-020-01809-1

29. Lee JH, Kim D, Oh YS, Jun HS. Lysophosphatidic acid signaling in diabetic nephropathy. *Int J Mol Sci* (2019) 20. doi: 10.3390/ijms20112850

30. Yung YC, Stoddard NC, Chun J. Lpa receptor signaling: pharmacology, physiology, and pathophysiology. *J Lipid Res* (2014) 55:1192–214. doi: 10.1194/jlr.R046458

31. Tager AM, LaCamera P, Shea BS, Campanella GS, Selman M, Zhao Z, et al. The lysophosphatidic acid receptor Lpa1 links pulmonary fibrosis to lung injury by mediating fibroblast recruitment and vascular leak. *Nat Med* (2008) 14:45–54. doi: 10.1038/nm1685

32. George J, Headen KV, Ogunleye AO, Perry GA, Wilwerding TM, Parrish LC, et al. Lysophosphatidic acid signals through specific lysophosphatidic acid receptor subtypes to control key regenerative responses of human gingival and periodontal ligament fibroblasts. *J Periodontol* (2009) 80:1338–47. doi: 10.1902/jop.2009.080624

33. Song HY, Lee MJ, Kim MY, Kim KH, Lee IH, Shin SH, et al. Lysophosphatidic acid mediates migration of human mesenchymal stem cells stimulated by synovial fluid of patients with rheumatoid arthritis. *Biochim Biophys Acta* (2010) 1801:23–30. doi: 10.1016/j.bbalip.2009.08.011

34. Wu Y, Jia H, Zhou H, Liu X, Sun J, Zhou X, et al. Immune and stromal related genes in colon cancer: analysis of tumour microenvironment based on the cancer genome atlas (Tcga) and gene expression omnibus (Geo) databases. *Scand J Immunol* (2022) 95:e13119. doi: 10.1111/sji.13119

35. Shi J, Jiang D, Yang S, Zhang X, Wang J, Liu Y, et al. Lpar1, correlated with immune infiltrates, is a potential prognostic biomarker in prostate cancer. *Front Oncol* (2020) 10:846. doi: 10.3389/fonc.2020.00846

36. Liu X, Guo H, Wei Y, Cai C, Zhang B, Li J. Tgf-B induces growth suppression in multiple myeloma mm.1s cells via E2f1. *Oncol Lett* (2017) 14:1884–8. doi: 10.3892/ol.2017.6360

37. Katoh M, Katoh M. Human fox gene family (Review). *Int J Oncol* (2004) 25:1495–500.

38. Zhang Y, Wang P. Foxf1 was identified as a novel biomarker of infantile hemangioma by weighted coexpression network analysis and differential gene expression analysis. *Contrast Media Mol Imaging* (2022) 2022:8981078. doi: 10.1155/2022/8981078

39. Walker N, Badri L, Wettlaufer S, Flint A, Sajjan U, Krebsbach PH, et al. Resident tissue-specific mesenchymal progenitor cells contribute to fibrogenesis in human lung allografts. *Am J Pathol* (2011) 178:2461–9. doi: 10.1016/j.ajpath.2011.01.058

40. Bian F, Lan YW, Zhao S, Deng Z, Shukla S, Acharya A, et al. Lung endothelial cells regulate pulmonary fibrosis through Foxf1/R-Ras signaling. *Nat Commun* (2023) 14:2560. doi: 10.1038/s41467-023-38177-2

41. Lee SY, Kim EK, Seo HB, Choi JW, Yoo JH, Jung KA, et al. Il-17 induced stromal cell-derived factor-1 and profibrotic factor in keloid-derived skin fibroblasts via the Stat3 pathway. *Inflammation* (2020) 43:664–72. doi: 10.1007/s10753-019-01148-1

42. Henderson NC, Rieder F, Wynn TA. Fibrosis: from mechanisms to medicines. *Nature* (2020) 587:555–66. doi: 10.1038/s41586-020-2938-9

43. Ma WT, Gao F, Gu K, Chen DK. The role of monocytes and macrophages in autoimmune diseases: A comprehensive review. *Front Immunol* (2019) 10:1140. doi: 10.3389/fimmu.2019.01140

44. Dong L, He Y, Cao Y, Wang Y, Jia A, Wang Y, et al. Functional differentiation and regulation of follicular T helper cells in inflammation and autoimmunity. *Immunology* (2021) 163:19–32. doi: 10.1111/imm.13282

45. Kamran N, Chandran M, Lowenstein PR, Castro MG. Immature myeloid cells in the tumor microenvironment: implications for immunotherapy. *Clin Immunol* (2018) 189:34–42. doi: 10.1016/j.clim.2016.10.008

46. Devaraj S, Glaser N, Griffen S, Wang-Polagruto J, Miguelino E, Jialal I. Increased monocytic activity and biomarkers of inflammation in patients with type 1 diabetes. *Diabetes* (2006) 55:774–9. doi: 10.2337/diabetes.55.03.06.db05-1417

frontiers | Frontiers in Immunology

TYPE Original Research
PUBLISHED 12 March 2024
DOI 10.3389/fimmu.2024.1324026



OPEN ACCESS

EDITED BY
Zhenghua Zhang,
Fudan University, China

REVIEWED BY
Michel Simon,
Université de Toulouse, France
Huijuan Liu,
Tianjin International Joint Academy of Biomedicine, China

*CORRESPONDENCE
Jin Kyeong Choi
jkchoi@jbnu.ac.kr

†These authors have contributed equally to this work

RECEIVED 18 October 2023
ACCEPTED 20 February 2024
PUBLISHED 12 March 2024

CITATION
Kim HE, Lee JY, Yoo D-H, Park H-H, Choi E-J, Nam K-H, Park J and Choi JK (2024) Imidazole propionate ameliorates atopic dermatitis-like skin lesions by inhibiting mitochondrial ROS and mTORC2. *Front. Immunol.* 15:1324026. doi: 10.3389/fimmu.2024.1324026



# Imidazole propionate ameliorates atopic dermatitis-like skin lesions by inhibiting mitochondrial ROS and mTORC2

Ha Eun Kim[1†], Jong Yeong Lee[1†], Dong-Hoon Yoo[2], Hyo-Hyun Park[3], Eun-Ju Choi[4], Kyung-Hwa Nam[5,6], Jin Park[5,6] and Jin Kyeong Choi[1*]

[1]Department of Immunology, Jeonbuk National University Medical School, Jeonju, Republic of Korea, [2]Department of Sports Rehabilitation and Exercise Management, University of Gyeongnam Geochang, Geochang-gun, Republic of Korea, [3]Department of Clinical Pathology, Daegu Health College, Daegu, Republic of Korea, [4]Department of Physical Education, College of Education, Daegu Catholic University, Gyeongsan, Republic of Korea, [5]Department of Dermatology, Jeonbuk National University Medical School, Jeonju, Republic of Korea, [6]Research Institute of Clinical Medicine of Jeonbuk National University-Biomedical Research Institute of Jeonbuk National University Hospital, Jeonju, Republic of Korea

**Background:** Imidazole propionate (IMP) is a histidine metabolite produced by some gut microorganisms in the human colon. Increased levels of IMP are associated with intestinal inflammation and the development and progression of cardiovascular disease and diabetes. However, the anti-inflammatory activity of IMP has not been investigated. This study aimed to elucidate the role of IMP in treating atopic dermatitis (AD).

**Methods:** To understand how IMP mediates immunosuppression in AD, IMP was intraperitoneally injected into a *Dermatophagoides farinae* extract (DFE)/1-chloro-2,4 dinitrochlorobenzene (DNCB)-induced AD-like skin lesions mouse model. We also characterized the anti-inflammatory mechanism of IMP by inducing an AD response in keratinocytes through TNF-α/IFN-γ or IL-4 stimulation.

**Results:** Contrary to the prevailing view that IMP is an unhealthy microbial metabolite, we found that IMP-treated AD-like skin lesions mice showed significant improvement in their clinical symptoms, including ear thickness, epidermal and dermal thickness, and IgE levels. Furthermore, IMP antagonized the expansion of myeloid (neutrophils, macrophages, eosinophils, and mast cells) and Th cells (Th1, Th2, and Th17) in mouse skin and prevented mitochondrial reactive oxygen species production by inhibiting mitochondrial energy production. Interestingly, we found that IMP inhibited AD by reducing glucose uptake in cells to suppress proinflammatory cytokines and chemokines in an AD-like *in vitro* model, sequentially downregulating the PI3K and mTORC2 signaling pathways centered on Akt, and upregulating DDIT4 and AMPK.

**Discussion:** Our results suggest that IMP exerts anti-inflammatory effects through the metabolic reprogramming of skin inflammation, making it a promising therapeutic candidate for AD and related skin diseases.

KEYWORDS

**imidazole propionate, atopic dermatitis, mitochondria ROS, mTORC2, AMPK, DDIT4**

# Introduction

Atopic dermatitis (AD) is a chronic inflammatory skin disease characterized by severe itching, skin dryness, recurrent eczematous lesions, and high susceptibility to infection (1). The disease is accompanied by the activation of the skin's innate immunity and exaggerated IgE sensitization to environmental allergens, and begins with a Th2 immune response that expands to adaptive immune responses involving Th1 and Th17 (2). The Th2 immune response is the primary cause of skin inflammation in AD (2). Blocking IL-4 and IL-13 receptors produced by Th2 cells has been clinically proven to be safe and effective, and is currently being applied as an alternative treatment for AD (3). Furthermore, phase II and III clinical trials of various biological and small-molecule antagonists targeting signal transduction pathways involved in the Th2 immune response are underway to develop therapies for AD (3).

Activation, proliferation, and differentiation of T helper cells are highly dependent on energy production and synthesis of metabolites (4). $CD4^+$ T cells are characterized by a preference for energy production via the mitochondrial pathway (5). Th2 cell differentiation requires extensive metabolic reprogramming in response to changes in intracellular metabolic requirements and nutrient exposure, which are primarily regulated by the mammalian target of rapamycin (mTOR) signaling (6). The mTOR complex integrates cytokine receptor signaling while regulating glucose, amino acid, and lipid metabolism (6). This requires the upregulation of glucose uptake (6). Previous studies have highlighted the importance of mTOR complex 2 (mTORC2; an mTOR complex) in Th2 cell differentiation in allergic diseases (7). mTORC2 promotes Th2 cell differentiation through various mechanisms, and as the Th2 cells enter inflamed tissue sites, they continue to differentiate through exposure to various inflammatory cytokines in the tissues (6). It also regulates reactive oxygen species (ROS) production and respiration in mitochondria (8). However, it is not yet clear how mTORC2 deregulation affects AD.

The recent discovery of disease-associated small microbiome molecules has led to a growing interest in their potential role in pathogenesis and as therapeutics (9, 10). Imidazole propionate (IMP) is a histidine metabolite produced by the gut microbiota (11). Elevated IMP levels have been associated with intestinal inflammation, cardiovascular disease, and an impaired glucose response in individuals with type 2 diabetes (11). IMP is also associated with the inhibition of insulin signaling through mTORC1 in the mTOR complex in mice and humans (12). Accumulating evidence suggests that imidazole and its derivatives possess a variety of pharmacological properties, including antifungal, antibacterial, anti-inflammatory, antiviral, and anticancer properties (13). However, studies on IMP are limited, and its effects on skin diseases have not been studied.

In this study, we investigated whether IMP suppresses skin inflammation in AD by regulating mTORC2 signaling and mitochondrial ROS. We found that IMP attenuated AD-associated inflammation and severity in both *in vivo* and *in vitro* models. These results indicate that IMP represents a potentially useful candidate for the treatment of Th2-driven inflammatory diseases, in addition to AD.

# Results

## IMP ameliorates the severity of AD-like skin lesions in a mouse model

In the present study, we investigated the potential therapeutic effects of IMP on AD-like skin inflammation using an AD-like skin lesion model. We used *Dermatophagoides farinae* extract (DFE) and 1-chloro-2,4 dinitrochlorobenzene (DNCB) to induce AD in the ear lobes of BALB/c mice by treating them for 28 days. Ear thickness was measured 24 h after the application of DFE or DNCB for AD-like skin lesions induction. IMP and Rapa were injected intraperitoneally every other day, three times a week, from day 7 to day 28 after induction of AD-like skin lesions. mTOR inhibitor Rapa was used as a positive control to investigate the possibility that IMP could inhibit the mTOR pathway in AD pathogenesis. The schematic diagram of AD-like skin lesions induction and IMP treatment are shown in Figure 1A. Disease severity was assessed by measuring the thickness, imaging, and histological analysis of the ear lobes. The ear thickness started to increase in the AD-like skin lesion mice 7 days after AD-like skin lesions induction, but was significantly reduced in the IMP-treated group (Figure 1B). The size and weight of the draining lymph nodes (auricular LNs) were also significantly reduced in the IMP-treated AD-like skin lesions group (Supplementary Figure S2). No change in body weight was observed in any of the groups following IMP administration (Figure 1C). Images of the mouse ears showed an inflammatory response with erythema, edema, keratinization, and scaling. These symptoms were ameliorated in the IMP-treated group (Figure 1D). Histopathological evaluation revealed significant thickening of the epidermis and dermis in AD-like skin lesion mice, which was significantly decreased in the AD-like skin lesion mice treated with IMP and Rapa (Figures 1E, F). In AD-like skin lesions, elevated IgE levels are associated with disease severity and IgE levels can be used to monitor treatment response (3). Our results showed that serum IgE levels were significantly lower in AD-like skin lesion mice treated with IMP (2 mg/mouse) than those in untreated AD-like skin lesion mice (Figure 1G). These findings suggest that IMP effectively mitigates the severity of AD-like skin lesions.

## IMP suppresses the expansion of inflammatory myeloid cells in the skin of AD-like skin lesion mice

Although Th2 cell-driven inflammatory responses are important in AD, various immune cells other than Th2 cells participate in the pathophysiology of AD. Myeloid cells (neutrophils, macrophages, eosinophils, and mast cells) play crucial roles in pruritus, barrier damage, and inflammation in AD

10.3389/fimmu.2024.1324026

(14). These pro-inflammatory myeloid cells are rare in normal skin but increase during inflammation, and their inhibition is associated with disease resolution (15, 16). Therefore, we isolated skin cells from the ear tissues of AD-like skin lesion mice and determined the inhibitory effects of IMP and Rapa on myeloid cells. Flow cytometric analysis showed that the frequency of myeloid cell infiltration in the skin was significantly reduced in a dose-dependent manner by the recruitment of neutrophils with the $CD11b^+Ly6G^+$ phenotype and macrophages with the $CD11b^+F4/80^+$ phenotype in the IMP-treated AD-like skin lesion mice compared to that in the AD-like skin lesion mice. Moreover, significant inhibition of mast cell expansion, characterized by eosinophils with the single-$F^+CD11b^+$ phenotype and mast cells with c-$kit^+Fc\varepsilon RIA^+$ phenotype, was also observed in AD-like skin lesion mice treated with IMP and Rapa compared to that in the untreated AD-like skin lesion mice (Figure 2). These results suggest that IMP markedly inhibits inflammatory cell infiltration in skin tissue.

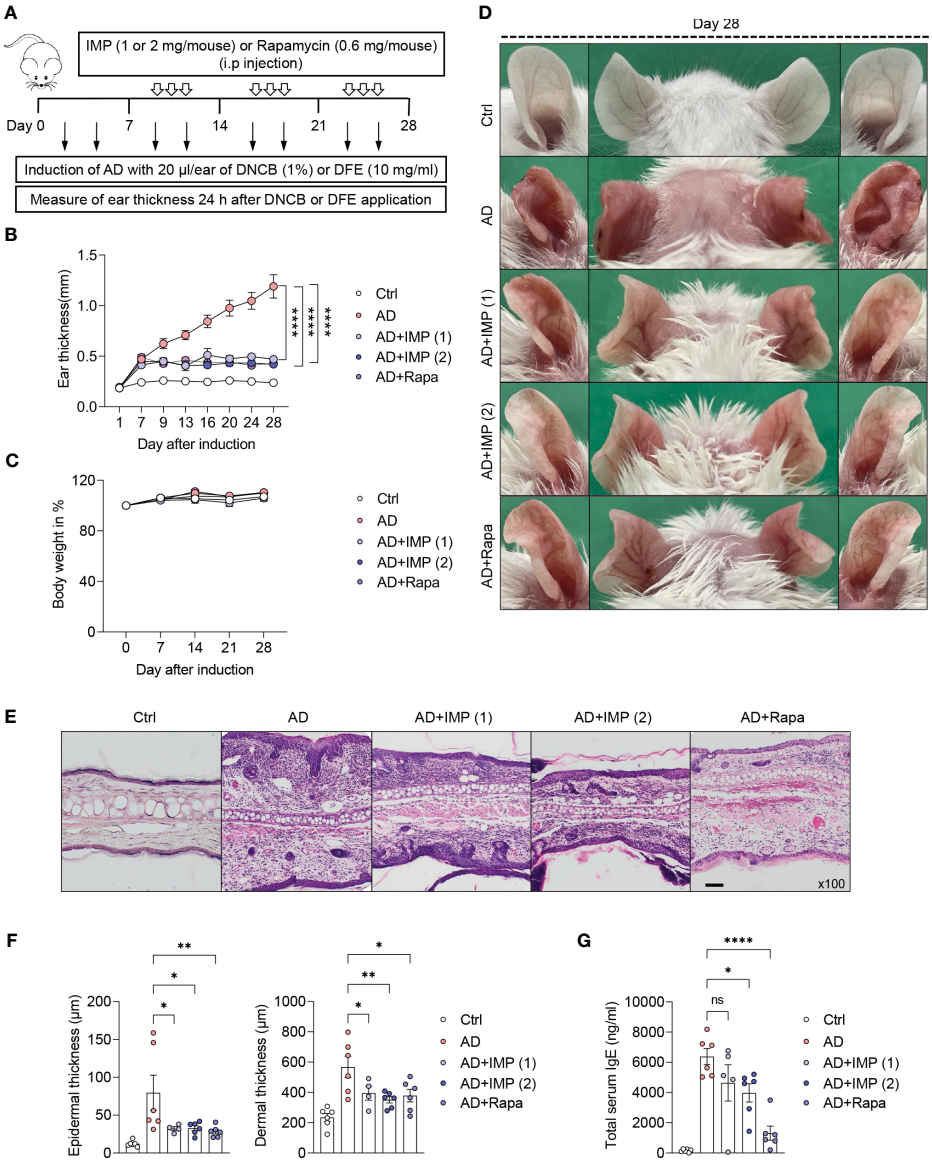


FIGURE 1
IMP attenuates the clinical symptoms of AD-like skin lesions in a mouse model. BALB/c mice were induced with DNCB and DFE, and treated with IMP (1 or 2 mg/mouse) or Rapa (0.6 mg/mouse). **(A)** Experimental design for the induction of AD-like skin lesions. The mice (n = 4–6/group) were divided into five groups. **(B)** Ear thickness was measured 24 h after DNCB or DFE application using a dial thickness gauge. **(C)** Mouse body weight was calculated as a percentage of the initial weight. **(D)** Images of the mouse ears from each representative group on day 28. **(E)** Representative photomicrographs of ear sections stained with hematoxylin and eosin (H&E) (×100 magnification; scale bar = 20 µm). **(F)** Epidermal and dermal thicknesses were measured using microphotographs of H&E-stained ear tissues. **(G)** Serum IgE levels were analyzed using ELISA. Data are presented as the mean ± standard error of mean (SEM). ****p < 0.0001, **p < 0.01, and *p < 0.05 indicate significant reduction compared to the AD group. Ctrl, control; AD, atopic dermatitis; DNCB, 2,4-dinitrochlorobenzene; DFE, *Dermatophagoides farina* extract; IMP, imidazole propionate; Rapa, rapamycin. ns: no significant.

10.3389/fimmu.2024.1324026

## IMP inhibits the expansion of Th1/Th2/Th17 cell immune responses and induces the expression of Foxp3$^+$ regulatory T cells in the skin of AD-like skin lesion mice

The acute onset of AD is characterized by infiltration of Th2 cells. In contrast, Th1 cells can be detected in chronic AD lesions as early as within an hour post-onset, alongside Th2 and Th17 cells (17). Therefore, CD4+ T helper cells are central to inducing AD, as highlighted in numerous studies, clinical trials, and mechanistic analyses, making them pivotal in the development of new therapeutic strategies (17). We isolated cells from the skin of AD and IMP-treated AD-like skin lesion mice, and investigated their antagonistic effects on Th1, Th2, and Th17 immune responses using intracellular cytokine staining. We found that the number of Th1 (CD4$^+$IFN-$\gamma^+$), Th2 (CD4$^+$IL-4$^+$), and Th17 (CD4$^+$IL-17A$^+$) cells were significantly reduced in the skin cells of both IMP- and Rapa-treated AD-like skin lesion mice, whereas this was not observed in AD-like skin lesion mice treated with Rapa alone (Figures 3A, B). We then analyzed the RNA expression of key cytokines produced by Th1, Th2, Th17, and Treg cells in the skin tissues. As predicted, the mRNA levels of cytokines produced by Th1 (*Ifnγ*), Th2 (*Il4*, *Il5*, *Il13*, and *Il31*), and Th17 (*Il17a*) were markedly reduced in the skin of IMP-treated AD-like skin lesion mice, providing clear evidence that IMP antagonizes T-cell responses during AD onset (Figure 3C). As Foxp3 has been reported to suppress T cell-mediated inflammatory responses in an AD-like skin lesions mouse model (18), we checked the RNA expression of Foxp3 to determine whether the IMP-mediated attenuation of Th1, Th2, and Th17 cells in AD was partially because of regulatory cells. We found that the expression of *Foxp3* was increased in the IMP-treated AD-like skin lesions group (Figure 3C).

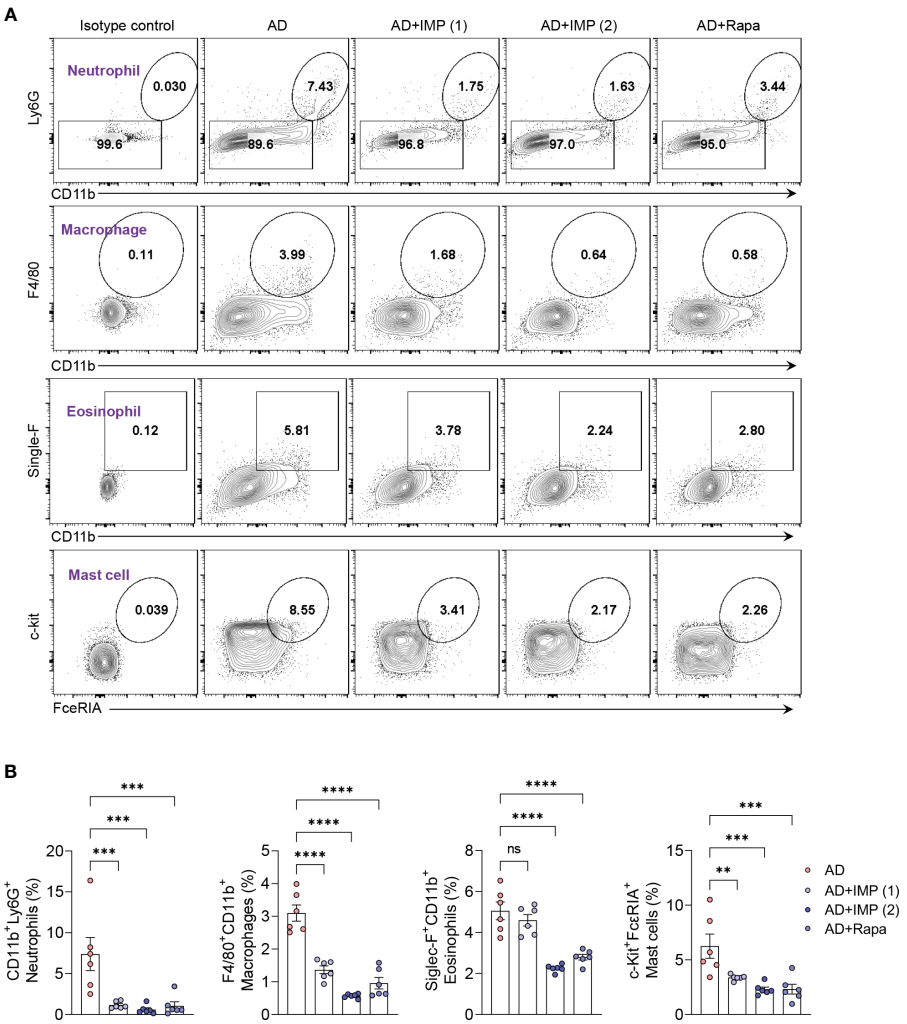


FIGURE 2
IMP inhibits the inflammatory myeloid cells in the skin of AD mice. **(A, B)** Representative flow cytometry plots and bar charts show percentage of CD11b$^+$Ly6G$^+$ (neutrophils), F4/80$^+$CD11b$^+$ (macrophages), single-F$^+$CD11b$^+$ (eosinophils), and c-Kit$^+$FcεRIA$^+$ (mast cells) in the ear skin cells (n = 6/group). Data are presented as the mean ± SEM. ****p < 0.0001, ***p < 0.001, and **p < 0.01 indicate significant reduction compared to the AD group. AD, atopic dermatitis; IMP, imidazole propionate; Rapa, rapamycin. ns: no significant.

## IMP alters energy metabolism and inhibits the production of mitochondrial ROS in the skin of AD-like skin lesion mice

Several physiological factors are involved in the severity and progression of AD, and measurement of energy metabolism and oxidative stress in the inflamed skin represent important markers for assessing the inflammatory state (19). In human skin inflammation, energy metabolism is highly dependent on the oxidative phosphorylation (OXPHOS) pathway (19). In this study, we extracted mouse ear skin cells 28 days after AD induction and combined the cells to measure the OCR, a key OXPHOS parameter. We found that basal and maximal OCR, mitochondrial respiratory capacity, ATP production rate, and ATP synthesis efficiency via oxygen consumption (coupling efficiency) were reduced in IMP-treated AD-like skin lesion mice compared to those in untreated AD-like skin lesion mice (Figure 4A). To understand how the mitochondrial metabolic profile changes under the influence of IMP, we investigated mitochondrial function in AD-like skin lesions mouse skin cells

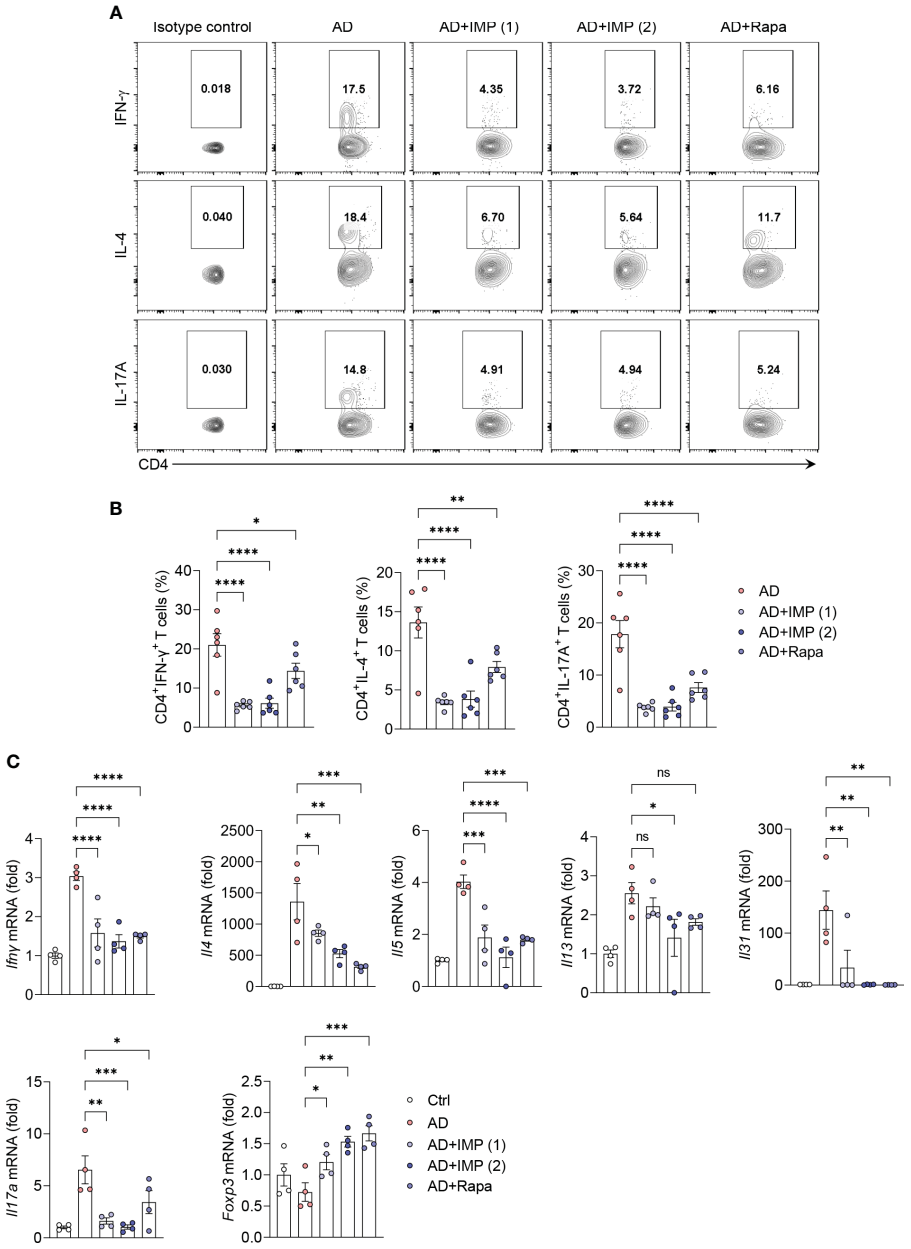


FIGURE 3
IMP regulates the T cell immune response in the inflamed skin of AD mice. **(A, B)** Representative flow cytometry plots and bar graphs showing percent $CD4^+$ T cells expressing IFN-γ, IL-4 or IL-17A in the ear skin cells (n = 6/group). **(C)** Gene expression of Th1 (*Ifnγ*), Th2 (*Il4*, *Il5*, *Il13*, and *Il31*), and Th17 (*Il17a*) cytokines and Treg (*Foxp3*) transcription factor in the ears of AD and IMP or Rapa-treated AD mice. To determine the cytokine expression in mice, the ears were excised on day 28. Gene expression was analyzed using real-time PCR (n = 4/group). The gene expression levels were normalized to that of β-actin. Data are presented as the mean ± SEM. ****p < 0.0001, ***p < 0.001, **p < 0.01, and *p < 0.05 indicate significant reduction compared to the AD group. Ctrl, control; AD, atopic dermatitis; IMP, imidazole propionate; Rapa, rapamycin. ns: no significant.

using MitoTracker™. Accumulation of dysfunctional mitochondria was observed in AD-like skin lesions mouse skin without IMP treatment, but this was reduced in the IMP- and Rapa-treated groups (Figure 4B). MitoSOX™, a mitochondria-specific ROS indicator, was used to measure mitochondrial ROS levels, and the assay revealed that ROS levels were increased in AD-like skin lesion mice, but decreased in the IMP- and Rapa-treated AD-like skin lesion groups (Figure 4C). These results suggest that the activated state of skin inflammatory cells in AD is associated with changes in metabolic processes, and that IMP inhibits mitochondrial dysfunction and ROS production.

## IMP inhibits glucose uptake in keratinocytes and regulates mTORC2 signaling to suppress inflammatory cytokines and chemokines

Next, we investigated the effects and mechanisms of IMP in an *in vitro* AD model. Keratinocytes in AD patients can amplify the recruitment and production of Th2 cell cytokines by releasing chemokines such as CCL17 and CCL22 (20). TNF-α has been reported to promote the production of CCL17 and CCL22 in keratinocytes, inducing features similar to atopic dermatitis (21, 22). In HaCaT cells, the levels of CCL17 and CCL22 are enhanced upon stimulation with TNF-α and IFN-γ (22, 23). Indeed, skin lesions in AD also show increased expression of CCL17 or CCL22 in response to elevated TNF-α and IFN-γ, and this has been used in numerous studies as an *in vitro* model mimicking AD (22, 24, 25). Based on these findings, we decided to apply this mechanism as an *in vitro* model for AD. Furthermore, we verified the efficacy of IMP in an AD environment *in vitro* using mouse primary keratinocytes induced with IL-4.

HaCaT cells were treated with different concentrations of IMP (5, 10, and 20 μg/mL) for 24 h to determine the effective concentration, and cell viability was measured using the MTT assay. The results showed that none of the concentrations of IMP tested affected the survival of HaCaT cells following 24 h of treatment (Supplementary Figure S3). Moreover, in the *in vitro* AD models using HaCaT cells or mouse primary keratinocytes stimulated with TNF-α/IFN-γ or IL-4, IMP treatment suppressed the gene expression of proinflammatory cytokines (TNF-α, IL-1β, and IL-6) and chemokines (CCL17 and CCL22) (Figure 5A and Supplementary Figure S4A). Based on the results of our *in vivo*

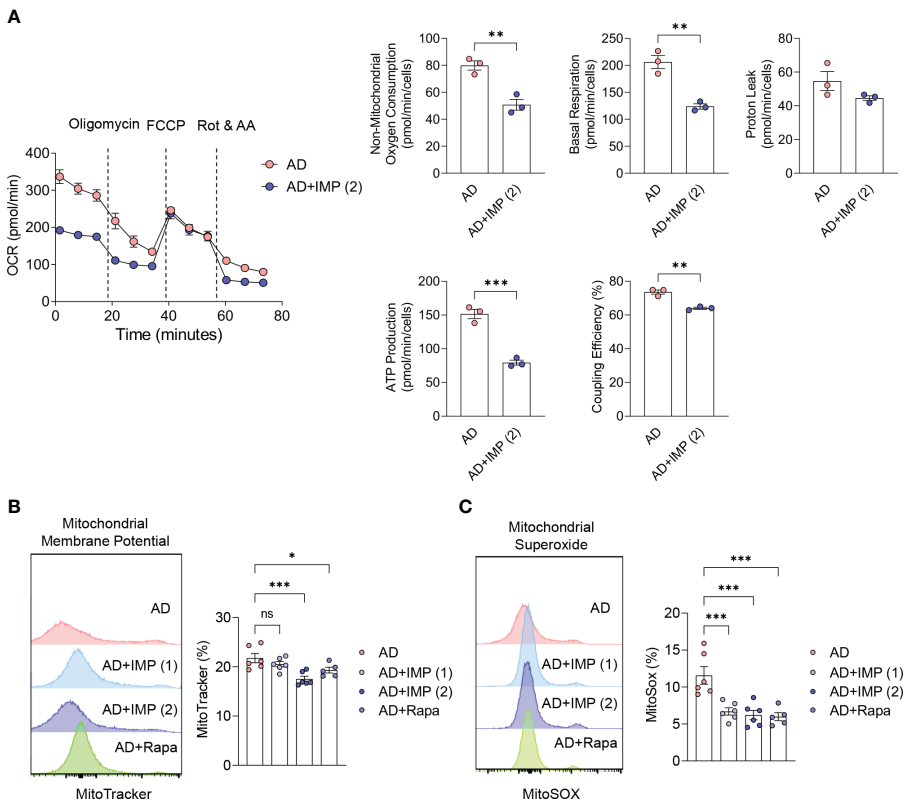


FIGURE 4
IMP inhibits mitochondrial ROS production by altering the inflammatory metabolic profile in AD skin. **(A)** Real-time changes in the oxygen consumption rate (OCR) of skin cells in response to oligomycin, FCCP, and Rot/AA. The bar charts show the mitochondrial oxygen consumption, basal and maximal respiratory capacity, proton leak, ATP production rate and coupling efficiency. Representative histograms and bar graphs showing total mitochondrial mass (n = 3/group). **(B)** and mitochondrial ROS production **(C)**. Mitochondrial mass and ROS were analyzed by flow cytometry in skin cells labeled with MitoTracker green or MitoSOX red (n = 6/group). Data are presented as the mean ± SEM. ***p < 0.001, **p < 0.01, and *p < 0.05 indicate significant reduction compared to the AD group. AD, atopic dermatitis; IMP, imidazole propionate; Rapa, rapamycin; OCR, oxygen consumption rate; FCCP, carbonyl cyanide-p-trifluoromethoxyphenylhydrazone; Rot/AA, rotenone and antimycin A; ATP, adenosine triphosphate; ROS, reactive oxygen species. ns: no significant.

10.3389/fimmu.2024.1324026

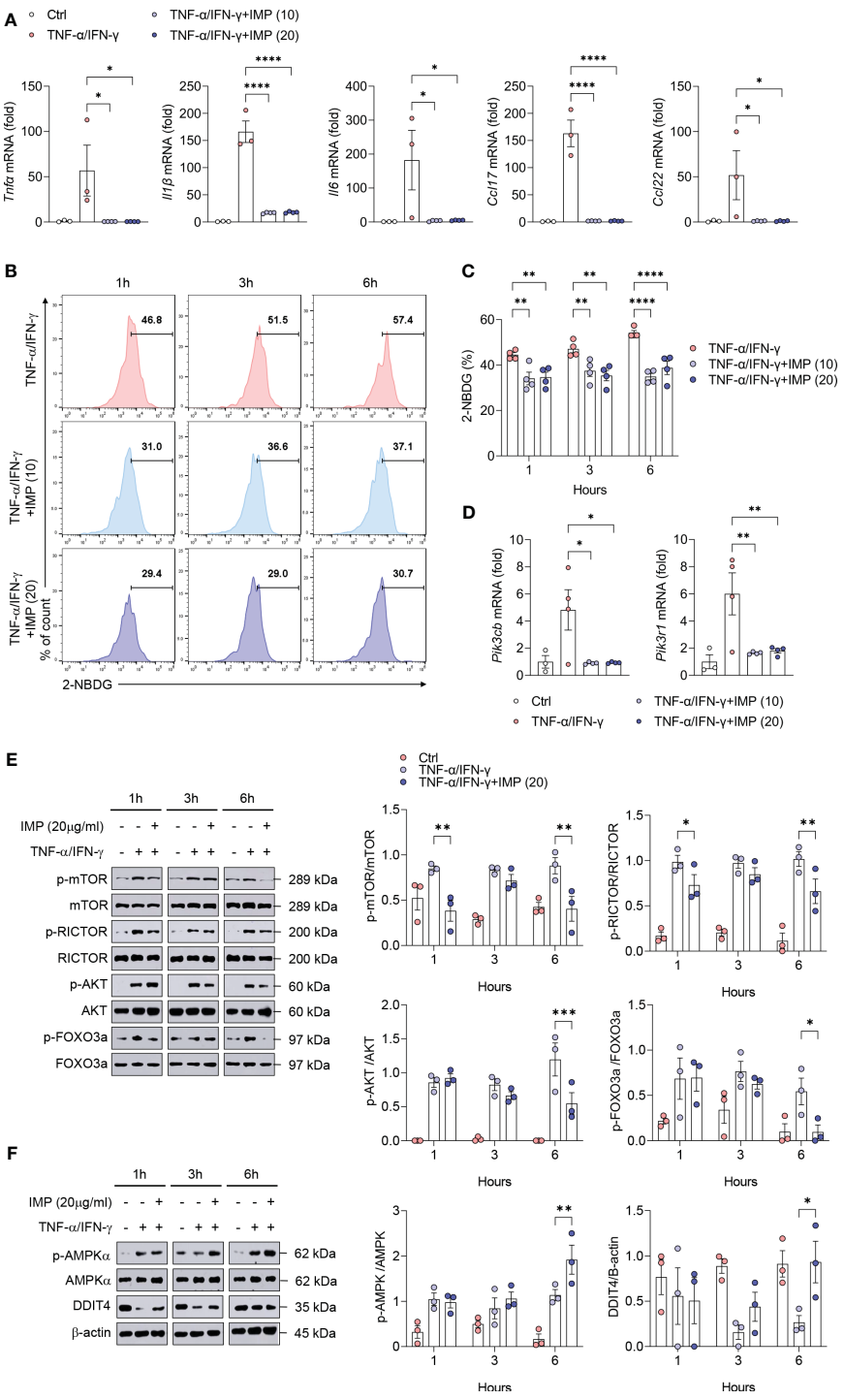


FIGURE 5
Induction of AMPK/DDIT4 by IMP inhibits mTORC2 signaling and reduces inflammatory cytokines and chemokines in AD *in vitro*. Human keratinocytes HaCaT cells were stimulated with TNF-α (10 ng/mL) and IFN-γ (10 ng/mL) in the presence or absence of IMP (10 or 20 μg/mL) for 6 h or indicated times (n = 3-4/group). **(A)** Gene expression of proinflammatory cytokines (*Tnfα*, *Il1β*, and *Il6*), and chemokines (*Ccl17 and Ccl22*) was analyzed using real-time PCR. **(B, C)** Representative histograms and bar graphs showing glucose uptake in HaCaT cells, which was determined by incubation with 2-NBDG for 2 h, followed by flow cytometry. **(D)** Gene expression of PI3K signaling molecules (*Pik3cb* and *Pik3r1*) was analyzed using real-time PCR. Protein expression of mTORC2 targets **(E)**, and that of AMPK and DDIT4 **(F)** in HaCaT cells stimulated in the presence or absence of IMP (20 μg/mL) was determined by western blotting. Data are presented as the mean ± SEM. ****p < 0.0001, ***p < 0.001, **p < 0.01, and *p < 0.05 indicate significant reduction compared to TNF-α/IFN-γ. IMP, imidazole propionate; 2-NBDG, 2-deoxy-2-[(7-nitro-2,1,3-benzoxadiazol-4-yl)amino]-D-glucose; mTOR, mammalian target of rapamycin; mTORC2, mammalian target of rapamycin complex 2; Rictor, rapamycin-insensitive companion of mammalian target of rapamycin; AKT, protein kinase B; FOXO3a, forkhead box O3a; AMPK, AMP-activated protein kinase; DDIT4, DNA-damage-inducible transcript 4.

experiments, we hypothesized that the inhibition of skin inflammation is related to glucose degradation. To test this hypothesis, HaCaT cells were stimulated with TNF-α/IFN-γ for 1, 3, and 6 h, and mouse primary keratinocytes were stimulated with IL-4 for 12, 24, and 48 h, respectively. Following treatment with IMPs, the intracellular glucose uptake status was determined by flow cytometry using the fluorescently-labeled glucose uptake molecule, 2-NBDG. The results showed an increase in glucose uptake at all time points for both TNF-α/IFN-γ-stimulated HaCaT cells and IL-4-stimulated mouse primary keratinocytes. In the IMP-treated group, glucose uptake was significantly reduced at all time points (Figure 5B, C and Supplementary Figures S4B, C). As an important metabolic regulator, mTOR significantly affects glucose metabolism (26). Therefore, we sought to determine whether IMP alters the global glucose metabolic pathway and modulates mTOR signaling. We found that IMP significantly inhibited the PI3Ks genes, *Pik3b* and *Pik3r1*, which encode transcription factors that mediate signals upstream of mTOR (Figure 5D). As inhibition of PI3K may affect mTOR signaling, we validated these results by analyzing the expression of downstream signaling targets of mTORC2, the mTOR complex related to the Th2 immune response, at various time points after treatment with IMP following stimulation with TNF-α/IFN-γ or IL-4 in HaCaT and mouse primary keratinocytes by western blotting. The results showed that TNF-α/IFN-γ stimulation increased the phosphorylation of mTOR, RICTOR, AKT, and FOXO3a, the downstream targets of mTORC2, whereas IMP impaired their activation (Figure 5E and Supplementary Figure S4D). AMPK and DDIT4 are negative regulators of mTORC2 and suppress Th2-mediated allergic immune responses (7, 27). Therefore, to investigate how IMP inhibits mTORC2 signaling, the activation status of AMPK and DDIT4 was determined by western blotting. We found that the phosphorylation of AMPK remained unchanged after 1 h of IMP treatment, but increased in the IMP-treated group, compared to TNF-α/IFN-γ alone, at 3 and 6 h. Similarly, activation of DDIT4 increased following 3 and 6 h of IMP-treatment (Figure 5F).

## Discussion

Microbial metabolites play key roles in various tissues and organs in the human body (28). These metabolites act on receptors at various sites, such as the intestine, liver, and central nervous system, and may contribute to metabolic diseases, such as obesity, type 2 diabetes, and cardiovascular disease (28). Microbially produced IMP has been found to be present at higher levels in the plasma of patients with prediabetes and type 2 diabetes. It acts as a negative regulator of type 2 diabetes through the p38/p62/mTORC1 pathway, and inhibits the glucose-lowering effects of metformin (12, 29). However, the role of IMP has not been investigated in skin diseases. In the present study, we found that IMP exerts anti-inflammatory effects on the skin, which is contrary to the findings of previous studies. Based on these findings, we sought to further investigate the role of IMP in skin inflammation, especially in AD, to evaluate the potential medical application of this microbial metabolite.

AD is characterized by intense pruritus, eczema, erythema, swelling, peeling, exudation, and scab formation on the skin, with epidermal barrier abnormalities, T cell-induced skin inflammation, and an increased IgE response in most patients (30). In contrast to the severe skin inflammation observed in AD mice, we found that AD mice treated with IMP showed attenuated disease severity, including inhibition of inflammatory cell infiltration in skin tissue and a significant reduction in serum IgE levels, suggesting that IMP attenuated the disease. AD is a chronic inflammatory skin disease caused by the complex interplay of immune responses (30). In particular, the interaction between myeloid and T cells has a major impact on the onset and progression of AD. In our study, we found that the expansion of neutrophils, macrophages, eosinophils, and mast cells was inhibited in the skin of AD-like skin lesion mice after IMP administration. This suggests that IMP reduces the ability of myeloid cells in the skin to present antigens to Th1/Th2/Th17 T cells, and inhibits T cell activation and subsequent cytokine production, which may impede the persistence and progression of AD inflammation. It is also worth noting that the suppression of Th1/Th2/Th17-produced cytokines and attenuation of inflammation in the skin tissues of IMP-treated AD-like skin lesion mice may also be correlated with the increased expression of Treg-expressing Foxp3 following IMP treatment.

In AD, the inflammatory response of Th cells is activated compared with that of naïve T cells, and promotes the inflammatory response by distorting the direction of OXPHOS metabolism in the mitochondria (31). In our study, the treatment of AD-like skin lesion mice with IMP decreased the OXPHOS activity in the skin. These data suggest that IMP reverses inflammation-related intracellular metabolic programs in T cells. Thus, IMP treatment decreased cytokine expression in Th1, Th2, and Th17 cells, whereas it was associated with increased Foxp3 expression in regulatory T cells.

Mitochondria play a crucial role in skin physiology (31). Their metabolic activity regulates keratinocyte differentiation by generating ROS (31, 32). However, excessive ROS production leads to mitochondrial dysfunction due to an increase in silver mitochondrial mass, which is associated with inflammatory signal activation and cell death (33). We found that treatment with IMP or Rapa reduced the accumulation of dysfunctional mitochondria in skin cells of the AD-like skin lesions mouse model and inhibited ROS production in these mitochondria. These findings suggest that mitochondrial accumulation and ROS production in skin cells are associated with AD pathogenesis and that IMP may directly improve mitochondrial function in AD-induced skin inflammatory cells.

Proliferating cells are more dependent on glucose uptake for growth than quiescent cells (34). Impaired glucose uptake contributes to skin damage and inflammation-related inhibition of keratinocyte proliferation, and is considered a novel strategy for the treatment of skin diseases (34). Previous reports have shown that IMP is significantly increased in patients with type 2 diabetes and impairs glucose tolerance and insulin signaling when

administered to mice, suggesting that it acts as a negative regulator (12). However, impaired glucose uptake in the inflamed skin environment is associated with suppression of inflammation (35). Our data showed that in an *in vitro* model of AD-like skin inflammation, IMP treatment resulted in reduced expression of Th2 recruitment chemokines and pro-inflammatory cytokines, and reduced glucose uptake levels (analyzed using 2-NBDG). These results demonstrate that IMP may inhibit inflammatory responses through impaired glucose binding in the AD skin inflammatory milieu, which is in contrast to the results of the limited studies on diseases associated with glucose tolerance and insulin resistance.

Our *in vivo* data showed that Rapa, used as a positive control, modulated mTOR phosphorylation to ameliorate clinical symptoms of AD by reducing epidermal and dermal thickness, inflammatory cell infiltration, and serum IgE and Th1/2 cytokine levels in the skin of AD-like skin lesion mice, which is consistent with previous studies (36). Furthermore, IMP showed similar effects as Rapa, suggesting that it may be directly involved in mTOR signaling in AD. Dysregulation of the PI3Kk/Akt/mTOR pathway is observed in skin cancer, psoriasis, and AD, and is associated with uncontrolled and excessive proliferation of inflammatory skin cells (37). mTOR forms two distinct protein complexes, mTORC1 and mTORC2, which play important roles in T-cell differentiation, skin morphology, and epidermal development (38). mTORC1 promotes Th17 differentiation, Foxp3 expression, and suppresses Treg cell status (39). mTORC2 (Rictor) is essential for Th1 and Th2 cell differentiation, and Akt activation (39). In T cells from pediatric AD patients, the PI3K/Akt pathway is abnormally activated (37). Rictor-deficient mice show filaggrin control of epidermal lipid synthesis and keratinization (40). mTORC2 regulates substrates such as forkhead box (Foxo) proteins O1 and O3 by targeting Akt, resulting in cell cycle suppression and regulation of Th1 transcription factors (38, 39). We found that the PI3K/Akt/mTOR pathway was activated in TNF-α/IFN-γ-stimulated HaCaT cells, an *in vitro* model of AD, and IMP-dependently inhibited mTOR, Rictor and Akt, and Forkhead box 3a phosphorylation. However, IMP did not affect the expression of the mTORC1 constituent protein Raptor and p70-S6K (Supplementary Figure S5). These results suggest that in skin inflammation, such as chronic AD with increased Th1/Th2 ratios, IMP may play an important role in maintaining immune cell homeostasis via the mTORC2 pathway. We further demonstrated that the activities of AMPK and DDIT4, which act as negative upstream regulators of AKT/mTOR, were increased by IMP. These results suggest that by upregulating AMPK and DDIT4, IMP may regulate the bioenergetic balance and overactivation of AD-associated skin inflammatory cells via mTORC2.

Metabolites are important molecules that drive energy production and conversion *in vivo*. Because of their reactivity, structural properties, and varying concentrations, they can change rapidly during metabolic processes in the body (4, 41). Therefore, some metabolites may participate in pro-inflammatory activities, whereas others may exhibit anti-inflammatory effects (41). Similarly, IMP may play a negative role in metabolic diseases associated with impaired glucose tolerance and insulin resistance; however, its anti-inflammatory effects remain unclear.

Our data revealed the regulatory capacity of IMP on mitochondrial function, ROS production, and mTORC2 activity, suggesting that IMP possesses anti-inflammatory effects and has potential as a novel alternative therapy for the treatment of AD, a T cell-mediated chronic skin inflammatory disease. Given these findings, further research is required to elucidate how metabolites, such as IMP, influence the interactions between the host and microbes in T-cell-driven skin diseases, and explore the potential to reverse their effects in specific disease contexts.

# Materials and methods

## Chemicals

The chemical structure of IMP is shown in Supplementary Figure S1. IMP and rapamycin (Rapa) were purchased from Sigma-Aldrich and Selleckchem, respectively.

## Cell culture and stimulation

The human keratinocyte cell line HaCaT was purchased from the CLS Cell Line Service (Eppelheim, Germany). The cells were cultured in Dulbecco's modified Eagle's medium (DMEM) supplemented with 10% fetal bovine serum (FBS) and antibiotics (100 U/mL penicillin G and 100 μg/mL streptomycin) at 37°C with 5% $CO_2$. To generate an *in vitro* AD model using the HaCaT cells, the cells were treated with 10 ng/mL each of recombinant human TNF-α and IFN-γ (both from R&D Systems). Simultaneously, the cells were treated with IMP (10 or 20 μg/mL).

## Mice

Six-week-old female BALB/c mice were purchased from Narabiotec Co. Ltd. (Seoul, Korea) and housed at 23 ± 2°C and 50 ± 5% humidity. The animal experiments were approved by the Animal Care and Use Committee of Jeonbuk National University Medical School (JBNU 2021-0169) and were conducted in accordance with the institutional guidelines.

## Induction of AD-like skin lesions in mouse ear

The mouse AD-like skin lesions model was induced according to the method described in our previous report (25). A schematic diagram of the experiment is shown in Figure 1A. The mice (n = 4 to 6) were randomly divided into five groups and the hair on the surfaces of both earlobes was stripped thrice using surgical tape (Nichiban, Tokyo, Japan). Then, 20 μL of 2,4-dinitrochlorobenzene (DNCB; 1% solution, dissolved in 1:3 acetone:olive oil, Sigma-Aldrich) was applied to both earlobes, followed by application of 20 μL of *Dermatophagoides farinae* extract (DFE; 10 mg/mL, dissolved in PBS plus 0.5% Tween 20, Greer Laboratory Inc.)

three days later. One week after the DNCB/DFE induction, the mice were injected intraperitoneally with IMP (1 or 2 mg/mouse) or Rapa (0.6 mg/mouse) thrice/week. All groups except the IMP and Rapa groups were injected with PBS. The ear thickness was measured 24 h after DNCB/DFE application using a dial thickness gauge (Mitutoyo Co., Tokyo, Japan). All mice were euthanized with $CO_2$ on day 28, and blood and tissue samples were collected and analyzed.

## Histology

Ear tissue was fixed in 4% formalin and embedded in paraffin. Sections (4 μm thick) of the ear tissue were stained with hematoxylin and eosin (H&E). Epidermal and dermal thickness, as well as inflammatory cell infiltration, were observed under a microscope. The thickness of the epidermis and dermis were measured based on the H&E staining pattern at ×100 magnification.

## Enzyme-linked immunosorbent assay

Serum IgE levels were measured on day 28 after the first induction using an IgE ELISA Kit (BD Biosciences, Franklin Lakes, NJ, USA) following the manufacturer's instructions.

## Florescence-activated cell sorting analysis

To detect intracellular cytokines in the skin cells, the cells were stimulated with phorbol-12-myristate-13-acetate (PMA; 20 ng/mL)/ionomycin (1 μg/mL) and Golgi Plug (BD biosciences) for 4 h. After stimulation, the cells were stained with Live/Dead™ Fixable Dead Cell dye (Thermo Fisher Scientific; diluted in PBS) for 15 min at room temperature and washed twice with cold PBS. For myeloid cell surface staining, antibodies were diluted 1:200 and incubated for 20 min at 4°C. After incubation, the samples were washed twice and staining buffer (BD Bioscience) was added. For T cell-producing cytokines, CD4 surface staining was performed followed by fixation and permeabilization using a Foxp3 Staining Kit (Thermo Fisher) and staining with IFN-γ, IL-4, IL-17A, and Foxp3 antibodies according to the manufacturer's protocol. The following antibodies were used: anti-mouse F4/80 (BD bioscience), anti-mouse CD11b (BD bioscience), anti-mouse Ly6G (BD bioscience), anti-mouse CD170 (Siglec-F) (Biolegend), anti-mouse CD117 (BD bioscience), anti-mouse FceR1a (BD bioscience), anti-mouse IFN-γ, anti-mouse IL-4, anti-mouse IL-17A, anti-mouse Foxp3 (Thermo), and isotype control (BD bioscience). All samples were collected using an Attune NxT acoustic focusing cytometer (Thermo Fisher Scientific). Live cells were gated based on FSC-A, SSC-A, and fixable viability live/dead dye, and then acquired with an Attune NxT acoustic focusing cytometer (Thermo Fisher). Data analysis was performed using the FlowJo (ver. 10.7.1) software.

## Real-time quantitative PCR

Total RNA was extracted from cultured cells and frozen tissues using the RNAIso Plus Reagent (Takara, Tokyo, Japan) according to the manufacturer's instructions. cDNA synthesis and RT-qPCR analyses were performed as described previously (42). The RNA samples were dissolved in RNase-free water (Thermo Fisher Scientific) and purified by phenol/chloroform extraction. The RevertAid™ First Strand cDNA Synthesis Kit (Thermo Fisher Scientific) was used for cDNA synthesis. The cDNA was then mixed with SYBR® Green PCR Master Mix (Applied Biosystems) along with the primers for qPCR. Gene expression of cytokines were analyzed using the StepOnePlus™ Real-Time PCR System (Thermo Fisher) according to the manufacturer-recommended PCR parameters. The primer sequences are listed Supplementary Table S1. Target gene expression was determined using the standard comparative ΔΔCt method and normalized to that of the housekeeping gene, β-actin.

## Oxygen consumption rate

Tissue cells isolated from the ear skin were pre-cultured in Seahorse XF RPMI medium (containing 10 mM XF glucose, 2 mM XF glutamine, and 1 mM XF pyruvate) at a density of $5 \times 10^5$ cells/well in poly D-lysine-coated XFp cell culture miniplates. The OCR was assessed using the XFp Cell Mito Stress Test Kit (Agilent) following the manufacturer's instructions and measured using a Seahorse XFp Analyzer (Agilent).

## Glucose uptake assay

Tissue cells from mouse ear skin ($5 \times 10^5$ cells/well) were seeded in a 96-well plate and incubated with 2-[N-(7-nitrobenz-2-oxa-1,3-diazol-4-yl) amino]-2-deoxy-D-glucose (2-NBDG, 0.01 mg/mL, Thermo Fisher) at 37°C for 30 min. Following incubation, the cells were washed twice with PBS and stained for 15 min at room temperature with Live/Dead™ Fixable Dead Cell dye (Thermo Fisher) to specifically detect the viable cells. The samples were analyzed using an Attune NxT acoustic focusing cytometer (Thermo Fisher).

## Western blotting

Cell lysates were prepared and western blotting was performed as described previously (42). Proteins were separated using 6%, 10%, or 12% sodium dodecyl sulfate-polyacrylamide gel electrophoresis. Proteins were detected using the following primary antibodies: anti-phospho-AMPKα (Cell Signaling Technology, clone 40H9), anti-AMPKα (Cell Signaling Technology), anti-phospho-mTOR (Cell Signaling Technology, clone D9C2), anti-mTOR (Cell Signaling Technology, clone 7C10), anti-β-actin (Cell Signaling Technology, clone 13E5), anti-DDIT4 (Proteintech), anti-phospho-

Rictor (Cell Signaling Technology, clone D30A3), anti-Rictor (Cell Signaling Technology, clone 53A2), anti-phospho-FoxO3a (Cell Signaling Technology, clone D18H8), anti-FoxO3a (Cell Signaling Technology, clone D19A7), anti-phospho-AKT (Cell Signaling Technology, clone Ser473), anti-AKT (Cell Signaling Technology, clone Ser473), anti-phospho-p70 S6 Kinase (Thr389) (Cell Signaling Technology, 9205S), anti p70 S6 Kinase (Cell Signaling Technology.9202S), anti-phospho-Raptor(Ser792) (Cell Signaling Technology, 2083S), and Raptor (24C12) (Cell Signaling Technology.2280S) antibodies. After the incubating with the corresponding secondary antibody, the ECL substrate (Thermo Fisher) signals were detected using an Amersham Imager 600 (Cytiva Life Sciences, GE HealthCare).

### Statistical analysis

Statistical analyses were performed using GraphPad Prism software (version 10.0). One-way analysis of variance (ANOVA) was used for the Holm-Šídák *post-hoc* test. Data are presented as mean ± standard error of the mean (SEM). Significance is indicated as follows: $*p < 0.05$; $**p < 0.01$; $***p < 0.001$; $****p < 0.0001$.

## Data availability statement

The original contributions presented in the study are included in the article/Supplementary Materials. Further inquiries can be directed to the corresponding author.

## Ethics statement

The animal study was approved by Animal Care and Use Committee of Jeonbuk National University Medical School (JBNU 2021-0169). The study was conducted in accordance with the local legislation and institutional requirements.

## Author contributions

HK: Data curation, Formal Analysis, Visualization, Writing – review & editing. JL: Data curation, Formal Analysis, Visualization, Writing – review & editing. DY: Data curation, Writing – review & editing. HP: Data curation, Writing – review & editing. EC: Data curation, Writing – review & editing. KN: Data curation, Methodology, Writing – review & editing. JP: Data curation, Methodology, Writing – review & editing. JC: Conceptualization, Funding acquisition, Investigation, Project administration, Supervision, Writing – original draft, Writing – review & editing.

## Funding

The author(s) declare financial support was received for the research, authorship, and/or publication of this article. This research was supported by National University Development Project at Jeonbuk National University in 2022.

## Conflict of interest

Author H-HP was employed by the company Aston Sci. Inc.

The remaining authors declare that the research was conducted in the absence of any commercial or financial relationships that could be construed as a potential conflict of interest.

## Publisher's note



## Supplementary material

The Supplementary Material for this article can be found online at: https://www.frontiersin.org/articles/10.3389/fimmu.2024.1324026/full#supplementary-material

## References

1. Langan SM, Irvine AD, Weidinger S. Atopic dermatitis. *Lancet*. (2020) 396:345–60. doi: 10.1016/S0140-6736(20)31286-1

2. Bieber T. Atopic dermatitis: an expanding therapeutic pipeline for a complex disease. *Nat Rev Drug Discovery*. (2022) 21:21–40. doi: 10.1038/s41573-021-00266-6

3. Torres T, Ferreira EO, Goncalo M, Mendes-Bastos P, Selores M, Filipe P. Update on atopic dermatitis. *Acta Med Port*. (2019) 32:606–13. doi: 10.20344/amp.11963

4. O'Neill LA, Kishton RJ, Rathmell J. A guide to immunometabolism for immunologists. *Nat Rev Immunol*. (2016) 16:553–65. doi: 10.1038/nri.2016.70

5. MacIver NJ, Michalek RD, Rathmell JC. Metabolic regulation of T lymphocytes. *Annu Rev Immunol*. (2013) 31:259–83. doi: 10.1146/annurev-immunol-032712-095956

6. Stark JM, Tibbitt CA, Coquet JM. The metabolic requirements of Th2 cell differentiation. *Front Immunol*. (2019) 10:2318. doi: 10.3389/fimmu.2019.02318

7. Pandit M, Timilshina M, Gu Y, Acharya S, Chung Y, Seo SU, et al. AMPK suppresses Th2 cell responses by repressing mTORC2. *Exp Mol Med*. (2022) 54:1214–24. doi: 10.1038/s12276-022-00832-x

8. Vlahakis A, Lopez Muniozguren N, Powers T. Mitochondrial respiration links TOR complex 2 signaling to calcium regulation and autophagy. *Autophagy*. (2017) 13:1256–7. doi: 10.1080/15548627.2017.1299314

9. Descamps HC, Herrmann B, Wiredu D, Thaiss CA. The path toward using microbial metabolites as therapies. *EBioMedicine*. (2019) 44:747–54. doi: 10.1016/j.ebiom.2019.05.063

10. Ma Y, Liu X, Wang J. Small molecules in the big picture of gut microbiome-host cross-talk. *EBioMedicine*. (2022) 81:104085. doi: 10.1016/j.ebiom.2022.104085

11. Molinaro A, Bel Lassen P, Henricsson M, Wu H, Adriouch S, Belda E, et al. Imidazole propionate is increased in diabetes and associated with dietary patterns and altered microbial ecology. *Nat Commun*. (2020) 11:5881. doi: 10.1038/s41467-020-20412-9

12. Koh A, Molinaro A, Stahlman M, Khan MT, Schmidt C, Manneras-Holm L, et al. Microbially Produced Imidazole Propionate Impairs Insulin Signaling through mTORC1. *Cell*. (2018) 175:947–61.e17. doi: 10.1016/j.cell.2018.09.055

13. Tolomeu HV, Fraga CAM. Imidazole: synthesis, functionalization and physicochemical properties of a privileged structure in medicinal chemistry. *Molecules*. (2023) 28:838. doi: 10.3390/molecules28020838

14. Fania L, Moretta G, Antonelli F, Scala E, Abeni D, Albanesi C, et al. Multiple roles for cytokines in atopic dermatitis: from pathogenic mediators to endotype-specific biomarkers to therapeutic targets. *Int J Mol Sci*. (2022) 23:2684. doi: 10.3390/ijms23052684

15. Dominguez PM, Ardavin C. Differentiation and function of mouse monocyte-derived dendritic cells in steady state and inflammation. *Immunol Rev*. (2010) 234:90–104.

16. Kasraie S, Werfel T. Role of macrophages in the pathogenesis of atopic dermatitis. *Mediators Inflamm*. (2013) 2013:942375. doi: 10.1155/2013/942375

17. Biedermann T, Skabytska Y, Kaesler S, Volz T. Regulation of T cell immunity in atopic dermatitis by microbes: the yin and yang of cutaneous inflammation. *Front Immunol*. (2015) 6:353. doi: 10.3389/fimmu.2015.00353

18. Fyhrquist N, Lehtimaki S, Lahl K, Savinko T, Lappetelainen AM, Sparwasser T, et al. Foxp3+ cells control Th2 responses in a murine model of atopic dermatitis. *J Invest Dermatol*. (2012) 132:1672–80. doi: 10.1038/jid.2012.40

19. Cibrian D, de la Fuente H, Sanchez-Madrid F. Metabolic pathways that control skin homeostasis and inflammation. *Trends Mol Med*. (2020) 26:975–86. doi: 10.1016/j.molmed.2020.04.004

20. Humeau M, Boniface K, Bodet C. Cytokine-mediated crosstalk between keratinocytes and T cells in atopic dermatitis. *Front Immunol*. (2022) 13:801579. doi: 10.3389/fimmu.2022.801579

21. Danso MO, van Drongelen V, Mulder A, van Esch J, Scott H, van Smeden J, et al. TNF-alpha and Th2 cytokines induce atopic dermatitis-like features on epidermal differentiation proteins and stratum corneum lipids in human skin equivalents. *J Invest Dermatol*. (2014) 134:1941–50. doi: 10.1038/jid.2014.83

22. Vestergaard C, Bang K, Gesser B, Yoneyama H, Matsushima K, Larsen CG. A Th2 chemokine, TARC, produced by keratinocytes may recruit CLA+CCR4+ lymphocytes into lesional atopic dermatitis skin. *J Invest Dermatol*. (2000) 115:640–6. doi: 10.1046/j.1523-1747.2000.00115.x

23. Xiao T, Kagami S, Saeki H, Sugaya M, Kakinuma T, Fujita H, et al. Both IL-4 and IL-13 inhibit the TNF-alpha and IFN-gamma enhanced MDC production in a human keratinocyte cell line, HaCaT cells. *J Dermatol Sci*. (2003) 31:111–7. doi: 10.1016/S0923-1811(02)00149-4

24. Horikawa T, Nakayama T, Hikita I, Yamada H, Fujisawa R, Bito T, et al. IFN-gamma-inducible expression of thymus and activation-regulated chemokine/CCL17 and macrophage-derived chemokine/CCL22 in epidermal keratinocytes and their roles in atopic dermatitis. *Int Immunol*. (2002) 14:767–73. doi: 10.1093/intimm/dxf044

25. Choi JK, Jang YH, Lee S, Lee SR, Choi YA, Jin M, et al. Chrysin attenuates atopic dermatitis by suppressing inflammation of keratinocytes. *Food Chem Toxicol*. (2017) 110:142–50. doi: 10.1016/j.fct.2017.10.025

26. Laplante M, Sabatini DM. mTOR signaling in growth control and disease. *Cell*. (2012) 149:274–93. doi: 10.1016/j.cell.2012.03.017

27. Coronel L, Hackes D, Schwab K, Riege K, Hoffmann S, Fischer M. p53-mediated AKT and mTOR inhibition requires RFX7 and DDIT4 and depends on nutrient abundance. *Oncogene*. (2022) 41:1063–9. doi: 10.1038/s41388-021-02147-z

28. Koh A, Backhed F. From association to causality: the role of the gut microbiota and its functional products on host metabolism. *Mol Cell*. (2020) 78:584–96. doi: 10.1016/j.molcel.2020.03.005

29. Koh A, Manneras-Holm L, Yunn NO, Nilsson PM, Ryu SH, Molinaro A, et al. Microbial Imidazole Propionate Affects Responses to Metformin through p38gamma-Dependent Inhibitory AMPK Phosphorylation. *Cell Metab*. (2020) 32:643–53.e4. doi: 10.1016/j.cmet.2020.07.012

30. Weidinger S, Beck LA, Bieber T, Kabashima K, Irvine AD. Atopic dermatitis. *Nat Rev Dis Primers*. (2018) 4:1. doi: 10.1038/s41572-018-0001-z

31. Feichtinger RG, Sperl W, Bauer JW, Kofler B. Mitochondrial dysfunction: a neglected component of skin diseases. *Exp Dermatol*. (2014) 23:607–14. doi: 10.1111/exd.12484

32. Hamanaka RB, Chandel NS. Mitochondrial metabolism as a regulator of keratinocyte differentiation. *Cell Logist*. (2013) 3:e25456. doi: 10.4161/cl.25456

33. Rizwan H, Pal S, Sabnam S, Pal A. High glucose augments ROS generation regulates mitochondrial dysfunction and apoptosis via stress signalling cascades in keratinocytes. *Life Sci*. (2020) 241:117148. doi: 10.1016/j.lfs.2019.117148

34. Zhang Z, Zi Z, Lee EE, Zhao J, Contreras DC, South AP, et al. Differential glucose requirement in skin homeostasis and injury identifies a therapeutic target for psoriasis. *Nat Med*. (2018) 24:617–27. doi: 10.1038/s41591-018-0003-0

35. Watson MJ, Vignali PDA, Mullett SJ, Overacre-Delgoffe AE, Peralta RM, Grebinoski S, et al. Metabolic support of tumour-infiltrating regulatory T cells by lactic acid. *Nature*. (2021) 591:645–51. doi: 10.1038/s41586-020-03045-2

36. Yang F, Tanaka M, Wataya-Kaneda M, Yang L, Nakamura A, Matsumoto S, et al. Topical application of rapamycin ointment ameliorates Dermatophagoides farina body extract-induced atopic dermatitis in NC/Nga mice. *Exp Dermatol*. (2014) 23:568–72. doi: 10.1111/exd.12463

37. Mercurio L, Albanesi C, Madonna S. Recent updates on the involvement of PI3K/AKT/mTOR molecular cascade in the pathogenesis of hyperproliferative skin disorders. *Front Med (Lausanne)*. (2021) 8:665647. doi: 10.3389/fmed.2021.665647

38. Ding X, Bloch W, Iden S, Ruegg MA, Hall MN, Leptin M, et al. mTORC1 and mTORC2 regulate skin morphogenesis and epidermal barrier formation. *Nat Commun*. (2016) 7:13226. doi: 10.1038/ncomms13226

39. Lee K, Gudapati P, Dragovic S, Spencer C, Joyce S, Killeen N, et al. Mammalian target of rapamycin protein complex 2 regulates differentiation of Th1 and Th2 cell subsets via distinct signaling pathways. *Immunity*. (2010) 32:743–53. doi: 10.1016/j.immuni.2010.06.002

40. Ding X, Willenborg S, Bloch W, Wickstrom SA, Wagle P, Brodesser S, et al. Epidermal mammalian target of rapamycin complex 2 controls lipid synthesis and filaggrin processing in epidermal barrier formation. *J Allergy Clin Immunol*. (2020) 145:283–300.e8. doi: 10.1016/j.jaci.2019.07.033

41. Zhang Y, Chen R, Zhang D, Qi S, Liu Y. Metabolite interactions between host and microbiota during health and disease: Which feeds the other? *BioMed Pharmacother*. (2023) 160:114295. doi: 10.1016/j.biopha.2023.114295

42. Lee JY, Lee JH, Lim HJ, Kim E, Kim DK, Choi JK. Aminooxy acetic acid suppresses Th17-mediated psoriasis-like skin inflammation by inhibiting serine metabolism. *Front Pharmacol*. (2023) 14:1215861. doi: 10.3389/fphar.2023.1215861

frontiers | Frontiers in Immunology

TYPE Brief Research Report
PUBLISHED 27 March 2024
DOI 10.3389/fimmu.2024.1347112



OPEN ACCESS

EDITED BY
Zhenghua Zhang,
Fudan University, China

REVIEWED BY
Zhang Chen,
Huazhong University of Science and Technology, China
Lei Jiang,
Guangdong Provincial People's Hospital, China
Georges Michel Nemer,
Hamad bin Khalifa University, Qatar

*CORRESPONDENCE
Haocheng Lu
luhc@sustech.edu.cn
Cuihong Lian
liancuihong@email.szu.edu.cn

†These authors have contributed equally to this work and shared the last authorship

RECEIVED 30 November 2023
ACCEPTED 18 March 2024
PUBLISHED 27 March 2024

CITATION
Hu W, Liu Y, Lian C and Lu H (2024) Genetic insight into putative causes of xanthelasma palpebrarum: a Mendelian randomization study. *Front. Immunol.* 15:1347112. doi: 10.3389/fimmu.2024.1347112



# Genetic insight into putative causes of xanthelasma palpebrarum: a Mendelian randomization study

Wenting Hu[1], Yaozhong Liu[2], Cuihong Lian[1*†] and Haocheng Lu[3*†]

[1]Department of Dermatology, Shenzhen Second People's Hospital, Shenzhen, Guangdong, China, [2]Department of Internal Medicine, Cardiovascular Center, University of Michigan Medical Center, Ann Arbor, MI, United States, [3]Department of Pharmacology, Joint Laboratory of Guangdong-Hong Kong Universities for Vascular Homeostasis and Diseases, School of Medicine, Southern University of Science and Technology, Shenzhen, Guangdong, China

Xanthelasma palpebrarum (XP) is the most common form of cutaneous xanthoma, with a prevalence of 1.1%~4.4% in the population. However, the cause of XP remains largely unknown. In the present study, we used Mendelian randomization to assess the genetic association between plasma lipids, metabolic traits, and circulating protein with XP, leveraging summary statistics from large genome-wide association studies (GWAS). Genetically predicted plasma cholesterol and LDL-C, but not HDL-C or triglyceride, were significantly associated with XP. Metabolic traits, including BMI, fasting glucose, type 2 diabetes, systolic and diastolic blood pressure, were not significantly associated with XP. Furthermore, we found genetically predicted 12 circulating proteins were associated with XP, including FN1, NTM, FCN2, GOLM1, ICAM5, PDE5A, C5, CLEC11A, CXCL1, CCL2, CCL11, CCL13. In conclusion, this study identified plasma cholesterol, LDL-C, and 12 circulating proteins to be putative causal factors for XP, highlighting the role of plasma cholesterol and inflammatory response in XP development.

KEYWORDS

**Mendelian randomization, Xanthelasma palpebrarum, plasma lipid, circulating protein, cytokine**

## 1 Introduction

Xanthelasma palpebrarum (XP) is the most common form of cutaneous xanthoma, usually manifesting as bilateral, symmetrical, soft, yellowish papules and plaques over the eyelid (1). A large cohort in Denmark shows that the prevalence of XP in the general population is about 4.4% (2). The prevalence varies in other studies (1.1%~4.4%) (3),

possibly due to its usually asymptomatic nature, and many patients do not get diagnosed. Patients often seek medical help because of its significant cosmetic burden and request treatment for these aesthetically undesirable facial lesions (4). Several therapeutic methods have been developed for XP, including surgical excision, laser therapy, chemical peeling, cryotherapy, radiofrequency ablation, plasma sublimation, and dermabrasion (5). Although surgical excision is the most common method, it could result in complications, such as scarring, dyspigmentation, and ectropion (5). Recurrence of XP is common, regardless of treatment method, ranging from 40% to 80% (6, 7). Currently, a gold-standard long-term treatment option has yet to be established (8), attributed to our limited understanding of the pathogenesis of XP.

XP lesions comprise mainly foamy histiocytes located within the upper reticular dermis or in perivascular and periadnexal areas, and the intracellular vacuoles contain esterified cholesterol and lipids, similar to evolving atheromas (4, 9). XP is a common complication in patients with familial hypercholesterolemia (10, 11). Many studies demonstrated that XP is associated with dyslipidemia, particularly high total cholesterol (TC) and high low-density lipoproteins (LDL) (12–14). From a meta-analysis of over 854 XP patients, XP patients had significantly higher serum levels of total cholesterol and LDL, higher apolipoprotein B, and relatively lower apolipoprotein A1. No significant difference in high-density lipoprotein (HDL), very low-density lipoprotein (VLDL), and triglyceride (TG) was observed between XP patients and the control population. Notably, about half of XP patients show normal lipid profiles (15). Nevertheless, it is still controversial whether hyperlipidemia is a cause of XP or just associated with XP because of possible potential confounding factors and reverse causation bias.

Mendelian randomization (MR) uses genetic variations to address causal relationships between modifiable or unmodifiable exposure and outcomes (16). MR is based on instrumental variable (IV) analysis. A validated IV is strongly related to exposure but not to the outcome, except through its association with exposure. The careful selection of IV could infer the causality between exposure and outcome in the presence of unobserved confounding factors. Here, we applied MR analysis to address the genetic causal effects of plasma lipids, metabolic traits, and circulating proteins on XP (17, 18) to investigate the molecular mechanisms and find potential drug targets for XP.

# 2 Method

## 2.1 Sources of exposure and outcome datasets

The study relied on publicly available summary statistics from large-scale GWAS. The datasets used in this study are listed in Supplementary Table 1. The FinnGen combines the imputed genotype and digital health record data from the Finnish population. It is the largest GWAS dataset available containing the XP phenotype with 228 cases and 344684 controls.

## 2.2 Selection of instrumental variables

We selected genome-wide significant single nucleotide polymorphisms (SNP) whose p-value is less than $5*10^{-8}$ for the plasmid lipid and metabolic traits. We excluded correlated SNPs whose linkage disequilibrium (LD) R2 > 0.001 in the 10,000kb region. We only keep the SNPs with F statistics > 10 to avoid weak IV bias. To prevent reverse correlation, we only included SNPs that explain a substantially larger variance of exposures than outcomes as calculated by the Steiger filter test (p< 0.05). IVs associated with possible confounding factors are removed by using PhenoScanner V2 tool (19).

For the circulating proteins, we used consortium of deCODE genetics (20), which contains the association between genetic variants and 4719 plasma proteins in 35,559 Icelanders (21). Valid SNPs were selected based on the following criteria: p-value< $5*10^{-8}$; Steiger filtering test p<0.05; cis-pQTL, which SNPs within 1MB from gene starting site; clumped to conditionally independent genetic IVs ($R^2$< 0.001 and kb=10,000). For proteins with more than 1 IV, the inverse variance-weighted (IVW) method was used; For proteins with only 1 IV, the Wald ratio method was used.

For the plasma inflammatory proteins, we used (1) GWAS results from The Cardiovascular Risk in Young Finns Study (YFS), which is a multicenter follow-up study with randomly chosen subjects from the Finnish cities of Helsinki, Kuopio, Oulu, Tampere, and Turku and their rural surroundings (22, 23). In this study, a total of 41 cytokines in the plasma were measured; (2) GWAS summary statistics from SCALLOP Consortium meta-analysis GWAS summary statistics for the Olink Inflammation panel (24). In this study, a genome-wide protein pQTL of 91 plasma proteins was measured using Olink Target platform in 14,824 participants. For both studies, valid SNPs were selected based on the following criteria: p-value< $5*10^{-8}$; Steiger filtering test p<0.05; both cis- and trans- SNPs were used; clumped to conditionally independent genetic IVs ($R^2$< 0.001 and kb=10,000). For proteins with more than 1 IV, the inverse variance-weighted (IVW) method was used; For proteins with only 1 IV, the Wald ratio method was used.

## 2.3 Two-sample Mendelian randomization

The two-sample MR was performed using TwoSampleMR (25) and MendelianRandomization (26) R package. For each exposure, we retrieved the summary statistics of selected IVs from the outcome dataset (27) to perform MR analysis. Data on exposure and outcome were then harmonized to ensure that the effect of an SNP on exposure and outcome corresponded with the same allele. $F$ statistics were calculated by sample size ($N$) and number of instruments ($K$) as: $F = (\frac{N-K-1}{K})(\frac{R^2}{1-R^2})$ $R^2$ is the variance in the exposure explained by the genetic variant, calculated as $R^2 = 2\beta_X^2 MAF(1 - MAF)$ ($MAF$ is the minor allele frequency). To avoid the weak IV bias, SNPs with $F$< 10 were excluded in the MR analysis. In the primary analysis, we used the inverse variance-weighted (IVW) method, which provided the highest precision,

assuming that all IVs are valid (28). The Wald ratio estimate of the $j$th variant is: $\hat{\theta}_j = \frac{\hat{\beta}_{Yj}}{\hat{\beta}_{Xj}}$ and its approximate standard error is $se(\hat{\theta}_j) = \left|\frac{se(\hat{\beta}_{Yj})}{\hat{\beta}_{Xj}}\right|$

The IVW estimate can be expressed as:

$$\hat{\theta}_{\mathrm{IVW}} = \frac{\sum_j \hat{\theta}_j \mathrm{se}(\hat{\theta}_j)^{-2}}{\sum_j \mathrm{se}(\hat{\theta}_j)^{-2}} = \frac{\sum_j \hat{\beta}_{Yj}\hat{\beta}_{Xj}\mathrm{se}(\hat{\beta}_{Yj})^{-2}}{\sum_j \hat{\beta}_{Xj}{}^2 \mathrm{se}(\hat{\beta}_{Yj})^{-2}}$$

The standard error of the IVW estimate is:

$$\mathrm{se}(\hat{\theta}_{\mathrm{IVW}}) = \sqrt{\frac{1}{\sum_j \hat{\beta}_{Xj}{}^2 \mathrm{se}(\hat{\beta}_{Yj})^{-2}}}$$

MR analyses were conducted using R (version 4.3.2) package "TwoSampleMR v0.5.8". The weighted median method is used, assuming that at least half of the IVs are valid. In addition, the MR-Egger method was used to correct the potential horizontal pleiotropy. The Cochran Q heterogeneity test (using TwoSampleMR::mr_heterogeneity function) was used to determine heterogeneity. The MR-Egger intercept test (using TwoSampleMR:: mr_pleiotropy_test function)was used to determine the unbalanced pleiotropy between exposure and outcome. The Steiger directionality test (using TwoSampleMR::directionality_test function) was used to determine the causal direction of the exposure and outcome. Sensitivity analysis was conducted by leave-one-out analysis (using TwoSampleMR:: mr_leaveoneout function). For circulating proteins and cytokines, the p-value was corrected by the FDR method.

# 3 Results

## 3.1 The causal effect of plasma lipids on XP

Based on the up-to-date largest GWAS study of XP from FinnGen Datafreeze 9 release and lipid traits from Global Lipids Genetics Consortium (2021), we assessed the causal effects of lipid traits and XP diseases, using two sample MR methods (Figure 1A; Supplementary Table 2). In the primary inverse variance weighted (IVW) analysis, we found that genetically predicted total cholesterol (Odds ratio, OR, 1.715; 95% confidence intercept, CI, 1.089 - 2.7; p = 0.020) and LDL (OR, 1.782; CI, 1.106-2.868; p = 0.017) were significantly associated with XP (Figures 1B, D). The leave-one-out analysis showed the robustness of the MR estimates (Figures 1C, E). The alternative analysis with the Weighted median and MR Egger method shows the same direction but did not reach significance, likely because they are of less power. For other lipid traits, including HDL (OR, 1.223; CI, 0.771-1.94; p = 0.393), non-HDL cholesterol (OR, 1.534; CI, 0.958-2.456; p = 0.075), and triglyceride (OR, 1.059; CI, 0.655-1.712; p = 0.814, the association did not reach statistical significance in primary IVW analysis.

## 3.2 The causal effect of metabolic traits on XP

XP was reported to be associated with other metabolic traits, including body weight, blood glucose, and blood pressure (29). We used large GWAS studies of BMI, diabetes, and blood pressure to assess their possible causality to XP (Figure 2; Supplementary Table 3). In primary IVW analysis, genetically predisposition of increased BMI (OR, 0.709; CI, 0.241-2.08; p = 0.531), fasting glucose (OR, 0.841; CI, 0.241-2.935; p = 0.786), type 2 diabetes mellitus (T2DM) (OR, 1.103; CI, 0.854-1.426; p = 0.452), systolic blood pressure (OR, 1.021; CI, 0.96-1.086; p = 0.509), diastolic blood pressure (OR, 1.116; CI, 0.955-1.303; p = 0.168) did not significantly increase the risk of XP. These metabolic traits did not significantly increase the risk of XP in alternative Weighted median and MR Egger methods.

## 3.3 Putative causal circulating proteins on XP

The development of XP involves the trans-endothelial migration of immune cells and their uptake of lipids. To identify the possible circulating proteins regulating these processes, we utilize the large-scale GWAS of circulating proteins (20). The protein quantitative trait loci (pQTLs) are used as genetic IVs in the MR study, and we integrate the plasma proteome with the XP GWAS (Figure 3; Supplementary Table 4). We found at least 1 SNPs as validated IV for 1199 circulating proteins and used these SNPs as genetic predictors of protein expression. Two sample MR analysis found 8 proteins with FDR corrected p-value< 0.05: fibronectin 1 (FN1, p = $5.15*10^{-13}$), neurotrimin (NTM, p = $8.24*10^{-10}$), ficolin 2 (FCN2, p = $2.06*10^{-8}$), Golgi membrane protein 1 (GOLM1, p = $5.61*10^{-7}$), intercellular adhesion molecule-5 (ICAM5, p = $3.9*10^{-4}$), phosphodiesterase 5A (PDE5A, p = $1.6*10^{-3}$), Complement C5 (C5, p = 0.031), C-type lectin domain containing 11A (CLEC11A, p = 0.033). Among them, FN1, NTM, ICAM5, and C5 were negatively associated with XP, while FCN2, GOLM1, PDE5A, and CLEC11A were positively associated with XP.

## 3.4 Putative causal circulating inflammatory proteins on XP

Inflammation plays an important role in various skin diseases, such as psoriasis and eczema. However, the role of inflammatory response in XP is still not clear. To address this question, we leveraged the GWAS data of inflammatory proteins (22–24). Using two-sample MR, we found that 3 out of 41 cytokines in Young Finns Study (Figure 4; Supplementary Table 5) were significantly associated with XP (FDR corrected p-value< 0.05), including C-X-C motif chemokine ligand 1 (CXCL1, also named GRO alpha, p = 0.0028), C-C motif chemokine ligand 2 (CCL2, also called MCP1, p = 0.0070), and C-C motif chemokine ligand 11 (CCL11, also name eotaxin, p = 0.026). In SCALLOP Consortium GWAS results, we found 2 out of 91 proinflammatory proteins were significantly associated with XP, including CCL2 (p = $9.724*10^{-9}$) and CCL13 ($2.096*10^{-6}$) (Supplementary Table 6). All the cytokines were positively associated with XP, indicating a possible role of inflammation in XP.

# 4 Discussion

XP is a relatively common skin disease, but the actual cause is still not clear. In this study, we used a two-sample MR analysis to

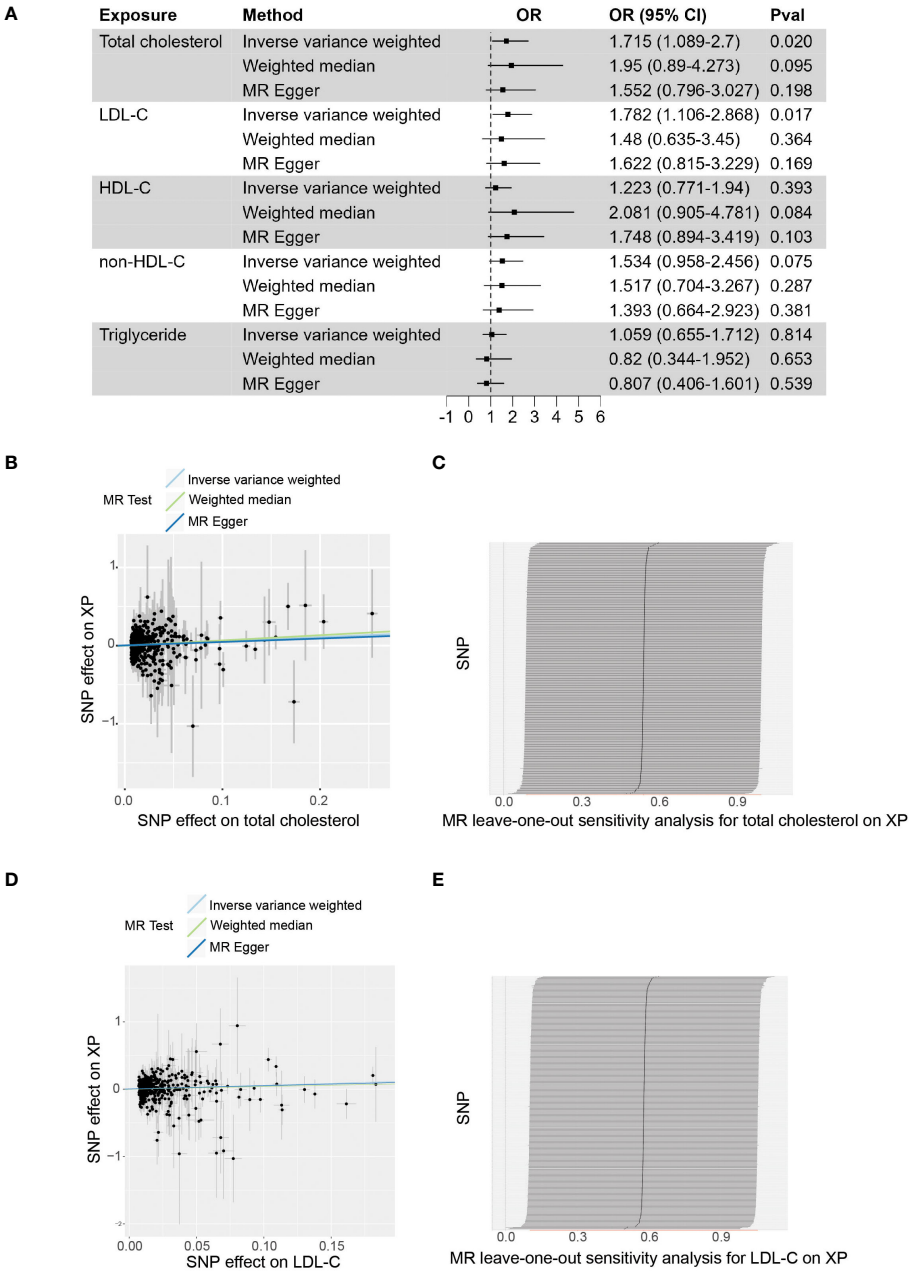


FIGURE 1
The causal effect of plasma lipids on XP. **(A)**, Forest plot to visualize the causal effect of plasma lipids on XP. **(B)**, Scatter plot to visualize the causal effect of plasma total cholesterol on XP. **(C)**, Leave-one-out plot to visualize the causal effect of total cholesterol on XP when leaving one SNP out. **(D)**, Scatter plot to visualize the causal effect of plasma LDL-C on XP. **(E)** Leave-one-out plot to visualize the causal effect of LDL-C on XP when leaving one SNP out. OR, Odds ratio; CI, confidence interval; Pval, p-value; LDL-C, low-density lipoprotein cholesterol; HDL-C, high-density lipoprotein cholesterol; non-HDL-C, non-high-density lipoprotein cholesterol.

investigate the risk factors and mechanism of XP. We used large lipid GWAS data and found that total cholesterol and LDL-C were causally associated with XP. In addition, to further understand the molecular mechanism of XP, in GWAS data of circulating protein and cytokines, we identified 8 circulating proteins and 3 inflammatory cytokines to be putative causes and potential therapeutic targets of XP in patients.

Many observation studies have reported that XP patients have significantly higher levels of cholesterol and LDL-C but various levels of triglycerides and HDL-C. Most studies only have tens or hundreds of individuals in the cohort, which limits the power of statistical analysis. XP is pathologically characterized by infiltration of lipid-rich foam cells in the demis, which shares many similarities with atherosclerosis. Given that high cholesterol, especially LDL-C is well established as a risk factor for atherosclerosis, XP is also often attributed to high plasma cholesterol. However, the causal effects of plasma lipids and XP is still not clear. The association of XP and high cholesterol could be attributed to other confounding factors, such as diet or lifestyle, which are difficult to exclude in observation studies. To address these issues, we conducted a comprehensive MR

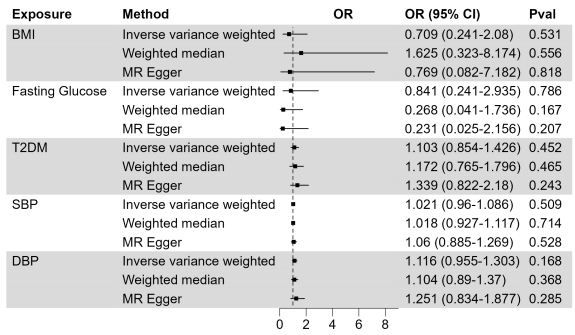


FIGURE 2
The causal effect of metabolic traits on XP. Forest plot to visualize the causal effect of BMI, fasting glucose, type 2 diabetes, systolic blood pressure, and diastolic blood pressure on XP. OR, Odds ratio; CI, confidence interval; Pval, p-value; BMI, body mass index; T2DM, Type 2 Diabetes Mellitus; SBP, systolic blood pressure; DBP, diastolic blood pressure.

analysis to determine the causality between plasma lipids and XP. The MR analysis used genetic variants as IV to test the causality and could overcome the problem of confounding factors and reverse causality. All the SNPs used in the study were listed in (Supplementary Table 7). We used the FinnGen Datafreeze 9 release (27) as the GWAS dataset for XP and the Global Lipids Genetics Consortium Results (GLGC) (30) as GWAS for plasma lipids. GLGC is a multi-ancestry meta-analysis of lipid levels in more than 1.65 million individuals. Two-sample MR analysis performed on these 2 datasets demonstrated that genetically predicted higher plasma total cholesterol and LDL-c, but neither triglycerides nor HDL-C were causally associated with XP. The horizontal pleiotropy was checked by Egger intercept, and heterogeneity was checked by Cochran's Q test. The alternative Weighted median and MR Egger test showed consistent direction but no significance, possibly due to the low accuracy of these methods compared with the primary IVW method. This analysis provides direct evidence that high plasma cholesterol and high LDL-C are both causal factors of XP, and cholesterol or LDL-C lowering therapy could be helpful in XP patients.

Many studies have shown that higher plasma lipids increase XP risk, but about half of XP patients exhibit a normal plasma lipid profile. This phenomenon indicates that there are additional pathways that determine XP development. In atherosclerosis development, the lesion is initiated by the trans-endothelial migration of monocytes into the aortic wall, followed by the uptake of lipids by monocyte-derived macrophage in the lesion (31). The infiltration of monocytes to tissue is regulated by many proinflammatory cytokines and chemotactic factors (32). To assess whether these processes contribute to lipid accumulation in the XP lesion, we used the pQTL data from a large GWAS dataset of circulating proteins and inflammatory cytokines to perform the two-sample MR analysis on XP. The analysis of circulating proteins showed that 8 proteins in the plasma could causally associate with XP, including FN1, NTM, FCN2, GOLM1, ICAM5, PDE5, C5, and CLEC11A (Figure 3).

Fibronectin (FN1) is a glycoprotein with multiple variants. FN1 is an extracellular matrix protein and plays an important role in cell adhesion, migration, growth, and differentiation (33, 34). Neurotrimin (NTM) is a neural cell adhesion molecule that regulates neurite outgrowth (35). Intriguingly, NTM is also implicated in several cardiovascular diseases, including heart failure (36), hypertension (37) and aneurysm (38). Ficolin2 (FCN2) is a soluble collagen-like protein that binds to pathogen pattern molecules (39) and is involved in innate immune defense (40). Golgi Membrane Protein 1 (GOLM1) is mainly located in the Golgi membrane and can also be secreted into circulation (41). Circulating GOLM1 can be used as an early diagnosis marker of hepatocellular carcinoma (42, 43). GOLM1 is also implicated in other cancers, including melanoma (44) and colon cancer (45). Intercellular adhesion molecule 5 (ICAM5) is an adhesion molecule important for the recruitment of inflammatory cells to the sites of inflammation. ICAM5 is also important for pathogen infection (46), auto-immune disease (47, 48), and nervous system (49, 50). Phosphodiesterase type 5A (PDE5A) selectively hydrolyzes cyclic GMP and is critical for maintaining cardiovascular homeostasis (51). PDE5 regulates vascular tone through the NO-cGMP pathway (52), and PDE5 inhibitors show promising results in treating heart ischemia injury (53, 54) and pathological hypertrophy (55). Complement factor C5 (C5) is a key component of the complement system and innate immune system. C5 is cleaved to C5a and C5b by C5 convertase. C5a functions as a potent chemotactic factor, and C5b facilitates the assembly of membrane attack complex (56). C5 inhibitors have been approved for the treatment of diseases of complement overactivation, including paroxysmal nocturnal hemoglobinuria, atypical hemolytic uremic syndrome, and vasculitis (57). C-type lectin domain family 11, member A (CLEC11A) is an osteogenic growth factor and is important for maintaining an adult skeleton (58, 59).

In the development of atherosclerosis, the recruitment of immune cells to the vascular wall is induced by several inflammatory cytokines and chemotactic factors. To address whether this process was also implicated in the accumulation of lipid-laden cells in the XP lesion, we utilized the GWAS dataset of 41 inflammatory cytokines in the blood (22, 23). In this dataset, we identified 3 cytokines, including CXCL1, CCL2, and CCL11, that were positively associated with XP. CXCL1 and its receptor CXCR2 signaling are crucial for monocyte infiltration into inflammatory tissues. CXCL1/CXCR2 signaling are widely studied in cardiovascular diseases, including cardiac hypertrophy (60), hypertension (61), aneurysm (62), and atherosclerosis (63). CCL11 [eosinophil chemotactic protein (Eotaxin)] has a selective role in the recruitment of eosinophils via activating CCR2, CCR3, and CCR5 receptors (64). Increased circulating CCL11 was implicated in several auto-immune and allergic diseases, including systemic lupus erythematosus (65), asthma (66), and multiple sclerosis (67). Importantly, the association between circulating CCL2 and XP was cross-validated in 2 different GWAS results. CCL2, also known as monocyte chemoattractant protein-1 (MCP-1), is a key chemoattractant protein for monocytes. By binding to its primary receptor, CCR2, CCL2 coordinates inflammatory monocytes traveling among bone marrow, blood, and

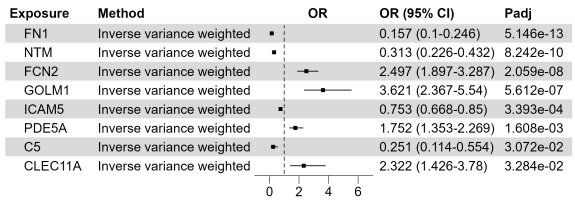


FIGURE 3
Putative causal circulating proteins on XP. Forest plot to visualize the causal effect of circulating proteins on XP. OR, Odds ratio; CI, confidence interval; Padj, FDR corrected p value. Candidates are selected based on the following criteria: MR results p-value (FDR adjusted)< 0.05; Egger Intercept P value > 0.05; Correct causal direction; Steiger P-value< 0.05; Q p value > 0.05.

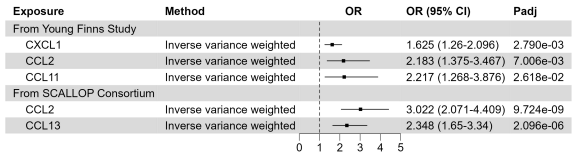


FIGURE 4
Putative causal inflammatory proteins on XP. Forest plot to visualize the causal effect of inflammatory proteins on XP. OR, Odds ratio; CI, confidence interval; Padj, FDR corrected p value. Candidates are selected based on the following criteria: MR results p-value (FDR adjusted)< 0.05; Egger Intercept P value > 0.05; Correct causal direction; Steiger P-value< 0.05; Q p value > 0.05.

inflammatory tissue (68). CCL2 can also regulate the migration and infiltration of other immune cells, including memory T lymphocytes and natural killer (NK) cells (69). CCL13 (MCP4) could induce the chemotaxis of multiple immune cells, including eosinophils, basophils, monocytes, macrophages, immature dendritic cells, and T cells (70). CCL13 is implicated in asthma, rheumatic diseases, skin conditions (atopic dermatitis and alopecia areata), and cancer (71). All of these cytokines are positively associated with XP and could potentially serve as novel therapeutic targets in XP.

Many studies reported the association between high plasma cholesterol and XP, but the mechanism of accumulation of lipids in the soft tissue is still not clear. XP is pathologically similar to atherosclerosis, characterized by infiltration of lipid-rich foam cells and proliferation of endothelial and fibroblastic cells (5). In the development of atherosclerosis, the infiltration of macrophages, followed by lipid uptake by infiltrated cells, is a key step in the progression of the disease. In this study, we found several plasma proteins involved in the inflammatory process (FCN2, C5, CXCL1, CCL2, CCL11, and CCL13) and cell adhesion (NTM and ICAM5) to be associated with XP. This information supports that local inflammation could be involved in the XP and deserves further investigation.

Our study has certain strengths. First, unlike observation studies, MR analysis could test the causality between exposures and outcomes, while observational studies could only provide association and easily flawed by the presence of confounding factors (72). Our result added the evidence that high cholesterol and LDL-C are causal factors of XP. Second, MR analysis could reduce confounding factors and reverse causation bias. Third, a large GWAS dataset provides adequate statistical power for the analysis. However, our study still has limitations. We acquired GWAS data for XP from FinnGen Data Freeze 9. This is the largest dataset containing results for the XP phenotype at present. However, in this dataset, only 228 cases of XP are reported, with 344,684 controls. The small number of cases may limit the statistical power of MR. In addition, MR analysis results can be violated by pleiotropy. In our study, the weighted median and MR-Egger methods provide a consistent direction as IVW, but the influence of horizontal pleiotropy still cannot be excluded. In addition, most of the GWAS studies are mainly from cohorts of European ancestry. It still requires further validation if the conclusion can be generalized to other populations.

## 5 Conclusions

Increased observational studies demonstrated that increased plasma cholesterol was a risk factor for XP. Our MR study further provided evidence for a causal link between plasma cholesterol, LDL-C, and XP, supporting the use of cholesterol-lowering drugs in treating XP. In addition, by analyzing the plasma proteins, we provided evidence that genetically predicted levels of 12 plasma proteins were associated with XP, highlighting the role of cell adhesion and inflammation in the development of XP.

## Data availability statement

The original contributions presented in the study are included in the article/Supplementary Material. Further inquiries can be directed to the corresponding authors.

## Author contributions

WH: Conceptualization, Data curation, Formal analysis, Methodology, Writing – original draft. YL: Investigation, Methodology, Supervision, Validation, Writing – review & editing. CL: Conceptualization, Supervision, Validation, Writing – review & editing. HL: Conceptualization, Data curation, Formal analysis, Funding acquisition, Writing – review & editing.

## Funding

The author(s) declare financial support was received for the research, authorship, and/or publication of this article. This research was funded by National Natural Science Foundation of China, grant number 82370490 and 32300958, Natural Science Foundation of Guangdong Province of China, grant number 2023A1515010489.

## Conflict of interest

The authors declare that the research was conducted in the absence of any commercial or financial relationships that could be construed as a potential conflict of interest.

## Publisher's note



## Supplementary material

The Supplementary Material for this article can be found online at: https://www.frontiersin.org/articles/10.3389/fimmu.2024.1347112/full#supplementary-material

SUPPLEMENTARY TABLE 1
The datasets used in this study.This table describes the sources of the datasets used in this study. N Cases, number of cases; N Controls, numbers of controls; DOI, digital object identifier.

SUPPLEMENTARY TABLE 2
MR results of plasma lipids to XP. This table is the MR results of total cholesterol, LDL-C, HDL-C, non-HDL-C, and TG to XP, corresponding to Figure 1. Method, methods used in MR analysis; N SNP, number of valid SNPs used in MR analysis; Beta, the effect estimated using the genetic variants; SE, standard deviation of beta; OR, Odds ratio with 95% confidence interval; Egger Intercept, the intercept term using MR-Egger method for assessing the pleiotropic effects; Egger Intercept P value, P value of MR-Egger method; Q value, the result of Cochran's Q test for evaluating the heterogeneity; Q p-value: P value of Cochran's Q test.

SUPPLEMENTARY TABLE 3
MR results of metabolic traits to XP. This table is the MR results of BMI, fasting glucose, type 2 diabetes, systolic blood pressure, and diastolic blood pressure to XP, corresponding to Figure 2. BMI, body mass index; Method, methods used in MR analysis; N SNP, number of valid SNPs used in MR analysis; Beta, the effect estimated using the genetic variants; SE, standard deviation of beta; OR, Odds ratio with 95% confidence interval; Egger Intercept, the intercept term using MR-Egger method for assessing the pleiotropic effects; Egger Intercept P value, P value of MR-Egger method; Q value, the result of Cochran's Q test for evaluating the heterogeneity; Q p value: P value of Cochran's Q test.

SUPPLEMENTARY TABLE 4
MR results of circulating proteins to XP. The protein quantitative trait loci (pQTLs) are used as genetic IVs in the MR study, and we integrate this plasma proteome with the XP GWAS, correspondent to Figure 3. Method, methods used in MR analysis; N SNP, number of valid SNPs used in MR analysis; Beta, the effect estimated using the genetic variants; SE, standard deviation of beta; P-value (FDR adjusted), false discovery rate adjusted P value for multiple testing correction; Egger Intercept, the intercept term using MR-Egger method for assessing the pleiotropic effects; Egger Intercept P value, P value of MR-Egger method; SNP r2 exposure, estimated variance explained in exposure; SNP r2 outcome, estimated variance explained in outcome; Correct causal direction, whether the assumption that exposure causes outcome is valid from MR Steiger test; Steiger P-value, P value of Steiger test; OR, Odds ratio; OR lci95, lower 95% confidence interval of OR; OR uci95, upper 95% confidence interval of OR; Q value, the result of Cochran's Q test for assessing the heterogeneity; Q p value: P value of Cochran's Q test.

SUPPLEMENTARY TABLE 5
MR results of circulating cytokines to XP. The GWAS data of circulating cytokines from Young Finns Study were used as exposure in MR analysis, corresponding to Figure 4. Method, methods used in MR analysis; N SNP, number of valid SNPs used in MR analysis; Beta, the effect estimated using the genetic variants; SE, standard deviation of beta; P-value (FDR adjusted), false discovery rate adjusted P value for multiple testing correction; Egger Intercept, the intercept term using MR-Egger method for assessing the pleiotropic effects; Egger Intercept P value, P value of MR-Egger method; SNP r2 exposure, estimated variance explained in exposure; SNP r2 outcome, estimated variance explained in outcome; Correct causal direction, whether the assumption that exposure causes outcome is valid from MR Steiger test; Steiger P-value, P value of Steiger test; OR, Odds ratio; OR lci95, lower 95% confidence interval of OR; OR uci95, upper 95% confidence interval of OR; Q value, the result of Cochran's Q test for assessing the heterogeneity; Q p value: P value of Cochran's Q test.

SUPPLEMENTARY TABLE 6
MR results of circulating inflammatory proteins to XP. The GWAS data of circulating inflammatory proteins from SCALLOP Consortium were used as exposure in MR analysis, corresponding to Figure 4. Method, methods used in MR analysis; N SNP, number of valid SNPs used in MR analysis; Beta, the effect estimated using the genetic variants; SE, standard deviation of beta; P-value (FDR adjusted), false discovery rate adjusted P value for multiple testing correction; Egger Intercept, the intercept term using MR-Egger method for assessing the pleiotropic effects; Egger Intercept P value, P value of MR-Egger method; SNP r2 exposure, estimated variance explained in exposure; SNP r2 outcome, estimated variance explained in outcome; Correct causal direction, whether the assumption that exposure causes outcome is valid from MR Steiger test; Steiger P-value, P value of Steiger test; OR, Odds ratio; OR lci95, lower 95% confidence interval of OR; OR uci95, upper 95% confidence interval of OR; Q value, the result of Cochran's Q test for assessing the heterogeneity; Q p value: P value of Cochran's Q test.

SUPPLEMENTARY TABLE 7
SNPs used for MR analysis. This table lists all SNPs used as IVs for MR analysis in this study, corresponding to Figures 1, 2. CHR, chromosome; POS, position on chromosome; Other allele, reference allele; Beta, the effect estimated using the genetic variants; SE, standard deviation of beta; F, F-statistic for average strength.

## References

1. Chang HC, Sung CW, Lin MH. Serum lipids and risk of atherosclerosis in xanthelasma palpebrarum: A systematic review and meta-analysis. *J Am Acad Dermatol.* (2020) 82:596–605. doi: 10.1016/j.jaad.2019.08.082

2. Christoffersen M, Frikke-Schmidt R, Schnohr P, Jensen GB, Nordestgaard BG, Tybjaerg-Hansen A. Xanthelasmata, arcus corneae, and ischaemic vascular disease and death in general population: prospective cohort study. *Bmj.* (2011) 343:d5497–d. doi: 10.1136/bmj.d5497

3. Namazi N, Amani M, Haghighi Morad M, Namazi N. Is normolipidemic xanthelasma palpebrarum an independent risk factor of atherosclerosis? *Int J Clin Practice.* (2021) 75:e14958. doi: 10.1111/ijcp.14958

4. Khode S, Tan SHT, Tan EA, Uppal S. Xanthelasma palpebrarum: more than meets the eye. *Indian J Otolaryngol Head Neck Surg.* (2019) 71:439–46. doi: 10.1007/s12070-018-1345-0

5. Malekzadeh H, Ormseth B, Janis JE. A practical review of the management of xanthelasma palpebrarum. *Plast reconstructive Surg Global Open*. (2023) 11:e4982. doi: 10.1097/GOX.0000000000004982

6. Nair PA, Singhal R. Xanthelasma palpebrarum - a brief review. *Clinical cosmetic investigational Dermatol*. (2018) 11:1–5. doi: 10.2147/CCID

7. Mendelson BC, Masson JK. Xanthelasma: follow-up on results after surgical excision. *Plast reconstructive surgery*. (1976) 58:535–8. doi: 10.1097/00006534-197611000-00001

8. Laftah Z, Al-Niaimi F. Xanthelasma: an update on treatment modalities. *J cutaneous aesthetic surgery*. (2018) 11:1–6. doi: 10.4103/JCAS.JCAS_56_17

9. Ferrando J, Bombi JA. Ultrastructural aspects of normolipidemic xanthomatosis. *Arch Dermatol Res*. (1979) 266:143–59. doi: 10.1007/BF00694624

10. Martin AC, Allen C, Pang J, Watts GF. Detecting familial hypercholesterolemia: The Jack and the Beanstalk principle. *J Clin Lipidol*. (2017) 11:575–8. doi: 10.1016/j.jacl.2017.02.003

11. Ceska R, Vrablík M, Horínek A. Familial defective apolipoprotein B-100: a lesson from homozygous and heterozygous patients. *Physiol Res*. (2000) 49 Suppl 1:S125–30.

12. Kim YG, Oh JW, Lee KC, Yoon SH. Clinical association between serum cholesterol level and the size of xanthelasma palpebrarum. *Arch Craniofacial Surgery*. (2022) 23:71–6. doi: 10.7181/acfs.2022.00185

13. Zhimin W, Hui W, Fengtao J, Wenjuan S, Yongrong L. Clinical and serum lipid profiles and LDLR genetic analysis of xanthelasma palpebrarum with nonfamilial hypercholesterolemia. *J Cosmetic Dermatol*. (2020) 19:3096–9. doi: 10.1111/jocd.13366

14. Rai A, Karki S, Prasad Sah S, Narayan Kamat L, Pradhan M. Dyslipidemia in patients with xanthelasma palpebrarum visiting the department of dermatology of a tertiary care centre: A descriptive cross-sectional study. *J Nepal Med Assoc*. (2022) 60:529–32. doi: 10.31729/jnma.7485

15. Bergman R. The pathogenesis and clinical significance of xanthelasma palpebrarum. *J Am Acad Dermatol*. (1994) 30:236–42. doi: 10.1016/S0190-9622(94)70023-0

16. Sanderson E, Glymour MM, Holmes MV, Kang H, Morrison J, Munafò MR, et al. Mendelian randomization. *Nat Rev Methods Primers*. (2022) 2:6. doi: 10.1038/s43586-021-00092-5

17. Huang Y, Liu Y, Ma Y, Tu T, Liu N, Bai F, et al. Associations of visceral adipose tissue, circulating protein biomarkers, and risk of cardiovascular diseases: A mendelian randomization analysis. *Front Cell Dev Biol*. (2022) 10. doi: 10.3389/fcell.2022.840866

18. Ning Z, Huang Y, Lu H, Zhou Y, Tu T, Ouyang F, et al. Novel drug targets for atrial fibrillation identified through mendelian randomization analysis of the blood proteome. *Cardiovasc Drugs Ther*. (2023). doi: 10.1007/s10557-023-07467-8

19. Kamat MA, Blackshaw JA, Young R, Surendran P, Burgess S, Danesh J, et al. PhenoScanner V2: an expanded tool for searching human genotype-phenotype associations. *Bioinf (Oxford England)*. (2019) 35:4851–3. doi: 10.1093/bioinformatics/btz469

20. Ferkingstad E, Sulem P, Atlason BA, Sveinbjornsson G, Magnusson MI, Styrmisdottir EL, et al. Large-scale integration of the plasma proteome with genetics and disease. *Nat Genet*. (2021) 53:1712–21. doi: 10.1038/s41588-021-00978-w

21. Wu Z, Yang KG, Lam TP, Cheng JCY, Zhu Z, Lee WY. Genetic insight into the putative causal proteins and druggable targets of osteoporosis: a large-scale proteome-wide mendelian randomization study. *Front Genet*. (2023) 14:1161817. doi: 10.3389/fgene.2023.1161817

22. Ahola-Olli AV, Würtz P, Havulinna AS, Aalto K, Pitkänen N, Lehtimäki T, et al. Genome-wide association study identifies 27 loci influencing concentrations of circulating cytokines and growth factors. *Am J Hum Genet*. (2017) 100:40–50. doi: 10.1016/j.ajhg.2016.11.007

23. Kalaoja M, Corbin LJ, Tan VY, Ahola-Olli AV, Havulinna AS, Santalahti K, et al. The role of inflammatory cytokines as intermediates in the pathway from increased adiposity to disease. *Obes (Silver Spring Md)*. (2021) 29:428–37. doi: 10.1002/oby.23060

24. Zhao JH, Stacey D, Eriksson N, Macdonald-Dunlop E, Hedman ÅK, Kalnapenkis A, et al. Genetics of circulating inflammatory proteins identifies drivers of immune-mediated disease risk and therapeutic targets. *Nat Immunol*. (2023) 24:1540–51. doi: 10.1038/s41590-023-01588-w

25. Agarwal K, Saikia P, Podder I. Metabolic syndrome and dyslipidemia in xanthelasma palpebrarum and associated risk–2 factors–A case-control study. *J Cosmetic Dermatol*. (2022) 21:7018–24. doi: 10.1111/jocd.15353

26. Yavorska OO, Burgess S. MendelianRandomization: an R package for performing Mendelian randomization analyses using summarized data. *Int J Epidemiol*. (2017) 46:1734–9. doi: 10.1093/ije/dyx034

27. Kurki MI, Karjalainen J, Palta P, Sipilä TP, Kristiansson K, Donner KM, et al. FinnGen provides genetic insights from a well-phenotyped isolated population. *Nature*. (2023) 613:508–18. doi: 10.1038/s41586-022-05473-8

28. Burgess S, Thompson SG. Mendelian randomization: methods for causal inference using genetic variants. (2021).

29. Agarwal K, Saikia P, Podder I. Metabolic syndrome and dyslipidemia in xanthelasma palpebrarum and associated risk-2 factors-A case-control study. *J Cosmet Dermatol*. (2022) 21:7018–24. doi: 10.1111/jocd.15353

30. Graham SE, Clarke SL, Wu KH, Kanoni S, Zajac GJM, Ramdas S, et al. The power of genetic diversity in genome-wide association studies of lipids. *Nature*. (2021) 600:675–9. doi: 10.1038/s41586-021-04064-3

31. Gimbrone MA Jr., García-Cardeña G. Endothelial cell dysfunction and the pathobiology of atherosclerosis. *Circ Res*. (2016) 118:620–36. doi: 10.1161/CIRCRESAHA.115.306301

32. Jaipersad AS, Lip GY, Silverman S, Shantsila E. The role of monocytes in angiogenesis and atherosclerosis. *J Am Coll Cardiol*. (2014) 63:1–11. doi: 10.1016/j.jacc.2013.09.019

33. Pankov R, Yamada KM. Fibronectin at a glance. *J Cell Sci*. (2002) 115:3861–3. doi: 10.1242/jcs.00059

34. Patten J, Wang K. Fibronectin in development and wound healing. *Adv Drug Deliv Rev*. (2021) 170:353–68. doi: 10.1016/j.addr.2020.09.005

35. Struyk AF, Canoll PD, Wolfgang MJ, Rosen CL, D'Eustachio P, Salzer JL. Cloning of neurotrimin defines a new subfamily of differentially expressed neural cell adhesion molecules. *J Neurosci*. (1995) 15:2141–56. doi: 10.1523/JNEUROSCI.15-03-02141.1995

36. Cao TH, Quinn PA, Sandhu JK, Voors AA, Lang CC, Parry HM, et al. Identification of novel biomarkers in plasma for prediction of treatment response in patients with heart failure. *Lancet*. (2015) 385 Suppl 1:S26. doi: 10.1016/S0140-6736(15)60341-5

37. McDonough CW, Warren HR, Jack JR, Motsinger-Reif AA, Armstrong ND, Bis JC, et al. Adverse cardiovascular outcomes and antihypertensive treatment: A genome-wide interaction meta-analysis in the international consortium for antihypertensive pharmacogenomics studies. *Clin Pharmacol Ther*. (2021) 110:723–32. doi: 10.1002/cpt.2355

38. Luukkonen TM, Pöyhönen M, Palotie A, Ellonen P, Lagström S, Lee JH, et al. A balanced translocation truncates Neurotrimin in a family with intracranial and thoracic aortic aneurysm. *J Med Genet*. (2012) 49:621–9. doi: 10.1136/jmedgenet-2012-100977

39. Garred P, Genster N, Pilely K, Bayarri-Olmos R, Rosbjerg A, Ma YJ, et al. A journey through the lectin pathway of complement-MBL and beyond. *Immunol Rev*. (2016) 274:74–97. doi: 10.1111/imr.12468

40. Garred P, Honoré C, Ma YJ, Munthe-Fog L, Hummelshøj T. MBL2, FCN1, FCN2 and FCN3-The genes behind the initiation of the lectin pathway of complement. *Mol Immunol*. (2009) 46:2737–44. doi: 10.1016/j.molimm.2009.05.005

41. Yan J, Zhou B, Li H, Guo L, Ye Q. Recent advances of GOLM1 in hepatocellular carcinoma. *Hepat Oncol*. (2020) 7:Hep22. doi: 10.2217/hep-2020-0006

42. Ye QH, Zhu WW, Zhang JB, Qin Y, Lu M, Lin GL, et al. GOLM1 modulates EGFR/RTK cell-surface recycling to drive hepatocellular carcinoma metastasis. *Cancer Cell*. (2016) 30:444–58. doi: 10.1016/j.ccell.2016.07.017

43. Chen J, Lin Z, Liu L, Zhang R, Geng Y, Fan M, et al. GOLM1 exacerbates CD8(+) T cell suppression in hepatocellular carcinoma by promoting exosomal PD-L1 transport into tumor-associated macrophages. *Signal Transduct Target Ther*. (2021) 6:397. doi: 10.1038/s41392-021-00784-0

44. Maas EJ, Wallingford CK, DeBortoli E, Smit DJ, Betz-Stablein B, Aoude LG, et al. GOLM1: expanding our understanding of melanoma susceptibility. *J Med Genet*. (2023) 60:835–7. doi: 10.1136/jmg-2023-109348

45. Pu Y, Song Y, Zhang M, Long C, Li J, Wang Y, et al. GOLM1 restricts colitis and colon tumorigenesis by ensuring Notch signaling equilibrium in intestinal homeostasis. *Signal Transduct Target Ther*. (2021) 6:148. doi: 10.1038/s41392-021-00535-1

46. Kousathanas A, Pairo-Castineira E, Rawlik K, Stuckey A, Odhams CA, Walker S, et al. Whole-genome sequencing reveals host factors underlying critical COVID-19. *Nature*. (2022) 607:97–103. doi: 10.1038/s41586-022-04576-6

47. Kim K, Brown EE, Choi CB, Alarcón-Riquelme ME, Kelly JA, Glenn SB, et al. Variation in the ICAM1-ICAM4-ICAM5 locus is associated with systemic lupus erythematosus susceptibility in multiple ancestries. *Ann Rheum Dis*. (2012) 71:1809–14. doi: 10.1136/annrheumdis-2011-201110

48. Chen G, Deutsch GH, Schulert GS, Zheng H, Jang S, Trapnell B, et al. Identification of distinct inflammatory programs and biomarkers in systemic juvenile idiopathic arthritis and related lung disease by serum proteome analysis. *Arthritis Rheumatol*. (2022) 74:1271–83. doi: 10.1002/art.42099

49. Pei YP, Wang YY, Liu D, Lei HY, Yang ZH, Zhang ZW, et al. ICAM5 as a novel target for treating cognitive impairment in fragile X syndrome. *J Neurosci*. (2020) 40:1355–65. doi: 10.1523/JNEUROSCI.2626-18.2019

50. Cheng K, Chen YS, Yue CX, Zhang SM, Pei YP, Cheng GR, et al. Calsyntenin-1 negatively regulates ICAM5 accumulation in postsynaptic membrane and influences dendritic spine maturation in a mouse model of fragile X syndrome. *Front Neurosci*. (2019) 13:1098. doi: 10.3389/fnins.2019.01098

51. Kass DA, Champion HC, Beavo JA. Phosphodiesterase type 5: expanding roles in cardiovascular regulation. *Circ Res*. (2007) 101:1084–95. doi: 10.1161/CIRCRESAHA.107.162511

52. Gebska MA, Stevenson BK, Hemnes AR, Bivalacqua TJ, Haile A, Hesketh GG, et al. Phosphodiesterase-5A (PDE5A) is localized to the endothelial caveolae and modulates NOS3 activity. *Cardiovasc Res*. (2011) 90:353–63. doi: 10.1093/cvr/cvq410

53. Dang TA, Kessler T, Wobst J, Wierer M, Braenne I, Strom TM, et al. Identification of a functional PDE5A variant at the chromosome 4q27 coronary artery disease locus in an extended myocardial infarction family. *Circulation*. (2021) 144:662–5. doi: 10.1161/CIRCULATIONAHA.120.052975

54. Zhang M, Kass DA. Phosphodiesterases and cardiac cGMP: evolving roles and controversies. *Trends Pharmacol Sci*. (2011) 32:360–5. doi: 10.1016/j.tips.2011.02.019

55. Kukreja RC. Phosphodiesterase-5 and retargeting of subcellular cGMP signaling during pathological hypertrophy. *Circulation.* (2012) 126:916–9. doi: 10.1161/CIRCULATIONAHA.112.124966

56. Horiuchi T, Tsukamoto H. Complement-targeted therapy: development of C5- and C5a-targeted inhibition. *Inflamm Regen.* (2016) 36:11. doi: 10.1186/s41232-016-0013-6

57. Mannes M, Dopler A, Zolk O, Lang SJ, Halbgebauer R, Höchsmann B, et al. Complement inhibition at the level of C3 or C5: mechanistic reasons for ongoing terminal pathway activity. *Blood.* (2021) 137:443–55. doi: 10.1182/blood.2020005959

58. Wang M, Guo J, Zhang L, Kuek V, Xu J, Zou J. Molecular structure, expression, and functional role of Clec11a in skeletal biology and cancers. *J Cell Physiol.* (2020) 235:6357–65. doi: 10.1002/jcp.29600

59. Hu Y, Zhang Y, Ni CY, Chen CY, Rao SS, Yin H, et al. Human umbilical cord mesenchymal stromal cells-derived extracellular vesicles exert potent bone protective effects by CLEC11A-mediated regulation of bone metabolism. *Theranostics.* (2020) 10:2293–308. doi: 10.7150/thno.39238

60. Wang L, Zhang YL, Lin QY, Liu Y, Guan XM, Ma XL, et al. CXCL1-CXCR2 axis mediates angiotensin II-induced cardiac hypertrophy and remodeling through regulation of monocyte infiltration. *Eur Heart J.* (2018) 39:1818–31. doi: 10.1093/eurheartj/ehy085

61. Mikolajczyk TP, Szczepaniak P, Vidler F, Maffia P, Graham GJ, Guzik TJ. Role of inflammatory chemokines in hypertension. *Pharmacol Ther*. (2021) 223:107799. doi: 10.1016/j.pharmthera.2020.107799

62. Anzai A, Shimoda M, Endo J, Kohno T, Katsumata Y, Matsuhashi T, et al. Adventitial CXCL1/G-CSF expression in response to acute aortic dissection triggers local neutrophil recruitment and activation leading to aortic rupture. *Circ Res.* (2015) 116:612–23. doi: 10.1161/CIRCRESAHA.116.304918

63. Zhou Z, Subramanian P, Sevilmis G, Globke B, Soehnlein O, Karshovska E, et al. Lipoprotein-derived lysophosphatidic acid promotes atherosclerosis by releasing CXCL1 from the endothelium. *Cell Metab*. (2011) 13:592–600. doi: 10.1016/j.cmet.2011.02.016

64. Ghafouri-Fard S, Shahir M, Taheri M, Salimi A. A review on the role of chemokines in the pathogenesis of systemic lupus erythematosus. *Cytokine.* (2021) 146:155640. doi: 10.1016/j.cyto.2021.155640

65. Pacheco-Lugo L, Sáenz-Garcia J, Navarro Quiroz E, González Torres H, Fang L, Díaz-Olmos Y, et al. Plasma cytokines as potential biomarkers of kidney damage in patients with systemic lupus erythematosus. *Lupus.* (2019) 28:34–43. doi: 10.1177/0961203318812679

66. Wu D, Zhou J, Bi H, Li L, Gao W, Huang M, et al. CCL11 as a potential diagnostic marker for asthma? *J asthma: Off J Assoc Care Asthma*. (2014) 51:847–54. doi: 10.3109/02770903.2014.917659

67. Ghafouri-Fard S, Honarmand K, Taheri M. A comprehensive review on the role of chemokines in the pathogenesis of multiple sclerosis. *Metab Brain Dis.* (2021) 36:375–406. doi: 10.1007/s11011-020-00648-6

68. Zhang H, Yang K, Chen F, Liu Q, Ni J, Cao W, et al. Role of the CCL2-CCR2 axis in cardiovascular disease: Pathogenesis and clinical implications. *Front Immunol.* (2022) 13:975367. doi: 10.3389/fimmu.2022.975367

69. Singh S, Anshita D, Ravichandiran V. MCP-1: Function, regulation, and involvement in disease. *Int Immunopharmacol.* (2021) 101:107598. doi: 10.1016/j.intimp.2021.107598

70. Mendez-Enriquez E, García-Zepeda EA. The multiple faces of CCL13 in immunity and inflammation. *Inflammopharmacology*. (2013) 21:397–406. doi: 10.1007/s10787-013-0177-5

71. Li LF, Dai F, Wang LL, Sun YT, Mei L, Ran Y, et al. CCL13 Hum diseases. *Front Immunol.* (2023) 14. doi: 10.3389/fimmu.2023.1176639

72. Kavoussi H, Ebrahimi A, Rezaei M, Ramezani M, Najafi B, Kavoussi R. Serum lipid profile and clinical characteristics of patients with xanthelasma palpebrarum. *Anais brasileiros dermatologia.* (2016) 91:468–71. doi: 10.1590/abd1806-4841.20164607

frontiers | Frontiers in Medicine

TYPE Review
PUBLISHED 28 March 2024
DOI 10.3389/fmed.2024.1335551



OPEN ACCESS

EDITED BY
Zhenghua Zhang,
Huashan Hospital, Fudan University, China

REVIEWED BY
Zlatko Kopecki,
University of South Australia, Australia
Francois Niyonsaba,
Juntendo University, Japan

*CORRESPONDENCE
Dongmei Shi
✉ shidongmei28@163.com

RECEIVED 09 November 2023
ACCEPTED 13 March 2024
PUBLISHED 28 March 2024

CITATION
Dong S, Li D and Shi D (2024) Skin barrier-inflammatory pathway is a driver of the psoriasis-atopic dermatitis transition. *Front. Med.* 11:1335551. doi: 10.3389/fmed.2024.1335551



# Skin barrier-inflammatory pathway is a driver of the psoriasis-atopic dermatitis transition

Sitan Dong[1], Dongmei Li[2] and Dongmei Shi[3]*

[1]College of Clinical Medicine, Jining Medical University, Jining, China, [2]Department of Microbiology and Immunology, Georgetown University Medical Center, Washington, DC, United States, [3]Department of Dermatology/Laboratory of Medical Mycology, Jining No.1 People's Hospital, Jining, China

As chronic inflammatory conditions driven by immune dysregulation are influenced by genetics and environment factors, psoriasis and atopic dermatitis (AD) have traditionally been considered to be distinct diseases characterized by different T cell responses. Psoriasis, associated with type 17 helper T (Th17)-mediated inflammation, presents as well-defined scaly plaques with minimal pruritus. AD, primarily linked to Th2-mediated inflammation, presents with poorly defined erythema, dry skin, and intense itching. However, psoriasis and AD may overlap or transition into one another spontaneously, independent of biological agent usage. Emerging evidence suggests that defects in skin barrier-related molecules interact with the polarization of T cells, which forms a skin barrier-inflammatory loop with them. This loop contributes to the chronicity of the primary disease or the transition between psoriasis and AD. This review aimed to elucidate the mechanisms underlying skin barrier defects in driving the overlap between psoriasis and AD. In this review, the importance of repairing the skin barrier was underscored, and the significance of tailoring biologic treatments based on individual immune status instead of solely adhering to the treatment guidelines for AD or psoriasis was emphasized.

KEYWORDS

**psoriasis, atopic dermatitis, overlap, skin barrier, tissue-resident memory T cell, antimicrobial peptides**

## 1 Introduction

Psoriasis and atopic dermatitis (AD) are two common chronic immune-inflammatory diseases, each marked by distinct clinical manifestations and immunological profiles. The acute phase of psoriasis typically results from activating type 17 helper T (Th17) cells and presents with well-defined erythematous scales accompanied by mild pruritus. The acute stage of AD commences with a Th2 cell-driven inflammatory response and elevated immunoglobulin E (IgE) levels, which leads to erythema with ill-defined borders and intense pruritus. Despite these contrasting presentations, some psoriasis patients exhibit AD-like symptoms, particularly during the acute phase. However, AD can manifest psoriasiform lichenified changes in its chronic stage (1, 2). This overlap between psoriasis and AD in clinical manifestations poses diagnostic challenges and impacts treatment decisions and clinical outcomes. Moreover, the clinical manifestations of these overlapping conditions can be influenced by various factors,

including the treatment regimens and immune status of individuals. Specifically, individuals with abnormalities in their skin barriers and immune responses may be more prone to exhibiting the overlapping symptoms of psoriasis and AD. The dynamic changes in local skin immunity can further contribute to the variability in clinical presentations.

Skin barriers encompass both physical and chemical components. Physical barriers are composed of keratinocytes (KCs), keratin, cornified cell envelope (CE), intercellular lipids, and skin connective structures, while chemical ones mainly comprise antimicrobial peptides (AMPs) and natural moisturizing factors (NMFs). Any impairment in these structures can predispose to a Th2 immune response.

The pathogenesis of AD and the subsequent "Atopic March" are attributed to a compromised skin barrier, which facilitates the increased penetration of external sensitized substances. The exposure of these heightened allergens triggers a systemic Th2 immune inflammation termed epithelial susceptibility (3). In addition, the interaction between Th2/Th17-related cytokines and skin structures or Kupffer cell (KC) cytokines establishes a cycle (loop) of skin barrier–inflammatory cytokine interactions. The coexistence of AD in psoriasis patients and vice versa (4–7) suggests the presence of shared pathogenic mechanisms driving the mutual conversion between the two diseases. This overlap is postulated to commence with Th2 inflammatory activation following the breakdown of the skin barrier due to genetic or other factors. In psoriasis, compromised skin barrier function may result from factors such as mechanical stimulation (intense scratching), a genetic mutation affecting epidermal barrier integrity, and the downregulation of barrier-related proteins because of dysregulated Th17-related cytokines (Supplementary Figure S1).

## 2 Keratin

Keratin, a cytoplasmic intermediate filament, serves as the primary structural protein of epidermal cells and ensures the integrity and resilience of the skin. Its proper expression orchestrated sequentially is fundamental for differentiating KCs across the various layers of the epidermis. Within the cytoplasm, keratin fibers typically aggregate into tension filaments and intricately weave a network structure. They are anchored to connective structures, such as desmosomes and half-desmosomes, and the extracellular matrix through transmembrane proteins, such as cadherins and integrins. These keratin networks interlink neighboring cells, which creates a cohesive framework. This unified structure not only shields the skin from external aggressors but also plays an important part in preserving the barrier function of the skin and safeguards against moisture loss and environmental insults.

### 2.1 Key keratins in psoriasis

As a fundamental structural protein in the epidermis, keratin10 (K10 or KRT10) plays a vital role in the hyperkeratosis and metabolic disorders of the skin. In psoriasis, various pathogenic mutations in *KRT10* have been identified in affected skin lesions, which indicates its involvement in the pathogenesis of psoriasis (8). Interestingly, the expression levels of K10 exhibit a negative correlation with the psoriasis area and severity index (PASI) (8). Moreover, therapeutic strategies that target the upregulation of K10 expression are promising in the management of psoriasis (9).

In response to skin barrier damage in healthy individuals, the expression of K1 and K10 is typically downregulated by differentiation-associated proteins, while that of K5 and K4 is upregulated by proliferative proteins. In addition, the expression of K6, K16, or K17, which is not normally expressed in KCs, is rapidly induced. Psoriasis patients often exhibit an "isomorphic reaction," where new lesions develop in areas of damaged skin. Intriguingly, the expression pattern of keratin genes in psoriasis lesions mirrors that of damaged skin in individuals without psoriasis (10, 11), which suggests that the overexpression of K6, K16, and K17 may contribute to the excessive proliferation of KCs within psoriasis lesions (10).

The presence of the K17–T cell–cytokine inflammatory loop in psoriasis lesions is implicated in the development and exacerbation of the condition via two distinct mechanisms. First, in this loop, KCs respond to external stimuli via various pattern recognitions (PRPs), factors, and cytokine receptors. This triggers downstream signaling pathways such as extracellular signal-regulated kinase (ERK) 1/2, protein 38 (p38), transcription factors such as signal transducer and activator of transcription 1 (STAT1), STAT3, and nuclear factor-E-2 correlation factor (Nrf2), and activator protein 1 (AP-1). The binding of these transcription factors to the K17 promoter results in the upregulated expression of K17. Concurrently, cytokines produced in the epidermis further activate the Nrf2 signaling pathway, which elevates the expression of K17 (12–15). Moreover, K17 can translocate to the nucleus, which induces the expression of cytokines such as interleukin (IL)-1β and chemokines, including C-X-C motif chemokine ligand (CXCL)-1, CXCL-10, CXCL-11, and chemokine ligand (CCL)-20. These molecules accelerate the differentiation of KCs and attract more T cells and neutrophils to psoriasis lesions, which contributes to disease progression.

Second, peptides derived from K17 exhibit molecular mimicry with the M protein of β-hemolytic *Streptococcus*. These peptides act as autoantigens, polarizing naive T cells into Th1, Th17, and Th22 cell subsets, which further promotes the development of psoriasis (16). The cytokines produced by these T cells, including interferon (IFN) -γ, IL-17A, IL-22, and tumor necrosis factor (TNF)-α, activate signaling pathways in KCs, which stimulates the expression of K17s and the proliferation of KCs. Thus, the K17–T cell–cytokine inflammatory loop plays a crucial role in the pathogenesis of psoriasis, with K17 serving as a central component of this loop (12, 16, 17). Furthermore, IL-22 may contribute to this loop by inhibiting the expression of K1 and K10 through activating STAT3 (18, 19).

### 2.2 Key keratins in AD

The involvement of the keratin-inflammatory cytokine pathway is also significant in the pathogenesis of AD. To be specific, K6 acts as an alarm protein in AD and triggers the generation of pro-inflammatory cytokines and AMPs. Variations in the *KRT6* gene have been associated with the onset, severity, progression, and outcomes of psoriasis and AD (10, 20), underscoring its importance in dermatological conditions. Damage to keratin proteins disrupts skin barrier integrity and initiates a subsequent Th2-type inflammatory response. In AD, Th2-related inflammatory cytokines such as IL-4 and

IL-13 downregulate the expression of key keratins such as K1 and K10, desmoglein (Dsg) 1, and desmocollin (Dsc) 1 (21). This dysregulation further exacerbates barrier dysfunction and helps perpetuate the inflammatory cascade characteristic of AD pathology.

## 2.3 Keratins for psoriasis–AD overlap

Psoriasis and AD may present distinct abnormalities in the keratin structure, but their shared consequence lies in disrupting the skin barrier. This disruption serves as a common pathway through which immune dysregulation occurs and potentially manifests as a Th2 immune disorder or a shift between Th17 and Th2 responses. Consequently, the compromised skin barrier exacerbates the chronic course and severity of psoriasis and AD individually and increases the likelihood of developing a psoriasis–AD overlap condition. In essence, the role of abnormal keratins in these dermatological conditions underlines the pivotal link between barrier integrity, immune dysregulation, and the clinical manifestations observed in patients with psoriasis, AD, and their overlap.

# 3 Cornified cell envelope

The cornified cell envelope (CE), a crucial component of the epidermis, is formed during the terminal differentiation of KCs. It consists of an insoluble tough outer membrane that forms the extensive cross-linking of various structural proteins and intercellular lipids. The CE comprises a complex network of cytoskeleton and keratin intermediate filament-related proteins. During the formation of the CE, keratin intermediate filaments and filaggrin (FLG) initially aggregate into bundles. After that, transglutaminase (TG)-1 catalyzes the connections among other structural proteins, including involucrin (IVL), loricrin (LOR), small proline-rich region proteins (SPRRs), trichohyalin, and late cornified envelope (LCE), as well as members of the S100 protein family (22–24). These interconnected proteins form a robust structural complex produced by KCs in the upper layers of the epidermis and serve as the foundation of the defense barrier of the skin.

Located at the q21.3 site on chromosome 1, the epidermal differentiation complex (EDC) encompasses a cluster of genes crucial for forming and maintaining the epidermal barrier. These genes can be categorized into three families. First, the KC envelope gene precursor family includes LOR, IVL, LCEs, and SPRRs. Second, the calcium-binding protein (S100) family contains EF-hand domains. Third, the fusion gene family is evolved from the above two, including FLG, Filaggrin-2 (FLG2), hornerin (HRNR), tripterygium hypoglaucum hutch (THH), trichohyalin-like-1 (TCHHL1), and cornulin (CRNN). The abnormal expression of any gene within the EDC, whether it encodes envelope structure proteins or enzymes involved in catalytic processes, can disrupt various differentiation stages of KCs. For instance, mutations in the FLG gene have been confirmed as a major predisposing factor for AD by triggering a Th2 immune response. Moreover, genes responsible for aggregating the keratinizing envelope within the EDC are also implicated in psoriasis (25). In psoriatic skin, a disruption in the formation of the cornified envelope (CE) could significantly compromise the barrier function of the skin (26), highlighting the importance of proper CE formation in maintaining skin health.

## 3.1 CE defects in psoriasis

In the past, it was widely believed that FLG plays a central pathogenic role in AD rather than psoriasis and psoriatic arthritis (27–30). However, the results obtained from recent studies challenge this notion, which suggests a broader role of FLG beyond AD condition and its potential association with psoriasis. For example, a study conducted in Taiwan revealed a high prevalence of the FLG P478S mutation among psoriatic patients (31). Additionally, the downregulated expression of FLG has been observed in some psoriasis patients even when identified FLG gene mutations are absent (29).

Moreover, caspase-14, a vital protease responsible for degrading FLG into NMFs, was shown to be downregulated in psoriatic hyperkeratotic skin lesions (32). The downregulation of caspase-14 indicates impaired FLG processing in psoriasis, which may contribute to the dysfunction of the skin barrier and exacerbate dry skin symptoms in psoriatic lesions. Similarly, an FLG-deficient mouse model exhibited skin inflammation dominated by Th17 responses (33). These findings collectively highlight the potential significance of FLG in psoriasis and underscore the need for further research into its role in the disease.

Mutations in six *LOR* genes have also been demonstrated in psoriasis (34), but their exact impact on the function of the CE remains unclear. Research on the LCE gene family has shown that LCE gene polymorphisms are associated with psoriasis (35, 36). The *LCE* gene family, composed of 18 members derived from *LCE1* to *LCE6*, is predominantly expressed in the skin and other keratinized epithelia. In particular, the deletion of LCE3B/C accounts for a significant proportion of psoriasis, akin to *FLG* mutations in AD (36–39). Unlike *FLG*, *LCE3B* and *LCE3C* show minimal expression in normal skin but are induced following skin damage, demonstrating their role in skin barrier repair. The inadequate post-injury repair of the skin barrier then leads to antigen penetration, which triggers toll-like receptors (TLRs) on Langerhans cell histiocytosis (LCH) or dendritic cells (DC) and subsequently activates Th17-mediated pathways involved in psoriasis (40). Further research should be conducted to examine the association of these proteins with the pathogenesis of psoriasis and AD.

CE component proteins such as FLG, LOR, and IVL are linked to Th1-, Th17-, and Th22-related cytokines. Specifically, the IL-17A-C/CAAT-enhancer-binding protein β (C/EBPB) pathway has been shown to upregulate *IVL* but downregulate *FLG* and *LOR* (41, 42). It has been found that IL-22 downregulates *FLG*, *LOR* (43), and *IVL* (42, 43) and also inhibits the expression of the EDC through the activation of the Janus kinase 1 (JAK1)-tyrosine kinase 2 (TYK2)-STAT3 pathway (43–47). Moreover, TNF-α is implicated in the downregulation of LOR expression (42). Interestingly, the level of LOR in psoriasis patients can be upregulated after using TNF-α antagonists. This suggests that TNF-α, a core pathogenic factor in psoriasis, may disrupt the skin barrier by downregulating LOR genes (48).

TG enzymes play a crucial role in maintaining the integrity of the skin barrier. TG1, TG3, and TG5 are primarily expressed in the epidermis and involved in the formation of the CE, while TG2 is predominantly expressed in the dermis and facilitates apoptosis and extracellular matrix formation. The expression levels of *TG1* and *TG2* in psoriasis patients are elevated compared to those in healthy individuals (49, 50) and positively correlated with levels of IL-6, CXCL8, and CCL20 (50). On the contrary, *TG3* is upregulated in psoriasis and acts as a protective factor by inhibiting the activation of

nuclear factor kappa-B (NF-κB) through the phosphorylated STAT3-ten-eleven translocase 3 (p-STAT3-TET3) pathway, which thereby reduces skin inflammation (51, 52). Collectively, these findings underscore the intricate involvement of CE component proteins in the pathogenesis of psoriasis and highlight their potential as therapeutic targets for managing skin barrier dysfunction and inflammation in psoriatic lesions.

## 3.2 CE defects in AD

In AD, *FLG* gene mutations or expression defects (3, 53) are considered a center factor in the "out-to-in" barrier pathogenesis observed in this condition (54–56). The resulting barrier defect gives rise to subsequent local and systemic Th2 immune responses, contributes to the early onset and persistence of AD (57, 58), and manifests as symptoms such as dry skin (59), eczema, and asthma (60, 61). Th2-related cytokines can further exacerbate barrier dysfunction by downregulating the expression of *FLG* (48, 62–66). For instance, IL-4 and IL-13 activate the JAK1/JAK2-STAT6/STAT3 pathway, which inhibits the expression of the *EDC* and downregulates *FLG*, *LOR,* and *IVL* (42). Furthermore, IL-13 triggers barrier dysfunction via the downregulation of the OVOL1-FLG axis and the upregulation of the periostin-IL-24 axis (67). The absence of LOR and IVL can further promote skin antigen penetration, increase atopic susceptibility, activate Th2 response, and perpetuate inflammatory loops.

Abnormal TG expression is also observed in AD patients, although the genetic variants of TG are not considered a significant factor in AD susceptibility (68). Instead, the abnormal expression of *TG2* is associated with eosinophilic bronchitis (EB), asthma, and other atopic diseases (69). Su et al. (68) showed that *TG1* and *TG3* messenger ribonucleic acid (mRNA) are significantly increased in the skin lesions of AD patients, which indicates that they are easily upregulated after inflammatory stimulation (68). However, conflicting results regarding *TG3* expression have been reported (70), with some studies suggesting a significant reduction in both AD and non-AD lesions. In AD, TG3 and tropomyosin (TMP) can activate the Th2 response (71), and specific IgE antibodies to TG3 and TMP have been detected. Currently, no correlation has been found between *LCE* gene mutation and atopic diseases (72, 73).

## 3.3 CE molecules in the psoriasis–AD overlap

In psoriasis–AD overlap, the cytokines associated with Th1, Th17, and Th22 responses in psoriasis are beneficial to downregulating the expression of *FLG*, *LOR,* and *IVL* (41–48). This downregulation of FLG activates the Th2 immune axis (3, 53–61), further exacerbating the inflammatory response. Additionally, the Th2 immune axis *per se* can also downregulate the expression of *FLG*, *LOR,* and *IVL* (42), which thus forms a feedback loop between the epidermal barrier and inflammatory factors. This dysregulation of both the epidermal barrier and immune response aggravates the disease condition and prolongs the chronic course of AD. This reciprocal regulation between T cells and the CE may represent a critical target for understanding the inter-transformation of psoriasis and AD, as well as the chronicity of psoriasis and AD.

# 4 Epidermal connection structure-related proteins

Epidermal connection structures, including tight junctions (TJs) and anchored connections such as desmosomes and half-desmosomes, are important to maintain the structural integrity and barrier function of the skin. Key proteins involved in these connection structures, such as claudins (CLDNs) and cadherins, are fundamental to their proper function. The aberrant expression of these proteins can disrupt barrier function, which leads to persistent inflammation and skin damage. This disruption ultimately contributes to the development of conditions such as AD and psoriasis and may facilitate their interconversion.

## 4.1 TJ: CLDN

As vital components of the skin barrier, TJs are predominantly located in the lateral membranes of granular KCs. Their main function lies in sealing KCs together, which prevents the entry of external antigens and microorganisms through the skin barrier. In addition, TJs also regulate substance transport, proliferation, and differentiation, as well as the polar secretion of lipids in epidermal cells. The structure integrity of TJs relies on a family of proteins known as CLDNs, which are encoded by *CLDN* genes. Numbered from CLDN1 to CLDN27 based on their order of discovery, CLDNs form the backbone of the TJ structure.

### 4.1.1 CLDNs in psoriasis

The expression levels of CLDN-1 and CLDN-7 are notably decreased in patients with psoriasis (74). As a member of the IL-1 cytokine family, IL-36γ is frequently over-expressed in psoriatic lesions, along with other IL-36 isomers. It has been identified that IL-36γ downregulates CLDN-1 and CLDN-7, which thereby compromises the integrity of TJs within the affected area and contributes to impaired skin barrier function (75). Additionally, the cytokines associated with the Th2/22 immune response are implicated in exerting negative effects on the expression of CLDN proteins (76).

### 4.1.2 CLDNs in AD

CLDN-1 and CLDN-4 are key components of the TJ of the epidermis, and their absence results in embryonic lethality owing to water loss and aberrant skin phenotypes (77). Mice lacking CLDN1 displayed severe impairment in skin barrier function and reduced *CLDN1* expression, which correlates with the activation of the Th2 immune pathway, elevated serum IgE levels, increased eosinophils (EOS), and heightened susceptibility to herpes simplex virus infection (78). In the context of AD, the decreased level of CLDN-1 induces the autonomous expression of IL-1β in KCs and promotes an epidermal inflammatory response upon exposure to non-pathogenic *Staphylococci*. Reversely, the increased level of CLDN-1 has been demonstrated to enhance barrier function and alleviate inflammation (79).

### 4.1.3 CLDNs in the psoriasis–AD overlap

Psoriasis and AD-associated cytokines have been observed to downregulate the expression of CLDNs, which disrupts the skin barrier (75, 76, 78). This dysregulation of CLDNs can lead to

compromised barrier integrity and accelerate the development of Th2-type inflammation, characteristic of AD. Consequently, CLDNs emerge as a critical component involved in both Th2 and IL-1β inflammatory pathways within the spectrum of psoriasis–AD overlap. This dual involvement of CLDNs underscores their potential significance in the pathogenesis of psoriasis–AD overlap, which indicates a mechanistic link between CLDN dysregulation and the convergence of these two dermatological conditions.

## 4.2 Anchored connections: CLDNs

### 4.2.1 CLDNs in psoriasis

CLDN proteins are vital for anchoring cellular connections, and their dysregulation is implicated in psoriasis pathogenesis. Specifically, several type I classical cadherins are associated with the development of psoriasis (80). In psoriasis vulgaris, the expression of E-cadherin, β-catenin, and T-cadherin is downregulated (81), whereas that of P-cadherin is upregulated (82). These changes may contribute to the excessive proliferation of KCs observed in psoriasis. The interaction between E-cadherin and integrin molecule αEβ7 (CD103) has been shown to aid the adhesion of lymphocytes to the skin epithelium. Abnormalities in this interaction can quicken the production of IL-17, leading to excessive epidermal hyperplasia and inflammatory leukocyte infiltration, thereby exacerbating psoriasis (83, 84). Furthermore, Dsg1, a critical component of desmosomes, is linked to psoriasis. Mice with the knocked-out *DSG1* gene exhibit the characteristics of an IL-17-skewed inflammatory signature. Current treatments that involve IL-12/23 antagonists have shown promising results in the improvement of psoriasis-related skin lesions (85).

### 4.2.2 Cadherins in AD

Cadherin defects are indeed observed in atopic dermatitis. Skin-derived group 2 innate lymphoid cells (ILC2) express skin-homing receptors and produce type 2 cytokines upon allergen infiltration through the skin. E-cadherin can inhibit the generation of type 2 cytokines (IL-4/IL-13) after ligating to ILC2. However, the downregulation of FLG, an important protein involved in maintaining the function of the skin barrier, results in that of E-cadherin. It is one of the important characteristics of AD. Consequently, the downregulation of E-cadherin caused by that of FLG leads to the loss of inhibition of ILC2 in AD patients, which increases the production of type 2 cytokines. As a result, E-cadherin is also important in the occurrence and development of AD (86–88). In addition, Th2 cytokine (IL-4) downregulates the expression of Dsg1 and reduces the number of desmosomes, which thereby compromises the integrity of the skin barrier (88).

### 4.2.3 Cadherins in the psoriasis–AD overlap

In the context of psoriasis–AD overlap, the downregulation of E/T-cadherin observed in psoriasis (80, 81) creates an environment conducive to producing Th2/Th17 inflammatory cytokines (83–88). These cytokines are pivotal in orchestrating the inflammatory response characteristic of both psoriasis and AD. To be specific, Th2 cytokines can downregulate the expression of Dsg1. The reduction in Dsg1 levels can lead to compromised barrier function and the skewness of subsequent inflammatory responses toward IL-17-skewed inflammation (85). Moreover, the dysregulation of cadherin expression may further perpetuate the inflammatory loop between psoriasis and AD. This interplay between multiple cadherins and inflammatory cytokines provides a potential mechanistic link for the overlap and interconversion of these two dermatological conditions.

# 5 Amps in psoriasis and AD

Chemical and physical barriers are essential components of cutaneous defense mechanisms. These barriers are primarily made up of AMPs, epidermal lipids, and NMFs (89). Among them, AMPs play a significant role in the chemical barrier of the skin. Apart from owing antimicrobial properties, AMPs are involved in various functions, including promoting cell migration, proliferation, and differentiation. They also modulate the expression of inflammatory factors and regulate the function of the skin barrier (90). In the skin, AMPs are primarily expressed constitutively or indelibly by stimuli such as microbial invasion or inflammation, KCs, and other cell types. Several key AMPs are found in human skin, including defensins, cathelicidin, ribonuclease 7 (RNase 7), psoriasin, and dermcidin (DCD). Studies have demonstrated that these AMPs involve the mechanisms underlying the development of psoriasis and AD (90).

## 5.1 Defensins

Defensins, a class of AMPs, are classified into three groups: α-defensins, β-defensins, and θ-defensins. Only α-defensins and β-defensins are expressed in humans (91). Human β-defensins (hBDs) 1–4 are expressed in leukocytes and epithelial cells (92). Despite the constitutive expression of hBD-1, hBD-2, and hBD-3, they are induced by factors such as skin barrier damage, microbial stimuli, and inflammation. Interestingly, hBD-2 is primarily resistant to Gram-negative bacteria, but hBD-3 demonstrates broad-spectrum antimicrobial activity against some microorganisms, including some multiple drug-resistant bacteria (93).

Immune disorders, barrier defects, and microbial invasion commonly found in psoriasis and AD can stimulate KCs, immune cells, and other cells to express excessive amounts of hBDs. These peptides function as antimicrobials, contribute to skin barrier repair, and modulate immune responses. Despite being elevated in the skin lesions of both psoriasis and AD patients, the expression levels of hBD-2 and hBD-3 are generally higher in psoriasis compared to AD (94). This disparity may explain why patients with AD are more prone to epidermal infections compared to those with psoriasis (95). Moreover, hBD-1 and hBD-3 are important in promoting the development and repair of TJs, crucial components of the physical barrier of the skin (96–98). In addition, hBD-3 can activate autophagy in KCs through the aryl hydrocarbon receptor (AhR) signaling pathway, which mitigates damage to the TJ barrier caused by IL-4 and IL-13 (99). It is believed that the defective expression of hBDs in AD, relative to psoriasis, is ascribed to the inhibition by Th2-type cytokines (100). Conversely, the upregulation of hBDs in psoriasis may be related to higher levels of IL-17, IL-22, and IFN-γ in the skin lesions of psoriasis patients (101). Furthermore, the modulation of T cell-mediated immune responses by hBDs enhances the generation of Th2 cytokines, IL-22, IFN-γ, and IL-10 while inhibiting the production of IL-17 (102, 103). As a result, hBDs may serve as a bridge for the

interplay between Th2/Th22 and Th1/Th17 immune responses. Agents targeting AMPs may have a potential impact on the overlap and transformation of psoriasis and AD.

## 5.2 Human cationic antimicrobial protein

Human cationic antimicrobial protein (hCAP) is among the earliest AMPs discovered in mammalian skin. Derived from hCAP, LL-37 is inducibly expressed in the presence of proteases (104) and present in different kinds of tissues and cells, including epithelial cells, KCs, and macrophages (105). Similar to other AMPs, hCAP is highly expressed when cells are stimulated by trauma, infection, or inflammation and acts as an antimicrobial agent and immunomodulator (106–109).

In psoriasis, LL-37 not only directly promotes the gene expression related to psoriasis (110) but also activates TLR7/8, which further enhances this gene expression. Additionally, it serves as a central player in the intricate interplay between various aspects of skin barriers, immunity, and autophagy. Its impact on the physical barrier of the skin and innate immunity involves a few mechanisms. For example, LL-37 forms complexes with self-deoxyribonucleic acid (DNA) released from apoptotic cells, which activates plasmacytoid dendritic cells (pDCs) via TLR9 and induces the production of interferon-α (IFN-α). Then, the increased level of IFN-α triggers the activation of myeloid DCs (mDCs) and T-cells, thereby promoting the inflammatory response and the development of skin lesions in psoriasis (111).

The second crucial function of LL-37 is to uphold the integrity of epidermal permeability and antimicrobial barriers. LL-37 is stored along with other AMPs, such as hBD-2, in epidermal lamellar bodies (LBs). The disruption of the permeability barrier leads to increased lipid synthesis and elevated mRNA and protein expression of LL-37 and hBD-2 homologs in mice. Conversely, the absence of hBD-2 delays the recovery of the permeability barrier, notwithstanding increased LL-37 expression, which indicates mutual regulation between epidermal permeability and antimicrobial barriers through AMPs (112). The modulation role of LL-37 in the skin's physical barrier results in the enhanced expression of TJ-related proteins, increased transepithelial resistance (TER), and reduced paracellular flux in the stratum corneum (SC). This process involves multiple signaling pathways and induces the expression of KC differentiation-specific proteins, which suggests that LL-37 contributes to maintaining the stability of the physical barrier while participating in cutaneous innate immunity (113). Moreover, studies have demonstrated that the restoration of the LL-37-mediated TJ barrier is associated with the activation of autophagy. In autophagy-deficient KCs and skin models, the TJ improvement induced by LL-37 was hindered, which suggests that LL-37 is capable of regulating the skin barrier by modulating autophagy (114).

In summary, the multifaceted roles of LL-37 highlight its significance in skin barrier function and immune modulation. Mast cell chemotaxis and IL-31 secretion are induced by hBDs and hCAP, which reveals their involvement in itch sensation, a common symptom in various skin diseases (115–117). Moreover, the upregulation of Th2-associated cytokines in the presence of hCAP indicates its role in promoting the inflammatory environment, potentially contributing to conditions such as psoriasis (118) and the overlap and transformation of psoriasis and AD. Considering these diverse functions, targeting LL-37 and related AMPs could provide therapeutic avenues for skin diseases featuring barrier dysfunction.

## 5.3 Psoriasin

Also known as S100A7, psoriasin plays a critical role in inflammatory cell chemotaxis, oxidative stress response, and the proliferation and differentiation of KCs. Expression levels of psoriasin are upregulated in the skin lesions of both psoriasis and AD (119–121).

Psoriasin production can be induced by an assortment of endogenous and exogenous factors and is involved in multiple signaling pathways, including AP-1, NF-κB, and STAT3. The activation of these pathways upregulates various pro-inflammatory cytokines, which directly or indirectly contribute to the pathogenesis of psoriasis and AD (122–125). In addition, several cytokines can induce the expression of S100A. IL-17, a crucial pro-inflammatory factor in psoriasis, is also important in both the acute and chronic phases of AD. IL-19, which enhances the action of IL-17A and induces IL-23, is part of the IL-23/IL-17 axis. It can also induce hBDs, which also cause the abnormal differentiation and proliferation of KCs (126). IL-1, IL-17, and IL-19 all upregulate the expression of S100A (126–128). IL-17 synergizes with IL-22 to induce the expression of S100A7, S100A8, and S100A9 (129). IL-36 also synergizes with IL-17A to induce the expression of S100A7 *in vitro* (130). In contrast to psoriasis-associated cytokines, however, Th2-associated cytokines, such as IL-4 and histamine, may hinder the expression of S100A7 in the skin (131, 132). Interestingly, Gittler et al. demonstrated an increase in S100A7, S100A8, and S100A9 genes, along with an increase in Th2/Th22 cytokines during the transition from the acute to the chronic stage of AD (129). Therefore, S100A may serve as a marker for the transition from the acute to chronic stage of AD. Additionally, chronic AD and psoriasis share overlapping immunologic and clinical features, which suggests that S100A may also play a pivotal role in psoriasis and AD.

Furthermore, akin to LL-37, S100A7 not only participates in innate immunity but also enhances the differentiation of KCs and increases the expression of epidermal differentiation markers. Similarly, it is beneficial to maintaining the stability of the skin barrier by regulating the expression of TJ-related proteins, a process modulated by glycogen synthase kinase 3 (GSK-3) and mitogen-activated protein kinase (MAPK) pathways (133). Similar to LL-37, S100A7 also serves as a crucial intersection of epidermal physical, immune, permeability, and antimicrobial barriers. The development of both psoriasis and AD involves multiple disruptions in the skin barrier and abnormalities in autophagy. Hence, AMPs such as LL-37 and S100A7 could present novel targets for treating these diseases characterized by skin barrier disorders in cases where it is challenging to distinguish between AD and psoriasis or when these conditions overlap. This approach could help avoid the direct use of potentially inappropriate immunosuppressive agents.

## 5.4 DCD

DCD, one of the AMPs with broad-spectrum activity, is produced by exocrine sweat glands and secreted onto the surface of the skin with sweat. It exerts its antimicrobial activity by inhibiting bacterial RNA

and protein expression (134). Unlike hBDs and hCAP, DCD secretion is not induced by skin injury or inflammation but rather regarded as a component of the innate defense of human skin (135). Abnormal levels of DCD are implicated in the pathogenesis of psoriasis and AD. The reduced expression of FLG leads to impaired sweat transport, which results in the accumulation of DCD in sweat glands and a decrease in sweat production (134). DCD-1 L stimulates the production of Th2 cytokines (IL-4, IL-13, and IL-31) and TNF-α by KCs (136). Moreover, it significantly upregulates the activation of NF-κB (137), a pathway involved in developing psoriasis. Furthermore, DCD-derived polypeptides such as DCD (86–103) activate mast cells and induce an inflammatory reaction, which thereby contributes to the occurrence and progression of psoriasis (138).

### 5.5 RNase7

RNase 7 is one of the primary AMPs secreted by KCs and acts as an alert protein in response to the disruption of the skin barrier. Its expression exhibits a significant elevation in the lesional skin of patients with AD or psoriasis compared to healthy individuals (139). RNase 7 promotes the recognition of self-DNA by plasmacytoid dendritic cells (pDCs) and facilitates their rapid sensing of bacterial DNA. Then, activated pDCs trigger a massive release of IFN-α (139). This mechanism aligns with the IFN-α expression induced by LL-37 and hBD-2/3 and is amplified by RNase 7 (140). Notably, pDCs and IFN-α are not only of importance to combat infections but also drive the initiation and progression of psoriasis and AD (141, 142). Furthermore, IL-17A and IFN-γ induce the expression of RNase 7 in KCs synergistically via STAT3 (143). Moreover, RNase7 downregulates Th2 cytokines (IL-4, IL-5, and IL-13) through the activation of GATA binding protein 3 (GATA3) (144). The protective role of RNase7 in AD appears to be well-established, although further studies are needed to fully understand its function.

## 6 Flightless I in psoriasis and AD

Flightless I (Flii), as a member of the gelsolin superfamily of proteins, is involved in various biological processes, including embryonic development, skin barrier repair, signaling, autophagy, and cancer onset and development. Emerging evidence shows that Flii is also significant in developing AD and psoriasis.

Skin barrier damage leads to the continuous invasion of allergens, which triggers immune activation and the development of immune-inflammatory skin diseases. Flii proteins act as negative regulators in the repair of skin barrier damage. With the over-expression of Flii in mice, the formation of hemidesmosomes is impaired, which affects the adhesion and migration of KCs (145). The over-expression of Flii in embryos decreases the expression of CLDN-1 and zonula occludens-2 (ZO-2), which are proteins associated with TJs (146). Despite being identified as a negative regulator of skin barrier repair, the exact mechanism by which Flii operates remains unclear and requires further investigation.

Elevated Flii expression has been observed in the skin lesions of patients with psoriasis. It has been shown that the use of neutralizing antibodies against Flii attenuates the inflammatory response induced by imiquimod in psoriasis mice (147). Regarding the fundamental role of the TLR4-NF-κB pathway in the pathogenesis of psoriasis (148), Flii may interfere with the binding of TLR4 to myeloid differentiation primary response protein 88 (MyD88), which thereby inhibits the NF-κB pathway (149). Resultantly, this leads to a reduction in the release of downstream inflammatory factors and a decrease in psoriasis symptoms.

In an ovalbumin (OVA)-induced mouse model of AD, the over-expression of Flii results in a Th2-skewed response that exacerbates the inflammatory response. Conversely, Flii heterozygous knockout mice exhibit significant Th1 immunoreactivity and reduced severity of AD and tissue inflammation (150). It was hypothesized in this study that Flii serves as a target protein contributing to the transition and overlap of psoriasis and AD. In psoriasis patients with epidermal over-expressing Flii, the disruption of the skin barrier promotes Th2 activation, which potentially causes the transition from psoriasis to AD. Further investigation into the intrinsic mechanism of the interaction between Flii and Th cells can provide valuable insights, which may represent a potential therapeutic target for skin inflammatory diseases featuring skin barrier dysfunction.

## 7 Autophagy in psoriasis and AD

Also called type II programmed cell death, autophagy is a cellular process in which damaged or aged macromolecules and organelles are degraded by lysosomal enzymes for self-digestion when cells are under external stress (151). It is a normal physiological process in the differentiation of KCs, regulating the inflammatory response and repairing the epidermal barrier (152). Nevertheless, the dysregulation of autophagy of KCs is also involved in the pathogenesis of psoriasis, AD, and other autoimmune skin diseases (153). Defective autophagy affects the differentiation of KCs, disrupts the skin barrier, and triggers inflammation, which leads to the increased production of inflammatory factors (154). Of note, a moisturizer with strong autophagy-stimulating properties has shown promising results in improving skin barrier function and alleviating itching in AD patients by promoting skin barrier restoration and inflammation control (155).

IL-17A, a key player in AD and psoriasis pathogenesis, negatively regulates autophagy and promotes inflammatory responses. KCs stimulated by IL-17 activate the phosphatidylinositol-3-hydroxy kinase (PI3K)/protein kinase B (AKT)/mammalian target of rapamycin (mTOR) signaling pathway, which inhibits the formation of autophagic vesicles and enhances autophagic flux, thereby suppressing autophagy while promoting cholesterol degradation (156, 157). Additionally, cis-Khellactone, an inhibitor of pro-inflammatory macrophages, promotes autophagy, reduces the infiltration of dermal macrophages in psoriasis, and markedly inhibits the production of IL-17A by Th17 cells (158). Thus, the inhibition of IL-17A may represent a potential therapeutic strategy for psoriasis and psoriasis-associated dyslipidemia by alleviating autophagy inhibition. Furthermore, metformin, a medicine commonly used to treat diabetes, has been shown to convert Th17 to Treg through enhanced autophagy (159). By reducing the number of Th17 cells and increasing that of Treg cells, metformin effectively enhances autophagy and may offer a therapeutic benefit to Th17-mediated psoriasis. Furthermore, KCs stimulated by a combination of psoriasis-associated cytokines (TNF-α, IL-1A, IL-17A, IL-22, and oncostatin M) activate autophagic

flux, which leads to recurrent psoriasis inflammation and increased skin barrier damage (157).

It has been shown that TNF-α, an important pro-inflammatory cytokine implicated in the pathogenesis of psoriasis, enhances the initiation of autophagosome formation but impairs subsequent processing, which leads to a negative impact on autophagy (160). In TNF-α-stimulated human immortal keratinocyte line (HaCaT) cells, the inhibitor of the wingless (Wnt)/β-catenin signaling pathway mitigates the pro-inflammatory and anti-autophagic effects of granulin precursor (PGRN) small interfering RNA (siRNA) (161). Moreover, both the number and activity of lysosomal components, including histone proteases D and L, were significantly reduced in KCs stimulated with TNF-α, which indicated impaired autophagy in AD and psoriasis (162, 163).

The protein sequestosome 1 (P62/SQSTM1), which acts as a selective autophagy receptor and a signaling hub, activates multiple inflammatory signaling pathways such as NF-κB and Nrf2 (160). The direct interaction between p62 and light chain (LC3) via the LC3-interacting region (LIR) domain facilitates the delivery of ubiquitinated protein aggregates to autophagic vesicles for selective autophagy (164). Increased p62 expression can upregulate various inflammatory signaling pathways associated with psoriasis and AD. In the TLR-NF-κB signaling pathway, the activation of TLR2/6 and TLR4 induces the autophagy pathway in human primary KCs and upregulates p62 expression (165). MyD88 and tumor necrosis factor receptor superfamily (TNFR)-associated factor 6, which are key signaling factors mediating TLR activation, play a critical role in autophagy development and p62 expression. Significant in the development of psoriasis and AD, Flii proteins hinder MyD88 binding to TLR4, which thus inhibits the TLR4-NF-κB pathway and cellular autophagy. Flii also disrupts selective autophagy by blocking the binding of p62 and LC3, thereby promoting the development of psoriasis and AD (166). The silencing of P62 results in the decreased expression of cytokines and AMPs in KCs, reduces NF-κB activity and decreases cell proliferation (165). In addition, the knockout of the AP1S3 gene associated with autophagosome formation leads to defective autophagy, increased p62 accumulation, and enhanced inflammation mediated by NF-κB and Nrf2 signaling pathways (167). Furthermore, the inactivation of the MAPK family in psoriasis decreases the autophagy of KCs, which correlates positively with the severity of psoriasis in patients and mouse models (168, 169). However, increased autophagy in KCs also results in the rapid degradation of proteins, including antigen proteins, despite exacerbating psoriasis and AD. This leads to increased recognition and presentation, which activates T helper cells (160). Moreover, the direct stimulation of the TCR enhances autophagy (170). Therefore, enhanced autophagy may promote T-cell survival and inflammatory responses, exacerbating psoriasis and AD.

Autophagy shares a common mechanism of action in psoriasis and AD, which signifies that abnormal cellular autophagy might play a significant role in the overlap, conversion, and development of psoriasis and AD. However, several questions remain unanswered, including whether autophagy promotes or attenuates skin inflammatory diseases, the pathways or mechanisms through which autophagy interacts with multiple immunoinflammatory factors, and how autophagy selectively promotes specific types of T cell differentiation. Controlling cellular autophagy could be a possible target for AD and psoriasis treatment.

## 8 Tissue-resident memory T cells and skin barrier interactions in psoriasis and AD

The recurrence of psoriasis and AD poses a significant challenge in treatment. It is currently proposed that the mechanism underlying the relapse of these conditions is closely related to the presence of tissue-resident memory T (TRM) within the skin barrier (171, 172). TRM leaves an "immune memory" in the skin even after the subsidence of inflammation (172). Upon the invasion of pathogens, initial T cells differentiate into effector and memory T cells, the latter of which is further classified into central memory T cells (TCM), effector memory T cells (TEM), and TRM (173). The residency and longevity of TRM within the skin are influenced by the interaction and regulation with KCs, fibroblasts, and other skin structural cells in the skin.

Unlike circulating T cells, TRM cannot migrate through the bloodstream and instead reside within skin tissues. This is primarily due to the binding of TRM to various ligands on the surface of KCs and its adherence to different structures within the skin barrier. TRM expresses specific markers such as CD69, CD103, and CD49a. CD103, the α chain of integrin αEβ7, binds to KC E-cadherin, which facilitates the adhesion of TRM to the epidermis and allows the residency of TRM in the skin (174). CD69 also contributes to the residency of TRM by downregulating the lymphoid tissue emigration pathway mediated by sphingosine-1-phosphate reporter 1 (S1PR1). CD49a binds to type IV collagen and mediates TRM residence within the basement membrane (175). In addition, the chemokine receptor 6 (CXCR6) C-X-C motif is expressed on human skin TRM cells, while its ligand CXCR16 is expressed on KCs, which enables the retention of TRM cells in the skin (176, 177). TRM cells are influenced by the epithelial immune microenvironment created by KCs and, in turn, activate and influence KCs. $CD49^{-}CD103^{+}CD8^{+}$ TRM cells mediating KC activation and epidermal proliferation promote the production of chemokines and AMPs, which leads to inflammation and relapse in psoriasis (178).

While substantial evidence shows that DCs and TRM cells such as Th2/Tc2, Th22/Tc22, and Th17/Tc17 are present in large numbers in lesions after the subsidence of inflammation in AD, their specific mechanisms in the recurrence of AD require further investigation (179). Moreover, TRM can persist in skin tissues for months to years and is primarily regulated by the local microenvironment (IL-7, IL-15, and transforming growth factor-β) generated by KCs and fibroblasts (180, 181). To sum up, the interaction between TRM cells and the skin barrier plays a key role in the recurrence of psoriasis and AD (Supplementary Figure S2).

## 9 Acute and chronic phases of psoriasis and AD with their overlap and interconversion

Typically, AD has been viewed as a Th2-driven immune-inflammatory disorder. However, emerging evidence indicates that AD involves activating multiple T-cell axes at different stages. During the chronic phase of AD, clinical and pathological features converge with psoriasis, which is attributed to the infiltration of similar subpopulations of Th cells. According to recent findings, the

heightened activation of Th2/Th22 occurs during the acute phase of AD, while the activation of Th1/Th17 progressively increases during the chronic phase (182). It is important to note that the transition from the acute to the chronic stage involves the persistent activation of Th2/Th22 and Th1/Th17 rather than a shift from Th2/Th22 to Th1/Th17 (129, 182, 183) (Supplementary Figure S3). Although the level of IL-17-producing cells is slightly higher in psoriasis patients than in those with severe AD, the difference shows no statistical significance (182). The presence of Th1/Th17 cells in chronic AD suggests a shared effector pathway with psoriasis, contributing to some of their clinical features and pathological similarities.

Interestingly, disorders affecting skin barrier-related factors have been reported to influence the polarity of Th cells. For instance, abnormalities in FLG may lead to Th2 polarity (57), whereas those in Dsg 1 may result in Th17 polarity (85). Consequently, variations in skin barrier impairments or disease during the development of psoriasis and AD can result in shifts in the dominance of Th cells and perpetuate a vicious cycle of skin barrier damage and inflammation. Clinically, this manifests as transformation, overlap, or exacerbation between psoriasis and AD. Future studies could investigate the impact of skin barrier-related factors and impairments in psoriasis and AD on aspects such as the rate and extent of transition between acute and chronic phases. Moreover, exploring whether biologics can be tailored based solely on immunologic type and the impact of Th1 and Th17 activation in the chronic phase of AD warrants investigation.

## 10 Conclusion

Skin barrier damage plays a crucial role in driving the progression of the spectrum of psoriasis/AD. Both psoriasis and AD involve skin barrier-inflammatory loops, contributing to disease exacerbation, overlap, and transformation. Various barrier factors, including keratin, CE, intercellular lipids, skin connective structure, and AMPs, participate in these inflammatory loops. It is speculated that the transition and overlap between psoriasis and AD are mediated through these skin barrier factors. Moreover, targeting skin barrier-associated factors may offer a more effective approach to modulating disease progression and transformation than solely focusing on inflammatory cytokines and signaling pathways. In the future, drugs targeting these skin barrier-associated factors could serve as upstream therapeutic targets to disrupt the barrier-inflammatory loop and attenuate disease progression and transformation. Importantly, it is proposed that psoriasis and AD inherently belong to the same disease spectrum. Their differences in clinical features are attributable to the predominance of T-cell axis activation under the influence of numerous factors. Hence, future treatments of psoriasis, AD, and overlapping psoriasis–AD conditions may directly target the immune activation state to select appropriate drugs and treatment modalities.

## Author contributions

SD: Writing – original draft. DL: Writing – review & editing. DS: Writing – review & editing.

## Funding

The author(s) declare financial support was received for the research, authorship, and/or publication of this article. This study was partly supported by grants from the National Natural Science Foundation of China (NM 82272358), the Traditional Chinese Medicine Science and Technology Program of Shandong Province (NM 2021 M080), and the Key R&D Program of Jining (NM 2023YXNS001).

## Conflict of interest

The authors declare that the research was conducted in the absence of any commercial or financial relationships that could be construed as a potential conflict of interest.

## Publisher's note



## Supplementary material

The Supplementary material for this article can be found online at: https://www.frontiersin.org/articles/10.3389/fmed.2024.1335551/full#supplementary-material

## References

1. Noda S, Suárez-Fariñas M, Ungar B, Kim SJ, de Guzman Strong C, Xu H, et al. The Asian atopic dermatitis phenotype combines features of atopic dermatitis and psoriasis with increased TH17 polarization. *J Allergy Clin Immunol*. (2015) 136:1254–64. doi: 10.1016/j.jaci.2015.08.015

2. Tokura Y, Hayano S. Subtypes of atopic dermatitis: from phenotype to endotype. *Allergol Int*. (2022) 71:14–24. doi: 10.1016/j.alit.2021.07.003

3. Dainichi T, Kitoh A, Otsuka A, Nakajima S, Nomura T, Kaplan DH, et al. The epithelial immune microenvironment (EIME) in atopic dermatitis and psoriasis. *Nat Immunol*. (2018) 19:1286–98. doi: 10.1038/s41590-018-0256-2

4. Kapila S, Hong E, Fischer G. A comparative study of childhood psoriasis and atopic dermatitis and greater understanding of the overlapping condition, psoriasis-dermatitis. *Australas J Dermatol*. (2012) 53:98–105. doi: 10.1111/j.1440-0960.2012.00878.x

5. Bozek A, Zajac M, Krupka M. Atopic dermatitis and psoriasis as overlapping syndromes. *Mediat Inflamm*. (2020) 2020:7527859. doi: 10.1155/2020/7527859. eCollection 2020

6. Barry K, Zancanaro P, Casseres R, Abdat R, Dumont N, Rosmarin D. Concomitant atopic dermatitis and psoriasis - a retrospective review. *J Dermatolog Treat*. (2021) 32:716–20. doi: 10.1080/09546634.2019.1702147

7. Schäbitz A, Eyerich K, Garzorz-Stark N. So close, and yet so far away: the dichotomy of the specific immune response and inflammation in psoriasis and atopic dermatitis. *J Intern Med*. (2021) 290:27–39. doi: 10.1111/joim.13235

8. Elango T, Sun J, Zhu C, Zhou F, Zhang Y, Sun L, et al. Mutational analysis of epidermal and hyperproliferative type I keratins in mild and moderate psoriasis vulgaris patients: a possible role in the pathogenesis of psoriasis along with disease severity. *Hum Genomics*. (2018) 12:27. doi: 10.1186/s40246-018-0158-2

9. Gao L, Dou J, Zhang B, Zeng J, Cheng Q, Lei L, et al. Ozone therapy promotes the differentiation of basal keratinocytes via increasing Tp63-mediated transcription of KRT10 to improve psoriasis. *J Cell Mol Med*. (2020) 24:4819–29. doi: 10.1111/jcmm.15160

10. Zhang X, Yin M, Zhang LJ. Keratin 6, 16 and 17-critical barrier Alarmin molecules in skin wounds and psoriasis. *Cells*. (2019) 8:807. doi: 10.3390/cells8080807

11. Yang L, Fan X, Cui T, Dang E, Wang G. Nrf2 promotes keratinocyte proliferation in psoriasis through up-regulation of keratin 6, keratin 16, and keratin 17. *J Invest Dermatol*. (2017) 137:2168–76. doi: 10.1016/j.jid.2017.05.015

12. Yang L, Jin L, Ke Y, Fan X, Zhang T, Zhang C, et al. E3 ligase Trim21 Ubiquitylates and stabilizes keratin 17 to induce STAT3 activation in psoriasis. *J Invest Dermatol*. (2018) 138:2568–77. doi: 10.1016/j.jid.2018.05.016

13. Zhang J, Li X, Wei J, Chen H, Lu Y, Li L, et al. Gallic acid inhibits the expression of keratin 16 and keratin 17 through Nrf2 in psoriasis-like skin disease. *Int Immunopharmacol*. (2018) 65:84–95. doi: 10.1016/j.intimp.2018.09.048

14. Jiang M, Li B, Zhang J, Hu L, Dang E, Wang G. Vascular endothelial growth factor driving aberrant keratin expression pattern contributes to the pathogenesis of psoriasis. *Exp Cell Res*. (2017) 360:310–9. doi: 10.1016/j.yexcr.2017.09.021

15. Lin Y, Zhang W, Li B, Wang G. Keratin 17 in psoriasis: current understanding and future perspectives. *Semin Cell Dev Biol*. (2022) 128:112–9. doi: 10.1016/j.semcdb.2021.06.018

16. Jin L, Wang G. Keratin 17: a critical player in the pathogenesis of psoriasis. *Med Res Rev*. (2014) 34:438–54. doi: 10.1002/med.21291

17. Fu M, Wang G. Keratin 17 as a therapeutic target for the treatment of psoriasis. *J Dermatol Sci*. (2012) 67:161–5. doi: 10.1016/j.jdermsci.2012.06.008

18. Depianto D, Kerns ML, Dlugosz AA, Coulombe PA. Keratin 17 promotes epithelial proliferation and tumor growth by polarizing the immune response in skin. *Nat Genet*. (2010) 42:910–4. doi: 10.1038/ng.665

19. Xiao CY, Zhu ZL, Zhang C, Fu M, Qiao HJ, Wang G, et al. Small interfering RNA targeting of keratin 17 reduces inflammation in imiquimod-induced psoriasis-like dermatitis. *Chin Med J*. (2020) 133:2910–8. doi: 10.1097/CM9.0000000000001197

20. Zhu AY, Mitra N, Margolis DJ. Longitudinal association of atopic dermatitis progression and keratin 6A. *Sci Rep*. (2022) 12:13629. doi: 10.1038/s41598-022-17946-x

21. Totsuka A, Omori-Miyake M, Kawashima M, Yagi J, Tsunemi Y. Expression of keratin 1, keratin 10, desmoglein 1 and desmocollin 1 in the epidermis: possible downregulation by interleukin-4 and interleukin-13 in atopic dermatitis. *Eur J Dermatol*. (2017) 27:247–53. doi: 10.1684/ejd.2017.2985

22. Kypriotou M, Huber M, Hohl D. The human epidermal differentiation complex: cornified envelope precursors, S100 proteins and the 'fused genes' family. *Exp Dermatol*. (2012) 21:643–9. doi: 10.1111/j.1600-0625.2012.01472.x

23. Uberoi A, Bartow-McKenney C, Zheng Q, Flowers L, Campbell A, Knight SAB, et al. Commensal microbiota regulates skin barrier function and repair via signaling through the aryl hydrocarbon receptor. *Cell Host Microbe*. (2021) 29:1235–1248.e8. doi: 10.1016/j.chom.2021.05.011

24. Karim N, Phinney BS, Salemi M, Wu PW, Naeem M, Rice RH. Human stratum corneum proteomics reveals cross-linking of a broad spectrum of proteins in cornified envelopes. *Exp Dermatol*. (2019) 28:618–22. doi: 10.1111/exd.13925

25. Qin D, Ma L, Qin L. Potential role of the epidermal differentiation complex in the pathogenesis of psoriasis. *Front Biosci*. (2022) 27:325. doi: 10.31083/j.fbl2712325

26. Candi E, Schmidt R, Melino G. The cornified envelope: a model of cell death in the skin. *Nat Rev Mol Cell Biol*. (2005) 6:328–40. doi: 10.1038/nrm1619

27. Henderson J, Northstone K, Lee SP, Liao H, Zhao Y, Pembrey M, et al. The burden of disease associated with filaggrin mutations: a population-based, longitudinal birth cohort study. *J Allergy Clin Immunol*. (2008) 121:872–7.e9. doi: 10.1016/j.jaci.2008.01.026

28. Lerbaek A, Bisgaard H, Agner T, Ohm Kyvik K, Palmer CN, Menné T. Filaggrin null alleles are not associated with hand eczema or contact allergy. *Br J Dermatol*. (2007) 157:1199–204. doi: 10.1111/j.1365-2133.2007.08252.x

29. Hüffmeier U, Traupe H, Oji V, Lascorz J, Ständer M, Lohmann J, et al. Loss-of-function variants of the filaggrin gene are not major susceptibility factors for psoriasis vulgaris or psoriatic arthritis in German patients. *J Invest Dermatol*. (2007) 127:1367–70. doi: 10.1038/sj.jid.5700720

30. Winge MC, Suneson J, Lysell J, Nikamo P, Liedén A, Nordenskjöld M, et al. Lack of association between filaggrin gene mutations and onset of psoriasis in childhood. *J Eur Acad Dermatol Venereol*. (2013) 27:e124–7. doi: 10.1111/j.1468-3083.2011.04403.x

31. Chang YC, Wu WM, Chen CH, Hu CF, Hsu LA. Association between P478S polymorphism of the filaggrin gene and risk of psoriasis in a Chinese population in Taiwan. *Arch Dermatol Res*. (2008) 300:133–7. doi: 10.1007/s00403-007-0821-2

32. Hoste E, Denecker G, Gilbert B, van Nieuwerburgh F, van der Fits L, Asselbergh B, et al. Caspase-14-deficient mice are more prone to the development of parakeratosis. *J Invest Dermatol*. (2013) 133:742–50. doi: 10.1038/jid.2012.350

33. Oyoshi MK, Murphy GF, Geha RS. Filaggrin-deficient mice exhibit TH17-dominated skin inflammation and permissiveness to epicutaneous sensitization with protein antigen. *J Allergy Clin Immunol*. (2009) 124:485–493.e1. doi: 10.1016/j.jaci.2009.05.042

34. Giardina E, Capon F, de Rosa MC, Mango R, Zambruno G, Orecchia A, et al. Characterization of the loricrin (LOR) gene as a positional candidate for the PSORS4 psoriasis susceptibility locus. *Ann Hum Genet*. (2004) 68:639–45. doi: 10.1046/j.1529-8817.2004.00118.x

35. Zhang XJ, Huang W, Yang S, Sun LD, Zhang FY, Zhu QX, et al. Psoriasis genome-wide association study identifies susceptibility variants within LCE gene cluster at 1q21. *Nat Genet*. (2009) 41:205–10. doi: 10.1038/ng.310

36. Sun L, Cao Y, He N, Han J, Hai R, Arlud S, et al. Association between LCE gene polymorphisms and psoriasis vulgaris among Mongolians from Inner Mongolia. *Arch Dermatol Res*. (2018) 310:321–7. doi: 10.1007/s00403-018-1813-0

37. Niehues H, van Vlijmen-Willems IM, Bergboer JG, Kersten FFJ, Narita M, Hendriks WJAJ, et al. Late cornified envelope (LCE) proteins: distinct expression patterns of LCE2 and LCE3 members suggest nonredundant roles in human epidermis and other epithelia. *Br J Dermatol*. (2016) 174:795–802. doi: 10.1111/bjd.14284

38. de Cid R, Riveira-Munoz E, Zeeuwen PL, Robarge J, Liao W, Dannhauser EN, et al. Deletion of the late cornified envelope LCE3B and LCE3C genes as a susceptibility factor for psoriasis. *Nat Genet*. (2009) 41:211–5. doi: 10.1038/ng.313

39. Karrys A, Rady I, Chamcheu RN, Sabir M, Mallick S, Chamcheu J, et al. Bioactive dietary VDR ligands regulate genes encoding biomarkers of skin repair that are associated with risk for psoriasis. *Nutrients*. (2018) 10:174. doi: 10.3390/nu10020174

40. Bergboer J, Zeeuwen P, Schalkwijk J. Genetics of psoriasis: evidence for epistatic interaction between skin barrier abnormalities and immune deviation. *J Invest Dermatol*. (2012) 132:2320–31. doi: 10.1038/jid.2012.167

41. Gutowska-Owsiak D, Schaupp AL, Salimi M, Selvakumar TA, McPherson T, Taylor S, et al. IL-17 downregulates filaggrin and affects keratinocyte expression of genes associated with cellular adhesion. *Exp Dermatol*. (2012) 21:104–10. doi: 10.1111/j.1600-0625.2011.01412.x

42. Furue M. Regulation of Filaggrin, Loricrin, and Involucrin by IL-4, IL-13, IL-17A, IL-22, AHR, and NRF2: pathogenic implications in atopic dermatitis. *Int J Mol Sci*. (2020) 21:5382. doi: 10.3390/ijms21155382

43. Noh M, Yeo H, Ko J, Kim HK, Lee CH. MAP17 is associated with the T-helper cell cytokine-induced down-regulation of filaggrin transcription in human keratinocytes. *Exp Dermatol*. (2010) 19:355–62. doi: 10.1111/j.1600-0625.2009.00902.x

44. Boniface K, Bernard FX, Garcia M, Gurney AL, Lecron JC, Morel F. IL-22 inhibits epidermal differentiation and induces proinflammatory gene expression and migration of human keratinocytes. *J Immunol*. (2005) 174:3695–702. doi: 10.4049/jimmunol.174.6.3695

45. Nograles KE, Zaba LC, Guttman-Yassky E, Fuentes-Duculan J, Suárez-Fariñas M, Cardinale I, et al. Th17 cytokines interleukin (IL)-17 and IL-22 modulate distinct inflammatory and keratinocyte-response pathways. *Br J Dermatol*. (2008) 159:1092–102. doi: 10.1111/j.1365-2133.2008.08769.x

46. Jin SH, Choi D, Chun YJ, Noh M. Keratinocyte-derived IL-24 plays a role in the positive feedback regulation of epidermal inflammation in response to environmental and endogenous toxic stressors. *Toxicol Appl Pharmacol*. (2014) 280:199–206. doi: 10.1016/j.taap.2014.08.019

47. Gutowska-Owsiak D, Schaupp AL, Salimi M, Taylor S, Ogg GS. Interleukin-22 downregulates filaggrin expression and affects expression of profilaggrin processing enzymes. *Br J Dermatol*. (2011) 165:492–8. doi: 10.1111/j.1365-2133.2011.10400.x

48. Kim BE, Howell MD, Guttman E, Gilleaudeau PM, Cardinale IR, Boguniewicz M, et al. TNF-α downregulates filaggrin and loricrin through c-Jun N-terminal kinase: role for TNF-α antagonists to improve skin barrier. *J Invest Dermatol*. (2011) 131:1272–9. doi: 10.1038/jid.2011.24

49. Su CC, Su TR, Lai JC, Tsay GJ, Lin HK. Elevated transglutaminase-2 expression in the epidermis of psoriatic skin and its role in the skin lesion development. *J Dermatol*. (2017) 44:699–702. doi: 10.1111/1346-8138.13742

50. Shin JW, Kwon MA, Hwang J, Lee SJ, Lee JH, Kim HJ, et al. Keratinocyte transglutaminase 2 promotes CCR6(+) γδT-cell recruitment by upregulating CCL20 in psoriatic inflammation. *Cell Death Dis*. (2020) 11:301. doi: 10.1038/s41419-020-2495-z

51. Ling S, Xu B, Luo Y, Fang X, Liu X, Wang A, et al. Transglutaminase 3 attenuates skin inflammation in psoriasis by inhibiting NF-κB activation through phosphorylated STAT3-TET3 signaling. *J Invest Dermatol*. (2022) 142:2968–2977.e10. doi: 10.1016/j.jid.2022.03.035

52. Piro MC, Ventura A, Smirnov A, Saggini A, Lena A, Mauriello A, et al. Transglutaminase 3 reduces the severity of psoriasis in Imiquimod-treated mouse skin. *Int J Mol Sci*. (2020) 21:1566. doi: 10.3390/ijms21051566

53. Cadau S, Gault M, Berthelemy N, Hsu CY, Danoux L, Pelletier N, et al. An inflamed and infected reconstructed human epidermis to study atopic dermatitis and skin care ingredients. *Int J Mol Sci*. (2022) 23:12880. doi: 10.3390/ijms232112880

54. Sandilands A, Terron-Kwiatkowski A, Hull PR, O'Regan GM, Clayton TH, Watson RM, et al. Comprehensive analysis of the gene encoding filaggrin uncovers prevalent and rare mutations in ichthyosis vulgaris and atopic eczema. *Nat Genet*. (2007) 39:650–4. doi: 10.1038/ng2020

55. Ruether A, Stoll M, Schwarz T, Schreiber S, Fölster-Holst R. Filaggrin loss-of-function variant contributes to atopic dermatitis risk in the population of northern Germany. *Br J Dermatol*. (2006) 155:1093–4. doi: 10.1111/j.1365-2133.2006.07500.x

56. Weidinger S, Rodríguez E, Stahl C, Wagenpfeil S, Klopp N, Illig T, et al. Filaggrin mutations strongly predispose to early-onset and extrinsic atopic dermatitis. *J Invest Dermatol*. (2007) 127:724–6. doi: 10.1038/sj.jid.5700630

57. Palmer CN, Irvine AD, Terron-Kwiatkowski A, Zhao Y, Liao H, Lee SP, et al. Common loss-of-function variants of the epidermal barrier protein filaggrin are a major predisposing factor for atopic dermatitis. *Nat Genet*. (2006) 38:441–6. doi: 10.1038/ng1767

58. Brown SJ, Sandilands A, Zhao Y, Liao H, Relton CL, Meggitt SJ, et al. Prevalent and low-frequency null mutations in the filaggrin gene are associated with early-onset and persistent atopic eczema. *J Invest Dermatol*. (2008) 128:1591–4. doi: 10.1038/sj.jid.5701206

59. Lagrelius M, Wahlgren CF, Bradley M, Melén E, Kull I, Bergström A, et al. Filaggrin gene mutations in relation to contact allergy and hand eczema in adolescence. *Contact Derm*. (2020) 82:147–52. doi: 10.1111/cod.13444

60. Basu K, Inglis SK, Bremner SA, Ramsay R, Abd A, Rabe H, et al. Filaggrin gene defects are associated with eczema, wheeze, and nasal disease during infancy: prospective study. *J Allergy Clin Immunol*. (2020) 146:681–2. doi: 10.1016/j.jaci.2020.02.036

61. Irvine AD, McLean WH, Leung DY. Filaggrin mutations associated with skin and allergic diseases. *N Engl J Med*. (2011) 365:1315–27. doi: 10.1056/NEJMra1011040

62. Howell MD, Kim BE, Gao P, Grant AV, Boguniewicz M, DeBenedetto A, et al. Cytokine modulation of atopic dermatitis filaggrin skin expression. *J Allergy Clin Immunol*. (2009) 124:R7–R12. doi: 10.1016/j.jaci.2009.07.012

63. Kim BE, Leung DY, Boguniewicz M, Howell MD. Loricrin and involucrin expression is down-regulated by Th2 cytokines through STAT-6. *Clin Immunol*. (2008) 126:332–7. doi: 10.1016/j.clim.2007.11.006

64. Takei K, Mitoma C, Hashimoto-Hachiya A, Takahara M, Tsuji G, Nakahara T, et al. Galactomyces fermentation filtrate prevents T helper 2-mediated reduction of filaggrin in an aryl hydrocarbon receptor-dependent manner. *Clin Exp Dermatol*. (2015) 40:786–93. doi: 10.1111/ced.12635

65. Takei K, Mitoma C, Hashimoto-Hachiya A, Uchi H, Takahara M, Tsuji G, et al. Antioxidant soybean tar Glyteer rescues T-helper-mediated downregulation of filaggrin expression via aryl hydrocarbon receptor. *J Dermatol*. (2015) 42:171–80. doi: 10.1111/1346-8138.12717

66. Tsuji G, Hashimoto-Hachiya A, Kiyomatsu-Oda M, Takemura M, Ohno F, Ito T, et al. Aryl hydrocarbon receptor activation restores filaggrin expression via OVOL1 in atopic dermatitis. *Cell Death Dis*. (2017) 8:e2931. doi: 10.1038/cddis.2017.322

67. Furue K, Ito T, Tsuji G, Ulzii D, Vu YH, Kido-Nakahara M, et al. The IL-13-OVOL1-FLG axis in atopic dermatitis. *Immunology*. (2019) 158:281–6. doi: 10.1111/imm.13120

68. Su H, Luo Y, Sun J, Liu X, Ling S, Xu B, et al. Transglutaminase 3 promotes skin inflammation in atopic dermatitis by activating monocyte-derived dendritic cells via DC-SIGN. *J Invest Dermatol*. (2020) 140:370–379.e8. doi: 10.1016/j.jid.2019.07.703

69. Chen L, Liu S, Xiao L, Chen K, Tang J, Huang C, et al. An initial assessment of the involvement of transglutaminase2 in eosinophilic bronchitis using a disease model developed in C57BL/6 mice. *Sci Rep*. (2021) 11:11946. doi: 10.1038/s41598-021-90950-9

70. Broccardo CJ, Mahaffey S, Schwarz J, Wruck L, David G, Schlievert PM, et al. Comparative proteomic profiling of patients with atopic dermatitis based on history of eczema herpeticum infection and *Staphylococcus aureus* colonization. *J Allergy Clin Immunol*. (2011) 127:186–193.e11, 193.e1-11. doi: 10.1016/j.jaci.2010.10.033

71. Sun J, Gu Y, Li K, Zhang JZ. Co-existence of specific IgE antibodies and T cells reactive to house dust mites and human transglutaminase3/tropomysin in patients with atopic dermatitis. *Eur J Dermatol*. (2021) 31:155–60. doi: 10.1684/ejd.2021.4018

72. Bergboer JG, Zeeuwen PL, Irvine AD, Weidinger S, Giardina E, Novelli G, et al. Deletion of late Cornified envelope 3B and 3C genes is not associated with atopic dermatitis. *J Invest Dermatol*. (2010) 130:2057–61. doi: 10.1038/jid.2010.88

73. Shen C, Gao J, Yin X, Sheng Y, Sun L, Cui Y, et al. Association of the late cornified envelope-3 genes with psoriasis and psoriatic arthritis: a systematic review. *J Genet Genomics*. (2015) 42:49–56. doi: 10.1016/j.jgg.2015.01.001

74. Kirschner N, Poetzl C, von den Driesch P, Wladykowski E, Moll I, Behne MJ, et al. Alteration of tight junction proteins is an early event in psoriasis: putative involvement of proinflammatory cytokines. *Am J Pathol*. (2009) 175:1095–106. doi: 10.2353/ajpath.2009.080973

75. Pan Y, Tang S, Xu L, Zheng S, Qiao J, Fang H. Expression and correlation of interleukin-36γ, claudin-1 and claudin-7 in psoriasis. *Indian J Dermatol Venereol Leprol*. (2019) 85:534–6. doi: 10.4103/ijdvl.IJDVL_640_18

76. Renert-Yuval Y, del Duca E, Pavel AB, Fang M, Lefferdink R, Wu J, et al. The molecular features of normal and atopic dermatitis skin in infants, children, adolescents, and adults. *J Allergy Clin Immunol*. (2021) 148:148–63. doi: 10.1016/j.jaci.2021.01.001

77. Tokumasu R, Tamura A, Tsukita S. Time- and dose-dependent claudin contribution to biological functions: lessons from claudin-1 in skin. *Tissue Barriers*. (2017) 5:e1336194. doi: 10.1080/21688370.2017.1336194

78. Leung DY. New insights into atopic dermatitis: role of skin barrier and immune dysregulation. *Allergol Int*. (2013) 62:151–61. doi: 10.2332/allergolint.13-RAI-0564

79. Bergmann S, von Buenau B, Vidal-y-Sy S, Haftek M, Wladykowski E, Houdek P, et al. Claudin-1 decrease impacts epidermal barrier function in atopic dermatitis lesions dose-dependently. *Sci Rep*. (2020) 10:2024. doi: 10.1038/s41598-020-58718-9

80. Takeichi M. The cadherin superfamily in neuronal connections and interactions. *Nat Rev Neurosci*. (2007) 8:11–20. doi: 10.1038/nrn2043

81. Li Z, Peng Z, Wang Y, Geng S, Ji F. Decreased expression of E-cadherin and beta-catenin in the lesional skin of patients with active psoriasis. *Int J Dermatol*. (2008) 47:207–9. doi: 10.1111/j.1365-4632.2007.03318.x

82. Zhou S, Matsuyoshi N, Takeuchi T, Ohtsuki Y, Miyachi Y. Reciprocal altered expression of T-cadherin and P-cadherin in psoriasis vulgaris. *Br J Dermatol*. (2003) 149:268–73. doi: 10.1046/j.1365-2133.2003.05464.x

83. Fukui T, Fukaya T, Uto T, Takagi H, Nasu J, Miyanaga N, et al. Pivotal role of CD103 in the development of psoriasiform dermatitis. *Sci Rep*. (2020) 10:8371. doi: 10.1038/s41598-020-65355-9

84. Brand A, Diener N, Zahner SP, Tripp C, Backer RA, Karram K, et al. E-cadherin is dispensable to maintain Langerhans cells in the epidermis. *J Invest Dermatol*. (2020) 140:132–142.e3. doi: 10.1016/j.jid.2019.06.132

85. Godsel LM, Roth-Carter QR, Koetsier JL, Tsoi LC, Huffine AL, Broussard JA, et al. Translational implications of Th17-skewed inflammation due to genetic deficiency of a cadherin stress sensor. *J Clin Invest*. (2022) 132:e144363. doi: 10.1172/JCI144363

86. Turner CT, Zeglinski MR, Richardson KC, Santacruz S, Hiroyasu S, Wang C, et al. Granzyme B contributes to barrier dysfunction in Oxazolone-induced skin inflammation through E-cadherin and FLG cleavage. *J Invest Dermatol*. (2021) 141:36–47. doi: 10.1016/j.jid.2020.05.095

87. Salimi M, Barlow JL, Saunders SP, Xue L, Gutowska-Owsiak D, Wang X, et al. A role for IL-25 and IL-33-driven type-2 innate lymphoid cells in atopic dermatitis. *J Exp Med*. (2013) 210:2939–50. doi: 10.1084/jem.20130351

88. Gao W, Gong J, Mu M, Zhu Y, Wang W, Chen W, et al. The pathogenesis of eosinophilic asthma: a positive feedback mechanism that promotes Th2 immune response via Filaggrin deficiency. *Front Immunol*. (2021) 12:672312. doi: 10.3389/fimmu.2021.672312

89. Eyerich S, Eyerich K, Traidl-Hoffmann C, Biedermann T. Cutaneous barriers and skin immunity: differentiating a connected network. *Trends Immunol*. (2018) 39:315–27. doi: 10.1016/j.it.2018.02.004

90. Nguyen H, Trujillo-Paez JV, Umehara Y, Yue H, Peng G, Kiatsurayanon C, et al. Role of antimicrobial peptides in skin barrier repair in individuals with atopic dermatitis. *Int J Mol Sci*. (2020) 21:7607. doi: 10.3390/ijms21207607

91. Schneider JJ, Unholzer A, Schaller M, Schäfer-Korting M, Korting HC. Human defensins. *J Mol Med (Berl)*. (2005) 83:587–95. doi: 10.1007/s00109-005-0657-1

92. Wiesner J, Vilcinskas A. Antimicrobial peptides: the ancient arm of the human immune system. *Virulence*. (2010) 1:440–64. doi: 10.4161/viru.1.5.12983

93. Harder J, Bartels J, Christophers E, Schroder JM. Isolation and characterization of human beta -defensin-3, a novel human inducible peptide antibiotic. *J Biol Chem*. (2001) 276:5707–13. doi: 10.1074/jbc.M008557200

94. Nomura I, Goleva E, Howell MD, Hamid QA, Ong PY, Hall CF, et al. Cytokine milieu of atopic dermatitis, as compared to psoriasis, skin prevents induction of innate immune response genes. *J Immunol*. (2003) 171:3262–9. doi: 10.4049/jimmunol.171.6.3262

95. Chieosilapatham P, Ogawa H, Niyonsaba F. Current insights into the role of human β-defensins in atopic dermatitis. *Clin Exp Immunol*. (2017) 190:155–66. doi: 10.1111/cei.13013

96. Hönzke S, Wallmeyer L, Ostrowski A, Radbruch M, Mundhenk L, Schäfer-Korting M, et al. Influence of Th2 cytokines on the Cornified envelope, tight junction proteins, and ß-Defensins in Filaggrin-deficient skin equivalents. *J Invest Dermatol*. (2016) 136:631–9. doi: 10.1016/j.jid.2015.11.007

97. Kiatsurayanon C, Niyonsaba F, Smithrithee R, Akiyama T, Ushio H, Hara M, et al. Host defense (antimicrobial) peptide, human β-defensin-3, improves the function of the epithelial tight-junction barrier in human keratinocytes. *J Invest Dermatol*. (2014) 134:2163–73. doi: 10.1038/jid.2014.143

98. Goto H, Hongo M, Ohshima H, Kurasawa M, Hirakawa S, Kitajima Y. Human beta defensin-1 regulates the development of tight junctions in cultured human epidermal keratinocytes. *J Dermatol Sci*. (2013) 71:145–8. doi: 10.1016/j.jdermsci.2013.04.017

99. Peng G, Tsukamoto S, Ikutama R, Nguyen HLT, Umehara Y, Trujillo-Paez JV, et al. Human β-defensin-3 attenuates atopic dermatitis-like inflammation through autophagy activation and the aryl hydrocarbon receptor signaling pathway. *J Clin Invest*. (2022) 132:e156501. doi: 10.1172/JCI156501

100. Alase A, Seltmann J, Werfel T, Wittmann M. Interleukin-33 modulates the expression of human β-defensin 2 in human primary keratinocytes and may influence the susceptibility to bacterial superinfection in acute atopic dermatitis. *Br J Dermatol*. (2012) 167:1386–9. doi: 10.1111/j.1365-2133.2012.11140.x

101. Kao CY, Chen Y, Thai P, Wachi S, Huang F, Kim C, et al. IL-17 markedly up-regulates beta-defensin-2 expression in human airway epithelium via JAK and NF-kappaB signaling pathways. *J Immunol*. (2004) 173:3482–91. doi: 10.4049/jimmunol.173.5.3482

102. Kanda N, Watanabe S. Increased serum human β-defensin-2 levels in atopic dermatitis: relationship to IL-22 and oncostatin M. *Immunobiology*. (2012) 217:436–45. doi: 10.1016/j.imbio.2011.10.010

103. Kanda N, Kamata M, Tada Y, Ishikawa T, Sato S, Watanabe S. Human β-defensin-2 enhances IFN-γ and IL-10 production and suppresses IL-17 production in T cells. *J Leukoc Biol*. (2011) 89:935–44. doi: 10.1189/jlb.0111004

104. Memariani H, Memariani M. Antibiofilm properties of cathelicidin LL-37: an in-depth review. *World J Microbiol Biotechnol*. (2023) 39:99. doi: 10.1007/s11274-023-03545-z

105. Scheenstra MR, van Harten RM, Veldhuizen E, Haagsman HP, Coorens M. Cathelicidins modulate TLR-activation and inflammation. *Front Immunol*. (2020) 11:1137. doi: 10.3389/fimmu.2020.01137

106. Steinstraesser L, Lam MC, Jacobsen F, Porporato PE, Chereddy KK, Becerikli M, et al. Skin electroporation of a plasmid encoding hCAP-18/LL-37 host defense peptide promotes wound healing. *Mol Ther*. (2014) 22:734–42. doi: 10.1038/mt.2013.258

107. Wei X, Zhang L, Yang Y, Hou Y, Xu Y, Wang Z, et al. LL-37 transports immunoreactive cGAMP to activate STING signaling and enhance interferon-mediated host antiviral immunity. *Cell Rep*. (2022) 39:110880. doi: 10.1016/j.celrep.2022.110880

108. Nagaoka I, Tamura H, Reich J. Therapeutic potential of cathelicidin peptide LL-37, an antimicrobial agent, in a murine Sepsis model. *Int J Mol Sci*. (2020) 21:5973. doi: 10.3390/ijms21175973

109. Fabisiak A, Murawska N, Fichna J. LL-37: cathelicidin-related antimicrobial peptide with pleiotropic activity. *Pharmacol Rep*. (2016) 68:802–8. doi: 10.1016/j.pharep.2016.03.015

110. Miura S, Garcet S, Li X, Cueto I, Salud-Gnilo C, Kunjravia N, et al. Cathelicidin antimicrobial peptide LL37 induces toll-like receptor 8 and amplifies IL-36γ and IL-17C in human keratinocytes. *J Invest Dermatol*. (2023) 143:832–841.e4. doi: 10.1016/j.jid.2022.10.017

111. Roby KD, Nardo AD. Innate immunity and the role of the antimicrobial peptide cathelicidin in inflammatory skin disease. *Drug Discov Today Dis Mech*. (2013) 10:e79–82. doi: 10.1016/j.ddmec.2013.01.001

112. Aberg KM, Man MQ, Gallo RL, Ganz T, Crumrine D, Brown BE, et al. Co-regulation and interdependence of the mammalian epidermal permeability and antimicrobial barriers. *J Invest Dermatol*. (2008) 128:917–25. doi: 10.1038/sj.jid.5701099

113. Akiyama T, Niyonsaba F, Kiatsurayanon C, Nguyen TT, Ushio H, Fujimura T, et al. The human cathelicidin LL-37 host defense peptide upregulates tight junction-related proteins and increases human epidermal keratinocyte barrier function. *J Innate Immun*. (2014) 6:739–53. doi: 10.1159/000362789

114. Ikutama R, Peng G, Tsukamoto S, Umehara Y, Trujillo-Paez JV, Yue H, et al. Cathelicidin LL-37 activates human keratinocyte autophagy through the $P2X_7$, mechanistic target of rapamycin, and MAPK pathways. *J Invest Dermatol*. (2023) 143:751–761.e7. doi: 10.1016/j.jid.2022.10.020

115. Chen X, Niyonsaba F, Ushio H, Nagaoka I, Ikeda S, Okumura K, et al. Human cathelicidin LL-37 increases vascular permeability in the skin via mast cell activation, and phosphorylates MAP kinases p38 and ERK in mast cells. *J Dermatol Sci*. (2006) 43:63–6. doi: 10.1016/j.jdermsci.2006.03.001

116. Subramanian H, Gupta K, Guo Q, Price R, Ali H. Mas-related gene X2 (MrgX2) is a novel G protein-coupled receptor for the antimicrobial peptide LL-37 in human mast cells: resistance to receptor phosphorylation, desensitization, and internalization. *J Biol Chem*. (2011) 286:44739–49. doi: 10.1074/jbc.M111.277152

117. Niyonsaba F, Ushio H, Hara M, Yokoi H, Tominaga M, Takamori K, et al. Antimicrobial peptides human beta-defensins and cathelicidin LL-37 induce the secretion of a pruritogenic cytokine IL-31 by human mast cells. *J Immunol*. (2010) 184:3526–34. doi: 10.4049/jimmunol.0900712

118. Kanda N, Hau CS, Tada Y, Sato S, Watanabe S. Decreased serum LL-37 and vitamin D3 levels in atopic dermatitis: relationship between IL-31 and oncostatin M. *Allergy*. (2012) 67:804–12. doi: 10.1111/j.1398-9995.2012.02824.x

119. Madsen P, Rasmussen HH, Leffers H, Honoré B, Dejgaard K, Olsen E, et al. Molecular cloning, occurrence, and expression of a novel partially secreted protein "psoriasin" that is highly up-regulated in psoriatic skin. *J Invest Dermatol*. (1991) 97:701–12. doi: 10.1111/1523-1747.ep12484041

120. Broome AM, Ryan D, Eckert RL. S100 protein subcellular localization during epidermal differentiation and psoriasis. *J Histochem Cytochem*. (2003) 51:675–85. doi: 10.1177/002215540305100513

121. D'Amico F, Trovato C, Skarmoutsou E, Rossi GA, Granata M, Longo V, et al. Effects of adalimumab, etanercept and ustekinumab on the expression of psoriasin (S100A7) in psoriatic skin. *J Dermatol Sci*. (2015) 80:38–44. doi: 10.1016/j.jdermsci.2015.07.009

122. Gläser R, Meyer-Hoffert U, Harder J, Cordes J, Wittersheim M, Kobliakova J, et al. The antimicrobial protein psoriasin (S100A7) is upregulated in atopic dermatitis and after experimental skin barrier disruption. *J Invest Dermatol*. (2009) 129:641–9. doi: 10.1038/jid.2008.268

123. Hofmann MA, Drury S, Fu C, Qu W, Taguchi A, Lu Y, et al. RAGE mediates a novel proinflammatory axis: a central cell surface receptor for S100/calgranulin polypeptides. *Cell*. (1999) 97:889–901. doi: 10.1016/S0092-8674(00)80801-6

124. Zackular JP, Chazin WJ, Skaar EP. Nutritional immunity: S100 proteins at the host-pathogen Interface. *J Biol Chem*. (2015) 290:18991–8. doi: 10.1074/jbc.R115.645085

125. Leclerc E, Fritz G, Vetter SW, Heizmann CW. Binding of S100 proteins to RAGE: an update. *Biochim Biophys Acta*. (2009) 1793:993–1007. doi: 10.1016/j.bbamcr.2008.11.016

126. Witte E, Kokolakis G, Witte K, Philipp S, Doecke WD, Babel N, et al. IL-19 is a component of the pathogenetic IL-23/IL-17 cascade in psoriasis. *J Invest Dermatol*. (2014) 134:2757–67. doi: 10.1038/jid.2014.308

127. Gläser R, Harder J, Lange H, Bartels J, Christophers E, Schröder JM. Antimicrobial psoriasin (S100A7) protects human skin from *Escherichia coli* infection. *Nat Immunol*. (2005) 6:57–64. doi: 10.1038/ni1142

128. Nukui T, Ehama R, Sakaguchi M, Sonegawa H, Katagiri C, Hibino T, et al. S100A8/A9, a key mediator for positive feedback growth stimulation of normal human keratinocytes. *J Cell Biochem*. (2008) 104:453–64. doi: 10.1002/jcb.21639

129. Gittler JK, Shemer A, Suárez-Fariñas M, Fuentes-Duculan J, Gulewicz KJ, Wang CQF, et al. Progressive activation of T(H)2/T(H)22 cytokines and selective epidermal proteins characterizes acute and chronic atopic dermatitis. *J Allergy Clin Immunol*. (2012) 130:1344–54. doi: 10.1016/j.jaci.2012.07.012

130. Carrier Y, Ma HL, Ramon HE, Napierata L, Small C, O'Toole M, et al. Inter-regulation of Th17 cytokines and the IL-36 cytokines in vitro and in vivo: implications in psoriasis pathogenesis. *J Invest Dermatol*. (2011) 131:2428–37. doi: 10.1038/jid.2011.234

131. Onderdijk AJ, Baerveldt EM, Kurek D, Kant M, Florencia EF, Debets R, et al. IL-4 downregulates IL-1β and IL-6 and induces GATA3 in psoriatic epidermal cells: route of action of a Th2 cytokine. *J Immunol*. (2015) 195:1744–52. doi: 10.4049/jimmunol.1401740

132. Kvarnhammar AM, Rydberg C, Järnkrants M, Eriksson M, Uddman R, Benson M, et al. Diminished levels of nasal S100A7 (psoriasin) in seasonal allergic rhinitis: an effect mediated by Th2 cytokines. *Respir Res*. (2012) 13:2. doi: 10.1186/1465-9921-13-2

133. Hattori F, Kiatsurayanon C, Okumura K, Ogawa H, Ikeda S, Okamoto K, et al. The antimicrobial protein S100A7/psoriasin enhances the expression of keratinocyte differentiation markers and strengthens the skin's tight junction barrier. *Br J Dermatol*. (2014) 171:742–53. doi: 10.1111/bjd.13125

134. Rieg S, Seeber S, Steffen H, Humeny A, Kalbacher H, Stevanovic S, et al. Generation of multiple stable dermcidin-derived antimicrobial peptides in sweat of different body sites. *J Invest Dermatol*. (2006) 126:354–65. doi: 10.1038/sj.jid.5700041

135. Rieg S, Garbe C, Sauer B, Kalbacher H, Schittek B. Dermcidin is constitutively produced by eccrine sweat glands and is not induced in epidermal cells under inflammatory skin conditions. *Br J Dermatol*. (2004) 151:534–9. doi: 10.1111/j.1365-2133.2004.06081.x

136. Paulmann M, Arnold T, Linke D, Özdirekcan S, Kopp A, Gutsmann T, et al. Structure-activity analysis of the dermcidin-derived peptide DCD-1L, an anionic antimicrobial peptide present in human sweat. *J Biol Chem*. (2012) 287:8434–43. doi: 10.1074/jbc.M111.332270

137. Niyonsaba F, Suzuki A, Ushio H, Nagaoka I, Ogawa H, Okumura K. The human antimicrobial peptide dermcidin activates normal human keratinocytes. *Br J Dermatol*. (2009) 160:243–9. doi: 10.1111/j.1365-2133.2008.08925.x

138. Che D, Jia T, Zhang X, Zhang L, du X, Zheng Y, et al. Dermcidin-derived polypeptides: DCD(86-103) induced inflammatory reaction in the skin by activation of mast cells via ST2. *Immunol Lett*. (2022) 251-252:29–37. doi: 10.1016/j.imlet.2022.09.008

139. Kopfnagel V, Wagenknecht S, Harder J, Hofmann K, Kleine M, Buch A, et al. RNase 7 strongly promotes TLR9-mediated DNA sensing by human Plasmacytoid dendritic cells. *J Invest Dermatol*. (2018) 138:872–81. doi: 10.1016/j.jid.2017.09.052

140. Tewary P, de la Rosa G, Sharma N, Rodriguez LG, Tarasov SG, Howard OMZ, et al. β-Defensin 2 and 3 promote the uptake of self or CpG DNA, enhance IFN-α production by human plasmacytoid dendritic cells, and promote inflammation. *J Immunol*. (2013) 191:865–74. doi: 10.4049/jimmunol.1201648

141. Chokshi A, Demory Beckler M, Laloo A, Kesselman MM. Paradoxical tumor necrosis factor-alpha (TNF-α) inhibitor-induced psoriasis: a systematic review of pathogenesis, clinical presentation, and treatment. *Cureus*. (2023) 15:e42791. doi: 10.7759/cureus.42791

142. Punnonen J, Punnonen K, Jansén CT, Kalimo K. Interferon (IFN)-alpha, IFN-gamma, interleukin (IL)-2, and arachidonic acid metabolites modulate IL-4-induced IgE synthesis similarly in healthy persons and in atopic dermatitis patients. *Allergy*. (1993) 48:189–95. doi: 10.1111/j.1398-9995.1993.tb00712.x

143. Simanski M, Rademacher F, Schröder L, Schumacher HM, Gläser R, Harder J. IL-17A and IFN-γ synergistically induce RNase 7 expression via STAT3 in primary keratinocytes. *PLoS One*. (2013) 8:e59531. doi: 10.1371/journal.pone.0059531

144. Kopfnagel V, Wagenknecht S, Brand L, Zeitvogel J, Harder J, Hofmann K, et al. RNase 7 downregulates TH2 cytokine production by activated human T cells. *Allergy*. (2017) 72:1694–703. doi: 10.1111/all.13173

145. Kopecki Z, Arkell R, Powell BC, Cowin AJ. Flightless I regulates hemidesmosome formation and integrin-mediated cellular adhesion and migration during wound repair. *J Invest Dermatol*. (2009) 129:2031–45. doi: 10.1038/jid.2008.461

146. Kopecki Z, Yang GN, Arkell RM, Jackson JE, Melville E, Iwata H, et al. Flightless I over-expression impairs skin barrier development, function and recovery following skin blistering. *J Pathol*. (2014) 232:541–52. doi: 10.1002/path.4323

147. Chong HT, Yang GN, Sidhu S, Ibbetson J, Kopecki Z, Cowin AJ. Reducing Flightless I expression decreases severity of psoriasis in an imiquimod-induced murine

model of psoriasiform dermatitis. *Br J Dermatol*. (2017) 176:705–12. doi: 10.1111/bjd.14842

148. Wen L, Zhang B, Wu X, Liu R, Fan H, Han L, et al. Toll-like receptors 7 and 9 regulate the proliferation and differentiation of B cells in systemic lupus erythematosus. *Front Immunol*. (2023) 14:1093208. doi: 10.3389/fimmu.2023.1093208

149. Mills SJ, Ahangar P, Thomas HM, Hofma BR, Murray RZ, Cowin AJ. Flightless I negatively regulates macrophage surface TLR4, delays early inflammation, and impedes wound healing. *Cells*. (2022) 11:2192. doi: 10.3390/cells11142192

150. Kopecki Z, Stevens NE, Chong HT, Yang GN, Cowin AJ. Flightless I alters the inflammatory response and autoantibody profile in an OVA-induced atopic dermatitis skin-like disease. *Front Immunol*. (2018) 9:1833. doi: 10.3389/fimmu.2018.01833

151. Simon HU, Friis R, Tait SW, Ryan KM. Retrograde signaling from autophagy modulates stress responses. *Sci Signal*. (2017) 10:eaag2791 pii. doi: 10.1126/scisignal.aag2791

152. Akinduro O, Sully K, Patel A, Robinson DJ, Chikh A, McPhail G, et al. Constitutive autophagy and Nucleophagy during epidermal differentiation. *J Invest Dermatol*. (2016) 136:1460–70. doi: 10.1016/j.jid.2016.03.016

153. Lowes MA, Suárez-Fariñas M, Krueger JG. Immunology of psoriasis. *Annu Rev Immunol*. (2014) 32:227–55. doi: 10.1146/annurev-immunol-032713-120225

154. Chikh A, Sanzà P, Raimondi C, Akinduro O, Warnes G, Chiorino G, et al. iASPP is a novel autophagy inhibitor in keratinocytes. *J Cell Sci*. (2014) 127:3079–93. doi: 10.1242/jcs.144816

155. Kwon SH, Lim CJ, Jung J, Kim HJ, Park K, Shin JW, et al. The effect of autophagy-enhancing peptide in moisturizer on atopic dermatitis: a randomized controlled trial. *J Dermatolog Treat*. (2019) 30:558–64. doi: 10.1080/09546634.2018.1544407

156. Varshney P, Saini N. PI3K/AKT/mTOR activation and autophagy inhibition plays a key role in increased cholesterol during IL-17A mediated inflammatory response in psoriasis. *Biochim Biophys Acta Mol basis Dis*. (2018) 1864:1795–803. doi: 10.1016/j.bbadis.2018.02.003

157. Wang Z, Zhou H, Zheng H, Zhou X, Shen G, Teng X, et al. Autophagy-based unconventional secretion of HMGB1 by keratinocytes plays a pivotal role in psoriatic skin inflammation. *Autophagy*. (2021) 17:529–52. doi: 10.1080/15548627.2020.1725381

158. Feng L, Song P, Xu F, Xu L, Shao F, Guo M, et al. cis-Khellactone inhibited the Proinflammatory macrophages via promoting autophagy to ameliorate Imiquimod-induced psoriasis. *J Invest Dermatol*. (2019) 139:1946–1956.e3. doi: 10.1016/j.jid.2019.02.021

159. Park MJ, Lee SY, Moon SJ, Son HJ, Lee SH, Kim EK, et al. Metformin attenuates graft-versus-host disease via restricting mammalian target of rapamycin/signal transducer and activator of transcription 3 and promoting adenosine monophosphate-activated protein kinase-autophagy for the balance between T helper 17 and Tregs. *Transl Res*. (2016) 173:115–30. doi: 10.1016/j.trsl.2016.03.006

160. Hailfinger S, Schulze-Osthoff K. Impaired autophagy in psoriasis and atopic dermatitis: a new therapeutic target. *J Invest Dermatol*. (2021) 141:2775–7. doi: 10.1016/j.jid.2021.06.006

161. Tian R, Li Y, Yao X. PGRN suppresses inflammation and promotes autophagy in keratinocytes through the Wnt/β-catenin signaling pathway. *Inflammation*. (2016) 39:1387–94. doi: 10.1007/s10753-016-0370-y

162. Klapan K, Frangež Ž, Markov N, Yousefi S, Simon D, Simon HU. Evidence for lysosomal dysfunction within the epidermis in psoriasis and atopic dermatitis. *J Invest Dermatol*. (2021) 141:2838–2848.e4. doi: 10.1016/j.jid.2021.05.016

163. Kopecki Z, Has C, Yang G, Bruckner-Tuderman L, Cowin A, Flightless I. A contributing factor to skin blistering in kindler syndrome patients. *J Cutan Pathol*. (2020) 47:186–9. doi: 10.1111/cup.13597

164. Ishii T, Warabi E, Siow R, Mann GE. Sequestosome1/p62: a regulator of redox-sensitive voltage-activated potassium channels, arterial remodeling, inflammation, and neurite outgrowth. *Free Radic Biol Med*. (2013) 65:102–16. doi: 10.1016/j.freeradbiomed.2013.06.019

165. Lee HM, Shin DM, Yuk JM, Shi G, Choi DK, Lee SH, et al. Autophagy negatively regulates keratinocyte inflammatory responses via scaffolding protein p62/SQSTM1. *J Immunol*. (2011) 186:1248–58. doi: 10.4049/jimmunol.1001954

166. He JP, Hou PP, Chen QT, Wang WJ, Sun XY, Yang PB, et al. Flightless-I blocks p62-mediated recognition of LC3 to impede selective autophagy and promote breast Cancer progression. *Cancer Res*. (2018) 78:4853–64. doi: 10.1158/0008-5472.CAN-17-3835

167. Mahil SK, Twelves S, Farkas K, Setta-Kaffetzi N, Burden AD, Gach JE, et al. AP1S3 mutations cause skin autoinflammation by disrupting keratinocyte autophagy and up-regulating IL-36 production. *J Invest Dermatol*. (2016) 136:2251–9. doi: 10.1016/j.jid.2016.06.618

168. Park A, Heo TH. IL-17A-targeting fenofibrate attenuates inflammation in psoriasis by inducing autophagy. *Life Sci*. (2023) 326:121755. doi: 10.1016/j.lfs.2023.121755

169. Zhou L, Wang J, Hou H, Li J, Li J, Liang J, et al. Autophagy inhibits inflammation via Down-regulation of p38 MAPK/mTOR signaling Cascade in endothelial cells. *Clin Cosmet Investig Dermatol*. (2023) 16:659–69. doi: 10.2147/CCID.S405068

170. Merkley SD, Chock CJ, Yang XO, Harris J, Castillo EF. Modulating T cell responses via autophagy: the intrinsic influence controlling the function of both antigen-presenting cells and T cells. *Front Immunol*. (2018) 9:2914. doi: 10.3389/fimmu.2018.02914

171. de Jesús-Gil C, Sans-de SanNicolàs L, García-Jiménez I, Ferran M, Celada A, Chiriac A, et al. The translational relevance of human circulating memory cutaneous lymphocyte-associated antigen positive T cells in inflammatory skin disorders. *Front Immunol*. (2021) 12:652613. doi: 10.3389/fimmu.2021.652613

172. Tian D, Lai Y. The relapse of psoriasis: mechanisms and mysteries. *JID Innov*. (2022) 2:100116. doi: 10.1016/j.xjidi.2022.100116

173. Ariotti S, Hogenbirk MA, Dijkgraaf FE, Visser LL, Hoekstra ME, Song JY, et al. T cell memory. Skin-resident memory $CD8^+$ T cells trigger a state of tissue-wide pathogen alert. *Science*. (2014) 346:101–5. doi: 10.1126/science.1254803

174. Watanabe R, Gehad A, Yang C, Scott LL, Teague JE, Schlapbach C, et al. Human skin is protected by four functionally and phenotypically discrete populations of resident and recirculating memory T cells. *Sci Transl Med*. (2015) 7:279ra39. doi: 10.1126/scitranslmed.3010302

175. Klicznik MM, Morawski PA, Höllbacher B, Varkhande SR, Motley SJ, Kuri-Cervantes L, et al. Human CD4(+)CD103(+) cutaneous resident memory T cells are found in the circulation of healthy individuals. *Sci Immunol*. (2019) 4:eaav8995. doi: 10.1126/sciimmunol.aav8995

176. Mackay LK, Minnich M, Kragten NA, Liao Y, Nota B, Seillet C, et al. Hobit and Blimp1 instruct a universal transcriptional program of tissue residency in lymphocytes. *Science*. (2016) 352:459–63. doi: 10.1126/science.aad2035

177. Zaid A, Hor JL, Christo SN, Groom JR, Heath WR, Mackay LK, et al. Chemokine receptor-dependent control of skin tissue-resident memory T cell formation. *J Immunol*. (2017) 199:2451–9. doi: 10.4049/jimmunol.1700571

178. Gallais Sérézal I, Hoffer E, Ignatov B, Martini E, Zitti B, Ehrström M, et al. A skewed pool of resident T cells triggers psoriasis-associated tissue responses in never-lesional skin from patients with psoriasis. *J Allergy Clin Immunol*. (2019) 143:1444–54. doi: 10.1016/j.jaci.2018.08.048

179. Migayron L, Merhi R, Seneschal J, Boniface K. Resident memory T cells in nonlesional skin and healed lesions of patients with chronic inflammatory diseases: appearances can be deceptive. *J Allergy Clin Immunol*. (2023):S0091-6749(23)01480-X pii. doi: 10.1016/j.jaci.2023.11.017

180. Schluns KS, Kieper WC, Jameson SC, Lefrançois L. Interleukin-7 mediates the homeostasis of naïve and memory CD8 T cells in vivo. *Nat Immunol*. (2000) 1:426–32. doi: 10.1038/80868

181. Quan C, Cho MK, Shao Y, Mianecki LE, Liao E, Perry D, et al. Dermal fibroblast expression of stromal cell-derived factor-1 (SDF-1) promotes epidermal keratinocyte proliferation in normal and diseased skin. *Protein Cell*. (2015) 6:890–903. doi: 10.1007/s13238-015-0198-5

182. Cesare AD, Meglio PD, Nestle FO. A role for Th17 cells in the immunopathogenesis of atopic dermatitis. *J Invest Dermatol*. (2008) 128:2569–71. doi: 10.1038/jid.2008.283

183. Jin M, Yoon J. From bench to clinic: the potential of therapeutic targeting of the IL-22 signaling pathway in atopic dermatitis. *Immune Netw*. (2018) 18:e42. doi: 10.4110/in.2018.18.e42

frontiers | Frontiers in Immunology

TYPE Original Research
PUBLISHED 10 June 2024
DOI 10.3389/fimmu.2024.1326728



OPEN ACCESS

EDITED BY
Dongqing Li,
Chinese Academy of Medical Sciences & Peking Union Medical College, China

REVIEWED BY
Masanori A. Murayama,
Kansai Medical University, Japan
Xiao Long,
Peking Union Medical College Hospital (CAMS), China

*CORRESPONDENCE
Ardeshir Bayat
ardeshir.bayat@uct.ac.za

RECEIVED 23 October 2023
ACCEPTED 09 April 2024
PUBLISHED 10 June 2024

CITATION
Sadiq A, Khumalo NP and Bayat A (2024) Development and validation of novel keloid-derived immortalized fibroblast cell lines. *Front. Immunol.* 15:1326728. doi: 10.3389/fimmu.2024.1326728



# Development and validation of novel keloid-derived immortalized fibroblast cell lines

Alia Sadiq, Nonhlanhla P. Khumalo and Ardeshir Bayat*

MRC Wound Healing and Keloid Research Unit, Hair and Skin Research Laboratory, Division of Dermatology, Department of Medicine, Faculty of Health Sciences, Groote Schuur Hospital, University of Cape Town, Cape Town, South Africa

Keloids are a common connective tissue disorder with an ill-understood etiopathogenesis and no effective treatment. This is exacerbated because of the absence of an animal model. Patient-derived primary keloid cells are insufficient as they age through passaging and have a limited supply. Therefore, there is an unmet need for development of a cellular model that can consistently and faithfully represent keloid's pathognomic features. In view of this, we developed keloid-derived immortalized fibroblast (KDIF) cell lines from primary keloid fibroblasts (PKF) by transfecting the human telomerase reverse transcriptase (h*TERT*) gene. The *TERT* gene encodes the catalytic subunit of the telomerase enzyme, which is responsible for maintaining the cellular replicative potential (cellular immortalization). Primary fibroblasts from keloid-specific lesional (peripheral, middle, and top) as well as extralesional sites were isolated and evaluated for cell line development and comparative cellular characteristics by employing qRT-PCR and immunofluorescence staining. Moreover, the immortalized behavior of KDIF cell lines was evaluated by comparing with cutaneous fibrosarcoma and dermatofibrosarcoma protuberans cell lines. Stable KDIF cell lines with elevated expression of h*TERT* exhibited the cellular characteristics of site-specific keloid fibroblasts. Histochemical staining for β-galactosidase revealed a significantly lower number of β-gal–positive cells in all three KDIF cell lines compared with that in PKFs. The cell growth curve pattern was studied over 10 passages for all three KDIF cell lines and was compared with the control groups. The results showed that all three KDIF cell lines grew significantly faster and obtained a fast growing characteristic as compared to primary keloid and normal fibroblasts. Phenotypic behavior in growth potential is an indication of h*TERT*-mediated immortalized transformation. Cell migration analysis revealed that the top and middle KDIF cell lines exhibited similar migration trend as site-specific PKFs. Notably, peripheral KDIF cell line showed significantly enhanced cell migration in comparison to the primary peripheral

fibroblasts. All KDIF cell lines expressed Collagen I protein as a keloid-associated fibrotic marker. Functional testing with triamcinolone inhibited cell migration in KDIF. ATCC short tandem repeat profiling validated the KDIF as keloid representative cell line. In summary, we provide the first novel KDIF cell lines. These cell lines overcome the limitations related to primary cell passaging and tissue supply due to immortalized features and present an accessible and consistent experimental model for keloid research.

KEYWORDS

**Keloid Disease, immortalized cell line, keloid scarring, keloid fibroblast, in vitro model, h*TERT*, stable transfection**

# 1 Introduction

Keloids are common fibroproliferative reticular dermal lesions of unknown etiopathogenesis, characterized clinically by an aggressive exophytic expansive growth into the surrounding skin with a high rate of recurrence post-therapy (1). Lack of relevant study models (including animal models as keloids only occur in human skin) (2) has been a challenging and rate-limiting issue for keloid research (3). Therefore, despite its inherent limitations compared with *in vivo* animal models, the use of *in vitro* monoculture studies using keloid-derived primary cultured fibroblasts has been invaluable in enabling studies in keloid pathobiology.

However, patient-derived primary cultured keloid fibroblasts are often scarce and insufficient as they age through passaging and have a limited supply. Additionally, keloid tissue is biologically heterogeneous with clinically distinct features within the lesion, including variable dermal cellularity, inflammatory infiltrate, and altered collagen I–III ratios (4), at margins (actively growing) compared with the center (dormant) of keloid (5), representing a variation at the cellular and molecular levels between central and peripheral keloid fibroblasts (6). This endotypic and phenotypic variation typically divides keloid into three distinct lesion-specific sites: (i) intralesional (keloid center), (ii) perilesional (keloid margin), and (iii) extralesional (normal appearing skin surrounding the lesion but distant to the margin) (7).

It has been established that *in vitro* disease–specific cell lines have lent themselves as an ideal option (a well-controlled system) to investigate the phenotypic and cellular characteristics of specific diseases. However, *in vitro* subculturing and maintenance cause aging (telomeric loss) in patient-derived primary cells (8). Significant telomeric loss was reported in keloids fibroblasts (9), resulting in a shorter lifespan and limiting the utility of keloid primary cells. Hence, induced overexpression of human telomerase reverse transcriptase (h*TERT*) has been envisioned as an attractive approach to extend lifespan of patient-derived primary cells, which is known as an "immortalized cell-line model approach." Induced immortalization bypasses cell events like replicative senescence and cellular crisis (10, 11). Thus, these cell lines act as a gold standard as they remain genetically identical, accessible, and consistent (12). Fibroblast cells have been considered as potential candidates to develop immortalized cell line for keloid disease as they have been implicated as an important contributor to keloid pathobiology and subsequent tissue formation (13, 14).

In view of this, we sectioned freshly obtained biopsies of keloid tissue into four specific sites: [i] top (papillary dermis of the intralesional center of keloid), (KT) [ii] middle (reticular dermis of the intralesional center of keloid) (KM), [iii] peripheral (margin of the keloid lesion) (KP), and [iv] extralesional tissue (KE) from the same donor (Figure 1C). Subsequently, these site-specific keloid tissue sections were used to isolate and develop keloid-derived immortalized fibroblast (KDIF) cell lines. The present study evaluated and compared the h*TERT* expression, immortalization, and characteristics/behavior (linked with immortalization) in primary keloid fibroblasts (PKFs) before and after genetic transfection (immortalization) (KDIF), having four distinct types of control groups. The control group included (i) normal fibroblasts (NFs) isolated from normal skin tissue, donated by a non-keloid–forming participant; (ii) extralesional keloid fibroblasts (KEs), as NFs isolated from normal (in appearance) skin adjacent to the keloid tissue, donated by a keloid participant; (iii) dermatofibrosarcoma protuberans (DFSP) fibroblasts, isolated from DFSP tissue; and (iv) fibrosarcoma fibroblasts (FSs) as established cancerous cell cultures, served as positive control for h*TERT* expression. Primary fibroblast cells from the PKF, KE, and NF groups are the representative of definite lifespan (non-immortalization character), whereas primary DFSP tissue–derived fibroblast cells and FS cells are the representative of indefinite lifespan (immortalization behavior). Hence, the evaluation of immortalization behavior was crucial to define a stable immortalization in genetically transformed primary fibroblasts. Once immortalization behavior was developed and established (stable transfection), KDIF cell lines were authenticated through short tandem repeat (STR) profiling by Amercican Type Culture Collection (ATCC). To our knowledge, we provide the first authenticated and functionally validated immortalized cell line for keloid disease.

# 2 Materials and methods

Here, we provide the concise summary of the key methods and procedures employed in the current study. The detailed method and associated references are available in SI Appendix 1.

## 2.1 Ethical approval

Ethical approval (HREC REF Number 493/2009, 30 October 2018) of this research study (Figures 1A–C) was obtained from the Human Research Ethics Committee, Faculty of Health Sciences, University of Cape Town, South Africa.

## 2.2 Tissue sampling and reference cell lines

Keloid participants (N = 3) were selected as donors for keloid lesional cutaneous tissue based on the study criteria. Keloid dermal tissue was dissected into four site-specific groups: (1) peripheral (margin of the keloid) (2), middle (deep reticular component of the center of keloid) (3), top (superficial papillary component of the center of keloid), and (4) keloid extralesional skin. Normal control skin tissue (non-keloid formers with no family history of keloid disease) samples were collected from healthy female participants (N = 3) during breast reduction surgery. Skin sarcoma tissue sample was donated from cases with a clinically and histologically confirmed DFSP condition (N = 2). All skin tissue samples were obtained from participants after receiving informed ethical consent. This study also included two fibroblastic sarcoma cell lines [Fsarc-01: HT-1080 (HT1080) (ATCC® CCL-121™) and Fsarc-02: HT-1080-Luc2 (ATCC® CCL-121-LUC2™)] and one DFSP cell line (DFSP-CL) (ATCC- Hs 63T) (ATCC CRL-7043) purchased from ATCC (USA) as the reference cell lines for comparitive studies (Supplementary Table 1). All keloid, normal, and DFSP skin samples were processed for primary fibroblasts culturing by the collagenase method and cultured according to the standard protocol (detailed method is available in SI Appendix 1).

## 2.3 h*TERT* expression (pre-transfection)

The h*TERT* gene (quantitative real-time PCR) and protein expression [immunofluorescence (IF) staining and flow cytometry] were studied in PKFs before transfection and compared with the control groups.

## 2.4 h*TERT* plasmid transfection and generation of stable cell lines

An h*TERT* immortalized cell system was used to develop immortalized keloid-derived fibroblast cell line through the following steps. (1) All three groups of PKF cultures were transfected with plasmid DNA (pGRN145, MBA-141™, ATCC) containing h*TERT* gene, separately. (2) The transiently transfected cell lines were treated with hygromycin B (*HygB*; an antibiotic marker for transfection), and resistant stable cell lines were selected and cloned. (3) Analysis of h*TERT* gene transfection at mRNA level was evaluated via quantitative real-time PCR (qRT-PCR), and protein expression was evaluated by flow cytometry. (4) The validation of cellular function of hTERT protein in cell senescence was assessed by senescence-associated ß-galactosidase histochemical staining assay in all three keloid-derived transformed fibroblast cell lines.

## 2.5 Defining cellular characteristics of keloid-derived immortalized fibroblasts

The stable transfected cell lines were evaluated for (a) cell viability, (b) cell growth curve, (c) cell cycle analysis, (d) cell migration, (e) cell invasion, (f) cellular senescence, and (g) hTERT protein expression via IF staining. The KDIF cell lines were validated by testing drug (triamcinolone) sensitivity on apoptosis, viability, and cell migration.

## 2.6 Authentication of cell line: Short Tandem Repeat (STR) profiling

All three cell lines (1. PT-KT-045-stb-CL, ATCC®, Cat. No. STRB3288; 2. PT-KM-045-stb-CL, ATCC®, Cat. No. STRB3289; and 3. PT-KP-045-stb-CL, ATCC®, Cat. No. STRB3289) were authenticated by ATCC STR profiling. Successfully transformed and actively growing cell lines were selected for cloning, stock preparation, and cryopreservation.

## 2.7 Statistical analysis

All experiments were conducted in triplicate, and the results were presented graphically as mean ± standard deviation (SD), 95% confidence interval, and percentage (%) when appropriate. The statistical analysis was carried out by Student's t-test, by using Microsoft Excel version 8. The data were also evaluated by applying two-way ANOVA and Tukey *post-hoc* test. Experiments were performed in triplicate and presented as mean ± S.D. The statistical significance level was set at $^{*}p < 0.05$, $^{**}p < 0.01$, and $^{***}p < 0.001$ (15).

# 3 Results

## 3.1 Primary site–specific keloid fibroblasts exhibited a comparatively low expression of h*TERT*

PKFs were isolated from four different sites (KT, KM, KP, and KE) of keloid skin tissue and then cultured and passaged three times (Figures 1A–C). Once cultures were established, we examined the

hTERT expression in PKFs at gene (qRT-PCR) and protein levels (IF) compared with the control groups (KE, NF, DFSP, and FS). The results from h*TERT* gene expression (qRT-PCR analysis) revealed no significant difference in relative gene expression (h*TERT*) between KT, KM, KP, and KE but showed a significantly lower h*TERT* gene expression (KT, 1.28 ± 0.22, $p < 0.023$; KP, 1.24 ± 0.43, $p < 0.04$; and KM, 1.11 ± 0.51, $p < 0.037$) compared to FS (FS, 1.80 ± 0.09) (Figure 1D). It is also noticed that h*TERT* expression was significantly lower in KT (1.28 ± 0.22, $p < 0.03$) and KM (1.11 ± 0.51, $p < 0.045$) compared with that in DFSP (1.75 ± 0.11). A significantly low h*TERT* expression was observed in KT (1.28 ± 0.22, p < 0.03) compared with that in NF (1.76 ± 0.13).

hTERT protein expression evaluated by flow cytometry Fluorescence-Activated Cell Sorting (FACS) in KT, KM, and KP was compared with that in the control groups (KE, NF, DFSP, and FS), which revealed a significantly higher percentage of hTERT-Fluorescein

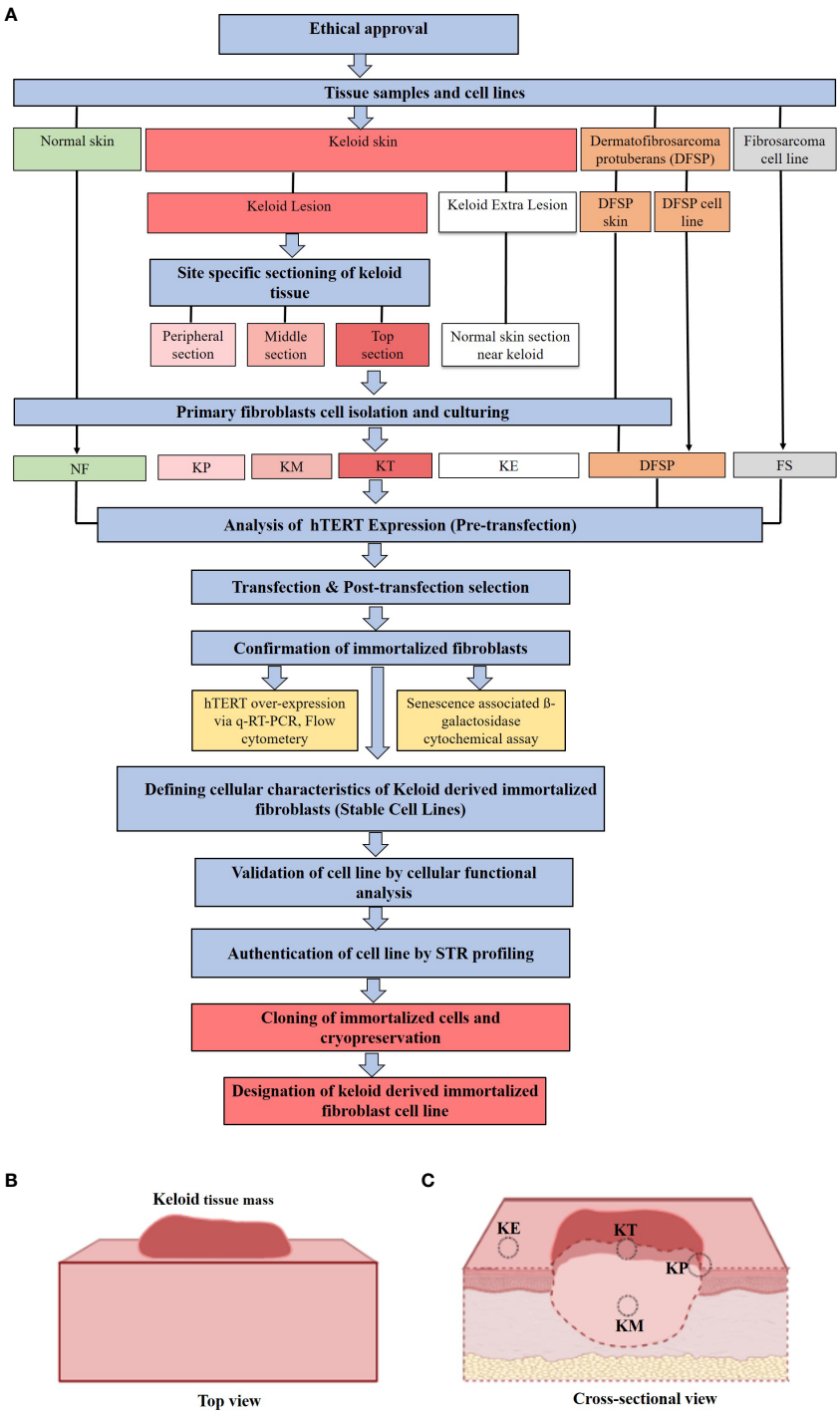


FIGURE 1 (Continued)

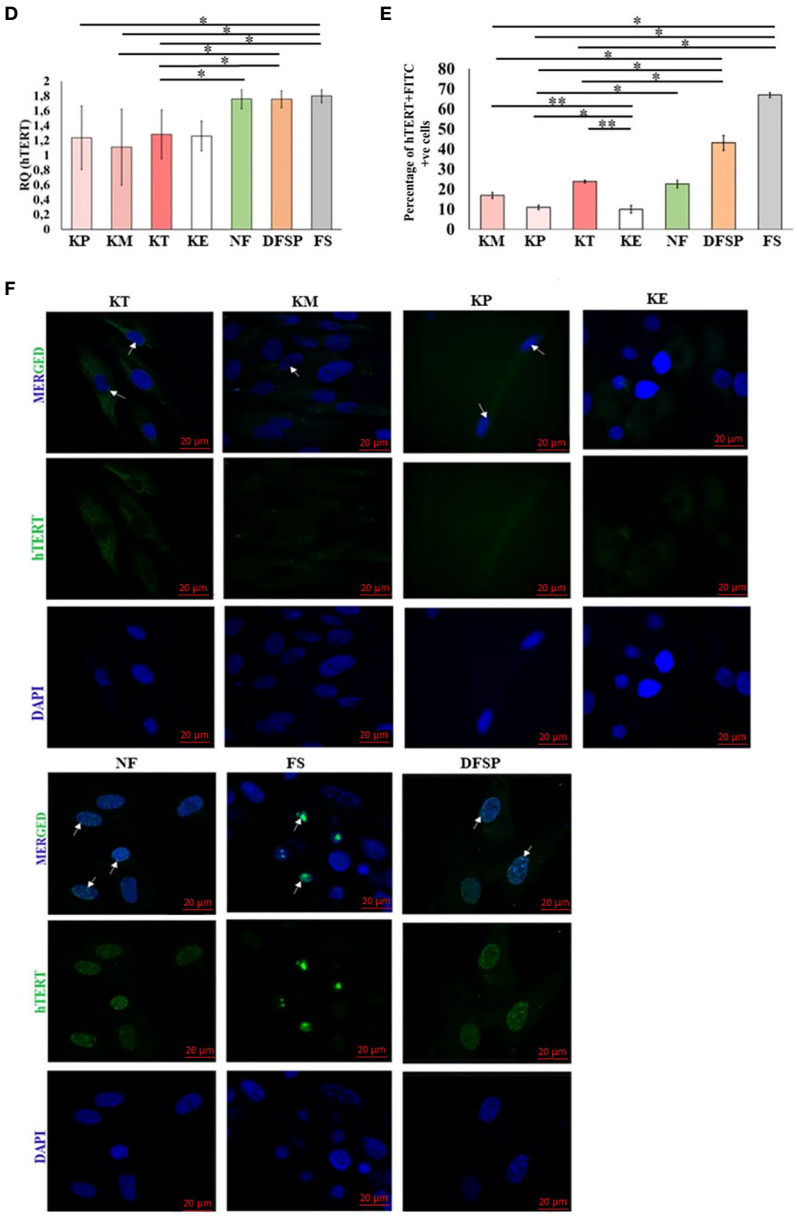


FIGURE 1 (Continued)
**(A)** Study methodology flow diagram. KP, keloid peripheral fibroblasts; KT, keloid top fibroblasts; KM, keloid middle fibroblasts; KE, keloid extralesional skin; NF, normal skin fibroblast; DFSP, dermatofibrosarcoma protuberans; FS, fibroblastic sarcoma cell line. **(B)** Overall bird's-eye view of keloid tissue mass. **(C)** Cross-sectional view of keloid tissue mass showing four different anatomical locations in relation to the lesion: (i) top of the keloid skin includes the superficial papillary dermis (KT), (ii) center keloid tissue includes the deep reticular dermis as middle of the keloid (KM), (iii) margin as peripheral part of keloid skin (KP), and (iv) neighboring normal appearing skin as keloid extralesional skin (KE), marked on keloid tissue mass for sectioning and isolation of site-specific primary keloid fibroblasts (PKFs). hTERT gene expression analysis in primary keloid fibroblasts (KP, KT, KM, and KE) and control groups (NF, DFSP, and FS) via **(D)** qRT-PCR and **(E)** protein expression by flow cytometry, and results were presented graphically as the percentage of hTERT-FITC–positive cells and **(F)** Immunofluorescence staining with hTERT-FITC (green, nuclear signal) and 4′,6-Diamidino-2-phenylindole dihydrochloride (DAPI) (blue, nuclear); scale bar, 20 µm. Experiments were performed in triplicate and analyzed by two-way ANOVA and significance levels set at $*P < 0.05$ and $**P < 0.01$.

isothiocyanate (FITC)–positive cell population in KT, KM, and KP (KT, 23.8 ± 0.69%, $p < 0.0004$; KP, 10.9 ± 1.03%, $p < 0.01$; and KM, 16.9 ± 1.5%, $p < 0.0004$) compared with that in KE (10 ± 1.84%) but significantly lower than that in FS (66.9 ± 1.2%, $p < 0.003$) and DFSP fibroblasts (43.1 ± 3.7%, $p < 0.01$). Furthermore, KP showed a significantly lower percentage of hTERT-FITC–positive cell population (10.9 ± 1.03%, $p < 0.41$) compared with NF (22.6 ± 1.84%) (Figure 1E). hTERT protein expression was also analyzed through IF analysis, and images showed no detectable nuclear signal in any of the primary keloid group compared to the control groups (Figure 1F).

## 3.2 Development of keloid-derived immortalized fibroblast cell lines by h*TERT* gene transfection and analysis via qRT-PCR and immunofluorescence techniques

hTERT gene transfection was performed by plasmid DNA gene (*pGRN145*; carrying h*TERT* gene) transfection using GeneXPlus Transfection Reagent (Materials and Methods section, SI Appendix 1). Post-transfection gene expression (h*TERT*) analysis was carried out in all three transfected cell lines (PT-KT-045, PT-KM-045, and PT-KP-045). Comparative hTERT gene expression was normalized with *GAPDH* (Glyceraldehyde-3-phosphate dehydrogenase) (Figure 2A). The results revealed a significantly increased expression (fold change) of h*TERT* gene in all three transfected keloid cell lines (KM, 1.67 ± 0.26, $p < 0.010$; KP, 1.5 ± 0.15, $p < 0.013$; and KT, 1.63 ± 0.14, $p < 0.027$) as compared to the non-transfected PKFs (KM, 0.70 ± 0.43; KP, 0.86 ± 0.15; and KT, 1.06 ± 0.34). Post-transfected protein expression of h*TERT* gene was also evaluated by IF staining and compared with non-transfected primary keloid cells. DFSP cells were included as positive control for nuclear hTERT signal. The results showed an hTERT nuclear protein expression (green nuclear expression marked with white arrow on image) in all transfected keloid fibroblasts, compared to the non-transfected PKFs (Figure 2B). Moreover, post-transfection analysis of hTERT protein expression showed that PT-KT-045 cell line exhibited a significantly higher percentage of cell population expressing positive hTERT-FITC signal (28.7 ± 1.3% $p < 0.002$) (Supplementary Figure S1). Histochemical staining for β-galactosidase, used as a marker of cell senescence, was also evaluated in hTERT-transfected cell lines. Significantly, a lower number of β-gal–positive cells were found in all three transfected cell lines (PT-KP-045, 12.8 ± 3.30%, $p < 0.0006$; PT-KT-045, 5.89 ± 2.19%, $p < 0.014$; and PT-KM-045, 11.6 ± 0.11%, $p < 0.002$) compared to KP (55.6 ± 2.4%), KT (29.47 ± 6.2%), KM (23.10 ± 1.4%), and NF (47.6 ± 4.6%, $p < 0.01$) (Figure 2C). These observations suggest possible phenotypic alterations, which are likely to be linked with hTERT transfection in all three transfected keloid cell lines.

## 3.3 Selection of stably transfected cell lines, propagation, and analysis

Post-transfection screening for stably transfected cells lines was carried out by selection of HygB (concentration ranges from 0 μg/mL tp 1,000 μg/mL)–resistant cells at 48-h antibiotic treatment, through the kill curve method and cell viability evaluated by employing 3-[4,5-dimethylthiazol-2-yl]-2,5 diphenyl tetrazolium bromide (MTT) assay (Supplementary Figures S2A–C). The antibiotic-resistant clones were then used for studying the cellular characteristics of KDIF cell lines (Supplementary Table 2).

## 3.4 Cellular characteristics of keloid-derived immortalized fibroblasts

We evaluated the cellular characteristics of KDIF such as viability, growth curve, cell cycle, migration, and invasion up to 10 passage number, compared with respective PKFs. The results from MTT assay revealed that metabolic activity (cell viability) of all three KDIF cell lines significantly increased (PT-KM-045, 68.6 ± 0.28%, $p < 2.84$ E-05; PT-KP-045, 63.12 ± 4.25%, $p < 0.013$; and PT-KT-045, 54.83 ± 6.30%, $p < 0.013$) compared to the respective primary keloid cells (KM, 20.33 ± 2.4%; KT, 11.03 ± 1.56%; and KP, 22.6 ± 2.7%) and NF (30.56 ± 1.6%, $p < 0.01$). Actively viable growing behavior of KDIF cell lines exhibited similarity to DFSP and FS fibroblast growth pattern (Figure 3A).

Cell migration potential of PKFs has been investigated previously (16). In our study, 48-h post-scratch assay revealed that PT-KT-045 and PT-KM-045 cell lines (63.0 ± 1.3%, $p < 0.6$, and 58.07 ± 2.23%, $p < 0.37$, respectively) exhibited a similar migration trend compared to primary KT and KM fibroblasts (63.63 ± 1.04% and 61.95% ± 2.93%, respectively) except PT-KP-045 cell line that showed a significantly enhanced cell migration (86.08 ± 1.60%, $p < 0.04$) in comparison to the primary KP fibroblasts (78.8 ± 5.15%) and NF fibroblasts (60.77 ± 3.17%). Both PT-KT-045 and PT-KM-045 cell lines exhibited (63.0 ± 1.3% and 58.07 ± 2.23%, respectively) a significantly lower migration potential compared to DFSP (70.80 ± 2.02%, $p < 0.004$) and FS (100 ± 1.2%, $p < 0.0003$) (Figure 3B; Supplementary Figure S3).

hTERT overexpression is known to activate invasive behavior in cells (17); therefore, we investigated the cellular invasive potential in all three KDIF cell lines. It was noticed that number of invasive cells were significantly higher in all KDIF cell lines (PT-KP-045, 171 ± 7.5, $p < 0.001$, PT-KM-045, 85 ± 10.3, $p < 0.003$ and PT-KT-045, 108.5 ± 9.8, $p < 0.007$) compared to NF (12.5±0.57). Notably, Both PT-KM-045 and PT-KP-045 cell lines showed significantly (85 ± 10.3, $p < 0.029$; 171 ± 7.5, $p < 0.002$, respectively) increased directional response (chemotaxis) towards growth factor fetal bovine serum (FBS), that resulted in their ability to migrate through a physical barrier towards chemo-attractant gradient, as compared to the primary KM and KP fibroblasts (26 ± 5.7 and 20.5 ± 2.9, respectively). Thus, hTERT overexpression in KDIF cell lines enhanced the cellular chemotaxis and directional response, indicating a similarity in behavior with DFSP and FS (Figures 3C, D).

The cell growth curve pattern had been studied over 10 passages for all three KDIF cell lines and compared with control groups. The results showed that all three KDIF cell lines grew significantly faster and obtained a fast growing characteristic at passage 9 (Figure 3E) compared to primary keloid and NFs. This phenotypic behavior in growth potential indicated the result of spontaneous hTERT-mediated immortalized transformation. Observations about cell viability and growth curve were further investigated by quantification of total DNA content at the G0, G1, S, and G2 phases of cell cycle in all three cell line's populations at 48-h and 12-day time points. Among all KDIF cell lines, PT-KT-045 cell line showed the highest percentage of cell population at the G1 phase (growth phase) (51.51 ± 0.23% $p < 0.016$) and at the S phase (36.15 ± 1.23% $p < 0.002$), at 48-h time point, that increased up to (83 ± 1.22% $p < 0.001$) the 12-day time point (Figure 3F), representing a fast growing cell line during early and late culture time points, which shows its active cell growth potential throughout the cell culturing.

10.3389/fimmu.2024.1326728

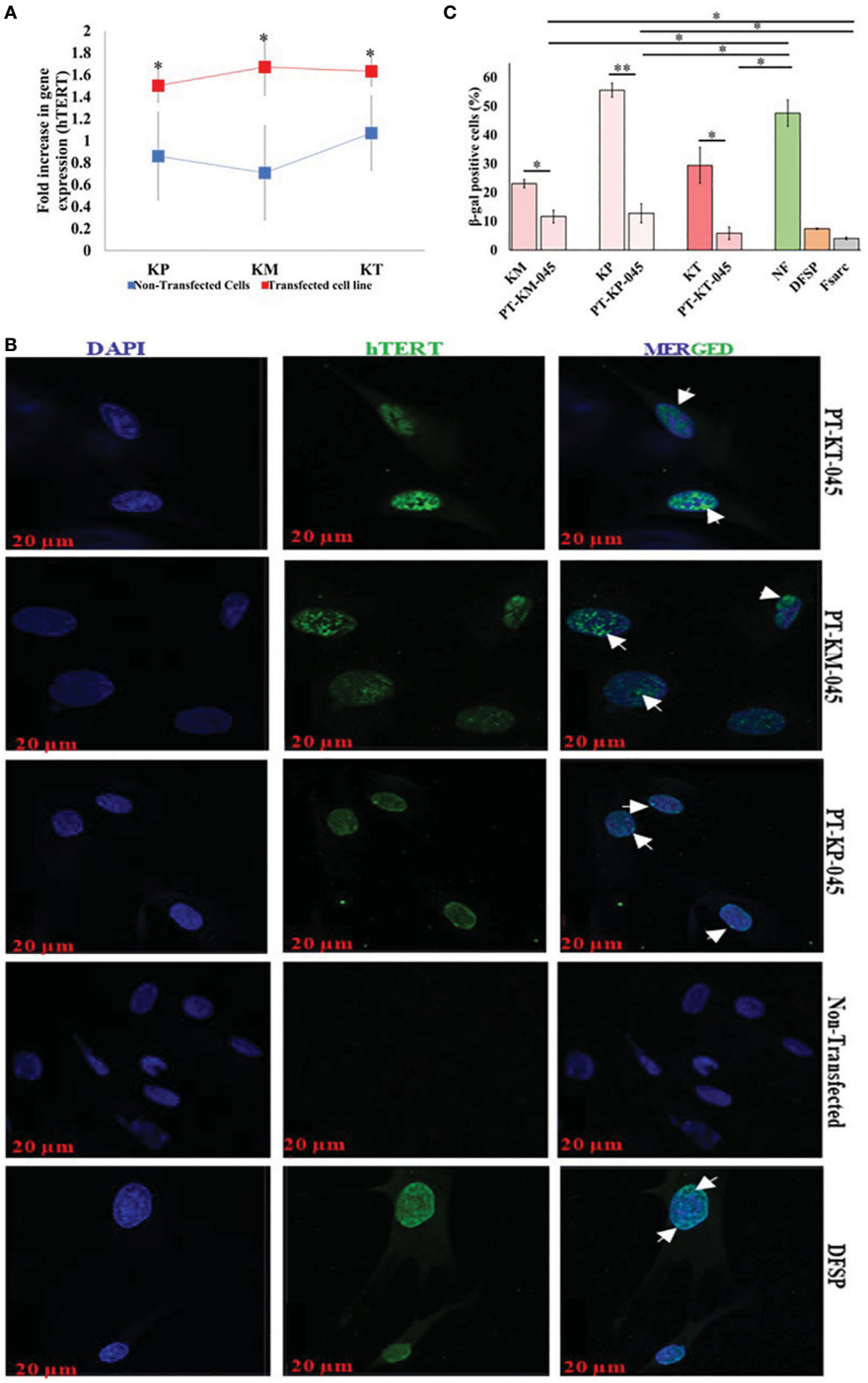


FIGURE 2
Immortalized Keloid cell line validation post-transfection. **(A)** qRT-PCR demonstrated an increase in h*TERT* gene expression (fold increase) between respective primary keloid cell lines (control, blue) and post-transfected cell lines (transfected, red). **(B)** Immunofluorescence staining with hTERT-FITC (green, nuclear signal) and DAPI (blue, nuclear); scale bar, 20 µm. **(C)** β-Galactosidase–associated senescence expressed as the percentage of stained cells and presented graphically. Experiments were performed in triplicate and presented as mean ± S.D. Significance levels were set at $*P < 0.05$ and $**P < 0.01$.

## 3.5 Validation of keloid-derived immortalized fibroblast cell lines

The immortalization of cells, through overexpression of telomerase (hTERT), has the advantage of maintaining a stable cellular phenotype as the cells remain diploid, but primary cultures from independent isolations can vary. Their overall growth characteristic and cellular response can also be altered due to introduced changes in their genetic makeup during the process of immortalization (18). Therefore, it is necessary to

10.3389/fimmu.2024.1326728

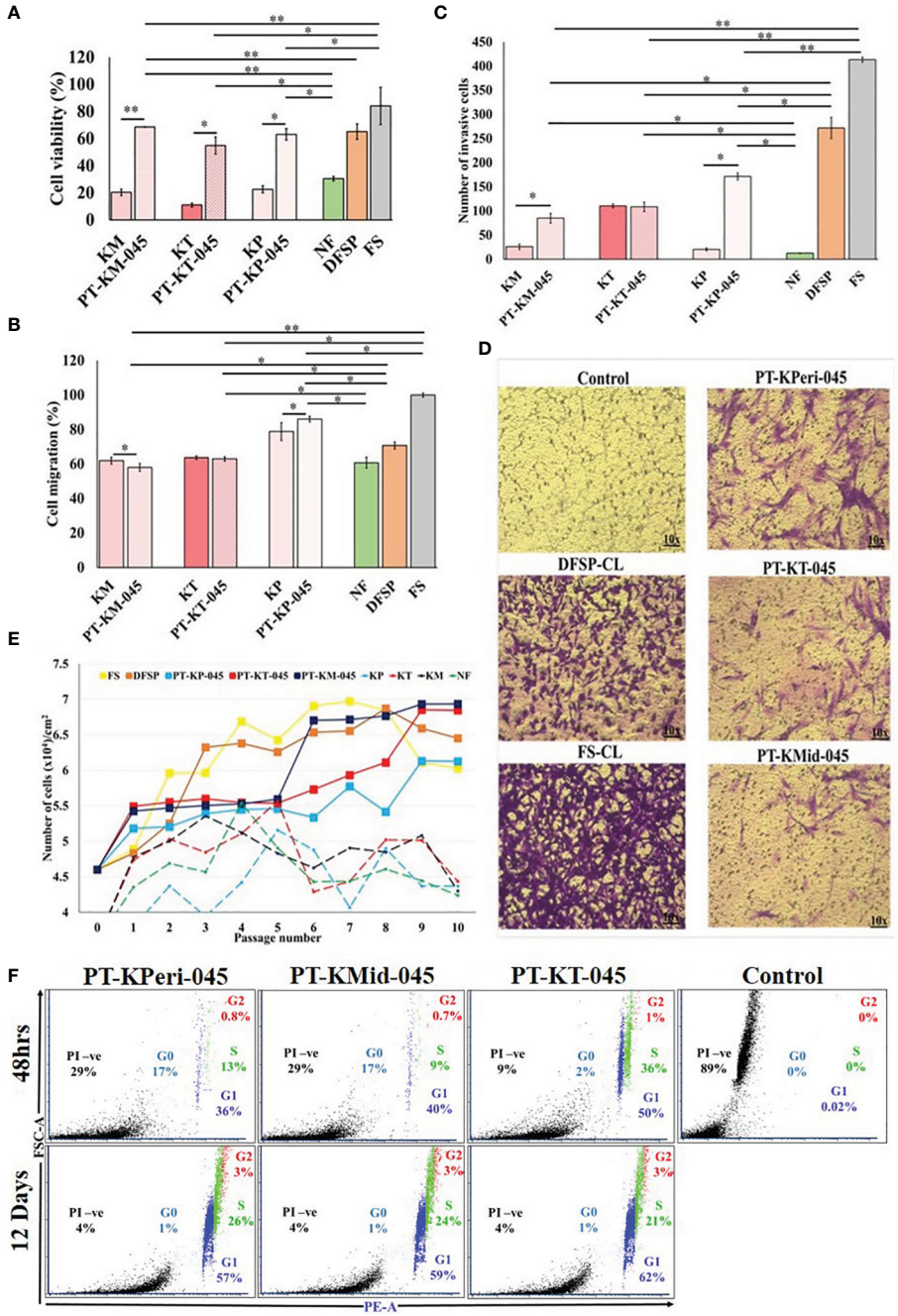


FIGURE 3
Cellular characteristics of keloid-derived immortalized fibroblast cell lines. **(A)** Cell viability, **(B)** cell migration, **(C)** cell invasion, **(D)** images showing a number of invading cells (image magnification, ×10), **(E)** population doubling assay, and **(F)** cell cycle analysis via flow cytometry using propidium iodide (PI) staining. Experiments were performed in triplicate and presented as mean ± S.D.). Significance levels were set at $^{*}P < 0.05$ and $^{**}P < 0.01$.

investigate and compare the cellular response of KDIF cell lines to see whether these cell lines represent keloid cell behavior or characteristics that would further validate their candidature as a representative model. Therefore, we studied the protein expression of collagen I in all three KDIF cell lines via IF staining. All three KDIF cell lines showed an increased protein expression of collagen I (Figure 4).

## 3.6 Functional validation: triamcinolone drug treatment decreased the cell viability and cell migration in KDIF and PKF cell lines

Studies have shown that triamcinolone and verapamil affect cell viability and induce apoptosis in PKFs (19–21) and are used clinically

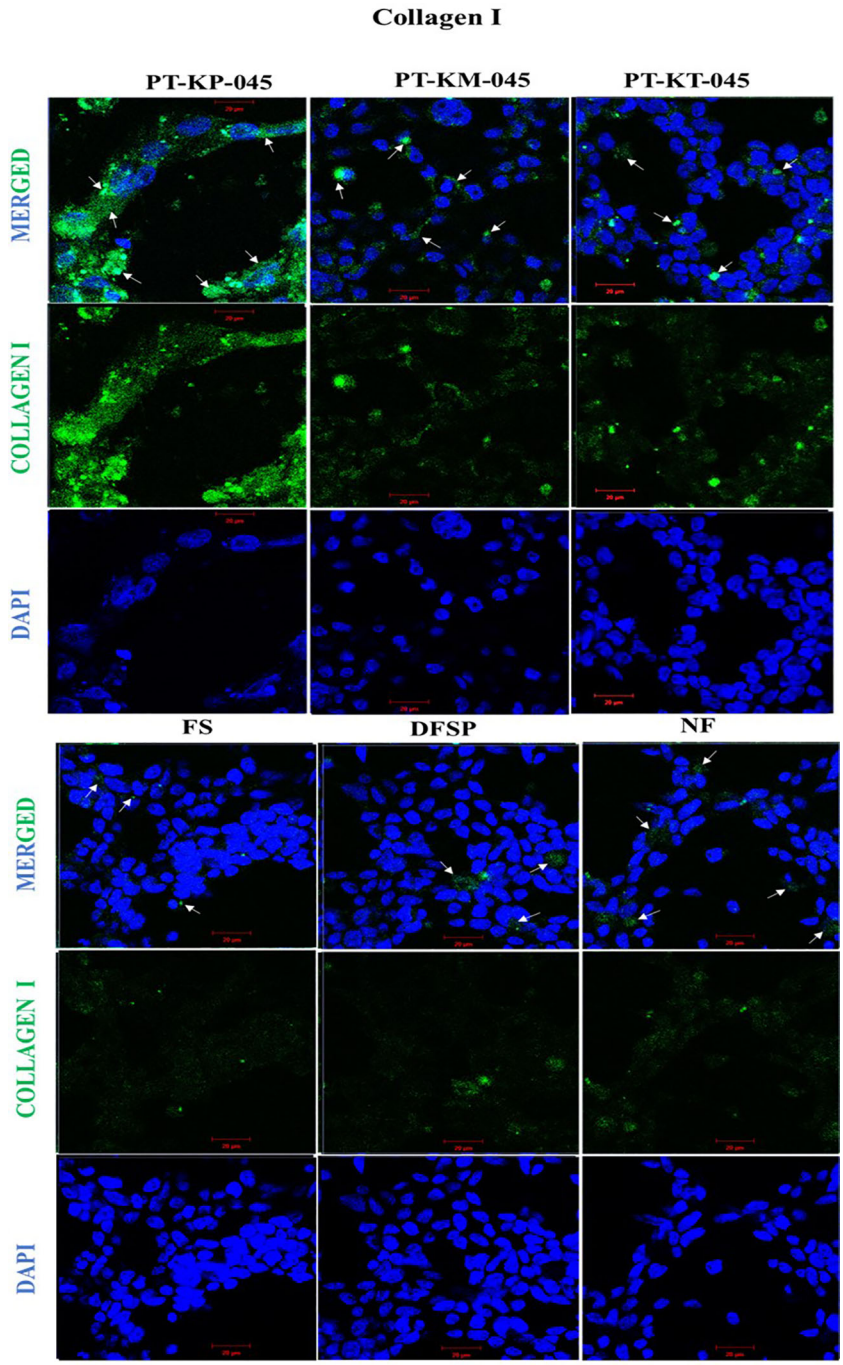


FIGURE 4
Immunofluorescence staining of increased collagen I protein expression in keloid cell lines compared with control. Cells were immunofluorescent labeled with anti-rabbit Alexa 488 (green, signal) marked with white arrows, and counterstained with DAPI (blue, nuclear signal) in transfected keloid fibroblasts group (PT-KP-045, PT-KT-045, and PT-KM-045) and DFSP, FS, and NF included as +ve control group. Scale bar set at 20 μm.

to treat keloids (22). Hence, KDIF cell lines were subjected to functional analysis and drug response studies for verapamil and triamcinolone. KDIF cell lines showed sensitivity to triamcinolone (100 μM each), which decreased cell viability significantly up to 20 ± 1.3% ($p < 0.02$) in all KDIF cell lines compared to the control group (untreated) (Figure 5A). Further investigation using annexin V apoptotic marker through flow cytometry analysis showed an increased percentage of cell population, positive for pre-apoptotic signal (Annexin V), in response to verapamil and, particularly, triamcinolone drug treatment (100 μM each) in KDIF (PT-KP-045, 22.4 ± 1.2%, $p < 0.001$; PT-KT-045, 21.7 ± 0.6%, $p < 0.003$; and PT-KM-045, 18.8 ± 0.7%, $p < 0.03$) as well as PKF cell line group (KP, 14.3 ± 0.2%, $p < 0.006$; KT, 16.2 ± 0.04%, $p < 0.01$; and KM, 15.5 ± 0.3%, $p < 0.025$) compared to the vehicle group (Figure 5B). These results confirmed the cellular response of KDIF cell lines toward drug treatment and represent PKF cell line's drug sensitivity particularly

for triamcinolone. Additionally, the effects of verapamil and triamcinolone (100 μM) on cell migration of KDIF and PKF cell lines were evaluated by employing an *in vitro* scratch assay at 24-h and 48-h time points. Triamcinolone significantly reduced the cell migration rate at both time points in all KDIF (PT-KP-045, 23.38 ± 4.50%, $p < 0.0002$; PT-KT-045, 13.64 ± 9.2%, $p < 0.004$; and PT-KM-045, 13.82 ± 2.11%, $p < 0.009$) as well as PKF cell lines (KP, 18.08 ± 6.9%, $p < 0.001$; KT, 11.84 ± 3.4%, $p > 0.7$; and KM, 15.40 ± 1.8%, $p < 0.009$) (Figure 5C), providing another supportive information about the representativeness of KDIF in terms of keloid behavior.

## 3.7 Authentication and designation

After functional validation, cell line identity and purity were evaluated for all three KDIF cell lines, by using standard genotyping

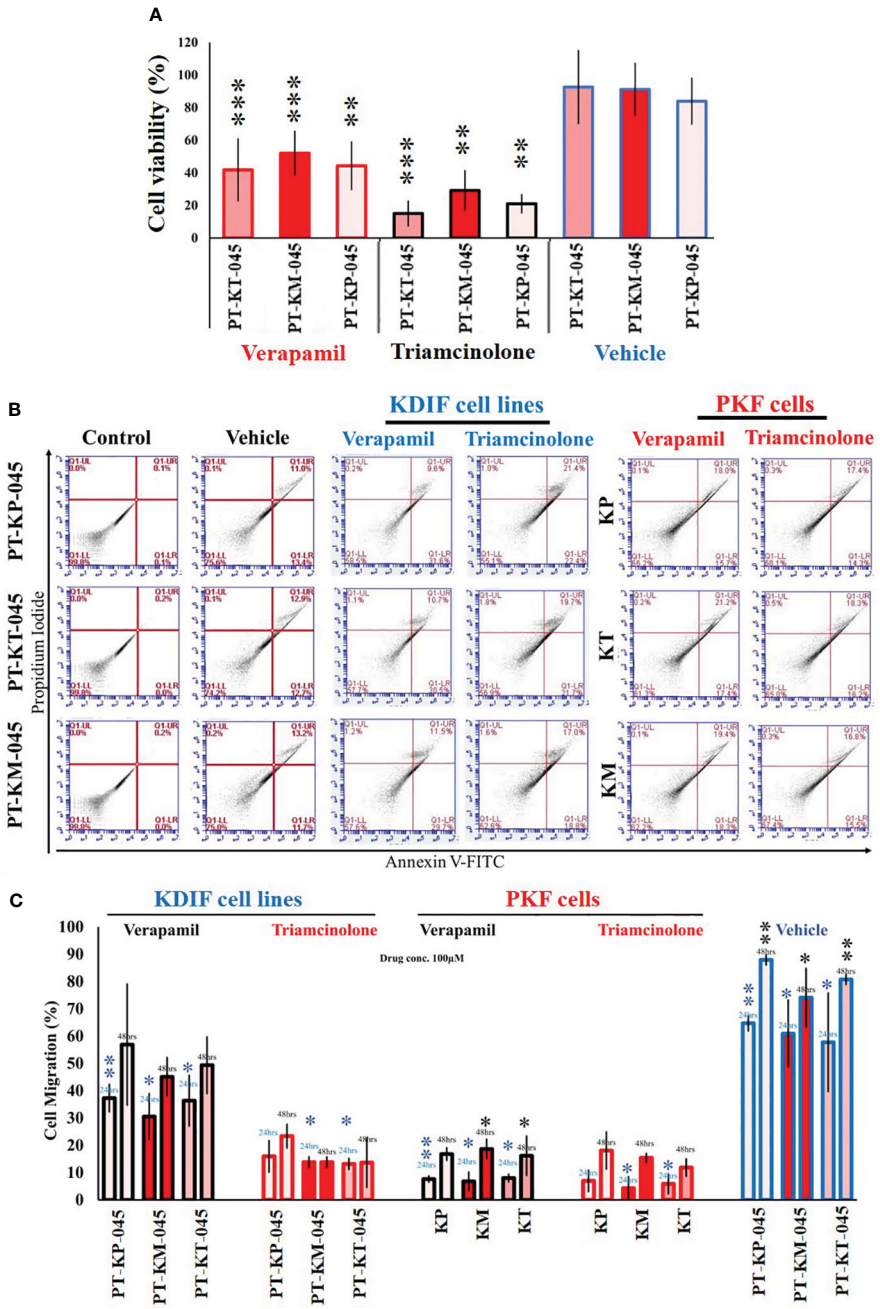


FIGURE 5
Functional validation of Keloid cell lines with drug testing. **(A)** Effect of verapamil and triamcinolone drug treatment (100 μM each) evaluated on cell viability of KDIF (PT-KT-045, PT-KM-045, and PT-KP-045) and percentage (%) cell viability was significantly decreased compared to vehicle group (untreated). **(B)** Effect of verapamil and triamcinolone drug treatment (100 μM each) evaluated on cellular apoptosis in KDIF, detected by staining with annexin V–conjugated FITC through flow cytometry. **(C)** Effects of verapamil and triamcinolone on cell migration represented graphically as the percentage (%) cell migration toward scratch zone at 24-h and 48-h time points. Experiments were performed in triplicate and presented as mean ± S.D.). Significance levels were set at $*p < 0.05$, $**p < 0.01$ and $***p < 0.001$.

technique such as the gold standard, STR profiling through ATCC services for human cell lines. Human cell line authentication assay identifies STR markers, which are short repetitive segments of DNA found between genes, at specific loci to established DNA fingerprints for every human cell line. This process involves PCR amplification of 17 most repetitive polymorphic markers plus Amelogenin gene in human genome and pattern use to develop unique identity profile of human cell lines. The results were presented as electropherogram showing the highest matches to the sample profile in the database along with the standard loci for each submitted cell line. First immortalized cell line labeled "PT-KT-045," derived from primary "Keloid Top fibroblasts (KT)" (ATCC®, Cat. No. STRB3288) (Figure 6A), shows no match with ATCC database at any of the Loci and is designated as "PT-KT-045-stb-CL" having unique STR identity. Electropherogram for the second immortalized cell line labeled "PT-KM-045," derived from

A

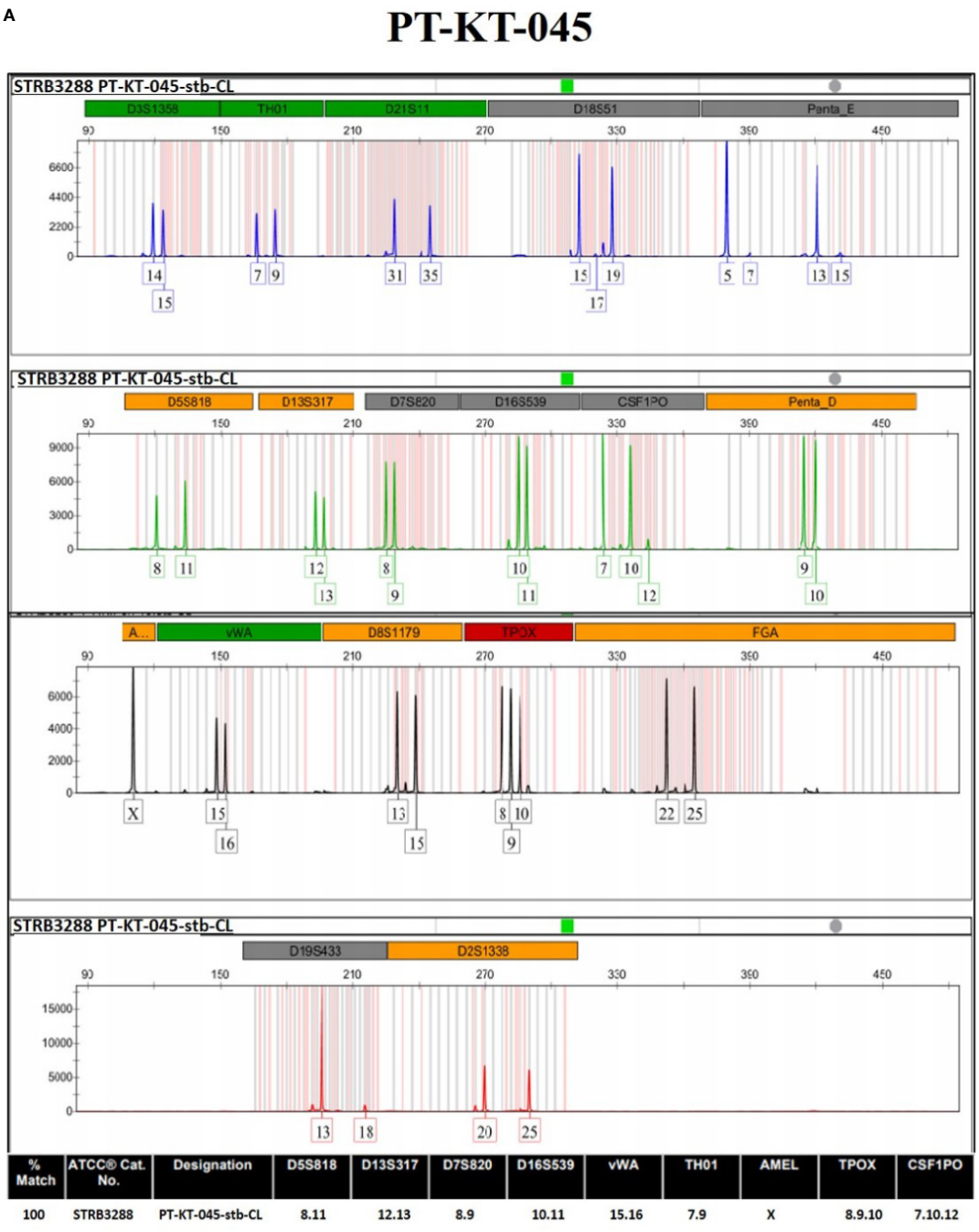


| % Match | ATCC® Cat. No. | Designation | D5S818 | D13S317 | D7S820 | D16S539 | vWA | TH01 | AMEL | TPOX | CSF1PO |
|---|---|---|---|---|---|---|---|---|---|---|---|
| 100 | STRB3288 | PT-KT-045-stb-CL | 8.11 | 12.13 | 8.9 | 10.11 | 15.16 | 7.9 | X | 8.9.10 | 7.10.12 |

FIGURE 6 (Continued)

**B**

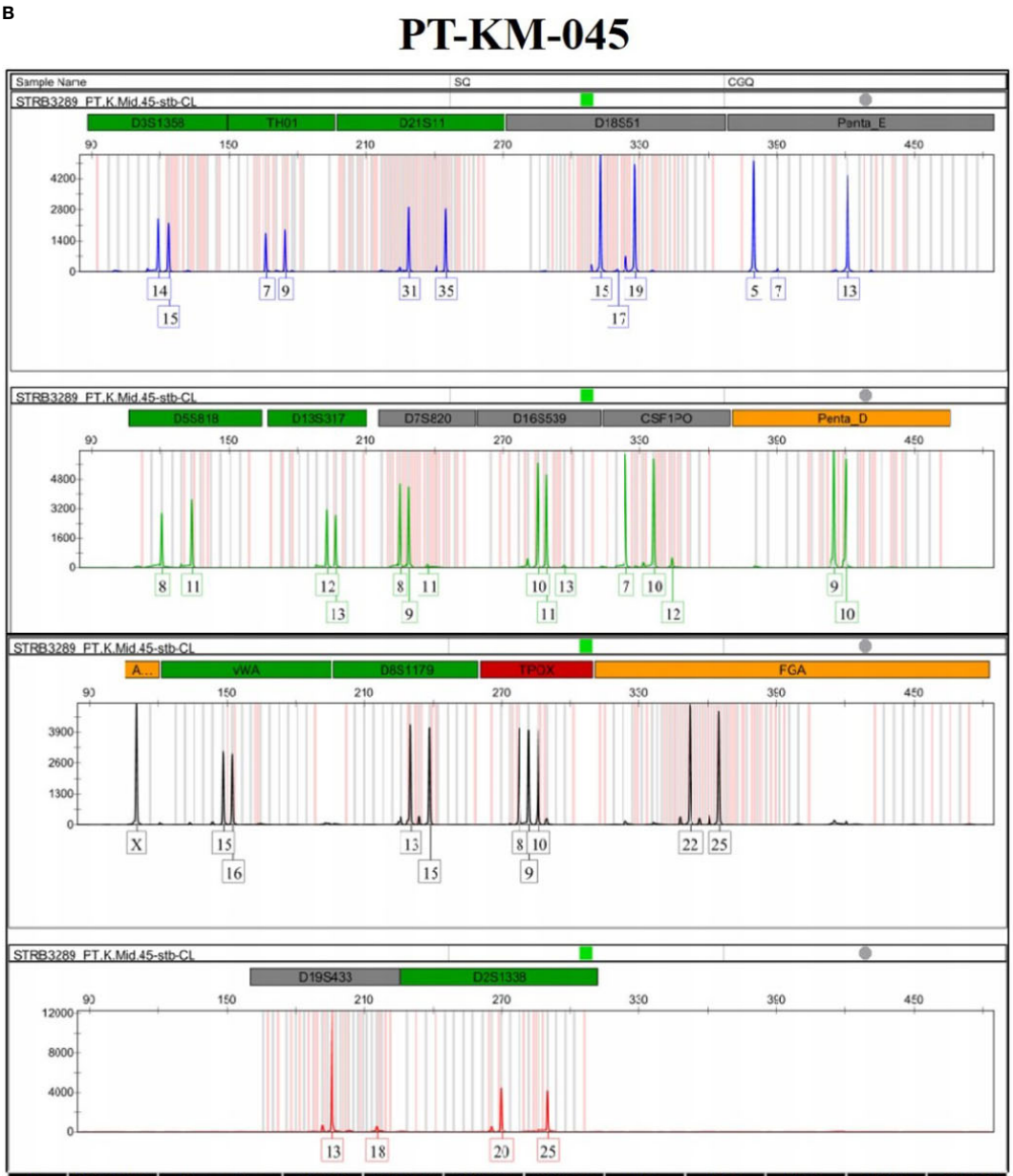


| % Match | ATCC® Cat. No. | Designation | D5S818 | D13S317 | D7S820 | D16S539 | vWA | TH01 | AMEL | TPOX | CSF1PO |
|---|---|---|---|---|---|---|---|---|---|---|---|
| 100 | STRB3289 | PT-KM-045-stb-CL | 8,11 | 12,13 | 8,9,11 | 10,11,13 | 15,16 | 7,9 | X | 8,9,10 | 7,10,12 |
| 82 | crl-3127 | UACC-1179; Breast Adenocarcinoma; Human (Homo sapiens) | 12 | 12 | 8,11 | 10,13 | 16 | 6 | X | 8 | 10 |

FIGURE 6 (Continued)

c

# PT-KP-045

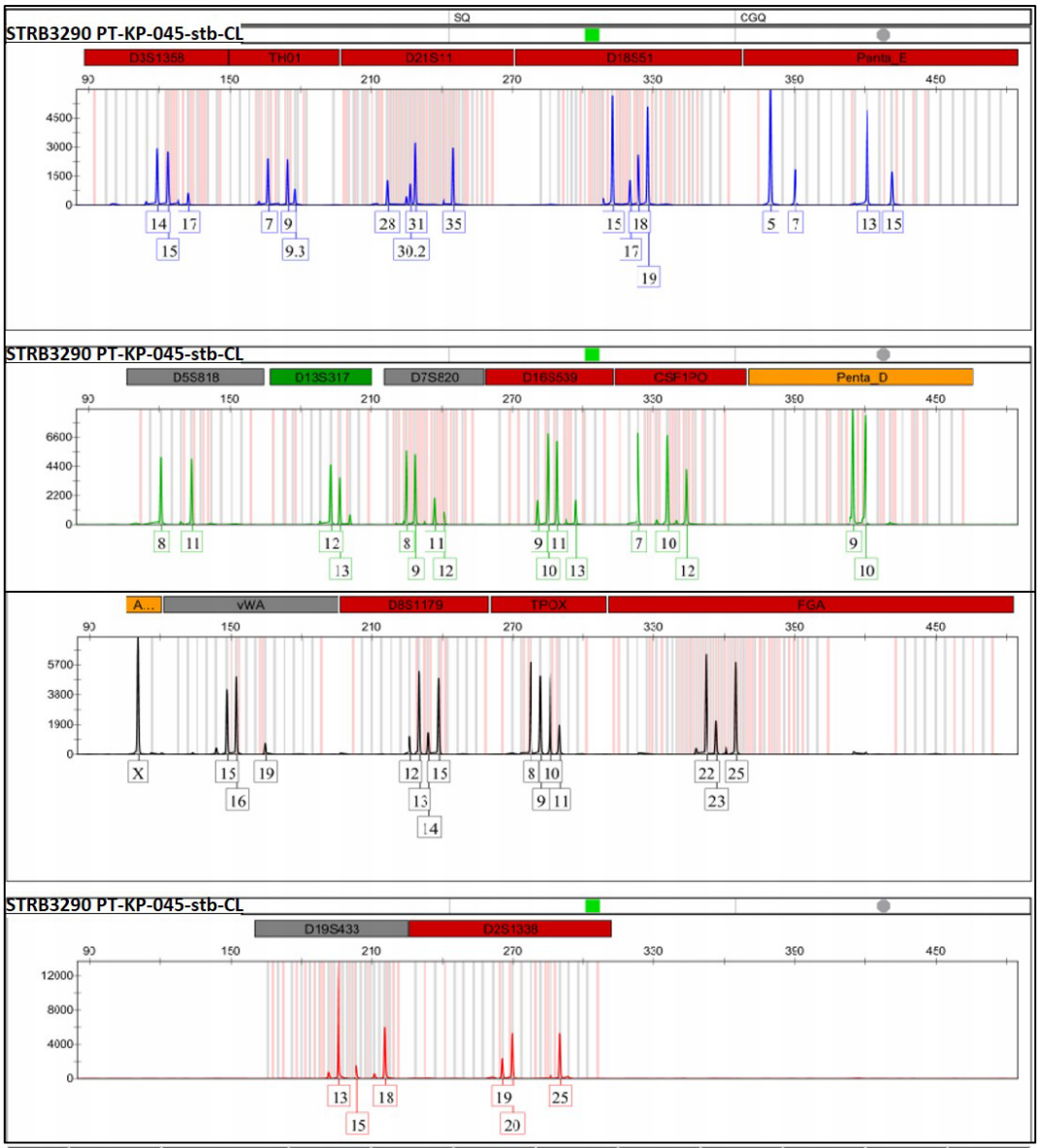


| % Match | ATCC® Cat. No. | Designation | D5S818 | D13S317 | D7S820 | D16S539 | vWA | TH01 | AMEL | TPOX | CSF1PO |
|---|---|---|---|---|---|---|---|---|---|---|---|
| 100 | STRB3290 | PT-KP-045-stb-CL | 8,11 | 12,13 | 8,9,11,12 | 9,10,11,13 | 15,16,19 | 7,9,9,3 | X | 8,9,10,11 | 7,10,12 |
| 81 | CRL-1573 | 293; Embryonic Kidney: Human (Homo sapiens) | 8,9 | 12,14 | 11,12 | 9,13 | 16,19 | 7,9,3 | X | 11 | 11,12 |

FIGURE 6 (Continued)
ATCC authentication of keloid-derived immortalized fibroblast cell lines via STR profiling. Electropherogram showing the 17 most repetitive polymorphic markers plus Amelogenin gene (D3S1358, TH01, D21S11, D18S51, Penta_E, D5S818, D13S317, D7S820, D16S539, CSF1PO, Penta_D, Amelogenin, vWA, D8S1179, TPOX, FGA, D19S433, and D2S1338) to develop the unique STR identity for **(A)** PT-KT-045, **(B)** PT-KM-045, and **(C)** PT-KP-045 human cell lines.

primary "Keloid Middle fibroblasts (KM)," is designated as "PT-KM-045-stb-CL" (ATCC®, Cat. No. STRB3289). It is showing 100% match for unique STR profile and 82% relatedness with UACC-1197 Breast Adenocarcinoma (crl-3127) from ATCC database (*Homo sapiens*) (Figure 6B). Third immortalized cell line labeled "PT-KP-045," derived from primary "Keloid Peripheral fibroblasts (KP)," designated as "PT-KP-045-stb-CL," (ATCC®, Cat. No. STRB3289), shows 100% match for unique STR profile and 81% relatedness with 293 embryonic kidney cells (*Homo Sapiens*) (CRL-1573) from ATCC database (Figure 6C). All results based on STR profiling confirmed that all three KDIF cell lines are authenticated as novel, clean, and originated from the same human source (female) (100% match), karyotypically normal and not contaminated with any other source.

# 4 Discussion

Lack of a relevant study model and the absence of an animal model pose a challenge in studying keloid pathobiology. In addition, patient-derived cultured PKFs are sub-optimal as they are heterogeneous in nature depending on lesional site of origin and have a limited lifespan as they age through passaging with a limited tissue supply. Thus, there is an unmet need to develop a robust and relevant cellular model that can faithfully represent keloid's pathognomic features.

Thus, we present, for the first time, KDIF cell lines from primary fibroblasts obtained from specific lesional sites (peripheral, middle, and top) within keloid tissue. We employed the strategy of overexpressing the h*TERT* gene to support the immortalized characteristic phenotype in keloid cell lines. For this purpose, specifically, we used the non-viral plasmid vector containing h*TERT* gene (pGRN145) as compared to available viral vectors (i.e., SV40), to eliminate any possibility of viral contamination in the genome of keloid fibroblast and to prevent the potential emergence of a cancerous phenotype in these cells. This approach was developed on the basis of the observation/knowledge that keloids exhibit a distinct nature compared to malignant tumors, which is clearly shown in our study by including two control groups of soft tissue carcinomas (1): DFSP and (2) FS. Through experiments utilizing qRT-PCR, flow cytometry, and IF techniques, we observed that the expression of the h*TERT* gene and protein in all three keloid site-specific primary fibroblasts (KT, KM, and KP) was lower when compared to DFSP and FS (as shown in Figures 1D–F).

Low hTERT expression in all PKF is responsible for limited lifespan in primary fibroblasts that can be counteracted by increased activity of telomerase, thus preserving telomere length and cellular functions (23). Hence, we envisioned this approach to extend the lifespan of patient-derived primary cells, which is known as the "immortalized cell line model approach" in order to induce overexpression of hTERT. Subsequently, we developed a KDIF cell line by introducing h*TERT* gene via transfection in all three site-specific PKF cells (peripheral, middle, and top keloid fibroblasts). Additionally, we demonstrated that stable KDIF cell lines showed enhanced expression of hTERT. The introduction of the h*TERT* gene is a widely used strategy to extend the lifespan of many cell types, and successful immortalization has, for instance, previously been reported in human retinal pigment epithelial cells (24).

Reconstitution of telomerase activity by induced expression of hTERT results in an immortal phenotype in various types of normal human cells, including fibroblasts. Despite transformation characteristics, it is unclear whether hTERT-immortalized cells are physiologically and biochemically the same as their normal counterparts (25). In view of the fact that continuous cell expansion always provides a selective advantage for rapid growth, the cellular phenotype can occasionally become biased because of the overgrowth of the most rapidly dividing cells, rather than the best differentiating cells (18). Therefore, we also evaluated the cellular as well as the functional characteristics of KDIF cell lines. Significantly improved cell viability and cell growth curve showed a fast growing trend in all three KDIF cell lines as a result of spontaneous hTERT-mediated immortal transformation. Observations about cell viability and growth curve were further evaluated by studying the cell cycle phase, in all three cell lines at 48-h and 12-day time point by flow cytometry. PT-KP-045 cell line was noticed as actively growing cells at the late stage of culturing and surpassing senescence. Furthermore, it was observed that all KDIF cell lines exhibited decreased senescence activity. Moreover, KDIF cell lines exhibited significantly increased cell migration and invasion, owing to hTERT overexpression, which is known to promote cell migration (16, 26, 27).

It is well recognized that increased Collagen I protein expression is associated with dermal fibrosis (28). Previous studies reported a significantly elevated protein expression of collagen 1 in keloid fibroblasts particularly at the growing margins of keloid scars (4). In this study, IF microscopy showed the increased expression of collagen 1 protein in every KDIF cell line, with notably abundant presence in PT-KP-045 cell line. Even though our preliminary testing on collagen 1 expression appears limited; this was conducted in order to provide additional insight into functional evaluation of our preliminary findings.

Furthermore, the use of triamcinolone for treating the keloid fibroblasts has been an active area of research (29–31), as it has shown effectiveness in modulating fibroblast activity (32). In our functional testing of drug efficacy on immortalized keloid fibroblast cell line, we specifically investigated that triamcinolone treatment–induced apoptosis affected viability and inhibited cell migration in KDIF cell lines as these are primary and core cellular characteristics identified during the fibroproliferative phenotypic development of keloids. These outcomes validate the responsiveness of KDIF cells to the drug and highlight the particular sensitivity of PKF cells to triamcinolone. This functional validation provides additional information about the representativeness of PKF as a suitable model for studying the cellular and therapeutic response of keloid fibroblasts in an *in vitro* research setting.

Moreover, human cell line identity and purity determination by "STR profiling" for all three KDIF cell lines established KDIF cell lines akin to standard cell lines exempted from genetic variation (genetically identical populations) and provided an unlimited cell population that overcomes the problem commonly encountered with limited supply of PKFs. In summary, these results demonstrate evident genetic, cellular, and biological alterations (h*TERT* gene–derived immortalization) in all KDIF cell lines as they represent

keloid cellular behavior and characteristics, confirming their candidature as a suitable in vitro model for research into keloids.

## Data availability statement

The original contributions presented in the study are included in the article/Supplementary Material. Further inquiries can be directed to the corresponding author.

## Ethics statement

The studies involving humans were approved by Human Research Ethics Committee (HREC REF Number 493/2009, Date 30/10/2018), Faculty of Health Sciences,University of Cape Town, South Africa. The studies were conducted in accordance with the local ethical guidelines and institutional requirements. The participants provided their written informed consent to participate in this study.

## Author contributions

AS: Data curation, Formal analysis, Investigation, Methodology, Validation, Visualization, Writing – original draft, Writing – review & editing. AB: Conceptualization, Formal analysis, Funding acquisition, Investigation, Methodology, Project administration, Resources, Supervision, Validation, Visualization, Writing – review & editing. NPK: Formal analysis, Funding acquisition, Investigation, Methodology, Project administration, Resources, Supervision, Validation, Visualization, Writing – review & editing.

## Funding

The author(s) declare financial support was received for the research, authorship, and/or publication of this article. This research project was funded by the South African Medical Research Council (Wound Healing and Keloid Research Unit) and the National Research Foundation (SARChI Chair in Dermatology).

## Acknowledgments

We are thankful to Prof. Hudson Donald and his team from Division of Plastic and Reconstructive Surgery, Groote Schuur Hospital, for facilitating the keloid and normal skin tissue sample collection. We are also thankful to Prof. Lydia Cairncross and her team from Department of Surgery, Groote Schuur Hospital, Cape Town, South Africa, for facilitating the DFSP skin tissue sample collection.

## Conflict of interest

The authors declare that the research was conducted in the absence of any commercial or financial relationships that could be construed as a potential conflict of interest.

## Publisher's note

All claims expressed in this article are solely those of the authors and do not necessarily represent those of their affiliated organizations, or those of the publisher, the editors and the reviewers. Any product that may be evaluated in this article, or claim that may be made by its manufacturer, is not guaranteed or endorsed by the publisher.

## Supplementary material

The Supplementary Material for this article can be found online at: https://www.frontiersin.org/articles/10.3389/fimmu.2024.1326728/full#supplementary-material

## References

1. Bayat A, Arscott G, Ollier WER, Ferguson MWJ, McGrouther DA. 'Aggressive keloid': A severe variant of familial keloid scarring. *J R Soc Med*. (2003) 96:554–5. doi: 10.1258/jrsm.96.11.554

2. Sharma JR, Lebeko M, Kidzeru EB, Khumalo NP, Bayat A. *In vitro* and ex vivo models for functional testing of therapeutic anti-scarring drug targets in keloids. *Adv Wound Care (New Rochelle)*. (2019) 8:655–70. doi: 10.1089/wound.2019.1040

3. Ud-Din S, Thomas G, Morris J, Bayat A. Photodynamic therapy: an innovative approach to the treatment of keloid disease evaluated using subjective and objective non-invasive tools. *Arch Dermatol Res*. (2013) 305:205–14. doi: 10.1007/s00403-012-1295-4

4. Syed F, Ahmadi E, Iqbal SA, Singh S, McGrouther DA, Bayat A. Fibroblasts from the growing margin of keloid scars produce higher levels of collagen I and III compared with intralesional and extralesional sites: clinical implications for lesional site-directed therapy. *Br J Dermatol*. (2011) 164:83–96. doi: 10.1111/bjd.2010.164.issue-1

5. Bayat A, Arscott G, Ollier WER, Fergusond MWJ, McGrouthera DA. Description of site-specific morphology of keloid phenotypes in an Afrocaribbean population. *J Plast Reconstr Aesthet Surg*. (2004) 57:122–33. doi: 10.1016/j.bjps.2003.11.009

6. Jumper N, Paus R, Bayat A. Functional histopathology of keloid disease. *Histol Histopathol*. (2015) 30:1033–57. doi: 10.14670/HH-11-624

7. Bagabir R, Syed F, Paus R, Bayat A. Long-term organ culture of keloid disease tissue. *Exp Dermatol*. (2012) 21:376–81. doi: 10.1111/j.1600-0625.2012.01476.x

8. Caley M, Wall IB, Peake M, Kipling D, Giles P, Thomas DW, et al. Development and characterisation of a Human Chronic Skin Wound Cell Line-Towards an alternative for animal Experimentation. *Int J Mol Sci*. (2018) 19:1001. doi: 10.3390/ijms19041001

9. De Felice B, Wilson RR, Nacca M. Telomere shortening may be associated with human keloids. *BMC Med Genet*. (2009) 10:110. doi: 10.1186/1471-2350-10-110

10. Kassem M, Abdallah BM, Yu Z, Ditzel N, Burns JS. The use of hTERT-immortalized cells in tissue engineering. *Cytotechnology*. (2004) 45:39–46. doi: 10.1007/s10616-004-5124-2

11. Cukusic A, Vidacek NS, Sopta M, Rubelj I. Telomerase regulation at the crossroads of cell fate. *Cytogenet Genome Res*. (2008) 122:263–72. doi: 10.1159/000167812

12. Niu N, Wang L. *In vitro* human cell line models to predict clinical response to anticancer drugs. *Pharmacogenomics*. (2015) 16:273–85. doi: 10.2217/pgs.14.170

13. Zhang X, Yin M, Zhang LJ. Keratin 6, 16 and 17-critical barrier alarmin molecules in skin wounds and psoriasis. *Cells*. (2019) 8:807. doi: 10.3390/cells8080807

14. Nangole FW, Agak GW. Keloid pathophysiology: fibroblast or inflammatory disorders? *JPRAS Open*. (2019) 22:44–54. doi: 10.1016/j.jpra.2019.09.004

15. Sadiq A, Shah A, Jeschke MG, Belo C, Hayat MQ, Murad S, et al. The role of serotonin during skin healing in post-thermal injury. *Int J Mol Sci*. (2018) 19:1034. doi: 10.3390/ijms19041034

16. Kim H, Anggradita LD, Lee S-J, Hur SS, Bae J, Hwang NS-Y, et al. Ameliorating fibrotic phenotypes of keloid dermal fibroblasts through an epidermal growth factor-mediated extracellular matrix remodeling. *Int J Mol Sci*. (2021) 22:2198. doi: 10.3390/ijms22042198

17. Park Y-J, Kim EK, Bae JY, Moon S, Kim J. Human telomerase reverse transcriptase (hTERT) promotes cancer invasion by modulating cathepsin D *via* early growth response (EGR)-1. *Cancer Lett*. (2016) 370:222–31. doi: 10.1016/j.canlet.2015.10.021

18. Robin JD, Wright WE, Zou Y, Cossette SC, Lawlor MW, Gussoni E. Isolation and immortalization of patient-derived cell lines from muscle biopsy for disease modelling. *J Vis Exp*. (2015) 95:e52307. doi: 10.3791/52307-v

19. Giugliano G, Pasqualib D, Notarob A, Brongoa S, Nicolettia G, D'Andreaa F, et al. Verapamil inhibits interleukin-6 and vascular endothelial growth factor production in primary cultures of keloid fibroblasts. *Br Assoc Plas Surg*. (2003) 56:804–9. doi: 10.1016/S0007-1226(03)00384-9

20. Chen AD, Chen RF, Li YT, Huang YT, Lin SD, Lai CS, et al. Triamcinolone acetonide suppresses keloid formation through enhancing apoptosis in a nude mouse model. *Ann Plast Surg*. (2019) 83:S50–4. doi: 10.1097/SAP.0000000000002090

21. Euler T, Valesky EM, Meissner M, Hrgovic I, Kaufmann R, Kippenberger S. Normal and keloid fibroblasts are differentially influenced by IFN-γ and triamcinolone as well as by their combination. *Wound Repair Regener*. (2019) 27:450–61. doi: 10.1111/wrr.12722

22. Kara K, Richard S. Treatment of keloids: A meta-analysis of intralesional triamcinolone, verapamil, and their combination. *Plast Reconstruct Surg*. (2022) 10:e4075. doi: 10.1097/GOX.0000000000004075

23. Vaiserman A, Krasnienkov D. Telomere length as a marker of biological age: state-of-the-art, open issues, and future perspectives. *Front Genet*. (2021) 11:630186. doi: 10.3389/fgene.2020.630186

24. Su F, Liu X, Liu G, Yu Y, Wang Y, Yaping J, et al. Establishment and evaluation of a stable cattle type II alveolar epithelial cell line. *PloS One*. (2013) 8:e76036. doi: 10.1371/journal.pone.0076036

25. Lindvall C, Hou M, Komurasaki T, Zheng C, Henriksson M, Sedivy JM, et al. Molecular characterization of human telomerase reverse transcriptase-immortalized human fibroblasts by gene expression profiling: activation of the epiregulin gene. *Cancer Res*. (2003) 63:1743–7.

26. Liu H, Liu Q, Ge Y, Zhao Q, Zheng X, Zhao Y. hTERT promotes cell adhesion and migration independent of telomerase activity. *Sci Rep*. (2016) 6:22886. doi: 10.1038/srep22886

27. Liu Q, Wang X, Jia Y, Long X, Yu N, Wang Y, et al. Increased blood flow in keloids and adjacent skin revealed by laser speckle contrast imaging. *Lasers Surg Med*. (2016) 48:360–4. doi: 10.1002/lsm.22470

28. Ashcroft KJ, Syed F, Bayat A. Site-specific keloid fibroblasts alter the behaviour of normal skin and normal scar fibroblasts through paracrine signalling. *PloS One*. (2013) 8:e75600. doi: 10.1371/journal.pone.0075600

29. McCoy BJ, Diegelmann RF, Cohen IK. *In vitro* inhibition of cell growth, collagen synthesis, and prolyl hydroxylase activity by triamcinolone acetonide. *Proc Soc Exp Biol Med*. (1980) 163:216–22. doi: 10.3181/00379727-163-40750

30. Oddera S, Cagnoni F, Mangraviti S, Giron-Michel J, Popova O, Canonica GW. Effects of triamcinolone acetonide on adult human lung fibroblasts: decrease in proliferation, surface molecule expression and mediator release. *Int Arch Allergy Immunol*. (2002) 129:152–9. doi: 10.1159/000065877

31. Yang TH, Gingery A, Thoreson AR, Larson DR, Zhao C, Amadio PC. Triamcinolone Acetonide affects TGF-β signaling regulation of fibrosis in idiopathic carpal tunnel syndrome. *BMC Musculoskelet Disord*. (2018) 19:342. doi: 10.1186/s12891-018-2260-y

32. Johnson BZ, Stevenson AW, Prêle CM, Fear MW, Wood FM. The role of IL-6 in skin fibrosis and cutaneous wound healing. *Biomedicines*. (2020) 8:101. doi: 10.3390/biomedicines8050101

# Frontiers in Immunology

**Explores novel approaches and diagnoses to treat immune disorders.**

The official journal of the International Union of Immunological Societies (IUIS) and the most cited in its field, leading the way for research across basic, translational and clinical immunology.

## Discover the latest Research Topics

See more →


**Frontiers**

Avenue du Tribunal-Fédéral 34
1005 Lausanne, Switzerland
frontiersin.org

**Contact us**

+41 (0)21 510 17 00
frontiersin.org/about/contact